



Universitat d'Alacant
Universidad de Alicante

Electrochemical functionalization of
nanostructured carbon material for
bioelectrochemical applications

Andrés Felipe Quintero Jaime



Tesis **Doctorales**

UNIVERSIDAD de ALICANTE

Unitat de Digitalització UA
Unidad de Digitalización UA



Universitat d'Alacant
Universidad de Alicante

Andrés Felipe Quintero Jaime

Electrochemical Functionalization of Nanostructured Carbon Materials for Bioelectrochemical Applications

Andrés Felipe Quintero Jaime

Universitat d'Alacant
Universidad de Alicante



Departamento de Química Física
Departamento de Química Inorgánica
Instituto Universitario de Materiales

**Electrochemical Functionalization of Nanostructured Carbon
Materials for Bioelectrochemical Applications**

Andrés Felipe Quintero Jaime

Tesis presentada para aspirar al grado de
DOCTOR por la Universidad de Alicante con
MENCIÓN DE DOCTOR INTERNACIONAL

DOCTORADO EN CIENCIA DE MATERIALES

Dirigida por:

Emilia Morallón Núñez
Catedrática de Química Física

Diego Cazorla Amorós
Catedrático de Química Inorgánica

ACKNOWLEDGEMENTS

First of all, I would like to express my deepest gratitude to my thesis supervisors, Prof. Dr. Emilia Morallón Núñez and Prof. Dr. Diego Cazorla Amorós for giving me the great opportunity to let me conduct this research through the scholarship and supporting me during my PhD, as well as his valuable guidance, comments and suggestions on the scientific work.

Special thanks to the Generalitat Valenciana for providing me the full scholarship of my PhD thesis through the Santiago Grisolia program.

I gratefully acknowledge to Prof. Dr Wolfgang Schuhmann and Dr. Felipe Conzuelo for accepting my invitation during my research stay in Electroanalitik und Sensorik group, and all the unconditional support.

I wish to express my gratitude to all my colleagues and professors in the group of electrocatalysis and electrochemical of polymers (GEPE), members of IUMA, friends from the electrochemistry groups and my friends in UA for all the great moments during this journey, making this 4 years one of the most beautiful experiences in my life, all of you are part of this ending.

Mi querida Lore, la verdad es que buena parte de esta recta final llena de altibajos y de esfuerzo sólo fue posible superarla gracias a ti, convirtiéndolos en momentos maravillosos, llevaderos e irreales, una madre putativa, y nunca podré expresar mi gratitud hacia ti.

Daniela me siento profundamente agradecido por darme todo ese apoyo incondicional y ese esfuerzo maravilloso, por estar en todo este proceso desde la distancia. Alemania fue absolutamente maravillosa con todo el brillo y alegría de tu amistad.

Ich möchte mich bedanken bei Daniela Wintrich und Alexander Boltz für eures Vertrauen, eure Unterstützung und wunderschöne Freundschaft, dass ihr mir gegeben habt. Ihr habt mir gezeigt, wie die Walle und Nordlichter aussehen. Ich habe schöne Erinnerungen an euch und an der schöne Zeit, die wir zusammen in Österreich verbracht haben. Wegen euch habe ich immer Wunsch nach Bochum zurückzukehren.

Also all the members in ELAN group for such wonderful moments out and inside the lab; and the great moments in the lunch, as well as the confidence during my 3 months in Germany.

A todos mis amigos y mi familia en Colombia y USA, infinitas gracias por toda esa incondicionalidad y apoyo en la distancia, las videollamadas y mensajes hicieron cada minuto más ameno.

Por ustedes...



Universitat d'Alacant
Universidad de Alicante

Papá



Universitat d'Alacant
Universidad de Alicante

*Leben heißt mehr Träume zu haben
als die Realität zerstören kann*

INDEX

Objectives and structure of the PhD Thesis

| | |
|---------------------------------|---|
| 1. Introduction | 1 |
| 2. Objectives of the PhD thesis | 1 |
| 3. Structure of the PhD Thesis | 2 |

Chapter 1: General Introduction

| | |
|--|----|
| 1. Nanostructured carbon materials | 11 |
| 1.1. Carbon nanotubes | 12 |
| 1.2. Graphene and Graphene oxide | 14 |
| 2. Surface chemistry of carbon materials | 15 |
| 2.1. Surface functionalization | 16 |
| 2.1.1. Non-covalent functionalization | 16 |
| 2.1.2. Covalent functionalization | 17 |
| 2.1.2.1. Oxygen functionalities | 19 |
| 2.1.2.2. Nitrogen functionalities | 20 |
| 2.1.2.3. Phosphorus species | 21 |
| 3. Electrochemical methods for functionalization | 22 |
| 3.1. Electrochemical non-covalent functionalization | 23 |
| 3.2. Electrochemical covalent functionalization | 23 |
| 4. Bioelectrochemical applications | 25 |
| 4.1. Electrochemical biofuel cells (EBFC) | 25 |
| 4.2. Sensors and Biosensors | 26 |
| 4.2.1. Electrochemical catalytic biosensors | 28 |
| 4.2.2. Electrochemical affinity biosensors | 30 |
| 4.3. Biorecognition molecules in bioelectrochemical application | 33 |
| 4.3.1. Soluble Glucose Dehydrogenase Pyrroloquinoleine quinone (PQQ-GDH) | 35 |
| 4.3.2. Glucose oxidase (GOx) | 36 |
| 4.3.3. Antibodies (Ab) | 37 |
| 4.4. Immobilization procedures of biorecognition elements | 38 |
| 4.4.1. Physical procedures of immobilization | 39 |
| 4.4.1.1. Adsorption | 39 |
| 4.4.1.2. Entrapment | 39 |
| 4.4.2. Chemical procedures of immobilization | 40 |
| 5. Analytes of study | 41 |
| 5.1. Detection of analytes in medical care | 42 |
| 5.1.1. Kallikrein-related peptidase 3 (KLK3) | 42 |

| | |
|-----------------------|----|
| 5.1.2. <i>Glucose</i> | 43 |
| 6. <i>References</i> | 45 |

Chapter 2: Techniques and Experimental Methods

| | |
|--|-----|
| 1. <i>Introduction</i> | 79 |
| 2. <i>Material and reagents</i> | 79 |
| 2.1. <i>Carbon materials</i> | 79 |
| 2.1.1. <i>Oxidized MWCNT and graphene-based materials</i> | 79 |
| 2.2. <i>Enzymes and antibodies</i> | 79 |
| 2.3. <i>Reagents</i> | 80 |
| 3. <i>Electrochemical techniques</i> | 81 |
| 3.1. <i>Cyclic Voltammetry (CV)</i> | 82 |
| 3.2. <i>Chronoamperometry (CA)</i> | 84 |
| 4. <i>Physicochemical characterization techniques</i> | 85 |
| 4.1. <i>Temperature Programmed Desorption (TPD)</i> | 85 |
| 4.2. <i>Physical Adsorption of Gases</i> | 86 |
| 4.2.1. <i>BET theory</i> | 89 |
| 4.3. <i>X-ray Photoelectron Spectroscopy (XPS)</i> | 90 |
| 4.4. <i>Raman Spectroscopy</i> | 91 |
| 5. <i>Analytical techniques</i> | 93 |
| 5.1. <i>Inductively Coupled Plasma Optical Emission Spectrometry (ICP-OES)</i> | 93 |
| 6. <i>Microscopy techniques</i> | 94 |
| 6.1. <i>Field Emission Scanning Electron Microscopy (FESEM)</i> | 95 |
| 6.2. <i>Transmission Electron Microscopy (TEM)</i> | 95 |
| 6.3. <i>Atomic Force Microscopy (AFM)</i> | 97 |
| 7. <i>Statistical analysis of data</i> | 99 |
| 7.1. <i>Statistical parameters for analysis of data: arithmetic average and standard deviation</i> | 99 |
| 7.1.1. <i>Measurements methods</i> | 99 |
| 7.1.1.1. <i>Calibration methods</i> | 100 |
| 7.1.1.1.1. <i>External calibration</i> | 100 |
| 7.1.1.1.2. <i>Unweighted calibration</i> | 100 |
| 7.1.1.2. <i>Standard addition method</i> | 100 |
| 7.1.2. <i>Analytical parameters</i> | 102 |
| 7.1.2.1. <i>Sensitivity</i> | 102 |
| 7.1.2.2. <i>Limit of detection and quantification</i> | 102 |
| 7.1.2.3. <i>Dynamic range, Linear range and working range</i> | 103 |
| 8. <i>References</i> | 104 |

Chapter 3: Electrochemical Functionalization of Single-Wall Carbon

Nanotubes with Phosphorus and Nitrogen Species

| | |
|---|-----|
| 1. Introduction | 113 |
| 2. Experimental | 115 |
| 2.1. Materials | 115 |
| 2.2. Surface functionalization with phosphorus and nitrogen species on SWCNT | 115 |
| 2.2.1. pH for the point of zero-charge (pH_{PZC}) | 115 |
| 2.2.2. Electrochemical modification with 4-amino phenyl phosphonic acid (4-APPA) | 116 |
| 2.2.3. Electrochemical characterization | 117 |
| 2.3. Physicochemical characterization | 117 |
| 3. Results and discussion | 118 |
| 3.1. Electrochemical functionalization of SWCNT in acid medium with phosphorus and nitrogen species | 118 |
| 3.1.1. Electrochemical oxidation of SWCNT in acid medium in presence of 4-APPA | 118 |
| 3.1.2. Electrochemical characterization of SWCNT functionalized with P and N | 120 |
| 3.2. Morphological characterization of SWCNT modified electrochemically with P and N species | 129 |
| 3.3. XPS analysis of P and N species on electrochemically modified SWCNT | 130 |
| 3.4. Raman spectroscopy of SWCNT electrochemically modified with 4-APPA | 134 |
| 4. Conclusions | 137 |
| 5. References | 137 |

Chapter 4: Effect of Surface Oxygen Groups in the Electrochemical Modification of Multi-Walled Carbon Nanotubes by 4-amino phenyl phosphonic acid

| | |
|---|-----|
| 1. Introduction | 149 |
| 2. Experimental | 151 |
| 2.1. Reagents and materials | 151 |
| 2.2. Electrochemical incorporation of phosphorus and nitrogen functionalities on CNTs | 151 |
| 2.2.1. Oxidation of pristine Multi-Walled Carbon Nanotubes | 151 |
| 2.2.2. Functionalization of MWCNTs and fMWCNTs with 4-APPA | 151 |
| 2.2.3. Electrochemical characterization | 152 |
| 2.3. Physicochemical characterization | 152 |

| | |
|--|-----|
| 3. Results and discussion | 153 |
| 3.1. <i>Physicochemical characterization of pristine MWCNTs and fMWCNT</i> | 153 |
| 3.2. <i>Electrochemical modification with 4-APPA</i> | 155 |
| 3.3. <i>Morphological characterization</i> | 165 |
| 3.4. <i>XPS characterization</i> | 166 |
| 3.5. <i>Raman spectroscopy</i> | 172 |
| 4. Conclusions | 175 |
| 5. References | 176 |

Annex to Chapter 4: Electrochemical Functionalization of Graphene-based Carbon Materials with Phosphorus and Nitrogen Species

| | |
|--|-----|
| 1. Experimental | 187 |
| 1.1. <i>Reagents</i> | 187 |
| 1.2. <i>Synthesis of graphene-based materials</i> | 187 |
| 1.2.1. <i>Graphene oxide</i> | 187 |
| 1.2.2. <i>Graphene oxide electrochemically reduced</i> | 187 |
| 1.2.3. <i>Graphene</i> | 188 |
| 1.3. <i>Electrochemical modification with 4-Aminophenyl phosphonic acid</i> | 188 |
| 1.4. <i>Electrochemical characterization</i> | 189 |
| 1.5. <i>Physicochemical characterization</i> | 189 |
| 2. Results and discussion | 189 |
| 2.1. <i>Electrochemical reduction of GO under neutral conditions</i> | 189 |
| 2.2. <i>Surface functionalization with 4-APPA</i> | 191 |
| 2.3. <i>XPS analysis of P and N species on electrochemically modified graphene-based materials</i> | 195 |
| 3. References | 201 |

Chapter 5: Electron Transfer Enhancement at Electrochemically Modified Multiwall Carbon Nanotubes based Bioelectrodes

| | |
|--|-----|
| 1. Introduction | 207 |
| 2. Experimental section | 208 |
| 2.1. <i>Materials</i> | 208 |
| 2.2. <i>Electrochemical modification of MWCNTs with 4-amino phenyl phosphonic acid</i> | 209 |
| 2.3. <i>Physicochemical characterization.</i> | 210 |
| 2.4. <i>Multi wall carbon nanotubes electrochemically modified with 4-APPA and PQQ-GDH</i> | 210 |
| 2.5. <i>Electrochemical characterization and biocatalytic activity</i> | |

| | |
|--|-----|
| <i>towards glucose oxidation</i> | 211 |
| 3. Results and discussion | 212 |
| 3.1. <i>Electrochemical modification of MWCTN with 4-APPA</i> | 212 |
| 3.2. <i>Electrochemical characterization of MWCNT modified with 4-APPA and PQQ-GDH</i> | 215 |
| 3.3. <i>Electrocatalytic response of MWCNT-APPA-X-GDH electrodes towards glucose oxidation</i> | 222 |
| 3.4. <i>Stability of MWCNT-APPA-X-GDH electrodes</i> | 228 |
| 4. Conclusions | 229 |
| 5. References | 230 |

Chapter 6: Single Wall Carbon Nanotubes-based Bioelectrodes Prepared by One-step Electrochemical Enzyme Entrapment

| | |
|---|-----|
| 1. Introduction | 239 |
| 2. Experimental | 240 |
| 2.1. <i>Reagents and equipment</i> | 240 |
| 2.2. <i>Electrochemical entrapment of enzyme</i> | 241 |
| 2.2.1. <i>Enzymatic electrolyte solutions</i> | 241 |
| 2.2.2. <i>One-step electrochemical synthesis of the bioelectrodes</i> | 242 |
| 2.3. <i>Physicochemical characterization</i> | 244 |
| 2.4. <i>Electrochemical characterization and catalytic activity towards glucose oxidation</i> | 245 |
| 3. Results and discussion | 246 |
| 3.1. <i>Electrochemical entrapment of s-GDH on SWCNT with 4-APPA using procedure 1</i> | 246 |
| 3.1.1. <i>Glucose oxidation on SWCNT-APPA-X@GDH/PQQ electrodes</i> | 249 |
| 3.2. <i>Immobilization of PQQ-GDH using procedure 2</i> | 253 |
| 3.2.1. <i>Electrochemical synthesis of SWCNT-APPA-X@PQQ-GDH electrodes</i> | 253 |
| 3.2.2. <i>Physicochemical characterization of SWCNT-APPA-X@PQQ-GDH electrodes</i> | 255 |
| 3.2.3. <i>Glucose oxidation on SWCNT-APPA-X@GDH-PQQ electrodes</i> | 259 |
| 3.2.4. <i>Stability and reproducibility</i> | 260 |
| 3.3. <i>Comparison between both procedures and drop-casting method.</i> | 261 |
| 4. Conclusions | 262 |
| 5. References | 263 |

Annex to Chapter 6: Single Wall Carbon Nanotubes-based Bioelectrodes Prepared by One-step Electrochemical Enzyme Entrapment

273

Chapter 7: Metal Free Electrochemical Glucose Biosensor based on N-doped Carbon Material

| | |
|--|-----|
| 1. Introduction | 291 |
| 2. Experimental section | 292 |
| 2.1. Materials | 292 |
| 2.2. Synthesis of PANI-TT | 293 |
| 2.3. Preparation of PANI-TT- GO_x modified electrode | 293 |
| 2.4. Physicochemical characterization | 294 |
| 2.5. Electrochemical characterization. | 295 |
| 3. Results and discussion | 296 |
| 3.1. Physicochemical characterization of PANI-TT | 296 |
| 3.2. Electrochemical behavior of PANI-TT- GO_x | 297 |
| 3.3. Electrocatalytic activity towards glucose oxidation | 302 |
| 3.4. Real samples | 308 |
| 3.5. Reproducibility and stability of PANI-TT- GO_x biosensors | 310 |
| 4. Conclusions | 311 |
| 5. References | 312 |

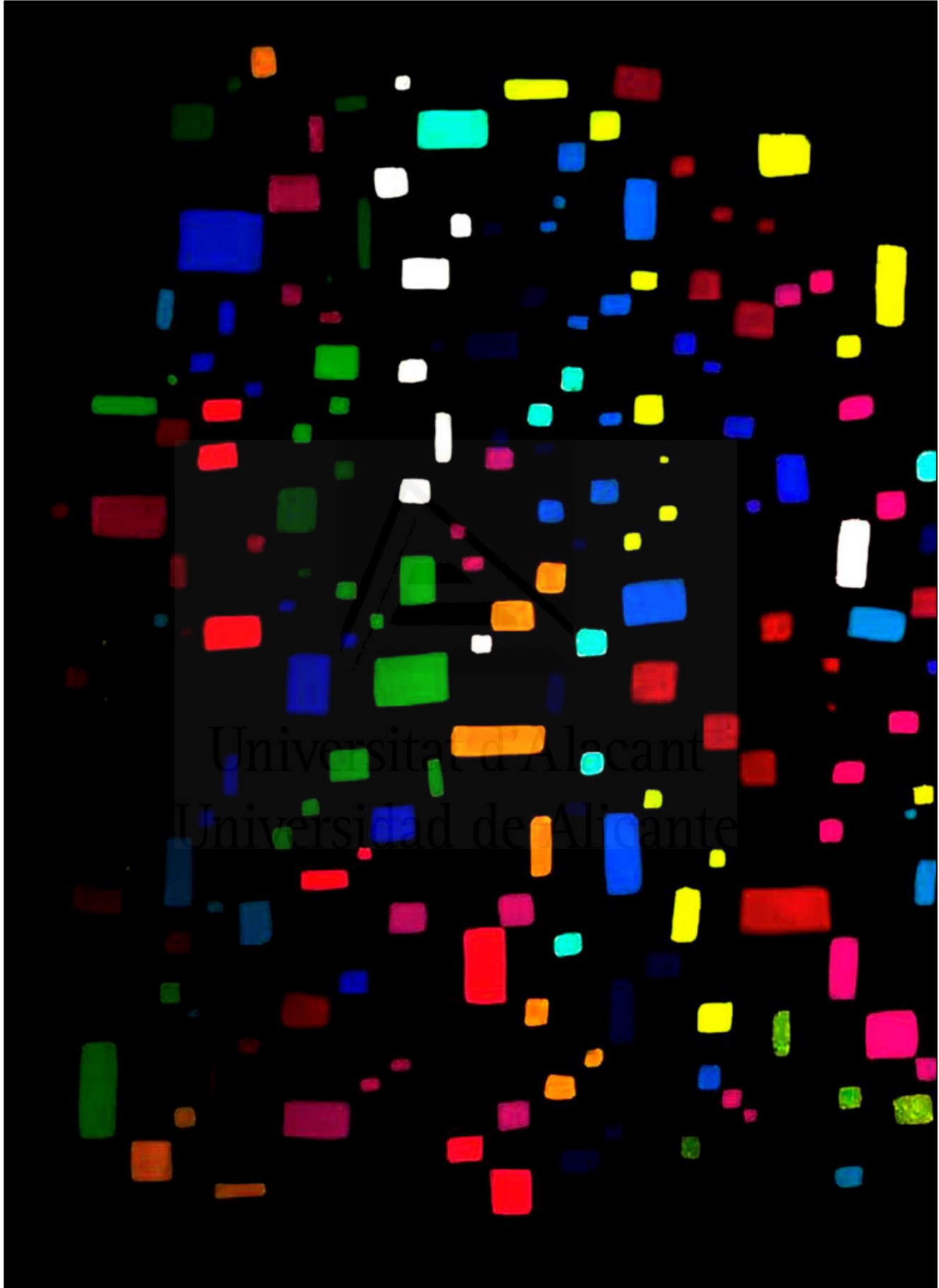
Chapter 8: Carbon Nanotubes Modified with Au for Electrochemical Detection of Prostate Specific Antigen: Effect of Au Nanoparticle Size Distribution

| | |
|--|-----|
| 1. Introduction | 323 |
| 2. Experimental | 325 |
| 2.1. Materials | 325 |
| 2.2. Preparation of the transducer material. Functionalized Multi-Wall Carbon Nanotubes (fMWCNT) with gold nanoparticles (AuNPs) | 326 |
| 2.2.1. Functionalization of Multi-Wall Carbon Nanotubes | 326 |
| 2.2.2. Gold nanoparticles synthesis | 326 |
| 2.2.3. fMWCNT decorated with AuNPs dispersion | 327 |
| 2.3. Immunosensor electrode preparation | 328 |
| 2.4. Electrochemical methods | 329 |
| 2.5. Physicochemical characterization | 329 |
| 3. Results and discussion | 330 |
| 3.1. fMWCNT-AuNPs electrodes characterization | 330 |

| | |
|---|------------|
| 3.1.1. <i>Physicochemical characterization</i> | 330 |
| 3.1.2. <i>Electrochemical characterization of fMWCNT-AuNPs</i> | 335 |
| 3.2. <i>Electrochemical characterization of the monoclonal antibodies immobilized on the fMWCNT-AuNPs samples</i> | 336 |
| 3.3. <i>Electrochemical performance of the PSA immunosensor</i> | 338 |
| 4. Conclusions | 346 |
| 5. References | 346 |
| Chapter 9: General conclusions | 357 |
| Capítulo 9: Conclusiones generales | 367 |
| Chapter 10: Resumen y conclusiones generales | 377 |



Universitat d'Alacant
Universidad de Alicante



Universitat d'Alicant
Universidad de Alicante

Chapter 0

Objectives and Structure of the PhD Thesis



Universitat d'Alacant
Universidad de Alicante

Objectives and structure of the PhD Thesis

1. Introduction

The present PhD thesis focuses on the development of different electrochemical methods for the functionalization of nanostructured carbon materials. Moreover, some chemical methods have also been studied. In the following chapters the different chemical and electrochemical procedures to obtain functional carbon materials are presented, their physicochemical, structural and electrochemical characterization, as well as, the performance as bioelectrodes and biosensors are also shown.

2. Objectives of the PhD thesis

The main objective of this PhD Thesis is the development of new electrochemical methods for functionalization of carbon materials for their further application as bioelectrodes and electrochemical biosensors, employing different bioelements. Based on this objective, the following specific objectives are presented:

- Electrochemical functionalization of nanostructured carbon materials (carbon nanotubes, graphene, graphene oxide, reduced graphene oxide) through the oxidation of 4-aminophenyl phosphonic acid (4-APPA) to introduce heteroatoms, such as N and P, on the carbon surface.
- Chemical functionalization with the incorporation of Au nanoparticles.
- Physicochemical, morphological and electrochemical characterization of the different functionalized carbon materials.
- Evaluate the applicability of the electrochemically functionalized carbon nanotubes in the immobilization of glucose dehydrogenase and the performance of the bioelectrodes to glucose oxidation.
- Development of a metal-free electrochemical biosensor of glucose employing N-doped carbon material prepared by carbonization of polyaniline.
- Develop a label-free electrochemical biosensor based on carbon nanotube modified with Au nanoparticles for the indirect immunodetection of the prostate specific antigen (PSA).

3. Structure of the PhD Thesis

The present PhD Thesis has been performed in the research groups Electrocatalysis and Polymer Electrochemistry (GEPE) and Carbon Materials and Environment (MCMA), belonging to the Materials Institute of the University of Alicante (IUMA).

- Chapter 1: General Introduction.

In this chapter an introduction of the main concepts and a specific description of the different carbon-based materials employed in this PhD Thesis, is performed. Furthermore, a description of the current procedures of surface modification, including electrochemical functionalization of carbon materials is presented. Moreover, the description of the different bioelectrodes and their application in bioelectrochemistry, including electrochemical biofuel cells and biosensors, is discussed. Then, the classification and the different immobilization procedures of bioelements have been presented.

- Chapter 2: Techniques and Methodology.

This chapter describes the different reagents, techniques and statistical methods employed during this PhD Thesis. A summary of the main concepts for each technique employed for physicochemical, morphological and electrochemical characterization is presented. Moreover, the different procedures, the accurate determination of the species of interest, different equations and statistical methods employed for the validation and reliability of the results obtained, are described in detail in this chapter.

- Chapter 3: Electrochemical Functionalization of Single Wall Carbon Nanotubes with Phosphorus and Nitrogen Species.

In this chapter, Single Wall Carbon Nanotubes (SWCNTs) have been successfully functionalized by electrochemical oxidation in presence of 4-amino phenyl phosphonic acid (4-APPA). Electrochemical modification has been performed by cyclic voltammetry using different upper potential limits, producing the incorporation of N and P functionalities on SWCNT through polymerization reactions. Electrochemical oxidation in presence of carbon nanotubes (CNTs) produces polymerization of 4-APPA, what has been related

to the interaction between monomer and the CNT surface. The voltammograms of the functionalized SWCNTs show different well-defined redox processes that are maintained at high pH. Raman spectroscopy shows that the structure of the SWCNT is maintained even at high potentials suggesting that oxidation selectively occurs in the 4-APPA monomer favoring polymer chain growth. The degree of modification of SWCNT can be easily controlled by selecting the electrochemical conditions.

Results of this chapter have been published in:

Quintero-Jaime, Andrés Felipe; Cazorla-Amorós, Diego; Morallón, Emilia. Electrochemical Functionalization of Single Wall Carbon Nanotubes with Phosphorus and Nitrogen Species, *Electrochimica Acta* (2020), 340, 135935

- Chapter 4: Effect of Surface Oxygen Groups in the Electrochemical Modification of Multi-Walled Carbon Nanotubes by 4-amino Phenyl Phosphonic Acid.

In this chapter, the electrochemical functionalization of pristine Multi-Walled Carbon Nanotubes (MWCNTs) and oxidized MWCNTs by nitric acid with 4-amino phenyl phosphonic acid (4-APPA) has been studied. Electrochemical modification has been carried out by cyclic voltammetry using different upper potential limits, what results in the incorporation of N and P functionalities through oligomerization and covalent attachment. The electrochemical characterization shows that there are important differences among the functionalized materials derived from the pristine MWCNTs or the oxidized materials. For the pristine MWCNTs, well-defined redox processes are observed. Characterization by X-Ray photoelectron spectroscopy, Raman spectroscopy and electron microscopy, show that oligomerization is easier for the pristine MWCNTs and the presence of oligomer chains are clearly distinguished for the lowest oxidation potentials. However, the presence of surface oxygen groups in the oxidized MWCNTs modify the interaction of the 4-APPA with the surface promoting mainly covalent attachment.

Results of this chapter have been published in:

Quintero-Jaime, Andrés Felipe. Cazorla-Amorós, Diego. Morallón, Emilia. Effect of Surface Oxygen Groups in the Electrochemical Modification of Multi-Walled Carbon Nanotubes by 4-amino Phenyl Phosphonic Acid, *Carbon* (2020), 165, pp. 328-339.

- Chapter 5: Electron Transfer Enhancement at Electrochemically Modified MWCNT with Phosphorous and Nitrogen Functionalities in Bioelectrode Synthesis.

In this chapter, Multi-Walled Carbon Nanotubes electrochemically modified with nitrogen and phosphorus species have been employed as a platform to immobilize glucose dehydrogenase pyrroloquinoline quinone dependent (PQQ-GDH) for the synthesis of biocatalysts. Depending on the upper potential limit applied during the electrochemical modification of MWCNTs, the nature and amount of the species incorporated on the carbon material surface can be selectively controlled. These incorporated species work as immobilization anchoring groups for the quinone oxidoreductase. The value of the upper potential limit used in the electrochemical modification influences the electron-transfer rate between the electrode and the enzyme. Then, the performance of the bioelectrodes in glucose oxidation and detection is improved by the electrochemical modification conditions, and the sensitivity towards glucose oxidation increases from 39.2 to 53.6 mA gMWCNT⁻¹ mM⁻¹ in a linear range between 0.1 to 1.2 mM. This electrochemical modification can be considered as a remarkable alternative for the synthesis of highly sensitive bioelectrodes.

This chapter contains some of the results obtained during the stay in the group “Elektroanalytik und Sensorik” in the department of Analytical Chemistry in Ruhr Universität (Bochum, Germany) under the supervision of the Prof. D. Wolfgang Schuhmann. It has been submitted for publication.

- Chapter 6: Single Wall Carbon Nanotubes-based Bioelectrodes Prepared by One-step Electrochemical Enzyme Entrapment.

In this chapter of the PhD Thesis, electrochemical entrapment of pyrroloquinoline quinone glucose dehydrogenase on Single Wall Carbon Nanotube electrodes was carried out by one-step during electrooxidation of 4-APPA. The adequate interaction between the functionalized SWCNTs and the enzyme can be achieved by making use of phosphorus groups during the electrochemical co-deposition films improving the electrocatalytic activity towards glucose oxidation. The sensitivity referred to the amount of enzyme, obtained for glucose oxidation (2.29 and 4.28 $\mu\text{A cm}^2 \text{mol}^{-1} \text{mM}^{-1}$) for the bioelectrodes synthesized at 1.15 V is improved in comparison with the drop-

casting method ($0.66 \mu\text{A cm}^2 \text{ mol}^{-1} \text{ mM}^{-1}$). Then, the one-step electrochemical entrapment in presence of 4-APPA, provides a good method for the development of bioelectrodes for glucose oxidation with high sensitivity and reproducibility.

This chapter shows some of the results obtained during the stay in the group “Elektroanalytik und Sensorik” in the department of Analytical Chemistry in Ruhr Universität (Bochum, Germany) under the supervision of the Prof. D. Wolfgang Schuhmann. It has been submitted for publication.

- Chapter 7: Metal Free Electrochemical Glucose Biosensor Based on N-doped Porous Carbon Material.

In this chapter, an enzymatic metal-free electrochemical biosensor based on immobilized glucose oxidase on a N-doped porous carbon material has been studied for the detection of glucose in different real samples. The N-doped carbon material, which contains quaternary nitrogen groups, has been obtained by heat treatment of polyaniline. These functionalities promote the electrocatalytic activity to oxygen reduction reaction. The electrochemical biosensor presents a remarkable electrochemical activity towards oxygen reduction reaction, being able to detect changes in oxygen concentration generated by the enzymatic oxidation of glucose, allowing the indirect detection of this compound in buffer solution (0.1 M PBS, pH=7.2). The metal-free electrochemical biosensor shows an outstanding performance, with a linear detection range between 5 μM and 5 mM, a high sensitivity of $23.57 \pm 1.77 \mu\text{A mM}^{-1} \text{ cm}^{-2}$ at -0.4 V vs. Ag/AgCl (3 M KCl). At these conditions, the addition of ascorbic acid, dopamine, uric acid and L-gluconic acid do not interfere with glucose determination. The method has been successfully applied to human urine and commercial sugary drink samples, without significant matrix effects, providing an alternative for glucose detection.

Results of this chapter have been submitted for publication in *Electrochimica Acta*.

- Chapter 8: Carbon Nanotubes Modified with Au for Electrochemical Detection of Prostate Specific Antigen: Effect of Au Nanoparticle Size Distribution.

In this chapter, different functionalized Multi-Walled Carbon Nanotube and gold nanoparticles (AuNPs) were synthesized as biosensor electrodes. These materials have been applied to the detection of the Prostate Specific Antigen (PSA). The synthesis of AuNPs was carried out using polyvinylpyrrolidone (PVP) as protecting agent. The PVP/Au molar ratio (0.5 and 50) controls the nanoparticle size distribution, obtaining a wide and narrow distribution with an average diameter of 9.5 nm and 6.6 nm, respectively. Nanoparticle size distribution shows an important effect in the electrochemical performance of the biosensor, increasing the electrochemical active surface area (EASA) and promoting the electron-transfer from the redox probe (Ferrocene/Ferrocenium) to the electrode. Furthermore, a narrow and small nanoparticle size distribution enhances the amount of antibodies immobilized on the transducer material and the performance during the detection of the PSA. Significant results were obtained for the quantification of PSA, with a limit of detection of 1 ng ml^{-1} and sensitivities of 0.085 and $0.056 \mu\text{A mL ng}^{-1}_{\text{PSA}}$ for the two transducer materials in only 5 minutes of detection.

Results of this chapter have been published in:

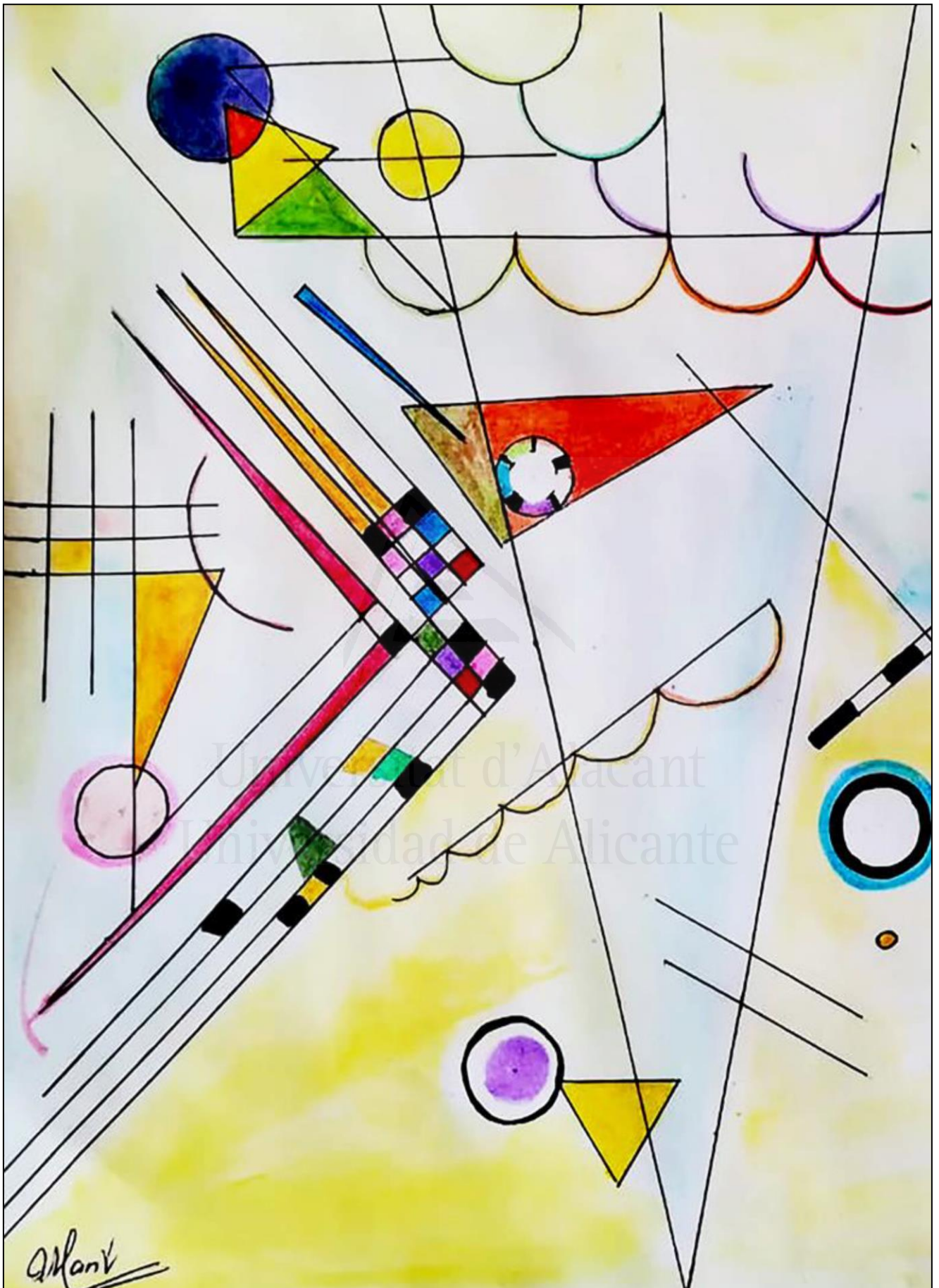
Quintero-Jaime, Andrés Felipe, Berenguer-Murcia, Ángel. Cazorla-Amorós, Diego. Morallón, Emilia. Carbon Nanotubes Modified with Au for Electrochemical Detection of Prostate Specific Antigen: Effect of Au Nanoparticle Size Distribution, *Frontiers in Chemistry* (2019), 7, 147.

- Chapter 9: General Conclusions

In this chapter the main conclusions of the PhD Thesis are presented.

- Chapter 10: Resumen y conclusiones generales.

Este capítulo contiene un resumen del trabajo de tesis que incluye una introducción general, un resumen de los resultados y de la discusión organizada de acuerdo con los capítulos presentados, incluyendo también las conclusiones generales de la tesis.



The background is an abstract watercolor painting. It features several prominent elements: a yellow circle with a dark blue center in the top left; a large blue circle with a yellow center in the middle right; a large black circle with a yellow and orange border and a red dot above it in the bottom right; and a complex geometric shape on the left composed of black, white, red, blue, and yellow segments. Thin black lines and a thick black curved line are scattered across the composition. The overall color palette is bright and varied, set against a light, textured background.

Chapter 1

General Introduction

Universitat d'Alacant
Universidad de Alicante

1. Nanostructured carbon materials

Carbon is one of the most versatile elements, in which the existence of four electrons facilitates the formation of covalent bonds with other C atoms, giving several allotropes, with specific structure and dimension, from 0D to 3D¹⁻⁴. The well-known allotropes of carbon include graphite, diamond and fullerenes, each of which can exist in a variety of materials with differing electrochemical properties.

The most common are based on the graphite structure, consisting of ideally infinite stacked sheets of grapheme layers. The carbon atoms in graphite are all sp² hybridized, with an intraplanar C-C bond length of 1.42 Å and interplanar spacing of 3.354 Å. Graphite based materials, for instance, may present excellent mechanical properties, high surface area and high electrical conductivity^{4,5}. For that reason, their application has been extended in different fields like energy storage and energy production^{6,7}, removal of pollutants^{3,8}, sensing/biosensing⁹⁻¹¹, medical-drugs releasing¹²⁻¹⁴, synthesis of composite material^{15,16}, catalysis^{17,18}, among others.

Carbon atoms in diamond are sp³ hybridized and with a tetrahedral geometry, with a C-C bond length of 1.54 Å, and usually contains dopants to provide sufficient electrical conductivity for electrochemical applications. The covalent bonds in diamond extend in the 3D space and the electrons are highly localized, what confers high hardness and thermal conductivity, low electrical conductivity and remarkable optical properties⁴.

Structural classification of carbon materials can be done considering the special dimension of the basic structural unit. Carbon materials with 0D structure, in which fullerenes can be found, are composed by a structure of pentagons and hexagons of carbon atoms bonded between them, generating single molecules with a closed tridimensional structure^{19,20}. Pentagons in the carbon material structure are responsible of the curvature, generating the characteristic closed cage structure of the fullerenes. The most stable structure is the C₆₀ that contains 12 pentagons and 20 hexagons of carbon atoms. Fullerenes with other number of carbon atoms have been reported in literature^{21,22}.

Carbon nanotubes are an example of 1D carbon materials, which consist on rolled-up graphene layers with its edges connected, which can be constituted by a single sheet of graphene (Single Walled CNT) or multiple sheets of graphene (Multi-Walled CNT)^{9,23,24}.

Graphene is a single-atom-thick sheet of hexagonally arranged, sp²-bonded carbon atoms that is not an integral part of a carbon material, but is freely suspended or adhered on a foreign substrate (2D structure)²⁵. Graphene has extraordinary mechanical, thermal and electrical properties²⁶.

Nowadays, research on carbon materials is rapidly growing, for example, in the development of porous and hierarchical structures, considering the strong influence that porosity presents in the properties of the material and, thus, in the applicability²⁷⁻²⁹. In principle, porous carbon materials are characterized by the presence of mainly sp² C-C bonds, arranged in graphene-like layers. In a simplified model of porosity, interlayer separation determines the formation of pores and, in the case of nanostructured porous carbons, the space between groups of graphene-domains can contribute to more ordered structured porosity in the resultant carbon materials^{30,31}. Methods of synthesis for these nanostructured porous materials use a nanostructured material of different composition which acts as a template. Generally, templates are based on polymers, mesoporous silica, zeolites, etc.^{7,30-33}.

Since in the present PhD Thesis different nanostructured carbon materials were employed as transducer materials to develop functional electrodes for applications in bioelectrochemistry, a detailed description of the specific carbon materials is presented in the following section.

1.1. Carbon nanotubes

Discovery of CNTs by Ijima in 1991 was performed by direct current arc-discharge evaporation of a carbon electrode at 100 torr, reaching high temperatures of around 2500°C, obtaining carbon materials with cylindrical structure with few nanometers of diameter³⁴. Carbon nanotubes can be classified into Single-Walled Carbon Nanotubes, which are conformed by a single graphene sheet rolled-up into a tube and Multi-Walled Carbon Nanotubes^{9,35,36}. In addition, MWCNTs can occur in various morphologies such as hollow tube, bamboo and herringbone, depending on their mode of

preparation³⁷. Interestingly, CNTs properties, especially electronic conductivity, has a strong dependence with the diameter of the tube and the wrapping angle of the graphene layer (helicity), giving place to a metallic and semiconducting behavior^{38,39}. Manufacturing synthesis processes of CNTs (i.e. Chemical Vapor Deposition, laser ablation) have focused in the selective synthesis of specific CNTs⁴⁰. configurations of the carbon nanotubes are determined by the wrapping vector (n,m) (Figure 1.1). Zigzag configuration occurs when $m = 0$ and armchair appears when $n = m$. All other tubes are of the ‘chiral’ type and have a finite wrapping angle ϕ between 0° and 30° ^{41,42}. Armchair tubes are metallic. For all other tubes (chiral and zigzag) there exist two possibilities. When $n-m=3l$ (where l is an integer), tubes are also expected to be metallic. In the case $n-m \neq 3l$, tubes are predicted to be semiconducting^{41,43}.

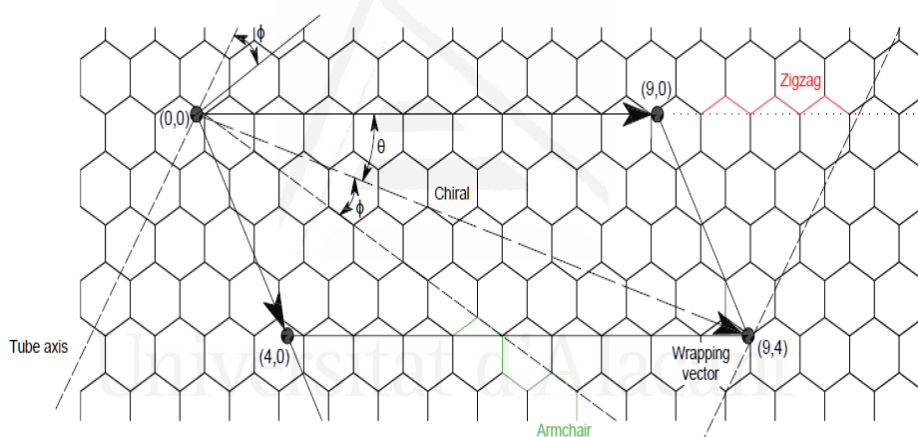


Figure 1.1. Construction of a carbon nanotube from a graphene sheet by rolling up the sheet along wrapping vector. (Adapted from: Wilder, J. W. G., Venema, L. C., Rinzler, A. G., Smalley, R. E., Dekker, C. Nature 391, 59-62 (1998)⁴¹).

In general, properties of CNTs are associated to the presence of high density of delocalized π orbitals in the outside part of the tube structure that facilitates the movement of the electrons through the material, promoting even a catalytic behavior for some reactions²⁴. Additionally, ordered structure of the carbon aromatic rings causes strong π - π interactions between CNTs which generates a stacking and agglomeration between them forming bundles³⁵. Non-

polar character of CNTs makes necessary the use of organic solvents for the proper management and further use of this material.

Even though CNTs properties make this material a promising candidate for different applications, direct use of CNTs has been limited as consequence of the difficult processability and dispersibility^{44,45}. Then, it is necessary the functionalization of CNTs without loss of properties and, for this reason, different methodologies of surface modification can be applied based on non-covalent interaction^{46,47}; or covalent modification⁴⁸.

1.2. Graphene and Graphene oxide

Graphene is a single-atom-thick sheet of hexagonally arranged, sp²-bonded carbon atoms that is not an integral part of a carbon material, but is freely suspended or adhered on a foreign substrate (2D structure)²⁵. One important aspect in the electronic-structure features of graphene is the high tendency of stacking of the graphene layers. Isolated graphene layer exhibits outstanding properties, including the highest room-temperature carrier mobility, a weak optical absorptivity (2.3%), high thermal conductivity (25 times that of silicon) and high mechanical strength (strongest nanomaterial measured, tensile strength of 130 GPa and a Young modulus of 1 TPa)⁴⁹.

Synthesis of graphene includes mechanical exfoliation of graphite, chemical vapor deposition (CVD), sublimation of silicon from SiC and reduction of graphene oxide; being the CVD the most scalable procedure to obtain high quality and controlled layers of graphene. However, time-consumption and high production costs make this procedure still no convenient for large scale graphene synthesis⁵⁰. Different approaches to scalable synthesis graphene from graphite have been attempted, throughout the formation of intercalation compounds which increase the interlayer distance^{51,52}. Another possibility involves the oxidation of graphite to obtain graphite oxide in which the sheets can be easily separated yielding graphene oxide. Thus, the oxidation treatments result in the incorporation of oxygen functional groups in the basal planes (carboxylic, hydroxyl and ether groups, for instance) and the material can be easily dispersed in polar media forming graphene oxide (GO)^{53,54}. However, incorporation of other kind of atoms or functionalities have been performed to obtain graphene layers⁵⁵⁻⁵⁷.

The first synthesis processes of graphene oxide were carried out in 1859 by Brodie⁵⁸, through the incorporation of oxygen in graphite using oxidizing reagents like HNO₃, KClO₃ or mixtures between KMnO₄ and H₂SO₄. Nowadays, Hummers and Offeman procedure with small modifications is the most accepted large-scale and cost-effective method for GO synthesis⁵⁹⁻⁶¹. Even though, unambiguous models of the GO structure do not exist as consequence of the complexity of the material, some models have attempted to explain the possible organization of the oxygen species and carbon atoms in the GO, being the model proposed by Lerf-Klinowski with some variations the most accepted (See Figure 1.2)^{62,63}.

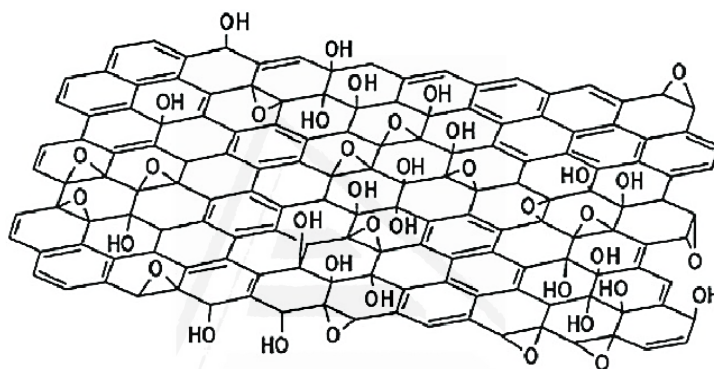


Figure 1.2. Graphene oxide model structure of Lerf-Klinowski (Adapted from: He, H., Klinowski, J. Foster, M., Lerf, A. Chem. Phys. Lett. 287 (1998) 53-56)⁶⁴.

One attractive interest for GO production lies in the use as precursor for graphene synthesis by thermal annealing or by reducing agents to restore the graphene structure^{65,66}. Unfortunately, reduction methods of GO require high temperatures, hazardous reagents and long-term reaction, making less cost-effective for scalable production of reduced graphene oxide⁶⁶; therefore current research in this field is focused in the development of GO reduction process which may overcome the disadvantages of the other methods; for instance, through electrochemical reduction in aqueous or organic media⁶⁷⁻⁷⁰.

2. Surface chemistry of carbon materials

Surface chemistry has a great influence on the physicochemical properties of the carbon materials. Therefore, their performance in applications such as the dispersion in liquids, the dispersion of metallic compounds and the

adsorption of vapors on carbons can be very different⁷¹⁻⁷⁴. Depending on the nature, concentration and distribution of the surface functional groups many authors have recognized that carbon materials can present high selectivity and catalytic activity towards specific reactions, i.e. oxidative dehydrogenation, dehydration of alcohols, NO_x/SO_x removal and liquid phase processes for the oxidation of contaminants⁷⁵⁻⁷⁷. Furthermore, surface functionalities provide acidic and basic behavior of the carbon material surface, which can act as cation and anion exchange sites, promoting an improved adsorption of species in the media for the further catalytic reaction¹⁸.

2.1. Surface functionalization

There are two functionalization methods, covalent and non-covalent functionalization, for modification of surface chemistry of the carbon materials^{74,78}.

2.1.1. Non-covalent functionalization

Non-covalent functionalization is a surface modification procedure in which, a target molecule (surfactant, polymers or aromatic compounds) is incorporated onto the carbon material surface through different kind of interactions, such as π - π stacking, adsorption forces, hydrophobic forces, electrostatic interactions, etc⁷⁹. Therefore, stability of the functionalities on the surface depends of the strength on the surface interactions. Given that, in these procedures formation of covalent bonds is avoided, π -conjugated structure and consequently most of the properties of the pristine material are preserved⁸⁰.

Generally, surfactants and polymers interact strongly with the π -conjugated structure, promoting an adsorption process onto the carbon material, which in some cases can be irreversible⁸¹. Additionally, polymerization and further attachment of organic chains or even biomolecules (DNA) have been performed employing the non-covalent functionalities on the carbon material surface⁸².

During the process of non-covalent functionalization, the target molecule creates a monolayer adsorbed on the carbon material surface; which in case of CNTs, wraps the tubular structure^{83,84}. Thus, one important feature in this kind of procedures is the nature of the functional molecule and its interaction with

the carbon surface; for example, previous studies have observed that depending on the difference of energy density between the functional molecule and the carbon material, stabilization of the system can be driven by the high π - π interaction or electrostatic interactions generated by the electron density⁸⁵. Unfortunately, functionalization by this way results in a difficult control of the degree of surface modification. In addition, the weak forces between the functionalities and the carbon material, and the environment-dependence nature of the interactions molecule-carbon material, can produce leaching and replacement of the functional molecule⁷⁹.

2.1.2. Covalent functionalization

Surface covalent functionalization procedures are based on the formation of covalent bonds through chemical reactions. First attempts of functionalization were developed under high oxidizing conditions, in which, oxygen functional groups (i.e. ether, carboxylic, lactones, hydroxyl, etc.) are incorporated in the structure of carbon materials^{24,79}. Nowadays, a wide variety of literature related with functionalization procedures follow the incorporation of other kind of species, based on the application of oxidative conditions⁸⁶, anchoring of molecules (grafting)⁸⁷ or even further polymerization reactions. Interestingly, through different organic reactions, the generation and anchoring of different functionalities have been possible. One example is shown in Figure 1.3, where different reactions of covalent chemical functionalization on CNTs are presented.

During the modification has been observed that functionalization conditions generate attacks on the carbon material edges and tips, on graphene and CNTs, respectively, but also in the graphene-layer and the sidewall on CNTs, breaking the sp^2 hybridization in the carbon material structure^{44,88,89}. Consequently, covalent functionalization leads not only to a surface modification but also to important structural changes in the carbon material, changing some of the intrinsic properties^{90,91}, being electrical conductivity one of the most affected during this kind of procedures⁸¹. Unfortunately, normal procedures of chemical functionalization lie in the use of high aggressive conditions: oxidative medium, high temperature and toxic chemical reagents; in which non-controlled degree of functionalization and selectivity of the species to incorporate can be achieved⁹².

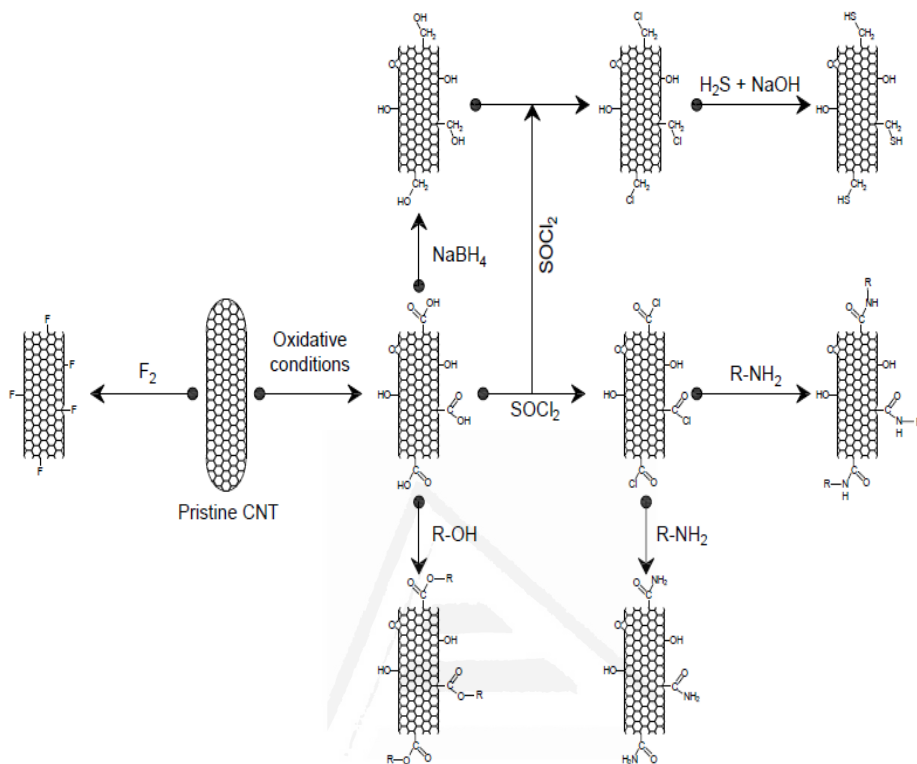


Figure 1.3. Schematic representation of covalent chemical functionalization procedures on CNTs.

In literature, functionalization procedures of CNTs involve the formation of highly reactive intermediate species, which attack the carbon atoms in the carbon material structure^{48,93}. Based on that, some mild alternatives of functionalization have emerged, taking advantage of the reactivity and catalytic effect of the π -conjugated carbon structure, which stabilizes the formation of radical species at lower temperatures and less aggressive conditions. Examples of these procedures have been employed in the functionalization by reduction of diazonium salts, halogenations, anchoring of amines or cycloadditions^{94–97}. Between all the alternatives for functionalization, application of electrochemical methods by oxidation or reduction to form radical species, has grown as a promising controlled and selective functionalization method^{98,99}.

2.1.2.1. Oxygen functionalities

In general, oxygen functionalities are inherently present in the carbon materials, as consequence of the reactivity of the carbon material with the environment during the synthesis process and storage, which also define the acid/basic properties of the carbon material surface^{100,101}. Surface oxygen species can be divided in mainly two groups based on the acid/basic nature¹⁰². Carboxylic acid, anhydrides and lactones tend to give an acid character to the carbon material surface, meanwhile, a neutral and weak basic behavior is observed in carbon materials with phenols, quinones, carbonyls and ethers.

Namely, procedures for functionalization with oxygen species involves the use of oxidative conditions in which the carbon material reacts with the oxidizing medium giving rise to the formation of the functionalities. Depending of the method, it is possible to control the nature of the functionality and even the location in the carbon material structure¹⁰³. Two different routes (dry and wet) highlight as traditional procedures to develop oxygen functionalities. In case of carbon nanotubes, the main carbon material employed in this PhD Thesis, first approaches of application of oxidative conditions can be tracked back to the initial procedures to open the end-caps of the carbon nanotubes using a thermal treatment at 700°C in gas phase using air, NO_x, O₃, among others, taking into account the high reactivity of this part of the CNTs^{74,104}. Interestingly, at the same time that tips of CNTs are opened, elimination of remaining amorphous carbon and functionalization of the surface of the CNTs can take place.

In contrast, wet route was developed as an alternative functionalization procedure in which an oxidant in aqueous solution promotes the oxidation of the carbon material³⁷. Different kind of agents have been employed (i.e. HNO₃, H₂SO₄, H₂SO₄:H₂O₂, HClO₄, H₂SO₄ and KMnO₄ or H₂SO₄ and K₂Cr₂O₇) in order to develop oxygen species^{105,106}, however, in some studies it has been observed that possible incorporation of other species such as sulphur can be achieved.

It is well-known that presence of surface oxygen groups enhances significantly the double-layer capacitance of the carbon materials and may provide faradic contribution to the stored charge¹⁰⁷⁻¹⁰⁹. Additionally, presence

of hydroxyl and carboxylic groups in the CNTs have been used to promote covalent linkages with small molecules¹¹⁰ and carbohydrates in enzymatic elements^{111,112}, facilitating immobilization of the bioelement, and improving the catalytic activity and even orientation of the bioelement¹⁰, what is of interest for biosensing applications. Furthermore, presence of these functionalities has been widely employed to promote different organic reactions such as incorporation of acyl-chloride groups, amidation, fluorination, hydrogenation, esterification, alkylation, cycle-addition and grafting of aromatic and aliphatic chains, working as platform for complexation⁵⁵, immobilization of metal cations¹¹³ or other biomolecules.

2.1.2.2. Nitrogen functionalities

Integration of carbon material in new technologies has involved the incorporation of different functionalities in order to modulate and adapt the carbon material properties, being the nitrogen species one of the most highlighted in many applications. Although nitrogen species can be found in the pristine carbon materials, nowadays different procedures of functionalization have been focused in generating specific nitrogen groups in the carbon material⁷⁴.

Nitrogen atoms can be directly attached to the carbon atoms network forming amine, pyridine, pyrrol species and quaternary nitrogen (also named as graphitic nitrogen), depending on the number of carbon atoms which are bonded with the nitrogen. Also, oxidized species of nitrogen functionalities as amides, pyridones or nitrogen oxides can be observed¹¹⁴. Nitrogen species may confer to the carbon material surface a basic character, hydrophilicity or higher stability, among other properties⁷⁴.

In literature different kind of procedures to incorporate N-functionalities in carbon materials have been intensively investigated. Most common procedures involve a treatment with a nitrogen precursor (i.e. urea, ammonia, melamine) in liquid or gas phase, in which a further process of thermal treatment is performed in order to stabilize or induce the formation of specific species^{74,114}. In this sense, another interesting route to obtain carbon materials with nitrogen functionalities is based on the use of a nitrogen source like polymers (i.e. Polypyrrole or Polyaniline)^{115,116} or organic compounds (i.e. acetonitrile)¹¹⁷

which impregnate or coat the carbon material surface. Then, a thermal treatment is applied to promote polycondensation reactions generating the functionalities¹¹⁴. Interestingly, studies have demonstrated that temperature of the thermal treatment has an important effect in the nature of the functionalities, taking into account that during the heating process, transformation of the N-functionalities occurs, producing a rearrangement of the nitrogen species^{118,119}.

Another interesting and widely used method to incorporate N-functionalities on surface lies on the reactions of amidation through previous oxygen functional groups in the carbon material surface. Two routes have been developed in this functionalization procedure. The first one involves an activation of a carboxylic group by formation of the acyl chloride (SOCl_2) and a subsequent amidation¹²⁰. For the second alternative, the amidation process can be carried out through activation of the carboxylic groups by reaction with carbodiimides¹²¹. In both cases, the presence of amide species have been employed to promote direct covalent immobilization of oligonucleotides and enzymes in biosensing application^{122,123}. Additionally, post thermal treatment favors the formation of pyridine, pyrrole, pyridine and quaternary nitrogen species, which have demonstrated an important enhancement in the electrochemical performance of the carbon material as electrocatalyst for oxygen reduction reaction¹²⁴.

2.1.2.3. Phosphorus species

Phosphorus species are another kind of functionalities that have received interest in the development of functional carbon materials. P incorporation in carbon material enhances their stability towards oxidation¹²⁵. It has also been reported that P increases efficiency of photocatalytic hydrogen evolution reaction, where incorporation of phosphorus in the structure of the carbon material produces a decrease in the band-gap and reduces the recombination of the electron-hole pairs¹²⁶. Furthermore, interesting approaches for development of wide-potential window and high oxidation resistance of carbon materials for electrochemical capacitors have been developed with outstanding results¹²⁷⁻¹²⁹.

Initial approaches of functionalization with phosphorus species were obtained during the carbonization of a carbon precursor in presence of a

phosphorus source, such as phosphoric acid, POCl_3 or phosphate solutions,^{125,129}. However, in the last years use of hydrothermal procedures in the synthesis of P functionalities have shown interesting results¹³⁰. In this process, phosphate, polyphosphate and phosphonate species can be incorporated in the carbon material structure. Another interesting route of P functionalization of carbon material has been carried out employing solvent-free reactions with organophosphorus compounds (triphenylphosphine) in a molten blend of carbon material, in this case SWNCTs, at mild conditions of temperature¹³¹.

Muleja et. al. have shown an interesting route of functionalization through the grafting of different phosphines onto the surface of MWCNTs using reactions of substitution of bromine species induced by arylation on the carbon material, obtaining structures which resembles the triphenylphosphine structure, for application as adsorbent of metals^{132,133}. In contrast to the oxidative treatment with phosphorus-based acids, during the chemical attachment of phosphine, radical species generated cause a nucleophilic attack to the carbon atoms network. In those cases P-C and P-O-C species are normally present in the carbon material surfaces^{134,135}. In this sense, incorporation of carbon materials containing organophosphorus compounds as phosphines, facilitates the complexation with metal cations such as Pd or Ni for catalysis, electrocatalysis applications, metal adsorption and sensing application field¹³⁶⁻¹³⁸.

3. Electrochemical methods for functionalization

The use of electrochemical methods in carbon materials has been extended to the application fields of energy production, energy-storage and biosensing devices^{23,139}. Besides, electrochemical procedures have raised as an alternative for scalable method of purification of carbon materials like CNTs and in the functionalization of carbon materials^{78,140,141}. This latter application has been intensively investigated, given that electrochemical methods can facilitate the formation of radical species by oxidative or reductive conditions to produce a covalent functionalization¹⁴². But also the polarization of the electrode can produce specific electrochemical reactions with species in the electrolyte, which are translated in non-covalent or covalent functionalization⁷⁴. Taking into account that chemical functionalization procedures require harsh operational conditions to promote the generation of active species and

consequently the surface incorporation¹⁴³, electrochemical procedures of functionalization provides milder conditions, at the same time, that offers a wide variety of parameters to obtain selective and controlled degree of modification⁷⁸.

3.1. Electrochemical non-covalent functionalization

Principle of polarization during the application of an electrochemical method (potentiostatic, galvanostatic or potenciodynamic) has been widely employed in the synthesis of composite materials in which mainly polymer layers are generated and deposited on the polarized electrode surface⁷⁴. Porous carbon materials and carbon nanotubes modified with polyaniline (PANI) have been widely explored^{144,145}, but other polymers have also been used¹⁴⁶, as promising electrodes for supercapacitors^{145,147}. Other approaches of non-covalent functionalization rely on the charge modulation of the electrode surface to attract a charged specie in solution, such as chitosan, poly(vinyl amine), among others, generating electrostatic interaction and then co-precipitation of the polymer film by a change from a charged state to a neutral stage^{148,149}. Those polymer chains can interact directly with the surface of the carbon material through π - π stacking between the aromatic compounds, CH- π interactions or electrostatic interactions^{150,151}. Eventually, during polarization process, anodic or cathodic, undesirable reactions such as electrolyte decomposition or oxidation of the electrode can also take place.

3.2. Electrochemical covalent functionalization

Initial approaches of electrochemical modification of carbon materials were based on the attachment of aromatic compounds, using diazonium salts and aromatic/aliphatic amines under reductive or oxidative polarizations, respectively^{152,153}. In those processes, radical formation is promoted by the polarization of the electrode, which presents a high selectivity to attack carbon structure producing the covalent bond^{154,155}. Attachment of the molecule, generally, promotes the formation of a non-electroactive layer, which growth (thickness) can be controlled varying different parameters like potential, time, current density, among others during the modification^{78,156}. Also, surface functionalities may act as initiator point for further polymerization and

growing (See Figure 1.4.)¹⁵⁷. Nevertheless, a continuous region with functional species is generated on the carbon surface.

Eventually, nature of the incorporated functionalities depends on the functional species employed in the electrolyte; for instance, diazonium salts generate functionalities with a high electrical insulating behavior, but with a remarkable tendency to produce covalent bonds with amino acid residues for immobilization of biocomponents^{97,158}. In contrast, other kind of electrochemical functionalization of CNTs, employing conjugated polymers as polyaniline, polypyrrole or other polymers, has been extensively investigated¹⁵⁹. In this case, high conductivity and good electron-transfer kinetics promote the formation of a composite material with good electrochemical activity¹⁶⁰.

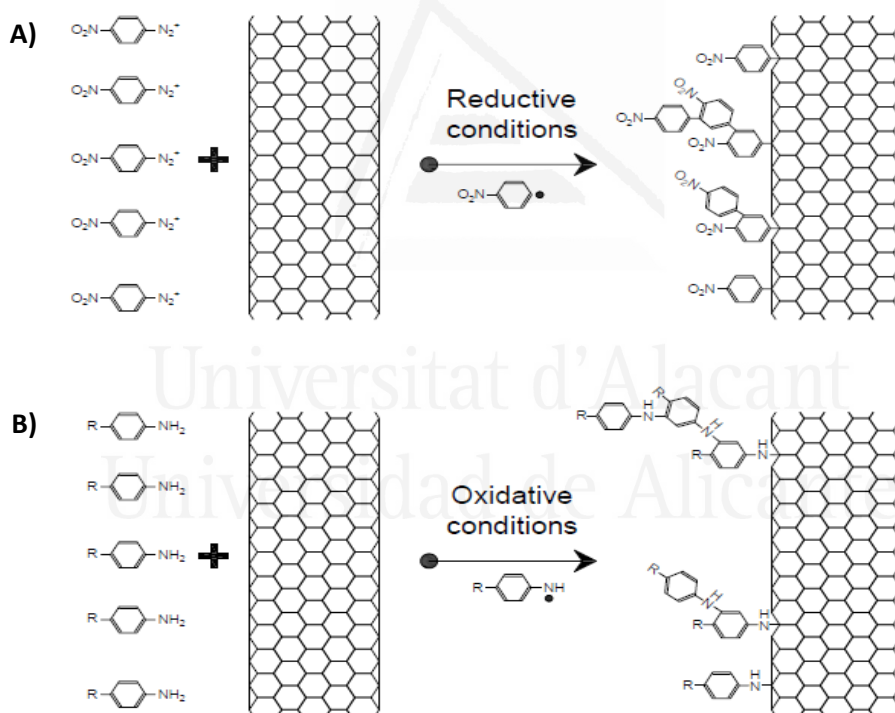


Figure 1.4. Examples of electrochemical functionalization of CNTs by: A) reductive conditions and B) oxidative conditions, employing diazonium salts and aromatic amines.

Unfortunately, high positive polarization of the carbon electrode can normally generate oxidation and corrosion of the carbon material, competition

with other oxidation reactions and loss in the stability of the electrolyte. In a previous research, high oxidative conditions promoted the increase in the surface oxygen species in a wide variety of carbon materials, including carbon nanotubes and activated carbons^{78,140,141}. Meanwhile, electrolysis procedures have been also developed on MWCNTs, promoting the halogenation with chlorine and bromine species; however, important structural changes such as broken-walls in the carbon nanotubes during the functionalization with those species are produced¹⁶¹.

Initial works under oxidative conditions, demonstrated that high anodic potentials are required for a proper radical formation, as has been observed in electrochemical modification of glassy carbon electrodes^{162,163}. Interestingly, curvature of the nanotubes, π -conjugated structure and high charge density provide catalytic activity towards oxidation of N-heterocyclic compounds in aqueous solution, offering the formation of different species on the surface as quinone groups¹⁶⁴. Examples of these works using substituted p-amino benzoic acids, combining a mechanism of covalent attachment of the molecule and non-covalent modification with homopolymers on CNTs, can be found in the literature⁹⁹.

4. Bioelectrochemical applications

In many aspects, biological processes have inspired the basis and fundamental principles of new technologies for different applications^{165,166}. In this sense, electrochemistry has gained a great interest as result of the considerable amount of biological process, which involves different chemical reactions, where electron transfer processes take place. Furthermore, the development of high performance bioelectrodes with high selectivity and efficiency, under considerable mild conditions generate a great interest^{167,168}, for those new technologies (i.e. fuel cells¹⁶⁹, biosensing¹⁷⁰ and photo-electrochemical energy harvesting assisted by photosystems¹⁷¹).

4.1. Electrochemical biofuel cells (EBFC)

EBFCs are a subcategory of the fuel cells, in which electrical energy is produced by the chemical conversion assisted by biomolecules, usually an enzymatic element, normally an oxidoreductase enzyme (redox enzyme), which catalyzes the oxidation or reduction of the specific reagent^{172,173}.

Most common configurations employ as cathode, electrodes modified with a laccase (Lc) or bilirubin oxidase (BOx), which present a high selectivity towards the oxygen reduction reaction (ORR)¹⁷⁴. However, other enzymatic elements (i.e. horse radish peroxidase-HRP) with high preference to reduction of hydrogen peroxide (H₂O₂) can be used in the biocathode¹⁷² (see Figure 1.5). In contrast, anodic reaction is carried out by the oxidation of reagents which act as fuel, commonly sugars, lactate, urea or alcohols. In this case, enzymatic reaction involves the oxidation of the component, producing electron transfer in the redox active center of the enzyme¹⁷⁵. Schematic EBFC is presented in Figure 1.5.

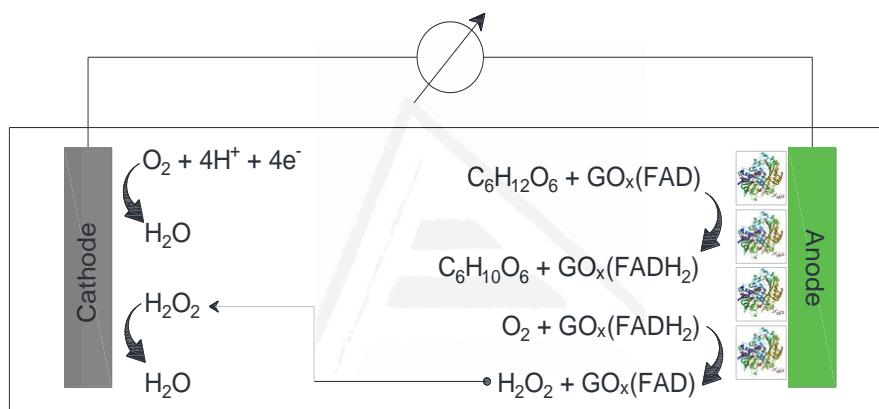


Figure 1.5. Scheme of a typical EBFC configuration.

Considering that performance of a device based on bioelectrochemistry has an important electrode-bioelement interaction dependence, high interest has been paid in the development of a wide variety of strategies for immobilizing the bioelement on the electrode^{156,176,177}. Between all of them, definitely, the use of electroactive compounds, such as conjugated-polymers, osmium hydrogels and carbon materials have demonstrated good immobilization properties¹⁷⁸⁻¹⁸⁰. Also, multi enzymatic platforms in bioelectrodes have provided a good route to generate cascade reactions with the different products generated by the enzymatic reactions, harvesting higher amount of electrons¹⁸¹.

4.2. Sensors and Biosensors

Chemical sensors are analytical devices, which transform a physical or chemical interaction, generated between a specific chemical species (analyte)

with a receptor element in the sensor surface, in a measurable and digitized signal which is correlated with the amount of the chemical species in the sample (Figure 1.6 includes a scheme for an electrochemical sensor). Depending on the transducer-principle, classification of the sensors has been established in optical, magnetic, thermometric, mass and electrochemical sensors^{182–185}.

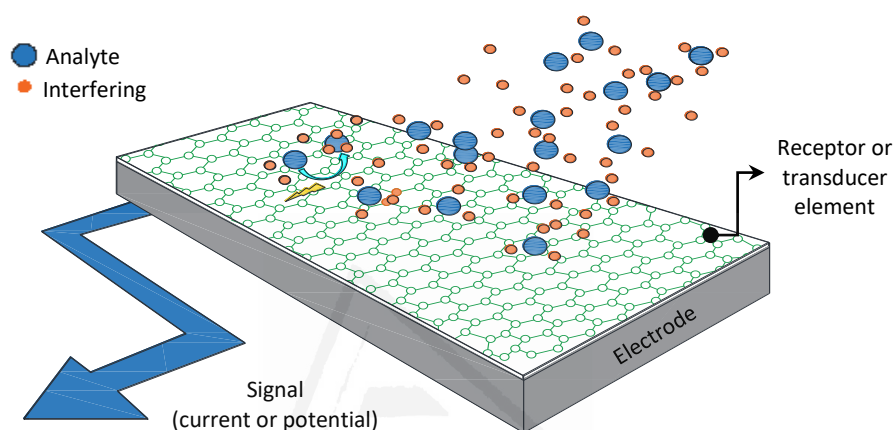


Figure 1.6. Scheme of an electrochemical sensor.

Nevertheless, within the different types of sensors, electrochemical sensors (potentiometric, impedimetric and amperometric) are highlighted as one the most applied, taking into account the easy miniaturization, portability, outstanding sensitivity and selectivity towards the species of interest¹⁸⁴.

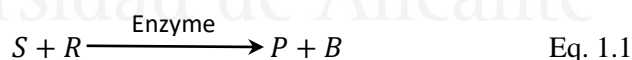
The use of a biological process with a selective mechanism of recognition combined with the high performance of the electrochemical sensor, constitutes the so-called electrochemical biosensors. These devices guarantee an accurate detection and quantification of chemical substances in biological fluids, considered an important aspect for a reliable clinical diagnostic of different diseases or medical disorders.

International Union of Pure and Applied Chemistry (IUPAC) defined an electrochemical biosensors as: “a self-contained integrated device, which is capable of providing specific quantitative or semi-quantitative analytical information using a biological recognition element (biochemical receptor) which is retained in direct spatial contact with an electrochemical transduction element. Because of their ability to be repeatedly calibrated, we

recommend that a biosensor should be clearly distinguished from a bioanalytical system, which requires additional processing steps, such as reagent addition”¹⁸⁶. Given that, biosensors use as receptor elements, biomolecules (enzymes, proteins, antibodies, nucleic acids, membranes, cells, and so on), the recognition processes are highly selective, allowing lower detection limits and higher selectivity and sensibility; in comparison with conventional sensors^{187,188}. Nowadays, classification of the biosensor has been widely debated; despite that 4 main groups have been proposed (affinity, catalytic, trans-membranes and cellular), many authors suggest that this classification can be simplified as biosensors of affinity and catalytic, considering that recognition element of the other 2 types of biosensors is based on the same principle as those mentioned before¹⁸⁹.

4.2.1. Electrochemical catalytic biosensors

Principle of catalytic biosensors is based on the use of a receptor-enzyme which generates a catalytic reaction with the species of interest (analyte), generating a consumption of species, at the same time that production of active species in the media takes place^{187,190}. Therefore, detection and quantification of the species of interest can be carried out in a direct or an indirect mode, through the electrochemical reactions with the enzyme or with the participating species (products or reagents) in the reaction, respectively. Oxidoreductase enzymes have served as recognition element for oxidation or dehydrogenation of the molecule of interest in a wide variety of electrochemical biosensors^{191,192}. The global reaction of a catalytic biosensor can be expressed as in Eq. 1.1.



In the equation, S represents the substrate, and the enzyme is selective to oxidize or reduce it. R is another species required for the reaction to take place (electron acceptor), P and B, are products generated. Nevertheless, during the enzymatic reaction, the substrate and the enzyme generate an enzymatic complex which promotes the oxidation/dehydrogenation reaction^{193,194}. Afterwards, the reduced enzyme transfers the electrons to the electron acceptor, which can be molecular oxygen, a redox mediator or even direct transfer from the enzyme to the electrode¹⁹⁵. Depending on how the transfer of

electrons occur, the catalytic biosensor is classified as 1st, 2nd and 3rd generation, as can be observed in Figure 1.7.

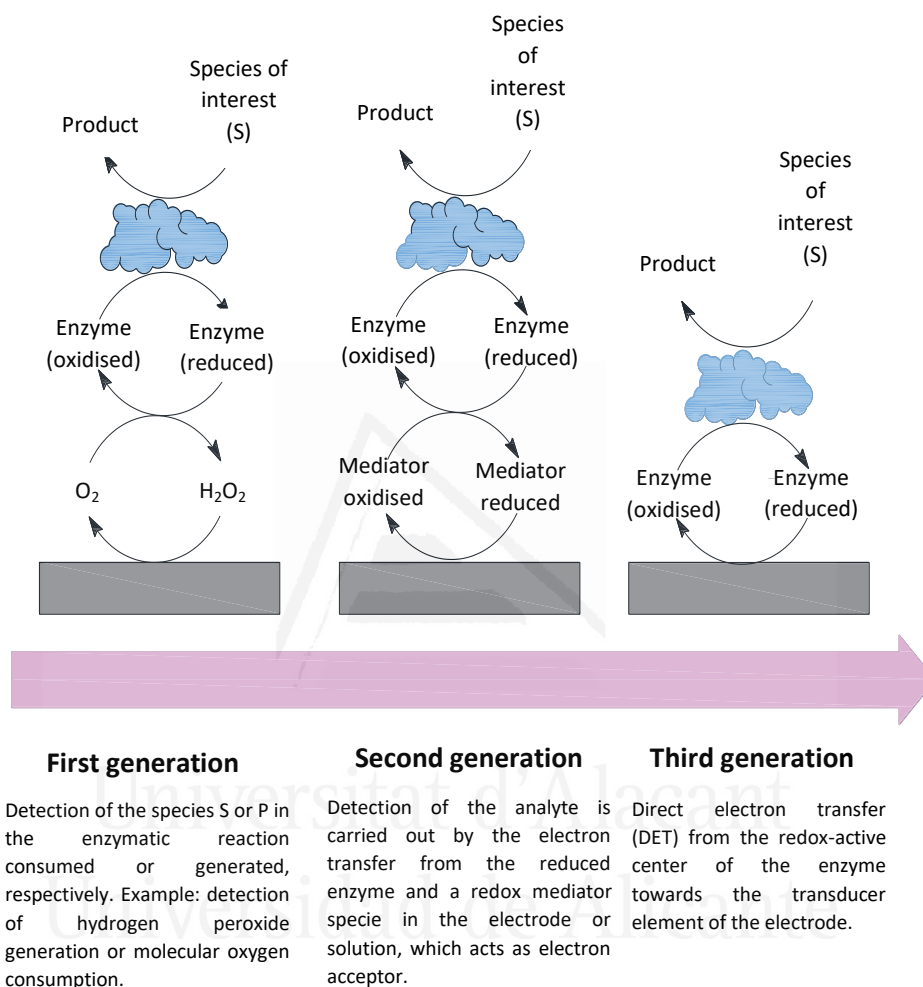


Figure 1.7. Classification of the catalytic biosensors.

Although, oxidoreductase enzymes have been extensively used in the detection of different analytes for biosensor applications, recent researches have employed bi- or multi-enzymatic systems for multiple detection of a variety of analytes in the same sample, and also for amplifying the sensing signal and enhancing the sensitivity towards the analyte of interest^{196,197}.

4.2.2. Electrochemical affinity biosensors

One important aspect in the sensing process of molecules in a complex matrix lies in the specificity that the biosensor presents towards the analyte. In this sense, multiple studies have focused in the use of bio-complexing agents, such as nucleic acids (DNA or aptamers) or antibodies, as bioreceptor elements for the detection and accurate quantification of specific analytes, giving rise to the affinity biosensors¹⁹⁸. In contrast with catalytic biosensors, where an oxidation or reduction reaction occurs by the interaction with the bioreceptor in the electrode, the bioreceptor element employed in the affinity biosensor has the capacity to adopt different three-dimensional conformations which permit the interaction with the analyte. In presence of the analyte, most of the bioreceptors suffer a conformational change forming a bonding in a specific site with the analyte. This active region is highly selective and specific, giving place to the formation of a stable complex-system, as can be observed in Figure 1.8¹⁹⁹

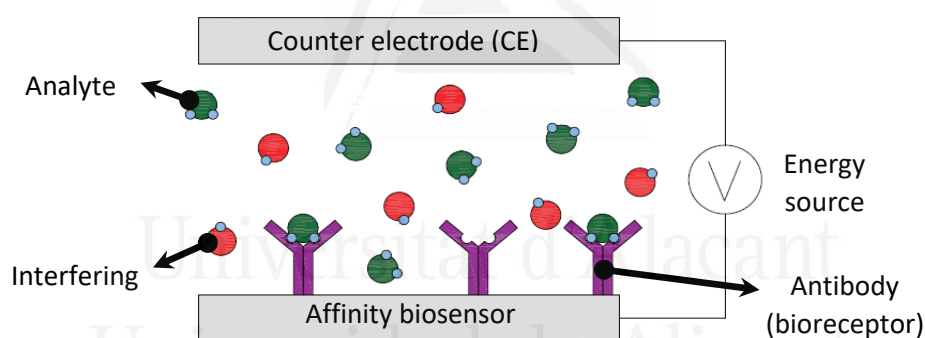


Figure 1.8. Electrochemical affinity biosensor.

Immunosensors, in which analytical detection is carried out by the use of different types of antibodies (IgG types-G immunoglobulin- immobilized onto the electrode surface), have demonstrated a promising alternative in the detection of biomarkers, virus, bacteria and pathogens²⁰⁰, as well as, chemical species which do not present electrochemical activity. Use of antibodies as elements for biorecognition has been extensively used, due to the high affinity constants between the antibody (Ab)/Antigen (Ag) of around $1 \times 10^5 - 1 \times 10^{12} \text{ mol}^{-1}$; thus, high selectivity and stability of the immunoreaction provide a proper detection of the analyte²⁰¹. Also, the lower limit of detection at around

nano- to femtomolar concentrations, makes this type of biosensors an alternative for detection of analytes at low-concentration^{202,203}.

Principle of immunosensor detection is essentially based on the recognition of molecular species through the affinity interaction between the antigen and the antibody. Essentially, the detection process of the target-molecule is performed by the changes in resistance, current, RI, capacitance, etc. due to the formation of immunocomplex antibody-antigen^{190,204}. In the conventional immunosensing process the Y-shaped antibody immobilized onto the electrode surface capture the antigen (target molecule) by binding with the specific region in the antibody, obtaining a direct measure of the analyte as consequence of the complex Ab-Ag formed. However, this method can involve low sensitivity, avoiding the accurate quantification^{190,205}.

Typical label-free assays for immunodetection have shown a remarkable performance, obtaining low detection limits and good lineal range. In label-free method, the immunocomplex (Ab-Ag) formed by the interaction of the antibody on the electrode surface with the antigen (target molecule), blocks the electrode surface of the immunosensor (see Figure 1.9-A). Considering the high molecular weight and the presence of long amino acid chains in the structure of the antigen molecules, steric effects are generated after the formation of the immunocomplex which create a hindrance for the emission of light, fluorescence or electron transfer of an electrochemical redox probe. At the same time, formation of the immunocomplex can be also related with variations on mass of the electrode that can be detected employing Quartz crystal microbalance (QCM)^{206,207}. In this way, concentration of the analyte can be correlated with the decrease of the signal-measured in the electrode.

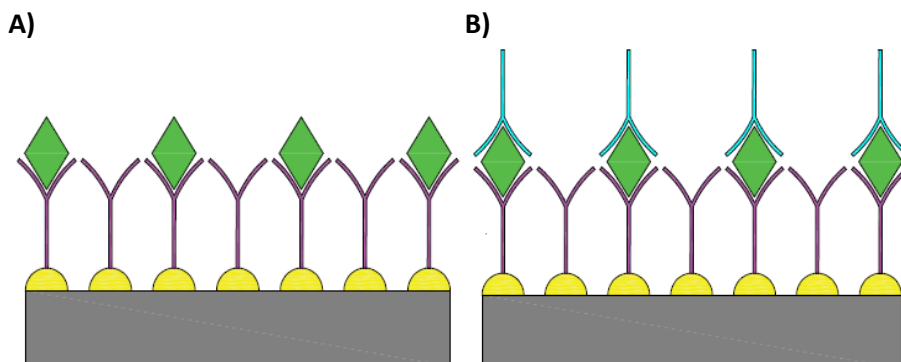


Figure 1.9. Label-free immunosensor platforms: A) label-free system with one antibody and B) label-free system with two antibodies (sandwich type).

Usually, species of interest in physiological fluids present low concentration, thus, the amount of immunocomplex Ag-Ab generated is very low, and then most of the immunosensors with the conventional label-free system show low sensitivity^{206,207}. For that reason, the coupling with a second antibody which increases the hindrance effect and then, the sensitivity is used (see Figure 1.9-B)^{208,209}.

Typical detectable signal of the target molecule in label-free method decreases with the increase of analyte concentration, thus a high background signal, implies the need of amplification of the signal to guarantee an accurate and reliable detection.

Recent works rapidly emerged employing the platform of a sandwich-type immunosensor, but in those cases the second antibody is modified with an indicator, such as an oxidoreductase enzyme, quantum dots, etc. which generates an increase in the variation of the signal by the addition of the analyte and the substrate of the enzyme, providing an improvement in the sensitivity and specificity^{210,211}. The most popular platforms include the use of a polyclonal antibody labeled with a peroxidase, the most commonly Horse Radish Peroxidase (HRP), to catalyze the hydrogen peroxide reduction in solution (see Figure 1.10), creating an amplification in the electrochemical signal^{212,213}.

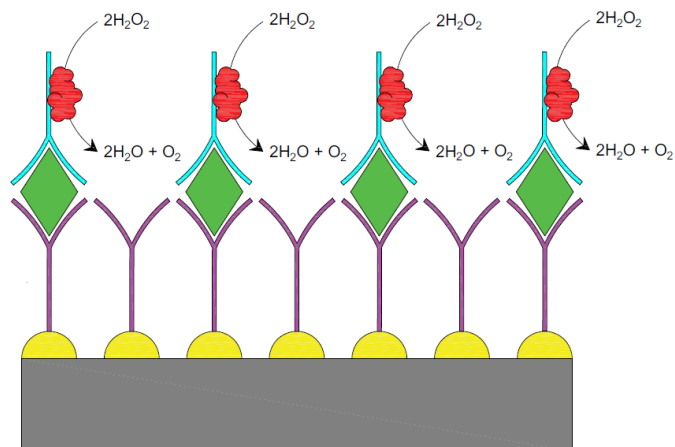


Figure 1.10. Sandwich-type immunosensor employing an antibody-labeled with an electroactive enzyme (HRP)

Continue efforts in research for the development of new immunosensor with sandwich-type configurations employing labeled antibodies have been developed in the last years, combining different bioactive enzymes (i.e. alkaline phosphatase), redox species (i.e. quinone, ferrocene-derivates or dyes), quantum dots (QDs), dendrimer systems and nanoparticles (i.e. Pd, Au)²¹⁴⁻²¹⁷. Use of nanoparticles guarantees the accurate immobilization of the antibodies on the electrode surface by covalent immobilization. Moreover, when the reaction $Ab_1-Ag-Ab_2$ takes place, some platforms employed nanoparticles which are immobilized with the rest of antibodies, which are not participating in the immunoreaction, avoiding non-specific adsorption and intensification of the signal.

4.3. Biorecognition molecules in bioelectrochemical application

The performance of the bioelectrochemical device depends on the selectivity and specificity between the bioelement and its substrate. Then, the proper selection of the biorecognition elements is crucial for sensing applications²¹⁸. Biorecognition elements are obtained isolating living systems to collect and purify the biomolecule from bacteria, plants or animals²¹⁹, including commercial and well-known enzymes as Glucose Oxidase (GOx), Horse Radish Peroxidase (HRP), Bilirubin Oxidase (Box), among others. Unfortunately, important features related with selectivity, stability of the

enzyme, deactivation and processability cannot be modified on them^{191,220}. Table 1.1 shows a classification of the biorecognition elements.

Table 1.1. Classification of current biorecognition elements employed in biosensing. Advantages and limitations²²¹.

| Recognition element | Sensor designation | Advantages | Limitations |
|-------------------------|---|--|--|
| Classical enzyme | Enzymatic-Catalytic biosensor | <ul style="list-style-type: none"> • High specificity • Simple procedure of immobilization | <ul style="list-style-type: none"> • Time-consumption during the purification • Costly • Low stability • Narrow temperature and pH conditions. |
| Antibodies | Immunosensor | <ul style="list-style-type: none"> • High specificity • High affinity | <ul style="list-style-type: none"> • Limited target molecules • Lack of stability • Use of animals for production • Laborious production |
| Nucleic acids | Genosensor | <ul style="list-style-type: none"> • Stability | <ul style="list-style-type: none"> • Limited target molecule |
| Cells | Cellular sensors | <ul style="list-style-type: none"> • Low-cost • Reduced purification requirements | -- |
| Aptamers | Aptasensor (DNA-RNA) and peptide sensor | <ul style="list-style-type: none"> • Easy to modify and design new structures • Control in the activity • Tunable selectivity by modification • Thermal stability • Synthesis <i>in-vitro</i> | -- |

4.3.1. Soluble Glucose Dehydrogenase Pyrroloquinoline quinone (PQQ-GDH)

Bacterial soluble glucose dehydrogenase from *Acinetobacter Calcoeticus* is a homodimer quinoprotein, in which a cofactor of 2,7,9-tricarboxy-1H-pyrrolo [2,3-f]-quinoline-4,5-dione, known as PQQ, catalyzes the oxidation of glucose into its corresponding lactone. The enzyme presents 3 cations of calcium in the structure, 2 for complex enzyme-cofactor stabilization and the third one required for the activation of the cofactor²²². Holo-enzyme is obtained by reconstruction of the apo-enzyme (s-GDH) in presence of PQQ and a Ca^{2+} precursor in neutral conditions^{223,224}. Isoelectric point of the enzyme is at around 9.5, being an alkaline enzyme, for that reason, at physiological conditions (pH=6-7.5) the enzyme is positively charged. Structure of the enzyme is shown in Figure 1.11.

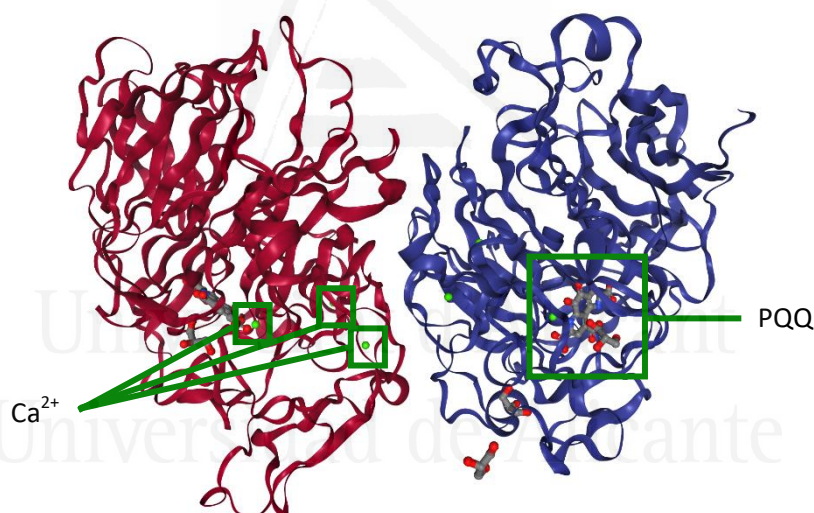


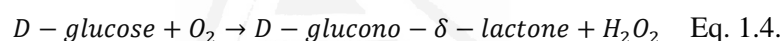
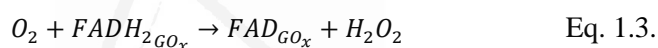
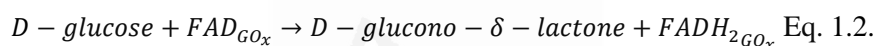
Figure 1.11. Structure of the *Acinetobacter Calcoeticus* PQQ-GDH showing a dimeric enzyme molecule (PDB ID: 1C9U).

The most important differences of PQQ-GDH, compared with other enzymes such as glucose oxidase (GOx), are its dependence toward oxygen concentration and its high catalytic efficiency, making this enzyme a promising candidate to be employed in the development of biocatalysts in bioanodes in BFCs and biosensors. Nevertheless, catalytic activity towards mono- and disaccharides to their corresponding lactones can produce

interference in the quantification of complex samples, where various saccharides can be present. This could lead to an overestimation of the target saccharide²²⁵.

4.3.2. Glucose oxidase (GOx)

The flavoprotein, glucose oxidase (β -D-glucose: oxygen 1-oxidoreductase, EC 1.1.3.4) is a homodimeric enzyme of 160 kDa of molecular weight (see Figure 1.12), which catalyzes the oxidation of the hydroxyl group of β -D-glucose employing molecular oxygen as electron acceptor species, producing β -D-glucono lactone and hydrogen peroxide, as is described below in the following equations²²⁶⁻²²⁹.



The oxidation process is carried out first by interactions of the domains in the enzyme and the substrate, then the non-bonded cofactor *Flavin adenine dinucleotide (FAD)* acts as active center and the oxidation reaction takes place^{230,231}. During this process, amine groups in the cofactor extract hydrogen from the glucose and incorporate them into the quinone structure of the FAD, giving place to a reduced form of the cofactor. Once, reduction of the cofactor ($FADH_2$) takes place (Eq. 1.2), oxygen oxidizes the cofactor, restoring the oxidation state of the cofactor in the glucose oxidase (Eq. 1.3)^{228,232}. In this process hydrogen peroxide is generated from the hydrogen extracted in Eq. 1.2 and the molecular oxygen in Eq. 1.3. Final reaction equation corresponds with Eq. 1.4.

First electrochemical biosensors for glucose detection in blood, employed either the detection of the increment in the H_2O_2 concentration or the consumption of molecular oxygen, giving place to the first generation glucose biosensor. Unfortunately, one important aspect in the correct performance of the GOx enzyme is the low stability by the increase in the H_2O_2 concentration and breakdown of the produced lactone to generate gluconic acid. This cause high oxidizing conditions and an increase in the local values of pH,

respectively. Both phenomena deactivate the enzyme, reducing the catalytic activity towards glucose oxidation. The use of redox mediators (i.e. ferrocene, ferrocyanide) as electron acceptor, allows the decrease in the working potential for glucose detection, avoiding the formation of H₂O₂ and interference effects of other components in the matrix, giving rise to the second generation electrochemical sensors.

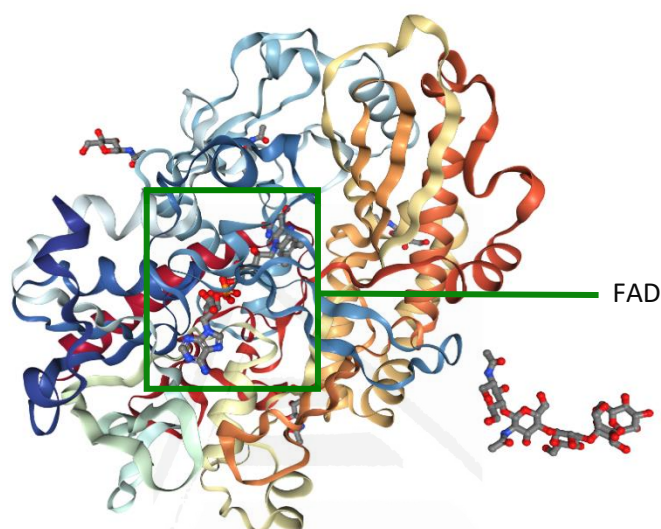


Figure 1.12. Structure of the *Aspergillus Niger* glucose oxidase (GOx) showing the component and redox active center (FAD) (PDB ID: 1GAL).

4.3.3. Antibodies (Ab)

Antibodies are glycoproteins generated in an organism as a response of the immune system for a foreign substance (antigen). Generally, antibodies can be divided in 5 different immunoglobulins (IgG, IgA, IgM, IgD y IgE); with a molecular weight between 25 and 150 kDa²³³. High interest in antibodies for biosensing raised as consequence of the high specificity and stability that this type of molecule presents to react with the antigen. Specifically, IgG are commonly used for different immunoassays and research in the development of immunosensors, due to the high concentration generated in the organism and remarkable specificity²³⁴. Morphological structure of the IgG is characterized by a Y-shape of the biomolecule, as can be observed in Figure 1.13^{235,236}.

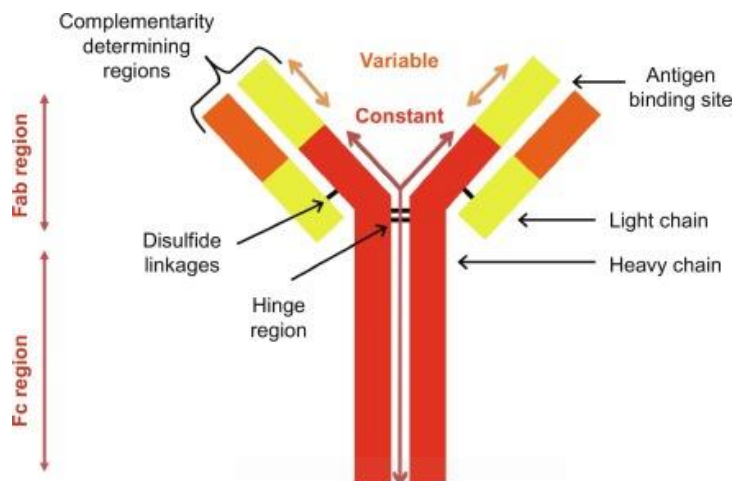


Figure 1.13. Schematic representation of an antibody for immunoassays (immunoglobulin G-IgG)²³⁷.

Y-shape structure is separated, basically, into two regions. The first region, related with the double-ended chains at the top of the antibody, well-known as Fab fragments (epitope), in which the existence of a variable and hypervariable regions with R-NH₂ groups, create an active site that recognizes a specific area of the antigen, promoting the recognition process and the formation of the immunocomplex Ab-Ag²³⁸. On the other hand, light chains in the Fab region of the IgG are bonded with a high molecular weight chain, corresponding with the Fc region, composed by high density carbohydrates and amino acids, which is bonded through disulfide linkages with the Fab region, generating a flexible region (hinge region). Fc fragment cannot interact with the antigen, thus, immunoreaction does not take place on this region. However, terminal groups of Fc region such as amine, carboxylic and thiol, mainly, have been widely employed to fix the antibody by covalent functionalization to amine-modified surface or gold surfaces, in many types of immunosensor platforms.

4.4. Immobilization procedures of biorecognition elements

Immobilization can be defined as a procedure in which a compound of interest (chemical molecule, enzyme, cells) is confined and localized in a defined and specific region, without modifying considerably its structure and properties²³⁹. In this sense, many approaches have been developed employing

physical and/or chemical methods to incorporate the bioelement in the electrode, maintaining its activity and enhancing the long-term stability²⁴⁰. Then, the immobilization process can be considered the triggering factor in the development of a good bioelectrochemical device²⁴¹.

In the next sections, a summary of the most important bioelements immobilization procedures are explained.

4.4.1. Physical procedures of immobilization

4.4.1.1. Adsorption

Adsorption process of immobilization can be considered the simplest procedure, based on the different non-covalent surface interaction as result of putting in contact the bioelement with the electrode surface. Those interactions can be generated by electrostatic interactions, π - π interactions, hydrophobic forces, hydrogen bonds and Van der Waals interactions, among others, between some specific points in the material and the bioelement^{242,243}. In this sense, isoelectric point of the bioelement is an important parameter to be considered in the application of this kind of immobilization procedure. Materials employed for adsorption process do not only involve flat surface electrodes, but also, some porous materials such as clays, α -Al₂O₃, mesoporous SiO₂, carbon materials and other ceramics, have been employed to promote the immobilization by adsorption process²⁴⁴⁻²⁴⁶. Simplicity of this procedure, makes it an easy scalable method in the fabrication of bioelectrodes, without important changes in the native bioelement, preventing denaturalization or variations in the catalytic activity²⁴⁷. Nevertheless, the nature of the different interactions between the immobilized molecule and the surface, generates weak binding and high reversibility of the adsorption/desorption process of the bioelement, since it is extremely susceptible to the pH variation, changes of solubility and temperature; resulting in a lower stability of the immobilization process.

4.4.1.2. Entrapment

The entrapment of molecules can be considered another physical immobilization procedure in which the molecule is confined by a physical barrier, generating a structured matrix of different nature, where the molecule

is enclosed²⁴⁸. The entrapment matrix can be colloidal phases, emulsion, fibers or polymers, which normally does not generate covalent bonds²⁴⁴. Classification of entrapment procedures can be appreciated in Table 1.2.

Table 1.2. Different entrapment procedures of molecules immobilization²⁴⁹

| Method of entrapment | Description |
|---|--|
| Cross-linking | In this procedure, the molecule is incorporated in an inorganic (sol-gel), organic (monomer or polymers) or enzymatic solution (Bovine serum albumin-BSA) creating a solution which is casted onto the surface of the electrode, letting it dry. Once, the solvent is removed the matrix precipitates around the enzyme, entrapping it. |
| Synthesis of composites | Entrapment takes place by the blending of the molecule to be immobilized and the material which works as electrode, obtaining a paste. Afterwards, electrode is manufactured and deposited, at the same time that the biomolecule is incorporated in the structure and interconnected in the own porosity of the materials. |
| Entrapment in perm-selective membranes | Immobilization in this case is carried out by the use of a membrane or a polymeric layer, deposited onto the surface of the electrode previously modified (by adsorption) with the molecule. In this case, the membrane generates a cage-like structure in which molecule cannot go away from the surface. In this case, the presence of a perm-selective layer provides a diffusional barrier and the diffusion of specific species may occur throughout the electrode, which in some cases improve the selectivity and avoid interference; sacrificing time-response of the electrode. |

4.4.2. Chemical procedures of immobilization

Chemical immobilization provides an effective route of immobilization based on the coupling and attachment of the biomolecule with the electrode material, through chemical reactions, and the formation of covalent chemical bonds²³⁹.

Covalent immobilization involves binding of some functional groups (amino, hydroxyl, thiol, carboxyl, imidazole, threonine, sulfhydryl, phenolic or indole) present in the amino acids-chain residues in the bioelement and other functional groups on the surface of the electrode or in the matrix employed for immobilization (polymeric or sol-gel matrix)^{250,251}. Recent efforts have been focused in the development of functionalization procedures with different molecules on the electrode surface, to incorporate useful functionalities to promote the immobilization of the bioelements^{252,253}.

The binding between the bioelement and the electrode might produce specific structural and conformational changes, which can produce either loss of the catalytic activity or denaturalization²⁵³⁻²⁵⁵. Nevertheless, some authors have claimed that at the same time that attachment of the element occurs, covalent immobilization can promote a better orientation of the bioelement, facilitating the charge-transfer with the electrode and the active center^{256,257}. Examples of those procedures use *Self-Assembled-Monolayer (SAM)* method or *cross-linking* agents^{202,258,259}, in which direct-electron transfer and retention of the catalytic activity can be achieved in some enzymes such as hemoglobin or glucose oxidase¹⁰. Additionally, combination of immobilization procedures between entrapment and covalent immobilization, have demonstrated good platforms in the development of electrochemical devices in sensing and BEFCs. Chitosan, conductive polymers and electroactive polymer based on Osmium complex, have demonstrated being proper matrix with considerable amount of functional groups, which can enhance the long-term stability of the enzyme and the electron transfer, working as nanowire²⁶⁰⁻²⁶³.

5. Analytes of study

Use of accurate methods for quantification of the concentration levels of different substances has embraced the attention of the research community in different application fields involving quality control, environmental control and health-care^{183,264}. For instance, following target species in a specific process in industry (i.e. fermentation, food processing) provides an outstanding alternative for control of the raw material (detection of contaminants as toxic pesticides, in case of vegetables and fruits) or during the fabrication process²⁶⁴⁻²⁶⁶. Additionally, detection and quantification processes

have been a powerful tool in the monitoring of biological components for treatment control, diseases detection and control of pathogen or virus²⁶⁷⁻²⁶⁹.

5.1. Detection of analytes in medical care

For many reasons, development of portable detection devices has been pervasively studied in medical field, focusing in the diagnostic of infectious diseases and bacteria. Due to their importance, blood glucose biosensors dominate around 85% of the current commercial market^{185,192}. Efforts for determination of glucose in other physiological fluids, development of continue monitoring procedures, non-invasive methods and determination of other important analytes in biological fluids in human being are still crucial for health-care. Examples of this research can be observed in the development of other biosensor platforms for detection of cholesterol^{270,271}, lactate²⁷², biomarkers (HER2, PSA)^{273,274}, DNA mutations²⁷⁵ and so on.

5.1.1. Kallikrein-related peptidase 3 (KLK3)

Kallikrein-related peptidase 3, is well-known also as the prostate-specific antigen (PSA); it is a single-polypeptide chain, from the group of glandular proteins present in human being, with a sequence of 240 amino acid residues (See Figure 1.14)²⁷⁶. KLK3 is an active serine protease of 34 kDa, which promotes the hydrolysis of the gel proteins in the seminal fluid, giving an important role in the liquefying of the seminal fluid²⁷⁷. PSA is released in the seminal fluid in a concentration range between 0.3-3 mg·mL⁻¹.

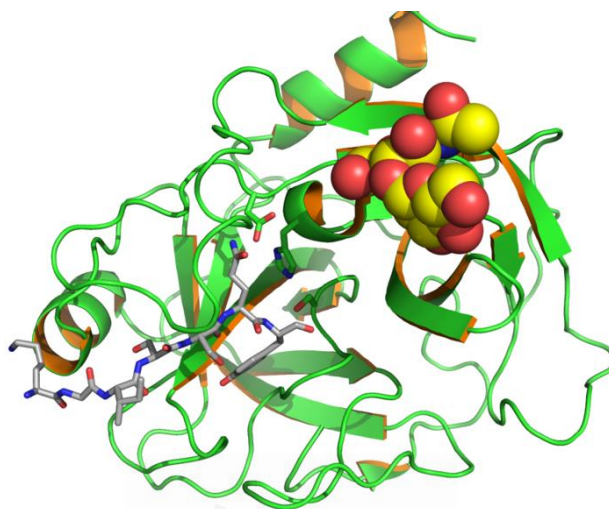


Figure 1.14. Single-polypeptide chain of PSA (PDB ID: 3HM8).

Clinical studies have demonstrated that epithelial cells in the prostate gland generate an over-expression in the production of PSA when prostate cancer is developed in men. Therefore, clinical use of PSA as a cancer biomarker has been widely studied for detection and control of prostate cancer by testing blood²⁷⁸. Unfortunately, lack of reliability in using PSA for prostate cancer diagnostic has been overshadowed by important key factors to be considered in the PSA measurement^{279,280}. On one hand, applicability of PSA as cancer biomarker lies in the fact that other prostate diseases can influence in the levels of PSA, specialty in first-stages of the prostate cancer, where PSA levels are slightly higher than 4 ngmL^{-1} ²⁸¹. On the other hand, important considerations such as previous preparation for blood harvesting and genetic facts have to be considered to avoid positive-false. For that reason, nowadays, detection of PSA in blood has been employed as a reliable tool for both, detection and control of advanced-stages of the prostate cancer and complementary test combined with other studies such as biopsy²⁸².

5.1.2. *Glucose*

Glucose is a water-soluble monosaccharide, synthesized mainly by plants and algae in the photosynthesis process from CO_2 and water in presence of sunlight. Additionally, glucose is present in the cellular structure of plants,

thus, glucose is the most abundant carbohydrate in nature, which is employed for a wide variety of organisms in the energy metabolism as energy source for all the biological processes. Normally, glucose presents 3 types of isomers α -glucose, β -glucose and δ -glucose; being the cyclizing forms (α - and δ -) the most stable ones in nature (see Figure 1.15).

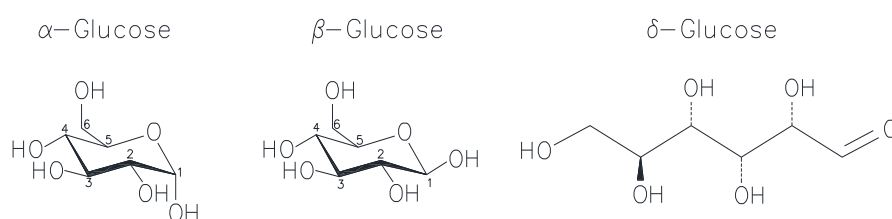


Figure 1.15. Different glucose isomers present in neutral conditions.

In general, glucose levels in animals play an important role in the metabolism, which triggers many important processes such as respiration or tissue/cellular growing²⁸³. As medical analyte, glucose has received an important attention in the control, mainly, of diabetes mellitus, which is a medical disorder caused by the deficiency of insulin in blood. Development of diabetes mellitus generates different medical disorders related with progressive deterioration of kidney function, death of blood tissue, heart attack and death in humans²²⁹. For that reason, methods for monitoring glucose levels in blood has increased importantly in the last decades, since the application of the first glucose biosensor proposed by Clark and Lyons in 1962, through the development of remarkable innovative strategies in the glycemc detection not only in blood, but also in urine, sweat or even tears, meanwhile miniaturization and implantation of sensing devices have been conceived as alternative for glucose monitoring^{12,284,285}.

Simultaneously, electrocatalytic oxidation of biomass and small molecules, employing oxidoreductase enzymes, has experienced a rapid development, specially, as an alternative to generate energy from their chemical conversion in neutral media or even physiological fluids, such as blood, serum, urine, tears and saliva; providing energy by use of a fuel cell configuration²⁸⁶⁻²⁸⁸. Important advantages in the application of these technologies lie in the use of neutral conditions, generation of clean by products and the use of abundant energy source (fuel)²⁸⁹. Considering that glucose is one of the most abundant

substances in nature, the use of this molecule to produce energy arises as a good alternative to green energy production in small electrical devices (i.e. biosensors).

6. References

- (1) Xiao, S.-X.; Huang, C.-S.; Li, Y.-L. Carbon Materials. In: Xu, R. Xu, Y, editor. *Modern Inorganic Synthetic Chemistry*, Second edition, Elsevier, Amsterdam, **2017**, pp. 429–462.
- (2) Inagaki, M. Kang, F. Introduction. In: Inagaki, M. Kang, F, editor. *Materials Science and Engineering of Carbon: Characterization*, Butterworth-Heinemann, Elsevier, Amsterdam, **2016**, pp. 1–6.
- (3) Mauter, M. S.; Elimelech, M. Environmental Applications of Carbon-Based Nanomaterials. *Environ. Sci. Technol.* **2008**, *42* (16), 5843–5859.
- (4) Pierson, H. O. The Element Carbon. In: Pierson, H, editor. *Graphite, Diamonds and Fullerenes*, William Andrew Publishing, Noyes Publications, Oxford, **1993**, pp. 11–42.
- (5) Pierson, H. O. Structure and Properties of Diamon and Diamond Polytypes. In: Pierson, H, editor. *Graphite, Diamonds and Fullerenes*, William Andrew Publishing, Noyes Publications, Oxford, **1993**, pp. 244–277.
- (6) Prasanth, R., Karthika-Ammini, S., Ge, L., Kumari-Thakur, M., Kumar-Thakur, V. Carbon Allotropes and Fascinated Nanostructures-The high-Impact Engineering Materials of the Millennium. In: T. Vijay Kumar, T. Manju Kumari, editor. *Chemical Functionalization of Carbon Materials-Chemistry and Applications*, Taylor and Francis group, CRC Press, Washington, **2016**, pp. 2-27.
- (7) Nishihara, H.; Kyotani, T. Templated Nanocarbons for Energy Storage. *Adv. Mater.* **2012**, *24* (33), 4473–4498.
- (8) Indrawirawan, S.; Sun, H.; Duan, X.; Wang, S. Nanocarbons in Different Structural Dimensions (0–3D) for Phenol Adsorption and Metal-Free Catalytic Oxidation. *Appl. Catal. B Environ.* **2015**, *179*, 352–362.

- (9) Eatemadi, A.; Daraee, H.; Karimkhanloo, H.; Kouhi, M.; Zarghami, N.; Akbarzadeh, A.; Abasi, M.; Hanifehpour, Y.; Joo, S. W. Carbon Nanotubes: Properties, Synthesis, Purification, and Medical Applications. *Nanoscale Res. Lett.* **2014**, *9* (1), 393.
- (10) González-Gaitán, C.; Ruiz-Rosas, R.; Morallón, E.; Cazorla-Amorós, D. Effects of the Surface Chemistry and Structure of Carbon Nanotubes on the Coating of Glucose Oxidase and Electrochemical Biosensors Performance. *RSC Adv.* **2017**, *7* (43), 26867–26878.
- (11) Abellán-Llobregat, A.; Vidal, L.; Rodríguez-Amaro, R.; Canals, A.; Morallón, E. Evaluation of Herringbone Carbon Nanotubes-Modified Electrodes for the Simultaneous Determination of Ascorbic Acid and Uric Acid. *Electrochim. Acta* **2018**, *285*, 284–291.
- (12) Scholten, K.; Meng, E. A Review of Implantable Biosensors for Closed-Loop Glucose Control and Other Drug Delivery Applications. *Int. J. Pharm.* **2018**, *544* (2), 319–334.
- (13) Yao, X.; Niu, X.; Ma, K.; Huang, P.; Grothe, J.; Kaskel, S.; Zhu, Y. Graphene Quantum Dots-Capped Magnetic Mesoporous Silica Nanoparticles as a Multifunctional Platform for Controlled Drug Delivery, Magnetic Hyperthermia, and Photothermal Therapy. *Small* **2017**, *13* (2), 1602225.
- (14) Zhao, X.; Liu, L.; Li, X.; Zeng, J.; Jia, X.; Liu, P. Biocompatible Graphene Oxide Nanoparticle-Based Drug Delivery Platform for Tumor Microenvironment-Responsive Triggered Release of Doxorubicin. *Langmuir* **2014**, *30* (34), 10419–10429.
- (15) Bose, S.; Kuila, T.; Mishra, A. K.; Rajasekar, R.; Kim, N. H.; Lee, J. H. Carbon-Based Nanostructured Materials and Their Composites as Supercapacitor Electrodes. *J. Mater. Chem.* **2012**, *22* (3), 767–784.
- (16) Liu, X.-W.; Sun, T.-J.; Hu, J.-L.; Wang, S.-D. Composites of Metal–Organic Frameworks and Carbon-Based Materials: Preparations, Functionalities and Applications. *J. Mater. Chem. A* **2016**, *4* (10), 3584–3616.
- (17) Tang, J.; Liu, J.; Torad, N. L.; Kimura, T.; Yamauchi, Y. Tailored Design of Functional Nanoporous Carbon Materials toward Fuel Cell Applications. *Nano Today* **2014**, *9* (3), 305–323.

- (18) Serp, P., Machado, B. Surface Chemistry of Nanostructured Carbon Materials and Preparation of Nanocarbon Supported Catalysts. In: Serp, P., Machado, B. Nanostructured Carbon Materials for Catalysis, The Royal Society of Chemistry, **2015**, pp. 163–222.
- (19) Krueger, A. Fullerenes – Cages Made from Carbon. In: Krueger, A. Carbon Materials and Nanotechnology. Wiley-VCH, Germany, **2010**, pp. 33–122.
- (20) Pierson, H. O. The Fullerene Molecules. In: Pierson, H, editor. Graphite, Diamonds and Fullerenes, William Andrew Publishing, Noyes Publications, Oxford, **1993**, pp. 356–373.
- (21) Badamshina, E.; Gafurova, M. Polymeric Nanocomposites Containing Non-Covalently Bonded Fullerene C60: Properties and Applications. *J. Mater. Chem.* **2012**, 22 (19), 9427–9438.
- (22) Bethune, D. S.; Johnson, R. D.; Salem, J. R.; de Vries, M. S.; Yannoni, C. S. Atoms in Carbon Cages: The Structure and Properties of Endohedral Fullerenes. *Nature* **1993**, 366 (6451), 123–128.
- (23) Pumera, M. The Electrochemistry of Carbon Nanotubes: Fundamentals and Applications. *Chem. – A Eur. J.* **2009**, 15 (20), 4970–4978.
- (24) Tasis, D.; Tagmatarchis, N.; Bianco, A.; Prato, M. Chemistry of Carbon Nanotubes. *Chem. Rev.* **2006**, 106 (3), 1105–1136.
- (25) Bianco, A.; Cheng, H.-M.; Enoki, T.; Gogotsi, Y.; Hurt, R. H.; Koratkar, N.; Kyotani, T.; Monthieux, M.; Park, C. R.; Tascon, J. M. D.; et al. All in the Graphene Family – A Recommended Nomenclature for Two-Dimensional Carbon Materials. *Carbon* **2013**, 65, 1–6.
- (26) Geim, A. K. Graphene: Status and Prospects. *Science* (80). **2009**, 324 (5934), 1530 LP – 1534.
- (27) Bleda-Martínez, M. J.; Lozano-Castelló, D.; Morallón, E.; Cazorla-Amorós, D.; Linares-Solano, A. Chemical and Electrochemical Characterization of Porous Carbon Materials. *Carbon* **2006**, 44 (13), 2642–2651.
- (28) Balandin, A. A. Thermal Properties of Graphene and Nanostructured Carbon Materials. *Nat. Mater.* **2011**, 10 (8), 569–581.

- (29) Liang, C.; Li, Z.; Dai, S. Mesoporous Carbon Materials: Synthesis and Modification. *Angew. Chemie Int. Ed.* **2008**, *47* (20), 3696–3717.
- (30) Sakintuna, B.; Yürüm, Y. Templated Porous Carbons: A Review Article. *Ind. Eng. Chem. Res.* **2005**, *44* (9), 2893–2902.
- (31) Lee, J.; Han, S.; Hyeon, T. Synthesis of New Nanoporous Carbon Materials Using Nanostructured Silica Materials as Templates. *J. Mater. Chem.* **2004**, *14* (4), 478–486.
- (32) Leyva-García, S.; Lozano-Castelló, D.; Morallón, E.; Cazorla-Amorós, D. Silica-Templated Ordered Mesoporous Carbon Thin Films as Electrodes for Micro-Capacitors. *J. Mater. Chem. A* **2016**, *4* (12), 4570–4579.
- (33) Leyva-García, S.; Nueangnoraj, K.; Lozano-Castelló, D.; Nishihara, H.; Kyotani, T.; Morallón, E.; Cazorla-Amorós, D. Characterization of a Zeolite-Templated Carbon by Electrochemical Quartz Crystal Microbalance and in Situ Raman Spectroscopy. *Carbon* **2015**, *89*, 63–73.
- (34) Iijima, S. Helical Microtubules of Graphitic Carbon. *Nature* **1991**, *354* (6348), 56–58.
- (35) Guldi, D. M., Martín, N. Carbon Nanotubes and Related Structures—Synthesis, Characterization, Functionalization and Applications, Wiley-VCH, T. J., Mölenbach, 2010.
- (36) Stankovich, S.; Dikin, D. A.; Dommett, G. H. B.; Kohlhaas, K. M.; Zimney, E. J.; Stach, E. A.; Piner, R. D.; Nguyen, S. T.; Ruoff, R. S. Graphene-Based Composite Materials. *Nature* **2006**, *442* (7100), 282–286.
- (37) Torres, T. Carbon Nanotubes and Related Structures. Synthesis, Characterization, Functionalization, and Applications. Edited by Dirk M. Guldi and Nazario Martín. *Angew. Chemie Int. Ed.* **2011**, *50* (7), 1473–1474.
- (38) Liu, J.; Wang, C.; Tu, X.; Liu, B.; Chen, L.; Zheng, M.; Zhou, C. Chirality-Controlled Synthesis of Single-Wall Carbon Nanotubes Using Vapour-Phase Epitaxy. *Nat. Commun.* **2012**, *3* (1), 1199.
- (39) Artyukhov, V. I.; Penev, E. S.; Yakobson, B. I. Why Nanotubes Grow

- Chiral. *Nat. Commun.* **2014**, *5* (1), 4892.
- (40) Schroeder, V.; Savagatrup, S.; He, M.; Lin, S.; Swager, T. M. Carbon Nanotube Chemical Sensors. *Chem. Rev.* **2019**, *119* (1), 599–663.
- (41) Wilder, J. W. G.; Venema, L. C.; Rinzler, A. G.; Smalley, R. E.; Dekker, C. Electronic Structure of Atomically Resolved Carbon Nanotubes. *Nature* **1998**, *391* (6662), 59–62.
- (42) Tomada, J.; Dienel, T.; Hampel, F.; Fasel, R.; Amsharov, K. Combinatorial Design of Molecular Seeds for Chirality-Controlled Synthesis of Single-Walled Carbon Nanotubes. *Nat. Commun.* **2019**, *10* (1), 3278.
- (43) Campidelli, S.; Meneghetti, M.; Prato, M. Separation of Metallic and Semiconducting Single-Walled Carbon Nanotubes via Covalent Functionalization. *Small* **2007**, *3* (10), 1672–1676.
- (44) Hirsch, A. Functionalization of Single-Walled Carbon Nanotubes. *Angew. Chemie Int. Ed.* **2002**, *41* (11), 1853–1859.
- (45) Lafuente, E.; Callejas, M. A.; Sainz, R.; Benito, A. M.; Maser, W. K.; Sanjuán, M. L.; Saurel, D.; de Teresa, J. M.; Martínez, M. T. The Influence of Single-Walled Carbon Nanotube Functionalization on the Electronic Properties of Their Polyaniline Composites. *Carbon* **2008**, *46* (14), 1909–1917.
- (46) Chen, J.; Collier, C. P. Noncovalent Functionalization of Single-Walled Carbon Nanotubes with Water-Soluble Porphyrins. *J. Phys. Chem. B* **2005**, *109* (16), 7605–7609.
- (47) Zhao, Y.-L.; Stoddart, J. F. Noncovalent Functionalization of Single-Walled Carbon Nanotubes. *Acc. Chem. Res.* **2009**, *42* (8), 1161–1171.
- (48) Dyke, C. A.; Tour, J. M. Covalent Functionalization of Single-Walled Carbon Nanotubes for Materials Applications. *J. Phys. Chem. A* **2004**, *108* (51), 11151–11159.
- (49) Deng, S.; Berry, V. Wrinkled, Rippled and Crumpled Graphene: An Overview of Formation Mechanism, Electronic Properties, and Applications. *Mater. Today* **2016**, *19* (4), 197–212.
- (50) Warner, J. H., Schäffel, F., Bachmatiuk, A., Rummeli, M.H. Methods

for Obtaining Graphene. In: Warner, J. H., Schäffel, F., Bachmatiuk, A., Rummeli, M.H., editor, Graphene-Fundamentals and emergent applications, Elsevier, Amsterdam, **2013**, pp. 129–228.

- (51) Loh, K. P.; Bao, Q.; Ang, P. K.; Yang, J. The Chemistry of Graphene. *J. Mater. Chem.* **2010**, *20* (12), 2277–2289.
- (52) Economopoulos, S. P.; Tagmatarchis, N. Chemical Functionalization of Exfoliated Graphene. *Chem. – A Eur. J.* **2013**, *19* (39), 12930–12936.
- (53) Dhakate, S. R.; Chauhan, N.; Sharma, S.; Tawale, J.; Singh, S.; Sahare, P. D.; Mathur, R. B. An Approach to Produce Single and Double Layer Graphene from Re-Exfoliation of Expanded Graphite. *Carbon* **2011**, *49* (6), 1946–1954.
- (54) Ang, P. K.; Wang, S.; Bao, Q.; Thong, J. T. L.; Loh, K. P. High-Throughput Synthesis of Graphene by Intercalation–Exfoliation of Graphite Oxide and Study of Ionic Screening in Graphene Transistor. *ACS Nano* **2009**, *3* (11), 3587–3594.
- (55) Ferrándiz-Saperas, M.; Ghisolfi, A.; Cazorla-Amorós, D.; Nájera, C.; Sansano, J. M. Multilayer Graphene Functionalized through Thermal 1,3-Dipolar Cycloadditions with Imino Esters: A Versatile Platform for Supported Ligands in Catalysis. *Chem. Commun.* **2019**, *55* (52), 7462–7465.
- (56) Avinash, M. B.; Subrahmanyam, K. S.; Sundarayya, Y.; Govindaraju, T. Covalent Modification and Exfoliation of Graphene Oxide Using Ferrocene. *Nanoscale* **2010**, *2* (9), 1762–1766.
- (57) Grayfer, E. D.; Nazarov, A. S.; Makotchenko, V. G.; Kim, S.-J.; Fedorov, V. E. Chemically Modified Graphene Sheets by Functionalization of Highly Exfoliated Graphite. *J. Mater. Chem.* **2011**, *21* (10), 3410–3414.
- (58) Brodie, B. C. XIII. On the Atomic Weight of Graphite. *Philos. Trans. R. Soc. London* **1859**, *149*, 249–259.
- (59) Dreyer, D. R.; Park, S.; Bielawski, C. W.; Ruoff, R. S. The Chemistry of Graphene Oxide. *Chem. Soc. Rev.* **2010**, *39* (1), 228–240.
- (60) Hummers, W. S.; Offeman, R. E. Preparation of Graphitic Oxide. *J. Am. Chem. Soc.* **1958**, *80* (6), 1339.

- (61) Staudenmaier, L. Verfahren Zur Darstellung Der Graphitsäure. *Berichte der Dtsch. Chem. Gesellschaft* **1898**, 31 (2), 1481–1487.
- (62) Lerf, A.; He, H.; Forster, M.; Klinowski, J. Structure of Graphite Oxide Revisited. *J. Phys. Chem. B* **1998**, 102 (23), 4477–4482.
- (63) Lerf, A.; He, H.; Riedl, T.; Forster, M.; Klinowski, J. ¹³C and ¹H MAS NMR Studies of Graphite Oxide and Its Chemically Modified Derivatives. *Solid State Ionics* **1997**, 101–103, 857–862.
- (64) He, H.; Klinowski, J.; Forster, M.; Lerf, A. A New Structural Model for Graphite Oxide. *Chem. Phys. Lett.* **1998**, 287 (1), 53–56.
- (65) Raidongia, K.; Tan, A. T. L.; Huang, J. Chapter 14 - Graphene Oxide: Some New Insights into an Old Material; Tanaka, K., Iijima, S. B. T.-C. N. and G. (Second E., Eds.; Elsevier: Oxford, ; pp. 341–374.
- (66) Pei, S.; Cheng, H.-M. The Reduction of Graphene Oxide. *Carbon* **2012**, 50 (9), 3210–3228.
- (67) Harima, Y.; Setodoi, S.; Imae, I.; Komaguchi, K.; Ooyama, Y.; Ohshita, J.; Mizota, H.; Yano, J. Electrochemical Reduction of Graphene Oxide in Organic Solvents. *Electrochim. Acta* **2011**, 56 (15), 5363–5368.
- (68) Toh, S. Y.; Loh, K. S.; Kamarudin, S. K.; Daud, W. R. W. Graphene Production via Electrochemical Reduction of Graphene Oxide: Synthesis and Characterisation. *Chem. Eng. J.* **2014**, 251, 422–434.
- (69) Shao, Y.; Wang, J.; Engelhard, M.; Wang, C.; Lin, Y. Facile and Controllable Electrochemical Reduction of Graphene Oxide and Its Applications. *J. Mater. Chem.* **2010**, 20 (4), 743–748.
- (70) Ping, J.; Wang, Y.; Fan, K.; Wu, J.; Ying, Y. Direct Electrochemical Reduction of Graphene Oxide on Ionic Liquid Doped Screen-Printed Electrode and Its Electrochemical Biosensing Application. *Biosens. Bioelectron.* **2011**, 28 (1), 204–209.
- (71) Strelko, V. V; Kartel, N. T.; Dukhno, I. N.; Kuts, V. S.; Clarkson, R. B.; Odintsov, B. M. Mechanism of Reductive Oxygen Adsorption on Active Carbons with Various Surface Chemistry. *Surf. Sci.* **2004**, 548 (1), 281–290.

- (72) Seredych, M.; Hulicova-Jurcakova, D.; Lu, G. Q.; Bandosz, T. J. Surface Functional Groups of Carbons and the Effects of Their Chemical Character, Density and Accessibility to Ions on Electrochemical Performance. *Carbon* **2008**, *46* (11), 1475–1488.
- (73) Lahaye, J.; Ehrburger, P. Surface Chemistry of Carbon: An Atomistic Approach. *Pure Appl. Chem.* **1989**, *61* (11), 1853–1858.
- (74) González Gaitán, Carolina. *Electrochemically modified carbon materials for applications in electrocatalysis and biosensors*. Directores: Ramiro Ruiz Rosas y Diego Cazorla Amorós. PhD thesis, Universidad de Alicante, Departamento de Química Inorgánica y Química Física, **2013**.
- (75) Soto, J.; Rosas, J. M.; Otero, J. C.; Rodríguez-Mirasol, J.; Cordero, T. Reaction Mechanisms of 2-Butanol Dehydration over a Phosphorus-Containing Activated Carbon Acid Catalyst. *J. Phys. Chem. C* **2018**, *122* (29), 16772–16778.
- (76) Valero-Romero, M. J.; Calvo-Muñoz, E. M.; Ruiz-Rosas, R.; Rodríguez-Mirasol, J.; Cordero, T. Phosphorus-Containing Mesoporous Carbon Acid Catalyst for Methanol Dehydration to Dimethyl Ether. *Ind. Eng. Chem. Res.* **2019**, *58* (10), 4042–4053.
- (77) Figueiredo, J. L.; Pereira, M. F. R. The Role of Surface Chemistry in Catalysis with Carbons. *Catal. Today* **2010**, *150* (1), 2–7.
- (78) González-Gaitán, C., Ruíz-Rosas, R., Morallón, E., Cazorla-Amorós, Diego. Electrochemical Methods to Functionalize Carbon Materials. In: T. Vijay Kumar, T. Manju Kumari, editor. *Chemical Functionalization of Carbon Materials-Chemistry and Applications*, Taylor and Francis group, CRC Press, Washington, **2016**, pp. 230-249.
- (79) Mubarak, N.M.M Sahu, J. N., Wong, J. R., Jayakumar, N. S., Ganesan, P., Abdullah, E. C. Overview on the Functionalization of Carbon Nanotubes. In: T. Vijay Kumar, T. Manju Kumari, editor. *Chemical Functionalization of Carbon Materials-Chemistry and Applications*, Taylor and Francis group, CRC Press, Washington, **2016**, pp. 82-101.
- (80) Jaisankar, S. N.; Haridharan, N.; Murali, A.; Sergii, P.; Špírková, M.; Mandal, A. B.; Matějka, L. Single-Electron Transfer Living Radical Copolymerization of SWCNT-g-PMMA via Graft from Approach.

Polymer **2014**, *55* (13), 2959–2966.

- (81) Chen, R. J.; Zhang, Y.; Wang, D.; Dai, H. Noncovalent Sidewall Functionalization of Single-Walled Carbon Nanotubes for Protein Immobilization. *J. Am. Chem. Soc.* **2001**, *123* (16), 3838–3839.
- (82) Wei, D.; Kvarnström, C.; Lindfors, T.; Ivaska, A. Electrochemical Functionalization of Single Walled Carbon Nanotubes with Polyaniline in Ionic Liquids. *Electrochem. commun.* **2007**, *9* (2), 206–210.
- (83) Bilalis, P.; Katsigiannopoulos, D.; Avgeropoulos, A.; Sakellariou, G. Non-Covalent Functionalization of Carbon Nanotubes with Polymers. *RSC Adv.* **2014**, *4* (6), 2911–2934.
- (84) O’Connell, M. J.; Boul, P.; Ericson, L. M.; Huffman, C.; Wang, Y.; Haroz, E.; Kuper, C.; Tour, J.; Ausman, K. D.; Smalley, R. E. Reversible Water-Solubilization of Single-Walled Carbon Nanotubes by Polymer Wrapping. *Chem. Phys. Lett.* **2001**, *342* (3), 265–271.
- (85) Georgakilas, V.; Otyepka, M.; Bourlinos, A. B.; Chandra, V.; Kim, N.; Kemp, K. C.; Hobza, P.; Zboril, R.; Kim, K. S. Functionalization of Graphene: Covalent and Non-Covalent Approaches, Derivatives and Applications. *Chem. Rev.* **2012**, *112* (11), 6156–6214.
- (86) Datsyuk, V.; Kalyva, M.; Papagelis, K.; Parthenios, J.; Tasis, D.; Siokou, A.; Kallitsis, I.; Galiotis, C. Chemical Oxidation of Multiwalled Carbon Nanotubes. *Carbon* **2008**, *46* (6), 833–840.
- (87) Munirasu, S.; Albuerne, J.; Boschetti-de-Fierro, A.; Abetz, V. Functionalization of Carbon Materials Using the Diels-Alder Reaction. *Macromol. Rapid Commun.* **2010**, *31* (6), 574–579.
- (88) Allongue, P.; Delamar, M.; Desbat, B.; Fagebaume, O.; Hitmi, R.; Pinson, J.; Savéant, J.-M. Covalent Modification of Carbon Surfaces by Aryl Radicals Generated from the Electrochemical Reduction of Diazonium Salts. *J. Am. Chem. Soc.* **1997**, *119* (1), 201–207.
- (89) Servinis, L.; Beggs, K. M.; Scheffler, C.; Wölfel, E.; Randall, J. D.; Gengenbach, T. R.; Demir, B.; Walsh, T. R.; Doeven, E. H.; Francis, P. S.; et al. Electrochemical Surface Modification of Carbon Fibres by Grafting of Amine, Carboxylic and Lipophilic Amide Groups. *Carbon* **2017**, *118*, 393–403.

- (90) Garg, A.; Sinnott, S. B. Effect of Chemical Functionalization on the Mechanical Properties of Carbon Nanotubes. *Chem. Phys. Lett.* **1998**, *295* (4), 273–278.
- (91) Meng, L.; Fu, C.; Lu, Q. Advanced Technology for Functionalization of Carbon Nanotubes. *Prog. Nat. Sci.* **2009**, *19* (7), 801–810.
- (92) Tuci, G.; Vinattieri, C.; Luconi, L.; Ceppatelli, M.; Cicchi, S.; Brandi, A.; Filippi, J.; Melucci, M.; Giambastiani, G. “Click” on Tubes: A Versatile Approach towards Multimodal Functionalization of SWCNTs. *Chem. – A Eur. J.* **2012**, *18* (27), 8454–8463.
- (93) Ying, Y.; Saini, R. K.; Liang, F.; Sadana, A. K.; Billups, W. E. Functionalization of Carbon Nanotubes by Free Radicals. *Org. Lett.* **2003**, *5* (9), 1471–1473.
- (94) He, M.; Swager, T. M. Covalent Functionalization of Carbon Nanomaterials with Iodonium Salts. *Chem. Mater.* **2016**, *28* (23), 8542–8549.
- (95) Rebelo, S. L. H.; Guedes, A.; Szefczyk, M. E.; Pereira, A. M.; Araújo, J. P.; Freire, C. Progress in the Raman Spectra Analysis of Covalently Functionalized Multiwalled Carbon Nanotubes: Unraveling Disorder in Graphitic Materials. *Phys. Chem. Chem. Phys.* **2016**, *18* (18), 12784–12796.
- (96) Pagona, G.; Karousis, N.; Tagmatarchis, N. Aryl Diazonium Functionalization of Carbon Nanohorns. *Carbon* **2008**, *46* (4), 604–610.
- (97) Zhang, Y.; Shen, Y.; Han, D.; Wang, Z.; Song, J.; Li, F.; Niu, L. Carbon Nanotubes and Glucose Oxidase Bionanocomposite Bridged by Ionic Liquid-like Unit: Preparation and Electrochemical Properties. *Biosens. Bioelectron.* **2007**, *23* (3), 438–443.
- (98) Bélanger, D.; Pinson, J. Electrografting: A Powerful Method for Surface Modification. *Chem. Soc. Rev.* **2011**, *40* (7), 3995–4048.
- (99) González-Gaitán, C.; Ruiz-Rosas, R.; Morallón, E.; Cazorla-Amorós, D. Functionalization of Carbon Nanotubes Using Aminobenzene Acids and Electrochemical Methods. Electroactivity for the Oxygen Reduction Reaction. *Int. J. Hydrogen Energy* **2015**, *40* (34), 11242–11253.

- (100) Such-Basáñez, I.; Román-Martínez, M. C.; Salinas-Martínez de Lecea, C. Ligand Adsorption on Different Activated Carbon Materials for Catalyst Anchorage. *Carbon* **2004**, *42* (7), 1357–1361.
- (101) Boehm, H. P. Some Aspects of the Surface Chemistry of Carbon Blacks and Other Carbons. *Carbon* **1994**, *32* (5), 759–769.
- (102) Barton, S. S.; Evans, M. J. B.; Halliop, E.; MacDonald, J. A. F. Acidic and Basic Sites on the Surface of Porous Carbon. *Carbon* **1997**, *35* (9), 1361–1366.
- (103) Lin, T.; Bajpai, V.; Ji, T.; Dai, L. Chemistry of Carbon Nanotubes. *Aust. J. Chem.* **2003**, *56* (7), 635–651.
- (104) Ajayan, P. M.; Ebbesen, T. W.; Ichihashi, T.; Iijima, S.; Tanigaki, K.; Hiura, H. Opening Carbon Nanotubes with Oxygen and Implications for Filling. *Nature* **1993**, *362* (6420), 522–525.
- (105) Wepasnick, K. A.; Smith, B. A.; Schrote, K. E.; Wilson, H. K.; Diegelmann, S. R.; Fairbrother, D. H. Surface and Structural Characterization of Multi-Walled Carbon Nanotubes Following Different Oxidative Treatments. *Carbon* **2011**, *49* (1), 24–36.
- (106) Li, Z.; Wang, L.; Li, Y.; Feng, Y.; Feng, W. Carbon-Based Functional Nanomaterials: Preparation, Properties and Applications. *Compos. Sci. Technol.* **2019**, *179*, 10–40.
- (107) Bleda-Martínez, M. J.; Pérez, J. M.; Linares-Solano, A.; Morallón, E.; Cazorla-Amorós, D. Effect of Surface Chemistry on Electrochemical Storage of Hydrogen in Porous Carbon Materials. *Carbon* **2008**, *46* (7), 1053–1059.
- (108) Salinas-Torres, D.; Shiraishi, S.; Morallón, E.; Cazorla-Amorós, D. Improvement of Carbon Materials Performance by Nitrogen Functional Groups in Electrochemical Capacitors in Organic Electrolyte at Severe Conditions. *Carbon* **2015**, *82*, 205–213.
- (109) Zhou, Z.; Zhang, Z.; Peng, H.; Qin, Y.; Li, G.; Chen, K. Nitrogen- and Oxygen-Containing Activated Carbon Nanotubes with Improved Capacitive Properties. *RSC Adv.* **2014**, *4* (11), 5524–5530.
- (110) MacMahon, S.; Fong, R.; Baran, P. S.; Safonov, I.; Wilson, S. R.; Schuster, D. I. Synthetic Approaches to a Variety of Covalently Linked

- Porphyrin–Fullerene Hybrids. *J. Org. Chem.* **2001**, *66* (16), 5449–5455.
- (111) Katz, E.; Willner, I. Biomolecule-Functionalized Carbon Nanotubes: Applications in Nanobioelectronics. *ChemPhysChem* **2004**, *5* (8), 1084–1104.
- (112) Burghard, M. Asymmetric End-Functionalization of Carbon Nanotubes. *Small* **2005**, *1* (12), 1148–1150.
- (113) Taylor, S. M.; Pătru, A.; Streich, D.; El Kazzi, M.; Fabbri, E.; Schmidt, T. J. Vanadium (V) Reduction Reaction on Modified Glassy Carbon Electrodes – Role of Oxygen Functionalities and Microstructure. *Carbon* **2016**, *109*, 472–478.
- (114) Shen, W.; Fan, W. Nitrogen-Containing Porous Carbons: Synthesis and Application. *J. Mater. Chem. A* **2013**, *1* (4), 999–1013.
- (115) Quílez-Bermejo, J.; Morallón, E.; Cazorla-Amorós, D. Oxygen-Reduction Catalysis of N-Doped Carbons Prepared via Heat Treatment of Polyaniline at over 1100 °C. *Chem. Commun.* **2018**, *54* (35), 4441–4444.
- (116) Zhang, W.; He, Y.-S.; Zhang, S.; Yang, X.; Yuan, X.; Ma, Z.-F. Effectively Incorporating Iron, Nitrogen, and Sulfur Functionalities on Carbon Surface for a Superior Electrocatalyst toward Oxygen Reduction Reaction. *Electrochem. commun.* **2017**, *81*, 34–37.
- (117) Liang, H.-W.; Zhuang, X.; Brüller, S.; Feng, X.; Müllen, K. Hierarchically Porous Carbons with Optimized Nitrogen Doping as Highly Active Electrocatalysts for Oxygen Reduction. *Nat. Commun.* **2014**, *5* (1), 4973.
- (118) Arrigo, R.; Hävecker, M.; Schlögl, R.; Su, D. S. Dynamic Surface Rearrangement and Thermal Stability of Nitrogen Functional Groups on Carbon Nanotubes. *Chem. Commun.* **2008**, No. 40, 4891–4893.
- (119) Pels, J. R.; Kapteijn, F.; Moulijn, J. A.; Zhu, Q.; Thomas, K. M. Evolution of Nitrogen Functionalities in Carbonaceous Materials during Pyrolysis. *Carbon* **1995**, *33* (11), 1641–1653.
- (120) Mostazo-López, M. J.; Ruiz-Rosas, R.; Morallón, E.; Cazorla-Amorós, D. Generation of Nitrogen Functionalities on Activated Carbons by

Amidation Reactions and Hofmann Rearrangement: Chemical and Electrochemical Characterization. *Carbon* **2015**, *91*, 252–265.

- (121) Nakajima, N.; Ikada, Y. Mechanism of Amide Formation by Carbodiimide for Bioconjugation in Aqueous Media. *Bioconjug. Chem.* **1995**, *6* (1), 123–130.
- (122) Huang, W.; Taylor, S.; Fu, K.; Lin, Y.; Zhang, D.; Hanks, T. W.; Rao, A. M.; Sun, Y.-P. Attaching Proteins to Carbon Nanotubes via Diimide-Activated Amidation. *Nano Lett.* **2002**, *2* (4), 311–314.
- (123) Baker, S. E.; Cai, W.; Lasseter, T. L.; Weidkamp, K. P.; Hamers, R. J. Covalently Bonded Adducts of Deoxyribonucleic Acid (DNA) Oligonucleotides with Single-Wall Carbon Nanotubes: Synthesis and Hybridization. *Nano Lett.* **2002**, *2* (12), 1413–1417.
- (124) Quílez-Bermejo, J.; González-Gaitán, C.; Morallón, E.; Cazorla-Amorós, D. Effect of Carbonization Conditions of Polyaniline on Its Catalytic Activity towards ORR. Some Insights about the Nature of the Active Sites. *Carbon* **2017**, *119*, 62–71.
- (125) Valero-Romero, M. J.; García-Mateos, F. J.; Rodríguez-Mirasol, J.; Cordero, T. Role of Surface Phosphorus Complexes on the Oxidation of Porous Carbons. *Fuel Process. Technol.* **2017**, *157*, 116–126.
- (126) Guo, S.; Deng, Z.; Li, M.; Jiang, B.; Tian, C.; Pan, Q.; Fu, H. Phosphorus-Doped Carbon Nitride Tubes with a Layered Micro-nanostructure for Enhanced Visible-Light Photocatalytic Hydrogen Evolution. *Angew. Chemie Int. Ed.* **2015**, *55* (5), 1830–1834.
- (127) Wen, Y.; Wang, B.; Huang, C.; Wang, L.; Hulicova-Jurcakova, D. Synthesis of Phosphorus-Doped Graphene and Its Wide Potential Window in Aqueous Supercapacitors. *Chem. – A Eur. J.* **2015**, *21* (1), 80–85.
- (128) Hou, H.; Shao, L.; Zhang, Y.; Zou, G.; Chen, J.; Ji, X. Large-Area Carbon Nanosheets Doped with Phosphorus: A High-Performance Anode Material for Sodium-Ion Batteries. *Adv. Sci.* **2017**, *4* (1), 1600243.
- (129) Berenguer, R.; Ruiz-Rosas, R.; Gallardo, A.; Cazorla-Amorós, D.; Morallón, E.; Nishihara, H.; Kyotani, T.; Rodríguez-Mirasol, J.; Cordero, T. Enhanced Electro-Oxidation Resistance of Carbon

- Electrodes Induced by Phosphorus Surface Groups. *Carbon* **2015**, *95*, 681–689.
- (130) Quesada-Plata, F.; Ruiz-Rosas, R.; Morallón, E.; Cazorla-Amorós, D. Activated Carbons Prepared through H₃PO₄-Assisted Hydrothermal Carbonisation from Biomass Wastes: Porous Texture and Electrochemical Performance. *Chempluschem* **2016**, *81* (12), 1349–1359.
- (131) Suri, A.; Chakraborty, A. K.; Coleman, K. S. A Facile, Solvent-Free, Noncovalent, and Nondisruptive Route To Functionalize Single-Wall Carbon Nanotubes Using Tertiary Phosphines. *Chem. Mater.* **2008**, *20* (5), 1705–1709.
- (132) Muleja, A. A.; Mbianda, X. Y.; Krause, R. W.; Pillay, K. Synthesis, Characterization and Thermal Decomposition Behaviour of Triphenylphosphine-Linked Multiwalled Carbon Nanotubes. *Carbon* **2012**, *50* (8), 2741–2751.
- (133) Adolph, M. A.; Xavier, Y. M.; Kriveshini, P.; Rui, K. Phosphine Functionalised Multiwalled Carbon Nanotubes: A New Adsorbent for the Removal of Nickel from Aqueous Solution. *J. Environ. Sci.* **2012**, *24* (6), 1133–1141.
- (134) Hamilton, C. E.; Barron, A. R. Phosphine Functionalized Single-Walled Carbon Nanotubes. *Main Gr. Chem.* **2009**, *8* (4), 275–281.
- (135) Marque, S.; Tordo, P. Reactivity of Phosphorus Centered Radicals. In: Majoral, J.-P. *New Aspects in Phosphorus Chemistry V.* Majoral, J.-P., Ed.; Springer Berlin Heidelberg: Berlin, Heidelberg, 2005; pp 43–76.
- (136) Fareghi-Alamdari, R.; Haqiqi, M. G.; Zekri, N. Immobilized Pd(0) Nanoparticles on Phosphine-Functionalized Graphene as a Highly Active Catalyst for Heck, Suzuki and N-Arylation Reactions. *New J. Chem.* **2016**, *40* (2), 1287–1296.
- (137) Georgakilas, V.; Kordatos, K.; Prato, M.; Guldi, D. M.; Holzinger, M.; Hirsch, A. Organic Functionalization of Carbon Nanotubes. *J. Am. Chem. Soc.* **2002**, *124* (5), 760–761.
- (138) Willocq, C.; Hermans, S.; Devillers, M. Active Carbon Functionalized with Chelating Phosphine Groups for the Grafting of Model Ru and Pd Coordination Compounds. *J. Phys. Chem. C* **2008**, *112* (14), 5533–

5541.

- (139) Fang, H.-T.; Liu, C.-G.; Liu, C.; Li, F.; Liu, M.; Cheng, H.-M. Purification of Single-Wall Carbon Nanotubes by Electrochemical Oxidation. *Chem. Mater.* **2004**, *16* (26), 5744–5750.
- (140) Berenguer, R.; Marco-Lozar, J. P.; Quijada, C.; Cazorla-Amorós, D.; Morallón, E. Effect of Electrochemical Treatments on the Surface Chemistry of Activated Carbon. *Carbon* **2009**, *47* (4), 1018–1027.
- (141) Berenguer, R.; Nishihara, H.; Itoi, H.; Ishii, T.; Morallón, E.; Cazorla-Amorós, D.; Kyotani, T. Electrochemical Generation of Oxygen-Containing Groups in an Ordered Microporous Zeolite-Templated Carbon. *Carbon* **2013**, *54*, 94–104.
- (142) Baibarac, M.; Lira-Cantú, M.; Oró-Solé, J.; Casañ-Pastor, N.; Gomez-Romero, P. Electrochemically Functionalized Carbon Nanotubes and Their Application to Rechargeable Lithium Batteries. *Small* **2006**, *2* (8-9), 1075–1082.
- (143) Wu, B.; Hu, D.; Kuang, Y.; Yu, Y.; Zhang, X.; Chen, J. High Dispersion of Platinum–Ruthenium Nanoparticles on the 3,4,9,10-Perylene Tetracarboxylic Acid-Functionalized Carbon Nanotubes for Methanol Electro-Oxidation. *Chem. Commun.* **2011**, *47* (18), 5253–5255.
- (144) Lei, Z.; Zhang, H.; Ma, S.; Ke, Y.; Li, J.; Li, F. Electrochemical Polymerization of Aniline inside Ordered Macroporous Carbon. *Chem. Commun.* **2002**, No. 7, 676–677.
- (145) Salinas-Torres, D.; Sieben, J. M.; Lozano-Castelló, D.; Cazorla-Amorós, D.; Morallón, E. Asymmetric Hybrid Capacitors Based on Activated Carbon and Activated Carbon Fibre–PANI Electrodes. *Electrochim. Acta* **2013**, *89*, 326–333.
- (146) Tam, P. D.; Hieu, N. Van. Conducting Polymer Film-Based Immunosensors Using Carbon Nanotube/Antibodies Doped Polypyrrole. *Appl. Surf. Sci.* **2011**, *257* (23), 9817–9824.
- (147) Salinas-Torres, D.; Sieben, J. M.; Lozano-Castello, D.; Morallón, E.; Burghammer, M.; Riekkel, C.; Cazorla-Amorós, D. Characterization of Activated Carbon Fiber/Polyaniline Materials by Position-Resolved Microbeam Small-Angle X-Ray Scattering. *Carbon* **2012**, *50* (3),

1051–1056.

- (148) Zhitomirsky, I. Electrophoretic Deposition of Organic–Inorganic Nanocomposites. *J. Mater. Sci.* **2006**, *41* (24), 8186–8195.
- (149) An, Q.; Rider, A. N.; Thostenson, E. T. Electrophoretic Deposition of Carbon Nanotubes onto Carbon-Fiber Fabric for Production of Carbon/Epoxy Composites with Improved Mechanical Properties. *Carbon* **2012**, *50* (11), 4130–4143.
- (150) Zhou, Y.; Fang, Y.; Ramasamy, R. P. Non-Covalent Functionalization of Carbon Nanotubes for Electrochemical Biosensor Development. *Sensors* **2019**, *19* (2), 392.
- (151) Hirsch, A.; Vostrowsky, O. Functionalization of Carbon Nanotubes. In: Schlüter, A. D. *Functional Molecular Nanostructures*, Schlüter, A. D. Ed.; Springer Berlin Heidelberg: Berlin, Heidelberg, **2005**; pp. 193–237.
- (152) Ghanem, M. A.; Kocak, I.; Al-Mayouf, A.; AlHoshan, M.; Bartlett, P. N. Covalent Modification of Carbon Nanotubes with Anthraquinone by Electrochemical Grafting and Solid Phase Synthesis. *Electrochim. Acta* **2012**, *68*, 74–80.
- (153) Bahr, J. L.; Yang, J.; Kosynkin, D. V; Bronikowski, M. J.; Smalley, R. E.; Tour, J. M. Functionalization of Carbon Nanotubes by Electrochemical Reduction of Aryl Diazonium Salts: A Bucky Paper Electrode. *J. Am. Chem. Soc.* **2001**, *123* (27), 6536–6542.
- (154) Kooi, S. E.; Schlecht, U.; Burghard, M.; Kern, K. Electrochemical Modification of Single Carbon Nanotubes. *Angew. Chemie Int. Ed.* **2002**, *41* (8), 1353–1355.
- (155) Gallardo, I.; Pinson, J.; Vilà, N. Spontaneous Attachment of Amines to Carbon and Metallic Surfaces. *J. Phys. Chem. B* **2006**, *110* (39), 19521–19529.
- (156) Kaur, N.; Thakur, H.; Prabhakar, N. Conducting Polymer and Multi-Walled Carbon Nanotubes Nanocomposites Based Amperometric Biosensor for Detection of Organophosphate. *J. Electroanal. Chem.* **2016**, *775*, 121–128.
- (157) Petrov, P.; Lou, X.; Pagnouille, C.; Jérôme, C.; Calberg, C.; Jérôme, R.

- Functionalization of Multi-Walled Carbon Nanotubes by Electrografting of Polyacrylonitrile. *Macromol. Rapid Commun.* **2004**, *25* (10), 987–990.
- (158) Zhang, Y.; Shen, Y.; Li, J.; Niu, L.; Dong, S.; Ivaska, A. Electrochemical Functionalization of Single-Walled Carbon Nanotubes in Large Quantities at a Room-Temperature Ionic Liquid Supported Three-Dimensional Network Electrode. *Langmuir* **2005**, *21* (11), 4797–4800.
- (159) Baibarac, M.; Baltog, I.; Godon, C.; Lefrant, S.; Chauvet, O. Covalent Functionalization of Single-Walled Carbon Nanotubes by Aniline Electrochemical Polymerization. *Carbon* **2004**, *42* (15), 3143–3152.
- (160) Zhang, T.; Nix, M. B.; Yoo, B.-Y.; Deshusses, M. A.; Myung, N. V. Electrochemically Functionalized Single-Walled Carbon Nanotube Gas Sensor. *Electroanalysis* **2006**, *18* (12), 1153–1158.
- (161) Unger, E.; Graham, A.; Kreupl, F.; Liebau, M.; Hoenlein, W. Electrochemical Functionalization of Multi-Walled Carbon Nanotubes for Solvation and Purification. *Curr. Appl. Phys.* **2002**, *2* (2), 107–111.
- (162) Adenier, A.; Chehimi, M. M.; Gallardo, I.; Pinson, J.; Vilà, N. Electrochemical Oxidation of Aliphatic Amines and Their Attachment to Carbon and Metal Surfaces. *Langmuir* **2004**, *20* (19), 8243–8253.
- (163) Malmos, K.; Iruthayaraj, J.; Pedersen, S. U.; Daasbjerg, K. General Approach for Monolayer Formation of Covalently Attached Aryl Groups Through Electrografting of Arylhydrazines. *J. Am. Chem. Soc.* **2009**, *131* (39), 13926–13927.
- (164) Mayuri, P.; Huang, S.-T.; Mani, V.; Kumar, A. S. A New Organic Redox Species-Indole Tetraone Trapped MWCNT Modified Electrode Prepared by in-Situ Electrochemical Oxidation of Indole for a Bifunctional Electrocatalysis and Simultaneous Flow Injection Electroanalysis of Hydrazine and Hydrogen Peroxide. *Electrochim. Acta* **2018**, *268*, 150–162.
- (165) Gebeshuber, I. C. Biotribology Inspires New Technologies. *Nano Today* **2007**, *2* (5), 30–37.
- (166) Rao, C. N. R.; Cheetham, A. K. Science and Technology of Nanomaterials: Current Status and Future Prospects. *J. Mater. Chem.*

2001, 11 (12), 2887–2894.

- (167) Rubianes, M. D.; Rivas, G. A. Enzymatic Biosensors Based on Carbon Nanotubes Paste Electrodes. *Electroanalysis* **2005**, 17 (1), 73–78.
- (168) Ivnitski, D.; Artyushkova, K.; Rincón, R. A.; Atanassov, P.; Luckarift, H. R.; Johnson, G. R. Entrapment of Enzymes and Carbon Nanotubes in Biologically Synthesized Silica: Glucose Oxidase-Catalyzed Direct Electron Transfer. *Small* **2008**, 4 (3), 357–364.
- (169) Cosnier, S.; Holzinger, M.; Le Goff, A. Recent Advances in Carbon Nanotube-Based Enzymatic Fuel Cells. *Front. Bioeng. Biotechnol.* **2014**, 2, 45.
- (170) Gross, A. J.; Holzinger, M.; Cosnier, S. Buckypaper Bioelectrodes: Emerging Materials for Implantable and Wearable Biofuel Cells. *Energy Environ. Sci.* **2018**, 11 (7), 1670–1687.
- (171) Zhao, F.; Wang, P.; Ruff, A.; Hartmann, V.; Zacarias, S.; Pereira, I. A. C.; Nowaczyk, M. M.; Rögner, M.; Conzuelo, F.; Schuhmann, W. A Photosystem I Monolayer with Anisotropic Electron Flow Enables Z-Scheme like Photosynthetic Water Splitting. *Energy Environ. Sci.* **2019**, 12 (10), 3133–3143.
- (172) Karimi, A.; Othman, A.; Uzunoglu, A.; Stanciu, L.; Andreescu, S. Graphene Based Enzymatic Bioelectrodes and Biofuel Cells. *Nanoscale* **2015**, 7 (16), 6909–6923.
- (173) Lee, J. Y.; Shin, H. Y.; Kang, S. W.; Park, C.; Kim, S. W. Use of Bioelectrode Containing DNA-Wrapped Single-Walled Carbon Nanotubes for Enzyme-Based Biofuel Cell. *J. Power Sources* **2010**, 195 (3), 750–755.
- (174) Umasankar, Y.; Brooks, D. B.; Brown, B.; Zhou, Z.; Ramasamy, R. P. Three Dimensional Carbon Nanosheets as a Novel Catalyst Support for Enzymatic Bioelectrodes. *Adv. Energy Mater.* **2014**, 4 (6).
- (175) Das, M.; Barbora, L.; Das, P.; Goswami, P. Biofuel Cell for Generating Power from Methanol Substrate Using Alcohol Oxidase Bioanode and Air-Breathed Laccase Biocathode. *Biosens. Bioelectron.* **2014**, 59, 184–191.
- (176) Pizzariello, A.; Stred'ansky, M.; Miertuš, S. A Glucose/Hydrogen

Peroxide Biofuel Cell That Uses Oxidase and Peroxidase as Catalysts by Composite Bulk-Modified Bioelectrodes Based on a Solid Binding Matrix. *Bioelectrochemistry* **2002**, *56* (1), 99–105.

- (177) Szczesny, J.; Marković, N.; Conzuelo, F.; Zacarias, S.; Pereira, I. A. C.; Lubitz, W.; Plumeré, N.; Schuhmann, W.; Ruff, A. A Gas Breathing Hydrogen/Air Biofuel Cell Comprising a Redox Polymer/Hydrogenase-Based Bioanode. *Nat. Commun.* **2018**, *9* (1), 4715.
- (178) Teanphonkrang, S.; Ernst, A.; Janke, S.; Chaiyen, P.; Sucharitakul, J.; Suginta, W.; Khunkaewla, P.; Schuhmann, W.; Schulte, A.; Ruff, A. Amperometric Detection of the Urinary Disease Biomarker P-HPA by Allosteric Modulation of a Redox Polymer-Embedded Bacterial Reductase. *ACS Sensors* **2019**, *4* (5), 1270–1278.
- (179) Pankratov, D.; Zhao, J.; Nur, M. A.; Shen, F.; Leech, D.; Chi, Q.; Pankratova, G.; Gorton, L. The Influence of Surface Composition of Carbon Nanotubes on the Photobioelectrochemical Activity of Thylakoid Bioanodes Mediated by Osmium-Complex Modified Redox Polymer. *Electrochim. Acta* **2019**, *310*, 20–25.
- (180) Xu, S.; Minteer, S. D. Pyrroloquinoline Quinone-Dependent Enzymatic Bioanode: Incorporation of the Substituted Polyaniline Conducting Polymer as a Mediator. *ACS Catal.* **2014**, *4* (7), 2241–2248.
- (181) Ruff, A.; Szczesny, J.; Marković, N.; Conzuelo, F.; Zacarias, S.; Pereira, I. A. C.; Lubitz, W.; Schuhmann, W. A Fully Protected Hydrogenase/Polymer-Based Bioanode for High-Performance Hydrogen/Glucose Biofuel Cells. *Nat. Commun.* **2018**, *9* (1), 3675.
- (182) Lin, Y.; Lu, F.; Tu, Y.; Ren, Z. Glucose Biosensors Based on Carbon Nanotube Nanoelectrode Ensembles. *Nano Lett.* **2004**, *4* (2), 191–195.
- (183) Kim, J.; Campbell, A. S.; de Ávila, B. E.-F.; Wang, J. Wearable Biosensors for Healthcare Monitoring. *Nat. Biotechnol.* **2019**, *37* (4), 389–406.
- (184) Ronkainen, N. J.; Halsall, H. B.; Heineman, W. R. Electrochemical Biosensors. *Chem. Soc. Rev.* **2010**, *39* (5), 1747–1763.
- (185) Mehrotra, P. Biosensors and Their Applications - A Review. *J. Oral Biol. Craniofacial Res.* **2016**, *6* (2), 153–159.

- (186) Thévenot, D. R.; Toth, K.; Durst, R. A.; Wilson, G. S. Electrochemical Biosensors: Recommended Definitions and Classification. International Union of Pure and Applied Chemistry (IUPAC), Analytical Chemistry Division, Commission on Biophysical Chemistry, Commission on Electroanalytical Chemistry, *Pure Appl. Chem.*, **1999**, *71*(12), 2333–2348.
- (187) Ziegler, C.; Göpel, W. Biosensor Development. *Curr. Opin. Chem. Biol.* **1998**, *2* (5), 585–591.
- (188) Dhand, C.; Das, M.; Datta, M.; Malhotra, B. D. Recent Advances in Polyaniline Based Biosensors. *Biosens. Bioelectron.* **2011**, *26* (6), 2811–2821.
- (189) Vo-Dinh, T. Biosensors and Biochips. In: Ferrari, M., Bashir, R., Wereley, S., editor, *BioMEMS and Biomedical Nanotechnology, Volume IV: Biomolecular Sensing, Processing and Analysis*, Springer, Boston, **2007**, pp. 1–20.
- (190) Walcarius, A.; Minter, S. D.; Wang, J.; Lin, Y.; Merkoçi, A. Nanomaterials for Bio-Functionalized Electrodes: Recent Trends. *J. Mater. Chem. B* **2013**, *1* (38), 4878–4908.
- (191) May, S. W. Applications of Oxidoreductases. *Curr. Opin. Biotechnol.* **1999**, *10* (4), 370–375.
- (192) Wang, J. Glucose Biosensors: 40 Years of Advances and Challenges. *Electroanalysis* **2002**, *10* (1), 107–119.
- (193) Kou, S. C.; Cherayil, B. J.; Min, W.; English, B. P.; Xie, X. S. Single-Molecule Michaelis–Menten Equations. *J. Phys. Chem. B* **2005**, *109* (41), 19068–19081.
- (194) Johnson, K. A.; Goody, R. S. The Original Michaelis Constant: Translation of the 1913 Michaelis–Menten Paper. *Biochemistry* **2011**, *50* (39), 8264–8269.
- (195) Heller, A.; Feldman, B. Electrochemical Glucose Sensors and Their Applications in Diabetes Management. *Chem. Rev.* **2008**, *108* (7), 2482–2505.
- (196) Leite, O. D.; Lupetti, K. O.; Fatibello-Filho, O.; Vieira, I. C.; Barbosa,

- A. de M. Synergic Effect Studies of the Bi-Enzymatic System Laccase–Peroxidase in a Voltammetric Biosensor for Catecholamines. *Talanta* **2003**, 59 (5), 889–896.
- (197) Bai, L.; Yuan, R.; Chai, Y.; Zhuo, Y.; Yuan, Y.; Wang, Y. Simultaneous Electrochemical Detection of Multiple Analytes Based on Dual Signal Amplification of Single-Walled Carbon Nanotubes and Multi-Labeled Graphene Sheets. *Biomaterials* **2012**, 33 (4), 1090–1096.
- (198) Vigneshvar, S.; Sudhakumari, C. C.; Senthilkumaran, B.; Prakash, H. Recent Advances in Biosensor Technology for Potential Applications – An Overview. *Front. Bioeng. Biotechnol.* **2016**, 4, 11.
- (199) Patel, D. J.; Suri, A. K. Structure, Recognition and Discrimination in RNA Aptamer Complexes with Cofactors, Amino Acids, Drugs and Aminoglycoside Antibiotics. *Rev. Mol. Biotechnol.* **2000**, 74 (1), 39–60.
- (200) Malhotra, B. D., Ali, M.A. Nanomaterials in Biosensors: Fundamentals and Applications. In: B.D. Malhotra, B. D., Ali, M.A., editors, Nanomaterials in Biosensors: Fundamentals and Applications, Elsevier, Amsterdam, William Andrew Publishing, **2018**, pp. 1–74.
- (201) Tajima, N.; Takai, M.; Ishihara, K. Significance of Antibody Orientation Unraveled: Well-Oriented Antibodies Recorded High Binding Affinity. *Anal. Chem.* **2011**, 83 (6), 1969–1976.
- (202) Rusling, J. F.; Sotzing, G.; Papadimitrakopoulou, F. Designing Nanomaterial-Enhanced Electrochemical Immunosensors for Cancer Biomarker Proteins. *Bioelectrochemistry* **2009**, 76 (1), 189–194.
- (203) Kavosi, B.; Salimi, A.; Hallaj, R.; Amani, K. A Highly Sensitive Prostate-Specific Antigen Immunosensor Based on Gold Nanoparticles/PAMAM Dendrimer Loaded on MWCNTS/Chitosan/Ionic Liquid Nanocomposite. *Biosens. Bioelectron.* **2014**, 52, 20–28.
- (204) Ju, H., Lai, G., Yan, F. Multianalyte immunoassay. In: Ju, H., Lai, G., Yan, F., editor, Immunosensing for Detection of Protein Biomarkers, Elsevier, Amsterdam, Glyn Jones, 2017, pp. 207–237.
- (205) Ju, H., Lai, G., Yan, F. Electrochemical immunosensing. In: Ju, H., Lai,

G., Yan, F., editor, *Immunosensing for Detection of Protein Biomarkers*, Elsevier, Amsterdam, Glyn Jones, 2017, pp. 77–110.

- (206) Okuno, J., Maehashi, K., Kerman, K., Takamura, Y., Matsumoto, K., Tamiya, E. Label-free immunosensor for prostate-specific antigen based on single-walled carbon nanotube array-modified microelectrodes, *Biosens. Bioelectron.* **2007**, 22 (9) 2377–2381.
- (207) Wang, H.; Zhang, Y.; Yu, H.; Wu, D.; Ma, H.; Li, H.; Du, B.; Wei, Q. Label-Free Electrochemical Immunosensor for Prostate-Specific Antigen Based on Silver Hybridized Mesoporous Silica Nanoparticles. *Anal. Biochem.* **2013**, 434 (1), 123–127.
- (208) Yu, X.; Munge, B.; Patel, V.; Jensen, G.; Bhirde, A.; Gong, J. D.; Kim, S. N.; Gillespie, J.; Gutkind, J. S.; Papadimitrakopoulos, F.; et al. Carbon Nanotube Amplification Strategies for Highly Sensitive Immunodetection of Cancer Biomarkers. *J. Am. Chem. Soc.* **2006**, 128 (34), 11199–11205.
- (209) Yan, M.; Zang, D.; Ge, S.; Ge, L.; Yu, J. A Disposable Electrochemical Immunosensor Based on Carbon Screen-Printed Electrodes for the Detection of Prostate Specific Antigen. *Biosens. Bioelectron.* **2012**, 38 (1), 355–361.
- (210) Yu, H.; Yan, F.; Dai, Z.; Ju, H. A Disposable Amperometric Immunosensor for α -1-Fetoprotein Based on Enzyme-Labeled Antibody/Chitosan-Membrane-Modified Screen-Printed Carbon Electrode. *Anal. Biochem.* **2004**, 331 (1), 98–105.
- (211) Tang, J.; Su, B.; Tang, D.; Chen, G. Conductive Carbon Nanoparticles-Based Electrochemical Immunosensor with Enhanced Sensitivity for α -Fetoprotein Using Irregular-Shaped Gold Nanoparticles-Labeled Enzyme-Linked Antibodies as Signal Improvement. *Biosens. Bioelectron.* **2010**, 25 (12), 2657–2662.
- (212) Liu, S.; Wang, Y.; Xu, W.; Leng, X.; Wang, H.; Guo, Y.; Huang, J. A Novel Sandwich-Type Electrochemical Aptasensor Based on GR-3D Au and Aptamer-AuNPs-HRP for Sensitive Detection of Oxytetracycline. *Biosens. Bioelectron.* **2017**, 88, 181–187.
- (213) Altintas, Z.; Uludag, Y.; Gurbuz, Y.; Tothill, I. E. Surface Plasmon Resonance Based Immunosensor for the Detection of the Cancer

- Biomarker Carcinoembryonic Antigen. *Talanta* **2011**, *86* (1), 377–383.
- (214) Villiers, C. Gold Nanoparticles for Sensors and Drug Delivery. In: Louis, C., Pluchery, O. Gold Nanoparticles for Physics, Chemistry and Biology, Imperial College Press, London, 2012, pp. 299-332.
- (215) Casado, C. M.; Cuadrado, I.; Morán, M.; Alonso, B.; García, B.; González, B.; Losada, J. Redox-Active Ferrocenyl Dendrimers and Polymers in Solution and Immobilised on Electrode Surfaces. *Coord. Chem. Rev.* **1999**, *185–186*, 53–80.
- (216) Yang, X.; Yuan, R.; Chai, Y.; Zhuo, Y.; Mao, L.; Yuan, S. Ru(Bpy)₃²⁺-Doped Silica Nanoparticles Labeling for a Sandwich-Type Electrochemiluminescence Immunosensor. *Biosens. Bioelectron.* **2010**, *25* (7), 1851–1855.
- (217) Amouzadeh Tabrizi, M.; Shamsipur, M.; Saber, R.; Sarkar, S.; Zolfaghari, N. An Ultrasensitive Sandwich-Type Electrochemical Immunosensor for the Determination of SKBR-3 Breast Cancer Cell Using RGO-TPA/FeHCFnano Labeled Anti-HCT as a Signal Tag. *Sensors Actuators B Chem.* **2017**, *243*, 823–830.
- (218) Pumera, M. Graphene in Biosensing. *Mater. Today* **2011**, *14* (7), 308–315.
- (219) Vo-Dinh, T.; Cullum, B. Biosensors and Biochips: Advances in Biological and Medical Diagnostics. *Fresenius. J. Anal. Chem.* **2000**, *366* (6), 540–551.
- (220) Bazin, I.; Tria, S. A.; Hayat, A.; Marty, J.-L. New Biorecognition Molecules in Biosensors for the Detection of Toxins. *Biosens. Bioelectron.* **2017**, *87*, 285–298.
- (221) Justino, C. I. L.; Freitas, A. C.; Pereira, R.; Duarte, A. C.; Rocha Santos, T. A. P. Recent Developments in Recognition Elements for Chemical Sensors and Biosensors. *TrAC Trends Anal. Chem.* **2015**, *68*, 2–17.
- (222) Oubrie, A.; Dijkstra, B. W. Structural Requirements of Pyrroloquinoline Quinone Dependent Enzymatic Reactions. *Protein Sci.* **2000**, *9* (7), 1265–1273.
- (223) Duine, J. A. Quinoproteins: Enzymes Containing the Quinonoid

Cofactor Pyrroloquinoline Quinone, Topaquinone or Tryptophan-Tryptophan Quinone. *Eur. J. Biochem.* **1991**, *200* (2), 271–284.

- (224) Lau, C.; Borgmann, S.; Maciejewska, M.; Ngounou, B.; Gründler, P.; Schuhmann, W. Improved Specificity of Reagentless Amperometric PQQ-SGDH Glucose Biosensors by Using Indirectly Heated Electrodes. *Biosens. Bioelectron.* **2007**, *22* (12), 3014–3020.
- (225) Stred'anský, M.; Monošík, R.; Mastihuba, V.; Šturdík, E. Monitoring of PQQ-Dependent Glucose Dehydrogenase Substrate Specificity for Its Potential Use in Biocatalysis and Bioanalysis. *Appl. Biochem. Biotechnol.* **2013**, *171* (4), 1032–1041.
- (226) Salimi, A.; Noorbakhsh, A. Layer by Layer Assembly of Glucose Oxidase and Thiourea onto Glassy Carbon Electrode: Fabrication of Glucose Biosensor. *Electrochim. Acta* **2011**, *56* (17), 6097–6105.
- (227) Wilson, R.; Turner, A. P. F. Glucose Oxidase: An Ideal Enzyme. *Biosens. Bioelectron.* **1992**, *7* (3), 165–185.
- (228) Bankar, S. B.; Bule, M. V.; Singhal, R. S.; Ananthanarayan, L. Glucose Oxidase — An Overview. *Biotechnol. Adv.* **2009**, *27* (4), 489–501.
- (229) Wang, J. Electrochemical Glucose Biosensors. *Chem. Rev.* **2008**, *108* (2), 814–825.
- (230) Wohlfahrt, G.; Trivić, S.; Zeremski, J.; Peričin, D.; Leskovac, V. The Chemical Mechanism of Action of Glucose Oxidase from *Aspergillus Niger*. *Mol. Cell. Biochem.* **2004**, *260* (1), 69–83.
- (231) Leskovac, V.; Trivić, S.; Wohlfahrt, G.; Kandrač, J.; Peričin, D. Glucose Oxidase from *Aspergillus Niger*: The Mechanism of Action with Molecular Oxygen, Quinones, and One-Electron Acceptors. *Int. J. Biochem. Cell Biol.* **2005**, *37* (4), 731–750.
- (232) Nakamura, S., Ogura, Y. Action Mechanism of Glucose Oxidase of *Aspergillus Niger*. *J. Biochem.* **1968**, *63* (3), 308–316.
- (233) Rispens, T., Vidarsson, G. Human IgG Subclasses. In: Ackerman, M. E., Nimmerjahn, F., editors, *Antibody Fc- Linking Adaptive and Innate Immunity*, Academic Press, Boston, **2014**, pp. 159–177.
- (234) Benvidi, A.; Firouzabadi, A. D.; Moshtaghiun, S. M.; Mazloum-

- Ardakani, M.; Tezerjani, M. D. Ultrasensitive DNA Sensor Based on Gold Nanoparticles/Reduced Graphene Oxide/Glassy Carbon Electrode. *Anal. Biochem.* **2015**, *484*, 24–30.
- (235) Szentivanyi, A., Maurer, P. H., Janicki, B. W. Antibodies Structure, Synthesis, Functiona, and Immunologic Intervention in Disease, first edition, Springer, New York, **1987**.
- (236) Cathou, R., Haber, E. Structure of the Antibody Combining Site. I. Hapten Stabilization of Antibody Conformation, *Biochem.* **1967**, *6*, 513-518.
- (237) Ju, H., Lai, G., Yan, F. Introduction. In: u, H., Lai, G., Yan, F., editor, Immunosensing for Detection of Protein Biomarkers, Elsevier, Amsterdam, Glyn Jones, 2017, pp. 1–30.
- (238) Schroeder, H. W.; Cavacini, L. Structure and Function of Immunoglobulins. *J. Allergy Clin. Immunol.* **2010**, *125* (2, Supplement 2), S41–S52.
- (239) Scouten, W. H.; Luong, J. H. T.; Stephen Brown, R. Enzyme or Protein Immobilization Techniques for Applications in Biosensor Design. *Trends Biotechnol.* **1995**, *13* (5), 178–185.
- (240) Bornscheuer, U. T. Immobilizing Enzymes: How to Create More Suitable Biocatalysts . *Angew. Chemie Int. Ed.* **2003**, *42* (29), 3336–3337.
- (241) Mateo, C.; Palomo, J. M.; Fernandez-Lorente, G.; Guisan, J. M.; Fernandez-Lafuente, R. Improvement of Enzyme Activity, Stability and Selectivity via Immobilization Techniques. *Enzyme Microb. Technol.* **2007**, *40* (6), 1451–1463.
- (242) Zhao, X. S.; Bao, X. Y.; Guo, W.; Lee, F. Y. Immobilizing Catalysts on Porous Materials. *Mater. Today* **2006**, *9* (3), 32–39.
- (243) Yu, C.-M.; Yen, M.-J.; Chen, L.-C. A Bioanode Based on MWCNT/Protein-Assisted Co-Immobilization of Glucose Oxidase and 2,5-Dihydroxybenzaldehyde for Glucose Fuel Cells. *Biosens. Bioelectron.* **2010**, *25* (11), 2515–2521.
- (244) Gamero-Quijano, A.; Huerta, F.; Morallón, E.; Montilla, F. Modulation of the Silica Sol–Gel Composition for the Promotion of Direct Electron

- Transfer to Encapsulated Cytochrome C. *Langmuir* **2014**, *30* (34), 10531–10538.
- (245) Santos, J. C. S. D.; Barbosa, O.; Ortiz, C.; Berenguer-Murcia, A.; Rodrigues, R. C.; Fernandez-Lafuente, R. Importance of the Support Properties for Immobilization or Purification of Enzymes. *ChemCatChem* **2015**, *7* (16), 2413–2432.
- (246) Garcia-Galan, C.; Berenguer-Murcia, Á.; Fernandez-Lafuente, R.; Rodrigues, R. C. Potential of Different Enzyme Immobilization Strategies to Improve Enzyme Performance. *Adv. Synth. Catal.* **2011**, *353* (16), 2885–2904.
- (247) Gao, Y.; Kyratzis, I. Covalent Immobilization of Proteins on Carbon Nanotubes Using the Cross-Linker 1-Ethyl-3-(3-Dimethylaminopropyl)Carbodiimide—a Critical Assessment. *Bioconjug. Chem.* **2008**, *19* (10), 1945–1950.
- (248) Brady, D.; Jordaan, J. Advances in Enzyme Immobilisation. *Biotechnol. Lett.* **2009**, *31* (11), 1639.
- (249) Pingarrón Carrazón, J. M.; Sánchez Batanero, P. Química Electroanalítica-Fundamentos y Aplicaciones; Síntesis S.A.: Madrid, España, 2003.
- (250) González-Arribas, E.; Bobrowski, T.; Di Bari, C.; Sliozberg, K.; Ludwig, R.; Toscano, M. D.; De Lacey, A. L.; Pita, M.; Schuhmann, W.; Shleev, S. Transparent, Mediator- and Membrane-Free Enzymatic Fuel Cell Based on Nanostructured Chemically Modified Indium Tin Oxide Electrodes. *Biosens. Bioelectron.* **2017**, *97*, 46–52.
- (251) Cao, L. Immobilised Enzymes: Science or Art? *Curr. Opin. Chem. Biol.* **2005**, *9* (2), 217–226.
- (252) Pedrosa, V. A.; Paliwal, S.; Balasubramanian, S.; Nepal, D.; Davis, V.; Wild, J.; Ramanculov, E.; Simonian, A. Enhanced Stability of Enzyme Organophosphate Hydrolase Interfaced on the Carbon Nanotubes. *Colloids Surfaces B Biointerfaces* **2010**, *77* (1), 69–74.
- (253) Feng, W.; Ji, P. Enzymes Immobilized on Carbon Nanotubes. *Biotechnol. Adv.* **2011**, *29* (6), 889–895.
- (254) Datta, S.; Christena, L. R.; Rajaram, Y. R. S. Enzyme Immobilization:

An Overview on Techniques and Support Materials. *3 Biotech* **2013**, *3* (1), 1–9.

- (255) Putzbach, W., Ronkainen, N.J. Immobilization Techniques in the Fabrication of Nanomaterial-Based Electrochemical Biosensors: A Review. *Sensors* **2013**, *13*, 4811–4840.
- (256) Wu, J. C. Y.; Hutchings, C. H.; Lindsay, M. J.; Werner, C. J.; Bundy, B. C. Enhanced Enzyme Stability Through Site-Directed Covalent Immobilization. *J. Biotechnol.* **2015**, *193*, 83–90.
- (257) López-Bernabeu, S.; Huerta, F.; Morallón, E.; Montilla, F. Direct Electron Transfer to Cytochrome c Induced by a Conducting Polymer. *J. Phys. Chem. C* **2017**, *121* (29), 15870–15879.
- (258) Göbel, G.; Schubart, I. W.; Scherbahn, V.; Lisdat, F. Direct Electron Transfer of PQQ-Glucose Dehydrogenase at Modified Carbon Nanotubes Electrodes. *Electrochem. commun.* **2011**, *13* (11), 1240–1243.
- (259) Wang, D.; Tan, Y. Electrodeposition of Enzymes-Integrated Mesoporous Composite Films by Interfacial Templating: A Paradigm for Electrochemical Biosensors. *Electrochim. Acta* **2014**, *116*, 495–503.
- (260) López-Bernabeu, S.; Gamero-Quijano, A.; Huerta, F.; Morallón, E.; Montilla, F. Enhancement of the Direct Electron Transfer to Encapsulated Cytochrome c by Electrochemical Functionalization with a Conducting Polymer. *J. Electroanal. Chem.* **2017**, *793*, 34–40.
- (261) Beissenhirtz, M. K.; Scheller, F. W.; Stöcklein, W. F. M.; Kurth, D. G.; Möhwald, H.; Lisdat, F. Electroactive Cytochrome c Multilayers within a Polyelectrolyte Assembly. *Angew. Chemie Int. Ed.* **2004**, *43* (33), 4357–4360.
- (262) Zhao, F.; Hartmann, V.; Ruff, A.; Nowaczyk, M. M.; Rögner, M.; Schuhmann, W.; Conzuelo, F. Unravelling Electron Transfer Processes at Photosystem 2 Embedded in an Os-Complex Modified Redox Polymer. *Electrochim. Acta* **2018**, *290*, 451–456.
- (263) Krajewska, B. Application of Chitin- and Chitosan-Based Materials for Enzyme Immobilizations: A Review. *Enzyme Microb. Technol.* **2004**, *35* (2), 126–139.

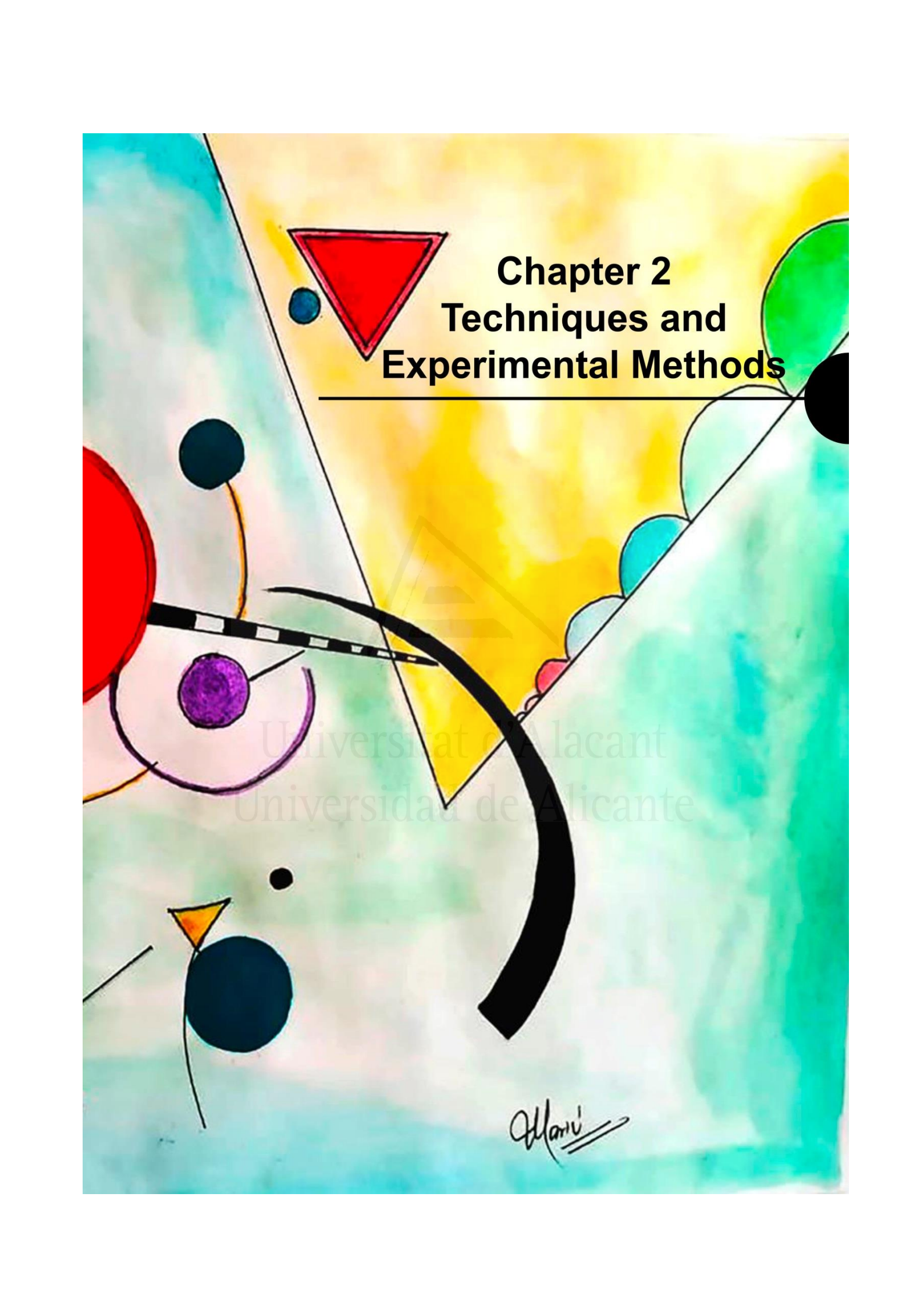
- (264) Arora, P.; Sindhu, A.; Dilbaghi, N.; Chaudhury, A. Biosensors as Innovative Tools for the Detection of Food Borne Pathogens. *Biosens. Bioelectron.* **2011**, *28* (1), 1–12.
- (265) Marty, J.-L.; Mionetto, N.; Noguier, T.; Ortega, F.; Roux, C. Enzyme Sensors for the Detection of Pesticides. *Biosens. Bioelectron.* **1993**, *8* (6), 273–280.
- (266) Vashist, S. K.; Venkatesh, A. G.; Mitsakakis, K.; Czilwik, G.; Roth, G.; von Stetten, F.; Zengerle, R. Nanotechnology-Based Biosensors and Diagnostics: Technology Push versus Industrial/Healthcare Requirements. *Bionanoscience* **2012**, *2* (3), 115–126.
- (267) Vashist, S. K. Point-of-Care Diagnostics: Recent Advances and Trends. *Biosensors* **2017**, *7* (4), 62.
- (268) Caygill, R. L.; Blair, G. E.; Millner, P. A. A Review on Viral Biosensors to Detect Human Pathogens. *Anal. Chim. Acta* **2010**, *681* (1), 8–15.
- (269) Ahmed, M. U.; Hossain, M. M.; Tamiya, E. Electrochemical Biosensors for Medical and Food Applications. *Electroanalysis* **2008**, *20* (6), 616–626.
- (270) Carrara, S.; Shumyantseva, V. V.; Archakov, A. I.; Samorì, B. Screen-Printed Electrodes Based on Carbon Nanotubes and Cytochrome P450sc for Highly Sensitive Cholesterol Biosensors. *Biosens. Bioelectron.* **2008**, *24* (1), 148–150.
- (271) Tan, X.; Li, M.; Cai, P.; Luo, L.; Zou, X. An Amperometric Cholesterol Biosensor Based on Multiwalled Carbon Nanotubes and Organically Modified Sol-Gel/Chitosan Hybrid Composite Film. *Anal. Biochem.* **2005**, *337* (1), 111–120.
- (272) Hernández-Ibáñez, N.; García-Cruz, L.; Montiel, V.; Foster, C. W.; Banks, C. E.; Iniesta, J. Electrochemical Lactate Biosensor Based upon Chitosan/Carbon Nanotubes Modified Screen-Printed Graphite Electrodes for the Determination of Lactate in Embryonic Cell Cultures. *Biosens. Bioelectron.* **2016**, *77*, 1168–1174.
- (273) Arkan, E.; Saber, R.; Karimi, Z.; Shamsipur, M. A Novel Antibody–Antigen Based Impedimetric Immunosensor for Low Level Detection of HER2 in Serum Samples of Breast Cancer Patients via Modification

of a Gold Nanoparticles Decorated Multiwall Carbon Nanotube-Ionic Liquid Electrode. *Anal. Chim. Acta* **2015**, *874*, 66–74.

- (274) Hong, W.; Lee, S.; Cho, Y. Dual-Responsive Immunosensor That Combines Colorimetric Recognition and Electrochemical Response for Ultrasensitive Detection of Cancer Biomarkers. *Biosens. Bioelectron.* **2016**, *86*, 920–926.
- (275) Song, K.-M.; Jeong, E.; Jeon, W.; Cho, M.; Ban, C. Aptasensor for Ampicillin Using Gold Nanoparticle Based Dual Fluorescence–Colorimetric Methods. *Anal. Bioanal. Chem.* **2012**, *402* (6), 2153–2161.
- (276) Lundwall, Å.; Brattsand, M. Kallikrein-Related Peptidases. *Cell. Mol. Life Sci.* **2008**, *65* (13), 2019–2038.
- (277) Lilja, H.; Ulmert, D.; Vickers, A. J. Prostate-Specific Antigen and Prostate Cancer: Prediction, Detection and Monitoring. *Nat. Rev. Cancer* **2008**, *8* (4), 268–278.
- (278) Zheng, G.; Patolsky, F.; Cui, Y.; Wang, W. U.; Lieber, C. M. Multiplexed Electrical Detection of Cancer Markers with Nanowire Sensor Arrays. *Nat. Biotechnol.* **2005**, *23* (10), 1294–1301.
- (279) Catalona, W. J.; Smith, D. S.; Ratliff, T. L.; Dodds, K. M.; Coplen, D. E.; Yuan, J. J. J.; Petros, J. A.; Andriole, G. L. Measurement of Prostate-Specific Antigen in Serum as a Screening Test for Prostate Cancer. *N. Engl. J. Med.* **1991**, *324* (17), 1156–1161.
- (280) Catalona, W. J., Richie, J. P., Ahmann, F. R., Hudson, M. A., Scardino, P.T., Flanigan, R. C., et. al. Comparison of Digital Rectal Examination and Serum Prostate Specific Antigen in the Early Detection of Prostate Cancer: Results of a Multicenter Clinical Trial of 6,630 Men. *J. Urol.* **1994**, *151* (5), 1283–1290.
- (281) Barry, M. J. Prostate-Specific–Antigen Testing for Early Diagnosis of Prostate Cancer. *N. Engl. J. Med.* **2001**, *344* (18), 1373–1377.
- (282) Partin, A. W.; Yoo, J.; Carter, H. B.; Pearson, J. D.; Chan, D. W.; Epstein, J. I.; Walsh, P. C. The Use of Prostate Specific Antigen, Clinical Stage and Gleason Score to Predict Pathological Stage in Men with Localized Prostate Cancer. *J. Urol.* **1993**, *150* (1), 110–114.

- (283) Galant, A. L.; Kaufman, R. C.; Wilson, J. D. Glucose: Detection and Analysis. *Food Chem.* **2015**, *188*, 149–160.
- (284) Heo, Y. J.; Takeuchi, S. Towards Smart Tattoos: Implantable Biosensors for Continuous Glucose Monitoring. *Adv. Healthc. Mater.* **2013**, *2* (1), 43–56.
- (285) Abellán-Llobregat, A.; Jeerapan, I.; Bandodkar, A.; Vidal, L.; Canals, A.; Wang, J.; Morallón, E. A Stretchable and Screen-Printed Electrochemical Sensor for Glucose Determination in Human Perspiration. *Biosens. Bioelectron.* **2017**, *91*, 885–891.
- (286) del Torno-de Román, L.; Navarro, M.; Hughes, G.; Esquivel, J. P.; Milton, R. D.; Minter, S. D.; Sabaté, N. Improved Performance of a Paper-Based Glucose Fuel Cell by Capillary Induced Flow. *Electrochim. Acta* **2018**, *282*, 336–342.
- (287) Yan, Y.; Fang, J.; Yang, Z.; Qiao, J.; Wang, Z.; Yu, Q.; Sun, K. Photoelectrochemical Oxidation of Glucose for Sensing and Fuel Cell Applications. *Chem. Commun.* **2013**, *49* (77), 8632–8634.
- (288) Liu, Y.; Dong, S. A Biofuel Cell Harvesting Energy from Glucose–Air and Fruit Juice–Air. *Biosens. Bioelectron.* **2007**, *23* (4), 593–597.
- (289) Bartlett, P. N. *Bioelectrochemistry: Fundamentals, Experimental Techniques and Applications*; John Wiley & Sons: Chichester, 2008.





Chapter 2
Techniques and
Experimental Methods

Universitat de València
Universidade de Alicante

Mani

1. Introduction

In this chapter the fundamental concepts of the different techniques employed for characterization and further evaluation of the performance of each material and electrode are presented. Furthermore, reagents and materials used during this PhD thesis are also presented. Nevertheless, specific experimental conditions will be explained in detail in each chapter.

2. Material and reagents

2.1. Carbon materials

During this PhD Thesis different nanostructured carbon materials, such as carbon nanotubes (CNTs) and graphene-based materials, were employed for the synthesis of the functional carbon materials. Commercial carbon nanotubes: Multi-Walled Carbon Nanotubes with 95% purity and Single-Walled Carbon Nanotubes with 99% purity were purchased from Cheap Tubes Inc.

2.1.1. Oxidized MWCNT and graphene-based materials.

In the case of MWCNTs, the oxidized MWCNTs (fMWCNTs) were obtained by functionalization in oxidative conditions in 3 M HNO₃ at 120°C for 24 hours under reflux conditions.

Graphene oxide was obtained by modified Hummer method employing graphite powder as precursor¹. Graphene suspensions were obtained following the procedure previously reported².

2.2. Enzymes and antibodies

Native human prostate specific antigen purified (PSA) and purified mouse monoclonal PSA antibody (Ab) (Purified IgG-Ab) were purchased from Bio-Rad Laboratories (Munich, Germany). Glucose oxidase (GO_x) from *Aspergillus Niger* Type VII, lyophilized ($\geq 100,000$ units g⁻¹) was obtained from Sigma-Aldrich.

Soluble apo-enzyme glucose dehydrogenase (s-GDH) was provided by Roche Diagnostics (Germany), which was reconstructed afterwards with pyrroloquinoline quinone (PQQ), following the next procedure: 36 mg of apo-enzyme s-GDH was dissolved in 10 mM (4-(2-hydroxyethyl)-1-piperazineethanesulfonic acid) (HEPES) Buffer solution (pH=7.0), 150 mM $\text{CaCl}_2 \cdot 2\text{H}_2\text{O}$ and 520 μM pyrroloquinoline quinone (PQQ) freshly prepared, attaining a concentration of 36 mg mL^{-1} . In this procedure, PQQ cofactor is introduced in the apo-enzyme structure as active center, and the complex is stabilized by the presence of three cations of calcium. At the same time, one of the calcium cations is required for the activation of the cofactor and oxidation of the substrate³.

2.3. Reagents

Depending on the type of modification made on the carbon materials different reagents were employed, thus, specific reagent for each modification procedure is described in detail in each chapter. Briefly, all reagents used for modification and characterizations are presented: sodium tetrachloroaurate (III) dihydrate ($\text{NaAuCl}_4 \cdot 2\text{H}_2\text{O}$, 99%), poly-n-vinylpyrrolidone (PVP, 40K), sodium hydroxide (NaOH, 99,99% purity), anhydrous ethylene glycol, methanol (+98%), HEPES ($\geq 99.5\%$ -titration), distilled aniline ACS reagent ($\geq 99.5\%$), ammonium persulphate ($\geq 98\%$ -BioXtra), D-(+)-Gluconic acid δ -lactone ($\geq 99\%$), D-(+)-Glucose ACS reagent, glutaraldehyde solution (50 wt. % in H_2O), L-Ascorbic acid reagent grade-Crystalline, Uric acid ($\geq 99\%$ -Crystalline) and pyrroloquinoline quinone ($\geq 95\%$ -HPLC), were purchased from Sigma-Aldrich.

Sulphuric acid (98%) analytical reagent and hydrochloric acid (37%) were obtained from VWR Chemicals. 4-Aminophenyl phosphonic acid (4-APPA, +98%) used as modifier agent was purchased from Tokyo Chemical Industry co (TCI). Potassium dihydrogen phosphate (KH_2PO_4) and ammonia solution (25%) were obtained from Merck. Dipotassium hydrogen phosphate (K_2HPO_4) and calcium chloride dehydrate were purchased from VWR Chemicals, respectively, and were used to prepare phosphate buffer solutions (0.01M PBS, pH=7.2 and 0.1M PBS, pH=7.2) to dissolve the immunoreagents and as electrolyte, unless otherwise noted. Ferrocenium hexafluorophosphate (Fc-97%), employed as redox probe, was purchased from Sigma Aldrich. All the

solutions were prepared using ultrapure water (18 MOhms·cm, Millipore® Milli-Q® water). The gases N₂ (99.999%) and H₂ (99.999%) were provided by Air Liquide.

3. Electrochemical techniques

Electrochemical techniques have been widely used to characterize and evaluate the performance of a material in a specific application. In the present work, cyclic voltammetry (CV) and chronoamperometry (CA) were employed in the functionalization, characterization and further evaluation of the different materials synthesized under different experimental conditions.

In order to perform the electrochemical measurements, a standard three electrode cell was used with a reference electrode (RE); a working electrode (WE), corresponding with the material to be measured; and a counter electrode (CE) which is an electrode with high surface area with respect to the working electrode. The cell was filled with the electrolyte with enough conductivity to avoid electrical resistance. A scheme of the standard electrochemical cell system employed is presented in Figure 2.1.

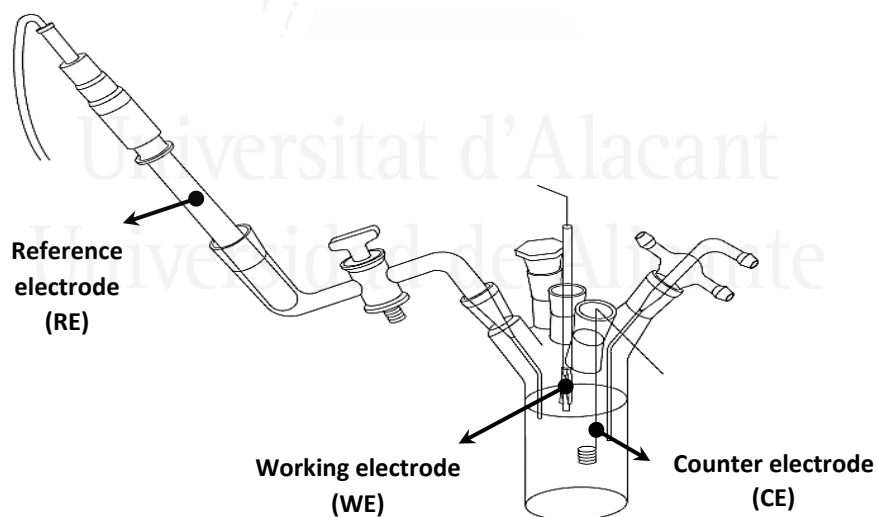


Figure 2.1. Scheme of the electrochemical standard cell set-up.

Electrochemical characterization methods, focus in the analysis of the different processes and interactions in the interphase between a solid electrode

and an electrolyte, when a stimulus (potential or current), is generated in the system. The nature of the induced current presents two different origins: a capacitive and a faradic contribution, which depend on the electrochemical processes, which occur at the interphase electrode-electrolyte⁴.

3.1. Cyclic Voltammetry (CV)

Cyclic voltammetry (CV) is one of the most employed electrochemical techniques for the characterization of electrode materials. CV is based on the application of a controlled potential, versus the reference electrode, to the working electrode, in which current goes through the working electrode and the counter electrode. In a cyclic voltammetry experiment, the current through the WE is measured, meanwhile the potential changes according with Eq. 2.1, using a constant potential scan rate⁴. Initially, the electrode is introduced at an initial potential, where non-faradic process takes place. Subsequently, the system is polarized between two potential limits (E_{upper} and E_{lower}) following a triangular wave (See Figure 2.2-A) according to the following equation:

$$E = E_0 \pm vt \quad \text{Eq. 2.1.}$$

Where E : potential, E_0 : Initial potential, v : scan rate and t : time. The potential scan is performed also in a reverse order, employing the same conditions, until a cycle is completed.

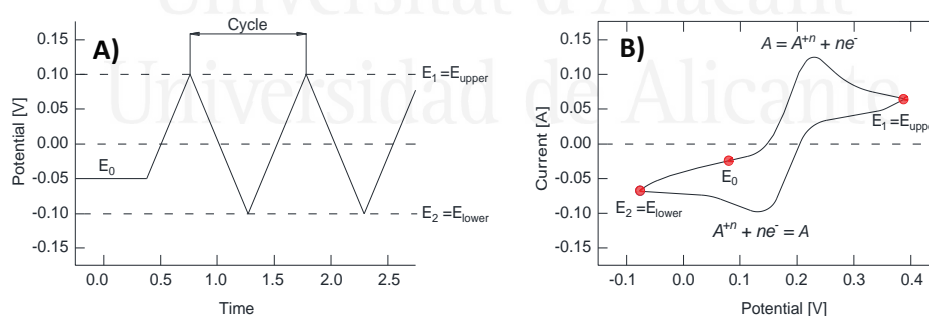
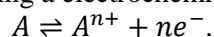


Figure 2.2. A) Triangular cyclic potential wave applied in time and B) cyclic voltammogram considering a electrochemical faradic redox process:



Once the potential is varied, the current generated for either faradic or capacitive processes, is registered versus the WE potential obtaining a cyclic

voltammogram. Figure 2.2-B shows a typical cyclic voltammogram for a redox process in solution. During the polarization of an electrode where a faradic process takes place, the electroactive species generates an increase in the current with the raising of the potential applied, due to the oxidation process. However, the current reaches a maximum value when all the species in the proximity of the interphase are oxidized, producing the peak of the process. Then, a decrease in current is observed, corresponding to a diffusion-controlled process, as consequence of the absence of species in the interphase electrode-electrolyte. The same behavior is observed for the reduction process in the reverse cycle. Depending on the conditions applied such as temperature, electrolyte, concentration, potential, species in solution, among others, the electrochemical behavior of the electrode differs and consequently the CV.

Electrochemical behavior for a carbon material presents the current associated with the capacitive contribution, delivered during the formation of the electrical double layer in the electrode-electrolyte interphase, where non-chemical reactions take place, which presents a quasi-rectangular shape as is described in Figure 2.3-A. Nevertheless, in the case of possible redox surface reactions, an additional contribution in current takes place, which appear as current peaks in the cyclic voltammogram, as can be observed in Figure 2.3-B.

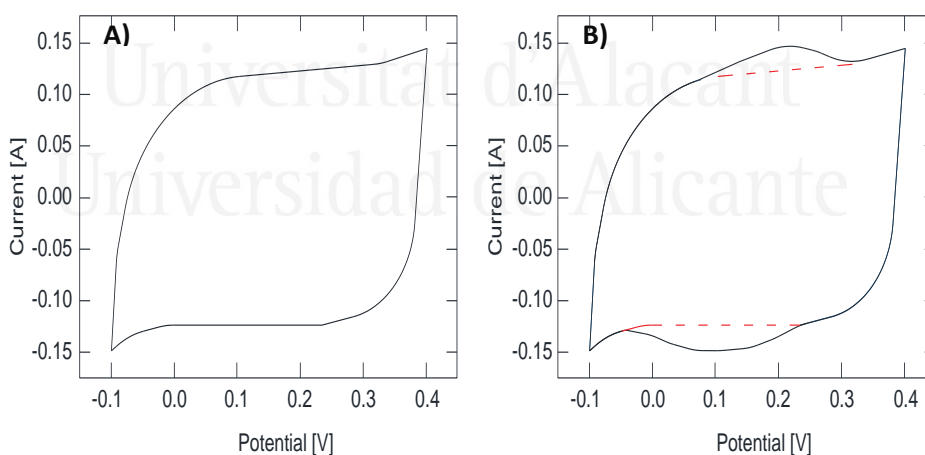


Figure 2.3. Cyclic voltammograms: A) Capacitive behavior and B) Faradic behavior.

3.2. Chronoamperometry (CA)

The chronoamperometry is an electrochemical technique, which is based on a potential step from an initial potential (E_0) to a final potential of interest (E_1). Then, the response of current with time corresponds to the chronoamperogram. Figure 2.4 shows schematically, the profiles obtained in a chronoamperometric test.

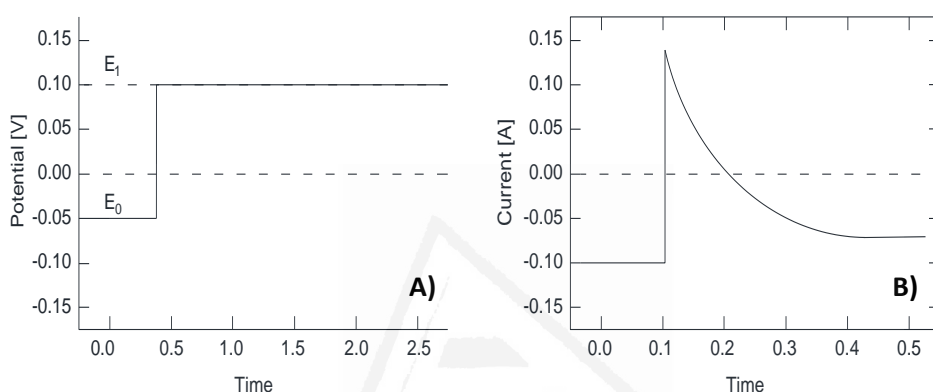


Figure 2.4. A) Potential profile versus time and B) Current profile versus time, in a chronoamperometric experiment during the application of a single potential-step.

Normally, at E_0 , no electrochemical reaction is produced and at E_1 , a faradic process takes place. In this sense, when the reaction is diffusion-controlled, the Cottrell equation is obeyed (Eq. 2.2.)^{4,5}.

$$i(t) = \frac{nFACD^{1/2}}{\pi^{1/2}t^{1/2}} = kt^{-1/2} \quad \text{Eq. 2.2.}$$

Nowadays, chronoamperometry has been widely employed for the determination of diffusion coefficients, stability and degradability of a catalyst, and as technique for the development of methods for quantification for sensors and biosensors⁶. In this last application, the electrode which acts as sensor, is polarized at a potential (E_1), where the analyte of interest is oxidized or reduced. Presence of the analyte generates a current which can be correlated with the concentration of the species. In this work, evaluation of the stability and applicability of the different materials as biosensors, has been made using the chronoamperometry technique⁷.

4. Physicochemical characterization techniques

Textural properties and surface chemistry of carbon materials have been considered crucial in electrocatalysis, energy storage, pollutant removal and biosensing applications, specially, taking into account that the tunability of those properties provides the carbon material the possibility to generate new and different properties in comparison with the pristine carbon material. Therefore, determination of the textural properties and surface chemistry has been necessary to understand the stability, chemical nature and distribution (homogeneity) of those surface functionalities. Physical adsorption of gases and Temperature Programmed Desorption (TPD) are two of the most powerful techniques for the characterization of those properties⁸.

4.1. Temperature Programmed Desorption (TPD)

TPD measurements have become a standard and useful technique for the analysis of the state of adsorbed surface species and been extensively used for characterizing the surface functionalities of carbon materials⁹⁻¹¹. Figure 2.5 shows the oxygen functional groups that can be found in carbon material surfaces.

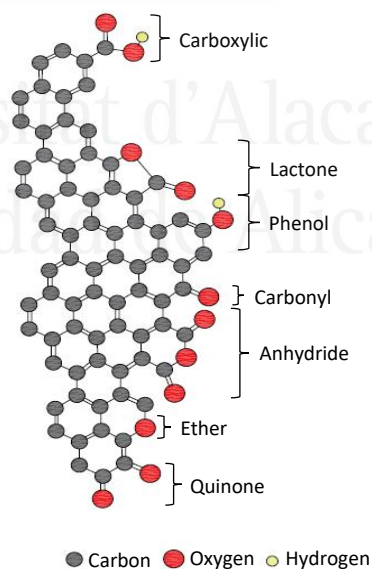


Figure 2.5. Scheme of the different oxygen surface groups present in carbon materials.

Applying a heating program to the sample in an inert atmosphere, decomposition of the different oxygen complexes of the carbon material occurs forming CO, CO₂ and H₂O. Decomposition of acidic groups as carboxylic, anhydrides, and lactones proceeds with CO₂ evolution at temperatures between 200°C and 700°C (anhydride groups also produce CO during their decomposition, that is, one CO and one CO₂ molecule per group), while neutral and basic groups as phenols, esters, carbonyls, and quinones decompose as CO at temperatures from 500°C to more than 1000°C^{9,12}.

In the present PhD Thesis, a TGA-DSC from TA Instruments, SDT Q600 coupled with a mass spectrometer Thermostar, Balzers, BSC 200 were employed for the detection and quantification of the gases generated during the temperature program. The procedure employed for TPD analysis was made employing 5-10 mg of carbon material sample and applying a helium flow of 100 ml min⁻¹, as carrier gas. The temperature program was performed from room temperature to 120°C at 20°C min⁻¹, maintaining this temperature for 2 hours, for sample drying; afterwards, the sample is submitted to a heating rate of 10°C min⁻¹ from 120°C to 950°C, keeping this temperature for 15 min.

4.2. Physical Adsorption of Gases

Adsorption isotherms have been widely employed in the characterization of textural properties of solid materials. Adsorption process is defined as the enrichment of fluid (liquid or gas) in a solid (or liquid) surface, at a determined temperature (See Figure 2.6), as consequence of the physical/chemical interaction between the fluid (adsorbate) and the solid-surface (adsorbent)¹³.

During the physical adsorption process of gases, a controlled dose of a specific gas is applied at constant temperature, until reaching the equilibrium. Considering that the concentration of the adsorbate in the monolayer is correlated with the specific surface area of the solid, this last parameter can be obtained.

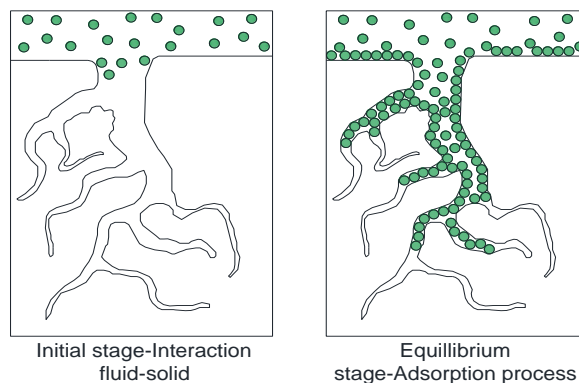


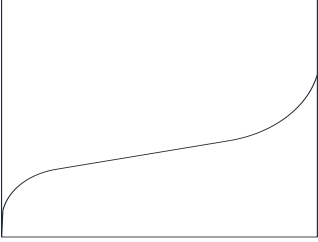

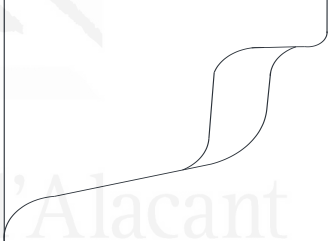
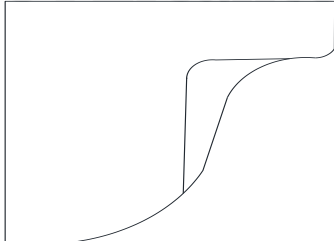
Figure 2.6. Scheme of the adsorption process in porous solid materials.

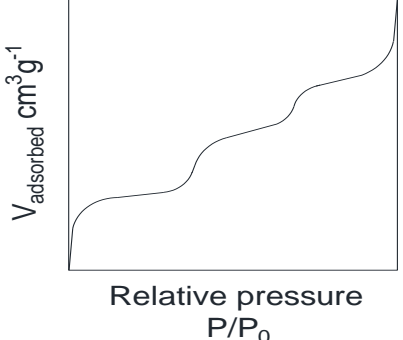
Isotherm adsorption with N_2 at 77K is the most used procedure for characterization and determination of porous texture parameters by adsorption process analysis. Unfortunately, N_2 as adsorbate at 77 K presents some diffusional problems that avoids the proper characterization of the narrow microporosity of materials (that is, pores of size below 0.7 nm). For that reason, CO_2 isotherms at 273K have been employed as complementary characterization.

Depending on the adsorption profiles ($V_{\text{gas adsorbed}}$ vs. P/P_0), IUPAC defines different types of isotherms which are correlated with some features of porous structure in solid materials (See Table 2.1).

Table 2.1. IUPAC Classification of Adsorption Isotherms for Gas-Solid Equilibria¹⁴.

| Isotherm | Features | Example |
|---------------|--|---------|
| Type I | Microporous solids- Monolayer adsorption model (Langmuir). | |

| | | |
|------------------------|---|--|
| <p>Type II</p> | <p>Non porous or macroporous solids</p> | <p>$V_{\text{adsorbed}} \text{ cm}^3 \text{ g}^{-1}$</p>  <p>Relative pressure P/P_0</p> |
| <p>Type III</p> | <p>Weak physical adsorption by multilayers</p> | <p>$V_{\text{adsorbed}} \text{ cm}^3 \text{ g}^{-1}$</p>  <p>Relative pressure P/P_0</p> |
| <p>Type IV</p> | <p>Hysteresis cycle associated with capillary condensation in mesoporous.</p> | <p>$V_{\text{adsorbed}} \text{ cm}^3 \text{ g}^{-1}$</p>  <p>Relative pressure P/P_0</p> |
| <p>Type V</p> | | <p>$V_{\text{adsorbed}} \text{ cm}^3 \text{ g}^{-1}$</p>  <p>Relative pressure P/P_0</p> |

| | | |
|-----------------------|--|--|
| <p>Type VI</p> | <p>Layer-by-layer adsorption on a highly uniform non-porous surface.</p> |  |
|-----------------------|--|--|

4.2.1. BET theory

Determination of specific surface area from the gas adsorption isotherm has been done by the use of the model of Brunauer, Emmett and Teller (BET). The theory is based on a kinetic semi-empirical approximation of the adsorption process, assuming multilayers of gas adsorbed on the material. In this model, the assumption of a Langmuir model is considered where no lateral interactions between the adsorbed molecules occur. Moreover, assumptions of condensation process, except in the first layer, and the formation of infinite number of layers at the saturation pressure are considered¹⁵. BET adsorption isotherm is expressed as:

$$\frac{P/P_0}{n(1-P/P_0)} = \frac{1}{n_m c} + \frac{(c-1)}{n_m c} \left(\frac{P}{P_0}\right) \quad \text{Eq. 2.3.}$$

Where P and P_0 are the equilibrium and the saturation pressures of the adsorbate, respectively, n is the adsorbed amount at a relative pressure (P/P_0), n_m is the adsorbed amount at the monolayer and C is a parameter related with the heat of adsorption.

Lineal representation of the experimental data obtained during a N_2 -77 K adsorption test according to Eq. 2.3 can be correlated to obtain the different parameters. In this case, the slope in the BET plot and the intercept are employed to determine the monolayer adsorbed quantity (n_m) and the BET constant (C). Specific surface area is obtained, taking into account the values of n_m using the following equation:

$$S = n_m \cdot a_m \cdot N_A \cdot 10^{-18} \quad \text{Eq. 2.4.}$$

Where, S is the specific surface area ($\text{m}^2 \text{g}^{-1}$), n_m is the amount of moles of N_2 adsorbed per gram of adsorbent in the monolayer determined by BET, a_m is the cross-sectional area of one adsorbate molecule ($\text{nm}^2 \text{molecule}^{-1}$, for N_2 at 77K it is 0.162 nm^2) and N_A is the Avogadro's number.

4.3. X-ray Photoelectron Spectroscopy (XPS)

X-ray Photoelectron Spectroscopy (XPS) is a technique widely employed in the study and characterization of solid surfaces in a depth range between 1-10 nm, through which it is possible to identify and quantify the chemical nature of the material¹⁶. The technique is based on the detection and quantification of the kinetic energy of the emitted electrons by the material, once is irradiated with a monochromatic beam which wavelength is in the X-ray range. Figure 2.7. shows the phenomenon of photoemission of electrons from an atom of a material during the irradiation with an X-ray beam.

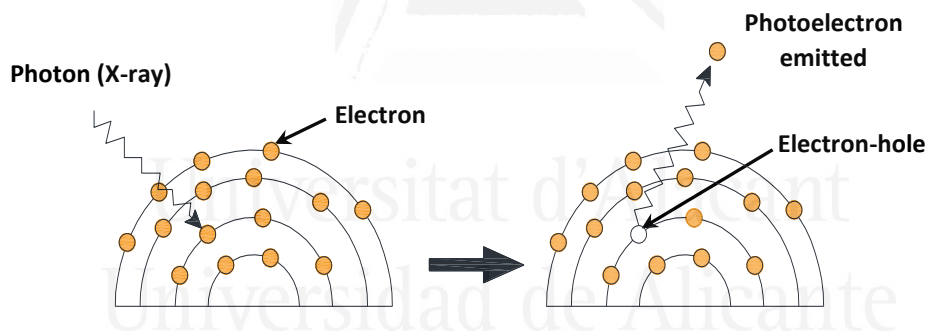


Figure 2.7. Photoemission of electrons during an XPS test.

During the process of photoemission of electrons, the X-ray impacts onto the material surface producing the emission of electrons with different kinetic energy. Based on that, Eq. 2.5 describes the energy of the photo-emitted electrons during the XPS phenomenon.

$$E_K = E_{h\nu} - E_b - \Phi \quad \text{Eq. 2.5.}$$

E_K is the kinetic energy of the emitted electron, $E_{h\nu}$ is the energy of the X-ray source employed for the equipment, E_b is the binding energy of the emitted electrons with respect to the Fermi level and Φ is the work function, associated with the spectrometer and the sample. A specific atom can present different types of emissions, arising from the internal orbitals of the atom or from the valence orbitals, therefore, different values of binding energy for a same species can be presented, which depends of the atom nature and oxidation state¹⁷.

Surface composition, degree of modification and nature of the different species in the materials employed in this work were studied using a VG-Microtech Mutilab 3000 spectrometer and an X-ray radiation source with a Mg anode ($K\alpha$ 1253.6 eV). This set-up employs a semi-spherical electron analyzer with 9 *channeltrons* (with a path energy between 2-200eV). The C1s peak position was set at 284.6 eV and used as reference. Deconvolution of the XPS peaks were done by least squares fitting using Gaussian-Lorentzian curves, while a Shirley line was used for the background determination^{18,19}.

4.4. Raman Spectroscopy

Raman spectroscopy is a powerful and complementary technique that provides important information in the characterization of carbon materials. The technique is based on the inelastic scattering phenomenon that radiation presents when interacts with the matter. Initially, radiation with a specific frequency, interacts with the sample; during this process most of the energy is scattered with the same frequency of the incident radiation, generating the Rayleigh scattering; however, small part of the light is absorbed and experiences inelastic scattering giving rise to the Stokes Raman or Anti-Stokes Raman scattering (See Figure 2.8)²⁰.

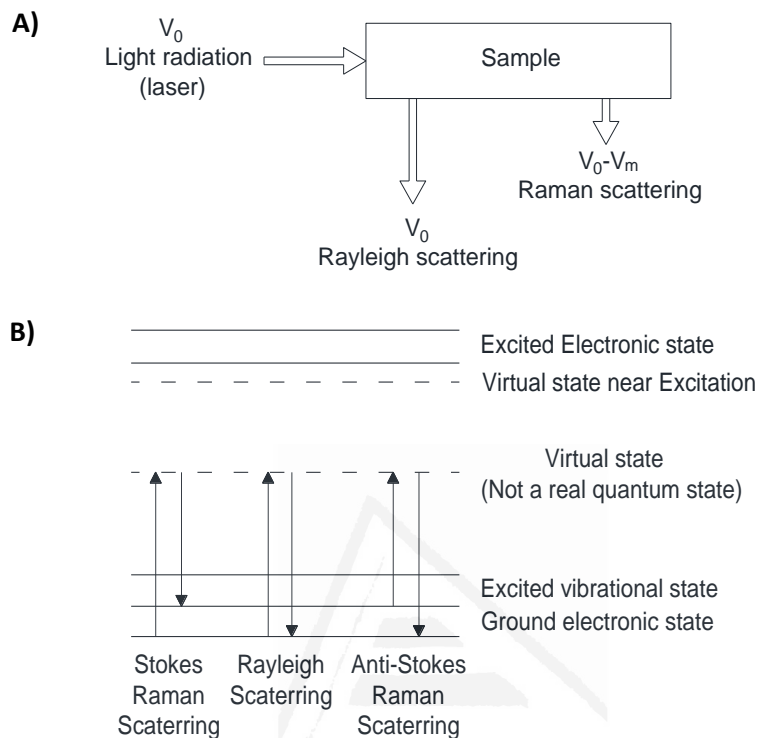


Figure 2.8. Scheme of light-radiation interaction with the matter: A) Scattering processes and B) Excitation-Emission process in a Raman experiment.

Depending on the final energy state of the molecule, two possible molecular energy levels can be presented, generating radiation with two different wavelengths. One of the emissions, characterized by the photon-emission from an excited level to a ground level with higher wavelength than the incident (the Radiation-Stokes lines). On the other hand, the second emission occurs from the excited state to a transition level with shorter wavelength than the incident (the Radiation-Anti-Stokes lines). Stokes process is more favored than Anti-Stokes process.

One important aspect of Raman scattering is that it is orders of magnitude less intense compared with other scattering phenomenon, what results in quite low sensitivity in some cases. Additionally, existence of emission processes like fluorescence can mask the signal of the Raman scattering. In this sense,

many approaches, to improve the Raman signal have been widely developed, as the use a monochromatic source of radiation, increasing sensibility of the detector, coupling with other radiation-emission phenomenon such as Plasmon, among others.

Absorption and excitation modes in Raman are determined by the change in the polarizability of the molecule during the interaction with the radiation, for instance, the molecular vibrations and displacement of the atoms from their equilibrium positions. Then, the intensity of Raman signal is also proportional to the magnitude of polarizability of the molecules. Since each molecule produces different characteristic vibrational energies, Raman spectrum provides a “fingerprint” for the identification and characterization of a material.

Raman spectra were obtained employing a Raman spectrometer model JASCO NRS-5100 with 300 mm of focal distance, coupled with a confocal microscope with an objective MPLFLN 20x and a solid-state laser (532 nm) with 4 mW in power. As detector, a charge-coupled device was employed, which was cooled by Peltier effect. Base line was corrected calibrating the line at 520 cm^{-1} in a pure silicon sample.

5. Analytical techniques

5.1. Inductively Coupled Plasma Optical Emission Spectrometry (ICP-OES)

ICP-OES is an important technique for quantification of a variety of a large number of elements which are present at very low concentrations in aqueous solution. With this technique, liquid samples are injected into a radiofrequency-induced argon plasma using one of a variety of nebulizers or sample introduction techniques. The sample mist reaching the plasma is quickly dried, vaporized, and energized through collisional excitation at high temperature²¹.

The torch or plasma source in the ICP-OES, consists of 4 concentric crystal-quartz tubes, which are surrounded by a cooled induction-coil where argon flows through it. In this system, the plasma is generated reaching a temperature of 10000°C . The plasma produces the ionization of the sample, which subsequently achieves the fundamental state, emitting radiation in the

UV-Visible spectrum, being the wave-length characteristic for each element. Emitted radiation is separated using a prism towards the detectors, which registers the intensity of the signal. A scheme of the performance of a ICP-OES can be observed in Figure 2.9. The intensity of the radiation generated can be correlated with the concentration of the species, establishing a procedure of quantification of the species in solution, through a calibration curve previously determined^{22,23}.

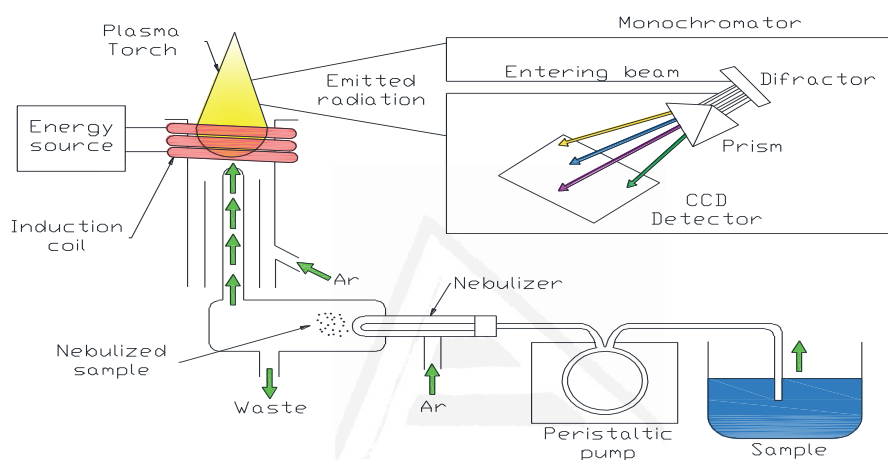


Figure 2.9. Scheme of parts and performance for a conventional ICP-OES system for the analysis of element of samples.

In this work, content of gold in the carbon material after the impregnation was determined by ICP-OES, which was performed in a Perkin Elmer 4300 spectrometer. To do this, 10 mg of the gold containing carbon nanotubes were submitted to an extraction of the metal employing a solution of aqua regia (HCl:HNO₃, 3:1) at 80°C for 6 hours. Afterwards the sample was filtered with nylon membrane (pore size of 450 nm) and diluted with ultrapure water, until achieving a concentration of 2% (w/w) HNO₃. Quantification of the amount of gold was determined employing the intensity of the emissions by a calibration curve of the metal.

6. Microscopy techniques

It is well recognized that nano and micrometric features in any material, specifically on surface, have an important effect in the bulk properties of a material. Morphology, porous structure, homogeneity, chemical distribution,

topology, among others, have been subject of study and an important tool to understand the applicability in specific fields. In the following sections, a short description of the microscopy techniques used in this PhD Thesis is presented.

6.1. Field Emission Scanning Electron Microscopy (FESEM)

Field Emission Scanning Electron Microscopy is a technique for morphological and chemical characterization of the material surface with higher resolution than the conventional SEM. In this case, a field emission cathode produces a highly focused beam of high and low energy electrons using low voltages (0.02-5 kV), in comparison with the thermionic system in the conventional SEM, avoiding over heating of the samples and possible sample damages.

The electron beam is composed by primary electrons which are irradiated over the surface of the sample. The interaction between the sample and the primary electrons generates the emission of electrons from the sample, named as secondary electrons, and X-ray fluorescence from which morphological and chemical information can be obtained²⁴.

Carbon materials morphology, structural changes after the functionalization and gold nanoparticle size distribution were analyzed in this PhD Thesis using a ZEISS Field Emission Scanning Electronic Microscopy model *Merlin VP Compact*, which is equipped with a BRUKER microanalysis system for EDX, model *Quantax 400*. In some cases, application of carbon coating was necessary to avoid charging of the sample and further degradation.

6.2. Transmission Electron Microscopy (TEM)

Transmission Electron Microscopy provides morphological and structural information of the sample. The technique uses an accelerated and thin electron beam, with energy between 100-200 keV that interacts with a very thin sample. Part of the electrons is transmitted through the sample that provides direct morphological and structural information. Other part of the electron beam is dispersed or absorbed by the sample producing different types of emission phenomena, such as secondary electrons, X-ray generation and Auger electrons. All the mentioned processes (i.e. transmission, dispersion and absorption) are employed to obtain information of the crystalline structure and

elemental chemical composition of the sample. Since the electrons have to pass through the sample, thin samples are required to guarantee the transmission of the electrons^{25,26}.

Conventional transmission electron microscopes consist of a combination of different lenses which resolve and amplify an image of the sample, in the same way that optical microscopes work. Radiation is generated by an electron gun, which is emitted by a Wolfram filament or a LaB₆ crystal. Electrons are generated applying a potential difference to the filament, accelerating them by the application of a negative potential of 100 kV and are focused through different condenser lenses towards the sample. Afterwards, electrons are collected and focused by the objective lens, generating a magnified image. This image is further magnified, due to the use of projector lenses, which at the same time control the amplification of the image in the fluorescence screen. Scheme of the structure, conformation and generation of the image using TEM can be observed in Figure 2.10²⁷.

Samples of the electrode materials studied in this PhD Thesis, were prepared by dispersion of the samples in isopropanol or DMF. Some drops of the dispersed material are deposited on a copper mesh and dried under room temperature and vacuum.

Universitat d'Alacant
Universidad de Alicante

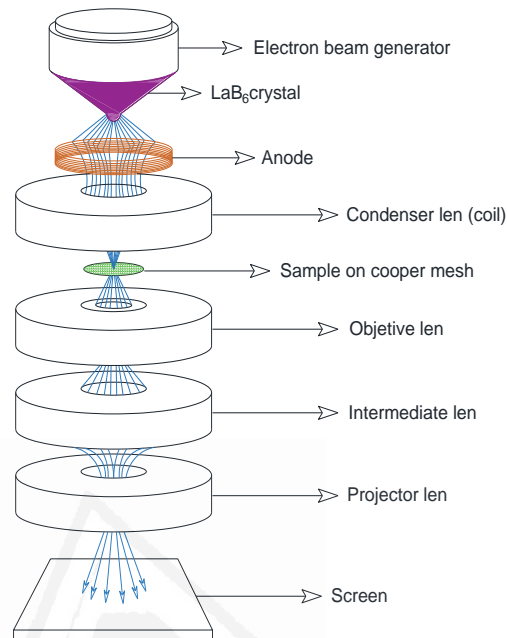


Figure 2.10. Scheme of the structure, organization and working of a conventional TEM.

TEM images were obtained from a transmission electron microscopy JEOL model JEM-2010 of 200 kV. The camera for acquisition of images is from GATAN model ORIUS SC600 and armed in the axis of the microscope in the bottom part and integrated with an acquisition system of images GATAN Digital Micrograph 1.80.70 for GMS 1.8.0.

6.3. Atomic Force Microscopy (AFM)

Atomic Force Microscopy is a technique of the family of scanning probes microscopy, for atomic and nanometer-scale characterization of the morphology and topology of solid surfaces. The operation principle and working set-up of AFM is closely related with the Scanning Tunneling Microscopy (STM), in which a xyz three dimensional positioning system localizes the detector in the specific position of evaluation. AFM detector corresponds to a cantilever with a sharp tip, microfabricated with silicon, silicon oxide or silicon nitride by photolithographic techniques²⁸.

Operation modes for AFM can be divided in two main groups, static and dynamic modes, based on the scanning of the tip or the sample. In contact mode, the sharp-tip drags the sample surface, producing deflections in the cantilever, thus, those deflections produce a mechanical signal in the piezoelectric which is translated in an electrical signal. However, signal in the test can be strongly influenced by the strong attractive forces between the tip and the sample which can pull the tip against the surface, therefore, contact mode is applied specially in surfaces where the overall force is repulsive²⁹.

In contrast, in non-contact mode (or semi-contact mode), especially the tapping-mode (oscillating mode), which was employed in this PhD Thesis, the cantilever is approached and positioned onto the solid surface at a frequency close to the frequency of resonance. During the operation, the system registers the deflection in the cantilever by the forces between the tip and the surface sample, such as Van de Waals forces and dipole-dipole interactions, electrostatic forces, among others. Deflection in the cantilever can be determined employing an interferometer or following the change in a light beam which impacts in the cantilever, as can be observed in Figure 2.11.

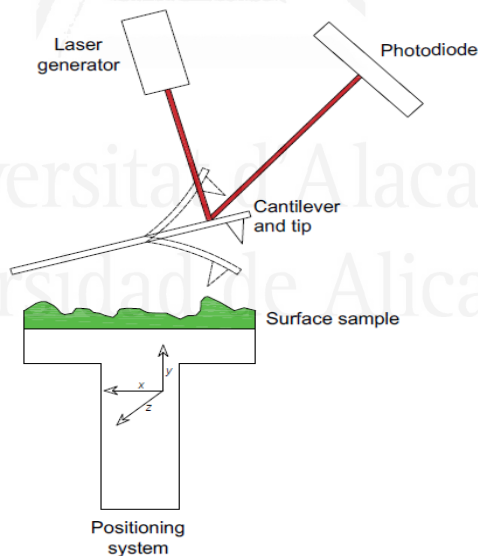


Figure 2.11. Standard set-up of AFM-Tapping mode.

AFM images were obtained from an atomic force microscope NT-MDT model Ntegra, coupled with high resolution Silicon AFM cantilever (NSG01

type), with a resonant frequency close to 150 kHz, was employed in semi-contact mode for the measurements of 10 x 10 μm. Scan rate of the cantilever was 0.5 Hz with a resolution of 256 points in the images.

7. Statistical analysis of data

Considering that part of the materials synthesized in this PhD Thesis are proposed as platforms for further development of bioelectrodes for sensing applications, some important analytical parameters have been determined to guarantee the proper evaluation of the developed materials. In this section, some analytical concepts, based on statistical analysis, are presented.

7.1. Statistical parameters for analysis of data: arithmetic average and standard deviation

The arithmetic average (\bar{x}) is defined as the average of a finite group of data, which is determined by the addition of all the measurements divided by the number of measurements (n) according to Eq. 2.6.

$$\bar{x} = \frac{\sum_{i=1}^n x_i}{n} \quad \text{Eq. 2.6.}$$

In case of determination of the reproducibility and precision between measurements, standard deviation provides in a quantitative way, the concordance between two or more measurements in the same conditions. This parameter can be determined following the Eq. 2.7.

$$S = \sqrt{\frac{\sum_{i=1}^n (x_i - \bar{x})^2}{n-1}} \quad \text{Eq. 2.7.}$$

7.1.1. Measurements methods

Instrumental methods for analytical quantification of species of interest are based on the development of a linear correlation between the signal and the concentration of the species. In this PhD Thesis the following calibration methods have been used.

7.1.1.1. Calibration methods

7.1.1.1.1. External calibration

External calibration is based on the use of standard solutions prepared for a known analyte concentration to obtain the calibration curve. In this technique, the lack of effect of matrix, which might produce a reduction or enhancement of signal by other component present together with the analyte of interest in the sample, allows the preparation of the samples with the analyte completely isolated of other external unknown compounds.

7.1.1.1.2. Unweighted calibration

Calibration curve is the result of the plot of concentration of the interest species in the analyte (x-axis values) and the signal produced (y-axis values). For analytical application, linear calibration curves with the equation: $y = m \cdot x + b$, where m is the slope and b the y-intercept, are required to validate the quantification method, guaranteeing an accurate measurement with low errors. Minimum of Least Squares is employed to determine the slope and intercept (m , b) parameters, applying low variance in the calibration curve points. Eq. 2.8 and 2.9 are employed to calculate the values of slope and intercept, respectively³⁰.

$$m = \frac{\sum_{i=1}^n \{(x_i - \bar{x})(y_i - \bar{y})\}}{\sum_{i=1}^n (x_i - \bar{x})^2} \quad \text{Eq. 2.8.}$$

$$a = \bar{y} - m \cdot \bar{x} \quad \text{Eq. 2.9.}$$

For estimation of the reliability of the linear fitting, the correlation coefficient (r) is determined following the Eq. 2.10:

$$r = \frac{\sum_{i=1}^n \{(x_i - \bar{x})(y_i - \bar{y})\}}{\sqrt{\sum_{i=1}^n (x_i - \bar{x})^2 \cdot \sum_{i=0}^n (y_i - \bar{y})^2}} \quad \text{Eq. 2.10.}$$

7.1.1.2. Standard addition method

During the use of external calibration curve, the presence of different species with the analyte of interest in real samples can generate an interference

in the measured signal and, consequently, an under or over estimation of the concentration of the analyte in the sample. Therefore, to overcome the effect of the matrix present in some cases in real samples, other methods have to be used for an accurate determination³¹. Attempts of this kind of analysis includes modification in the detection system, dilution³², separation/extraction of components³¹ and development of protocols and procedures of calibration, as standard addition method in which different standards with a similar matrix of the real sample or even with the real sample itself, are employed in the determination of the target analyte.

In the standard addition method, linear calibration curve is determined employing same volumes of standards, which are prepared with the real sample (at around 6 different standards), in which a known amount of the analyte is added into the matrix. Signal produced by the standard solutions is measured and correlated with the concentration of analyte in the different samples. Concentration of the real sample is determined by extrapolation of the calibration curve to the intercept with the X axis (when $y = 0$) as can be observed in Figure 2.12. The absolute value of this concentration corresponds with the concentration of the analyte in the real sample evaluated.

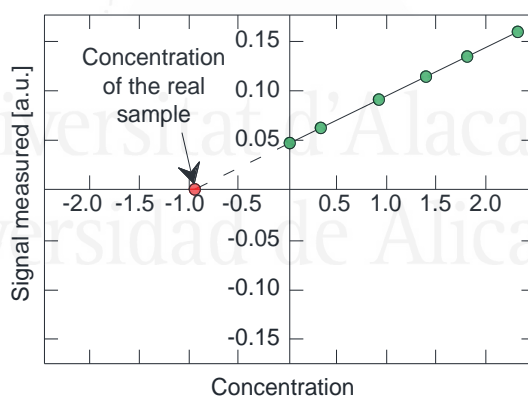


Figure 2.12. Determination of the concentration of a real sample by the standard addition method.

Unfortunately, application of this procedure for quantification of the analyte requires the construction of the calibration curve employing the problem sample, implying in the use of high amount of sample and the construction of a calibration curve for each problem sample. In this PhD

This thesis, standard addition method was employed as a quantification method applied on real samples in urine to take into account the effect of the matrix.

7.1.2. Analytical parameters

7.1.2.1. Sensitivity

Sensitivity can be defined as the ability that a method, equipment or test presents to distinguish minimum significance variation or difference of a specific parameter (current, potential, resistivity, etc.) of the system, with the concentration of the analyte. In this sense, sensitivity can be determined experimentally as the slope of the calibration curve.

7.1.2.2. Limit of detection and quantification

Limit of detection (LOD) has been defined, based on the International Union of Pure and Applied Chemistry (IUPAC), which has adopted the definition given by the International Standardization Organization (document ISO 11843) as “the lowest quantity of a substance that can be distinguished from the absence of that substance (a blank value) within a stated confidence limit”^{33,34}, following:

$$LOD = x_{bi} + ks_{bi} \quad \text{Eq. 2.11.}$$

Where x_{bi} is the mean of the blank measurements, s_{bi} is the standard deviation of the blank measurements, and k is a numerical factor chosen according to the confidence level desired³⁵. Even though, several approaches have been used to determine correctly the detection limit of an analytical method, nowadays, definition of an entirely clear criterion for LOD determination has not been accepted. For example, a normal criterion is defined as the concentration of analyte which produces a signal equal to the blank plus 3 times the standard deviation of the blank, in accordance, with the IUPAC definition. However, the variation can be 2, 4 or 10 times the standard deviation for more conservative LOD. Another alternative for estimation of the LOD commonly accepted is from an experimental method, in which LOD is obtained afterwards successive additions of the diluted analyte to obtain a notable variation in the signal. In the case of limit of quantification (LOQ), it is considered as the lowest concentration in a sample that can be quantified

with an acceptable level of accuracy and precision³⁶. In this sense, LOQ was determined experimentally as described in Eq. 2.12.

$$LOQ = 3.3LOD \quad \text{Eq. 2.12.}$$

7.1.2.3. Dynamic range, Linear range and working range

Dynamic range is defined as the interval of concentration in which the signal varies (increasing or decreasing) with the concentration of the analyte, associated with the calibration curve of the method of quantification. Nevertheless, dynamic range may present a non-constant signal variation with the concentration, making difficult to fix an accurate range; therefore, an instrumental range in which change in the signal presents a steady behavior is required for analytical purposes. In this sense, determination of a steady region in the dynamic range, where the change of signal and concentration presents a linear correlation, called linear dynamic range (linear range), is the most employed for quantification of species in an analytical method.

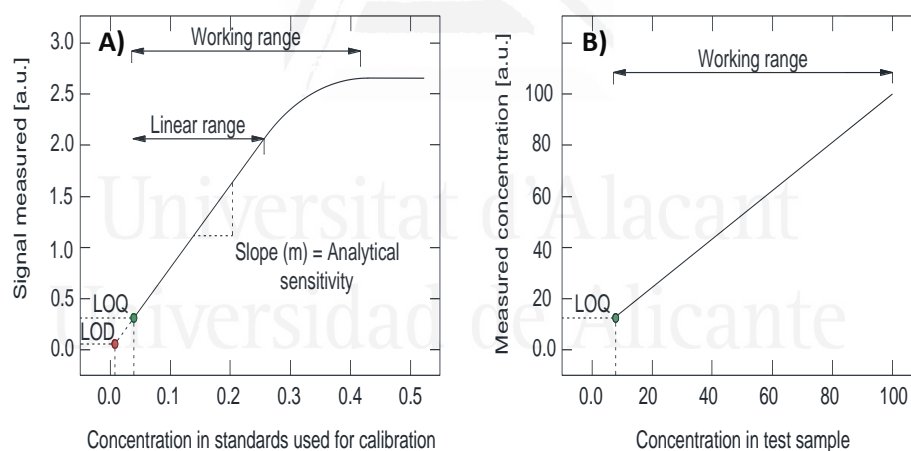


Figure 2.13. A) Typical example of response curve obtained in a detection method and B) Comparison curve obtained with a measurement procedure where the test sample was determined and plotted against the real concentration of the sample.

On the other hand, working range is defined as the concentration interval over which the method provides results with an acceptable uncertainty. The lower end of the working range is bounded by the limit of quantification LOQ.

The upper end of the working range is defined by concentrations at which significant anomalies in the analytical sensitivity are observed. Limits of the linear range, conventionally, are fixed between the LOQ, as lower limit, and the upper value of the linear dynamic range where anomalies of the sensitivity are observed^{37,38}.

8. References

- (1) Marcano, D. C.; Kosynkin, D. V.; Berlin, J. M.; Sinitskii, A.; Sun, Z.; Slesarev, A.; Alemany, L. B.; Lu, W.; Tour, J. M. Improved Synthesis of Graphene Oxide. *ACS Nano* **2010**, *4* (8), 4806–4814.
- (2) Ferrándiz-Saperas, M.; Ghisolfi, A.; Cazorla-Amorós, D.; Nájera, C.; Sansano, J. M. Multilayer Graphene Functionalized through Thermal 1,3-Dipolar Cycloadditions with Imino Esters: A Versatile Platform for Supported Ligands in Catalysis. *Chem. Commun.* **2019**, *55* (52), 7462–7465.
- (3) Pinyou, P.; Ruff, A.; Pöller, S.; Ma, S.; Ludwig, R.; Schuhmann, W. Design of an Os Complex-Modified Hydrogel with Optimized Redox Potential for Biosensors and Biofuel Cells. *Chem. – A Eur. J.* **2016**, *22* (15), 5319–5326.
- (4) Bard, A.; Faulkner, L. *Electrochemical Methods: Fundamental and Applications*, 2nd ed.; Harris, D., Swain, E., Aiello, E., Eds.; John Wiley & Sons, Ltd: Austin, **2000**.
- (5) Pingarrón Carrazón, J. M.; Sánchez Batanero, P. *Química Electroanalítica-Fundamentos y Aplicaciones; Síntesis S.A, Madrid, España, 2003*.
- (6) Bansod, B.; Kumar, T.; Thakur, R.; Rana, S.; Singh, I. A Review on Various Electrochemical Techniques for Heavy Metal Ions Detection with Different Sensing Platforms. *Biosens. Bioelectron.* **2017**, *94*, 443–455.
- (7) Wang, J. *Analytical Electrochemistry*, 2nd ed.; Wiley-VCH, **2006**.
- (8) Boehm, H. P. *Some Aspects of the Surface Chemistry of Carbon*

Blacks and Other Carbons. *Carbon* **1994**, *32* (5), 759–769.

- (9) Figueiredo, J. L.; Pereira, M. F. R.; Freitas, M. M. A.; Órfão, J. J. M. Modification of the Surface Chemistry of Activated Carbons. *Carbon* **1999**, *37* (9), 1379–1389.
- (10) Otake, Y.; Jenkins, R. G. Characterization of Oxygen-Containing Surface Complexes Created on a Microporous Carbon by Air and Nitric Acid Treatment. *Carbon* **1993**, *31* (1), 109–121.
- (11) Calo, J. M.; Cazorla-Amorós, D.; Linares-Solano, A.; Román-Martínez, M. C.; De Lecea, C. S.-M. The Effects of Hydrogen on Thermal Desorption of Oxygen Surface Complexes. *Carbon* **1997**, *35* (4), 543–554.
- (12) Román-Martínez, M. C.; Cazorla-Amorós, D.; Linares-Solano, A.; de Lecea, C. S.-M. Tpd and TPR Characterization of Carbonaceous Supports and Pt/C Catalysts. *Carbon* **1993**, *31* (6), 895–902.
- (13) Rackley, S. A. Adsorption capture systems. In: Racklet, S. A., editor, *Carbon Capture and Storage*, second edition, Butterworth-Heinemann, Boston, **2017**, pp. 151–185.
- (14) Donohue, M. D.; Aranovich, G. L. Classification of Gibbs Adsorption Isotherms. *Adv. Colloid Interface Sci.* **1998**, *76–77*, 137–152.
- (15) Brunauer, S.; Emmett, P. H.; Teller, E. Adsorption of Gases in Multimolecular Layers. *J. Am. Chem. Soc.* **1938**, *60* (2), 309–319.
- (16) Tougaard, S. Surface Nanostructure Determination by X-ray Photoemission Spectroscopy Peak Shape Analysis. *J. Vac. Sci. Technol. A* **1996**, *14* (3), 1415–1423.
- (17) Mello-Castanho, S. R. Espectroscopia Fotoelectrónica de Rayos-X. *Sociedad Española de Cerámica y Vidrio*, **1997**.
- (18) Cordero-Lanzac, T.; Rosas, J. M.; García-Mateos, F. J.; Ternero-Hidalgo, J. J.; Palomo, J.; Rodríguez-Mirasol, J.; Cordero, T. Role of

Different Nitrogen Functionalities on the Electrochemical Performance of Activated Carbons. *Carbon* **2018**, *126*, 65–76.

- (19) Quílez-Bermejo, J.; Morallón, E.; Cazorla-Amorós, D. Oxygen-Reduction Catalysis of N-Doped Carbons Prepared via Heat Treatment of Polyaniline at over 1100 °C. *Chem. Commun.* **2018**, *54* (35), 4441–4444.
- (20) Larkin, P. *Infrared and Raman Spectroscopy: Principles and Spectral Interpretation*, 2nd ed.; Elsevier: Stamford, **2018**.
- (21) Novaes, C. G.; Bezerra, M. A.; da Silva, E. G. P.; Santos, A. M. P. dos; Romão, I. L. da S.; Santos Neto, J. H. A Review of Multivariate Designs Applied to the Optimization of Methods Based on Inductively Coupled Plasma Optical Emission Spectrometry (ICP OES). *Microchem. J.* **2016**, *128*, 331–346.
- (22) Skoog, D.; Holler, J.; Neiman, T.; Holler, J. *Principios de Análisis Instrumental*, 6th ed.; González, S. C., Ed.; Mc Graw-Hill S.A., **2000**.
- (23) Montaser, A. *Inductively Coupled Plasma Mass Spectrometry*; Montaser, A., Ed.; Wiley-VCH: Washington, **1998**.
- (24) Kulkarni, V. S., Shaw, C. *Microscopy Techniques*. In: Kulkarni, V. S., Shaw, C., editors, *Essential Chemistry for Formulators of Semisolid and Liquid Dosages*, Academic Press, Boston, **2016**, pp. 183–192.
- (25) Pérez-Arantegui, J., Mulvey, P. *Microscopy techniques-Electron Microscopy*, in: P. Worsfold, A. Townshend, C.B.T.-E. of A.S. (Second E. Poole (Eds.)), Elsevier, Oxford, **2005**, pp. 114–124.
- (26) Kunitake, M., Watanabe, S. Ohira, A. *Scanning Probe Microscopy Techniques for Modern Nanomaterials*. In: Imae, T., editor, *Nanolayer Research-Methodology and Technology for Green Chemistry*, Elsevier, Amsterdam, **2017**, pp. 77–114.
- (27) Williams, D.; Carter, B. *Transmission Electron Microscopy-Part 1*, 2nd ed., Springer, Ed.; Springer: Boston, **2009**.

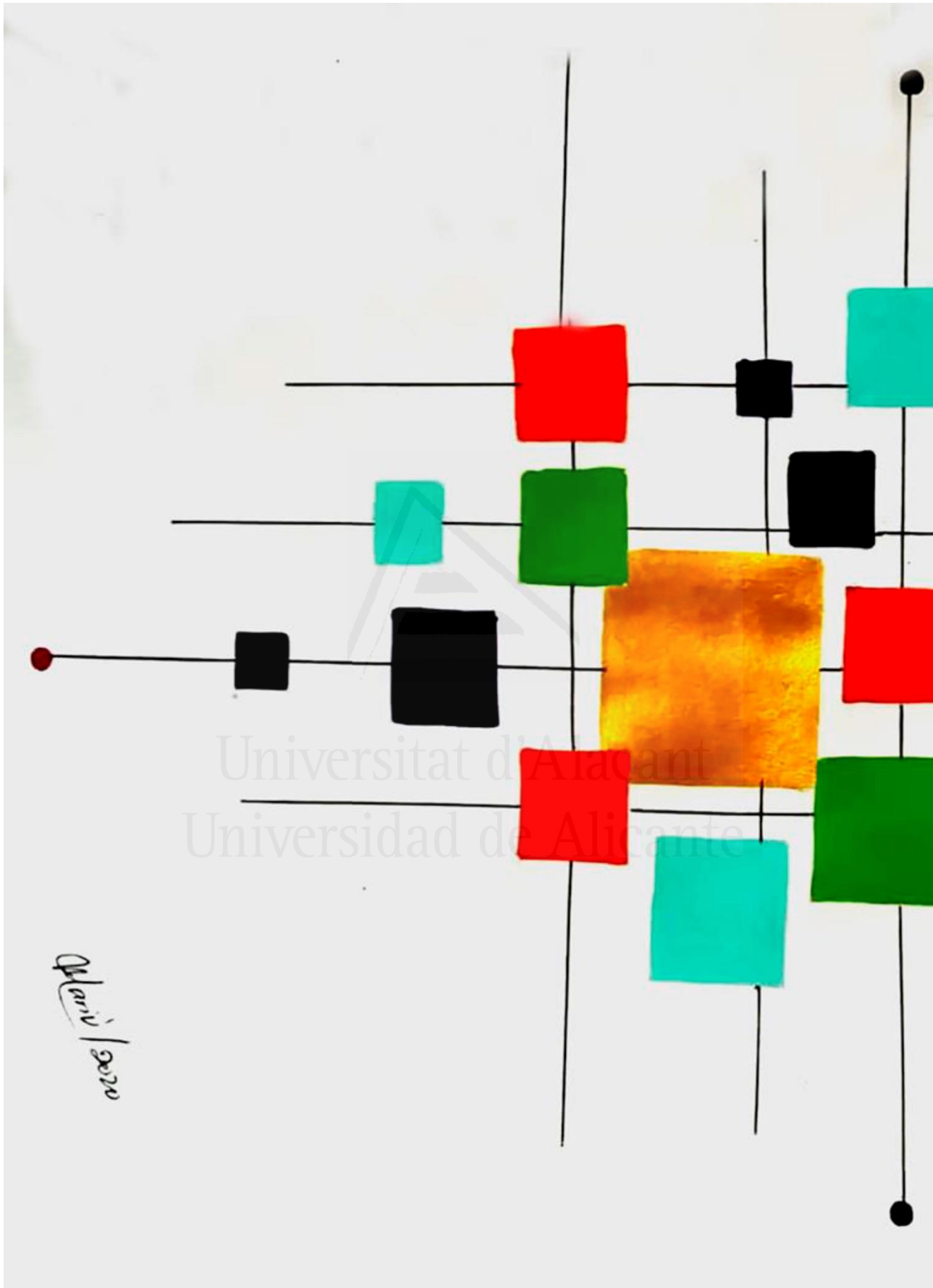
- (28) Haugstad, G. Atomic Force Microscopy: Understanding Basic Modes and Advanced Applications, 1st ed., John Wiley & Sons, Inc., **2012**.
- (29) Magonov, S.; Whangbo, M.-H. Surface Analysis with STM and AFM: Experimental and Theoretical Aspects of Image Analysis, 1st ed., Wiley-VCH, **1995**.
- (30) Miller, J. N. Basic Statistical Methods for Analytical Chemistry. Part 2. Calibration and Regression Methods. A Review. *Analyst* **1991**, *116* (1), 3–14.
- (31) Hajšlová, J.; Zrostlíková, J. Matrix Effects in (Ultra)Trace Analysis of Pesticide Residues in Food and Biotic Matrices. *J. Chromatogr. A* **2003**, *1000* (1), 181–197.
- (32) Ferrer, C.; Lozano, A.; Agüera, A.; Girón, A. J.; Fernández-Alba, A. R. Overcoming Matrix Effects Using the Dilution Approach in Multiresidue Methods for Fruits and Vegetables. *J. Chromatogr. A* **2011**, *1218* (42), 7634–7639.
- (33) Allegrini, F.; Olivieri, A. C. IUPAC-Consistent Approach to the Limit of Detection in Partial Least-Squares Calibration. *Anal. Chem.* **2014**, *86* (15), 7858–7866.
- (34) Amatore, C.; Da Mota, N.; Sella, C.; Thouin, L. General Concept of High-Performance Amperometric Detector for Microfluidic (Bio)Analytical Chips. *Anal. Chem.* **2008**, *80* (13), 4976–4985.
- (35) McNaught, A. D.; Wilkinson, A. *Compendium of Chemical Terminology-IUPAC*, 2nd ed., McNaught, A. D., Wilkinson, A., Eds., Blackwell Scientific Publications, Oxford, **2019**.
- (36) Şengül, Ü. Comparing Determination Methods of Detection and Quantification Limits for Aflatoxin Analysis in Hazelnut. *J. Food Drug Anal.* **2016**, *24* (1), 56–62.
- (37) Loconto, P. Trace Environmental Quantitative Analysis: Principles, Techniques and Applications, 2nd ed., Francis, T. & Ed.; CRC Press,

Boca Raton, **2005**.

- (38) Vallée-Bélisle, A.; Ricci, F.; Plaxco, K. W. Engineering Biosensors with Extended, Narrowed, or Arbitrarily Edited Dynamic Range. *J. Am. Chem. Soc.* **2012**, *134* (6), 2876–2879.



Universitat d'Alacant
Universidad de Alicante

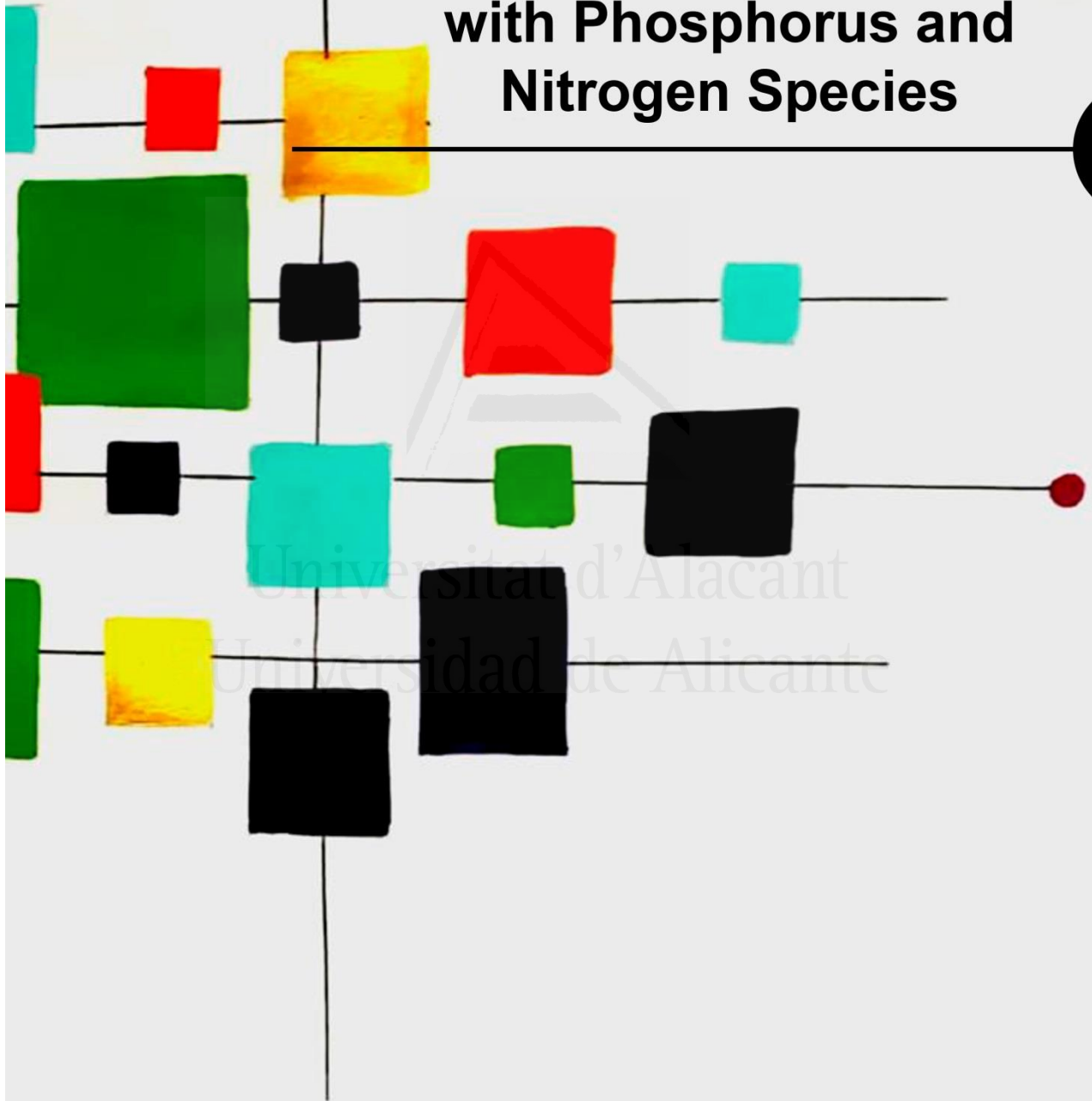


Universitat d'Alicant
Universidad de Alicante

Artur / 2020

Chapter 3

Electrochemical Functionalization of Single- Wall Carbon Nanotubes with Phosphorus and Nitrogen Species



Universitat d'Alacant
Universidad de Alicante

1. Introduction

Since their discovery, nanocarbon materials, such as carbon nanotubes (CNTs), have attracted the attention of researchers due to their outstanding mechanical, optical, chemical and electronic properties. However, these intrinsic properties are not usually obtained due to the difficulty in preparing high purity CNT with the desired structure, and their tendency to bundling¹. This last aspect results in an important limitation from an application point of view since it impedes their effective dispersion in a solvent and their processability. Thus, one important aspect to facilitate further potential applications of CNTs lies in the proper surface modification to overcome the high van der Waals interactions between tubes, allowing their effective dispersion and proper processability^{2,3}. There are different methodologies for CNT functionalization, which can be classified as covalent and non-covalent functionalization techniques³⁻⁸. An interesting approach for surface modification of CNTs involves the integration of the CNTs with other functional components, which synergistically offers novel materials with potential applicability^{4,8-10}.

In terms of functionalization, SWCNT present high sensitivity to the experimental conditions of functionalization, which may generate important changes in the pristine material, producing the modification of their intrinsic properties, for instance electrical conductivity and mechanical properties¹¹⁻¹³. Therefore, mild surface-modification procedures that do not produce significant alterations in the SWCNT structure, are necessary for the design of new functional materials based on carbon nanotubes¹⁴.

Some examples of non-covalent functionalization of SWCNT are based on the adsorption and wrapping of the SWCNT surface, through electrostatic interactions, π - π stacking, hydrophobic forces or hydrogen bonds, with different types of conjugated polymers^{13,15}, metal nanoparticles¹⁶, porphyrins, etc.¹⁷⁻¹⁹.

Although, non-covalent functionalization of SWCNT does not produce significant damage in the carbon nanotube structure, the weak interaction between the functional molecule and the CNTs may not offer high stability, producing leaching and loss of the properties achieved after the functionalization⁹. In this context, incorporation of functional groups through

covalent bonds in the CNTs side-wall or tips, results in functionalities on CNTs with higher stability^{20,21}. Covalent functionalization can be carried out employing oxidative conditions, generating different surface oxygen groups, what is very useful for CNTs processing^{12,22,23}. Furthermore, other kind of functionalization based on different reactions such as fluorination, hydrogenation, esterification, alkylation, etc., has been employed in CNT covalent functionalization^{12,24,25}. Unfortunately, most of the covalent functionalization procedures induce defects, which severely deteriorate the SWCNT structure and properties^{8,26}. Therefore, development of non-damaging functionalization procedures of SWCNT, which may preserve as much as possible the properties of the pristine material, is an important challenge.

In the last decades, generation of highly reactive radicals under oxidative or reductive conditions by electrochemical methods (i.e., so-called electrografting methods), to anchor different functional molecules, such as diazonium salts, aliphatic and aromatic compounds, has emerged as a powerful methodology for covalent functionalization in different surfaces such as metals, oxides and carbon materials^{8,27-29}.

In previous studies done in our research group, MWCNTs and zeolite templated carbon (ZTC) were submitted to mild oxidative conditions in presence of different amino-containing compounds producing functionalization with different redox processes^{30,31}. However, modifier agent (4-aminobenzyl phosphonic acid) is not directly bonded to the aromatic ring of the carbon material structure, as consequence of its low reactivity, did not produce a significant incorporation of phosphorus in the carbon nanotube. In this work, we carried out a systematic study of the effect of the oxidation potential, using 4-aminophenyl phosphonic acid (4-APPA) applying cyclic voltammetry for the functionalization of SWCNT, in order to achieve the co-doping of the SWCNT with N and P surface species, but avoiding important damage of the SWCNT. Interestingly, the degree of electrochemical modification of SWCNT surface can be easily controlled by selecting the electrochemical conditions.

2. Experimental

2.1. Materials

Single-Wall Carbon nanotubes (SWCNT) with purity 99% (1-4 nm of diameter) with 3-30 μm length were purchased to Cheap Tubes Inc. (Cambridgeport, USA). Specific surface area, obtained by the Brunauer, Emmett and Teller (BET) method, is $587\text{ m}^2\text{ g}^{-1}$ and the total amount of surface oxygen was determined by temperature programmed desorption, is $277\text{ }\mu\text{mol g}^{-1}$.³²

N, N-Dimethylformamide (DMF), extra pure, was provided by Scharlau and used as solvent to disperse the SWCNT. Sulphuric acid (98%) analytical reagent to prepare the electrolyte, was obtained from VWR Chemicals. 4-amino phenyl phosphonic acid (4-APPA, +98%), used as modifier agent, was purchased from Tokyo Chemical Industry co (TCI). Potassium dihydrogen phosphate (KH_2PO_4) and dipotassium hydrogen phosphate trihydrate ($\text{K}_2\text{HPO}_4\cdot 3\text{H}_2\text{O}$) for preparation of 0.1 M PBS (pH=7.2) were obtained from Merck and VMR Chemicals, respectively. Potassium Hydroxide (KOH, 85%) was purchased from VWR Chemicals. All the solutions were prepared using ultrapure water (18 MOhms cm, Purelab Ultra Elga equipment). The gases N_2 (99.999%) and H_2 (99.999%) were provided by Air Liquide.

2.2. Surface functionalization with phosphorus and nitrogen species on SWCNT

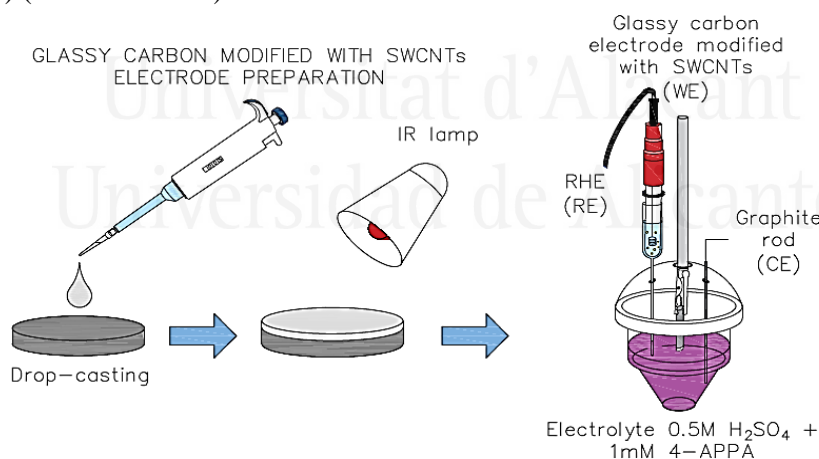
2.2.1. pH for the point of zero-charge (pH_{PZC})

The determination of the pH_{PZC} has been done using the method described in the literature³³. Different amounts of SWCNT (0.05, 0.1, 0.5, 1, 5 and 10 %w/w) were put in contact with ultrapure water. Samples were sonicated for 10 minutes and subsequently, immersed in a thermostatic bath at 25°C and under stirring for 24 hours (equilibrium time). After this time, the samples were filtered and the pH of the solution obtained was measured. The pH_{PZC} for the SWCNT was 6.3.

2.2.2. Electrochemical modification with 4-amino phenyl phosphonic acid (4-APPA)

The working electrode for electrochemical modification was prepared using glassy carbon (GC) as support, modified with the SWCNT. 1 mg of SWCNT was dispersed in DMF employing an ultrasonic cold-bath for 45 minutes, achieving a dispersion of 1 mg mL^{-1} SWCNTs. Prior to the deposition of SWCNT, GC surface (3 mm diameter) was sanded with emery paper and polished using 1 and $0.05 \text{ }\mu\text{m}$ alumina slurries, then rinsed with ultrapure water. Afterwards, $5 \text{ }\mu\text{L}$ aliquot of the dispersion was dropped onto the electrode surface and dried under an infrared lamp to remove the solvent. This procedure was repeated twice until completing $10 \text{ }\mu\text{L}$ of the SWCNT suspension on the surface.

Electrochemical modification of SWCNT was performed using an Autolab PGSTAT 302 (Metrohm Netherlands) potentiostat, with a standard three-electrode cell configuration, in which the glassy carbon electrode modified with SWCNT was the working electrode (WE), a graphite rod was used as counter electrode (CE) and a reversible hydrogen electrode (RHE) introduced in the same electrolyte but without 4-APPA, was used as reference electrode (RE) (see Scheme 3.1).



Scheme 3.1. Experimental procedure for the electrochemical functionalization of SWCNT with 4-APPA.

Electrochemical modification was carried out by cyclic voltammetry in aqueous solution $0.5 \text{ M H}_2\text{SO}_4 + 1 \text{ mM APPA}$ in a deoxygenated cell by

bubbling nitrogen. Modification of carbon material was achieved submitting the sample to 10 cycles at 10 mV s^{-1} , in different potential windows, increasing the positive potential. After electrochemical treatment, electrodes were washed with excess of water, removing the remaining electrolyte.

2.2.3. *Electrochemical characterization*

Electrochemical behavior of the SWCNT modified with 4-APPA was evaluated by cyclic voltammetry in different electrolytes (acid, neutral and alkaline electrolytes), employing a three electrode cell configuration, where, glassy carbon modified with SWCNT functionalized with 4-APPA, was the working electrode (WE), a graphite rod was the counter electrode (CE) and a reversible hydrogen electrode (RHE) introduced in the same electrolyte, was the reference electrode (RE). Potential range was fixed between 0 and 1 V at 50 mV s^{-1} .

2.3. *Physicochemical characterization*

X-Ray photoelectron spectroscopy (XPS) was performed in a VG-Microtech Mutilab 3000 spectrometer using an Al K α radiation (1253.6 eV). The deconvolution of the XPS peaks for C1s, O2p, P2p and N1s was done by least squares fitting using Gaussian-Lorentzian curves, while a Shirley line was used for the background determination. The P2p spectra have been analyzed considering the spin-orbit splitting into P2p $_{3/2}$ and P2p $_{1/2}$ with a 2:1 peak area ratio and an energy separation of 0.87 eV.

Transmission electron microscopic measurements (TEM) were carried out using JEOL TEM, JEM-2010 model, INCA Energy TEM 100 model, and GATAN acquisition camera.

Raman spectra were collected with a Jasco NRS-5100 spectrometer with a focal distance of 300 mm. A solid-state laser (532 nm) with 3.9 mW was used. The spectra were acquired for 120 s. The Raman set-up was coupled to a microscope with an objective of 20 magnifications (MPLFLN 20x). Previous to the analysis, calibration of the spectrometer was performed with a Si slice ($521 \pm 2 \text{ cm}^{-1}$), checking the shifting in the line at 520 cm^{-1} and correcting the base line to eliminate the effect of the fluorescence.

3. Results and discussion

3.1. Electrochemical functionalization of SWCNT in acid medium with phosphorus and nitrogen species

3.1.1. Electrochemical oxidation of SWCNT in acid medium in presence of 4-APPA

In order to establish the most adequate conditions for electrochemical functionalization of SWCNT surfaces with phosphorus and nitrogen species employing 4-APPA, the upper potential limit was stepwise opened from 0.8 to 1.8 V, as can be observed in Figure 3.1-A.

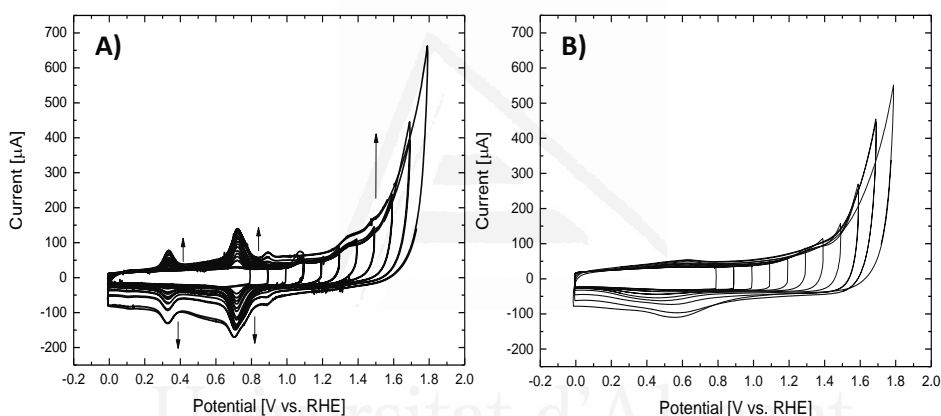


Figure 3.1. Cyclic voltammograms during the first cycle of the open stepwise potential window for: A) SWCNT in 0.5 M H_2SO_4 + 1 mM 4-APPA and B) SWCNT in 0.5 M H_2SO_4 at 50 mV s^{-1} .

In presence of 4-APPA in the electrolyte, a highly reversible process appears in the voltammograms at 0.68 V, when the upper potential limit reaches values of 0.8 V. The intensity of this redox process increases with the number of cycles, as can be observed in Figure 3.1-A. Moreover, when the positive potential increases, irreversible anodic waves at around 1.1 V and 1.4 V appear, that can be associated with the oxidation of 4-APPA, together with an increase in current at higher potentials similar to what is observed in the voltammogram of the SWCNT in absence of 4-APPA (Figure 3.1-B). However, the current is higher in presence of 4-APPA. Additionally, the increase in the double-layer capacitance and the development of an additional

redox process at 0.31 V are also observed. This redox process increases with the number of cycles.

Considering the previous electrochemical stepwise potential study in SWCNT, different upper potential limits were chosen. Surface functionalization of SWCNT has been studied using different electrode samples at each potential. Figure 3.2 shows the voltammograms obtained for the different positive potentials studied in absence and in presence of 4-APPA in the electrolyte. For all the potentials evaluated, the voltammograms for the SWCNT modified electrodes in 0.5 M H₂SO₄ in absence of 4-APPA (black line in Figure 3.2), present the development of a broad redox process at around 0.5 V that corresponds to the formation of oxygen functionalities³⁴, as consequence of the electrooxidation of SWCNT. This redox process increases with the positive potential limit as well as its irreversibility (Figure 3.2-E).

Once the 4-APPA is incorporated in the electrolyte (red lines in cyclic voltammograms in Figure 3.2), an over-oxidation current at higher potential is observed for all the upper potentials studied, related with the contribution of 4-APPA to the oxidation current. Figure 3.2-A shows the voltammograms when the upper potential limit is 1.0 V. It is clear the appearance of a reversible redox process at 0.71 V (peak C) that increases with the number of cycles. When the upper potential limit is 1.2 V, an irreversible oxidation peak at 1.1 V (See Figure 3.2-B) is clearly observed during the first cycle that decreases with the number of cycles. Moreover, the current of the first redox process at 0.71 V increases with the number of cycles, in comparison with Figure 3.2-A. At the same time, other redox processes at 0.33 V (peak B) and 0.53 V (peak D) are also observed. Further polarization above 1.2 V (Figure 3.2-C and 3.2-D), produces the increase in the current of these redox processes and their relative current depends on the potential. The appearance of these processes can be related with the formation of electroactive species, such as oxidative radicals, dimers or oligomers on the SWCNT surface.

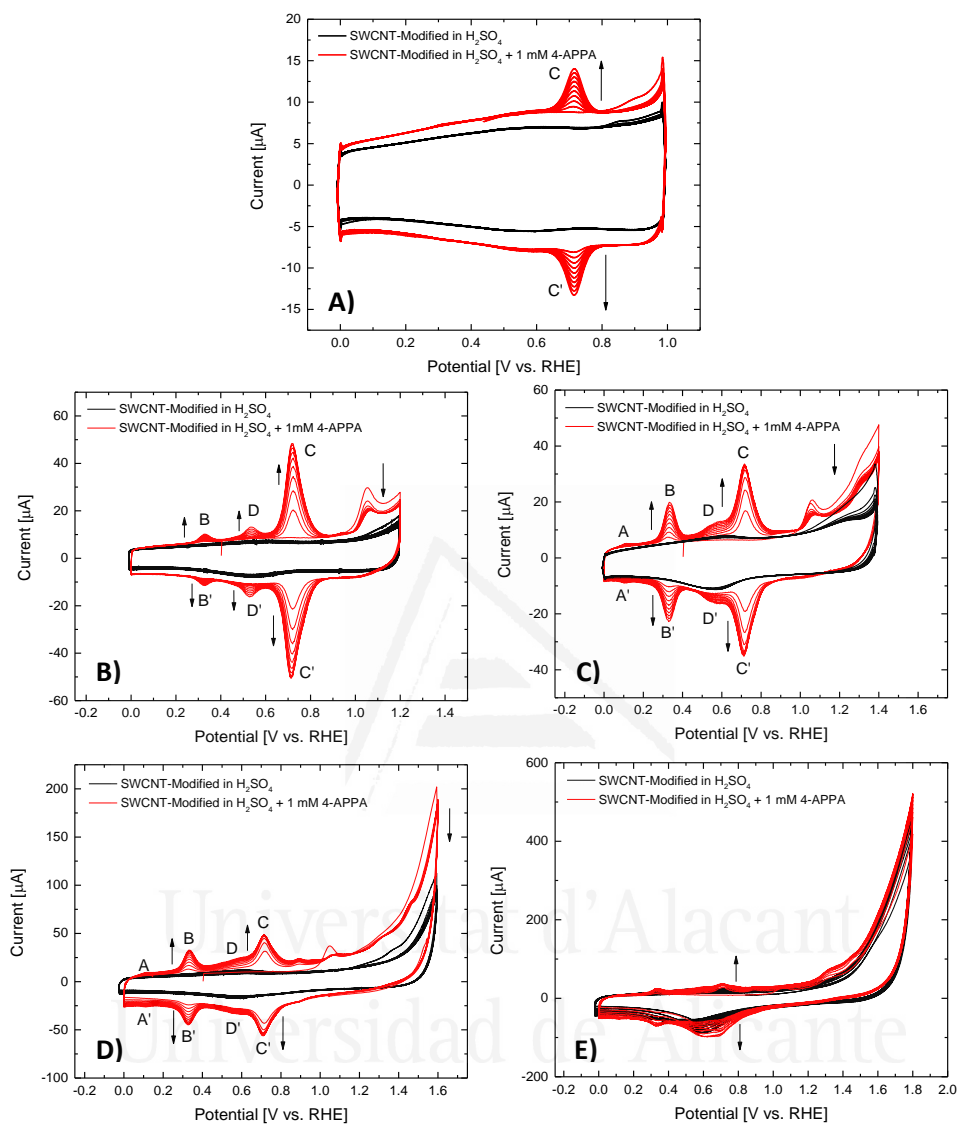


Figure 3.2. Cyclic voltammograms obtained during 10 cycles for a SWCNT electrode in 0.5 M H_2SO_4 (Black lines) and 0.5 M H_2SO_4 + 1 mM 4-APPA (Red lines) at 10 mV s^{-1} under N_2 atmosphere at different positive potential limits: A) 1.0 V, B) 1.2 V, C) 1.4 V, D) 1.6 V and E) 1.8 V.

3.1.2. Electrochemical characterization of SWCNT functionalized with P and N

Evidence of the functionalization with P and N species in the SWCNT was verified by cyclic voltammetry in acid media without presence of the 4-APPA

in the solution. Figure 3.3 shows the voltammograms of the functionalized SWCNTs prepared at different potentials as explained in the previous section (See Figure 3.2). The voltammograms of the SWCNT submitted to the same polarization conditions in absence of 4-APPA are also presented for comparison purposes (Black lines).

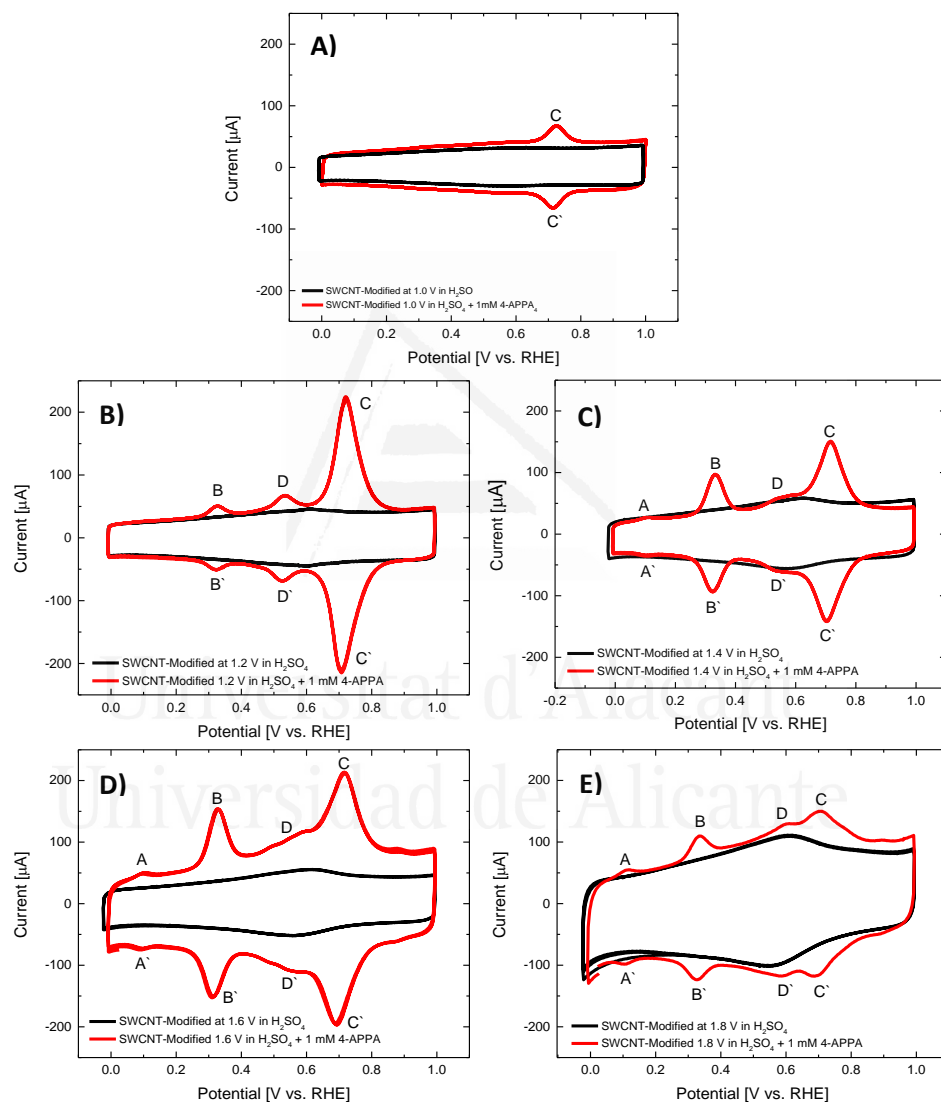


Figure 3.3. Steady state voltammograms for the modified SWCNTs in absence (black line) and presence (red line) of 4-APPA at different potential: A) 1.0 V, B) 1.2 V, C) 1.4 V, D) 1.6 V and E) 1.8 V in 0.5 M H₂SO₄, $v_{scan}=50 \text{ mV s}^{-1}$, under N₂ atmosphere.

After the electrochemical modification process, the electrode was removed from the 4-APPA containing solution, washed with ultrapure water and introduced in a 0.5 M H₂SO₄ solution in absence of 4-APPA to carry out the experiments in Figure 3.3. In terms of the different electrochemical processes observed in acidic conditions in the SWCNT after modification, all the oxidation/reduction processes induced in the CNTs present high stability with cycling between 0 and 1 V, suggesting a good anchoring of the electroactive species on the CNT surface. Moreover, the modified SWCNTs show an outstanding increase in the current density, corresponding to an increase in the stored-charge, which is proportional to the increase of the upper potential limit until 1.6 V. The values of stored-charge measured after modification at potentials higher than 1.2 V, is above 200 % of the initial value of the pristine SWCNT (Table 3.1).



Universitat d'Alacant
Universidad de Alicante

Table 3.1. Electrochemical parameters for the different electrochemical processes in SWCNT modified with 4-APPA at different potentials. All the values were determined for the cyclic voltammograms at $v_{\text{scan}}=50 \text{ mV s}^{-1}$.

| Upper potential limit [V vs. RHE] | Total stored-charge [μC]* | | | ΔE^A [mV] | ΔE^B [mV] | ΔE^C [mV] | ΔE^D [mV] | $I^{\text{ox}}/I^{\text{red}}_A$ | $I^{\text{ox}}/I^{\text{red}}_B$ | $I^{\text{ox}}/I^{\text{red}}_C$ | $I^{\text{ox}}/I^{\text{red}}_D$ |
|--------------------------------------|---|------|----------|----------------------|----------------------|----------------------|----------------------|----------------------------------|----------------------------------|----------------------------------|----------------------------------|
| | Acid | PBS | Alkaline | | | | | | | | |
| | Pristine | 612 | 427 | | | | | | | | |
| 1.0 | 736 | 600 | 660 | -- | 3 | 10 | -- | -- | 0.95 | 1 | -- |
| 1.2 | 1136 | 570 | 530 | -- | 3 | 14 | 7 | -- | 0.99 | 1 | 0.99 |
| 1.4 | 1076 | 1260 | 1030 | 1 | 8 | 14 | 10 | 0.79 | 1 | 1 | 0.97 |
| 1.6 | 1869 | 1260 | 1130 | 10 | 15 | 23 | 18 | 0.70 | 1 | 1 | 1 |
| 1.8 | 1849 | 1510 | 1490 | 15 | 9 | 21 | 11 | 0.56 | 0.88 | 1 | 1 |

*Stored-charge was determined in 0.5 M H_2SO_4 , 0.1M PBS (pH=7.2) and 0.1 M KOH.

Universidad de Alicante

The electrochemical study with the scan rate of the modified SWCNT electrodes can be observed in Figure 3.4 in acid media. In all cases, linear-dependence behavior of the oxidation and reduction currents with the scan rate is observed for all the redox processes formed during the functionalization (See Figure 3.5), indicating that all of them are processes related with species confined on surface³⁵.

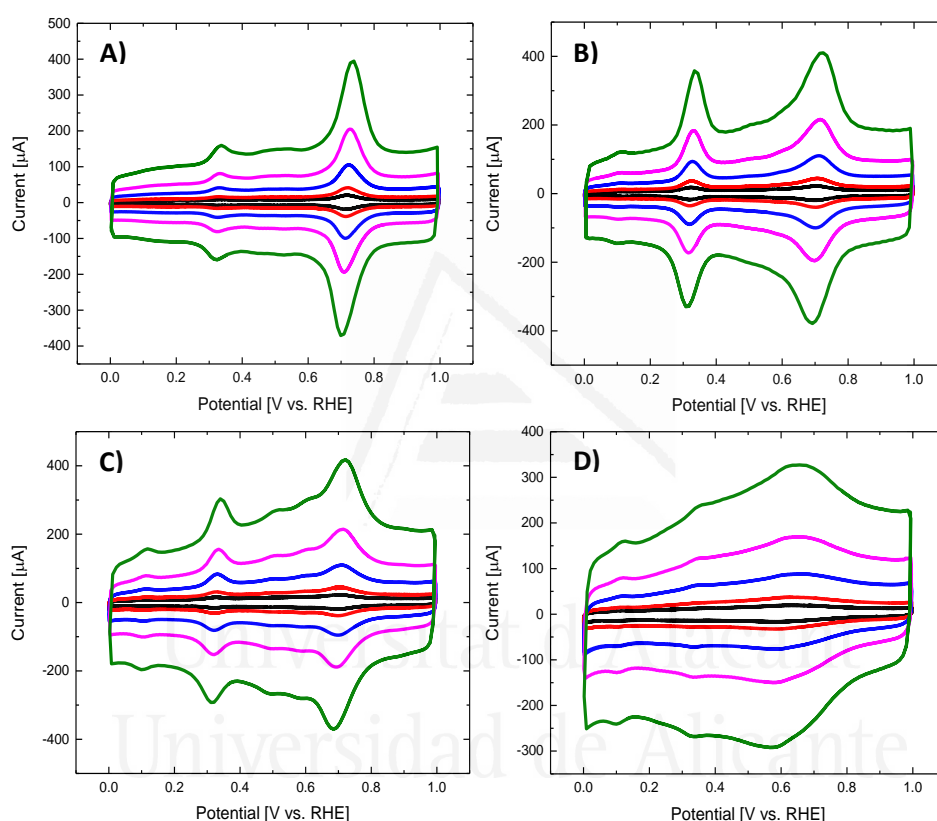


Figure 3.4. Cyclic voltammetry of SWCNT electrochemical modified with 4-APPA at different potential: A) 1.2 V, B) 1.4 V, C) 1.6 V and D) 1.8 V in 0.5 M H₂SO₄ at different v_{scan} (black-10 mV s⁻¹, red-20 mV s⁻¹, blue-50 mV s⁻¹, pink-100 mV s⁻¹ and green 200 mV s⁻¹) under N₂ atmosphere.

Values of peak potential separation for all the redox processes are lower than 25 mV and current ratio I_{ox}/I_{red} are close to one for processes B, C and D, suggesting that the electroactive functionalities incorporated onto the SWCNT present a highly reversible behavior (See Table 3.1). When the oxidation potential is 1.8 V, a decrease in the redox processes is clearly observed in the

voltammogram (Figure 3.3-E), which can be a consequence of an over oxidation that can produce oxidative degradation of the species present on the surface.

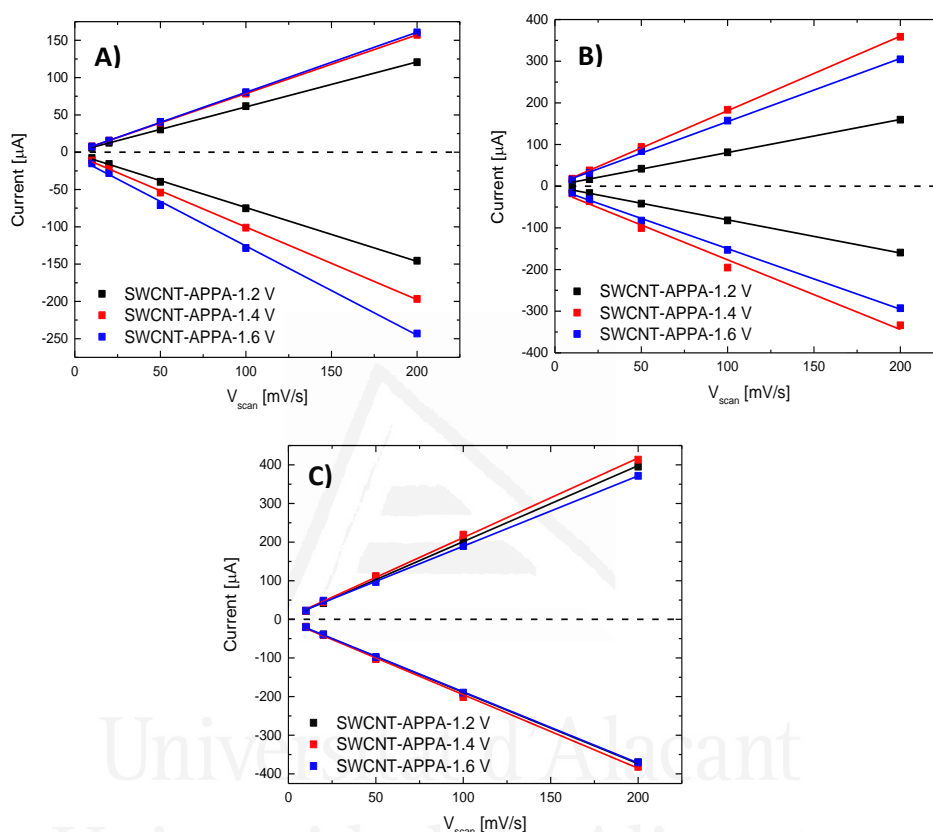


Figure 3.5. Plot of cathodic and anodic peak currents vs. v_{scan} for SWCNTs electrochemical modified at different potential with 4-APPA in 0.5 M H_2SO_4 : A) Process A, B) Process B and C) Process C.

The obtained results could be explained considering aniline-based compounds polymerization although covalent bonding with the SWCNT cannot be discarded. It is well-known that aniline-based compounds oxidize with the formation of radicals that can react giving polyaniline-type products^{36–38}. The redox processes observed with a high reversibility are in agreement with the formation of polyaniline-based oligomers. In polyaniline, redox processes, related with the change of the oxidation states from leucoemeraldine to emeraldine and emeraldine to pernigraniline in the polymer

chain, appear at around 0.3 and 0.7 V vs. RHE in acid conditions, respectively^{39,40}. However, the high reversibility and symmetry of the redox processes suggest that covalently bound redox species may also exist. In fact, another possibility that has to be considered is that the amine radical could also react with the SWCNT, promoting the formation of N-C bonds and producing a covalent attachment of the 4-APPA molecule on the carbon nanotubes surface. Polymerization could further proceed through these covalently bonded species. However, electroactivity for the 4-APPA molecule covalently attached to the SWCNT surface, if it occurs, should not result in well-defined redox processes as observed in Figure 3.3 due to the expected energy heterogeneity arisen from the different sites of the SWCNT where the attachment may occur (i.e., the tip or the wall of the CNT). Nevertheless, these interesting redox processes should be subject of further research, although it cannot be discarded that the strong interaction between the polymer and the SWCNT may be the responsible for the high reversibility observed due to an enhanced electron transfer.

The first step in the polymerization of 4-APPA is the adsorption of the monomer on the SWCNT. At the experimental conditions used (0.5 M H₂SO₄) the monomer will be fully protonated forming phosphonic acid and anilinium cations. Since the SWCNT have a low oxygen content and have not been subjected to any oxidation treatment ($\text{pH}_{\text{pzc}} = 6.3$), at the pH of the experiments, the surface will be positively charged. Consequently, the adsorption of the 4-APPA molecule will not occur through the protonated amine group due to repulsive electrostatic interactions and dispersive interactions (i.e., π - π interactions) would be the main adsorption mechanism^{41,42}. This means that although the surface coverage by 4-APPA will not be high, the adsorption of the molecules will mainly occur parallel to the SWCNT surface. Thus, at oxidation conditions, the 4-APPA radicals could be formed at the surface of the SWCNT and react with other adsorbed (or covalently bonded) molecules forming the oligomers with the expected electroactivity from the N species. This possibility will be further reinforced with the characterization of the obtained materials presented in the next sections. It must be noted that 4-APPA oligomerization is not observed on platinum electrodes, in which polyaniline growth is straightforward, being necessary the addition of aniline to produce co-polymerization⁴³. This suggests

that monomer adsorption and orientation on the electrode determine the polymerization reaction.

Electrochemical properties of surface functionalities onto the SWCNT have an important dependence with the pH. This can be observed in Figure 3.6, for SWCNT electrochemically modified in different electrolytes. In general, with increasing the pH, the current of the processes decreases (or even disappears) and the peak separation increases. Thus, at neutral pH (0.1 M PBS solution at pH = 7.2), redox processes present an increase in the peak separation or even a loss of electroactivity. At alkaline pH, the reduction of the electrochemical activity of the redox processes is remarkable and only redox process C is observed. Increase in the peak separation of the electrochemical processes can be a result of the loss of reversibility of the surface redox processes with the increase of pH^{44,45}. This behavior with the pH is in agreement with polyaniline-type products that loss their electroactivity with the increase of the pH.

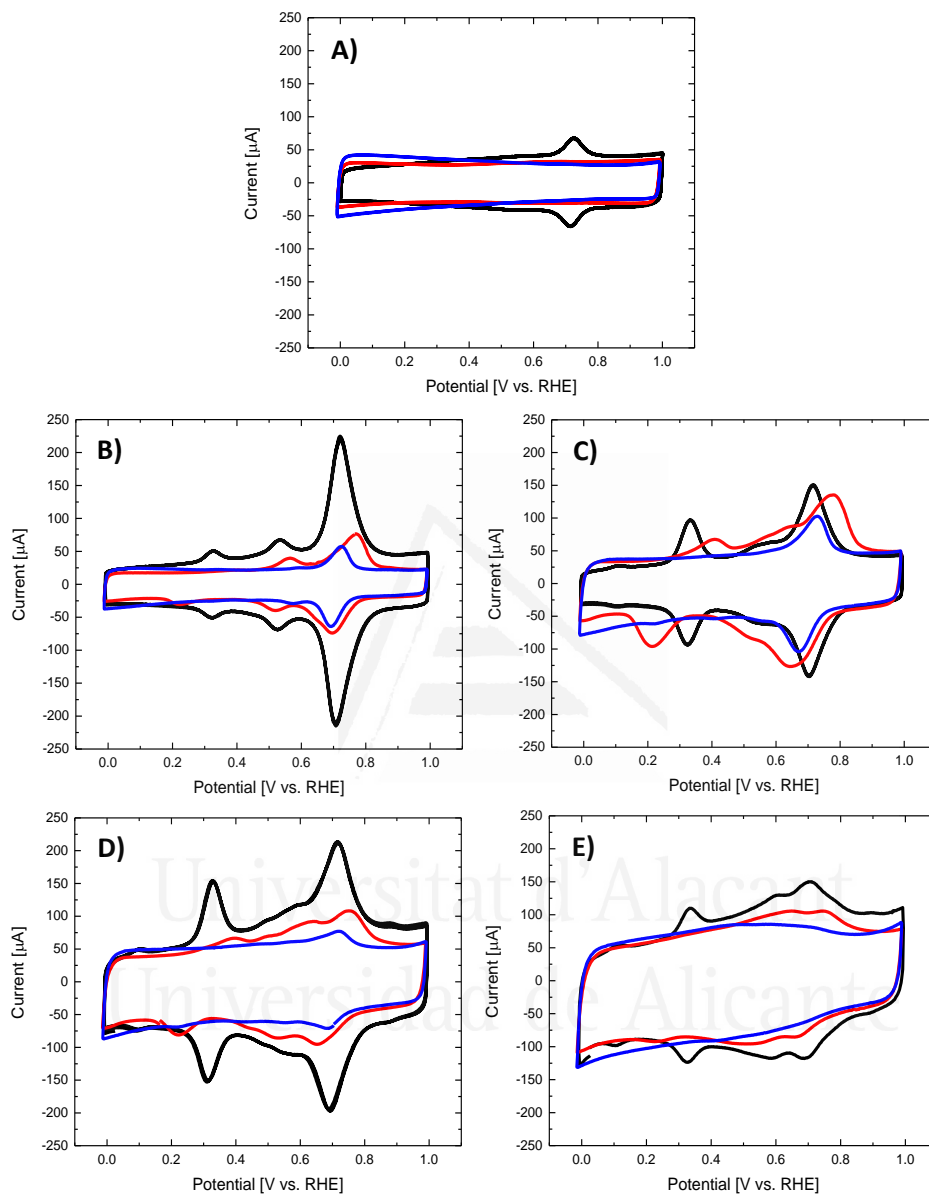


Figure 3.6. Steady state voltammograms for the modified SWCNT with 4-APPA at: A) 1.0 V, B) 1.2 V, C) 1.4 V, D) 1.6 V and E) 1.8 V in 0.5 M H₂SO₄ (Black lines), 0.1 M PBS (pH = 7.2-Red lines) and 0.1 M KOH (Blue lines) at 50 mV s⁻¹ under N₂ atmosphere.

3.2. Morphological characterization of SWCNT modified electrochemically with P and N species

Figure 3.7 shows the TEM images for pristine SWCNT and the same carbon nanotubes after electrochemical modification with 4-APPA at the different anodic potentials.

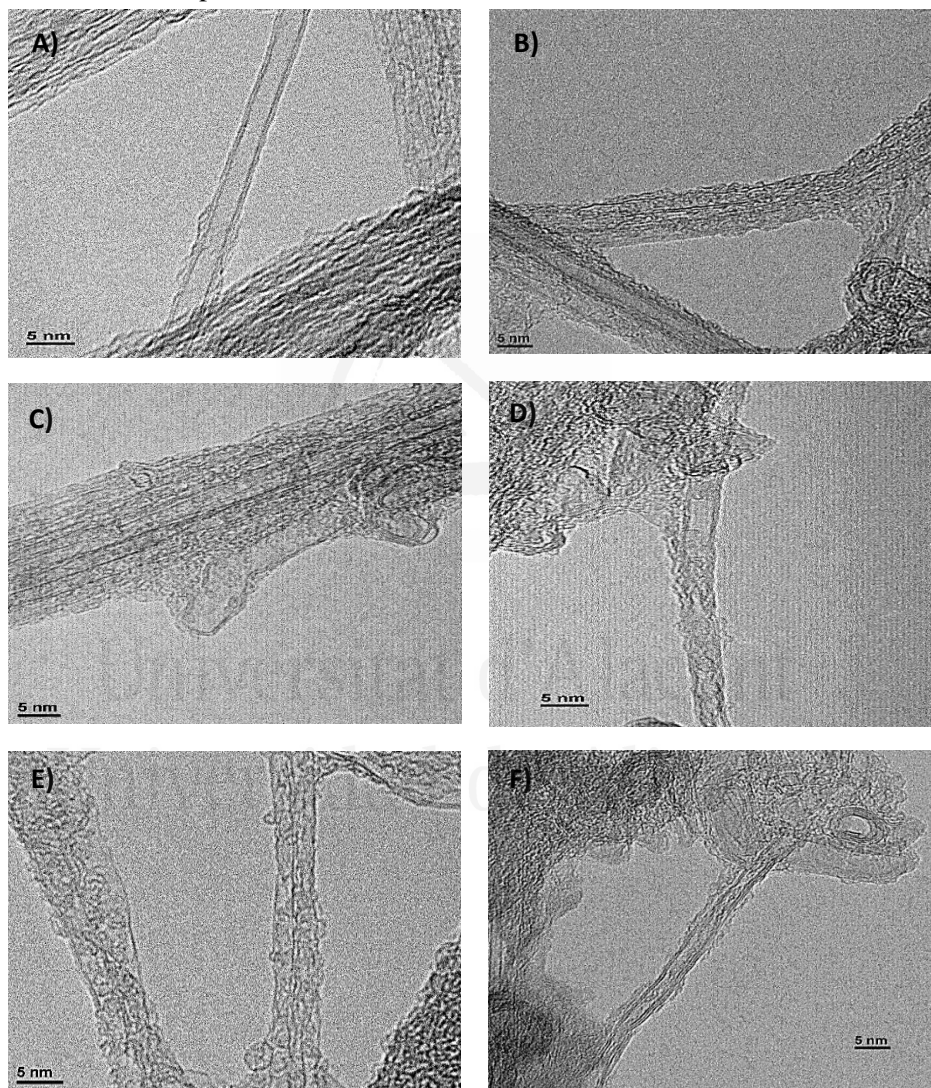


Figure 3.7. TEM micrographs for SWCNT electrochemical modified with 4-APPA at: A) Pristine, B) 1.0 V, C) 1.2 V, D) 1.4 V, E) 1.6 V and F) 1.8 V vs. RHE.

SWCNT presents the typical tubular structure formed by one-two layers of rolled-graphene layers (Figure 3.7-A). Once SWCNT are modified with 4-APPA, a deposited material on the SWCNT is clearly observed, which morphology seems to be dependent on the applied potential during the functionalization. This is a direct proof of polymerization of 4-APPA onto the SWCNT. The formed oligomers are wrapping the CNT surface and when the applied potential is 1 or 1.2 V, uniform layers of the oligomers can be clearly observed, what is in agreement with the proposed reaction mechanism (Figure 3.7-B and C). However, at higher potentials, the deposited material has not such homogeneity and even discontinuous, or not linear chains can be observed. This can be due to the strong oxidation conditions, which generate oxygen functional groups on the CNT that modifies the orientation of the 4-APPA molecules, producing less ordered and shorter polymer chains (Figure 3.7-D, E and F).

Interestingly, non-important structural changes, such as broken-walls of SWCNTs can be observed, suggesting that, despite the high oxidative conditions used, destruction and morphological changes on the SWCNTs shape are not very important, being the oxidation mainly focused on the 4-APPA polymerization and further attachment or adsorption on surface of the species generated during the functionalization.

3.3. XPS analysis of P and N species on electrochemically modified SWCNT

The degree of incorporation of O, N and P species, and the chemical nature of the different surface functionalities incorporated on the SWCNT were studied by XPS. Table 3.2 summarizes the amount of O, N and P incorporated in the SWCNT during the electrochemical modification.

Table 3.2. Chemical composition obtained from XPS of the electrochemical modified SWCNT with 4-APPA.

| Applied potential [V vs. RHE] | %O (at) | %N (at) | %P (at) | N/P* |
|----------------------------------|---------|---------|---------|------|
| Pristine | 3.13 | 0.37 | 0.00 | -- |
| 1.2 | 3.93 | 0.60 | 0.15 | 1.5 |
| 1.4 | 5.03 | 0.83 | 0.24 | 1.9 |
| 1.6 | 6.81 | 1.24 | 0.5 | 1.7 |
| 1.8 | 12.66 | 1.58 | 0.44 | 2.8 |

*The N content of the pristine SWCNT has been subtracted for the calculation.

The electrochemical modification at 1 V (Figure 3.3-A) shows redox processes in the sample, suggesting the incorporation of functionalities on the CNT surface. However, the low amount of N and P detected, close to the detection limit of the technique, makes impossible a proper quantification of these species in the modified SWCNT. This indicates that the electrochemical characterization has better sensitivity to surface modification than other techniques. For this reason, the data at 1 V are not included in the table. The results obtained for higher potentials show that the nitrogen content increases with the upper positive potential limit. The content of phosphorus also increases with the potential; however, at 1.8 V the amount of phosphorus decreases, probably due to the oxidation of the phosphonic groups to phosphoric groups that can be further hydrolyzed (See Table 3.2). The ratio N/P is between 1.5 and 1.9 for all the studied potentials except for 1.8 V, indicating that the incorporation of the 4-APPA maintains both functional groups although some phosphonic groups are lost at these conditions. The oxygen content does not experience a strong increase until the highest potentials are reached and at which less ordered and shorter polymer chains are observed. This means that at this potential, a strong oxidation of the polymer and also of the SWCNT may occur.

Figure 3.8 presents the XPS N1s spectra for the SWCNT modified at different upper potential limits, showing different species depending on the applied potential. The region between 398.5 and 400.1 eV can be assigned to

neutral amines and imines species, respectively, generated during the oxidation of 4-APPA which are also observed in PANI, and are in agreement with the formation of oligomer/polymeric chains^{40,46,47}. A third peak at around 402 eV is also observed in all the potentials. This peak can be associated with more oxidized nitrogen species^{47,48}. These oxidized nitrogen species increase significantly in the SWCNT modified at 1.8 V, in agreement with what has been observed in other amine-containing molecules, electrochemically attached on different materials surfaces^{49,50}.

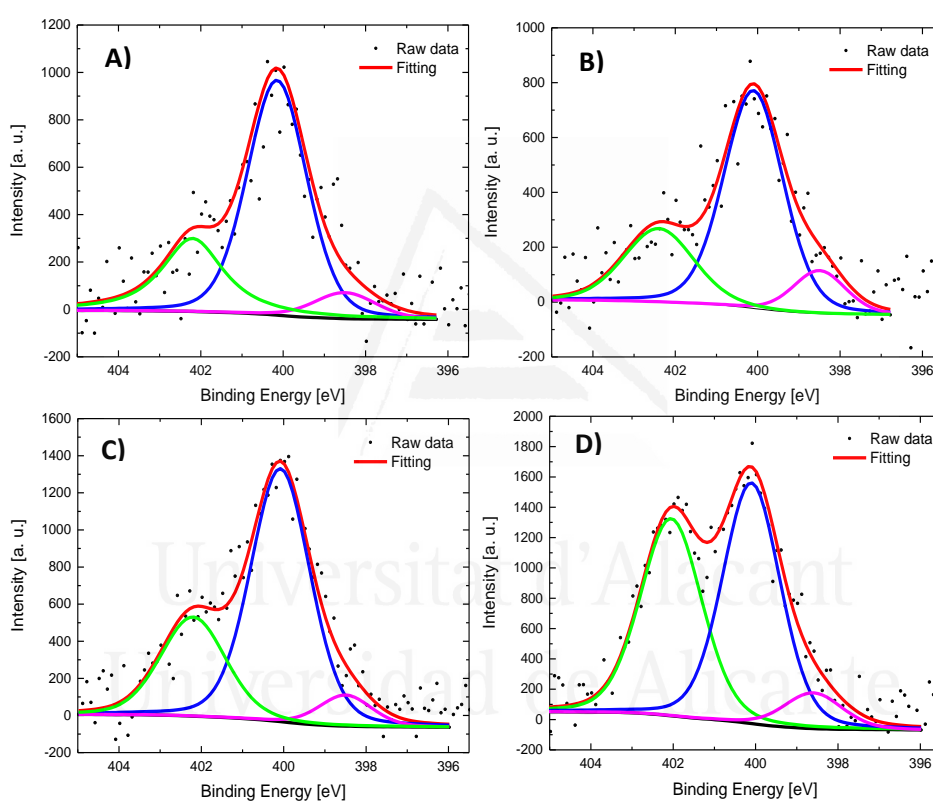


Figure 3.8. N1s XPS spectra for SWCNT electrochemical modified with 4-APPA at different oxidation potentials: A) 1.2 V, B) 1.4 V, C) 1.6 V and D) 1.8 V vs. RHE.

Regarding the P2p spectra in Figure 3.9, two asymmetric doublets are observed (the XPS for the sample prepared at 1.2 V is not deconvoluted because of the low amount of P, making the spectrum very noisy). The first contribution at 132.6 eV can be associated with the binding energy of C-P-O species^{51,52}, in agreement with the presence of the phosphonic group^{53,54}. A

second contribution at 133.3 eV can be related to C-O-P species that are formed as consequence of the oxidation of the phosphonic group to phosphoric group^{51,52,55,56}.

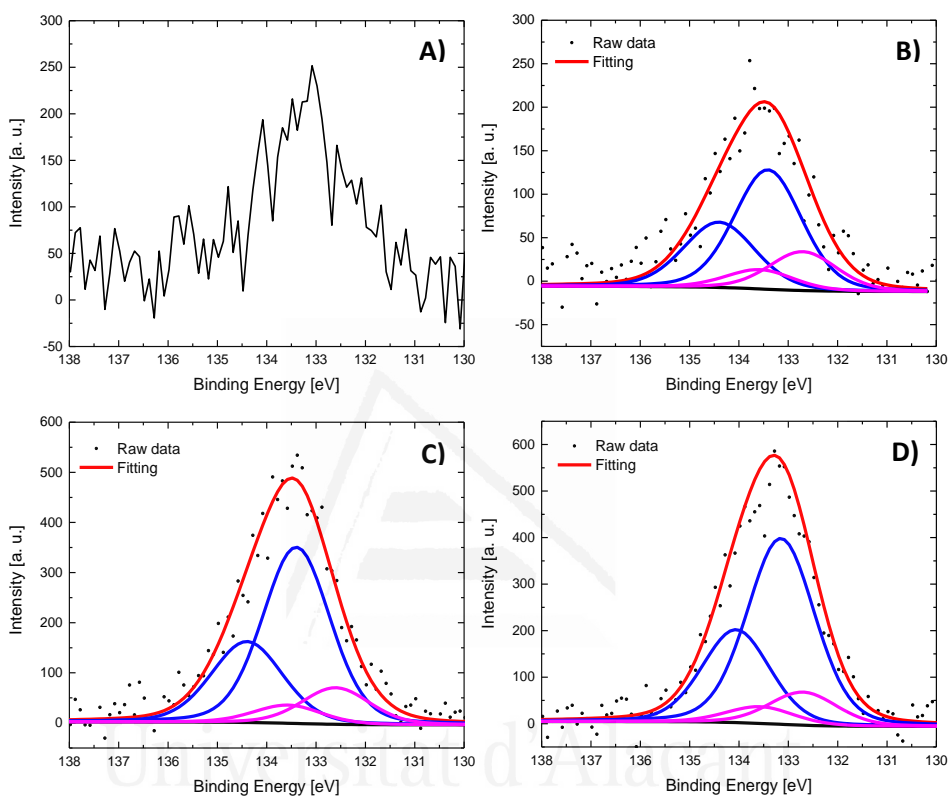


Figure 3.9. P2p XPS spectra for SWCNT electrochemically modified with 4-APPA at different oxidation potentials: A) 1.2 V, B) 1.4 V, C) 1.6 V and D) 1.8 V vs. RHE.

Table 3.3 presents the atomic percentage for each N and P species determined by XPS for the modified SWCNTs. In the case of nitrogen important changes can be observed at 1.8 V where nitrogen species, corresponding with neutral species, decrease with the corresponding increase in oxidized nitrogen species. This is especially remarkable at the highest potential in which different nitrogen species compared to polyaniline³⁵ must be present at the surface. It must be noted that oxidized nitrogen is, in all the cases, higher than for phosphonic acid ring-substituted polyanilines prepared via direct chemical phosphonation⁵⁷. Interestingly, phosphorus species

associated with the phosphonic moieties present a constant value until a positive potential limit of 1.4 V and its contribution decreases at 1.6 and 1.8 V. Table 3.3 shows that the main P-species corresponds to phosphoric acid functionality (C-O-P) as consequence of the oxidation of the phosphonic group.

Table 3.3. Distribution of N1s contributions for SWCNT electrochemically modified with 4-APPA at different potentials.

| Potential applied [V vs. RHE] | % Neutral N species (398.5 and 400.1 eV) | % Oxidized nitrogen (402.2 eV) | C-O-P (133.3 eV) | C-P-O (132.6 eV) |
|-------------------------------|--|--------------------------------|------------------|------------------|
| 1.2 | 73 | 27 | 71 | 29 |
| 1.4 | 75 | 25 | 75 | 25 |
| 1.6 | 72 | 28 | 83 | 17 |
| 1.8 | 57 | 43 | 85 | 15 |

*All the percentages correspond with the total amount of each N1s and P2p determined.

3.4. Raman spectroscopy of SWCNT electrochemically modified with 4-APPA

Raman spectroscopy was employed to analyze the structural and physicochemical changes produced by the electrochemical modification of the SWCNT with 4-APPA. Raman spectra in Figure 3.10-A for pristine SWCNT and electrochemically modified with 4-APPA, present mainly two contributions associated with C-C vibration, the G (1585 cm^{-1}) and D (1350 cm^{-1}) bands, corresponding to an ideal graphitic lattice vibration mode and with a disorder-induced band, respectively⁵⁸⁻⁶⁰.

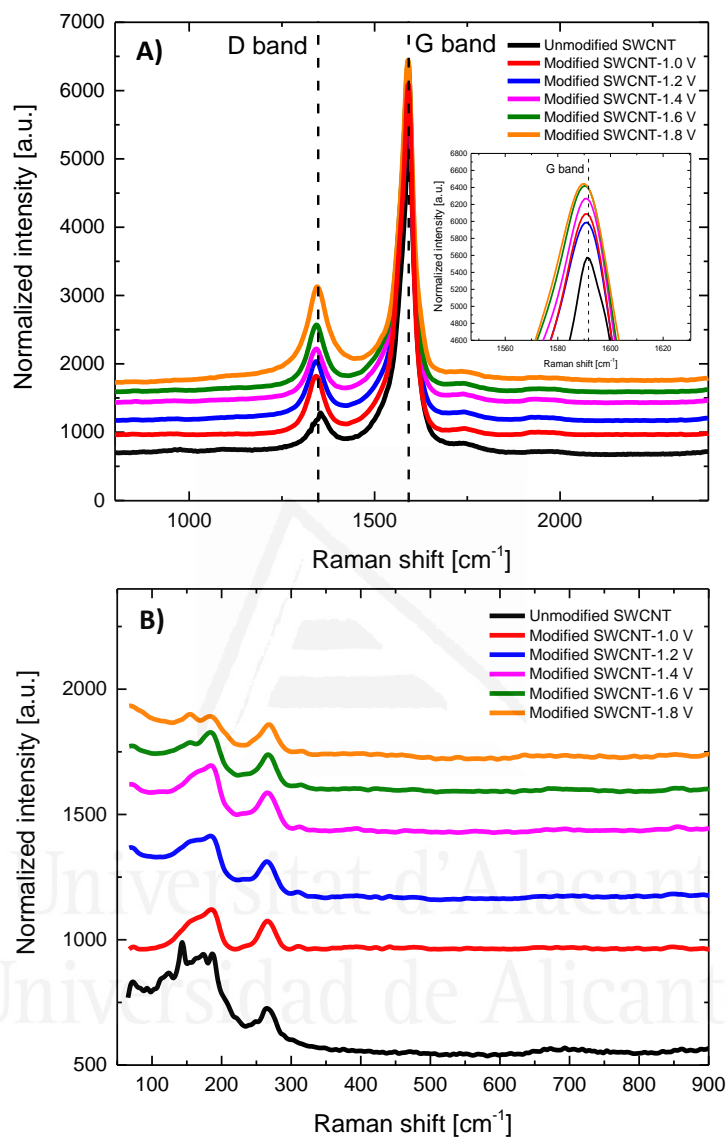


Figure 3.10. Raman spectra of SWCNT electrochemically modified with 4-APPA at different potentials: A) D and G band region, and B) RBM region of SWCNT.

It can be observed a similar Raman spectrum for all the modified SWCNT. However, the electrochemical modification causes an increase in the ratio of the relative intensities for these two bands (I^D/I^G), as can be observed in Figure 3.11. Moreover, the intensity and the position of the G-Band change with the

functionalization from 1592 cm^{-1} for the pristine SWCNTs to 1589 cm^{-1} for the functionalized SWCNTs at 1.8V. This could indicate changes in the electronic structure, in doping or in the resonance conditions of the SWCNTs contributing to G-Band⁶¹. However, this shift is especially important for the highest potentials used at which the changes in the morphology are clearly observed by TEM. These changes are in agreement with the reaction with 4-APPA species to promote the attachment, the interaction of polymer chains adsorbed onto the CNT and the defects induced in the CNT by electrooxidation.

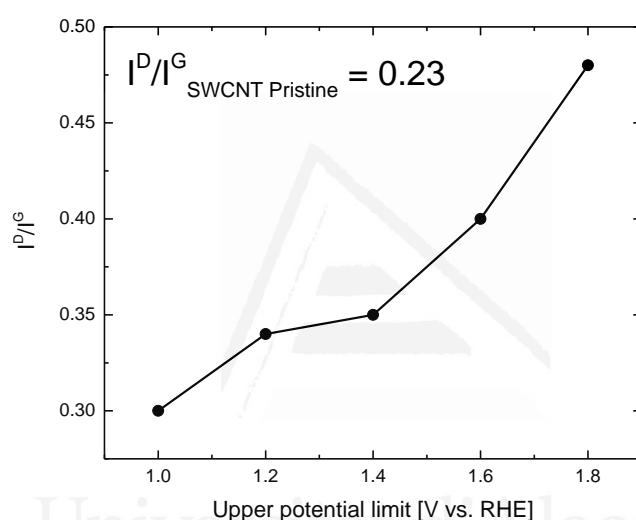


Figure 3.11. Plot I^D/I^G relative intensities as a function of the upper potential limit during the electrochemical modification of SWCNT with 4-APPA.

In the case of SWCNT, it is well-known that Radial Breathing Mode (RBM) is an environment sensitive property and it is related to the diameter of the tube^{60,62-64}. These Raman spectra regions are included in Figure 3.10-B. Interestingly, the main features of this region do not significantly change with the functionalization and only some contributions at lower frequencies present a decrease of the intensity with the upper potential limit of functionalization. The diameter of the pristine and modified SWCNT has been determined from the RBM region. The obtained values are between 1.1 to 2.3 nm in all cases. These values are in agreement with the TEM micrographs analyzed previously (Figure 3.7). In spite of the application of oxidative conditions and functionalization process in the CNT, the RBM region is still clearly observed and with small changes, suggesting that SWCNTs maintain their tubular

structure without suffering strong damages during the electrochemical functionalization. In this sense electrochemical modification produces low structural changes in the CNTs with high increase in the N and P species, even at the high positive potential limit used for the modification, what is in agreement with most of the functionalization occurring by wrapping the SWCNT by 4-APPA-based polymer, as deduced from TEM.

4. Conclusions

Functionalization of SWCNT with N and P functional groups was achieved by electrochemical oxidation of 4-APPA by cyclic voltammetry. The electrochemical oxidation selectively produces attachment of electroactive species and oligomer layers that wrap the surface of the SWCNT. Increase in the positive potential of the electrochemical modification demonstrated a high influence in the degree of incorporation of N and P species. Thus, when an upper potential limit of 1.6 V is used, the highest P incorporation is reached and further potential increase causes loss of P-species probably due to hydrolysis reactions. Several surface redox processes that depend on the applied potential are clearly observed in the voltammograms of the functionalized SWCNT. These redox processes present an important pH dependence. The well-defined redox processes observed suggests good interaction between the SWCNTs and the functionalities attached and oligomer adsorbed homogeneously on surface. This conclusion is supported by TEM and Raman spectroscopy. However, the high reversibility and symmetry of the redox processes suggest that covalently bound redox species may also exist.

The high selectivity of the electrochemical process towards monomer oxidation, even at high potentials, and the precise control of the degree of modification of the CNT surface by selecting the electrochemical conditions, makes this method an alternative procedure for electrochemical co-functionalization with P and N species with the generation of electroactive materials.

5. References

- (1) Inagaki, M.; Kang, F.; Toyoda, M.; Konno, I. *Advanced Materials Science and Engineering of Carbon*; Butterworth-Heinemann, Elsevier: Tsinghua, China, **2014**.

- (2) Dinadayalane, T. C.; Leszczynski, J. Comparative Theoretical Study on the Positional Preference for Functionalization of Two OH and SH Groups with (5,5) Armchair SWCNT. *J. Phys. Chem. C* **2013**, *117* (27), 14441–14450.
- (3) Naqvi, S. T. R.; Rasheed, T.; Hussain, D.; Najam ul Haq, M.; Majeed, S.; shafi, S.; Ahmed, N.; Nawaz, R. Modification Strategies for Improving the Solubility/Dispersion of Carbon Nanotubes. *J. Mol. Liq.*, **2020**, *297*, 111919.
- (4) Li, Z.; Wang, L.; Li, Y.; Feng, Y.; Feng, W. Carbon-Based Functional Nanomaterials: Preparation, Properties and Applications. *Compos. Sci. Technol*, **2019**, *179*, 10–40.
- (5) Ata, M. S.; Poon, R.; Syed, A. M.; Milne, J.; Zhitomirsky, I. New Developments in Non-Covalent Surface Modification, Dispersion and Electrophoretic Deposition of Carbon Nanotubes. *Carbon*, **2018**, *130*, 584–598.
- (6) Wang, C.; Xia, K.; Wang, H.; Liang, X.; Yin, Z.; Zhang, Y. Advanced Carbon for Flexible and Wearable Electronics. *Adv. Mater.* **2019**, *31* (9), 1801072.
- (7) Oueiny, C.; Berlioz, S.; Patout, L.; Perrin, F. X. Aqueous Dispersion of Multiwall Carbon Nanotubes with Phosphonic Acid Derivatives. *Colloids Surfaces A Physicochem. Eng. Asp.* **2016**, *493*, 41–51.
- (8) González-Gaitán, C.; Ruíz-Rosas, R.; Morallón, E.; Cazorla-Amorós, D. Electrochemical Methods to Functionalize Carbon Materials. In: Vijay Kumar, T.; Manju Kumari, T.; editor. *Chemical Functionalization of Carbon Materials-Chemistry and Applications*, Taylor and Francis group, CRC Press, Washington, **2016**, pp. 230-249.
- (9) Jaisankar, S. N.; Haridharan, N.; Murali, A.; Sergii, P.; Špírková, M.; Mandal, A. B.; Matějka, L. Single-Electron Transfer Living Radical Copolymerization of SWCNT-g-PMMA via Graft from Approach. *Polymer* **2014**, *55* (13), 2959–2966.
- (10) Sun, Y.-P.; Fu, K.; Lin, Y.; Huang, W. Functionalized Carbon Nanotubes: Properties and Applications. *Acc. Chem. Res.* **2002**, *35* (12), 1096–1104.
- (11) Komarova, N. S.; Krivenko, A. G.; Ryabenko, A. G.; Naumkin, A. V. Active Forms of Oxygen as Agents for Electrochemical Functionalization of SWCNTs. *Carbon* **2013**, *53*, 188–196.

- (12) Mubarak, N. M.; Sahu, J. N.; Wong, J. R.; Jayakumar, N. S.; Ganesan, P.; Abdullah, E. C. Overview on the Functionalization of Carbon Nanotubes. In: Vijay Kumar, T.; Manju Kumari, T.; editor. *Chemical Functionalization of Carbon Materials-Chemistry and Applications*, Taylor and Francis group, CRC Press, Washington, **2016**, pp. 230-249.
- (13) Lee, J. U.; Huh, J.; Kim, K. H.; Park, C.; Jo, W. H. Aqueous Suspension of Carbon Nanotubes via Non-Covalent Functionalization with Oligothiophene-Terminated Poly(Ethylene Glycol). *Carbon* **2007**, *45* (5), 1051–1057.
- (14) Boháčová, M.; Zetková, K.; Knotek, P.; Bouša, D.; Friess, K.; Číhal, P.; Lanč, M.; Hrdlička, Z.; Sofer, Z. Mildly Oxidized SWCNT as New Potential Support Membrane Material for Effective H₂/CO₂ Separation. *Appl. Mater. Today* **2019**, *15*, 335–342.
- (15) Kumar, D.; Jha, P.; Chouksey, A.; Rawat, J. S. B. S.; Tandon, R. P.; Chaudhury, P. K. 4-(Hexafluoro-2-Hydroxy Isopropyl)Aniline Functionalized Highly Sensitive Flexible SWCNT Sensor for Detection of Nerve Agent Simulant Dimethyl Methylphosphonate. *Mater. Chem. Phys.* **2016**, *181*, 487–494.
- (16) Adekunle, A. S.; Pillay, J.; Ozoemena, K. I. Probing the Electrochemical Behaviour of SWCNT–Cobalt Nanoparticles and Their Electrocatalytic Activities towards the Detection of Nitrite at Acidic and Physiological PH Conditions. *Electrochim. Acta* **2010**, *55* (14), 4319–4327.
- (17) Chen, R. J.; Zhang, Y.; Wang, D.; Dai, H. Noncovalent Sidewall Functionalization of Single-Walled Carbon Nanotubes for Protein Immobilization. *J. Am. Chem. Soc.* **2001**, *123* (16), 3838–3839.
- (18) Ebrahim-Habibi, M.-B.; Ghobeh, M.; Mahyari, F. A.; Rafii-Tabar, H.; Sasanpour, P. An Investigation into Non-Covalent Functionalization of a Single-Walled Carbon Nanotube and a Graphene Sheet with Protein G: A Combined Experimental and Molecular Dynamics Study. *Sci. Rep.* **2019**, *9* (1), 1273.
- (19) Fraser, R. A.; Stoeffler, K.; Ashrafi, B.; Zhang, Y.; Simard, B. Large-Scale Production of PMMA/SWCNT Composites Based on SWCNT Modified with PMMA. *ACS Appl. Mater. Interfaces* **2012**, *4* (4), 1990–1997.
- (20) Ntim, S. A.; Sae-Khow, O.; Witzmann, F. A.; Mitra, S. Effects of

Polymer Wrapping and Covalent Functionalization on the Stability of MWCNT in Aqueous Dispersions. *J. Colloid Interface Sci.* **2011**, *355* (2), 383–388.

- (21) Aravind, S. S. J.; Baskar, P.; Baby, T. T.; Sabareesh, R. K.; Das, S.; Ramaprabhu, S. Investigation of Structural Stability, Dispersion, Viscosity, and Conductive Heat Transfer Properties of Functionalized Carbon Nanotube Based Nanofluids. *J. Phys. Chem. C* **2011**, *115* (34), 16737–16744.
- (22) Ramanathan, T.; Fisher, F. T.; Ruoff, R. S.; Brinson, L. C. Amino-Functionalized Carbon Nanotubes for Binding to Polymers and Biological Systems. *Chem. Mater.* **2005**, *17* (6), 1290–1295.
- (23) Martínez, M. T.; Callejas, M. A.; Benito, A. M.; Cochet, M.; Seeger, T.; Ansón, A.; Schreiber, J.; Gordon, C.; Marhic, C.; Chauvet, O.; et al. Sensitivity of Single Wall Carbon Nanotubes to Oxidative Processing: Structural Modification, Intercalation and Functionalisation. *Carbon* **2003**, *41* (12), 2247–2256.
- (24) Ma, P.-C.; Siddiqui, N. A.; Marom, G.; Kim, J.-K. Dispersion and Functionalization of Carbon Nanotubes for Polymer-Based Nanocomposites: A Review. *Compos. Part A Appl. Sci. Manuf.* **2010**, *41* (10), 1345–1367.
- (25) Holzinger, M.; Abraham, J.; Whelan, P.; Graupner, R.; Ley, L.; Hennrich, F.; Kappes, M.; Hirsch, A. Functionalization of Single-Walled Carbon Nanotubes with (R-)Oxycarbonyl Nitrenes. *J. Am. Chem. Soc.* **2003**, *125* (28), 8566–8580.
- (26) Theodore, M.; Hosur, M.; Thomas, J.; Jeelani, S. Influence of Functionalization on Properties of MWCNT–Epoxy Nanocomposites. *Mater. Sci. Eng. A* **2011**, *528* (3), 1192–1200.
- (27) Bélanger, D.; Pinson, J. Electrografting: A Powerful Method for Surface Modification. *Chem. Soc. Rev.* **2011**, *40* (7), 3995–4048.
- (28) Ghanem, M. A.; Kocak, I.; Al-Mayouf, A.; AlHoshan, M.; Bartlett, P. N. Covalent Modification of Carbon Nanotubes with Anthraquinone by Electrochemical Grafting and Solid Phase Synthesis. *Electrochim. Acta* **2012**, *68*, 74–80.
- (29) Allongue, P.; Delamar, M.; Desbat, B.; Fagebaume, O.; Hitmi, R.; Pinson, J.; Savéant, J.-M. Covalent Modification of Carbon Surfaces by Aryl Radicals Generated from the Electrochemical Reduction of

Diazonium Salts. *J. Am. Chem. Soc.* **1997**, *119* (1), 201–207.

- (30) González-Gaitán, C.; Ruiz-Rosas, R.; Morallón, E.; Cazorla-Amorós, D. Functionalization of Carbon Nanotubes Using Aminobenzene Acids and Electrochemical Methods. Electroactivity for the Oxygen Reduction Reaction. *Int. J. Hydrogen Energy* **2015**, *40* (34), 11242–11253.
- (31) González-Gaitán, C.; Ruiz-Rosas, R.; Nishihara, H.; Kyotani, T.; Morallón, E.; Cazorla-Amorós, D. Successful Functionalization of Superporous Zeolite Templated Carbon Using Aminobenzene Acids and Electrochemical Methods. *Carbon* **2016**, *99*, 157–166.
- (32) Gabe, A.; Ruiz-Rosas, R.; Morallón, E.; Cazorla-Amorós, D. Understanding of Oxygen Reduction Reaction by Examining Carbon-Oxygen Gasification Reaction and Carbon Active Sites on Metal and Heteroatoms Free Carbon Materials of Different Porosities and Structures. *Carbon* **2019**, *148*, 430–440.
- (33) Such-Basáñez, I.; Román-Martínez, M. C.; Salinas-Martínez de Lecea, C. Ligand Adsorption on Different Activated Carbon Materials for Catalyst Anchorage. *Carbon* **2004**, *42* (7), 1357–1361.
- (34) Salinas-Torres, D.; Huerta, F.; Montilla, F.; Morallón, E. Study on Electroactive and Electrocatalytic Surfaces of Single Walled Carbon Nanotube-Modified Electrodes. *Electrochim. Acta* **2011**, *56* (5), 2464–2470.
- (35) Bard, A.; Faulkner, L. *Electrochemical Methods: Fundamental and Applications*, 2nd ed., John Wiley & Sons, Ltd, Austin, **2000**.
- (36) Probst, M.; Holze, R. A Systematic Spectroelectrochemical Investigation of Alkyl-Substituted Anilines and Their Polymers. *Macromol. Chem. Phys.* **1997**, *198* (5), 1499–1509.
- (37) Nateghi, M. R.; Zahedi, M.; Mosslemin, M. H.; Hashemian, S.; Behzad, S.; Minnai, A. Autoacceleration/Degradation of Electrochemical Polymerization of Substituted Anilines. *Polymer* **2005**, *46* (25), 11476–11483.
- (38) Benyoucef, A.; Huerta, F.; Ferrahi, M. I.; Morallon, E. Voltammetric and in Situ FT-IRS Study of the Electropolymerization of o-Aminobenzoic Acid at Gold and Graphite Carbon Electrodes: Influence of PH on the Electrochemical Behaviour of Polymer Films. *J. Electroanal. Chem.* **2008**, *624* (1), 245–250.

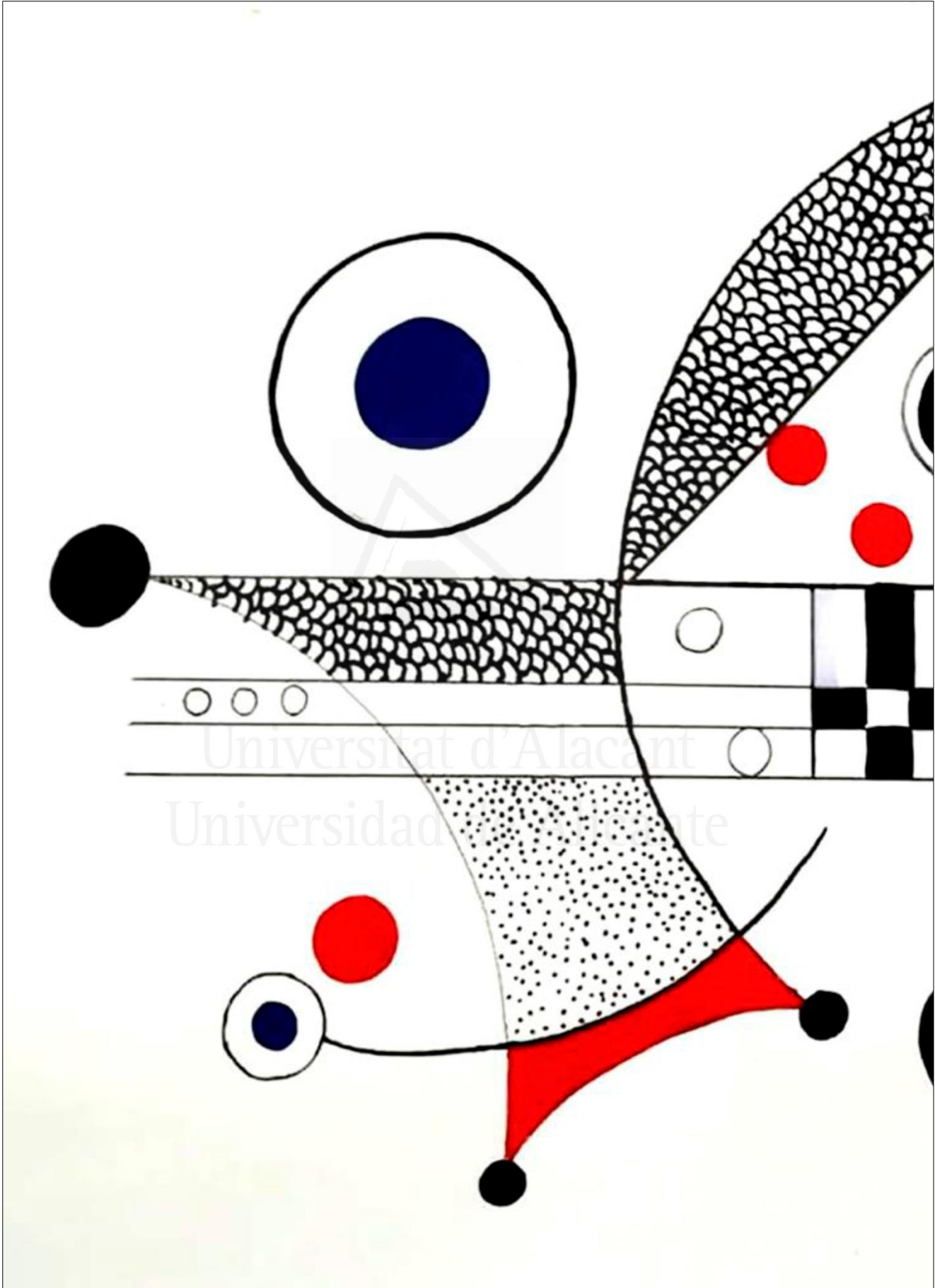
- (39) Wang, B.; Tang, J.; Wang, F. Electrochemical Polymerization of Aniline. *Synth. Met.* **1987**, *18* (1), 323–328.
- (40) Quílez-Bermejo, J.; Ghisolfi, A.; Grau-Marín, D.; San-Fabián, E.; Morallón, E.; Cazorla-Amorós, D. Post-Synthetic Efficient Functionalization of Polyaniline with Phosphorus-Containing Groups. Effect of Phosphorus on Electrochemical Properties. *Eur. Polym. J.* **2019**, *119*, 272–280.
- (41) Radovic, L. R.; Silva, I. F.; Ume, J. I.; Menéndez, J. A.; Leon, C. A. L. Y.; Scaroni, A. W. An Experimental and Theoretical Study of the Adsorption of Aromatics Possessing Electron-Withdrawing and Electron-Donating Functional Groups by Chemically Modified Activated Carbons. *Carbon* **1997**, *35* (9), 1339–1348.
- (42) Radovic, L. R.; Moreno-Castilla, C.; Rivera-Utrilla, J. Carbon Materials as adsorbents in aqueous solution. In: Radovic, L. R. editor. Chemistry and physics of carbon, Vol 27, Marcel Dekker, CRC Press, New York, **2000**. pp. 227-405.
- (43) Martínez-Sánchez, B. Síntesis y Caracterización Electroquímica de Polianilinas Modificadas Con Grupos Fosfónicos., Universidad de Alicante, **2019**.
- (44) Tang, H.; Kitani, A.; Yamashita, T.; Ito, S. Highly Sulfonated Polyaniline Electrochemically Synthesized by Polymerizing Aniline-2,5-Disulfonic Acid and Copolymerizing It with Aniline. *Synth. Met.* **1998**, *96* (1), 43–48.
- (45) Jürmann, G.; Schiffrin, D. J.; Tammeveski, K. The PH-Dependence of Oxygen Reduction on Quinone-Modified Glassy Carbon Electrodes. *Electrochim. Acta* **2007**, *53* (2), 390–399.
- (46) Wang, Z.; Dong, Y.; Li, H.; Zhao, Z.; Bin Wu, H.; Hao, C.; et. al. Enhancing lithium–sulphur battery performance by strongly binding the discharge products on amino-functionalized reduced graphene oxide, *Nat. Commun.* **2014**, *5*, 5002.
- (47) Abidi, M.; López-Bernabeu, S.; Huerta, F.; Montilla, F.; Besbes-Hentati, S.; Morallón, E. Spectroelectrochemical Study on the Copolymerization of O-Aminophenol and Aminoterephthalic Acid. *Eur. Polym. J.* **2017**, *91*, 386–395.
- (48) Cordero-Lanzac, T.; Rosas, J. M.; García-Mateos, F. J.; Ternero-Hidalgo, J. J.; Palomo, J.; Rodríguez-Mirasol, J.; Cordero, T. Role of

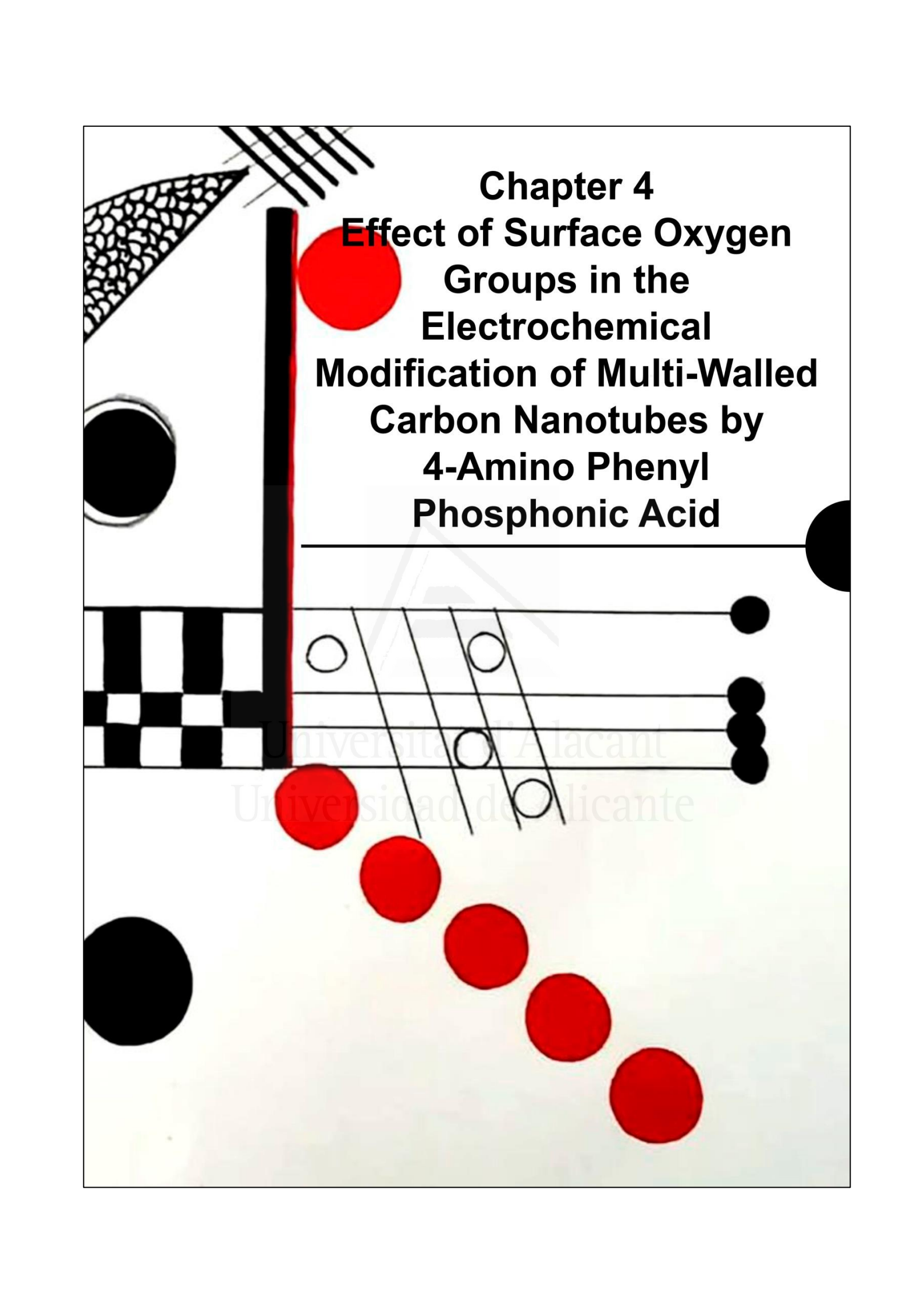
Different Nitrogen Functionalities on the Electrochemical Performance of Activated Carbons. *Carbon* **2018**, *126*, 65–76.

- (49) Baskar, S.; Liao, C.-W.; Chang, J.-L.; Zen, J.-M. Electrochemical Synthesis of Electroactive Poly(Melamine) with Mechanistic Explanation and Its Applicability to Functionalize Carbon Surface to Prepare Nanotube–Nanoparticles Hybrid. *Electrochim. Acta* **2013**, *88*, 1–5.
- (50) Adenier, A.; Chehimi, M. M.; Gallardo, I.; Pinson, J.; Vilà, N. Electrochemical Oxidation of Aliphatic Amines and Their Attachment to Carbon and Metal Surfaces. *Langmuir* **2004**, *20* (19), 8243–8253.
- (51) Berenguer, R.; Ruiz-Rosas, R.; Gallardo, A.; Cazorla-Amorós, D.; Morallón, E.; Nishihara, H.; Kyotani, T.; Rodríguez-Mirasol, J.; Cordero, T. Enhanced Electro-Oxidation Resistance of Carbon Electrodes Induced by Phosphorus Surface Groups. *Carbon* **2015**, *95*, 681–689.
- (52) Quesada-Plata, F.; Ruiz-Rosas, R.; Morallón, E.; Cazorla-Amorós, D. Activated Carbons Prepared through H₃PO₄-Assisted Hydrothermal Carbonisation from Biomass Wastes: Porous Texture and Electrochemical Performance. *Chempluschem* **2016**, *81* (12), 1349–1359.
- (53) Chen, Y.; Guo, L.-R.; Chen, W.; Yang, X.-J.; Jin, B.; Zheng, L.-M.; Xia, X.-H. 3-Mercaptopropylphosphonic Acid Modified Gold Electrode for Electrochemical Detection of Dopamine. *Bioelectrochemistry* **2009**, *75* (1), 26–31.
- (54) Yang, D.-S.; Bhattacharjya, D.; Inamdar, S.; Park, J.; Yu, J.-S. Phosphorus-Doped Ordered Mesoporous Carbons with Different Lengths as Efficient Metal-Free Electrocatalysts for Oxygen Reduction Reaction in Alkaline Media. *J. Am. Chem. Soc.* **2012**, *134* (39), 16127–16130.
- (55) Paniagua, S. A.; Hotchkiss, P. J.; Jones, S. C.; Marder, S. R.; Mudalige, A.; Marrikar, F. S.; Pemberton, J. E.; Armstrong, N. R. Phosphonic Acid Modification of Indium–Tin Oxide Electrodes: Combined XPS/UPS/Contact Angle Studies. *J. Phys. Chem. C* **2008**, *112* (21), 7809–7817.
- (56) Koh, S. E.; McDonald, K. D.; Holt, D. H.; Dulcey, C. S.; Chaney, J. A.; Pehrsson, P. E. Phenylphosphonic Acid Functionalization of Indium Tin Oxide: Surface Chemistry and Work Functions. *Langmuir* **2006**,

22 (14), 6249–6255.

- (57) Amaya, T.; Kurata, I.; Inada, Y.; Hatai, T.; Hirao, T. Synthesis of Phosphonic Acid Ring-Substituted Polyanilines via Direct Phosphonation to Polymer Main Chains. *RSC Adv.* **2017**, *7* (62), 39306–39313.
- (58) Leyva-García, S.; Morallón, E.; Cazorla-Amorós, D.; Béguin, F.; Lozano-Castelló, D. New Insights on Electrochemical Hydrogen Storage in Nanoporous Carbons by in Situ Raman Spectroscopy. *Carbon* **2014**, *69*, 401–408.
- (59) Leyva-García, S.; Nueangnoraj, K.; Lozano-Castelló, D.; Nishihara, H.; Kyotani, T.; Morallón, E.; Cazorla-Amorós, D. Characterization of a Zeolite-Templated Carbon by Electrochemical Quartz Crystal Microbalance and in Situ Raman Spectroscopy. *Carbon* **2015**, *89*, 63–73.
- (60) Dresselhaus, M. S.; Jorio, A.; Saito, R. Characterizing Graphene, Graphite, and Carbon Nanotubes by Raman Spectroscopy. *Annu. Rev. Condens. Matter Phys.* **2010**, *1* (1), 89–108.
- (61) Voggu, R.; Rout, C. S.; Franklin, A. D.; Fisher, T. S.; Rao, C. N. R. Extraordinary Sensitivity of the Electronic Structure and Properties of Single-Walled Carbon Nanotubes to Molecular Charge-Transfer. *J. Phys. Chem. C* **2008**, *112* (34), 13053–13056.
- (62) Gupta, R.; Singh, B. P.; Singh, V. N.; Gupta, T. K.; Mathur, R. B. Origin of Radial Breathing Mode in Multiwall Carbon Nanotubes Synthesized by Catalytic Chemical Vapor Deposition. *Carbon* **2014**, *66*, 724–726.
- (63) Ruiz-Soria, G.; Susi, T.; Sauer, M.; Yanagi, K.; Pichler, T.; Ayala, P. On the Bonding Environment of Phosphorus in Purified Doped Single-Walled Carbon Nanotubes. *Carbon* **2015**, *81*, 91–95.
- (64) Wang, P.-C.; Liao, Y.-C.; Lai, Y.-L.; Lin, Y.-C.; Su, C.-Y.; Tsai, C.-H.; Hsu, Y.-J. Conversion of Pristine and P-Doped Sulfuric-Acid-Treated Single-Walled Carbon Nanotubes to n-Type Materials by a Facile Hydrazine Vapor Exposure Process. *Mater. Chem. Phys.* **2012**, *134* (1), 325–332.



The background features a complex abstract design. On the left, there is a vertical black bar with a red stripe on its right edge. To its left are a checkered square pattern, a black circle, and a textured, fan-like shape. In the top left corner, there are several parallel diagonal lines. The right side of the page is decorated with a vertical stack of black circles and a larger black circle at the bottom right. The title text is centered in the upper right quadrant.

Chapter 4
Effect of Surface Oxygen
Groups in the
Electrochemical
Modification of Multi-Walled
Carbon Nanotubes by
4-Amino Phenyl
Phosphonic Acid

Universidad de Alicante
Universidad de Alicante

1. Introduction

Carbon nanotubes (CNTs) have attracted important attention over the last decades in many scientific and nanotechnology applications, due to the remarkable chemical stability, biocompatibility, catalytic and electronic properties¹. These carbon materials can be modified through non-covalent or covalent interactions in the tip and/or the sidewall of the nanotubes¹⁻³. Nowadays, tailoring the type of surface functionalities incorporated is desirable in order to develop new properties in the CNTs and improve their application in different areas like electrocatalysis and biosensing, for example⁴⁻⁶. CNTs functionalization through covalent or non-covalent methods can be a route for carbon material heteroatom doping (i.e., insertion of heteroatoms in the carbon structure); for example, by applying further heat treatments.

Heteroatom doping of the carbon surface is a promising method for modifying the properties of carbon materials, which has brought remarkable improvement, for example, in the electrocatalytic behavior towards oxidation-reduction reactions, such as oxygen evolution reaction (OER)^{7,8}, oxygen reduction reaction (ORR)^{8,9} and hydrogen evolution reaction (HER)^{8,10}. Surface modification of CNTs with nitrogen groups has been widely studied. The unique structure and surface properties of nitrogen-doped carbon nanotubes leads to a better dispersion of Pt that produces higher catalytic activity toward ORR¹¹. Additionally, recent studies have proved the high catalytic activity for ORR of N-doped carbon materials, rising as a promising alternative in the development of catalysts for fuel cells⁹. Oxygen, nitrogen and phosphorus-doping are promising candidates to introduce functionalities, which can increase the active sites for different reactions^{12,13}. Regarding P-doping of carbon materials, Berenguer et al. showed an important improvement in the stability of activated carbons towards electrochemical oxidation¹⁴.

Carbon materials functionalization can be done through covalent and non-covalent methods¹⁻³. Covalent functionalization methods employ conditions that may generate important structural changes, which can either deteriorate their structure or inhibit some of their properties. Non covalent functionalization methods are the preferred methods when it is necessary to maintain the electronic properties of the CNT.

Chemical methods are the most used for CNT functionalization. In these methods, usually the CNT are oxidized to incorporate oxygen functionalities. It can be carried out using wet methods (for example nitric acid water solutions) or dry oxidation methods where the carbon surface is exposed to an oxidizing gas, usually air, at mild temperatures². Subsequently, those functionalities are either directly used or employed as intermediates to apply different organic chemistry routes, for example to introduce acyl-chloride groups and further substitution by other groups such as amines; which are useful for the grafting of other molecules, immobilization of bioreceptor elements such as DNA or the complexation of metals for sensing and electroanalysis applications¹⁵⁻¹⁸. Fluorination, hydrogenation, esterification, alkylation and cycle-addition and functionalization via in situ diazonium compounds, are other examples that can be found for CNTs surface chemistry modification^{2,19-21}. Nevertheless, chemical functionalization involves in most of the cases aggressive conditions (i.e., oxidative media), high temperature, toxic chemical reagents, etc., which in some cases produce non-controlled functionalization degree and might promote the damaging and collapse of the CNT structure²².

On the other hand, electrochemically assisted modification of carbon materials has emerged in the last two decades as a flexible, simple and effective tool for controlled functionalization of carbon materials². These methods are a promising alternative for functionalization and grafting of molecules in carbon materials, obtaining high selectivity towards the desired functional group without damage of the CNT structure^{6,23}.

Considering the importance to develop procedures for CNTs surface functionalization, which can provide controlled and non-damaging modification of CNT, in this study we use electrochemical methods for surface functionalization of multi-walled carbon nanotubes (MWCNTs) by electrochemical oxidation in presence of 4-amino phenyl phosphonic acid (4-APPA) in aqueous solution. This will permit to incorporate both N and P heteroatoms on the MWCNTs which are of great interest for different applications. In addition, we have studied the effect of the surface oxygen groups of the MWCNTs on the functionalization. The results show that the degree of functionalization, electroactivity and stability of the different incorporated functionalities, is very much dependent on the surface oxygen groups present in the MWCNTs surface.

2. Experimental

2.1. Reagents and materials

Multi-Walled Carbon Nanotubes with purity 95% (8 nm of diameter) with 10-30 μm length were purchased to Cheap Tubes Inc. (Cambridgeport, USA). Nitric acid (65%) from Panreac was employed to incorporate surface oxygen groups in the MWCNTs and also to remove the metal impurities in the CNTs. N, N-Dimethylformamide (DMF), extra pure, was provided by Scharlau and used as solvent to disperse the non-oxidized CNTs.

Sulphuric acid (98%) analytical reagent to prepare the electrolyte, was obtained by VWR Chemicals. 4-amino phenyl phosphonic acid (4-APPA, +98%) used as modifier agent was purchased from Tokyo Chemical Industry co (TCI). Potassium dihydrogen phosphate (KH_2PO_4) was obtained from Merck. Dipotassium hydrogen phosphate tri hydrate ($\text{K}_2\text{HPO}_4 \cdot 3\text{H}_2\text{O}$) and Potassium Hydroxide (KOH, 85%) were purchased from VWR Chemicals, respectively. All the solutions were prepared using ultrapure water (18 $\text{M}\Omega$ cm, Purelab Ultra Elga equipment). The gases N_2 (99.999%) and H_2 (99.999%) were provided by Air Liquide.

2.2. Electrochemical incorporation of phosphorus and nitrogen functionalities on CNTs

2.2.1. Oxidation of pristine Multi-Walled Carbon Nanotubes

MWCNTs were subjected to oxidation with nitric acid solution, according to the following procedure. In a two-necked, round-bottom flask, 200 mg of MWCNT were added in 100 mL of 3 M HNO_3 at 120°C for 24 hours under reflux conditions. MWCNTs were separated after 24 hours, filtered, washed with ultrapure water until the pH was neutral and dried in vacuum at 60°C for 24 hours, and weighed. The sample was named as fMWCNTs.

2.2.2. Functionalization of MWCNTs and fMWCNTs with 4-APPA

Working electrode was prepared using 1 mg mL^{-1} of a dispersion of each type of CNTs. DMF was used for MWCNTs and water for fMWCNTs, because the presence of surface oxygen groups improves the dispersibility in aqueous solution. Prior to the deposition of CNTs, glassy carbon electrode

surface (3 mm diameter) was sanded with emery paper and polished using 1 and 0.05 μm alumina slurries and then rinsed with ultrapure water. Afterwards, 10 μL aliquot of the dispersion was dropped onto the glassy carbon (GC) surface and dried under an infrared lamp to remove the solvent.

Electrochemical modification was performed by cyclic voltammetry in presence of 4-APPA, using an eDAQ Potentiostat (EA163 model) coupled to a wave generator (EG&G Parc Model 175) and the data acquisition was done with an eDAQ e-corder 410 unit (Chart and Scope Software), using a standard three-electrode cell configuration. The CNTs were the working electrode (WE), a graphite rod was used as counter electrode (CE) and a reversible hydrogen electrode (RHE) introduced in the same electrolyte without 4-APPA, was the reference electrode (RE). Electrochemical modification was carried out in 0.5 M H_2SO_4 + 1 mM 4-APPA aqueous solution in a deoxygenated cell by bubbling nitrogen. The CNTs were submitted to 10 cycles at 10 mV s^{-1} by cyclic voltammetry using different positive potential limits. After electrochemical treatment, carbon electrodes were washed with excess of water, removing the remaining electrolyte.

2.2.3. *Electrochemical characterization*

Electrochemical behavior of the CNTs functionalized with 4-APPA were evaluated in 0.5 M H_2SO_4 solution without 4-APPA, employing a three-electrode configuration cell. The potential range was fixed between 0 and 1.0 V vs. RHE at 50 mV s^{-1} .

2.3. *Physicochemical characterization*

X-Ray photoelectron spectroscopy (XPS) was performed in a VG-Microtech Mutilab 3000 spectrometer and Al $\text{K}\alpha$ radiation (1253.6 eV). The deconvolution of the XPS P2p and N1s peaks was done by least squares fitting using Gaussian-Lorentzian curves, while a Shirley line was used for the background determination. The P2p spectra have been analyzed considering the spin-orbit splitting into P2p_{3/2} and P2p_{1/2} with a 2:1 peak area ratio and 0.87 eV splitting²⁴.

Transmission electron microscopy measurements (TEM) were carried out using JEOL TEM, JEM-2010 model, INCA Energy TEM 100 model, and GATAN acquisition camera.

Temperature programmed desorption (TPD) experiments were performed in a DSC-TGA equipment (TA Instruments, SDT 2960 Simultaneous) coupled to a mass spectrometer (Thermostar, Balzers, GSD 300 T3) which was used to follow the m/z lines ascribed to the decomposition of surface functional groups from the surface of the carbon materials. The thermobalance was purged for 2 hours under a helium flow rate of 100 mL min^{-1} and then heated up to 950°C (heating rate $20^\circ\text{C min}^{-1}$).

The textural properties of the materials have been evaluated by N_2 adsorption isotherms at -196°C in an automatic adsorption system (Autosorb-6, Quantachrome). Prior to the measurements, the samples were degassed at 250°C for 4 h. Apparent surface areas have been determined by BET method (S_{BET}) and total micropore volumes (pores of size $< 2 \text{ nm}$) have been assessed by applying the Dubinin-Radushkevich (DR) equation to the N_2 adsorption isotherms. Mesoporous volume (V_{meso}) was determined from the difference between the volume of microporous (V_{DR}) and the volume adsorbed at a relative pressure of 0.9.

Raman spectra were collected with a Jasco NRS-5100 spectrometer. A 3.9 mW He-Ne laser at 633 nm was used. The spectra were acquired for 120 s. The detector was a Peltier cooled charge coupled device (CCD) (1024×255 pixels). Calibration of the spectrometer was performed with a Si slice ($521 \pm 2 \text{ cm}^{-1}$).

3. Results and discussion

3.1. Physicochemical characterization of pristine MWCNTs and fMWCNT

MWCNTs and fMWCNTs were studied by temperature programmed desorption (TPD) in order to analyze the surface oxygen groups incorporated during the oxidation with HNO_3 . Figure 4.1 shows the evolution of CO and CO_2 during the TPD for pristine MWCNTs and fMWCNTs. Table 4.1 reports the amount of CO and CO_2 desorbed, as well as the total oxygen amount (calculated as $\text{CO} + 2\text{CO}_2$) obtained from the TPD experiments for both samples. In the case of pristine MWCNTs CO and CO_2 desorptions are very small and can be associated with the presence of some surface oxygen groups, most of them, at the end-tips of the CNTs. In the case of fMWCNT, the oxidation treatment increases the amount of surface oxygen groups, as

deduced from the increase of CO and CO₂ evolution. Surface oxygen groups decompose as CO₂ between 200-400°C, 400-550°C and 700-900°C associated with carboxylic acid, anhydrides and lactones, respectively²⁵⁻²⁷. The CO profile of fMWCNT shows main desorption peaks above 600°C associated with phenol and carbonyl/quinone groups²⁵⁻²⁹. The contribution below 600°C corresponds to anhydrides^{27,29}. The results from the nitric acid treatment are in agreement with previous studies from our research group²⁹ and the abundant literature regarding wet oxidation of porous carbons (See for example, references^{25,26,28}).

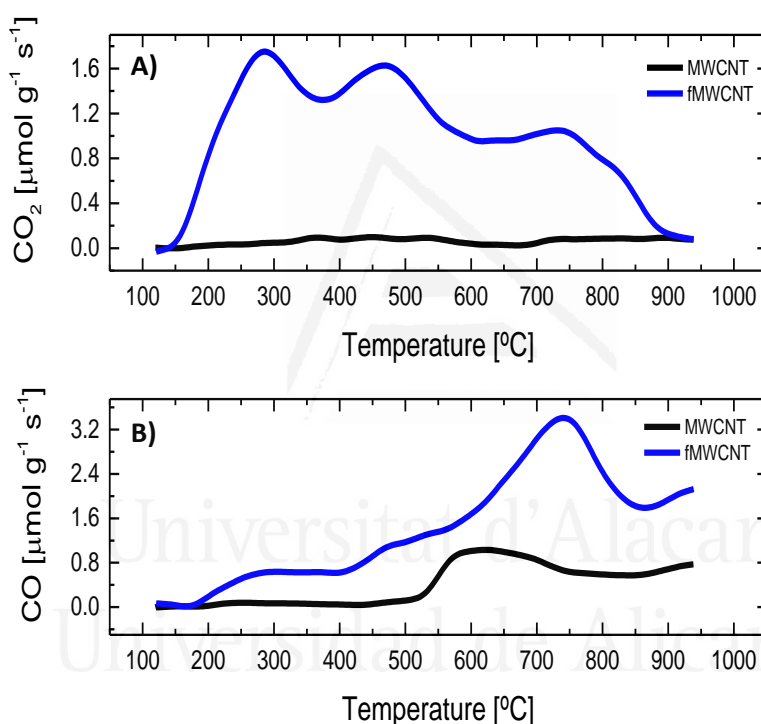


Figure 4.1. TPD profiles for: A) CO₂ and B) CO for pristine MWCNTs and fMWCNTs.

Additionally, this oxidation treatment causes an increase in the specific surface of the MWCNTs from 208 m² g⁻¹ for pristine MWCNTs to 460 m² g⁻¹ for fMWCNTs as can be observed in the N₂ isotherms in Figure 4.2 and Table 4.1.

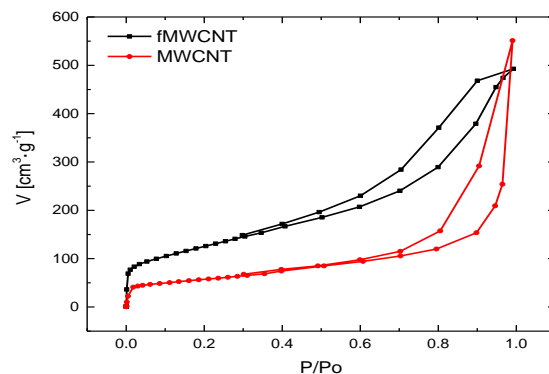


Figure 4.2. N₂ adsorption isotherms at -196 °C for MWCNTs and fMWCNTs samples.

Table 4.1. Porous texture and surface chemistry characterization for both carbon nanotubes.

| Surface chemistry | | | |
|---------------------|---|---|---|
| Sample | CO ₂ / μmol g ⁻¹ | CO / μmol g ⁻¹ | Total O / μmol g ⁻¹ |
| MWCNT | 148 | 954 | 1250 |
| fMWCNT | 2477 | 3502 | 8456 |
| Textural properties | | | |
| Sample | S _{BET} / m ² g ⁻¹ | V _{DR} (N ₂) / cm ³ g ⁻¹ | V _{meso} (N ₂) / cm ³ g ⁻¹ |
| MWCNT | 208 | 0.08 | 0.29 |
| fMWCNT | 460 | 0.18 | 0.57 |

3.2. Electrochemical modification with 4-APPA

Optimal electrochemical functionalization conditions for MWCNTs and fMWCNTs with 4-amino phenyl phosphonic acid were established by step-wise opening of the upper potential limit of the cyclic voltammogram from 0.8 to 1.8 V, in presence and absence of the 4-APPA (Figure 4.3).

The voltammograms for MWCNT until 1.2 V present the typical rectangular-shape capacitive behavior with lack of redox processes^{30,31}; however, when the upper potential limit increases over 1.4 V, oxidation/reduction processes appear at around 0.6 V, which can be associated with the surface oxygen groups produced during the oxidation of the CNTs at high potentials³². In contrast, fMWCNTs present from the first cycle the oxidation/reduction processes at around 0.6 V, which are related with the surface oxygen groups produced with the nitric acid treatment^{29,32}. In this case,

treatment with nitric acid solution induces the formation of different oxygen functionalities, among which quinone species have electrochemical activity at those potential ranges²⁹. Interestingly, negligible increase in the current of these processes is observed when the upper potential limit increases; suggesting that additional oxidation of the fMWCNTs during the electrochemical treatment is not significant.

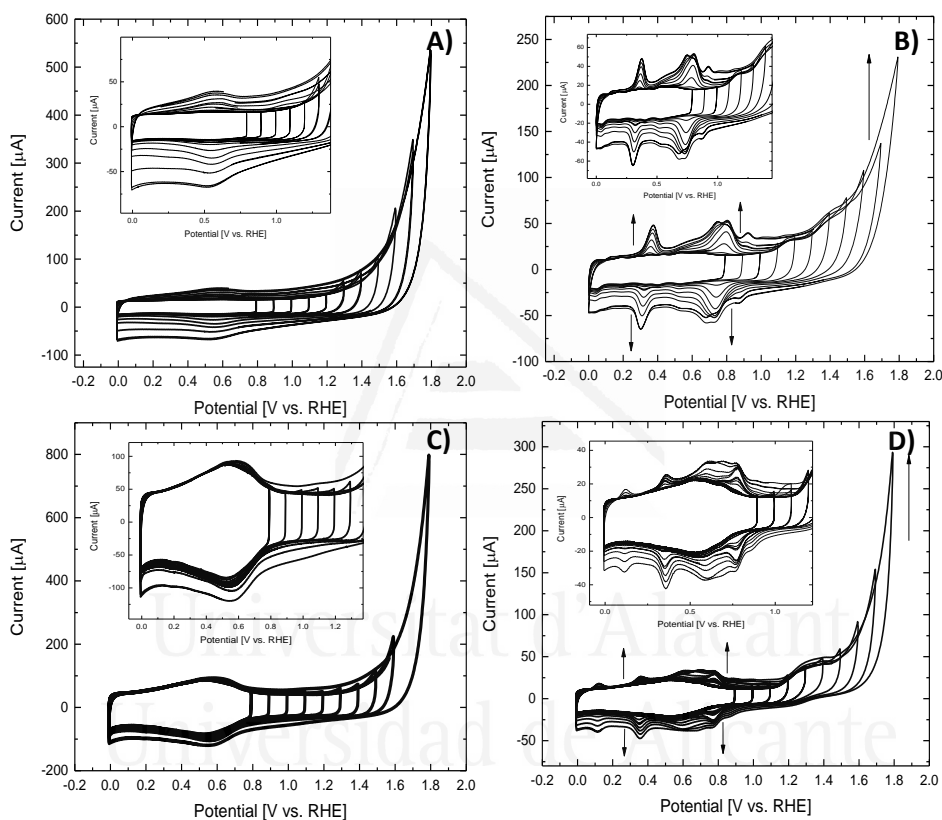


Figure 4.3. Cyclic voltammograms of the open step-wise positive potential limit for: A) MWCNT in 0.5 M H_2SO_4 , B) MWCNT in 0.5 M H_2SO_4 + 1 mM 4-APPA, C) fMWCNT in 0.5 M H_2SO_4 and D) fMWCNT in 0.5 M H_2SO_4 + 1 mM 4-APPA.

Once, 4-APPA is incorporated in the electrolyte (Figures 4.3-B and 4.3-D), no variation of the electrochemical behavior for both carbon nanotube samples occurs until 1.0 V. When the potential increases to values higher than 1 V, an over oxidation current at higher potentials occurs and different redox processes are observed in the voltammograms at around 0.75, 0.31 and 0.12 V,

suggesting the formation of different electrochemical species from the 4-APPA oxidation. Continuous increase in the upper potential limit generates other redox processes in the whole voltammogram, which at the same time shows an important increase in the electric charge with cycling.

From these results, the direct oxidation of both CNTs was performed with different samples in absence (black line) and presence (red line) of the 4-APPA in the electrolyte and at different positive potential limits (Figures 4.4 and 4.5).

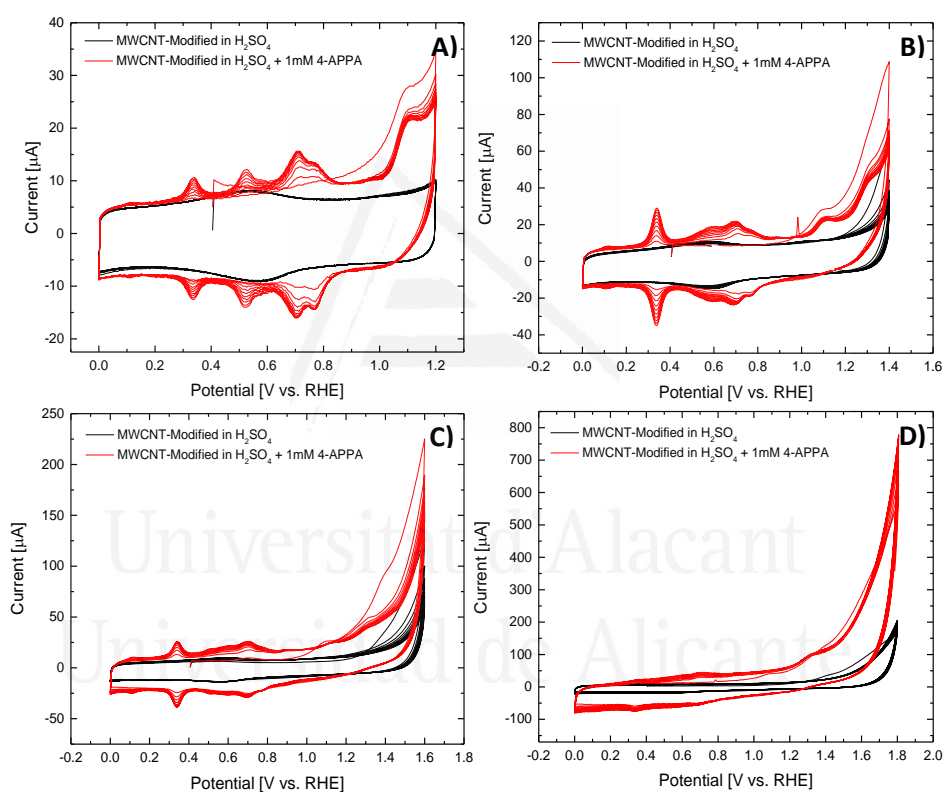


Figure 4.4. Electrochemical functionalization of MWCNT in 0.5 M H_2SO_4 (Black line) and 0.5 M H_2SO_4 + 1 mM 4-APPA (Red line) at 10 mV s^{-1} , 10 cycles under N_2 atmosphere at different potentials: A) 1.2, B) 1.4, C) 1.6 and D) 1.8 V.

Interestingly, both CNTs show the formation of different redox processes during the oxidation of 4-APPA, and the increase in their current with cycling. It is well-known that oxidation of substituted anilines produces the

polymerization of the molecule through the formation of aniline-type polymers^{33,34}. Then, the oxidation of 4-APPA can promote the formation of species that can be covalently anchored on the CNT surface or oligomers, composed of more than two molecules of 4-APPA, that interact with the surface of the CNTs through non-covalent interaction. However, the electrochemical homopolymerization of 4-APPA on platinum electrodes is not produced, being necessary the copolymerization with aniline³⁵

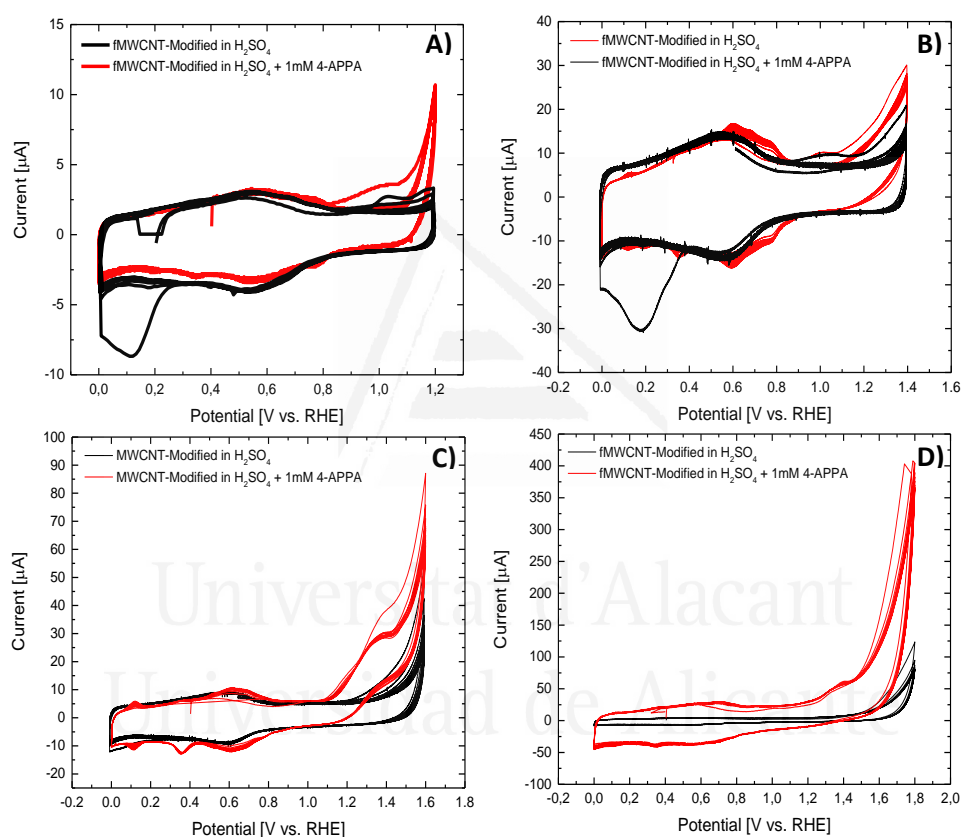


Figure 4.5. Electrochemical functionalization of fMWCNT in 0.5 M H_2SO_4 (Black line) and 0.5 M H_2SO_4 + 1 mM 4-APPA (Red line) at 10 mV s^{-1} , 10 cycles under N_2 atmosphere at different potentials: A) 1.2, B) 1.4, C) 1.6 and d) 1.8 V.

In this sense, Figure 4.6 shows the cyclic voltammograms obtained during the subsequent characterization of the different modified MWCNTs and fMWCNTs electrodes in acid media. Interestingly, well defined redox peaks

observed at high potential (processes B and C) in the electrochemically modified MWCNTs do not appear in the electrochemically modified fMWCNTs, where only process A is clearly distinguished. In this last case, an increase in the charge is observed with respect to the fMWCNT treated up to the same potential limit; however, the shapes of the voltammograms are similar to that of the fMWCNTs. These results indicate that the presence of the surface oxygen groups in the fMWCNTs affects the electrochemical oxidation of 4-APPA and the interaction with the CNT surface.



Universitat d'Alacant
Universidad de Alicante

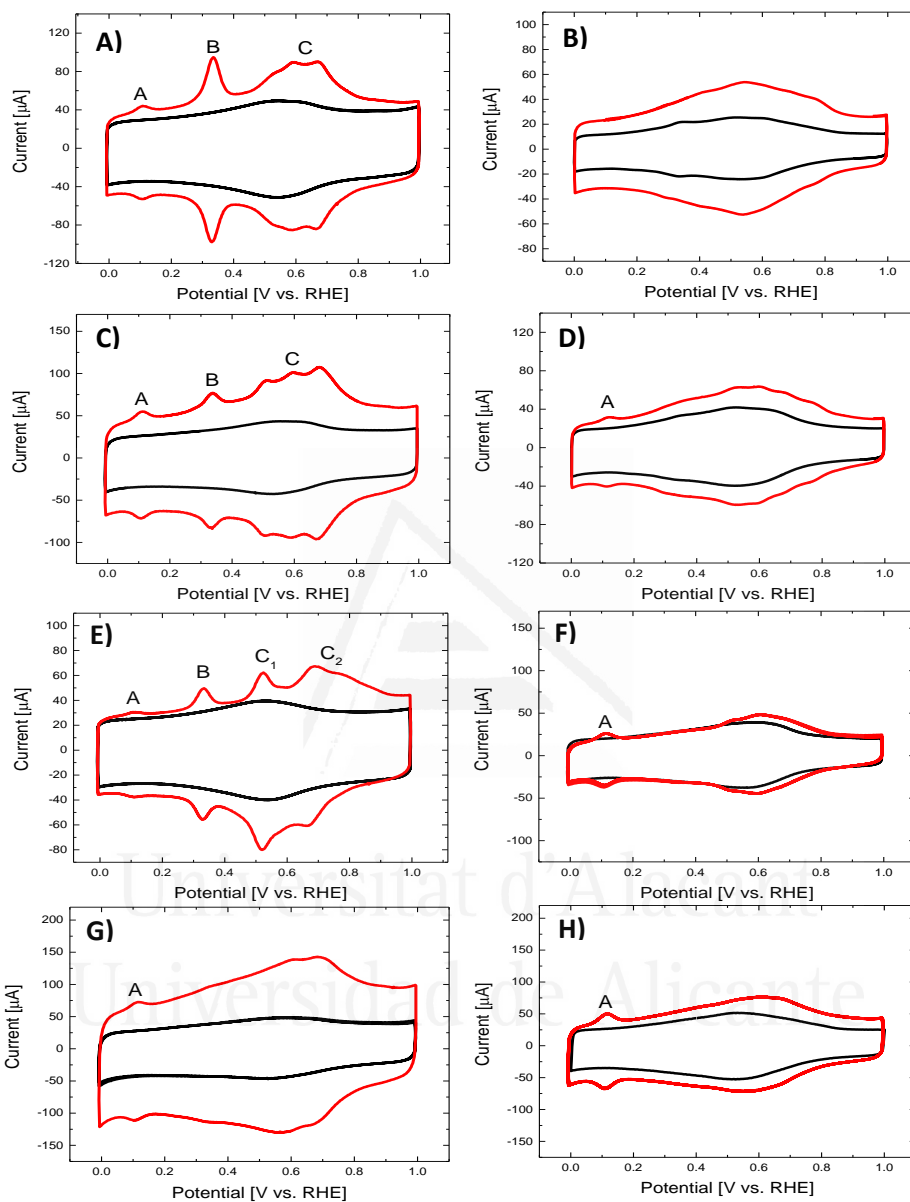


Figure 4.6. Cyclic voltammograms in 0.5 M H_2SO_4 at 50 mV s^{-1} of both CNTs after electrochemical modification in absence (black line) and presence (red line) of 4-APPA: A) MWCNTs modified at 1.2 V, B) fMWCNTs modified at 1.2 V, C) MWCNTs modified at 1.4 V, D) fMWCNTs modified at 1.4 V, E) MWCNTs modified at 1.6 V, F) fMWCNTs modified at 1.6 V, G) MWCNTs modified at 1.8 V, and H) fMWCNTs modified at 1.8 V.

As has been proposed for SWCNT, two different phenomena can be considered during the electrochemical oxidation in presence of 4-APPA. The first one, could be associated with a covalent attachment of the amino phenyl phosphonic acid onto the carbon nanotube through the formation of C_{CNT-N} . The second one phenomenon that can occur during the electrochemical functionalization, is the formation and growing of different oligomers, which can interact with the carbon nanotube walls. At the conditions used in the electrochemical oxidation, the phosphonic and the amine groups are protonated and the interaction with the surface of pristine MWCNT should mainly occur through π - π interactions between the aromatic ring of the 4-APPA molecule and the surface of the CNTs³⁶, what may favor oligomerization reactions, thus producing electroactive species as observed in the voltammograms. In the case of the oxidized MWCNT, the presence of surface oxygen groups decreases the point of zero charge of the fMWCNT sample what would favor 4-APPA adsorption. However, the presence of electron withdrawing oxygen groups decreases the π electron density of the fMWCNT and, consequently the dispersive potential, what may result in an important decrease in 4-APPA adsorption, since the adsorption of aromatic compounds in carbon materials may be determined by dispersive forces³⁷. In addition, the surface oxygen groups may also modify the orientation of the 4-APPA molecule, thus reducing the incorporation of 4-APPA parallel to the surface of the CNTs. All these factors contribute to impeding the oligomerization reaction.

The current peak of the different redox processes observed in the voltammograms of the MWCNTs and fMWCNTs functionalized with 4-APPA (See Figure 4.7 and 4.8), shows a linear-dependence with the scan rate what indicates that redox processes are surface-controlled processes³⁸. At the same time, the values of the peak potential separation for all the redox processes are lower than 50 mV and the ratio of the peak currents (I_{ox}/I_{red}) is near 1 for redox processes B and C (See Table 4.2) suggesting a reversible behavior. Slope of the linear-fitting with the scan rate (v_{scan}) can be associated with the coverage of the active species on the surface³⁸. The decrease in the slope with the potential (See Figure 4.8), observed in process B for MWCNTs, suggests that a high oxidation potential over 1.4 V causes a decrease in the concentration of the surface species. This could be a consequence of an over oxidation of those species generated during the electrochemical functionalization onto the CNTs.

Thus, in the case of the oxidation in absence of 4-APPA, the no appearance of clear redox processes in the voltammograms indicates the formation pseudocapacitive processes due to electroactive species with slightly different energy formed at the MWCNT surface, that is, electroactive oxygen functional groups. However, in presence of 4-APPA and for pristine MWCNTs, a highly homogenous material seems to be formed what is in agreement with oligomerization. Some contribution from covalent 4-APPA molecules attachment on the CNT wall should not be discarded in both cases although the heterogeneity of the different sites where the reaction may occur would produce wider peaks.

Table 4.2. Electrochemical parameters for the different electrochemical processes on carbon nanotubes modified with 4-APPA at different potentials in 0.5 M H₂SO₄.

| Carbon nanotube | Upper potential limit [V vs. RHE] | E ^A [mV] | E ^B [mV] | E ^C [mV] | I ^{ox} /I ^{red} _A | I ^{ox} /I ^{red} _B |
|-----------------|-----------------------------------|---------------------|---------------------|---------------------|--|--|
| MWCNT | 1.2 | 1.5 | 4.9 | -- | 0.81 | 0.88 |
| | 1.4 | 3.4 | 6.1 | -- | 0.83 | 0.97 |
| | 1.6 | 5.0 | 4.5 | -- | 0.76 | 0.91 |
| | 1.8 | 10 | -- | -- | 0.65 | -- |
| fMWCNT | 1.2 | -- | 5.5 | 11.4 | -- | 1 |
| | 1.4 | 4.2 | 7.1 | 13.9 | 0.76 | 0.96 |
| | 1.6 | 8.0 | 8.2 | 0 | 0.72 | 1 |
| | 1.8 | 8.0 | -- | -- | 0.72 | -- |

All the values were determined for the CVs at $v_{\text{scan}} = 50 \text{ mV s}^{-1}$.

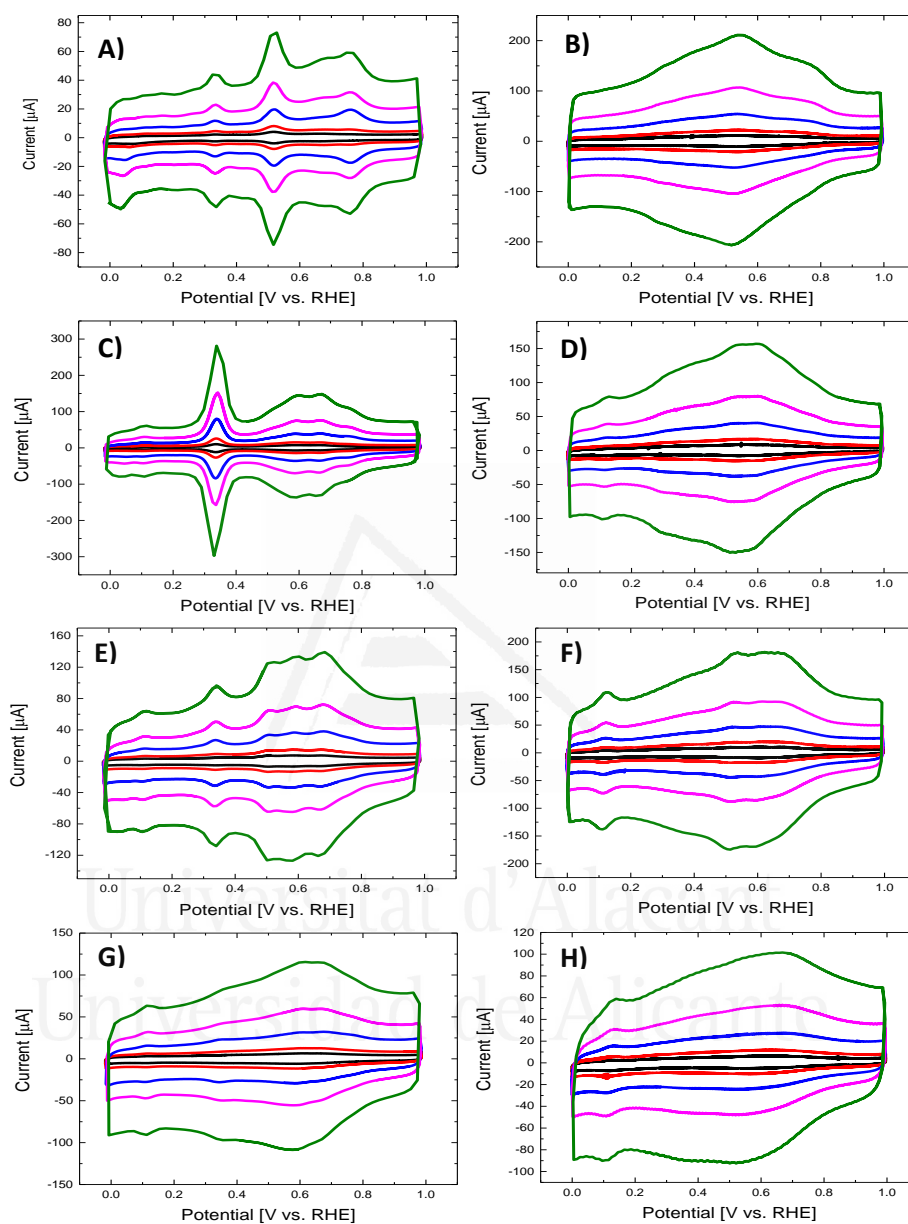


Figure 4.7. Cyclic voltammograms in 0.5 M H_2SO_4 at different v_{scan} (black: 10, red: 20, blue: 50, pink: 100 and green: 200 mV s^{-1}) after electrochemical modification with 4-APPA for: A) MWCNTs modified at 1.2 V, B) fMWCNTs modified at 1.2 V, C) MWCNTs modified at 1.4 V, D) fMWCNTs modified at 1.4 V, E) MWCNTs modified at 1.6 V, F) fMWCNTs modified at 1.6 V, G) MWCNTs modified at 1.8 V, and H) fMWCNTs modified at 1.8 V.

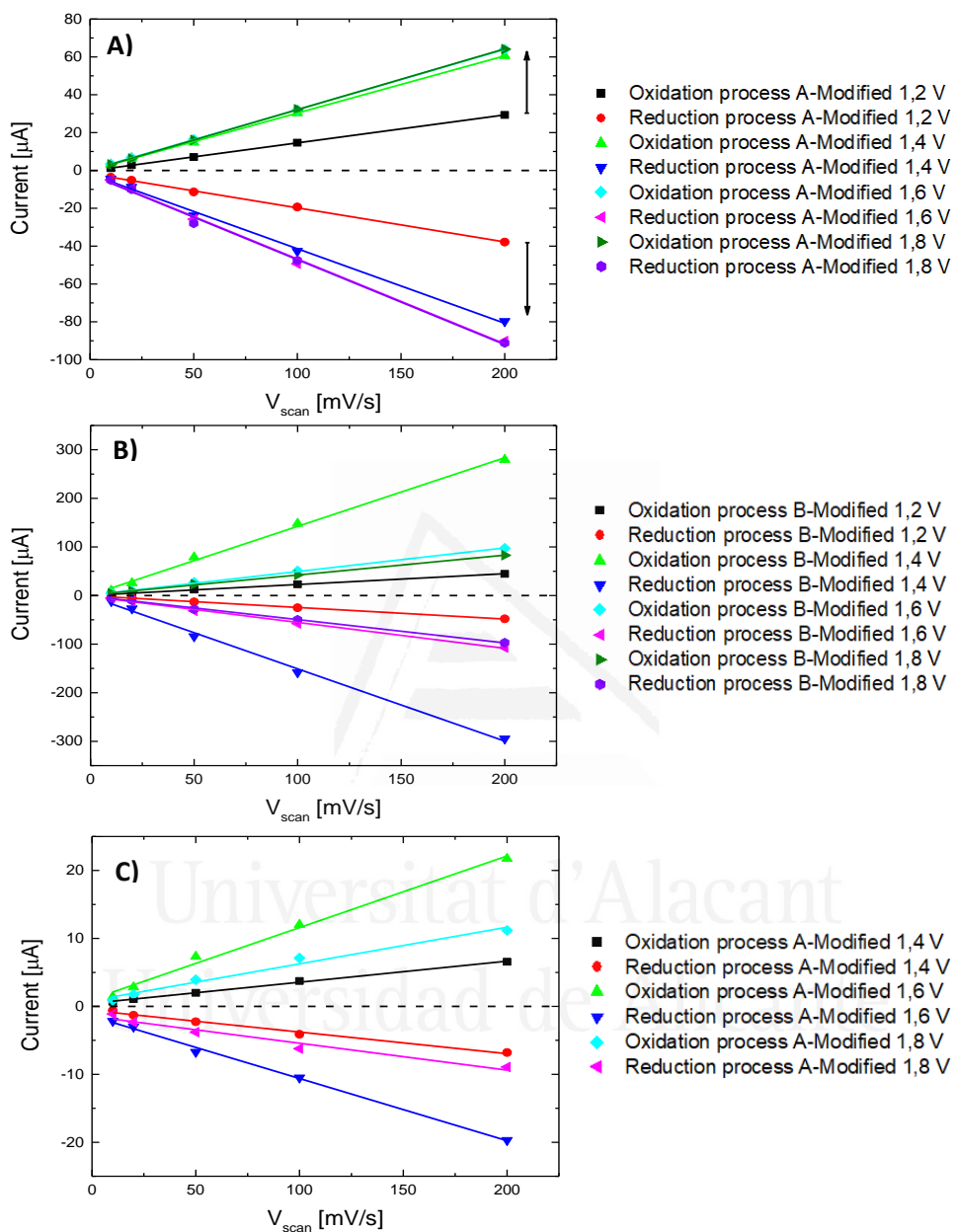


Figure 4.8. Plot of cathodic and anodic peaks vs. v_{scan} for process A and B in different carbon nanotubes electromodified at different potential with 4-APPA in 0.5 M H_2SO_4 : A) Process A of MWCNTs, B) Process B of MWCNTs and C) Process A of fMWCNTs.

3.3. Morphological characterization

Figure 4.9 shows the TEM images of the pristine MWCNTs, the fMWCNTs and after electrochemical functionalization at different potentials.

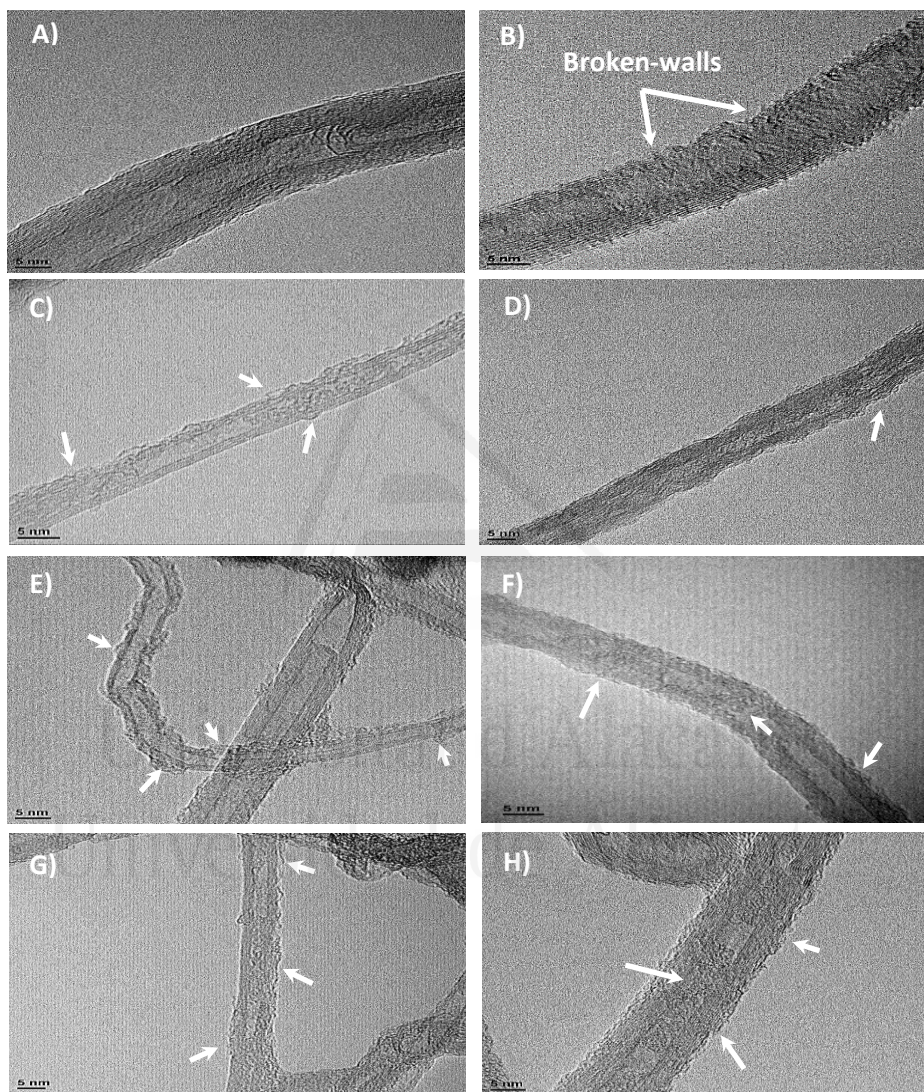


Figure 4.9. TEM images of: A) MWCNTs, B) fMWCNTs, C) MWCNTs modified at 1.2 V, D) fMWCNTs modified at 1.2 V, E) MWCNTs modified at 1.6 V, F) fMWCNTs modified at 1.6 V, G) MWCNTs modified at 1.8 V and H) fMWCNTs modified at 1.8 V. All the modified CNT in presence of 4-APPA.

Pristine MWCNTs in Figure 4.9-A show a typical tubular shape; on the other hand, fMWCNTs, which were oxidized with nitric acid, present important morphological changes with high amount of wall defects, as can be observed in Figure 4.9-B, where broken-walls can be found. These results are in agreement with the N₂ adsorption results in which the BET surface area increases with the nitric acid treatment. Then, this treatment may permit that the inner side of the nanotubes could be accessible to the electrolyte.

Figures 4.9-C to 4.9-H show the TEM images of the CNTs modified by electrochemical oxidation in presence of 4-APPA at different upper potential limits. The formation of agglomerates can be clearly observed onto the surface of samples MWCNT in all the positive potential limits used. These agglomerates are clearly observed in the MWCNTs surface compared to fMWCNTs, suggesting that oligomer chains are formed during the electrochemical modification with the 4-APPA, which can be anchored and adsorbed on the surface of the MWCNTs. Interestingly, no important structural changes, as broken-walls in the graphene layers of the MWCNT sample can be observed, suggesting that despite the oxidative conditions used during the electrochemical modification most of the oxidation occurs in the 4-APPA molecules which have higher reactivity.

In the case of fMWCNTs the same structures surrounding the CNT walls are also observed although in lower quantities; however, in these samples, the presence of these oligomers seem to be also observed in some cases inside the nanotubes (Figures 4.9-F and 4.9-H), what is in agreement with the wall discontinuities observed for this material that permit the monomer and electrolyte molecules to enter into the inner part of the fMWCNT.

3.4. XPS characterization

Incorporation of different species on the CNTs surface was studied by XPS analysis. Table 4.3 summarizes the amount of O, N and P incorporated in the CNTs.

Table 4.3. Composition obtained from XPS of the electrochemical modified MWCNTs and fMWCNT with 4-APPA at different positive potentials.

| Carbon nanotube | Upper potential limit [V vs. RHE] | O (at%) | N (at%) | P (at%) |
|------------------------|--|----------------|----------------|----------------|
| MWCNT | Pristine | 1.79 | 0.0 | 0.0 |
| | 1.2 | 2.53 | 0.49 | 0.25 |
| | 1.4 | 5.35 | 0.97 | 0.58 |
| | 1.6 | 7.00 | 1.05 | 0.46 |
| | 1.8 | 10.64 | 1.10 | 0.27 |
| fMWCNT | Pristine | 8.60 | 0.65 | 0.02 |
| | 1.2 | 9.30 | 0.89 | 0.15 |
| | 1.4 | 13.68 | 2.17 | 0.82 |
| | 1.6 | 10.28 | 1.56 | 0.47 |
| | 1.8 | 13.67 | 1.90 | 0.43 |

Oxygen content increases with the upper potential limit in modified MWCNTs sample. This can be understood considering that, at the same time that functionalization and oligomer-chains formation take place, oxidative conditions promote the over oxidation of the oligomers and of the CNT in some extent. However, in the case of fMWCNTs the oxygen content seems to reach a maximum value for oxidation potentials above 1.4 V. Due to the initial strong degree of oxidation of this material, the incorporation of further oxygen species is smaller compared to the MWCNTs sample which has an initial low oxygen content (Table 4.3). In the case of nitrogen content, it reaches a maximum value for oxidation potentials above 1.4 V for both CNTs samples. On the contrary, phosphorus species show a maximum value of concentration at 1.4 V, for both materials. Therefore, a desorption or decomposition process of the phosphorus groups take place at higher upper potential limits probably due to oxidation of phosphonic groups followed by hydrolysis reactions.

Figure 4.10 presents the XPS spectra for the CNTs modified at different positive potentials. Both CNTs show a N1s signal that can be deconvoluted into two or three contributions, which relative intensity is dependent on the functionalization potential. The three contributions observed appear at 398.5,

400 and 402.2 eV. The first and second can be assigned to imine and amine species, respectively, related to the formation of oligomers similar to polyaniline structure^{39,40}. The peak at 402.2 eV appears for oxidation potentials over 1.2 V for the MWCNTs and increases with increasing the oxidation potential. It can be associated with oxidized and positively charged nitrogen species formed from the over oxidation of the oligomers at these high potentials. This tendency is also observed for the modified fMWCNTs sample; however, it must be noted that this material already contains N corresponding mainly to oxidized N species due to the nitric acid oxidation pretreatment (See Table 4.1), what explains that this peak is also observed for the lowest oxidation potential used.



Universitat d'Alacant
Universidad de Alicante

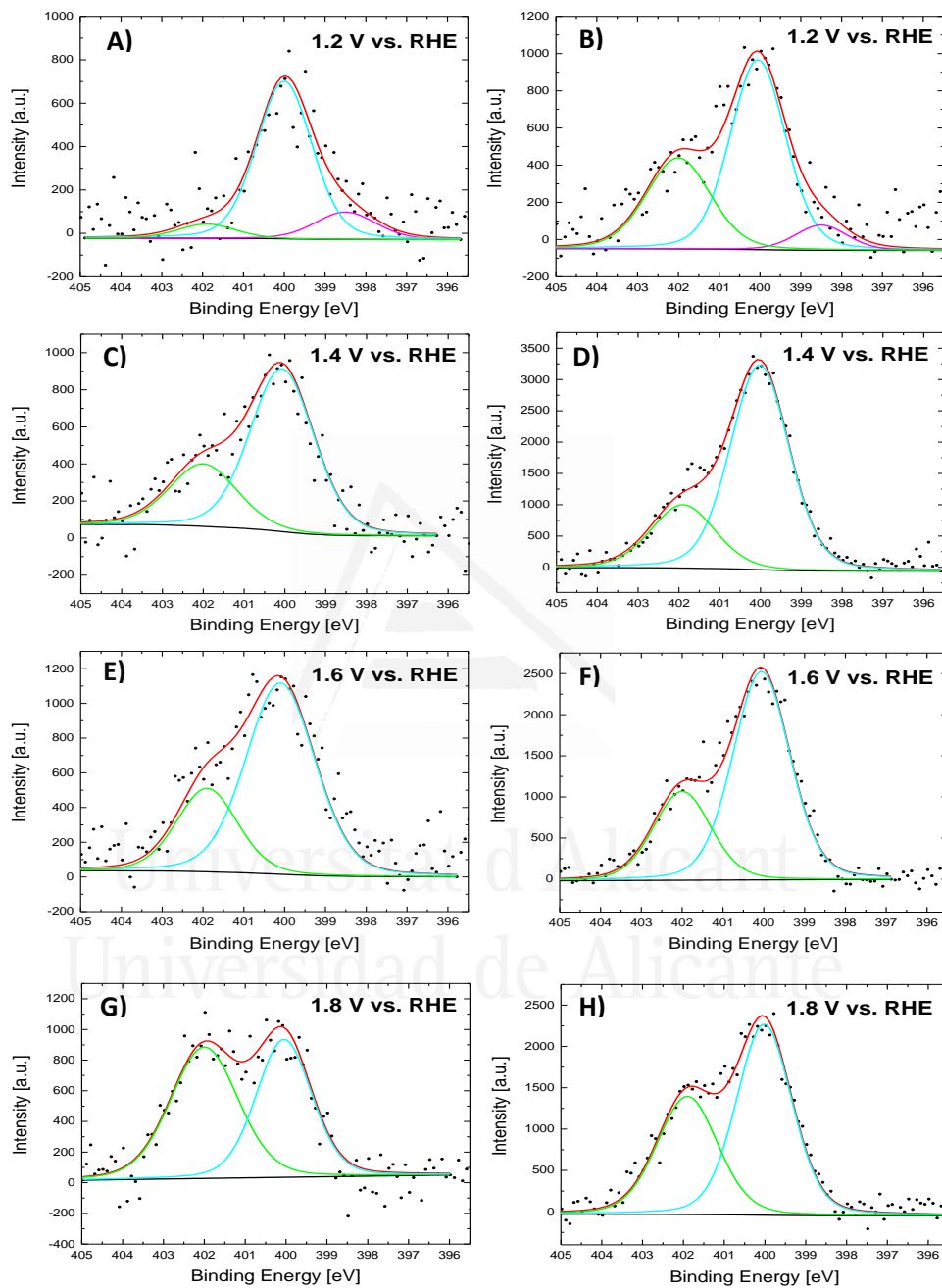


Figure 4.10. N1s XPS spectra for CNT electrochemically modified with 4-APPA at different applied potentials: A), C), E) and G) corresponds with MWCNTs, B), D), F) and H) corresponds with fMWCNTs.

Regarding the P2p spectra of the functionalized CNTs, phosphorus species present a main peak at 133.5 eV that can be deconvoluted into two contributions (Figure 4.11). The first doublet at 132.6 and 133.5 eV is associated with C-P-O species, corresponding to phosphonic group^{35,41,42}. A second major contribution at 133.3 and 134.2 eV is clearly observed that can be associated to phosphoric species (C-O-P)⁴³ as consequence of the oxidation of the phosphonic group during the electrochemical oxidation conditions.



Universitat d'Alacant
Universidad de Alicante

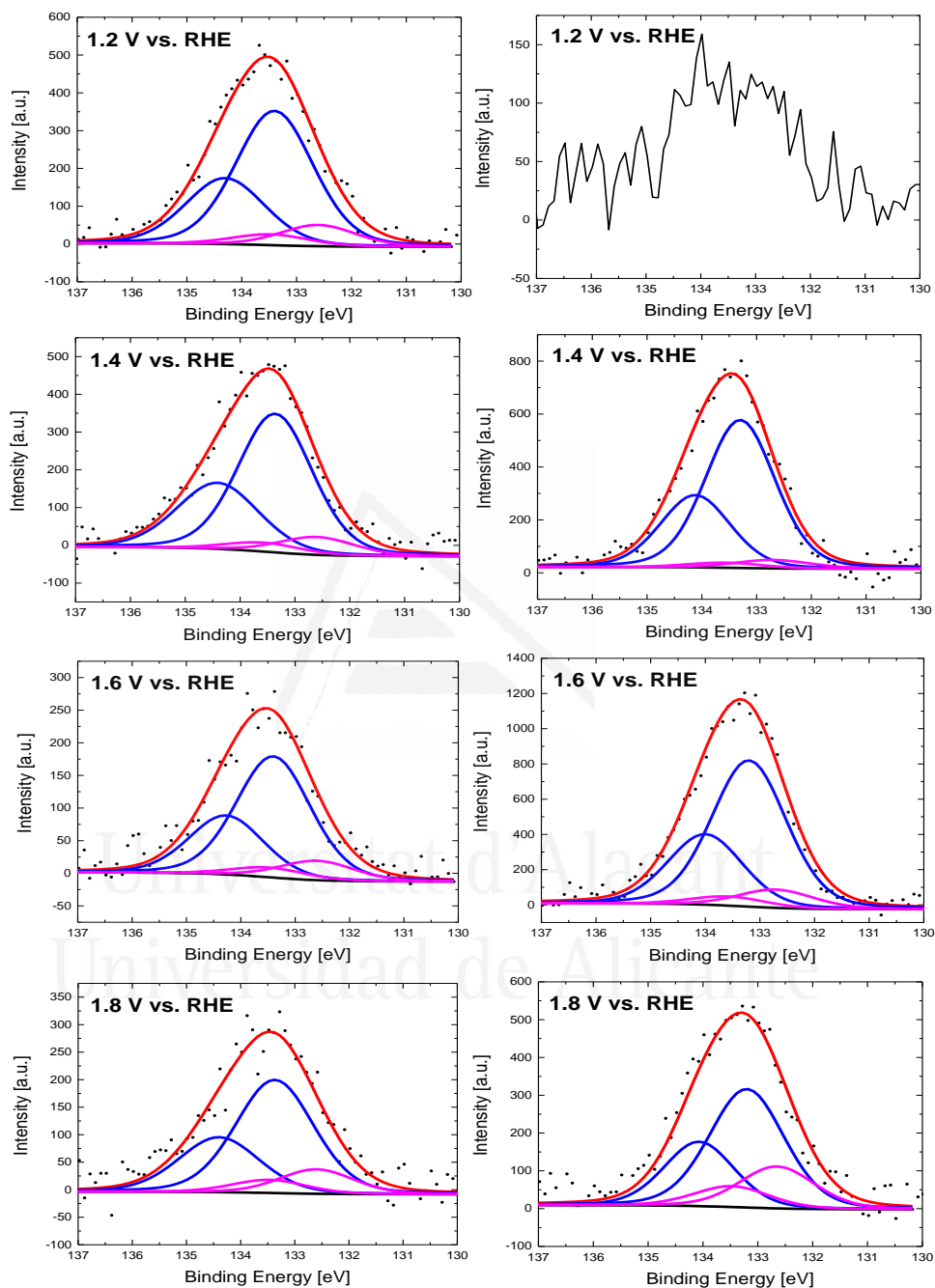


Figure 4.11. P2p XPS spectra for CNT electrochemically modified with 4-APPA at different upper positive limits: plots on right correspond with MWCNTs and plots in left correspond with fMWCNTs.

Table 4.4 shows the percentage of distribution for the main N and P species determined by XPS for the different functionalized CNTs. In the case of MWCNTs sample, the amount of neutral N species decreases with potential with a corresponding increase in oxidized N. However, in fMWCNT the amount of neutral nitrogen species is lower since the lowest potential used and do not suffer critical oxidation, suggesting that an important amount of 4-APPA is bonded to the CNT through reactions with surface oxygen groups or surface defects. In the case of phosphorus species, most of them correspond to oxidized phosphorus species.

Table 4.4. Distribution of N1s and P2p contributions for MWCNT and fMWCNT electrochemical modified with 4-APPA at different potentials.

| Carbon nanotube | Upper potential limit [V vs. RHE] | % Neutral N species | % Oxidized nitrogen | % C-O-P (133.3 eV) | % C-P-O (132.6 eV) |
|-----------------|-----------------------------------|---------------------|---------------------|--------------------|--------------------|
| MWCNT | 1.2 | 93 | 7 | 86 | 14 |
| | 1.4 | 71 | 29 | 89 | 11 |
| | 1.6 | 72 | 28 | 87 | 13 |
| | 1.8 | 46 | 54 | 83 | 17 |
| fMWCNT | 1.2 | 67 | 33 | -- | -- |
| | 1.4 | 75 | 25 | 89 | 11 |
| | 1.6 | 70 | 30 | 94 | 6 |
| | 1.8 | 60 | 40 | 74 | 26 |

*All the percentages correspond with the total amount of each N1s and P2p determined.

3.5. Raman spectroscopy

Structural and physicochemical changes were studied by Raman spectroscopy for the pristine MWCNTs and after the electrochemical modification. Figure 4.12 presents the Raman spectra recorded for MWCNTs, fMWCNTs and after electrochemical modification with 4-APPA. The first-order G and D bands (at around 1585 and 1350 cm^{-1} , respectively) are observed in all the spectra. These bands are characteristic of graphene based carbon materials, the G band corresponds to an ideal graphitic lattice vibration

mode and the D band is related to the presence of defects⁴⁴⁻⁴⁷. More specifically, D band is related to the presence of amorphous carbon⁴⁵. In the case of fMWCNTs, the D band increases compared to MWCNTs due to the nitric acid treatment that produces important damage and carbon material removal from the tube walls. In the fMWCNTs sample a shoulder at around 1620 cm^{-1} is observed that can be associated to D' band (Figure 4.12-D) due to defects along the tube induced by functionalization and strain in the C-C carbon bonds⁴⁵⁻⁴⁶.

A low intensity band at around 1150 cm^{-1} can be clearly observed for MWCNTs after modification with 4-APPA (Figure 4.12-A). This band can be associated to C-O stretching mode in P-O-C_{aromatic} species⁴⁸ or to C-N-C asymmetric stretching in quinoid structure^{34,48-50}. This feature is in agreement with oligomer formation; however, this band is not clearly distinguished for fMWCNTs derived materials, what is in agreement with the lower degree of oligomer incorporation that can be achieved for the functionalized material.

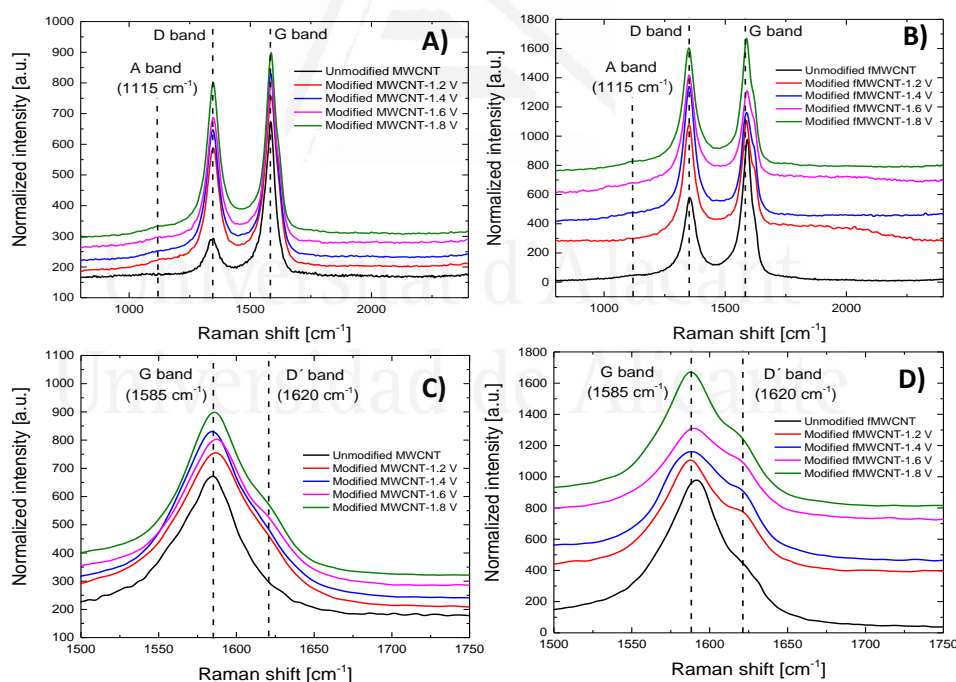


Figure 4.12. Raman spectra of carbon nanotubes electrochemically modified with 4-APPA at different positive potentials: A) MWCNTs, B) fMWCNTs, C) enlargement of G and D' region for MWCNTs and D) enlargement of G and D' region for fMWCNTs.

Once MWCNTs and fMWCNTs are submitted to a high anodic polarization in presence of 4-APPA, the D and D' bands increase. In the case of MWCNTs a shoulder at around 1620 cm^{-1} can be distinguished and the D' band increases importantly for fMWCNTs. The anodic polarization is inducing the formation of defects which is more important for fMWCNT. Those defects, which are present in a higher concentration for fMWCNTs, can be anchoring points for 4-APPA thus unfavouring the oligomerization process.

Figure 4.13 presents the I^D/I^G and $I^{D'}/I^G$ ratios calculated after deconvolution of the G band. For curve fitting, Lorentzian shape has been used for G band and Gaussian shape for D' band⁵¹. The evolution of I^D/I^G and $I^{D'}/I^G$ ratios with potential follows a similar trend; in the case of MWCNT materials they increase with potential and for fMWCNTs it goes through a maximum. In addition, the I^D/I^G and $I^{D'}/I^G$ ratios are higher for fMWCNTs derived materials for all the potentials studied except for the sample prepared at 1.8 V. The increase in the ratio of bands for functionalized MWCNTs indicates some oxidation of the pristine MWCNTs generating defects. It must be noted that there is an important increase after modifying the material at 1.2 V compared to the pristine MWCNTs and, afterwards, the increase is not important until 1.6 V. However, the increase of the ratio from the pristine fMWCNTs to the modification at 1.2 V is not so high because the functionalization with HNO_3 already produces important amount of defects in the MWCNT. Upon modification of fMWCNTs with increasing potential the ratios I^D/I^G and $I^{D'}/I^G$ goes through a maximum indicating that at such potential some removal of the most reactive carbon sites and amorphous carbon may occur through carbon gasification reactions or the formation of species in solution. This is in agreement with previous observations with nanostructured carbon materials⁴⁷.

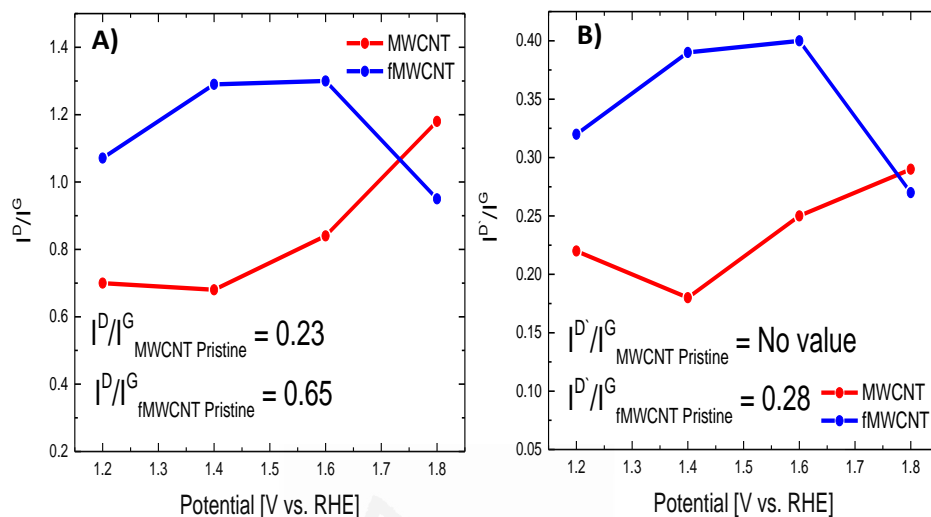


Figure 4.13. A) I^D/I^G ratio and B) I^D/I^G , both as a function of the positive potential limit used in the electrochemical modification with 4-APPA.

4. Conclusions

MWCNTs and fMWCNTs were functionalized successfully with N and P species during electrochemical oxidation of 4-APPA employing cyclic voltammetry. The oxidation of 4-APPA promotes the formation of electroactive oligomers onto the CNT surface; however, covalently bonded redox species cannot be discharged. It has been observed a negative effect of the surface oxygen groups in the degree of functionalization. Thus for the fMWCNT the amount of phosphorus incorporated is lower than in the non-oxidized MWCNTs. However, the amount of P incorporated shows a maximum in both CNTs at an upper potential limit of 1.4 V; further potential increase causes an over oxidation of the oligomers or the oxidation of the phosphorus groups without producing sever damage of the carbon nanotube structure.

In the case of MWCNTs, different redox processes with high reversibility are observed, which produces a remarkable increase in the electric charge stored compared to the pristine MWCNTs. In addition, oligomer chains are clearly observed by TEM. In the case of the fMWCNTs, the oligomerization reaction is not favored compared to the pristine MWCNTs. In this material, the presence of electron withdrawing oxygen groups that decrease the π electron

density of the CNTs and modify the orientation of the 4-APPA molecule, thus reducing the incorporation of 4-APPA parallel to the surface of the CNTs, impeding the oligomerization reaction.

The evolution of I^D/I^G and $I^{D'}/I^G$ Raman band ratios with potential in presence of 4-APPA follows a similar trend for functionalized MWCNTs and functionalized fMWCNTs. For MWCNTs they increase importantly from 1.4 V, indicating that some oxidation of the MWCNTs occurs from this potential, generating defects. However, in the case of fMWCNTs these ratios go through a maximum indicating that some loss of carbon material occurs through carbon gasification reactions or the formation of species in solution. These reactions may also make difficult the functionalization by 4-APPA.

Thus, the presence of surface oxygen groups in the MWCNTs is detrimental to achieve the functionalization through oligomerization reactions, being covalent attachment the prevailing mechanism.

5. References

- (1) Hirsch, A. Functionalization of Single-Walled Carbon Nanotubes. *Angew. Chemie Int. Ed.* **2002**, *41* (11), 1853–1859.
- (2) González-Gaitán, C.; Ruíz-Rosas, R.; Morallón, E.; Cazorla-Amorós, D. Electrochemical Methods to Functionalize Carbon Materials. In: Vijay Kumar, T.; Manju Kumari, T., editor. *Chemical Functionalization of Carbon Materials-Chemistry and Applications*, Taylor and Francis group, CRC Press, Washington, **2016**, pp. 230-249.
- (3) Mallakpour, S.; Soltanian, S. Surface Functionalization of Carbon Nanotubes: Fabrication and Applications. *RSC Adv.* **2016**, *6* (111), 109916–109935.
- (4) Hu, L.; Hecht, D. S.; Grüner, G. Carbon Nanotube Thin Films: Fabrication, Properties, and Applications. *Chem. Rev.* **2010**, *110* (10), 5790–5844.
- (5) Georgakilas, V.; Bourlinos, A.; Gournis, D.; Tsoufis, T.; Trapalis, C.; Mateo-Alonso, A.; Prato, M. Multipurpose Organically Modified Carbon Nanotubes: From Functionalization to Nanotube Composites. *J. Am. Chem. Soc.* **2008**, *130* (27), 8733–8740.

- (6) González-Gaitán, C.; Ruiz-Rosas, R.; Morallón, E.; Cazorla-Amorós, D. Functionalization of Carbon Nanotubes Using Aminobenzene Acids and Electrochemical Methods. Electroactivity for the Oxygen Reduction Reaction. *Int. J. Hydrogen Energy* **2015**, *40* (34), 11242–11253.
- (7) Li, J.-C.; Hou, P.-X.; Zhao, S.-Y.; Liu, C.; Tang, D.-M.; Cheng, M.; Zhang, F.; Cheng, H.-M. A 3D Bi-Functional Porous N-Doped Carbon Microtube Sponge Electrocatalyst for Oxygen Reduction and Oxygen Evolution Reactions. *Energy Environ. Sci.* **2016**, *9* (10), 3079–3084.
- (8) Tang, C.; Titirici, M.-M.; Zhang, Q. A Review of Nanocarbons in Energy Electrocatalysis: Multifunctional Substrates and Highly Active Sites. *J. Energy Chem.* **2017**, *26* (6), 1077–1093.
- (9) Quílez-Bermejo, J.; Morallón, E.; Cazorla-Amorós, D. Oxygen-Reduction Catalysis of N-Doped Carbons Prepared via Heat Treatment of Polyaniline at over 1100 °C. *Chem. Commun.* **2018**, *54* (35), 4441–4444.
- (10) Qu, K.; Zheng, Y.; Zhang, X.; Davey, K.; Dai, S.; Qiao, S. Z. Promotion of Electrocatalytic Hydrogen Evolution Reaction on Nitrogen-Doped Carbon Nanosheets with Secondary Heteroatoms. *ACS Nano* **2017**, *11* (7), 7293–7300.
- (11) Chen, Y.; Wang, J.; Liu, H.; Banis, M. N.; Li, R.; Sun, X.; Sham, T.-K.; Ye, S.; Knights, S. Nitrogen Doping Effects on Carbon Nanotubes and the Origin of the Enhanced Electrocatalytic Activity of Supported Pt for Proton-Exchange Membrane Fuel Cells. *J. Phys. Chem. C* **2011**, *115* (9), 3769–3776.
- (12) Sajjadi, S.; Ghourchian, H.; Rahimi, P. Different Behaviors of Single and Multi Wall Carbon Nanotubes for Studying Electrochemistry and Electrocatalysis of Choline Oxidase. *Electrochim. Acta* **2011**, *56* (26), 9542–9548.
- (13) Cruz-Silva, E.; Cullen, D. A.; Gu, L.; Romo-Herrera, J. M.; Muñoz-Sandoval, E.; López-Urías, F.; Sumpter, B. G.; Meunier, V.; Charlier, J.-C.; Smith, D. J.; et al. Heterodoped Nanotubes: Theory, Synthesis, and Characterization of Phosphorus–Nitrogen Doped Multiwalled

Carbon Nanotubes. *ACS Nano* **2008**, 2 (3), 441–448.

- (14) Berenguer, R.; Ruiz-Rosas, R.; Gallardo, A.; Cazorla-Amorós, D.; Morallón, E.; Nishihara, H.; Kyotani, T.; Rodríguez-Mirasol, J.; Cordero, T. Enhanced Electro-Oxidation Resistance of Carbon Electrodes Induced by Phosphorus Surface Groups. *Carbon* **2015**, 95, 681–689.
- (15) Ramanathan, T.; Fisher, F. T.; Ruoff, R. S.; Brinson, L. C. Amino-Functionalized Carbon Nanotubes for Binding to Polymers and Biological Systems. *Chem. Mater.* **2005**, 17 (6), 1290–1295.
- (16) Lafuente, E.; Callejas, M. A.; Sainz, R.; Benito, A. M.; Maser, W. K.; Sanjuán, M. L.; Saurel, D.; de Teresa, J. M.; Martínez, M. T. The Influence of Single-Walled Carbon Nanotube Functionalization on the Electronic Properties of Their Polyaniline Composites. *Carbon* **2008**, 46 (14), 1909–1917.
- (17) Cañete-Rosales, P.; González, M.; Ansón, A.; Martínez, M. T.; Yáñez, C.; Bollo, S. Electrochemical characterization of oligonucleotide-carbon nanotube functionalized using different strategies, *Electrochim. Acta.* **2014**, 140, 489–496.
- (18) M.L. Ramírez, C.S. Tettamanti, F.A. Gutierrez, J.M. Gonzalez-Domínguez, A. Ansón-Casaos, J. Hernández-Ferrer, M.T. Martínez, G.A. Rivas, M.C. Rodríguez, Cysteine functionalized bio-nanomaterial for the affinity sensing of Pb(II) as an indicator of environmental damage, *Microchem. J.* **2018**, 141, 271–278.
- (19) Ma, P.-C.; Siddiqui, N. A.; Marom, G.; Kim, J.-K. Dispersion and Functionalization of Carbon Nanotubes for Polymer-Based Nanocomposites: A Review. *Compos. Part A Appl. Sci. Manuf.* **2010**, 41 (10), 1345–1367.
- (20) Holzinger, M.; Abraham, J.; Whelan, P.; Graupner, R.; Ley, L.; Hennrich, F.; Kappes, M.; Hirsch, A. Functionalization of Single-Walled Carbon Nanotubes with (R-)Oxycarbonyl Nitrenes. *J. Am. Chem. Soc.* **2003**, 125 (28), 8566–8580.
- (21) González-Domínguez, J. M., M. González, A. Ansón-Casaos, A.M.

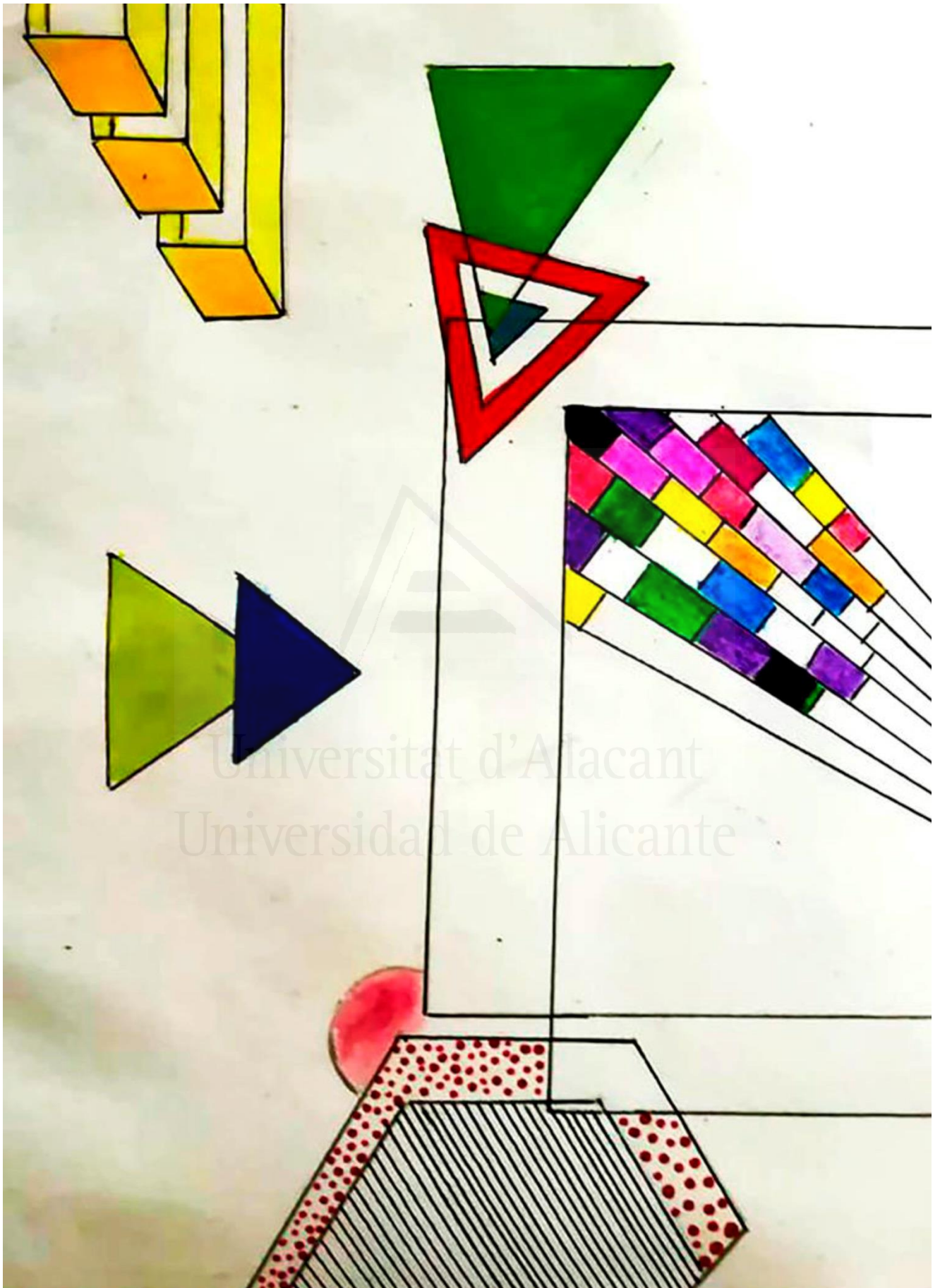
- Díez-Pascual, M.A. Gómez, M.T. Martínez, Effect of Various Aminated Single-Walled Carbon Nanotubes on the Epoxy Cross-Linking Reactions, *J. Phys. Chem. C* **2011**, *115*, 7238–7248.
- (22) Tuci, G.; Vinattieri, C.; Luconi, L.; Ceppatelli, M.; Cicchi, S.; Brandi, A.; Filippi, J.; Melucci, M.; Giambastiani, G. “Click” on Tubes: A Versatile Approach towards Multimodal Functionalization of SWCNTs. *Chem. – A Eur. J.* **2012**, *18* (27), 8454–8463.
- (23) Bélanger, D.; Pinson, J. Electrografting: A Powerful Method for Surface Modification. *Chem. Soc. Rev.* **2011**, *40* (7), 3995–4048.
- (24) Cordero-Lanzac, T.; García-Mateos, F. J.; Rosas, J. M.; Rodríguez-Mirasol, J.; Cordero, T. Flexible Binderless Capacitors Based on P- and N-Containing Fibrous Activated Carbons from Denim Cloth Waste. *Carbon* **2018**, *139*, 599–608.
- (25) Boehm, H. P. Surface Oxides on Carbon and Their Analysis: A Critical Assessment. *Carbon* **2002**, *40* (2), 145–149.
- (26) Figueiredo, J. L.; Pereira, M. F. R.; Freitas, M. M. A.; Órfão, J. J. M. Modification of the Surface Chemistry of Activated Carbons. *Carbon* **1999**, *37* (9), 1379–1389.
- (27) Román-Martínez, M. C.; Cazorla-Amorós, D.; Linares-Solano, A.; de Lecea, C. S.-M. Tpd and TPR Characterization of Carbonaceous Supports and Pt/C Catalysts. *Carbon* **1993**, *31* (6), 895–902.
- (28) Moreno-Castilla, C.; López-Ramón, M. V; Carrasco-Marín, F. Changes in Surface Chemistry of Activated Carbons by Wet Oxidation. *Carbon* **2000**, *38* (14), 1995–2001.
- (29) Bleda-Martínez, M. J.; Lozano-Castelló, D.; Morallón, E.; Cazorla-Amorós, D.; Linares-Solano, A. Chemical and Electrochemical Characterization of Porous Carbon Materials. *Carbon* **2006**, *44* (13), 2642–2651.
- (30) Salinas-Torres, D.; Huerta, F.; Montilla, F.; Morallón, E. Study on Electroactive and Electrocatalytic Surfaces of Single Walled Carbon Nanotube-Modified Electrodes. *Electrochim. Acta* **2011**, *56* (5), 2464–2470.

- (31) González-Gaitán, C.; Ruiz-Rosas, R.; Morallón, E.; Cazorla-Amorós, D. Effects of the Surface Chemistry and Structure of Carbon Nanotubes on the Coating of Glucose Oxidase and Electrochemical Biosensors Performance. *RSC Adv.* **2017**, *7* (43), 26867–26878.
- (32) Zaragoza-Martín, F.; Sopeña-Escario, D.; Morallón, E.; de Lecea, C. S. M. Pt/Carbon Nanofibers Electrocatalysts for Fuel Cells. Effect of the Support Oxidizing Treatment. *J. Power Sources* **2007**, *171* (2), 302–309.
- (33) Lindfors, T.; Ivaska, A. PH Sensitivity of Polyaniline and Its Substituted Derivatives. *J. Electroanal. Chem.* **2002**, *531* (1), 43–52.
- (34) Benyoucef, A.; Huerta, F.; Vázquez, J. L.; Morallon, E. Synthesis and in Situ FTIRS Characterization of Conducting Polymers Obtained from Aminobenzoic Acid Isomers at Platinum Electrodes. *Eur. Polym. J.* **2005**, *41* (4), 843–852.
- (35) Martínez-Sánchez, B. *Síntesis y Caracterización Electroquímica de Polianilinas Modificadas con Grupos Fosfónicos*, Universidad de Alicante, Master thesis, **2019**.
- (36) Radovic, L. R.; Silva, I. F.; Ume, J. I.; Menéndez, J. A.; Leon, C. A. L. Y.; Scaroni, A. W. An Experimental and Theoretical Study of the Adsorption of Aromatics Possessing Electron-Withdrawing and Electron-Donating Functional Groups by Chemically Modified Activated Carbons. *Carbon* **1997**, *35* (9), 1339–1348.
- (37) Rivera-Utrilla, J.; Sánchez-Polo, M. The Role of Dispersive and Electrostatic Interactions in the Aqueous Phase Adsorption of Naphthalenesulphonic Acids on Ozone-Treated Activated Carbons. *Carbon* **2002**, *40* (14), 2685–2691.
- (38) Bard, A.; Faulkner, L. *Electrochemical Methods: Fundamental and Applications*, 2nd ed.; Harris, D., Swain, E., Aiello, E., Eds.; John Wiley & Sons, Ltd: Austin, **2000**.
- (39) Chan, H. S. O.; Ng, S. C.; Sim, W. S.; Tan, K. L.; Tan, B. T. G. Preparation and Characterization of Electrically Conducting Copolymers of Aniline and Anthranilic Acid: Evidence for Self-Doping

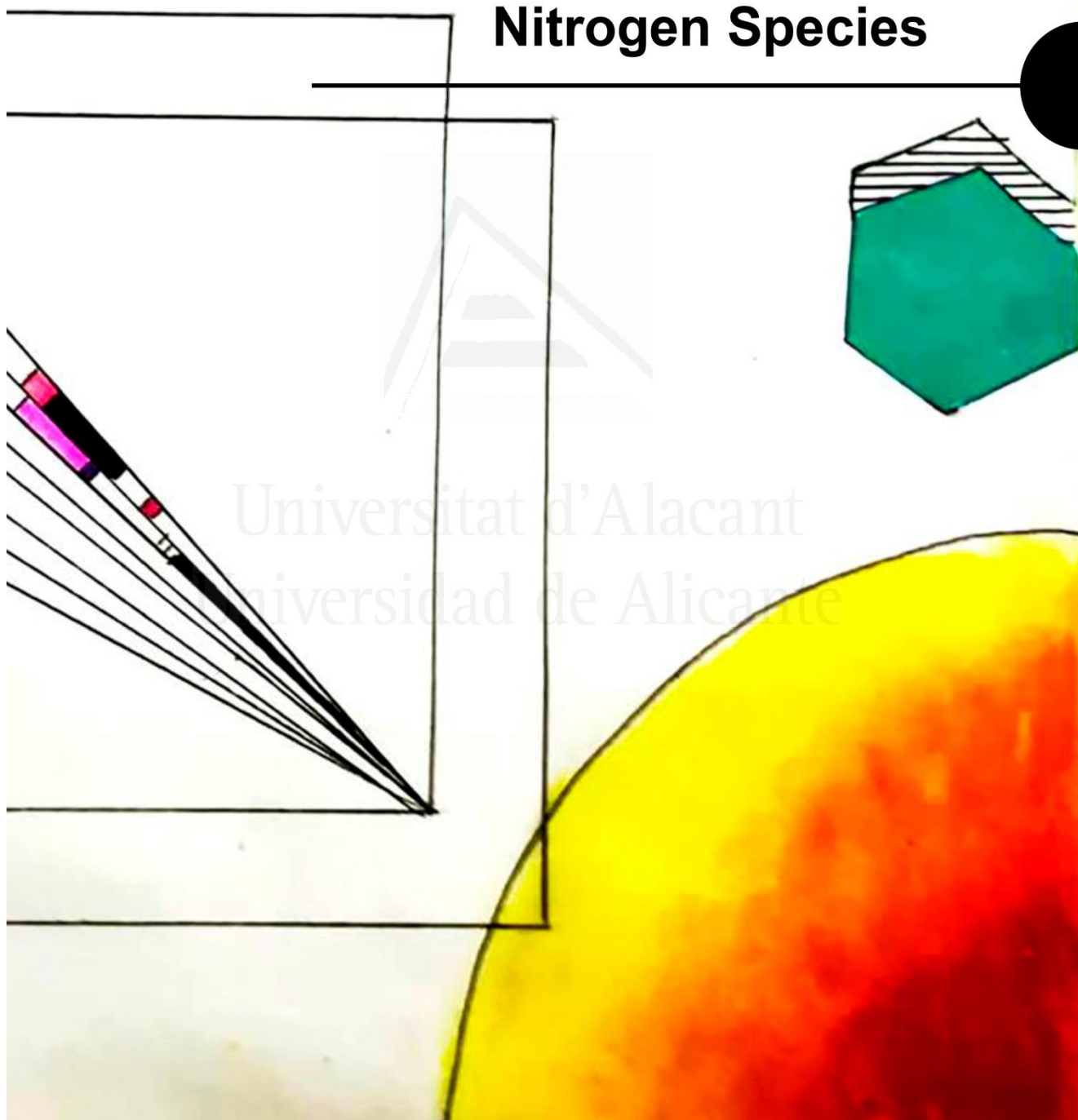
- by x-Ray Photoelectron Spectroscopy. *Macromolecules* **1992**, *25* (22), 6029–6034.
- (40) Quílez-Bermejo, J.; Ghisolfi, A.; Grau-Marín, D.; San-Fabián, E.; Morallón, E.; Cazorla-Amorós, D. Post-Synthetic Efficient Functionalization of Polyaniline with Phosphorus-Containing Groups. Effect of Phosphorus on Electrochemical Properties. *Eur. Polym. J.* **2019**, *119*, 272–280.
- (41) Chen, Y.; Guo, L.-R.; Chen, W.; Yang, X.-J.; Jin, B.; Zheng, L.-M.; Xia, X.-H. 3-Mercaptopropylphosphonic Acid Modified Gold Electrode for Electrochemical Detection of Dopamine. *Bioelectrochemistry* **2009**, *75* (1), 26–31.
- (42) Yang, D.-S.; Bhattacharjya, D.; Inamdar, S.; Park, J.; Yu, J.-S. Phosphorus-Doped Ordered Mesoporous Carbons with Different Lengths as Efficient Metal-Free Electrocatalysts for Oxygen Reduction Reaction in Alkaline Media. *J. Am. Chem. Soc.* **2012**, *134* (39), 16127–16130.
- (43) Quesada-Plata, F.; Ruiz-Rosas, R.; Morallón, E.; Cazorla-Amorós, D. Activated Carbons Prepared through H₃PO₄-Assisted Hydrothermal Carbonisation from Biomass Wastes: Porous Texture and Electrochemical Performance. *Chempluschem* **2016**, *81* (12), 1349–1359.
- (44) Ferrari, A. C. Raman Spectroscopy of Graphene and Graphite: Disorder, Electron–Phonon Coupling, Doping and Nonadiabatic Effects. *Solid State Commun.* **2007**, *143* (1), 47–57.
- (45) Lehman, J. H.; Terrones, M.; Mansfield, E.; Hurst, K. E.; Meunier, V. Evaluating the Characteristics of Multiwall Carbon Nanotubes. *Carbon* **2011**, *49* (8), 2581–2602.
- (46) Chakrapani, N.; Curran, S.; Wei, B.; Ajayan, P. M.; Carrillo, A.; Kane, R. S. Spectral Fingerprinting of Structural Defects in Plasma-Treated Carbon Nanotubes. *J. Mater. Res.* **2003**, *18* (10), 2515–2521.
- (47) Leyva-García, S.; Nueangnoraj, K.; Lozano-Castelló, D.; Nishihara, H.; Kyotani, T.; Morallón, E.; Cazorla-Amorós, D. Characterization of a

- Zeolite-Templated Carbon by Electrochemical Quartz Crystal Microbalance and in Situ Raman Spectroscopy. *Carbon* **2015**, 89, 63–73.
- (48) Sócrates, G. Infrared and Raman Characteristic Group Frequencies. Tables and Charts, 3rd ed. Jhon Wiley & Sons, Ltd, Chichester, UK, 2004.
- (49) Cotarelo, M. A.; Huerta, F.; Quijada, C.; Mallavia, R.; Vázquez, J. L. Synthesis and Characterization of Electroactive Films Deposited from Aniline Dimers. *J. Electrochem. Soc.*, **2006**, 153 (7) D114-D122.
- (50) Geniès, E. M.; Penneau, J. F.; Lapkowski, M.; Boyle, A.. Electropolymerisation Reaction Mechanism of Para-Aminodiphenylamine. *J. Electroanal. Chem. Interfacial Electrochem.* **1989**, 269 (1), 63–75.
- (51) Antunes, E. F.; Lobo, A. O.; Corat, E. J.; Trava-Airoldi, V. J.; Martin, A. A. et. al. Comparative Study of First- and Second-Order Raman Spectra of MWCNT at Visible and Infrared Laser Excitation. *Carbon* **2006**, 44 (11), 2202–2211.

Universitat d'Alacant
Universidad de Alicante



Annex to Chapter 4 Electrochemical Functionalization of Graphene-Based Materials with Phosphorus and Nitrogen Species



1. Experimental

1.1. Reagents

Sulphuric acid (98%) analytical reagent was obtained from VWR Chemicals. 4-amino phenyl phosphonic acid (4-APPA, +98%), used as modifier agent, was purchased from Tokyo Chemical Industry co (TCI). Sodium sulfate (Na_2SO_4) (99%) was obtained from Merck. All the solutions were prepared using ultrapure water (18 M Ω cm, Purelab Ultra Elga equipment). The gases N_2 (99.999%) and H_2 (99.999%) were provided by Air Liquide.

1.2. Synthesis of graphene-based materials

1.2.1. Graphene oxide

Synthesis of graphene oxide (GO) was performed using the modified Hummers method¹. Graphite powder is treated under acidic and oxidant conditions to promote the exfoliation of the graphene-sheets, incorporating high amount of surface oxygen groups, making easy the dispersion in polar media.

The working electrode for electrochemical modification was prepared using glassy carbon (GC), as support, modified with the GO. 1 mg of GO was dispersed in ultrapure water employing an ultrasonic cold-bath for 45 minutes, achieving a dispersion of 1 mg mL⁻¹ of GO. Prior to the casting, the glassy carbon electrode surface (3 mm diameter) was sanded with emery paper and polished using 1 and 0.05 μm alumina slurries, then rinsed with ultrapure water. Afterwards, 5 μL aliquot of the dispersion was dropped onto the glassy carbon surface and dried under an infrared lamp to remove the solvent. This procedure was repeated twice.

1.2.2. Graphene oxide electrochemically reduced

The electrochemical reduction of GO was carried out by cyclic voltammetry conditions using an eDAQ Potentiostat (EA163 model) coupled to a EG&G Parc Model 175 wave generator and the data acquisition was performed with a eDAQ e-corder 410 unit (Chart and Scope Software), using a standard three-electrode cell configuration. The glassy carbon electrode

modified with GO was the working electrode (WE), a graphite rod as counter electrode (CE) and a reversible hydrogen electrode (RHE), introduced in the working electrolyte, the reference electrode. The procedure consisted in the application of 20 cycles in a potential range between -1.0 to 1.0 V, at a scan rate of 50 mV s^{-1} in a deoxygenated solution of $0.1 \text{ M Na}_2\text{SO}_4$. Afterwards electrodes are washed with excess of ultrapure water and stored for further modification or characterization.

1.2.3. Graphene

Graphene suspensions were obtained following the procedure previously reported³: 500 mg of graphite were heated at 930°C for 1 h under 100 mL min^{-1} flow of nitrogen. Subsequently, graphite was dispersed in 100 mL of N-Methyl-2-Pyrrolidone (NMP) and sonicated in an ultrasound bath for 2 h. Insoluble particles are removed after letting stand the suspension for 5 days. Supernatant is collected and weighed, determining the final concentration of the suspension at about 0.3 mg mL^{-1} . 5 μL of graphene suspension in NMP was deposited on the polished glassy carbon electrode surface and dried in vacuum. This procedure was repeated 6 times to achieve a total mass of 9 μg . Graphene samples are named as K14.

1.3. Electrochemical modification with 4-amino phenyl phosphonic acid

Electrochemical modification of graphene-based materials was performed using an Autolab PGSTAT 302 (Metrohm Netherlands) potentiostat, with a standard three-electrode cell configuration, in which the glassy carbon electrode modified with graphene-based materials was the working electrode (WE), a graphite rod was used as counter electrode and a reversible hydrogen electrode introduced in the same electrolyte but without 4-APPA, was used as reference electrode. Electrochemical modification was carried out in aqueous solution $0.5 \text{ M H}_2\text{SO}_4 + 1 \text{ mM APPA}$ in a deoxygenated cell by bubbling nitrogen. Electrochemical modification of graphene-based materials was achieved by cyclic voltammetry submitting the sample to 10 cycles at 10 mV s^{-1} , in different potential windows. After electrochemical treatment, electrodes were washed with excess of water, removing remaining electrolyte.

1.4. Electrochemical characterization

Electrochemical behavior of the graphene-based materials unmodified and modified with 4-APPA was evaluated by cyclic voltammetry in acid medium, employing a three electrode configuration cell, where, glassy carbon modified with graphene-based materials functionalized with 4-APPA, was the working electrode (WE), a graphite rod was the counter electrode (CE) and a reversible hydrogen electrode (RHE) introduced in the same electrolyte, was the reference electrode (RE). Potential range was fixed between 0 and 1 V at 50 mV s^{-1} , for all the characterization.

1.5. Physicochemical characterization

X-Ray photoelectron spectroscopy (XPS) was performed in a VG-Microtech Mutilab 3000 spectrometer using an Al K α radiation (1253.6 eV). The deconvolution of the XPS peaks for C1s, O2p, P2p and N1s was done by least squares fitting using Gaussian-Lorentzian curves, while a Shirley line was used for the background determination. The P2p spectra have been analyzed considering the spin-orbit splitting into P2p $_{3/2}$ and P2p $_{1/2}$ with a 2:1 peak area ratio and an energy separation of 0.87 eV⁴.

2. Results and discussion

2.1. Electrochemical reduction of GO under neutral conditions

Figure A-4.1 shows the voltammogram performed during the electrochemical reduction of GO in an extended potential cycling (-1.0 to 1.0 V vs. RHE) in neutral conditions. During the first cycle of polarization at lower potential limit a high reduction current with an on-set potential at -0.5 V is observed, due to the reduction of GO. The intensity of this current decreases with cycling. Additionally, two different phenomena take place during the electrochemical reduction of GO. The first one, involves the increase in the voltammetric charge associated with the double-layer process and the second includes the appearance of one redox process at 0.6 V during the positive scan which intensity increases with cycling. After 20 cycles at these conditions, the reduced graphene oxide is obtained (rGO).

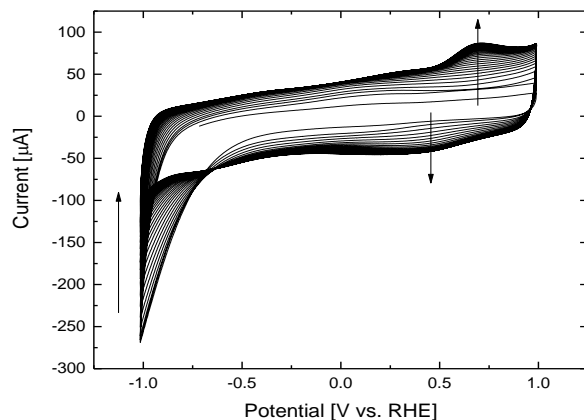


Figure A-4.1. Cyclic voltammograms of electrochemical reduction of GO electrode in 0.1 M Na_2SO_4 at 50 mV s^{-1} , 20 consecutive cycles.

Figure A-4.2 shows the voltammograms obtained during the 20 cycle for GO and rGO in 0.5 M H_2SO_4 .

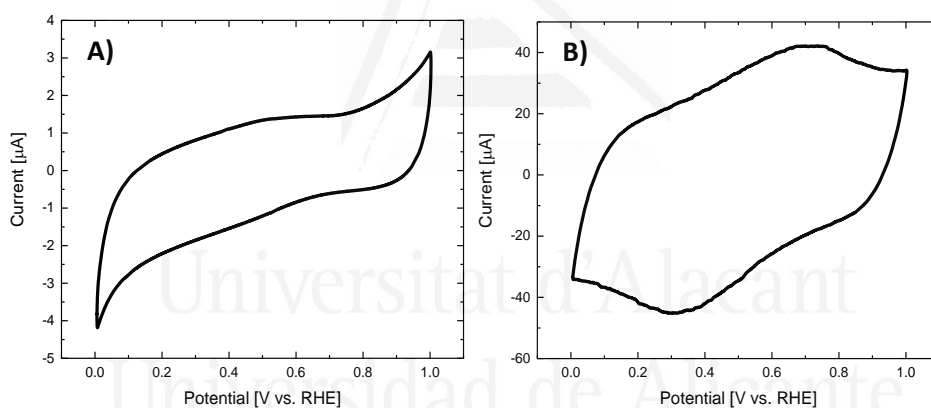


Figure A-4.2. Cyclic voltammograms for: A) GO and B) rGO (after electrochemical reduction) in 0.5 M H_2SO_4 at 50 mV s^{-1} under N_2 atmosphere.

The GO presents the voltammogram of a carbon material with low conductivity, a tilted voltammogram and low value of double layer capacitance, as consequence of the high concentration of defects in the graphene layer (Figure A-4.2-A). However, the voltammogram for rGO shows important differences with respect to the GO. First, an important increase in the current is observed, which is related with a higher surface area after the electrochemical reduction. Furthermore, one redox process at around 0.65 V in

the positive scan, with a separation of peak potential of 0.4 V can be related with remaining electroactive surface oxygen groups in the graphene layer^{5,6}.

2.2. Surface functionalization with 4-APPA

Figure A-4.3 shows the cyclic voltammograms of the upper potential limit stepwise opened from 1.0 to 1.8 V in presence of 4-APPA (Figure A-4.3-B and A-4.3-D) and in absence of 4-APPA (Figure A-4.3, A and C) for GO and rGO, respectively.

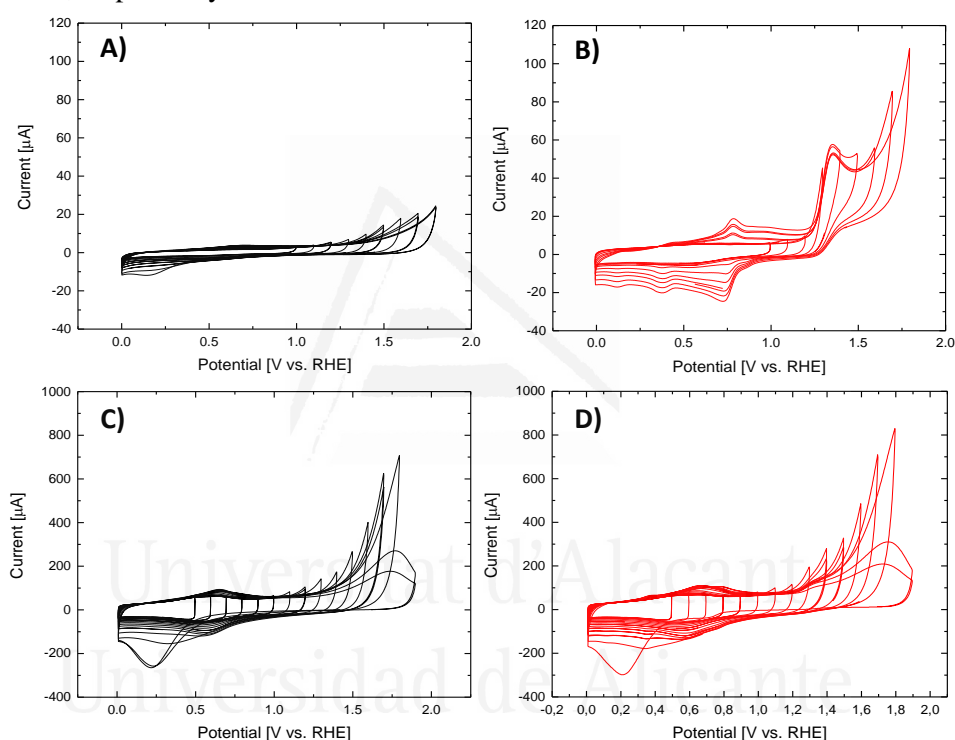


Figure A-4.3. Cyclic voltammograms during the first cycle of the open stepwise potential window for: A) GO in 0.5 M H_2SO_4 , B) GO in 0.5 M $\text{H}_2\text{SO}_4 + 1 \text{ mM}$ 4-APPA, C) rGO in 0.5 M H_2SO_4 and D) rGO in 0.5 M $\text{H}_2\text{SO}_4 + 1 \text{ mM}$ 4-APPA.

In presence of 4-APPA, GO and rGO present a different voltammetric behavior. Thus, the oxidation of 4-APPA on GO electrode shows a clear irreversible oxidation peak at 1.35 V. After this oxidation peak, several redox processes appear in the voltammogram during the negative scan to less positive potentials. However, the voltammetric profiles of the rGO in presence

of 4-APPA are very similar to those obtained with rGO in absence of 4-APPA (Figure A-4.3-C and A-4.3-D).

Higher polarization above 1.2 V generates an irreversible anodic peak associated with the oxidation of 4-APPA in the two carbon materials, being less important its contribution in the rGO. In the reverse scan, different redox processes at 0.75, 0.35 and 0.12 V appear in the GO. In contrast, rGO does not show significant redox processes to those observed during the oxidation of rGO in absence of 4-APPA (See Figure A-4.3-C), suggesting that a growing and deposition of the oligomer layer occurs in a less extension than in the case of GO and the oxidation of the rGO is more important than the oxidation of 4-APPA.

The electrochemical modification of 4-APPA was performed using K14 sample, as can be observed in the cyclic voltammograms (Figure A-4.4) from 0.5 to 1.8 V vs. RHE. It can be observed a similar voltammetric behavior to GO, being observed in this case the presence of an oxidation current at the same potential than for GO.

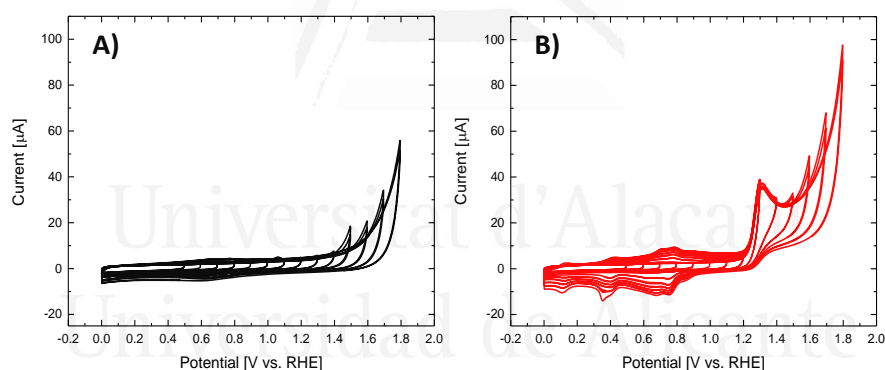


Figure A-4.4. Cyclic voltammograms during the first cycle of the open stepwise potential window for: A) graphene K14 in 0.5 M H₂SO₄ and B) graphene K14 in 0.5 M H₂SO₄+ 1 mM 4-APPA at 50 mV s⁻¹.

Based on the stepwise upper potential limit study, two upper potential limits were chosen (1.5 and 1.8 V) for the functionalization of the materials. Figure A-4.5 shows the voltammograms for GO and rGO during the oxidation in absence (black voltammograms) and in presence of 4-APPA (red voltammograms) in the solution. Once electrochemical modification with 4-APPA is carried out (red lines CVs in Figure A-4.5) a clear oxidation peak is

observed in GO; however, this oxidation is overlapped with the oxidation of the carbon material in the case of rGO. For K14 graphene, the oxidation of 4-APPA at 1.5 and 1.8 V (Data not shown) presents similar behavior to that observed with GO.

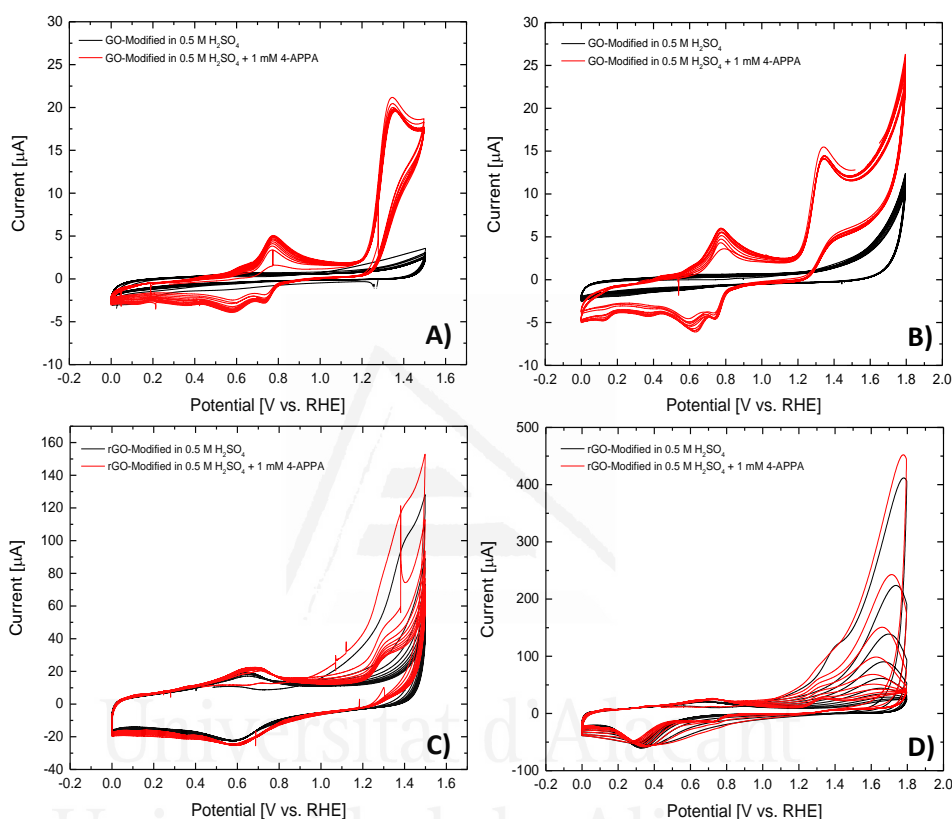


Figure A-4.5. Cyclic voltammograms obtained during 10 cycles for a GO and rGO electrodes in 0.5 M H₂SO₄ (Black lines) and 0.5 M H₂SO₄ + 1 mM 4-APPA (Red lines) at 10 mV s⁻¹ under N₂ atmosphere at different positive potential limits: A) GO-1.5 V, B) GO-1.8 V, C) rGO-1.5 V and D) rGO-1.8 V.

The clear irreversible oxidation current observed in the case of GO at 1.35 V has not been observed in previous studies with CNTs (chapter 3 and chapter 4). In this carbon material, the development of redox processes with an oxidation peak at 0.77 V and the corresponding reduction peaks at 0.75 and 0.58 V are clearly observed.

Figure A-4.6 shows the voltammograms in 0.5 M H₂SO₄ for the carbon material after the electrochemical modification. The black lines correspond to

the voltammograms of the carbon materials oxidized at the same potential but in absence of 4-APPA in the solution.

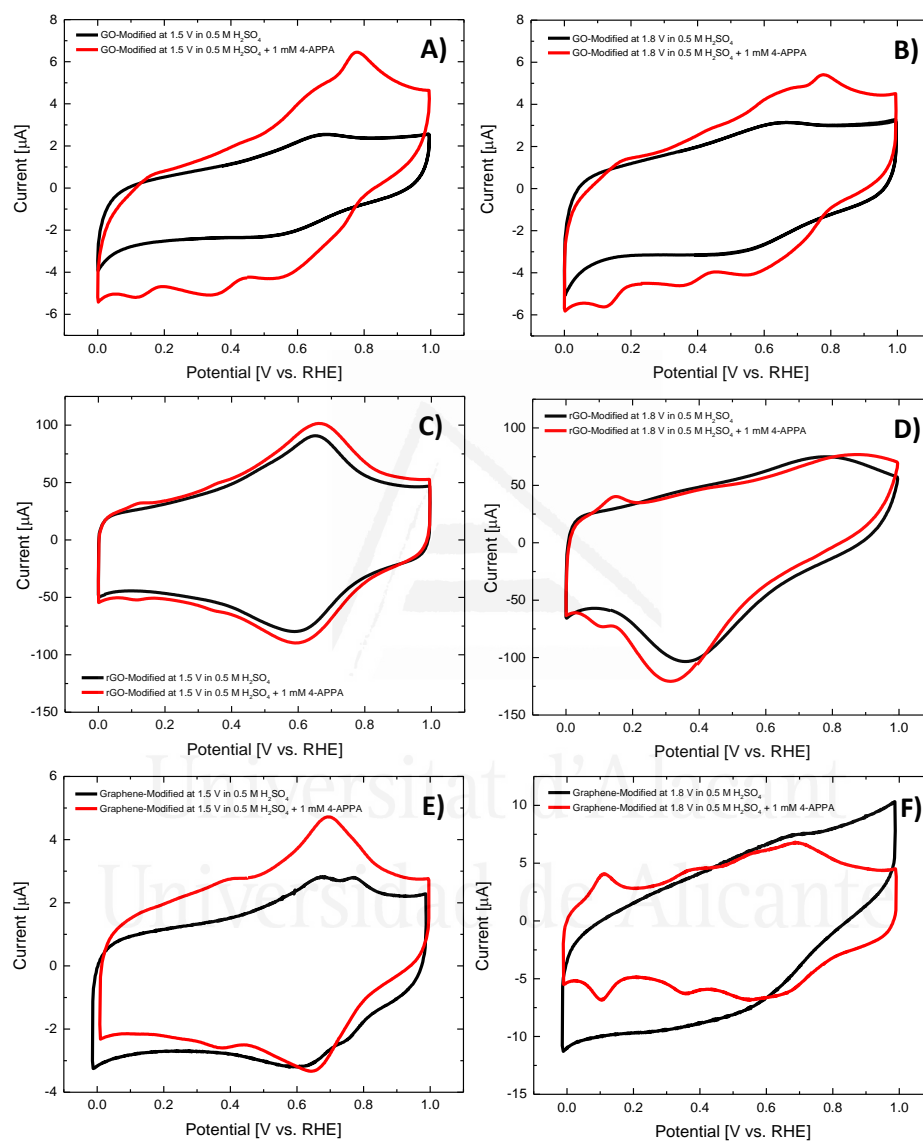


Figure A-4.6. Steady state CVs in 0.5 M H₂SO₄ for graphene-based materials electrochemically modified in absence (black line) and in presence (red line) of 4-APPA: A) GO, 1.5 V, B) GO, 1.8 V, C) rGO, 1.5 V, D) rGO, 1.8 V E) graphene K14 modified at 1.5 V and F) graphene K14 modified at 1.8 V, at 50 mV s⁻¹

For GO the appearance of different redox processes at 0.77 and 0.65 V (the reduction processes appear at 0.56, 0.35 and 0.11 V) are the most representatives. The increase in the potential limit of modification does not produce an important change in the voltammogram, only a decrease in the voltammetric charge can be appreciated, which could be related with a degradation of the oligomers produced during the oxidation of 4-APPA as has been observed for other substituted polyanilines⁷⁻¹⁰. Interestingly, for K14 electrodes (Figure A-4.6, E and F), the voltammograms show reversible redox processes at 0.67 and 0.38 V in both potentials studied. On the other hand, a third contribution at lower potential 0.11 V appears when the upper potential limit is 1.8 V. In case of graphene oxidized at 1.8 V in absence of 4-APPA, a tilted voltammogram is observed indicative of a resistive behavior as consequence of the oxidation of the graphene structure. However, once functionalization with 4-APPA is carried out, the resistive behavior is not observed despite the high conditions of oxidation and reversible redox processes are clearly observed. In this sense, the polymer/oligomer formed on the graphene surface can hinder its oxidation, protecting the material from the degradation.

For rGO, no significant differences can be observed in the voltammograms with respect to the obtained after oxidation in absence of 4-APPA (Figure A-4.6, C and D), only a small increase in voltammetric charge can be appreciated when the oxidation is produced in presence of 4-APPA. In this case, a small and reversible redox process at a 0.12 V is observed after the electrochemical treatment in presence of 4-APPA at 1.8 V. This result indicates that in this rGO the oxidation of the carbon material is produced in larger extension than the oxidation of 4-APPA.

2.3. XPS analysis of P and N species on electrochemically modified graphene-based materials

The amount of N and P species, and their chemical nature, incorporated on the GO and rGO were studied by XPS. Table A-4.1 summarizes the amount of O, N and P incorporated in the graphene-based materials during the electrochemical modification.

Table A-4.1. Chemical composition obtained from XPS of electrochemical modified graphene-based materials with 4-APPA.

| Graphene-based material | Upper limit potential [V vs. RHE] | O (at%) | N (at%) | P (at%) |
|-------------------------|-----------------------------------|---------|---------|---------|
| GO | Pristine | 24.3 | 0.86 | -- |
| | 1.5 | 22.2 | 0.71 | 1.14 |
| | 1.8 | 29.7 | 1.54 | 0.61 |
| rGO | Pristine | 20.1 | 1.39 | -- |
| | 1.5 | 23.0 | 1.37 | 0.52 |
| | 1.8 | 21.5 | 1.03 | 0.65 |
| Graphene K14 | 1.5 | 22.9 | 2.96 | 0.78 |
| | 1.8 | 12.6 | 1.6 | 0.55 |

It can be observed that for GO the amount of nitrogen increases with the upper potential limit from 1.5 to 1.8 V (Table A-4.1). Nevertheless, high polarization over 1.5 V causes a decrease in the concentration of phosphorus content, probably due to the overoxidation of the polymeric species formed during the oxidation and the oxidation of the phosphonic groups to phosphoric groups that can be hydrolyzed. The XPS data of N and P for rGO show a low amount of these two species in the surface. This result is in agreement with the behavior observed in voltammograms, where similar electrochemical behavior was observed in absence and in presence of 4-APPA in the solution, which could suggest a low degree of functionalization. Moreover, in the case of rGO a non-clear dependence with the upper potential limit is observed. In the case of K14 sample, a high amount of N and P is obtained at lower potential limit that decreases with the increase in potential (Table A-4.1). However, in case of GO and rGO, the amount of N mainly at 1.5 V cannot be distinguished from the amount of the pristine sample, indicating that the functionalization is more difficult than in the case of carbon nanotubes.

Deconvolution of N1s spectra in Figure A-4.7 presents the different species of nitrogen produced after the electrochemical modification of GO, rGO and K14 with 4-APPA at the two potentials evaluated. In case of both GO and rGO, the main peak can be deconvoluted in two peaks with binding energy of

399.8 and 402 eV, which can be assigned with the presence of amine and oxidized nitrogen species, consequence of the formation of oligomer/polymeric chains and N functionalities on the surface^{10-13,14}. Nevertheless, rGO shows an additional contribution at lower energy binding at around (~398.5 eV) related with presence of imines. The second contribution at 402 eV increases with the increase of the upper potential limit due to oxidation of N species into oxidized nitrogen species^{9,11}. The same behavior as for GO is observed for K14.

Regarding the P2p spectra, deconvolution of the phosphorus species might be carried out in one or two asymmetric doublets, as can be observed in Figure A-4.8. For GO and rGO electrode modified at a potential of 1.5 V, the spectra show a first contribution at 132.6 eV, associated in the literature with the binding energy of C-P-O species^{15, 16}, in agreement with the presence of the phosphonic group. Furthermore, a second contribution at 133.3 eV related with the C-O-P species appears that increases with the upper potential limit, as consequence of the oxidation of the phosphonic group to phosphoric group. However, when GO is electrochemically modified at a potential of 1.8 V, phosphorus species shows an important shift to higher binding energy at 134.1 eV, related with oxidized phosphorus species in which higher oxygen interaction is present, in concordance with values reported in literature for this species in carbon materials^{11, 17,18}.

Table A-4.2. Chemical distribution of the N and P species obtained from XPS of electrochemical modified graphene-based materials with 4-APPA.

| Graphene-based material | Upper potential limit [V vs. RHE] | More oxidized P (134.1 eV) | C-O-P (133.3 eV) | C-P-O (132.6 eV) | Imines (398.5 eV) | Neutral amines (399.8 eV) | Oxidized nitrogen species (~402 eV) |
|-------------------------|-----------------------------------|----------------------------|------------------|------------------|-------------------|---------------------------|-------------------------------------|
| GO | 1.5 | - | 44 | 56 | -- | 87 | 13 |
| | 1.8 | 100 | - | - | -- | 40 | 60 |
| rGO | 1.5 | - | 66 | 34 | 12 | 74 | 14 |
| | 1.8 | - | 53 | 47 | 11 | 77 | 12 |
| Graphene K14 | 1.5 | - | 60 | 40 | -- | 59 | 41 |
| | 1.8 | - | 66 | 34 | -- | 21 | 79 |

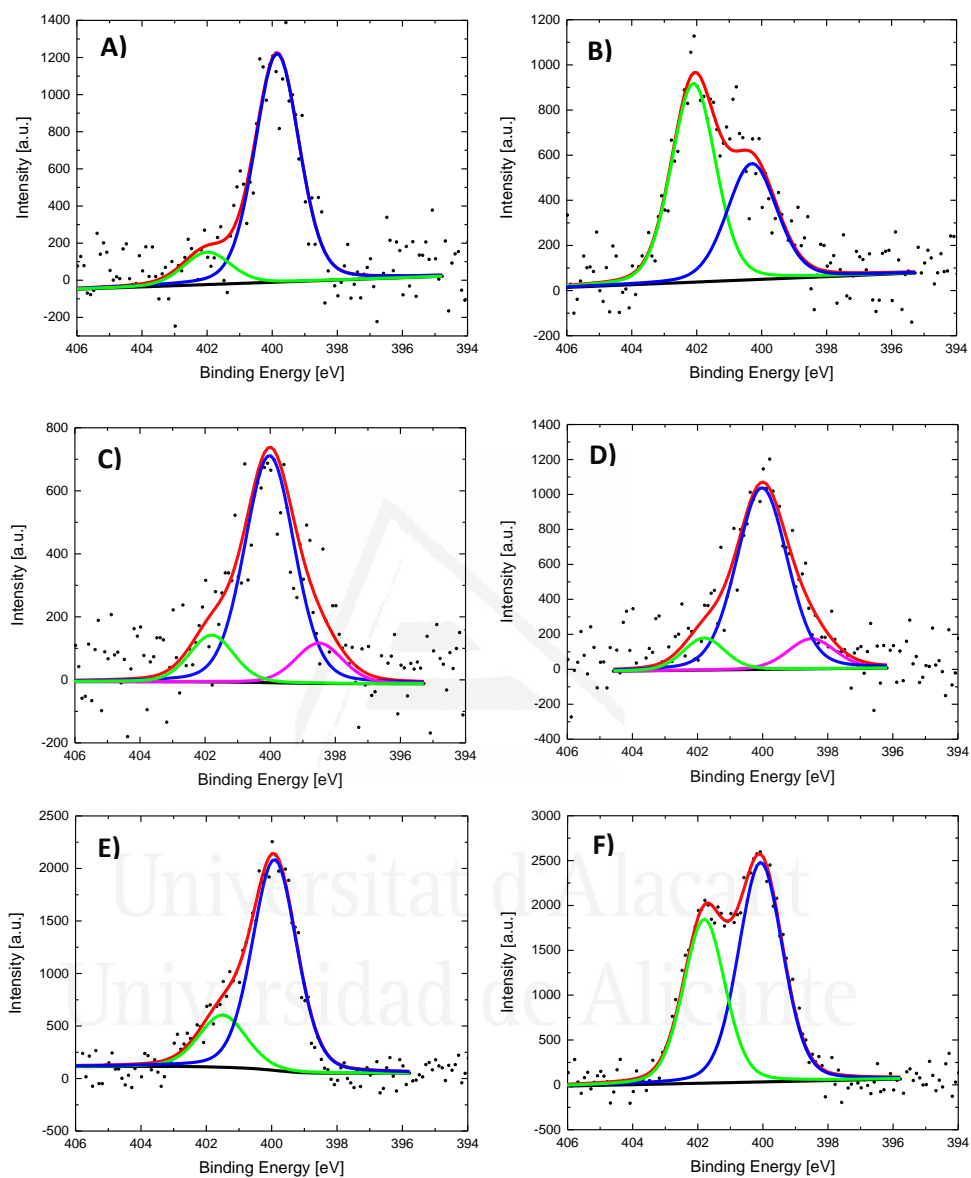
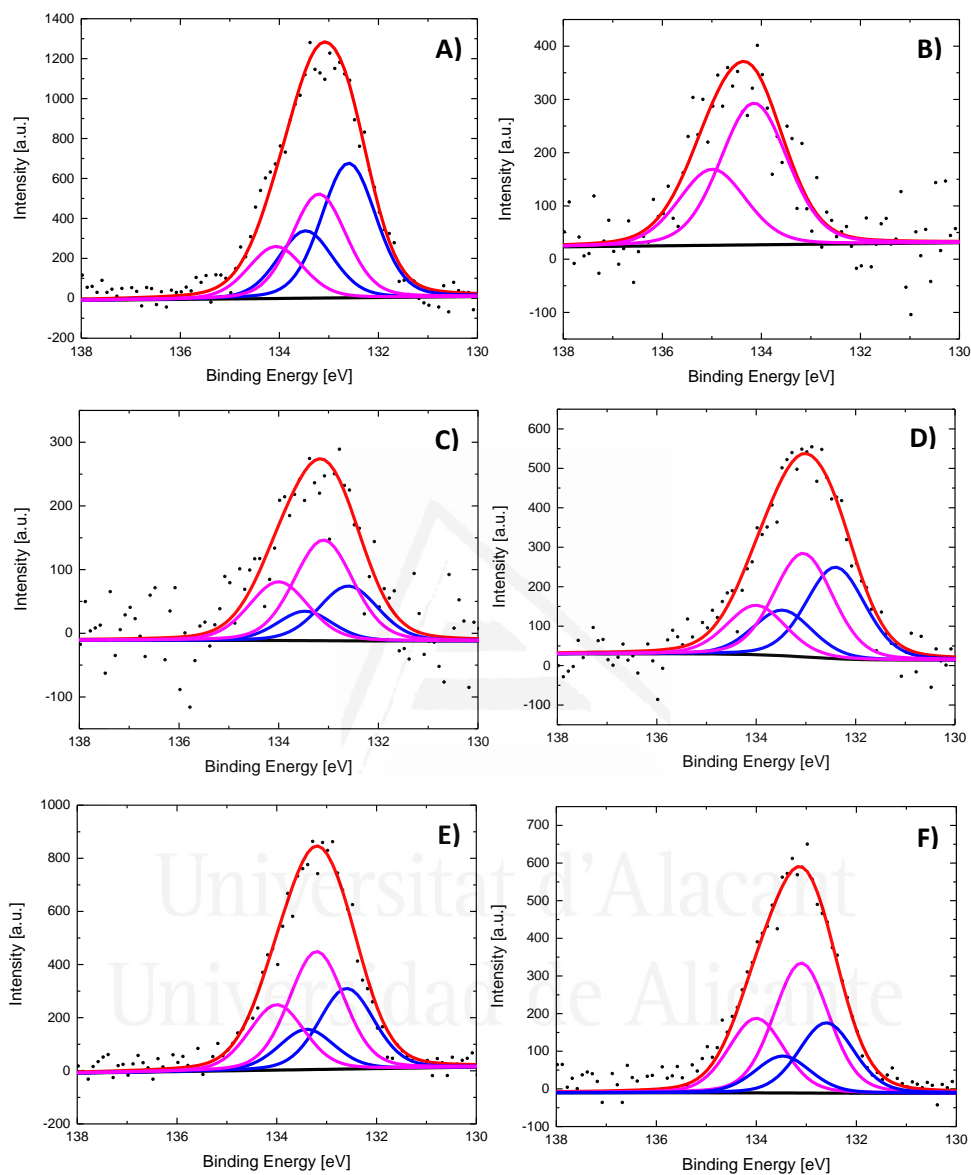


Figure A-4.7. N1s XPS spectra deconvoluted for GO and rGO electrochemical modified with 4-APPA at different oxidation potential: A) GO modified at 1.5 V, B) GO modified at 1.8 V, C) rGO modified at 1.5 V, D) rGO modified at 1.8 V, E) graphene K14 modified at 1.5 V and F) graphene K14 modified at 1.8 V.



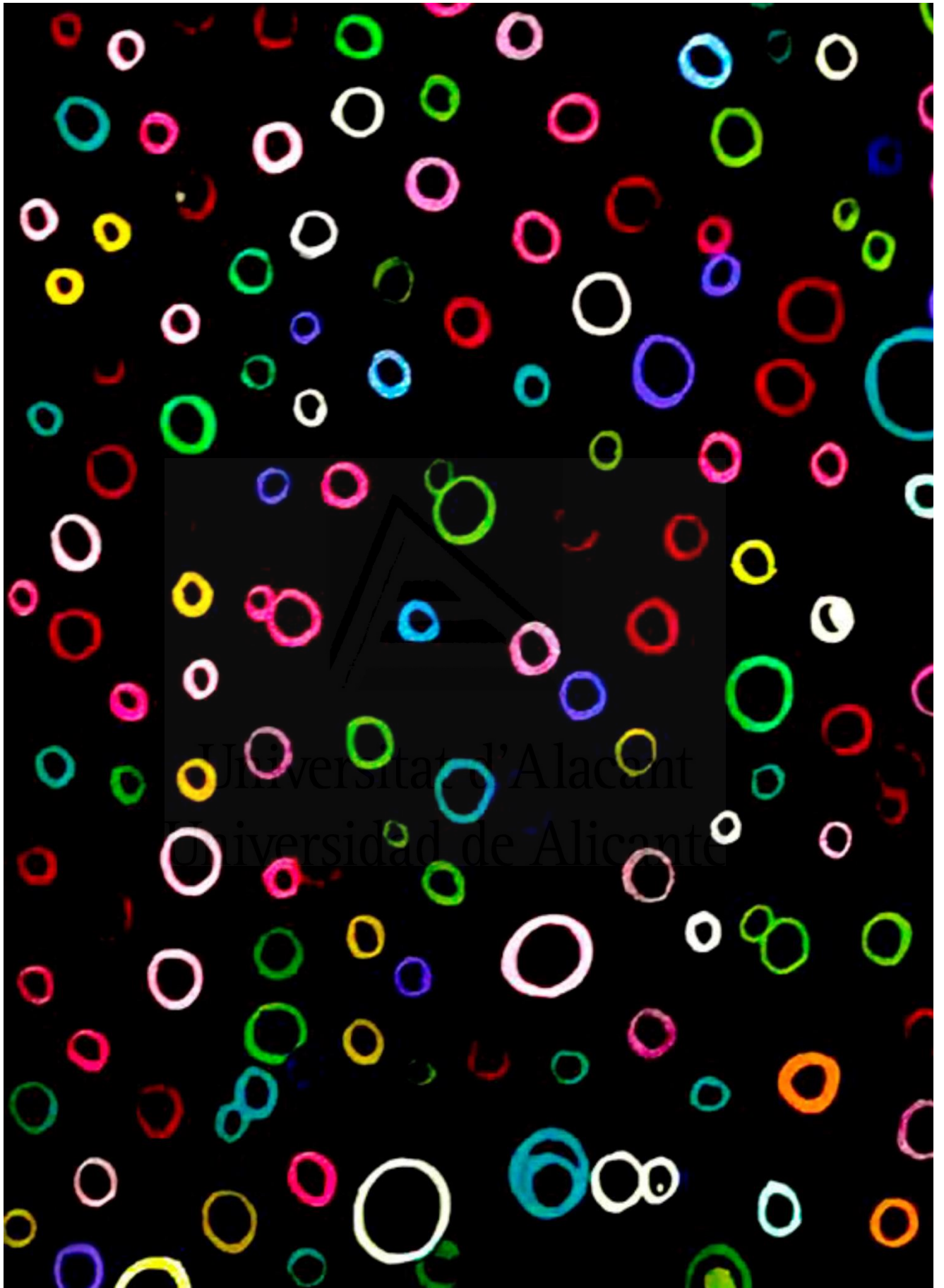
FigureA-4.8. P2p XPS spectra for GO, rGO and K14 electrochemical modified with 4-APPA at different oxidation potential: A) GO modified at 1.5 V, B) GO modified at 1.8 V, C) rGO modified at 1.5 V, D) rGO modified at 1.8 V, E) graphene K14 modified at 1.5 V and F) graphene K14 modified at 1.8 V.

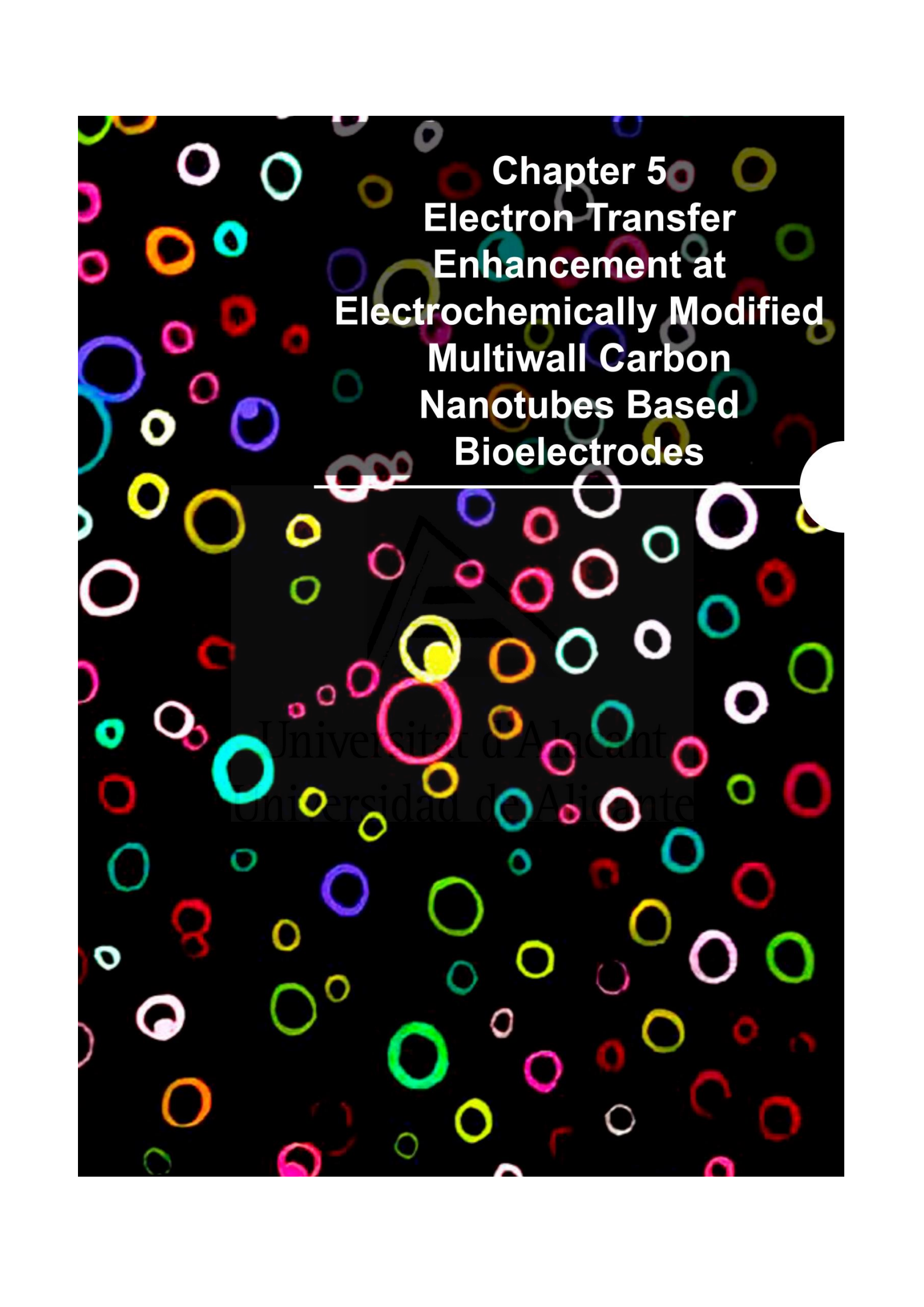
3. References

- (1) Marcano, D. C.; Kosynkin, D. V.; Berlin, J. M.; Sinitskii, A.; Sun, Z.; Slesarev, A.; Alemany, L. B.; Lu, W.; Tour, J. M. Improved Synthesis of Graphene Oxide. *ACS Nano* **2010**, *4* (8), 4806–4814.
- (2) Shao, Y.; Wang, J.; Engelhard, M.; Wang, C.; Lin, Y. Facile and Controllable Electrochemical Reduction of Graphene Oxide and Its Applications. *J. Mater. Chem.* **2010**, *20* (4), 743–748.
- (3) Ferrándiz-Saperas, M.; Ghisolfi, A.; Cazorla-Amorós, D.; Nájera, C.; Sansano, J. M. Multilayer Graphene Functionalized through Thermal 1,3-Dipolar Cycloadditions with Imino Esters: A Versatile Platform for Supported Ligands in Catalysis. *Chem. Commun.* **2019**, *55* (52), 7462–7465.
- (4) Cordero-Lanzac, T., García-Mateos, F. J., Rosas, J. M., Rodríguez-Mirasol, J., Cordero, T. Flexible Binderless Capacitors Based on P- and N-Containing Fibrous Activated Carbons from Denim Cloth Waste. *Carbon* **2018**, *139*, 599–608.
- (5) Toh, S. Y.; Loh, K. S.; Kamarudin, S. K.; Daud, W. R. W. Graphene Production via Electrochemical Reduction of Graphene Oxide: Synthesis and Characterisation. *Chem. Eng. J.* **2014**, *251*, 422–434.
- (6) Salinas-Torres, D.; Huerta, F.; Montilla, F.; Morallón, E. Study on Electroactive and Electrocatalytic Surfaces of Single Walled Carbon Nanotube-Modified Electrodes. *Electrochim. Acta* **2011**, *56* (5), 2464–2470.
- (7) Probst, M.; Holze, R. A Systematic Spectroelectrochemical Investigation of Alkyl-Substituted Anilines and Their Polymers. *Macromol. Chem. Phys.* **1997**, *198* (5), 1499–1509.
- (8) Nateghi, M. R.; Zahedi, M.; Mosslemin, M. H.; Hashemian, S.; Behzad, S.; Minnai, A. Autoacceleration/Degradation of Electrochemical Polymerization of Substituted Anilines. *Polymer* **2005**, *46* (25), 11476–11483.
- (9) Benyoucef, A.; Huerta, F.; Ferrahi, M. I.; Morallon, E. Voltammetric and in Situ FT-IRS Study of the Electropolymerization of o-Aminobenzoic Acid at Gold and Graphite Carbon Electrodes: Influence of PH on the Electrochemical Behaviour of Polymer Films. *J. Electroanal. Chem.* **2008**, *624* (1), 245–250.
- (10) Wang, B.; Tang, J.; Wang, F. Electrochemical Polymerization of

Aniline. *Synth. Met.* **1987**, *18* (1), 323–328.

- (11) Quílez-Bermejo, J.; Ghisolfi, A.; Grau-Marín, D.; San-Fabián, E.; Morallón, E.; Cazorla-Amorós, D. Post-Synthetic Efficient Functionalization of Polyaniline with Phosphorus-Containing Groups. Effect of Phosphorus on Electrochemical Properties. *Eur. Polym. J.* **2019**, *119*, 272–280.
- (12) Abidi, M.; López-Bernabeu, S.; Huerta, F.; Montilla, F.; Besbes-Hentati, S.; Morallón, E. Spectroelectrochemical Study on the Copolymerization of O-Aminophenol and Aminoterephthalic Acid. *Eur. Polym. J.* **2017**, *91*, 386–395.
- (13) Wang, Z.; Dong, Y.; Li, H.; Zhao, Z.; Bin Wu, H.; Hao, C.; Liu, S.; Qiu, J.; Lou, X. W. (David). Enhancing Lithium–Sulphur Battery Performance by Strongly Binding the Discharge Products on Amino-Functionalized Reduced Graphene Oxide. *Nat. Commun.* **2014**, *5*, 5002.
- (14) Cordero-Lanzac, T.; Rosas, J. M.; García-Mateos, F. J.; Ternero-Hidalgo, J. J.; Palomo, J.; Rodríguez-Mirasol, J.; Cordero, T. Role of Different Nitrogen Functionalities on the Electrochemical Performance of Activated Carbons. *Carbon* **2018**, *126*, 65–76.
- (15) Berenguer, R.; Ruiz-Rosas, R.; Gallardo, A.; Cazorla-Amorós, D.; Morallón, E.; Nishihara, H.; Kyotani, T.; Rodríguez-Mirasol, J.; Cordero, T. Enhanced Electro-Oxidation Resistance of Carbon Electrodes Induced by Phosphorus Surface Groups. *Carbon* **2015**, *95*, 681–689.
- (16) Quesada-Plata, F.; Ruiz-Rosas, R.; Morallón, E.; Cazorla-Amorós, D. Activated Carbons Prepared through H₃PO₄-Assisted Hydrothermal Carbonisation from Biomass Wastes: Porous Texture and Electrochemical Performance. *Chempluschem* **2016**, *81* (12), 1349–1359.
- (17) Ruiz-Soria, G.; Susi, T.; Sauer, M.; Yanagi, K.; Pichler, T.; Ayala, P. On the Bonding Environment of Phosphorus in Purified Doped Single-Walled Carbon Nanotubes. *Carbon* **2015**, *81*, 91–95.
- (18) Valero-Romero, M. J.; García-Mateos, F. J.; Rodríguez-Mirasol, J.; Cordero, T. Role of Surface Phosphorus Complexes on the Oxidation of Porous Carbons. *Fuel Process. Technol.* **2017**, *157*, 116–126.



The background of the slide is a black field filled with numerous small, colorful circles in various sizes and colors, including red, green, blue, yellow, orange, and white. The circles are scattered across the entire page, creating a vibrant, abstract pattern.

Chapter 5 Electron Transfer Enhancement at Electrochemically Modified Multiwall Carbon Nanotubes Based Bioelectrodes

Universitat d'Alicant
Universidad de Alicante

1. Introduction

In many applications, electron-transfer (ET) between the enzymatic element immobilized in an electrode and the substrate is so far the triggering factor for an optimal operation of any bioelectrochemical devices. Nevertheless, the embedded redox-active center of the enzyme, for example oxidoreductases, in the amino acids structure makes difficult the direct electron transfer (DET) in the biocatalyst electrode^{1,2}. Therefore, continued efforts have focused on facilitating and promoting the ET from the redox center in the enzyme towards the electrode. Different immobilization methods have been extensively used to keep the activity of the enzyme, improving the orientation of the enzyme or even “wiring” the active center of the enzyme with the transducer, providing a path for a DET mechanism³⁻⁶. Unfortunately, denaturalization and conformational changes in the bioenzymatic element are produced during the immobilization process, that can decrease their stability and catalytic behavior⁶.

Carbon nanotubes (CNTs) have been employed as platforms in the development of biocatalysts in biosensing and bioelectrodes for electrochemical energy generation due to the remarkable chemical stability, biocompatibility, catalytic and electronic properties^{7,8}. Moreover, some studies have suggested that the structural features of the CNTs can reduce the distance between the active-center of the enzyme and the electrode surface^{8,9}. One important aspect that promotes the versatility of CNTs applications, lies in their tunable-surface chemistry that can be done through different procedures including non-covalent or covalent functionalization methods^{10,11}. In this sense, modification of CNTs by surface functionalities provides an outstanding route for synthesis of active materials with enhanced properties for specific applications.

First approaches of functionalization were focused in the oxidation of CNTs, employing acid solutions to incorporate oxygen functionalities, such as carboxylic moieties, which can anchor the amine-terminal groups in the enzyme structure with the CNT surface, promoting the immobilization of the bioelement¹². Nowadays, other reactions, (i.e. amidation, hydrogenation, electrografting, etc.), based on the generation of radical species of high reactivity that can react with the carbon atoms in the CNT structure, have

become a promising route in the assembling of building blocks for the synthesis of improved biocatalysts¹³⁻¹⁶.

Functionalization of CNTs surface with different type of active species by chemical and electrochemical modification procedures have demonstrated being effective for anchoring surface functionalities that can interact covalently with amino acids in the enzymes^{13,17-19}. For example, carbon nanotube surface modified with maleimide groups by electrografting of primary amines, were used to elaborate the surface-modified electrode which shows high catalytic currents and long-term storage stability⁵.

In this work, Multi Wall Carbon Nanotubes (MWCNTs) electrochemically functionalized with N and P species have been synthesized, obtaining electroactive species for the development of bioelectrodes as platforms for biosensors and biofuel cell applications. The functional carbon materials promote a good electron-transfer between a quinone oxidoreductase glucose dehydrogenase (PQQ-GDH), employed as enzymatic model element, and the electrode. Thus, a biofunctional metal-free MWCNTs electrode is developed in which the amount phosphorus and nitrogen species introduced on the carbon nanotube surface can be controlled. Depending of the upper potential limit of electrochemical modification, operational stability, electron-transfer kinetics, catalytic activity and sensitivity towards glucose oxidation can be significantly improved, providing an interesting platform for developing high performance bioelectrodes with good interaction with the enzymatic element.

2. Experimental section

2.1. Materials

MWCNT with purity 95% (8 nm of diameter), 10-30 μm of length were purchased to Cheap Tubes Inc. (Cambridgeport, USA). N,N-Dimethylformamide (DMF), extra pure, provided by Scharlau, was used as solvent to disperse the CNTs. Specific surface area, obtained from N_2 adsorption isotherms at $-196\text{ }^\circ\text{C}$ in an automatic adsorption system (Autosorb-6, Quantachrome) and using the Brunauer, Emmett and Teller (BET) method, is $208\text{ m}^2\text{ g}^{-1}$.

Soluble apo-enzyme glucose dehydrogenase (sGDH) was provided by Roche Diagnostics (Germany). Sulphuric acid (98%) analytical reagent to

prepare the electrolyte, was obtained from VWR Chemicals. 4-amino phenyl phosphonic acid (4-APPA, +98%) was purchased to Tokyo Chemical Industry co (TCI-Belgium). Potassium dihydrogen phosphate (KH_2PO_4) and dipotassium hydrogen phosphate tri hydrate ($\text{K}_2\text{HPO}_4 \cdot 3\text{H}_2\text{O}$), obtained from VWR Chemicals, were used to prepare phosphate buffer solution (0.1 M PBS, pH=7.2). (4-(2-hydroxyethyl)-1-piperazineethanesulfonic acid) (HEPES) ($\geq 99.5\%$ -titration), D-(+)-Glucose ACS reagent and pyrroloquinoline quinone (PQQ) ($\geq 95\%$ -HPLC) were purchased from Sigma-Aldrich. All the solutions were prepared using ultrapure water (18 M Ω cm, Purelab Ultra Elga equipment). The gases Ar (99.999%) and H₂ (99.999%) were provided by Air Liquide.

Electrochemical measurements were performed in a BIOLOGIC SP-300 potentiostat and a standard three-electrode cell configuration, in which glassy carbon (GC) electrodes modified with the MWCNTs were the working electrode (WE), a graphite rod was used as counter electrode (CE) and a Ag/AgCl (3 M KCl) introduced in the same electrolyte and connected with the working solution through a Lugging capillary, was used as reference electrode (RE). The potentials are referred to this reference electrode, and in order to compare with the potentials used in the other chapters of this PhD Thesis, the following equivalence should be applied: 0.97, 1.17 and 1.37 V correspond to 1.2, 1.4 and 1.6 V vs. RHE, respectively.

2.2. Electrochemical modification of MWCNTs with 4-amino phenyl phosphonic acid.

Dispersions of 1 mg mL⁻¹ of MWCNTs in DMF were prepared. Prior to the deposition of MWCNTs, the glassy carbon (GC) surface (3 mm diameter) was sanded with emery paper and polished using 1 and 0.05 μm alumina slurries, then rinsed with ultrapure water. Afterwards, 5 μL aliquot of the MWCNTs dispersion was dropped onto the GC surface and dried under an infrared lamp to remove the solvent. This procedure was repeated twice until completing 10 μL of the carbon material suspension on the electrode.

The electrochemical modification of MWCNTs was performed by cyclic voltammetry in a deoxygenated 0.5 M H₂SO₄ + 1 mM 4-APPA aqueous solution. During the measurement inert gas (Ar) flow was maintained. Modification of carbon material was achieved submitting the sample to 10

cycles at 10 mV s^{-1} , reaching different upper potential limit. After electrochemical treatment, carbon electrodes were washed with excess of ultrapure water, removing remaining electrolyte.

1.3 Physicochemical characterization.

X-Ray photoelectron spectroscopy (XPS) was performed in a VG-Microtech Mutilab 3000 spectrometer and Al K α radiation (1253.6 eV). The P2p spectra have been analyzed considering the spin-orbit splitting into P2p $_{3/2}$ and P2p $_{1/2}$ with a 2:1 peak area ratio and 0.87 eV splitting²⁰.

Scanning electron micrographs were taken using an ORIUS SC600 model Field Emission Scanning Electron Microscopy (FE-SEM) and a ZEISS microscope, Merlin VP Compact model. Samples are coated with a thin layer of carbon to avoid decomposition of the enzyme and the different oligomers incorporated by the electrochemical modification of 4-APPA.

2.4. Multi wall carbon nanotubes electrochemically modified with 4-APPA and PQQ-GDH

Glassy carbon electrodes modified with MWCNT functionalized with 4-APPA were modified with PQQ-GDH as a bioactive species.

Firstly, the s-GDH were reconstructed with PQQ, following this procedure: 36 mg of s-GDH were dissolved in 10 mM HEPES Buffer solution (pH=7.0), 150 mM CaCl $_2$ ·2H $_2$ O and 520 μ M of PQQ freshly prepared, attaining a concentration of 36 mg mL $^{-1}$ of PQQ-GDH. In this procedure, PQQ cofactor is introduced in the apo-enzyme structure as active center, and the complex is stabilized by the presence of three calcium cations²¹. At the same time, one of the calcium cations is required for the activation of the cofactor and oxidation with the substrate (glucose). Enzymatic solution was treated at 1600 rpm for 30 min in vortex and stored at 4°C till being used.

Bioelectrodes were synthesized dropping 5 μ L aliquot of the enzymatic solution onto the MWCNT functionalized with 4-APPA. The aliquot was dried at 4°C for 1 hour, promoting the incubation process of the enzyme onto the surface electrode. Subsequent washing with 0.1 M PBS (pH=7.2) removes the non-immobilized enzymes and the electrode was dried under Ar flow. Surface

concentration of PQQ-GDH was calculated from the redox processes in the voltammogram using Eq. 5.1.

$$\Gamma = \frac{Q}{nFA} \quad \text{Eq. 5.1}$$

Where Γ is the surface concentration of PQQ-GDH (mol m^{-2}), n is the number of electrons in the redox reaction, F is the Faraday constant (C mol^{-1}), A is the electrode-surface area (m^2) and Q is the charge (C) obtained from the integration of the anodic peak associated with the redox process of the enzyme.

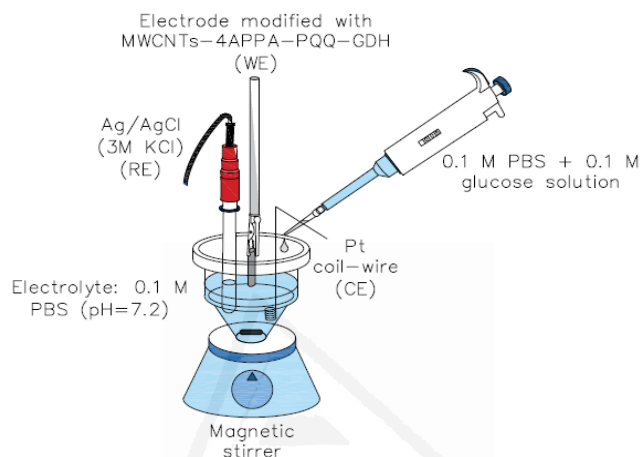
Apparent electron-transfer constant (k_s^{app}) for the redox-active center of the PQQ-GDH in the electrochemically modified MWCNTs with 4-APPA at different upper potential limits, was estimated using the Laviron's model²². Values of k_s^{app} were estimated for each electrode prepared in this work considering the Laviron's formalism based on the classical Butler–Volmer theory²³.

2.5. Electrochemical characterization and biocatalytic activity towards glucose oxidation

Electrochemical behavior of MWCNTs modified with 4-APPA and PQQ-GDH (MWCNT-PQQ-GDH) was evaluated in 0.1 M PBS solution (pH=7.2), in absence and presence of glucose using cyclic voltammetry.

On the other hand, electrochemical catalytic behavior towards glucose oxidation was studied by chronoamperometry in the same electrochemical cell configuration. Considering that oxidation process of glucose by the PQQ-GDH has no oxygen dependence, room atmosphere conditions were used. The different electrodes were stabilized at 0.35 V in 0.1 M PBS (pH=7.2) solution during 1 h previous to the addition of glucose. After this time, aliquots of 0.1 M glucose solution were added to the electrochemical cell, obtaining concentrations between 5 μM to 6 mM. During the chronoamperometry, stirring conditions are maintained to improve the flux of glucose towards the electrode surface. Scheme 5.1 shows the electrochemical set-up. Cyclic voltammetry was employed at the beginning and at the end of the test to control that the characteristic of the electrode is maintained during the study. All measurements were carried out in triplicate with three electrodes prepared

in the same conditions. Moreover, the limit of detection (LOD) was determined empirically, by progressively measuring more diluted concentrations of the analyte. The LOD was the lowest concentration whose signal could be clearly distinguished from the blank. Moreover, the limit of quantification (LOQ) was calculated as 3.3 times the LOD (LOQ = 3.3LOD).



Scheme 5.1. Electrochemical set-up configuration for studying the catalytic activity of MWCNT electrochemical modified with 4-APPA and PQQ-GDH towards glucose oxidation.

In this work, the electrodes prepared are named as MWCNT-APPA-X for those prepared without enzyme, being X the upper potential limit that was employed for the electrochemical modification, and MWCNT-APPA-X-GDH for the electrode with the PQQ-GDH immobilized.

Electrochemical stability of the different electrodes was determined by two different chronoamperometry experiments. In the first experiment, MWCNT-APPA-X-GDH electrodes were polarized from the open circuit potential to 0.35 V. In case of the first stability test, the electrodes are maintained for 10 min at this potential, then an aliquot of 0.1 M of glucose is added to achieve a concentration of 20 mM. The electrodes were stored at 4°C and tested each day in the same conditions for 8 days. The second stability test consists on maintaining the electrode at the potential of 0.35 V for 24 hours without addition of glucose under continued stirring conditions.

3. Results and discussion

3.1. Electrochemical modification of MWCTN with 4-APPA

Cyclic voltammograms during electrochemical oxidation of 4-APPA on MWCNT at different upper potential limits are shown in Figure 5.1.

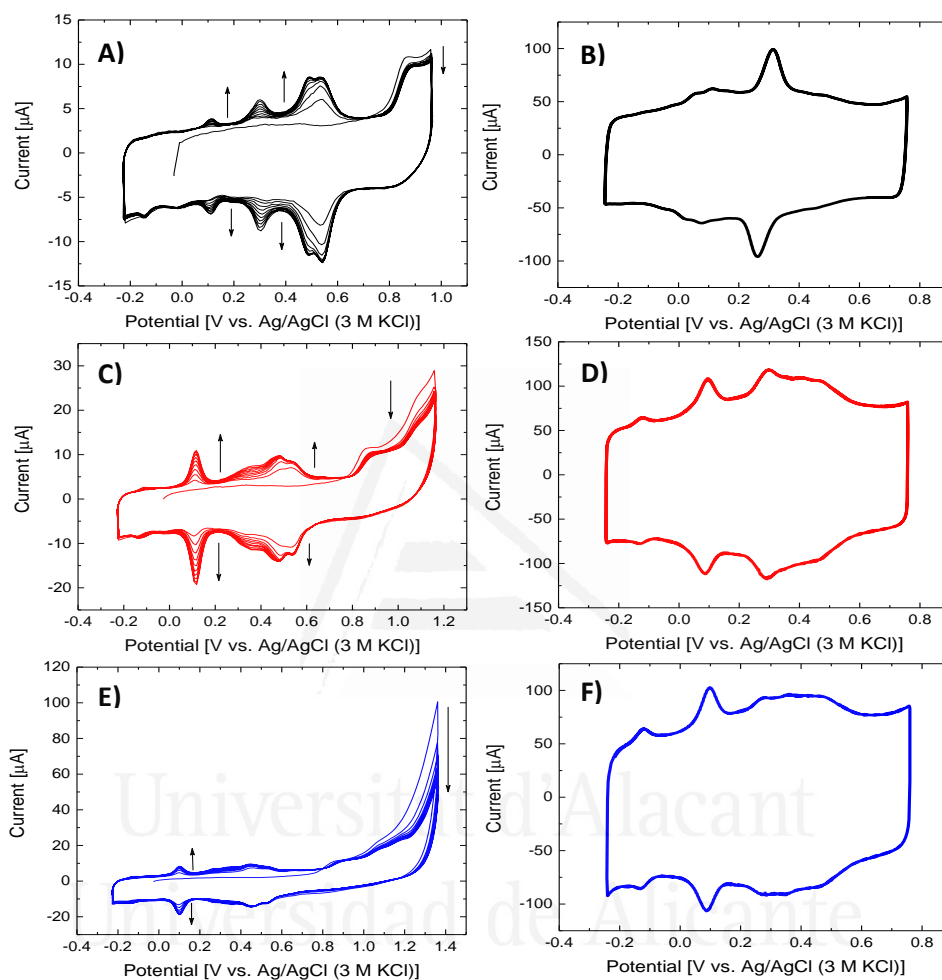


Figure 5.1. Cyclic voltammograms of MWCNT in 0.5 M H_2SO_4 + 1 mM 4-APPA at 10 mV s^{-1} , 10 cycles under Ar atmosphere at different upper potential limits: A) 0.97 V, C) 1.17 V and E) 1.37 V. Cyclic voltammograms for MWCNT-APPAX electrodes in 0.5 M H_2SO_4 , B) MWCNT-APPAX-0.97, D) MWCNT-APPAX-1.17 and F) MWCNT-APPAX-1.37 at 50 mV s^{-1} , under Ar atmosphere.

Irreversible oxidation peaks can be observed at potentials higher than 0.8 V that correspond to the oxidation of 4-APPA (Fig. 5.1-A, 5.1-D and 5.1-E). During oxidation of 4-APPA, oligomer chains as well as covalently bonded species to the surface of the MWCNTs can be produced²⁴. Presence of those

species on the surface can generate different highly reversible redox processes in the voltammogram in absence of 4-APPA in the solution (Figure 5.1-B, 5.1-D and 5.1-F).

Continuous cycling of the electrode in presence of 4-APPA generates an increase in the charge of the different reversible redox processes observed between -0.2 and 0.7 V. Figure 5.2-A shows the value of charge determined from the voltammogram normalized to the amount of MWCNT deposited. It can be observed that these values increase with the upper potential limit used in the oxidation of 4-APPA reaching values twice of the initial for the MWCNTs only with the polarization at 0.97 V and more than 4 times for the highest potential studied.

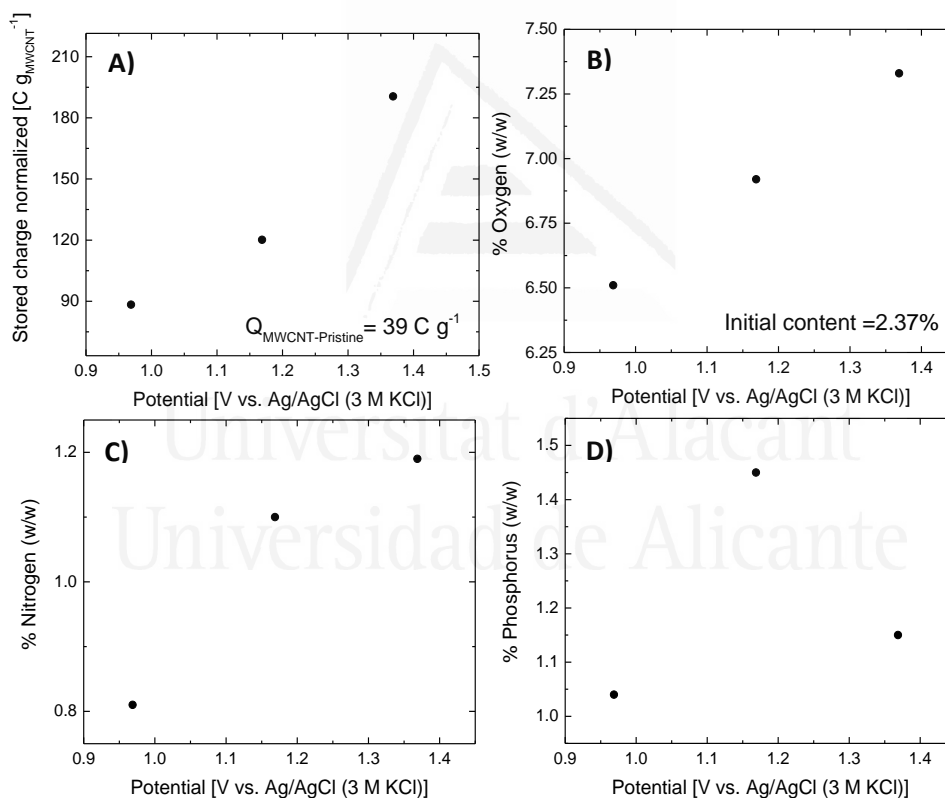


Figure 5.2. A) Charge normalized vs. upper potential limit used in the 4-APPA oxidation, B) Amount of oxygen vs. upper potential limit, C) Amount of nitrogen vs. upper potential limit and D) Amount of phosphorus vs. upper potential limit. Note: Charge was determined in a potential range of 0.63 V and at scan rate of 50 mV s⁻¹, under Ar atmosphere.

Figure 5.2-B, 5.2-C and 5.2-D shows the amount of oxygen, nitrogen and phosphorus determined by XPS, respectively, for the MWCNT-APPA electrodes at different upper potential limits. Quantification by XPS elucidates the degree of modification and incorporation of heteroatoms on the MWCNT surface (See Figure 4.10 and 4.11)

The amount of oxygen and nitrogen on the MWCNT-APPA-X surfaces (Figures 5.2-B and 5.2-C), shows a direct dependence with the upper potential limit used in the oxidation. The oxidative conditions at higher potential promotes the incorporation of oxygen functionalities in the MWCNT, oligomer chains adsorbed on the surface and covalently bonded APPA species²⁴. Interestingly, phosphorus content shows a maximum value of incorporation at 1.17 V, suggesting that oxidation at higher potentials favors phosphonic acid oxidation and desorption due to hydrolysis reactions.

3.2. *Electrochemical characterization of MWCNT modified with 4-APPA and PQQ-GDH*

The bioelectrodes should be stable at pH close to the physiological one, then it is important to characterize the synthesized electrodes under these conditions. Figure 5.3 shows the electrochemical response of MWCNT-APPA-X electrodes in 0.1 M PBS (pH=7.2). Pristine MWCNTs presents a quasi-rectangular shape at these conditions; however, the MWCNT-APPA-X samples show different redox processes as in the case of acidic conditions but with lower current, thus indicating that they maintain the electroactivity at this pH.

Universidad de Alicante

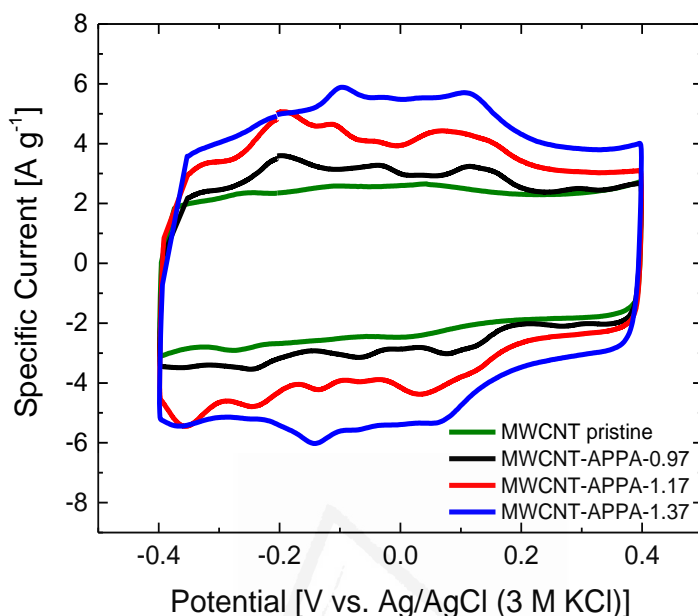


Figure 5.3. Cyclic voltammograms for the MWCNT and MWCNT-APPA-X electrodes in 0.1 M PBS (pH = 7.2) at 50 mV s^{-1} under Ar atmosphere.

Figure 5.4 shows the cyclic voltammograms of the electrodes after immobilization of the PQQ-GDH. It can be observed a small decrease of the double-layer charge with respect to the MWCNT-APPA-X for all the electrodes. Additionally, a clear electrochemical redox couple is observed in all the modified MWCNT-APPA-X-GDH electrodes, at the same formal potential (E^0) of about -0.12 V , which can be assigned to the two-electron redox process of the PQQ in the active-redox center of the holo-enzyme PQQ-GDH in neutral conditions²⁵. This result is in agreement with other electrochemical behaviors observed for immobilized PQQ-GDH using different electrodes^{26,27}.

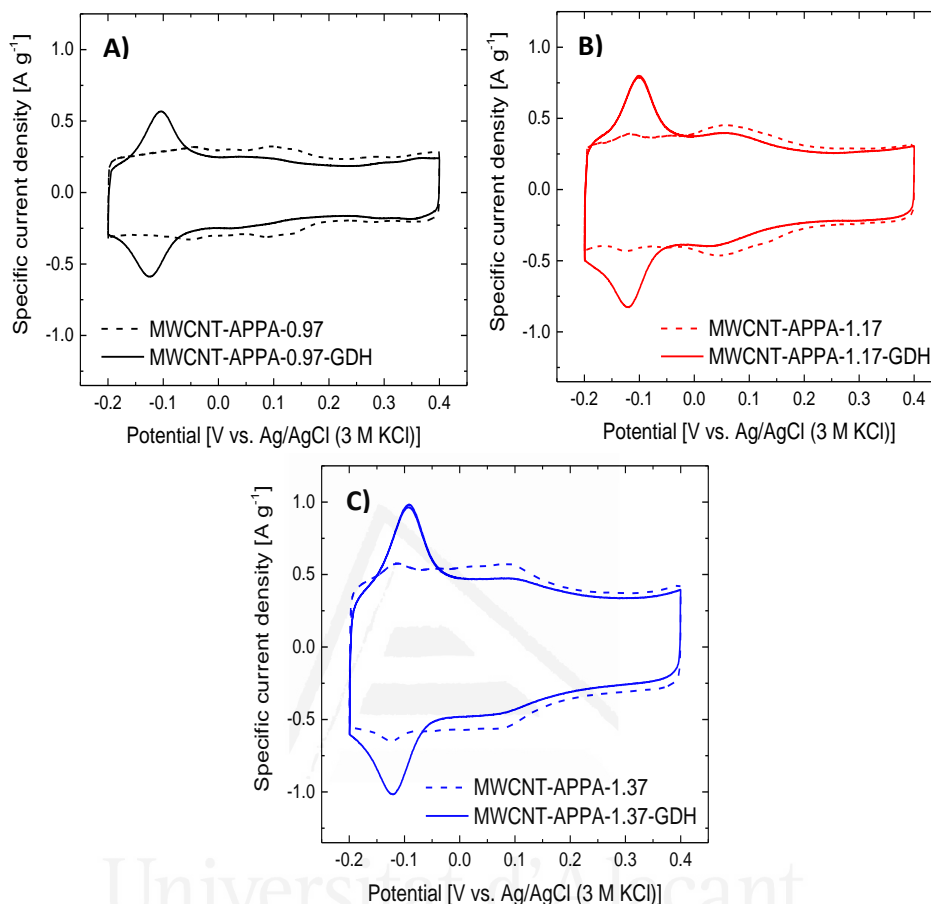


Figure 5.4. Cyclic voltammograms of MWCNT-APPA and MWCNT-APPA-X-GDH at different upper potential limits of modification: A) 0.97 V, B) 1.17 V and C) 1.37 V in 0.1 M PBS (pH = 7.2), at 5 mV s^{-1} under Ar atmosphere.

The peak potential separation associated with the PQQ active center in the holo-enzyme has values corresponding to a theoretical reversible two-electron transfer process at 5 mV s^{-1} ($\sim 29 \text{ mV}$)²⁸, which is in agreement with the values of the $I_{\text{anodic}}/I_{\text{cathodic}}$ ratio ~ 1 . Taking into account the pH conditions, the redox process of the cofactor in the enzyme can be a process in which the formation of intermediate quinone species and one protonation of the PQQ can take place²⁹.

Table 5.1 shows the values of surface coverage of PQQ-GDH for the different electrodes. These values change similarly as the phosphorus content

(Figure 5.2-D), reaching the maximum value for the MWCNT modified with APPA at 1.17 V, which is the one with the highest phosphorus content. This can be consequence of the electrostatic interaction between the PQQ-GDH, which presents a net positive charge at the pH conditions employed during the immobilization process³⁰ and the different deprotonated terminal groups in the phosphorus moieties³¹ incorporated on the MWCNTs surface.

Table 5.1. Electrochemical parameters associated with the PQQ-GDH electron-transfer process on MWCNT-APPA-X-GDH electrodes.

| Upper potential limit [V] | Γ^{**} [mol cm ⁻²] | ΔE^{**} [mV] | k_s^{app} [s ⁻¹] | i_a [A g ⁻¹]* | i_c [A g ⁻¹]* | $\frac{i_a}{i_c}$ |
|----------------------------------|--|-------------------------|-----------------------------------|--------------------------------|--------------------------------|-------------------|
| 0.97 | 1.76x10 ⁻¹¹ | 22 | 69.2 | 0.27 | 0.29 | 0.94 |
| 1.17 | 2.23x10 ⁻¹¹ | 20 | 71.5 | 0.43 | 0.39 | 1.10 |
| 1.37 | 1.56x10 ⁻¹¹ | 30 | 81.7 | 0.43 | 0.36 | 1.20 |

*Anodic and cathodic current density and charge of the PQQ-GDH were determined subtracting the contribution of the MWCNT-APPA-X without enzyme.

**Values determined at 5 mV s⁻¹

Electrochemical study with the scan rate shows a linear-dependence behavior of the oxidation and reduction currents, associated with the two electron-transfer process for the active redox center of the enzyme immobilized onto the modified MWCNTs (See Figures 5.5). This corresponds to a surface confined redox process³²⁻³⁴, confirming the confinement of the enzyme by the functional groups on the MWCNT surface. Interestingly, the slope of the linear-fitting with the scan rate (v_{scan}), could be related with the concentration of the active species on the surface (coverage of PQQ-GDH)^{35,36}, which shows a maximum value for the MWCNT-APPA-1.17 electrode, in agreement with the results in Table 5.1, which confirms that a higher concentration of enzyme is reached with this electrode.

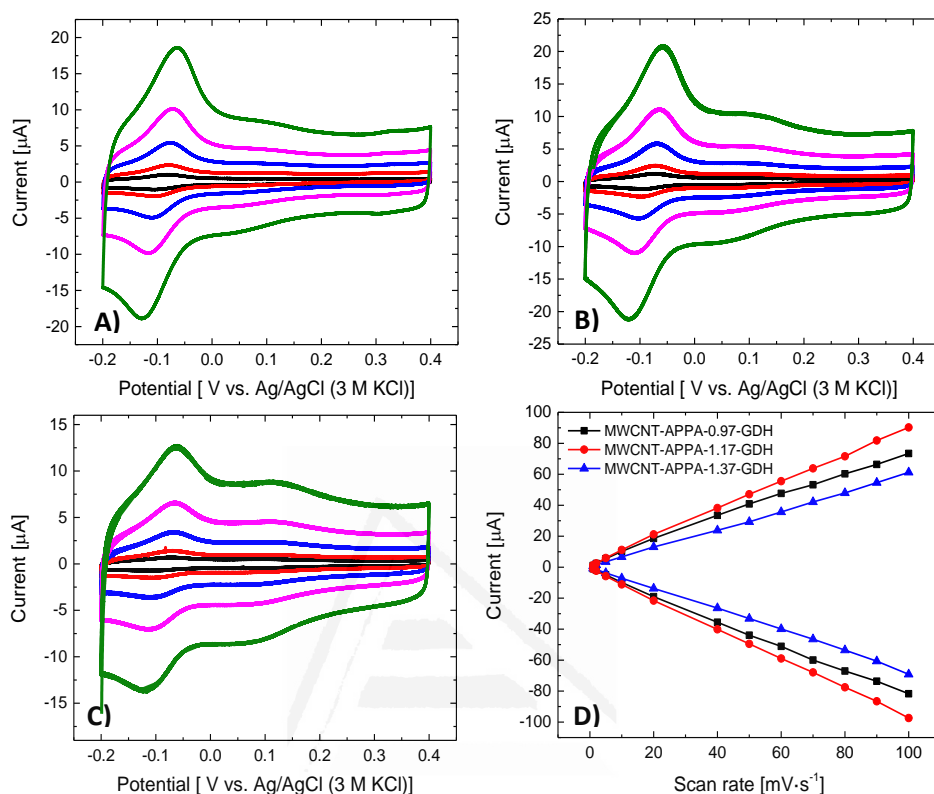


Figure 5.5. A-C) Cyclic voltammetry of MWCNT-APPA-X-GDH electrodes synthesized at different upper potential limits: A) 0.97, B) 1.17 and C) 1.37 V in 0.1 M PBS (pH = 7.2) at different v_{scan} (black: 1 mV s^{-1} , red: 2 mV s^{-1} , blue: 5 mV s^{-1} , pink: 10 mV s^{-1} and green: 20 mV s^{-1}) under Ar atmosphere. D) Plot of cathodic and anodic peak currents vs. v_{scan} for the redox processes of the PQQ-GDH in MWCNT-APPA-X-GDH electrodes in 0.1 M PBS (pH = 7.2).

The apparent rate constant, k_s^{app} , (Table 5.1) was calculated, and values between 69 and 82 s^{-1} are obtained from the Trumpet-plots (See Figure 5.6). An increase of the k_s^{app} with the upper potential limit suggests that the interaction between the MWCNT-APPA electrodes and PQQ-GDH is improved, providing a fast electron-transfer between the electrode and the redox-active center of the enzyme.

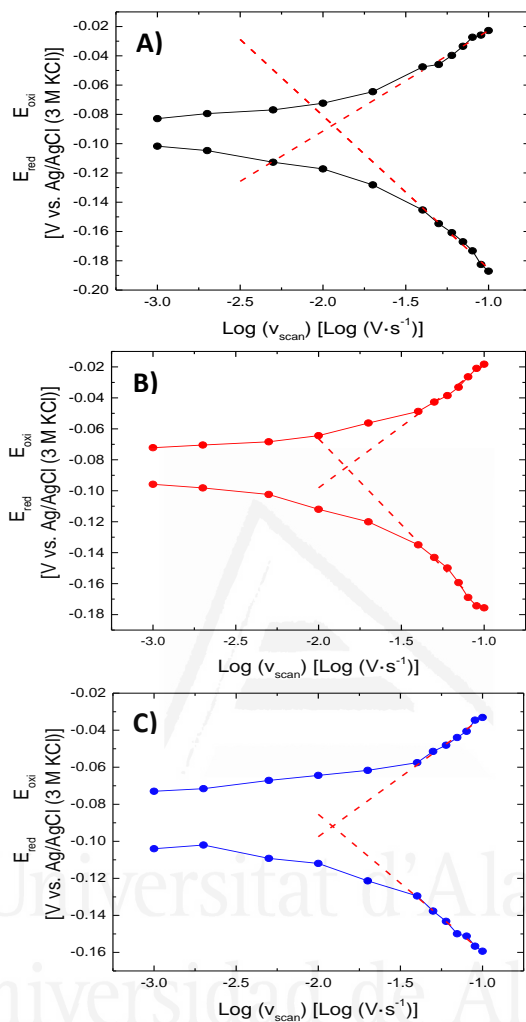


Figure 5.6. Trumpet plots of the anodic and cathodic peak potential (E_p) vs. the logarithm of scan rate ($\log_{10} v_{scan}$), the linear fitting at scan rates from 1 mV s^{-1} to 200 mV s^{-1} for MWCNT-APPA-X-GDH at different upper potential limits: A) 0.97, B) 1.17 and C) 1.37 V.

The morphological characterization obtained by FESEM of the MWCNT-APPA-X and MWCNT-APPA-GDH synthesized are presented in Figure 5.7.

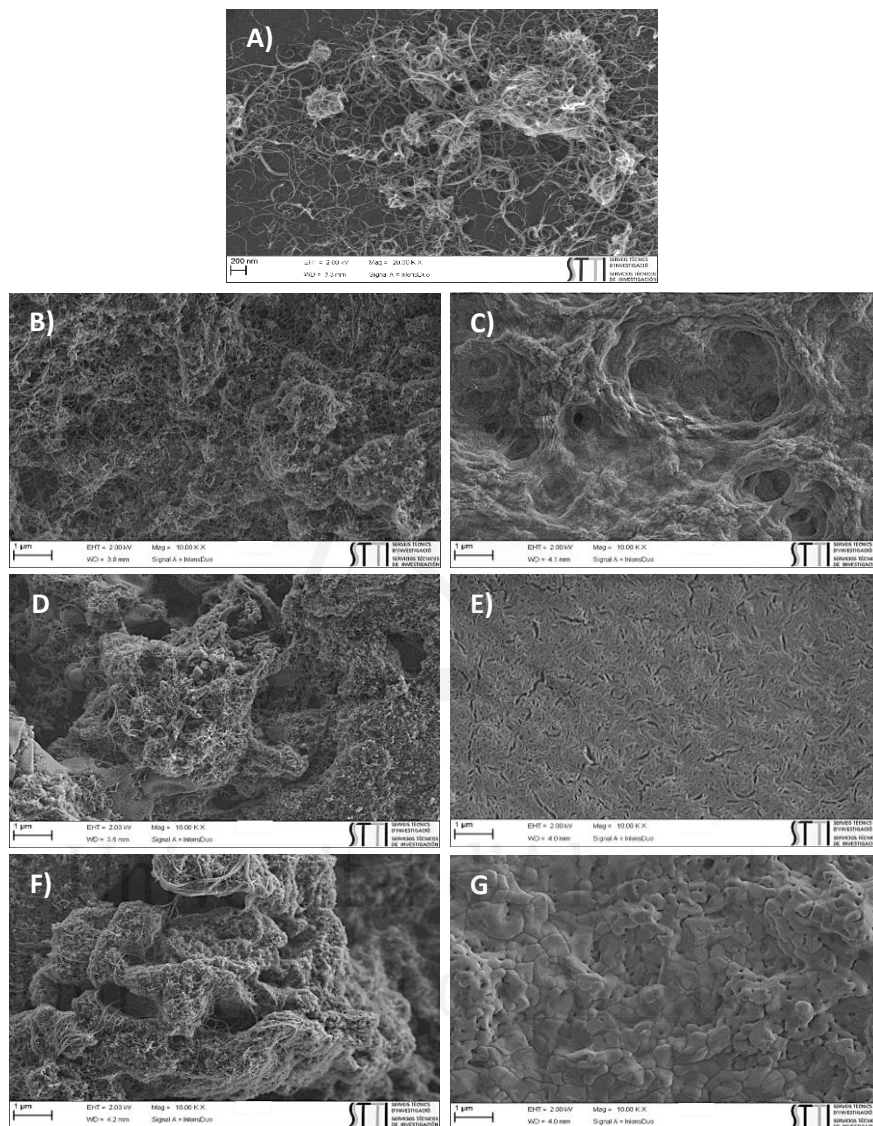


Figure 5.7. FESEM micrographs of A) MWCNT, B) MWCNT-APPA-0.97, D) MWCNT-APPA-1.17 and F) MW CNT-APPA-1.37 V. C) MWCNT-APPA-0.97-GDH, E) MWCNT-APPA-1.17-GDH and G) MWCNT-APPA-1.37-GDH.

Morphology of the deposits of MWCNTs modified with 4-APPA can be observed in Figure 5.7. Typical bundles can be observed in the deposits of MWCNTs (see Figure 5.7-A) and the modified MWCNTs with 4-APPA.

However, the oxidation of MWCNTs in presence of 4-APPA causes the formation of a thin film and small deposits on the MWCNTs surface, related with the oligomer chains formed. Once, PQQ-GDH is immobilized on the MWCNTs electrochemically modified (See Figure 5.7-B, 5.7-D and 5.7-F), the formation of a continuous enzymatic coating can be appreciated in all the electrodes; nevertheless, depending on the applied potential for the modification with APPA, the morphology of the coating changes considerably. Electrodes modified at 0.97 V presents a coating of PQQ-GDH, which resembles the roughness and bundles-like structure of the MWCNTs; suggesting a low thickness of the enzymatic coating. Increase of the applied potential promotes the immobilization of a dense and thick coating with presence of porosity and sponge-like texture for the potential of 1.17 V and a more defined globular morphology is observed at 1.37 V.

3.3. Electrocatalytic response of MWCNT-APPA-X-GDH electrodes towards glucose oxidation

Figure 5.8-A, 5.8-C and 5.8-E shows the cyclic voltammograms in presence and absence of glucose for the MWCNT-APPA-X-GDH electrodes. It can be observed for the three electrodes the appearance of an oxidation current upon addition of glucose. The current starts from a potential of about -120 mV and increases with respect to the blank voltammogram (in absence of glucose) with the potential. The non-functionalized MWCNTs do not show this oxidation current in presence of glucose (Data not shown). Figures 5.8-B, 5.8-D and 5.8-F show the chronoamperogram obtained with the same electrodes at 0.35 V and the response when the glucose is added in a concentration of 20 mM. After the addition of glucose, the current increases as consequence of the catalytic activity of the enzyme. The bioelectrode modified at 1.37 V shows the highest values of current change (Δi) of $1.47 \text{ A} \cdot \text{g}_{\text{MWCNT}}^{-1}$ by cyclic voltammetry and $3.06 \text{ } \mu\text{A}$ by chronoamperometry; in contrast with the other potentials studied for the modification of the MWCNTs, where this value is $0.49 \text{ A}_{\text{MWCNT}} \cdot \text{g}^{-1}$ and $0.89 \text{ } \mu\text{A}$ for both electrodes. This behavior can be correlated with the apparent rate constant (Table 5.1). It can be observed that this value is higher for the MWCNT-APPA-1.37-GDH electrode. In this sense, despite the lower amount of immobilized enzyme in the MWCNT-APPA-1.37-GDH electrode, the enzyme has better orientation what permits that the redox-active center of PQQ-GDH be located closer to the surface, improving the direct electron transfer to the electrode.

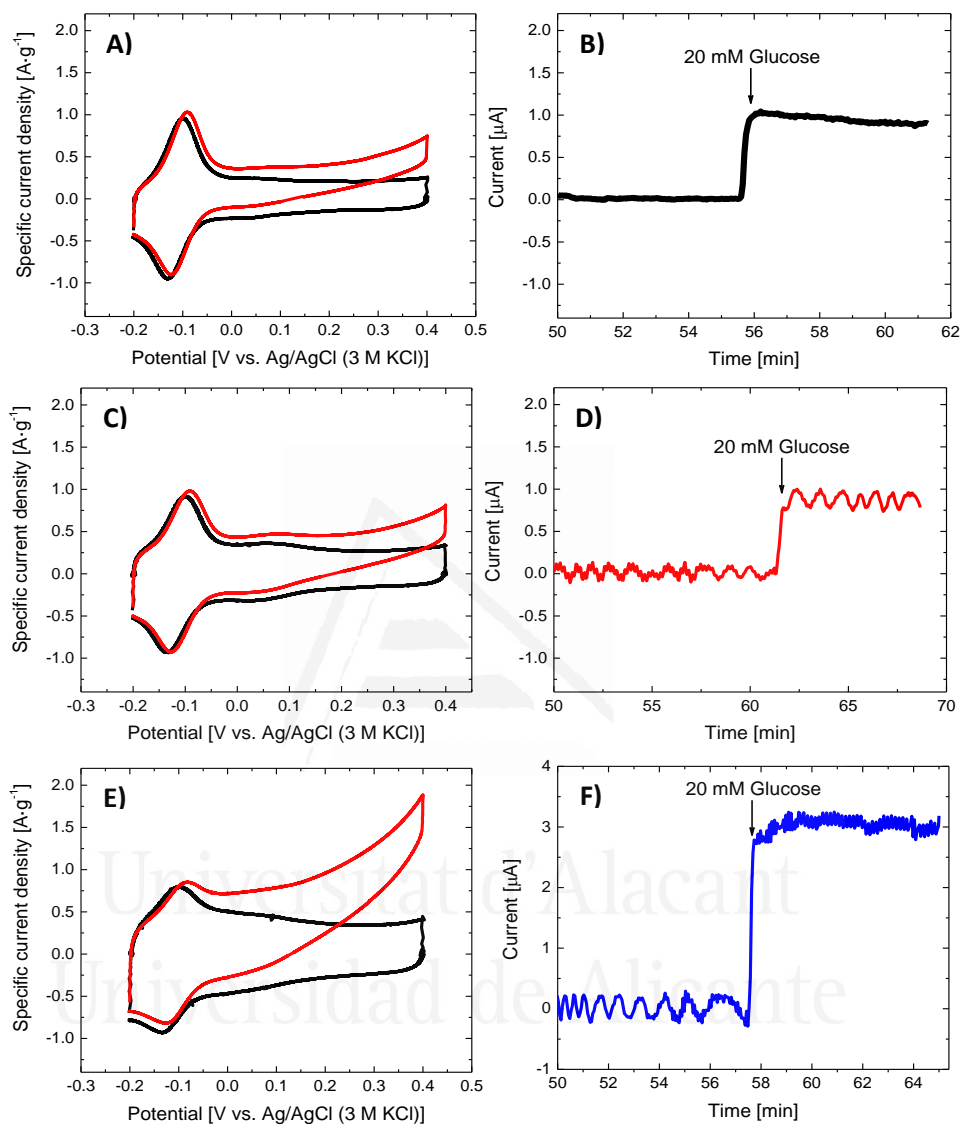


Figure 5.8. Cyclic voltammograms for MWCNT-APPA-X-GDH electrodes in 0.1 M PBS (pH = 7.2) in absence (black line) and presence (red line) of 20 mM glucose at 5 mV s^{-1} under Ar atmosphere: A) 0.97, C) 1.17 and E) 1.37 V. Amperometric response at 0.35 V of MWCNT-APPA-X-GDH modified at B) 0.97, D) 1.17 and F) 1.37 V, after the addition of 0.1 M of glucose in 0.1 M PBS (pH = 7.2) to achieve 20 mM of glucose in solution under room atmosphere and stirring conditions.

Regarding the electrocatalytic behavior and activity of the enzyme immobilized in the different modified MWCNT electrodes, Figures 5.9-A, 5.9-C and 5.9-E show the chronoamperometry profiles carried out at 0.35 V under stirring condition for glucose oxidation in the concentration range between 5.0 μ M and 6.0 mM in PBS (pH = 7.2). All the electrodes present a rapid response to the change in the glucose concentration. Limit of detection (LOD) was determined empirically, as the lowest concentration of glucose whose signal can be clearly distinguished from the background current, showing for the electrodes modified at 1.17 and 1.37 V values of 5 μ M. In contrast, bioelectrodes synthesized at 0.97 V presents a LOD of 10 μ M.

Figure 5.9-B, 5.9-D and 5.9-F shows the calibration curves for the MWCNT-APPA-X-GDH electrodes that present a Michaelis-Menten behavior, in which a linear range at low glucose concentration is observed; afterwards, a plateau zone appears corresponding to the saturation of the enzyme. In the case of MWCNT-APPA-1.17-GDH and MWCNT-APPA-1.37-GDH electrodes, calibration curves at low values of glucose concentration (less than 0.1 M) show a change in the slope, which can suggest that either surface chemistry changes or modifications in the oligomer chain structure, due to swelling for example, can produce modification in the interaction enzyme-electrode, affecting the diffusion of the substrate and product towards the enzyme and through the electrode surface^{39,40}. Thus, best linear calibration range was determined between 0.1 and 1.0 mM for all the electrodes.

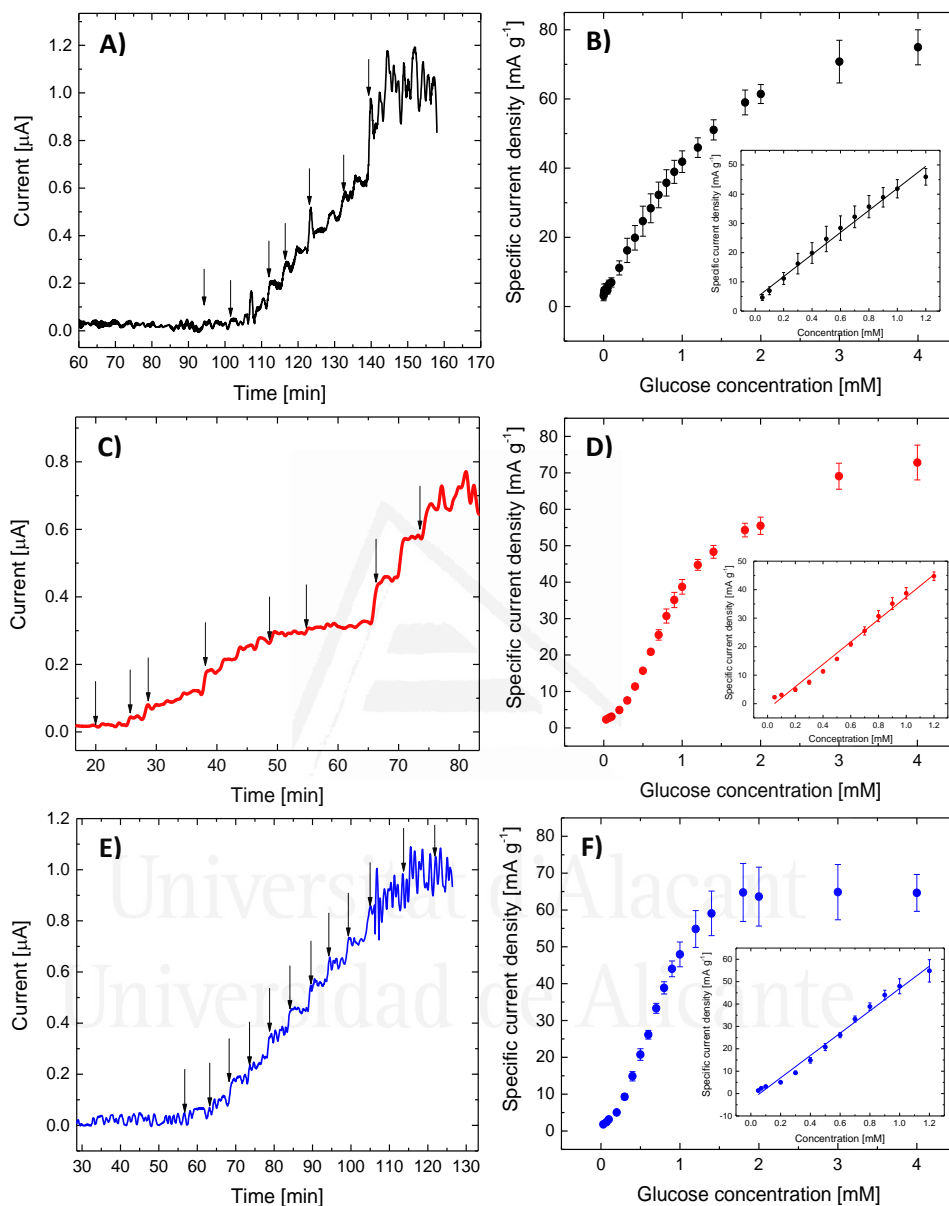


Figure 5.9. Chronoamperometry profiles at 0.35 V in 0.1 M PBS (pH=7.2) to successive addition of glucose (marked with arrows), from 5 μM to 6 mM, A) MWCNT-APP-0.97-GDH, C) MWCNT-APP-1.17-GDH and E) MWCNT-APP-1.37-GDH. Calibration curves: B) MWCNT-APP-0.97-GDH, D) MWCNT-APP-1.17-GDH and F) MWCNT-APP-1.37-GDH. Inset: Calibration curve in the concentration range between 0.1 to 1.0 mM.

Interestingly, sensitivity of the electrodes presents an important enhancement with the increase in the upper potential limit used in the electrochemical modification of MWCNTs, obtaining at 1.37 V a value 37% higher than for the electrode modified at 0.97 V (Table 5.2). This is most likely due to the faster kinetics in the electron-transfer process between the enzyme redox-active center and the electrode surface, in agreement with the increase in the k_s^{app} . Moreover, taking into account that the active center of the enzyme is a probe with external-electron transfer mechanism, the functionalities incorporated during the electrochemical modification, could facilitate the transfer of electrons, as a mediating process, because the redox processes observed in the functionalized MWCNT-APPA appear at higher potentials than the redox process associated to the redox active center of the enzyme⁴¹.

Table 5.2. Analytical figures of merit for the quantification of glucose for MWCNT-APPA-X-GDH electrodes.

| Parameter | Upper potential limit of synthesis [V vs. Ag/AgCl] | | |
|--|--|------------|------------|
| | 0.97 | 1.17 | 1.37 |
| Sensitivity [mA g _{MWCNT} ⁻¹ mM ⁻¹] | 39.2 ± 2.8 | 42.2 ± 4.5 | 53.6 ± 4.7 |
| R ² | 0.995 | 0.990 | 0.992 |
| Linear range (mM) | 0.1-1.2 | 0.1-1.2 | 0.1-1.2 |
| LOD (mM) | 0.01 | 0.005 | 0.005 |
| LOQ (mM) | 0.033 | 0.0165 | 0.0165 |
| K _m ^{app} (mM) | 2.5 | 2.7 | 1.6 |

*All the parameters were determined employing 3 different electrodes synthesized at the same electrochemical conditions.

The apparent Michaelis-Menten constant (K_m^{app}) (Table 5.2), characteristic parameter for the enzyme-electrode interaction, was experimentally determined by the Lineweaver-Burk fitting, obtaining values of 2.5, 2.7 and 1.6 mM for the three electrodes electrochemical modified at 0.97, 1.17 and 1.37 V, respectively (Figure 5.10). These values are in agreement with the values for PQQ-GDH in solution, which is between 0.5-22 mM, and also with

previous works in which this parameter presents values between 0.2 to 3 mM⁴² when the enzyme is immobilized.

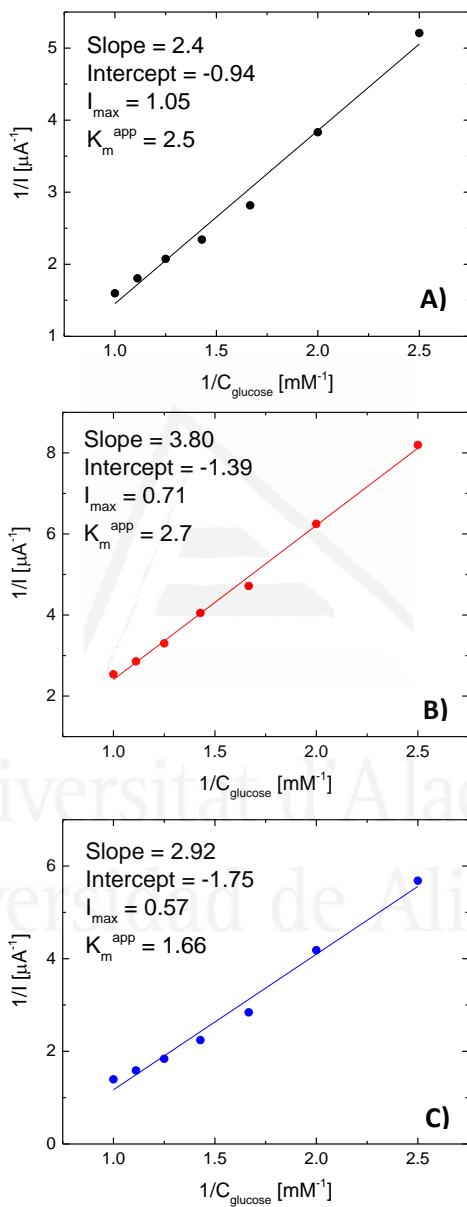


Figure 5.10. Lineweaver-Burk fitting MWCNT-APPA-X-GDH synthesized at different upper potential limits: A) 0.97, B) 1.17 and C) 1.37 V.

The lower value is obtained with MWCNT-APPA-1.37-GDH electrode, what indicates the high affinity of the enzyme to the substrate (glucose in this case). Despite the fact that a strong interaction between the enzyme and the substrate decreases the concentration of saturation of the enzyme towards glucose detection, as consequence of the impediment effect towards the interaction with the glucose, this interaction produces an increase in the sensitivity of the bioelectrode. Then, low values of K_m^{app} from an analytical point of view are correlated with an increase in the sensitivity and a reduction in the concentration of saturation⁴³.

3.4. Stability of MWCNT-APPA-X-GDH electrodes

Operational long-term stability was evaluated by measuring the current change (with respect to the current of the blank) after the addition 20 mM glucose, for 8 days. Bioelectrodes were stored at 4°C in 0.1 M PBS (pH=7.2). Figure 5.11-A shows the evolution of the catalytic glucose oxidation current each day.

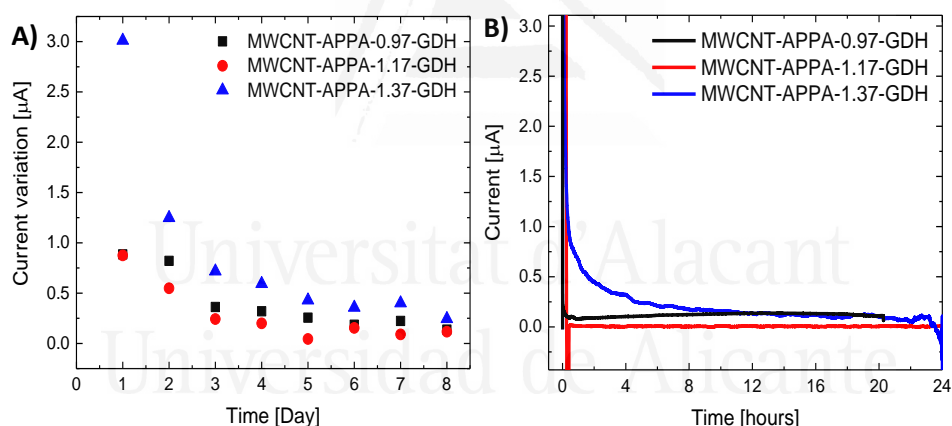


Figure 5.11. A) Stability of MWCNT-APPA-X-GDH electrodes. Conditions: Chronoamperometry at 0.35 V in 0.1 M PBS (pH=7.2) in presence of 20 mM glucose evaluated for 8 days and B) Chronoamperometry during glucose oxidation on MWCNT-APPA-X-GDH electrodes in 0.1 M PBS (pH=7.2) at 0.35 V, under stirring conditions and room atmosphere.

The figure shows a decrease in the 8th day of around 90% of the initial current for all the bioelectrodes. This decrease is more important in the MWCNT-APPA-1.37-GDH electrode. The decrease in the catalytic activity seems to be related mainly to a possible desorption of the enzyme immobilized

on the electrode which could be related with the protonation of the phosphorus species on the MWCNT surface, as result of a local pH change generated during oxidation of glucose⁴⁴. Then, electrostatic interaction between the positively charged enzyme and the phosphorus groups could be responsible for the immobilization of the enzyme. This behavior can also be confirmed by the decrease in the charge associated with the redox process of the active center of the enzyme (PQQ), after 3 hours at 0.35 V in presence of 6 mM glucose (Figure not shown).

It is important to point out that MWCNT-APPA-1.37-GDH electrode presents the highest decrease in the catalytic current with time, but this electrode still provides the highest current during the test.

Additional long-term stability test under continuous operation during 24 hours in 0.1 M PBS (pH=7.2) solution at 0.35 V was also carried out (Figure 5.11-B), demonstrating that no important change in the current is observed in all the electrodes.

4. Conclusions

The electrochemical modification of MWCNT with 4-APPA has demonstrated the incorporation of different phosphorus and nitrogen surface species which promote the immobilization of PQQ-GDH. The bioelectrodes have been used in the oxidation of glucose at physiological pH. Depending of the upper potential limit used in the electrochemical modification of MWCNTs, morphological features of the enzymatic coating and interaction with the enzymatic element improve the electron-transfer kinetics, obtaining values for apparent electron transfer rate constants from 69 to 82 s⁻¹. This good electron transfer could be associated with a better orientation of the redox-active center of the enzyme to the electrode. Moreover, the different biocatalytic electrodes show different amounts of immobilized enzyme, oxidation catalytic current and sensitivity towards glucose oxidation.

The MWCNT-APPA-1.37-GDH bioelectrode shows the highest values of glucose oxidation current (1.47 A g⁻¹ obtained by cyclic voltammetry and 3.06 μA obtained by chronoamperometry). The sensitivity obtained for this electrode is 53.63 ± 4.72 mA g_{MWCNT}⁻¹ mM⁻¹. Therefore, the electrochemical modification of MWCNTs with phosphorus and nitrogen species coming from oxidation of 4-APPA, can be considered as a promising alternative to control

and improve the electrochemical performance of biocatalysts for further applications as biosensors.

5. References

- (1) Léger, C.; Bertrand, P. Direct Electrochemistry of Redox Enzymes as a Tool for Mechanistic Studies. *Chem. Rev.* **2008**, *108* (7), 2379–2438.
- (2) Katz, E.; Willner, I. Integrated Nanoparticle–Biomolecule Hybrid Systems: Synthesis, Properties, and Applications. *Angew. Chemie Int. Ed.* **2004**, *43* (45), 6042–6108.
- (3) Wang, D.; Tan, Y. Electrodeposition of Enzymes-Integrated Mesoporous Composite Films by Interfacial Templating: A Paradigm for Electrochemical Biosensors. *Electrochim. Acta* **2014**, *116*, 495–503.
- (4) Schubart, I. W.; Göbel, G.; Lisdat, F. A Pyrroloquinolinequinone-Dependent Glucose Dehydrogenase (PQQ-GDH)-Electrode with Direct Electron Transfer Based on Polyaniline Modified Carbon Nanotubes for Biofuel Cell Application. *Electrochim. Acta* **2012**, *82*, 224–232.
- (5) Al-Lolage, F. A.; Meneghello, M.; Ma, S.; Ludwig, R.; Bartlett, P. N. A Flexible Method for the Stable, Covalent Immobilization of Enzymes at Electrode Surfaces. *ChemElectroChem* **2017**, *4* (6), 1528–1534.
- (6) Datta, S.; Christena, L. R.; Rajaram, Y. R. S. Enzyme Immobilization: An Overview on Techniques and Support Materials. *Biotech.* **2013**, *3* (1), 1–9.
- (7) Leech, D.; Kavanagh, P.; Schuhmann, W. Enzymatic Fuel Cells: Recent Progress. *Electrochim. Acta* **2012**, *84*, 223–234.
- (8) Lin, Y.; Lu, F.; Tu, Y.; Ren, Z. Glucose Biosensors Based on Carbon Nanotube Nanoelectrode Ensembles. *Nano Lett.*, **2004**, *4* (2), 191–195.
- (9) Bartlett, P. N. *Bioelectrochemistry: Fundamentals, Experimental Techniques and Applications*. 1st ed., John Wiley & Sons, Ltda, Southampton, UK, **2008**.
- (10) Li, Z.; Wang, L.; Li, Y.; Feng, Y.; Feng, W. Carbon-Based Functional Nanomaterials: Preparation, Properties and Applications. *Compos. Sci. Technol.* **2019**, *179*, 10–40.
- (11) Naqvi, S. T. R.; Rasheed, T.; Hussain, D.; Najam ul Haq, M.; Majeed, S.; shafi, S.; Ahmed, N.; Nawaz, R. Modification Strategies for Improving the Solubility/Dispersion of Carbon Nanotubes. *J. Mol. Liq.*

2020, 297, 111919.

- (12) Ramanathan, T.; Fisher, F. T.; Ruoff, R. S.; Brinson, L. C. Amino-Functionalized Carbon Nanotubes for Binding to Polymers and Biological Systems. *Chem. Mater.* **2005**, *17* (6), 1290–1295.
- (13) Adenier, A.; Chehimi, M. M.; Gallardo, I.; Pinson, J.; Vilà, N. Electrochemical Oxidation of Aliphatic Amines and Their Attachment to Carbon and Metal Surfaces. *Langmuir* **2004**, *20* (19), 8243–8253.
- (14) Malmos, K.; Iruthayaraj, J.; Pedersen, S. U.; Daasbjerg, K. General Approach for Monolayer Formation of Covalently Attached Aryl Groups Through Electrografting of Arylhydrazines. *J. Am. Chem. Soc.* **2009**, *131* (39), 13926–13927.
- (15) Sarauli, D.; Xu, C.; Dietzel, B.; Schulz, B.; Lisdat, F. Differently Substituted Sulfonated Polyanilines: The Role of Polymer Compositions in Electron Transfer with Pyrroloquinoline Quinone-Dependent Glucose Dehydrogenase. *Acta Biomater.* **2013**, *9* (9), 8290–8298.
- (16) Banerjee, S.; Hemraj-Benny, T.; Wong, S. S. Covalent Surface Chemistry of Single-Walled Carbon Nanotubes. *Adv. Mater.* **2005**, *17* (1), 17–29.
- (17) Bousquet, A.; Awada, H.; Hiorns, R. C.; Dagron-Lartigau, C.; Billon, L. Conjugated-Polymer Grafting on Inorganic and Organic Substrates: A New Trend in Organic Electronic Materials. *Prog. Polym. Sci.* **2014**, *39* (11), 1847–1877.
- (18) Patolsky, F.; Weizmann, Y.; Willner, I. Long-Range Electrical Contacting of Redox Enzymes by SWCNT Connectors. *Angew. Chemie Int. Ed.* **2004**, *43* (16), 2113–2117.
- (19) Ma, P.-C.; Siddiqui, N. A.; Marom, G.; Kim, J.-K. Dispersion and Functionalization of Carbon Nanotubes for Polymer-Based Nanocomposites: A Review. *Compos. Part A Appl. Sci. Manuf.* **2010**, *41* (10), 1345–1367.
- (20) Thermo scientific XPS simplified [Online], Thermo scientific XPS, Phosphorus (2020). Available at: <https://xpssimplified.com/elements/phosphorus.php#appnotes> [Accessed 2018 March 3].
- (21) Pinyou, P.; Ruff, A.; Pöller, S.; Ma, S.; Ludwig, R.; Schuhmann, W. Design of an Os Complex-Modified Hydrogel with Optimized Redox

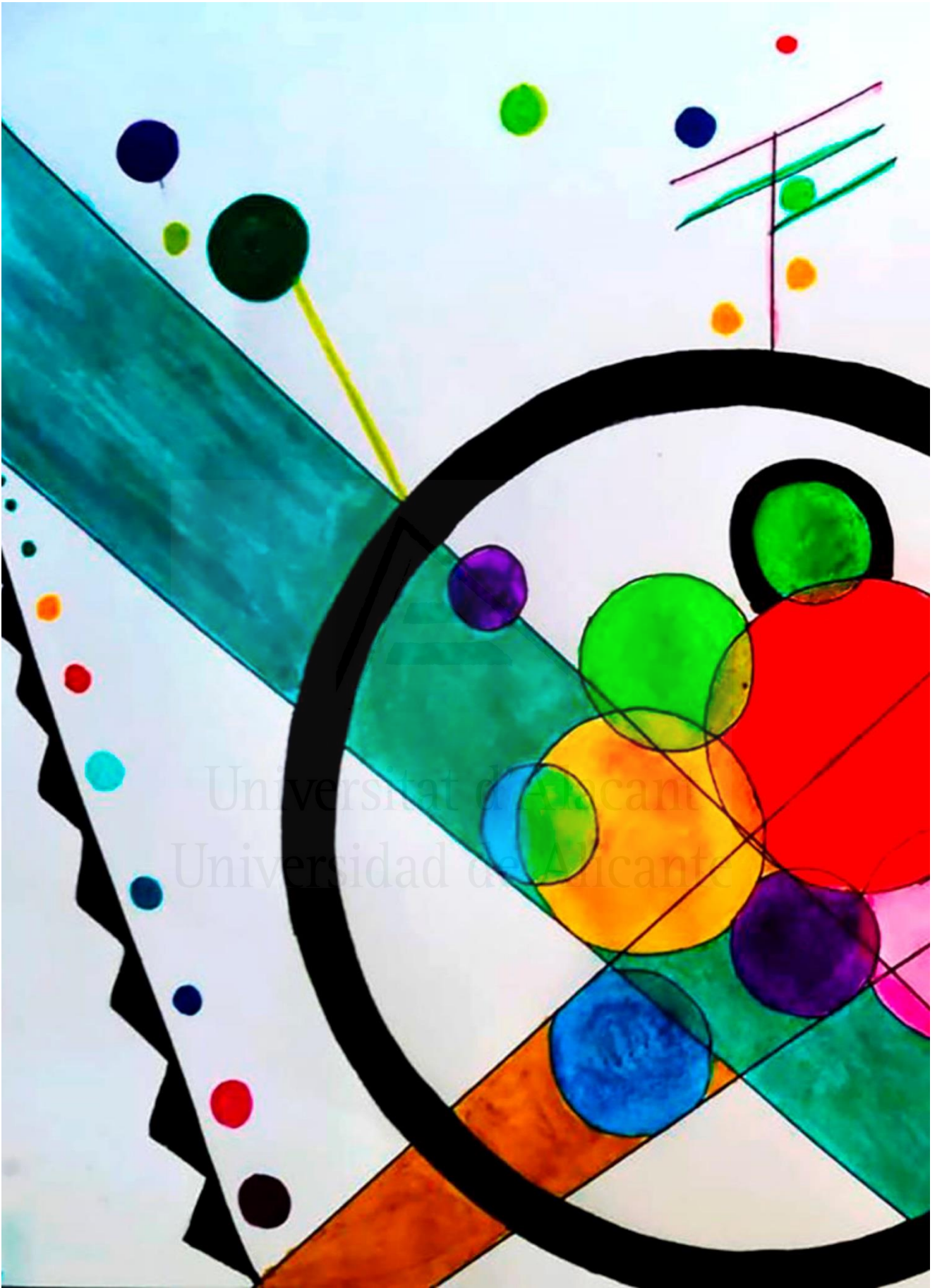
- Potential for Biosensors and Biofuel Cells. *Chem. – A Eur. J.* **2016**, *22* (15), 5319–5326.
- (22) Laviron, E. General Expression of the Linear Potential Sweep Voltammogram in the Case of Diffusionless Electrochemical Systems. *J. Electroanal. Chem. Interfacial Electrochem.* **1979**, *101* (1), 19–28.
- (23) Drummond, T. G.; Hill, M. G.; Barton, J. K. Electron Transfer Rates in DNA Films as a Function of Tether Length. *J. Am. Chem. Soc.* **2004**, *126* (46), 15010–15011.
- (24) Quintero-Jaime, A.; Cazorla-Amorós, D.; Morallón, E. Effect of Surface Oxygen Groups in the Electrochemical Modification of Multiwall Carbon Nanotubes by 4-Amino Phenyl Phosphonic Acid. *Carbon* **2020**, *165*, 328–339.
- (25) Reddy, S. Y.; Bruce, T. C. Mechanism of Glucose Oxidation by Quinoprotein Soluble Glucose Dehydrogenase: Insights from Molecular Dynamics Studies. *J. Am. Chem. Soc.* **2004**, *126* (8), 2431–2438.
- (26) Tanne, C.; Göbel, G.; Lisdat, F. Development of a (PQQ)-GDH-Anode Based on MWCNT-Modified Gold and Its Application in a Glucose/O₂-Biofuel Cell. *Biosens. Bioelectron.* **2010**, *26* (2), 530–535.
- (27) Flexer, V.; Durand, F.; Tsujimura, S.; Mano, N. Efficient Direct Electron Transfer of PQQ-Glucose Dehydrogenase on Carbon Cryogel Electrodes at Neutral pH. *Anal. Chem.* **2011**, *83* (14), 5721–5727.
- (28) Shinohara, H.; Khan, G. F.; Ikariyama, Y.; Aizawa, M. Electrochemical Oxidation and Reduction of PQQ Using a Conducting Polypyrrole-Coated Electrode. *J. Electroanal. Chem. Interfacial Electrochem.* **1991**, *304* (1), 75–84.
- (29) Katz, E.; Schlereth, D. D.; Schmidt, H.-L. Electrochemical Study of Pyrroloquinoline Quinone Covalently Immobilized as a Monolayer onto a Cystamine-Modified Gold Electrode. *J. Electroanal. Chem.* **1994**, *367* (1), 59–70.
- (30) Kim, Y.-P.; Park, S. J.; Lee, D.; Kim, H.-S. Electrochemical Glucose Biosensor by Electrostatic Binding of PQQ-Glucose Dehydrogenase onto Self-Assembled Monolayers on Gold. *J. Appl. Electrochem.* **2012**, *42* (6), 383–390.
- (31) Yasutaka, K.; Takato, Y.; Takashi, K.; Kohsuke, M.; Hiromi, Y. Enhancement in Adsorption and Catalytic Activity of Enzymes

- Immobilized on Phosphorus- and Calcium-Modified MCM-41. *J. Phys. Chem. B* **2011**, *115* (34), 10335–10345.
- (32) Ratautas, D.; Lauryėnas, A.; Dagys, M.; Marcinkeviėienė, L.; Meškys, R.; Kulys, J. High Current, Low Redox Potential Mediatorless Bioanode Based on Gold Nanoparticles and Glucose Dehydrogenase from *Ewingella Americana*. *Electrochim. Acta* **2016**, *199*, 254–260.
- (33) Liu, J.; Wang, X.; Wang, T.; Li, D.; Xi, F.; Wang, J.; Wang, E. Functionalization of Monolithic and Porous Three-Dimensional Graphene by One-Step Chitosan Electrodeposition for Enzymatic Biosensor. *ACS Appl. Mater. Interfaces* **2014**, *6* (22), 19997–20002.
- (34) Sajjadi, S.; Ghourchian, H.; Rahimi, P. Different Behaviors of Single and Multi Wall Carbon Nanotubes for Studying Electrochemistry and Electrocatalysis of Choline Oxidase. *Electrochim. Acta* **2011**, *56* (26), 9542–9548.
- (35) Wang, Y.; Joshi, P. P.; Hobbs, K. L.; Johnson, M. B.; Schmidtke, D. W. Nanostructured Biosensors Built by Layer-by-Layer Electrostatic Assembly of Enzyme-Coated Single-Walled Carbon Nanotubes and Redox Polymers. *Langmuir* **2006**, *22* (23), 9776–9783.
- (36) Casado, C. M.; Cuadrado, I.; Morán, M.; Alonso, B.; García, B.; González, B.; Losada, J. Redox-Active Ferrocenyl Dendrimers and Polymers in Solution and Immobilised on Electrode Surfaces. *Coord. Chem. Rev.* **1999**, *185–186*, 53–80.
- (37) Göbel, G.; Schubart, I. W.; Scherbahn, V.; Lisdat, F. Direct Electron Transfer of PQQ-Glucose Dehydrogenase at Modified Carbon Nanotubes Electrodes. *Electrochem. commun.* **2011**, *13* (11), 1240–1243.
- (38) Sarauli, D.; Xu, C.; Dietzel, B.; Schulz, B.; Lisdat, F. A Multilayered Sulfonated Polyaniline Network with Entrapped Pyrroloquinoline Quinone-Dependent Glucose Dehydrogenase: Tunable Direct Bioelectrocatalysis. *J. Mater. Chem. B* **2014**, *2* (21), 3196–3203.
- (39) Barwe, S.; Andronescu, C.; Pöller, S.; Schuhmann, W. Codeposited Poly(Benzoxazine) and Os-Complex Modified Polymethacrylate Layers as Immobilization Matrix for Glucose Biosensors. *Electroanalysis* **2015**, *27* (9), 2158–2163.
- (40) Andronescu, C.; Pöller, S.; Schuhmann, W. Electrochemically Induced Deposition of Poly(Benzoxazine) Precursors as Immobilization Matrix

for Enzymes. *Electrochem. commun.* **2014**, *41*, 12–15.

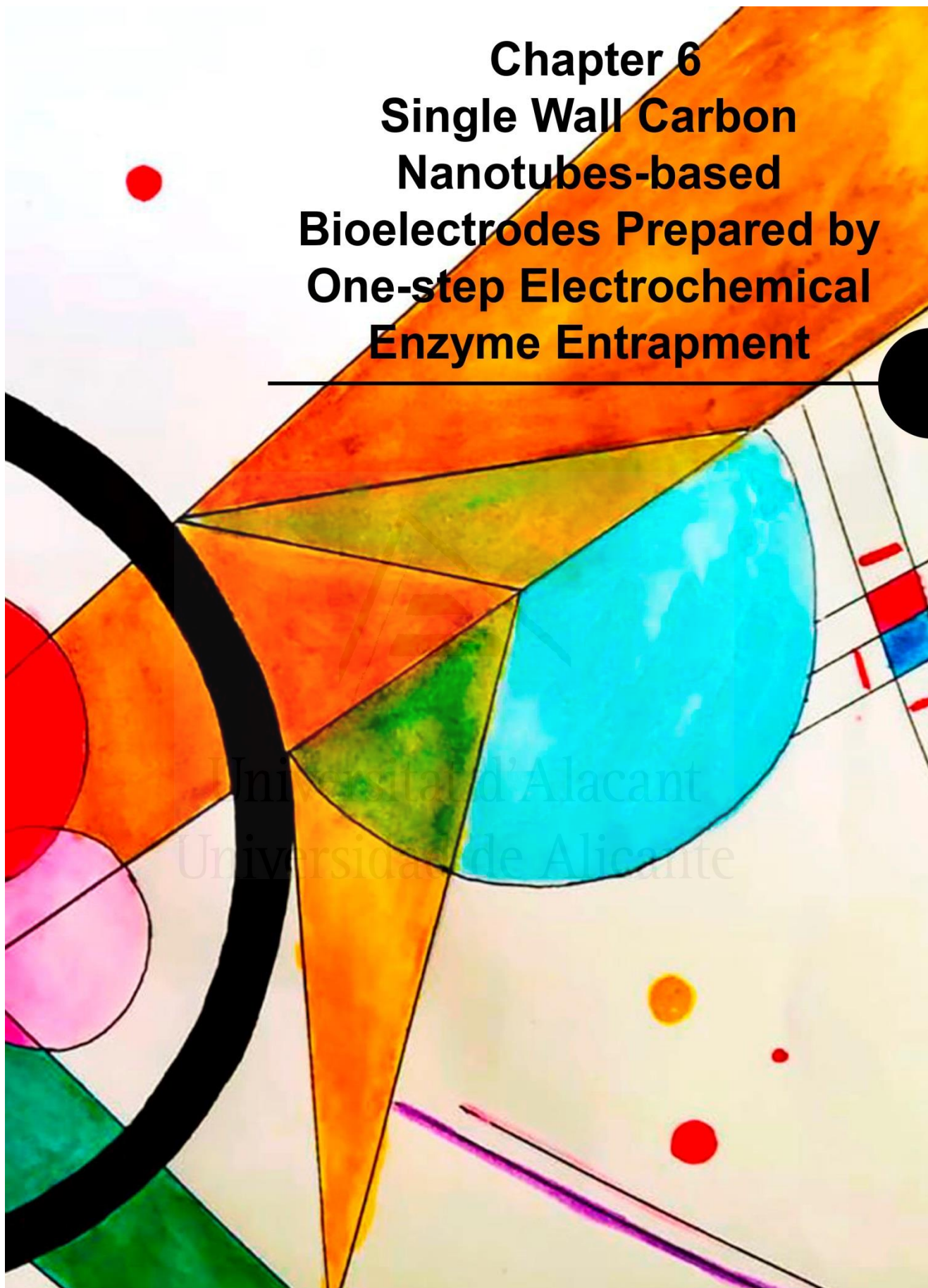
- (41) Lopez, R. J.; Babanova, S.; Artyushkova, K.; Atanassov, P. Surface Modifications for Enhanced Enzyme Immobilization and Improved Electron Transfer of PQQ-Dependent Glucose Dehydrogenase Anodes. *Bioelectrochemistry* **2015**, *105*, 78–87.
- (42) Fusco, G.; Göbel, G.; Zanoni, R.; Kornejew, E.; Favero, G.; Mazzei, F.; Lisdat, F. Polymer-Supported Electron Transfer of PQQ-Dependent Glucose Dehydrogenase at Carbon Nanotubes Modified by Electropolymerized Polythiophene Copolymers. *Electrochim. Acta* **2017**, *248*, 64–74.
- (43) Pingarrón Carrazón, J. M.; Sánchez Batanero, P. Química Electroanalítica-Fundamentos y Aplicaciones. 1st ed., Síntesis S.A, Madrid, España, 2003.
- (44) Chen, Y.; Yang, X.-J.; Guo, L.-R.; Jin, B.; Xia, X.-H.; Zheng, L.-M. Direct Electrochemistry of Cytochrome c on a Phosphonic Acid Terminated Self-Assembled Monolayers. *Talanta* **2009**, *78* (1), 248–252.

Universitat d'Alacant
Universidad de Alicante



Chapter 6
Single Wall Carbon
Nanotubes-based
Bioelectrodes Prepared by
One-step Electrochemical
Enzyme Entrapment

Universitat d'Alacant
Universidad de Alicante



1. Introduction

The design of bioelectrodes has received great attention as a fundamental part in technologies for green-energy production based on electrochemical biofuel cells (EBFC), food chemistry and biosensing¹⁻³. These active bioelectrodes are important to obtain fast response, high sensitivity and stable biocatalysts. In this sense, the current research has mainly focused in the development of scalable, controlled and reproducible procedures of biocatalyst synthesis, which may also enhance the interaction between the enzyme and the electrode, promoting an efficient electron-transfer⁴⁻⁶. Unfortunately, the electron-transfer between the redox center in the enzyme, like glucose oxidase (GOx), glucose dehydrogenase (s-GDH), laccase oxidase (Lc), etc., and the electrode is normally hindered by the structure of the enzyme, that buries the redox cofactor⁷⁻⁹.

Herein lies the importance of development of immobilization methods during the synthesis of the biocatalyst, in which the appropriate assembling of confined enzymatic element without affecting its catalytic activity is of great relevance^{1,10}. Besides, orientation and even interconnection of the redox cofactor with the electrode surface can provide platforms for fast and efficient electron transfer^{11,12} by an electron-hopping mechanism^{5,13,14} or direct electron transfer^{15,16}, which confers high efficiency and performance of the bioelectrode.

Despite the wide variety of immobilization procedures, like covalent linkage, adsorption, electrostatic interaction and crosslinking, the confining of the enzyme into an inorganic (i.e. sol-gel) or polymeric matrix provides an interesting route to generate a close interaction between the electrode and the enzyme^{9,17,18}. Additionally, entrapment assisted by electrochemical methods affords an easy, scalable and controlled preparation of the bioelectrode^{1,19-21}. The entrapment based on the electrochemical deposition of a polymer with other components like chitosan is considered as a simple, fast, uniform and controllable immobilization route^{22,23}. However, in these examples, the polymers have low conductivity and lack of electroactivity, what makes that the mediation of electron transfer is impeded. However, the entrapment in redox active polymers based on osmium complex or its copolymers with non-electroactive polymers have demonstrated outstanding performance not only in the proper immobilization of the enzymatic element, but also in the

improvement of the electron transfer^{11,13,24}. Moreover, other redox species like ferrocene-derivatives, methyl viologen or Ru-complex have also been employed with remarkable results²⁵⁻²⁷.

Conjugated polymers, such as polyaniline (PANI), polypyrrole (Py) and poly(3-4 ethylenedioxythiophene) (PEDOT), can offer a good platform as matrix for electrochemical enzyme entrapment, especially considering the easy and well-known polymerization mechanism and remarkable conductivity²⁸⁻³¹. Moreover, the incorporation of redox species and the use of substituents in the monomer precursor have improved the redox behavior of the polymer, generating electrochemical functional groups which facilitates the electron transfer^{31,32}.

In the present work, two different routes for the synthesis of bioelectrodes have been studied. In these routes, electrochemical entrapment of pyrroloquinoline quinone dependent glucose dehydrogenase (s-GDH) during oxidation of 4-APPA on single wall carbon nanotubes electrodes, has been employed. The proposed method provides a methodology for electrochemical immobilization of the enzyme by one-step, in which the direct entrapment of the reconstructed enzyme can be done. Interestingly, catalytic activity of the bioelectrode depends on the upper potential limit used in the electrochemical entrapment. The synthesized electrodes have demonstrated a good performance towards glucose oxidation with good sensitivity and reproducibility.

2. Experimental

2.1. Reagents and equipment

Single Wall Carbon nanotubes (SWCNT) with purity 99% (1-4 nm of diameter) with 3-30 μm length were purchased to Cheap Tubes Inc. (Cambridgeport, USA). Specific surface area, obtained by the Brunauer, Emmett and Teller (BET) method, is $587 \text{ m}^2 \text{ g}^{-1}$.

Soluble apo-enzyme glucose dehydrogenase (s-GDH) was obtained from Roche Diagnostics (Germany). 4-amino phenyl phosphonic acid (4-APPA, +98%) used as modifier agent was purchased to Tokyo Chemical Industry co (TCI-Belgium). Potassium dihydrogen phosphate (KH_2PO_4) and dipotassium hydrogen phosphate tri hydrate ($\text{K}_2\text{HPO}_4 \cdot 3\text{H}_2\text{O}$) were purchased from VWR

Chemicals, and they were used to prepare phosphate buffer solution (0.1M PBS, pH = 7.2). 4-(2-hydroxyethyl)-1-piperazineethanesulfonic acid (HEPES) ($\geq 99.5\%$ -titration), D-(+)-Glucose ACS reagent, pyrroloquinoline quinone ($\geq 95\%$ -HPLC) and dimethylformamide (DMF) were purchased from Sigma-Aldrich. All the solutions were prepared using ultrapure water (18 MOhms cm, Purelab Ultra Elga equipment). Ar (99.999%) and H₂ (99.999%) were provided by Air Liquide.

2.2. Electrochemical entrapment of enzyme

2.2.1. Enzymatic electrolyte solutions

Firstly, 10 mM HEPES aqueous buffer solution (pH = 5.0) was prepared which contains 150 mM CaCl₂, 0.1 M KCl and 1 mM 4-APPA. This solution is named as HEPES electrolyte. Depending on the synthesis procedure (Scheme 1), the model enzyme (soluble glucose dehydrogenase) can be incorporated into the buffer solution in different ways as follows:

Solution 1 for procedure 1: apo-enzyme s-GDH is dissolved in the HEPES electrolyte until a concentration of 5 mg mL⁻¹ is obtained.

Solution 2 for procedure 2: Firstly, reconstruction of the s-GDH is carried out with PQQ following the next steps. Step 1, 36 mg of apo-enzyme s-GDH was dissolved in 10 mM HEPES buffer solution (pH = 7.0) with 150 mM CaCl₂ and 520 μ M of PQQ freshly prepared, attaining a concentration of 36 mg mL⁻¹. This enzymatic solution was mixed at 1600 rpm for 30 min in vortex and stored at 4°C until its use. In this procedure, PQQ cofactor is introduced in the apo-enzyme structure as active center and the complex is stabilized by the presence of three calcium cations³³. Step 2, in order to avoid further mediating effects of the free PQQ which can be adsorbed onto the electrode surface, a purification process is carried out. The 36 mg mL⁻¹ solution of PQQ-GDH was treated in a centrifugal concentrator Eppendorf (VIVASPIN 500) with a membrane of 10 kDa. Centrifugation is carried out at 8000 rpm during 25 min. Step 3, an aliquot of this enzymatic PQQ-GDH solution is added in the 10 mM HEPES (pH = 7.0), 150 mM CaCl₂ and 0.1 M KCl solution to attain a final concentration of 5 mg mL⁻¹ by vortex at 1200 rpm. All the enzyme solutions are stored at 4°C until its use.

2.2.2. *One-step electrochemical synthesis of the bioelectrodes*

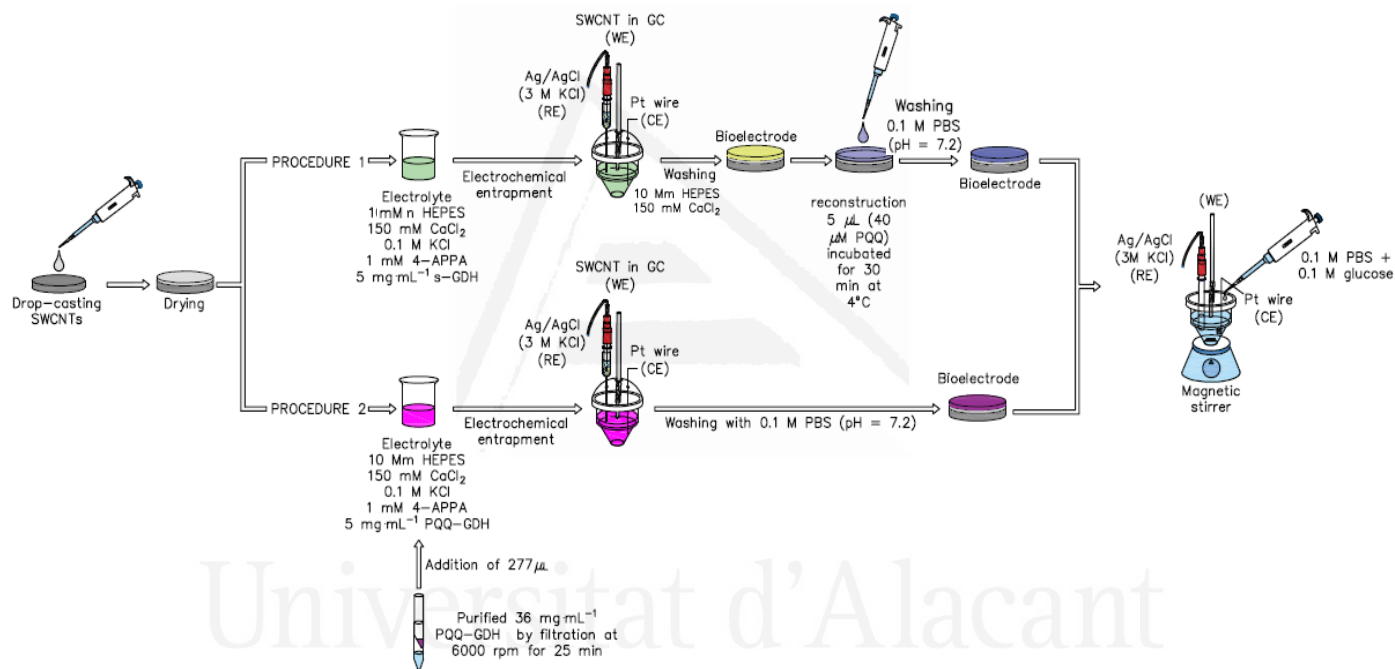
The working electrode for the electrochemical modification was prepared using a glassy carbon rod (GC) as support, modified with the SWCNT. 1 mg of SWCNT was dispersed in DMF employing an ultrasonic cold-bath for 45 minutes, achieving a dispersion of 1 mg mL⁻¹ SWCNTs. Prior to the deposition of SWCNTs, glassy carbon electrode surface (3 mm diameter) was sanded with emery paper and polished using 1 and 0.05 μm alumina slurries, then rinsed with ultrapure water in ultrasonic bath. Afterwards, 5 μL aliquot of the dispersion was dropped onto the glassy carbon surface and dried under an infrared lamp to remove the solvent. This procedure was repeated twice until completing 10 μL of the SWCNT suspension on the surface.

Electrochemical entrapment of the enzyme on the SWCNT electrode was performed using two procedures by cyclic voltammetry submitting the sample to 50 cycles at 50 mV s⁻¹, at different upper potential limits. The equipment used was an Autolab PGSTAT 302 (Metrohm Netherlands) bipotentiostat station, in which glassy carbon electrode modified with the SMCNTs was the working electrode (WE), a platinum wire as counter electrode (CE) and a Ag/AgCl (3 M KCl) introduced in a Lugging capillary with the same electrolyte without 4-APPA and enzyme, as reference electrode (RE). Electrolyte employed was a deoxygenated HEPES electrolyte with 5 mg mL⁻¹ of the enzyme in both procedures.

Solution 1 and solution 2 are used in the electrochemical immobilization using procedure 1 and procedure 2, respectively. Depending on the procedure employed (Scheme 1), after the electrochemical immobilization, the bioelectrodes were washed with excess of 0.1 M PBS solution (pH = 7.2) (procedure 2) or with 10 mM HEPES, 150 mM CaCl₂ (procedure 1). In procedure 1, after electrochemical immobilization, an aliquot of 5 μL of a solution of 40 μM PQQ in buffer solution (10 mM HEPES, 150 mM CaCl₂) was dropped on the electrode and incubated at 4°C for 30 min³⁴. Afterwards, the electrodes were rinsed with 0.1 M PBS solution (pH = 7.2).

In procedure 2, the electrochemical immobilization of the GDH and PQQ is done in one step.

Stepwise representation for the synthesis of the bioelectrodes, employing both procedures is presented in Scheme 6.1.



Scheme 6.1. Electrochemical immobilization of s-GDH on SWCNT with 4-APPA using two procedures.

In procedure 1, the electrodes are named as SWCNT-APPA-X@GDH and SWCNT-APPA-X@GDH/PQQ before and after the addition of PQQ, respectively. In the case of procedure 2, the electrodes are named as SWCNT-APPA-X@PQQ-GDH. For electrodes synthesized in the same conditions but without the presence of enzyme the nomenclature employed was SWCNT-APPA-X. In all the cases, X represents the upper potential limit that was employed for the electrochemical entrapment.

An additional SWCNT-APPA-1.15 electrode was prepared for comparison purposes in which the enzyme was immobilized by drop-casting of 5 μL of 36 mg mL^{-1} of PQQ-GDH (SWCNT-APPA-X@PQQ-GDH_{drop casting}).

The surface concentration of the PQQ that is related with the reconstructed enzyme, was determined from the charge of the redox process in the cyclic voltammograms using the following equation (Eq. 6.1):

$$\Gamma = \frac{Q}{nFA} \quad \text{Eq. 6.1}$$

Where Γ is the surface concentration of PQQ-GDH (mol cm^{-2}), n is the number of transferred electrons, F is the Faraday constant (96485 C mol^{-1}), A is the active surface area (m^2), which was determined using the specific surface area of the deposited SWCNT in the same electrolyte. Q is the electrical charge obtained from the integration of the anodic peak associated with the cofactor in the enzyme. The charge contribution of the SWCNT-APPA-X electrode without enzyme was subtracted.

2.3. Physicochemical characterization

X-Ray photoelectron spectroscopy (XPS) was performed in a VG-Microtech Mutilab 3000 spectrometer using Al $K\alpha$ radiation (1253.6 eV). The deconvolution of the XPS C1s, O2p, P2p and N1s was done by least squares fitting using Gaussian-Lorentzian curves, while a Shirley line was used for the background determination. The P2p spectra have been analyzed considering the spin-orbit splitting into 2p_{3/2} and 2p_{1/2} with a 2:1 peak area ratio and 0.87 eV splitting³⁵.

Scanning electron micrographs were taken using an ORIUS SC600 model Field Emission Scanning Electron Microscopy (FESEM) and a ZEISS microscope, Merlin VP Compact model. Samples are coated with a thin layer

of carbon to avoid decomposition of the enzyme and the different oligomers incorporated by the electrochemical modification of 4-APPA.

AFM images were obtained from an atomic force microscope NT-MDT model Ntegra, coupled with high resolution Silicon AFM cantilever (NSG01 type), with a resonant frequency close to 150 kHz. It was employed in semi-contact mode for the measurements of 10 x 10 μm . Scan rate of the cantilever was 0.5 Hz with a resolution of 256 points in the images.

2.4. Electrochemical characterization and catalytic activity towards glucose oxidation

Electrochemical behavior of biocatalyst was evaluated in 0.1 M PBS (pH = 7.2) solution, in presence and absence of glucose, employing a three electrode configuration cell, where, bioelectrodes were the working electrode (WE), a platinum wire as counter electrode (CE) and a Ag/AgCl (3 M KCl) electrode introduced in the electrochemical cell as reference electrode (RE). In order to compare with the other chapters of this PhD Thesis, the following equivalence should be done: 0.75, 0.95 and 1.15 correspond to 1.2, 1.4 and 1.6 V vs. RHE, respectively. Characterization was performed at room atmosphere conditions, taking into account the non O₂-dependence of the enzyme.

Electrochemical catalytic behavior towards glucose oxidation was determined by chronoamperometry, in the same electrochemical cell configuration previously mentioned. In a typical measurement, before the addition of glucose, the working electrode is stabilized at 0.35 V in 0.1M PBS (pH = 7.2) solution under room atmosphere conditions and, subsequently, aliquots from a 0.1 M glucose solution were added to the electrochemical cell, obtaining glucose concentrations between 5 μM to 10 mM. The time between aliquots was established in 5 min, to guarantee a stabilization of the current after glucose addition. During the chronoamperometry, stirring conditions are maintained during all the experiment. Cyclic voltammetry was employed at the beginning and the end of the chronoamperometry to follow changes in the electrode.

Moreover, for comparison purposes, SWCNTs were used without any modification as support of the PQQ-GDH. The characterization of this electrode by cyclic voltammetry and chronoamperometry in presence and

absence of glucose is presented in Figure A-6.1; the results confirm that this electrode is not active for oxidation of glucose.

3. Results and discussion

3.1. Electrochemical entrapment of *s*-GDH on SWCNT with 4-APPA using procedure 1.

The potentiodynamic electrochemical entrapment of apo-enzyme *s*-GDH using procedure 1 at different upper potential limits (See Figure A-6.2), shows the presence of an irreversible oxidation peak at 0.69 V in the first cycle, which can be associated with the oxidation of the 4-APPA. After this first cycle, different redox processes appear in the voltammogram at lower potentials which charge increases with cycling the electrode; at the same time, the current associated with the oxidation of the 4-APPA decreases. This voltammetric behavior is similar to that observed in absence of GDH in the solution and it has been previously observed in acid media³⁶. The observed processes were associated to the functionalization of SWCNT with the species produced during oxidation of 4-APPA. In presence of the apo-enzyme no significant changes are observed in the voltammograms and similar redox process are observed, what indicates that the electrochemical functionalization of SWCNT is also being produced.

Figure 6.1 shows the electrochemical characterization of the different electrodes in PBS electrolyte (pH=7.2) obtained in presence and absence of GDH at different upper potential limits. It can be observed in all cases that the oxidation of 4-APPA (Figure 6.1-A) generates stable electrochemical surface redox processes related with the species formed during SWCNT functionalization. These redox processes are reversible, and their charge increases with the upper potential limit used in the functionalization. Moreover, these redox processes are stable at this pH. When the electrochemical functionalization is done in presence of *s*-GDH (Figure 6.1-B), the double layer charge between -0.2 and 0 V, decreases that can be associated to the blockage of the SWCNT surface by the enzyme. Moreover, an additional redox peak (A-A') is observed in the SWCNT-APPA-X@GDH electrodes. The presence of the apo-enzyme in the electrode tends to generate a more resistive behavior, observed in the slightly tilted voltammograms, but the

main redox processes are clearly observed in the voltammogram (See Figure 6.1-B).

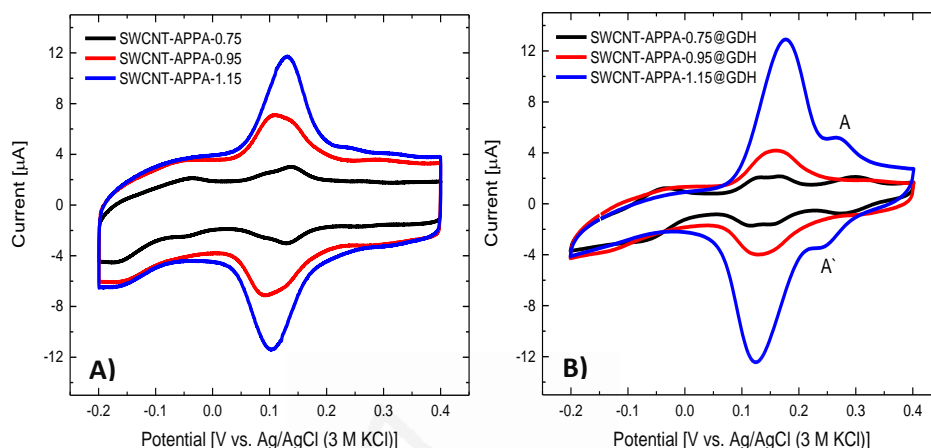


Figure 6.1. Cyclic voltammograms of: A) SWCNT-APPA-X and B) SWCNT-APPA-X@GDH electrodes. Electrochemical modification was carried out at different upper potential limits (0.75 V in black line, 0.95 V in red line and 1.15 V in blue line) at 50 mV s^{-1} for 50 cycles under Ar atmosphere. 0.1 M PBS (pH = 7.2) under room atmosphere conditions at 5 mV s^{-1}

Table 6.1 shows the XPS quantification for SWCNT-APPA-X electrodes. It can be observed that the amount of N is always higher than that of P and that the amount of N remains almost constant from an upper potential limit of 0.75 V, whereas the amount of P increases with the upper potential limit. This behavior is different to the observed during the functionalization in sulfuric acid³⁶, in which an increase of both N and P were observed. In this HEPES electrolyte, the amount of both P and N is higher than the incorporated in acidic conditions and, interestingly, the amount of P is significantly higher than in acidic conditions. No further potentials were evaluated because an additional experiment of electrochemical polarization at 1.35 V produced the disappearance of the redox process and a large oxidation current (See Figure A-6.3).

Table 6.1. Quantification of surface species by XPS and distribution of N and P contributions for SWCNT-APPA-X modified in HEPES electrolyte at different potentials.

| Upper potential limit [V vs. Ag/AgCl (3 M KCl)] | Ca (at%) | O (at%) | N (at%) | P (at%) | N/P* | % Neutral N species (398.5 and 400.1 eV) | % Oxidized nitrogen (401.5 eV) | % C-O-P (133.3 eV) | % C-P-O (132.6 eV) |
|---|----------|---------|---------|---------|------|--|--------------------------------|--------------------|--------------------|
| Pristine | -- | 3.1 | 0.37 | 0.0 | -- | -- | -- | -- | -- |
| 0.75 | -- | 7.2 | 1.67 | 0.23 | 5.7 | 94 | 6 | 67 | 33 |
| 0.95 | 0.24 | 8.0 | 1.41 | 0.51 | 2.0 | 95 | 5 | 59 | 41 |
| 1.15 | 0.48 | 8.5 | 1.70 | 0.88 | 1.5 | 90 | 10 | 61 | 39 |

*The N content of the pristine SWCNT has been subtracted for the calculation.

In terms of the different contributions of N and P species, XPS N1s spectra shows (Figure A-6.4) a peak at around 400.1 eV in all the potentials studied. The main important contributions are related with the presence of neutral amines and imines species with binding energies at around 400.1 and 398.5 eV, respectively^{36,37}. Furthermore, a small contribution associated with oxidized nitrogen species at binding energy around 401.5 eV are observed. Despite the polarization conditions used, no important changes are appreciated in the distribution of the species in the electrode.

In case of P2p spectra (Figure A-6.5), two asymmetric doublets appear. The first one at 132.6 eV, associated with the binding energy of C-P-O species, in agreement with the phosphonic group of the 4-APPA precursor³⁶, and the second at 133.3 eV related to phosphoric species (C-O-P) generated from the electrochemical oxidation of the phosphonic group at the anodic polarization conditions^{36,38}.

3.1.1. Glucose oxidation on SWCNT-APPA-X@GDH/PQQ electrodes

The electrodes prepared using procedure 1 have been used in the oxidation of glucose in order to check their electrocatalytic activity. The SWCNT-APPA-X@GDH electrodes do not oxidize glucose (See Figure A-6.6), due to the absence of the cofactor (PQQ). In all cases, a decrease in the charge of the different redox processes are observed.

Therefore, the heterogeneous reconstitution of the GDH enzyme, considering that it is immobilized on the electrode surface, was carried out by drop-casting of the cofactor (PQQ) onto the SWCNT-APPA-X@GDH electrodes (procedure 1)³⁹. Figures 6.2-A, 6.2-C and 6.2-E (dotted lines) show the cyclic voltammograms for the SWCNT-APPA-X@GDH/PQQ electrodes. It can be clearly observed the appearance of a redox couple at around -0.11 V, which can be assigned to the two-electron transfer of the PQQ^{40,41}, suggesting that the entrapped apo-enzyme was successfully reconstructed^{42,43}.

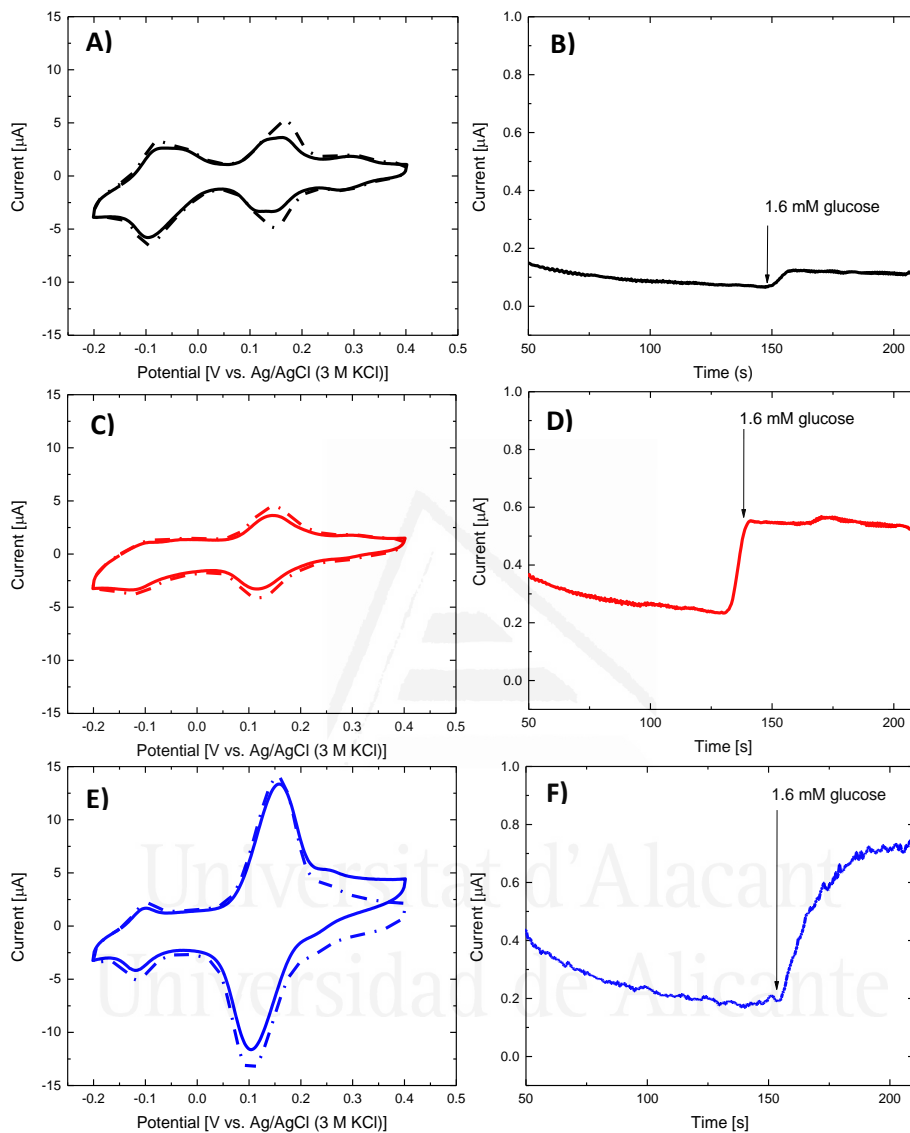


Figure 6.2. Electrocatalytic performance of SWCNT-APPA-X@GDH/PQQ towards glucose oxidation synthesized at different upper potential limits (0.75 (A,B), 0.95 (C,D) and 1.15 (E,F)). A, C and E) Cyclic voltammogram in absence (dotted line) and presence (solid line) of 4 mM glucose, in 0.1 M PBS (pH = 7.2) at room atmosphere conditions at 5 mV s^{-1} ($n=3$). B, D and F) Chronoamperometry response of SWCNT-APPA-X@GDH/PQQ in 0.1 M PBS (pH = 7.2) at room atmosphere conditions at a fixed potential of 0.35 V before and after the addition of 1.6 mM glucose.

In presence of glucose (Figures 6.2-A, 6.2-C and 6.2-E, solid lines), the voltammetric charges decrease, and the SWCNT-APPA-1.15@GDH/PQQ electrode (Figure 6.2-E) shows an oxidation current at more positive potentials, which can be associated to the oxidation of glucose in solution, producing an oxidation current of 2.3 μA at 0.4 V. Chronoamperometry response at 0.35 V (Figures 6.2-B, 6.2-D and 6.2-F) demonstrates that when glucose is introduced in the solution in a concentration of 1.6 mM, all the electrodes present electrocatalytic activity towards glucose oxidation, confirming that the immobilized enzyme maintains its catalytic activity.

The electrocatalytic activity is higher for the sample functionalized at 1.15 V. This can be explained considering either that the amount of immobilized enzyme is higher when the potential reaches a value of 1.15 V (the amount of functionalities in the SWCNT-APPA-1.15/GDH electrode is the highest, See Figure 6.1) or that the chemical interaction between the enzyme and the functionalized SWCNT favors the most adequate orientation of the enzyme that improves the electron transfer with the electrode.

The favored interaction between the enzyme and the functionalized SWCNT can be understood considering that at the pH conditions used, the acidic phosphorus groups are deprotonated whereas the enzyme (with an isoelectric point ~ 9.5) presents a net positive charge^{30,44}. In this sense, P species can facilitate the electron transfer with the electrode, as has been observed with other negatively charged functional groups in polyaniline-based polymers and sulphonic-containing electrodes^{45,46} and phosphorus-containing electrodes and other redox enzymes^{47,48}.

Surface concentration (Γ) of the enzyme was calculated from the reversible redox process at -0.11V and the values obtained for the SWCNT-APPA-X@GDH/PQQ electrodes are at around $2.57 \pm 0.73 \times 10^{-10} \text{ mol cm}^{-2}$. Then, in the three electrodes the amount of reconstructed enzyme is similar; however, the electrocatalytic response towards glucose oxidation is higher in the SWCNT-APPA-1.15X@GDH/PQQ electrode. Then, this electrode is used for the glucose oxidation with different concentrations. Figure 6.3-A shows the chronoamperometry curves obtained at 0.35 V under stirring condition for glucose concentrations between 5.0 μM and 4.0 mM in 0.1 M PBS (pH = 7.2) for the SWCNT-APPA-1.15@GDH/PQQ electrode. It can be observed an increase in the current after the addition of aliquots of glucose.

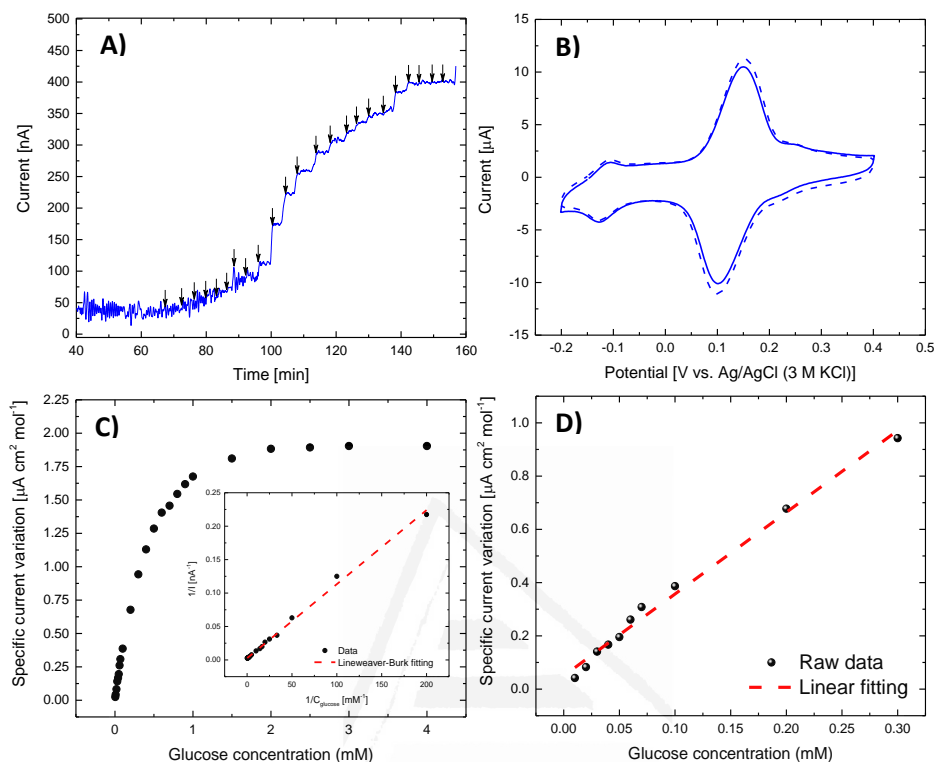


Figure 6.3. A) Chronoamperometric curve for SWCNT-APPA-1.15@GDH/PQQ electrode at 0.35 V for different concentrations of glucose: 0.005, 0.01, 0.02, 0.03, 0.04, 0.05, 0.06, 0.07, 0.1, 0.2, 0.3, 0.4, 0.5, 0.6, 0.7, 0.8, 0.9, 1, 1.5, 2, 2.5, 3 and 4 mM under room atmosphere conditions, B) Cyclic voltammograms of SWCNT-APPA-1.15@GDH/PQQ electrode before (dash line) and after (solid line) the oxidation of glucose, C) Calibration curve. Inset: Lineweaver-Burk plot and D) Linear regression fitting.

Cyclic voltammograms before and after the detection of glucose in Figure 6.3-B confirms the stability of the electrode. Figure 6.3-C shows the calibration curve (variation of the current normalized to the surface concentration of enzyme versus glucose concentration) which presents the Michaelis-Menten behavior. The linear fitting for the electrode is obtained in the concentration range between 10 μM to 300 μM , with a sensitivity of $3.07 \mu\text{A cm}^2 \text{mol}^{-1} \text{mM}^{-1}$ ($R^2=0.99$) as can be observed in Figure 6.3-D. The limit of detection (LOD) was determined empirically, as the lowest concentration of glucose whose signal can be clearly distinguished from the background current, having a value of 5 μM . Apparent Michaelis-Menten

constant (K_m^{app}) for the enzymatic biosensor, which is an important parameter regarding the interaction between the immobilized enzyme and its substrate, was experimentally estimated by the Lineweaver-Burk fitting of the double reciprocal plot, obtaining a value of around 0.42 mM (See Figure 6.3-C-Inset), which is similar to the values in solution (0.5-22 mM)³⁰, but lower than those reported previously for other biosensors^{42,49}. The low value of K_m^{app} obtained suggests high affinity between the enzyme and the substrate.

Once electrochemical behavior previously studied, demonstrated the applicability of the electrochemical entrapment of s-GDH employing anodic oxidation with 4-APPA, and subsequent reconstruction of the enzyme (procedure 1), experiments with direct electrochemical entrapment of reconstructed PQQ-GDH were carried out (procedure 2) in order to analyze the viability of a one-step synthesis of the biocatalyst.

3.2. Immobilization of PQQ-GDH using procedure 2.

3.2.1. Electrochemical synthesis of SWCNT-APPA-X@PQQ-GDH electrodes

Figures 6.4-A, 6.4-C and 6.4-E show the cyclic voltammograms of the electrochemical entrapment of reconstructed glucose dehydrogenase using procedure 2 at different upper potential limits. Irreversible oxidation of 4-APPA is observed from 0.69 V as well as several redox processes at less positive potentials which intensity increases with cycling. The voltammetric profiles obtained are similar to those resulting in procedure 1, although there are some differences in the relative intensities of the redox processes. Similarly, to what was observed in procedure 1 the immobilization of the enzyme and electrochemical functionalization of the SWCNTs occur at the same time.

Figures 6.4-B, 6.4-D and 6.4-F contain the voltammograms of the SWCNT-APPA-X@PQQ-GDH electrodes in 0.1M PBS (pH = 7.2). It can be observed in all the cases the presence of a redox processes at -0.11 V associated to the PQQ in the enzyme^{40,50}. This indicates the adequate electron transfer between the enzyme and the electrode. In this case, the surface concentration obtained is $5.77 \pm 0.80 \times 10^{-11} \text{ mol cm}^{-2}$ for SWCNT-APPA-1.15@PQQ-GDH, a value lower than the obtained with procedure 1.

Moreover, the redox process associated with the functionalities produced by oxidation of 4-APPA appear in all voltammograms at 0.13 V.

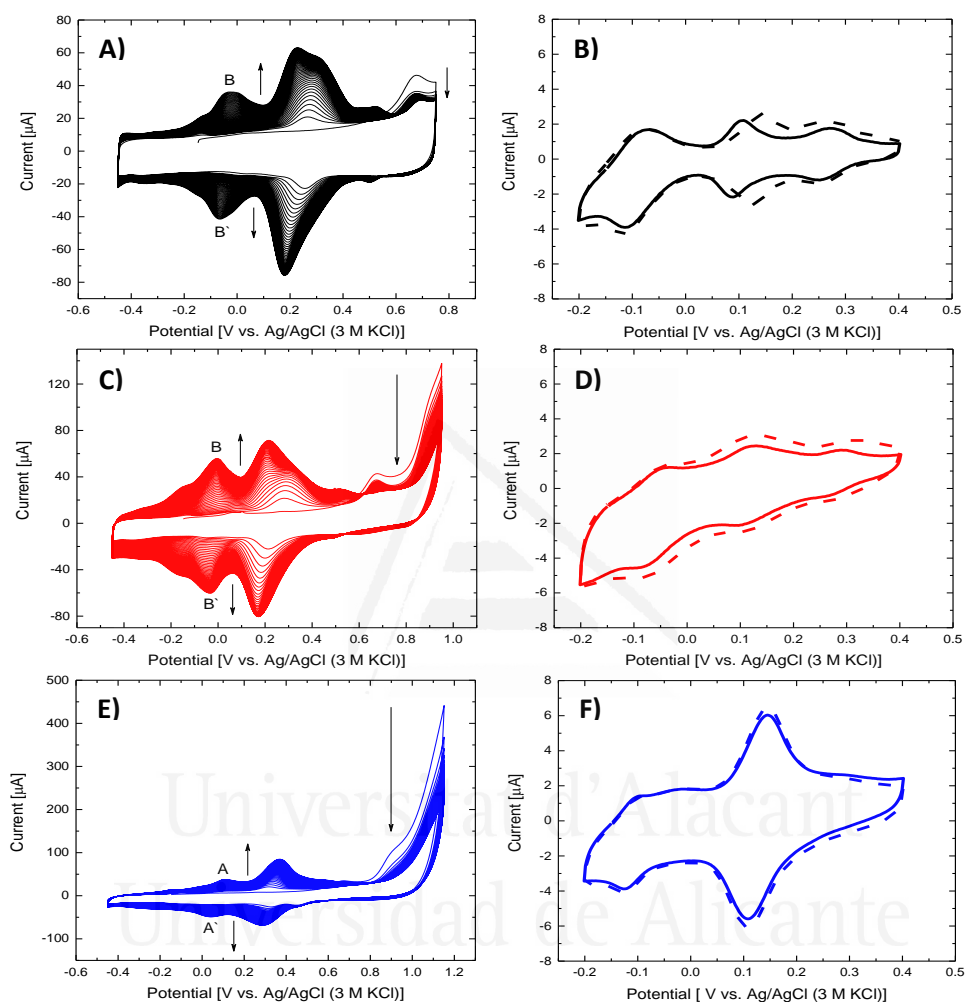


Figure 6.4. Cyclic voltammograms during electrochemical entrapment of purified PQQ-GDH solution on SWCNT at different upper potential limit (0.75 (A,B), 0.95 (C,D) and 1.15 (E,F)) in HEPES electrolyte + 5 mg mL⁻¹ PQQ-GDH (pH=5.0) at 50 mV s⁻¹ for 50 cycles under Ar atmosphere: A) 0.75 V, C) 0.95 V and E) 1.15 V. Electrochemical characterization by cyclic voltammetry of SWCNT-APPA-X@PQQ-GDH in absence (dashed line) and presence (solid line) of 4 mM of glucose in 0.1 M PBS (pH = 7.2) under room atmosphere conditions at 5 mV s⁻¹ (n=3), being: B) 0.75 V, D) 0.95 V and F) 1.15 V.

3.2.2. *Physicochemical characterization of SWCNT-APPA-X@PQQ-GDH electrodes*

The results of XPS analysis of the bioelectrodes are shown in Table 6.2. The amount of nitrogen detected is much higher than the observed in the functionalized SWCNT in absence of enzyme (SWCNT-APPA-X electrodes in Table 6.1), showing the incorporation of the enzyme and the contribution of the nitrogen-containing groups to N1s peak. The XPS spectra presented in Figure A-6.7 for all the samples, show the presence of two N species at around 398.5 eV and 400 eV. The species at 400 eV, which is the one with the highest intensity, can be assigned to the amide species of the peptide chain and the peak at 398.5 eV could be related to imine species⁵¹.

In the case of P2p spectra (Figure A-6.8), two asymmetric doublets appear in all the electrodes. The position of these peaks is similar to the observed in the SWCNT-APPA-X electrodes (Table 6.1); however, the percentage of these species changes and depends on the potential conditions used (Table 6.2). Interestingly, when the entrapment is done at 0.95 or 1.15 V, the main P peak is that corresponding to phosphonic species (i.e., C-P-O 2p_{3/2} peak at 132.5 eV). This result indicates that the presence of enzyme stabilizes the phosphonic group avoiding their oxidation which can be a consequence of the interaction between this group and the enzyme.

Table 6.2. Quantification of surface species by XPS and distribution of N, Ca, O and P contributions for SWCNT-APPA-X@PQQ-GDH synthesized in HEPES electrolyte at different potentials in presence of 5 mg mL⁻¹ PQQ-GDH.

| Upper potential limit [V vs. Ag/AgCl (3 M KCl)] | Ca (at%) | O (at%) | N (at%) | P (at%) | % Imines (398.5 eV) | % Amides (400 eV) | C-O-P 133.3 eV | C-P-O 132.6 eV |
|--|---------------------|--------------------|--------------------|--------------------|--------------------------------|------------------------------|---------------------------|---------------------------|
| Pristine | -- | 3.1 | 0.37 | 0.0 | -- | -- | -- | -- |
| 0.75 | 0.19 | 9.9 | 6.4 | 1.7 | -- | 100 | 62 | 38 |
| 0.95 | 0.12 | 18.6 | 25.9 | 0.5 | 34 | 66 | 10 | 90 |
| 1.15 | 0.56 | 24.1 | 13.6 | 3.1 | 12 | 88 | 14 | 86 |

Figure 6.5 shows the morphology of the SWCNT-APPA-X@PQQ-GDH electrodes synthesized at the different upper potential limits. Once electrochemical entrapment is performed, the surface of the SWCNT is covered by a smooth and globular coating, which morphology and thickness depends on the upper potential limit employed during the entrapment. In case of SWCNT-APPA-0.75@PQQ-GDH (Figure 6.5-B) the appearance of isolated enzymatic/APPA deposits can be observed between the interconnected bundles of the SWCNTs. However, when potential increases, the amount of deposit, distribution and thickness increase and the formation of a smooth surface can be observed (Figures 6.5-C to 6.5-F). However, the morphology is different to the electrode prepared in absence of enzyme (see sample SWCNT-APPA-1.15, Figures A-6.9-C and A-6.9-D). The formation of the enzymatic/APPA deposit on the electrode surface is the responsible for the strong changes in morphology observed. The presence of the enzyme during the electrochemical entrapment generates a globular-like structure that makes smoother the surface as observed by AFM microscopy (Figure A-6.10).

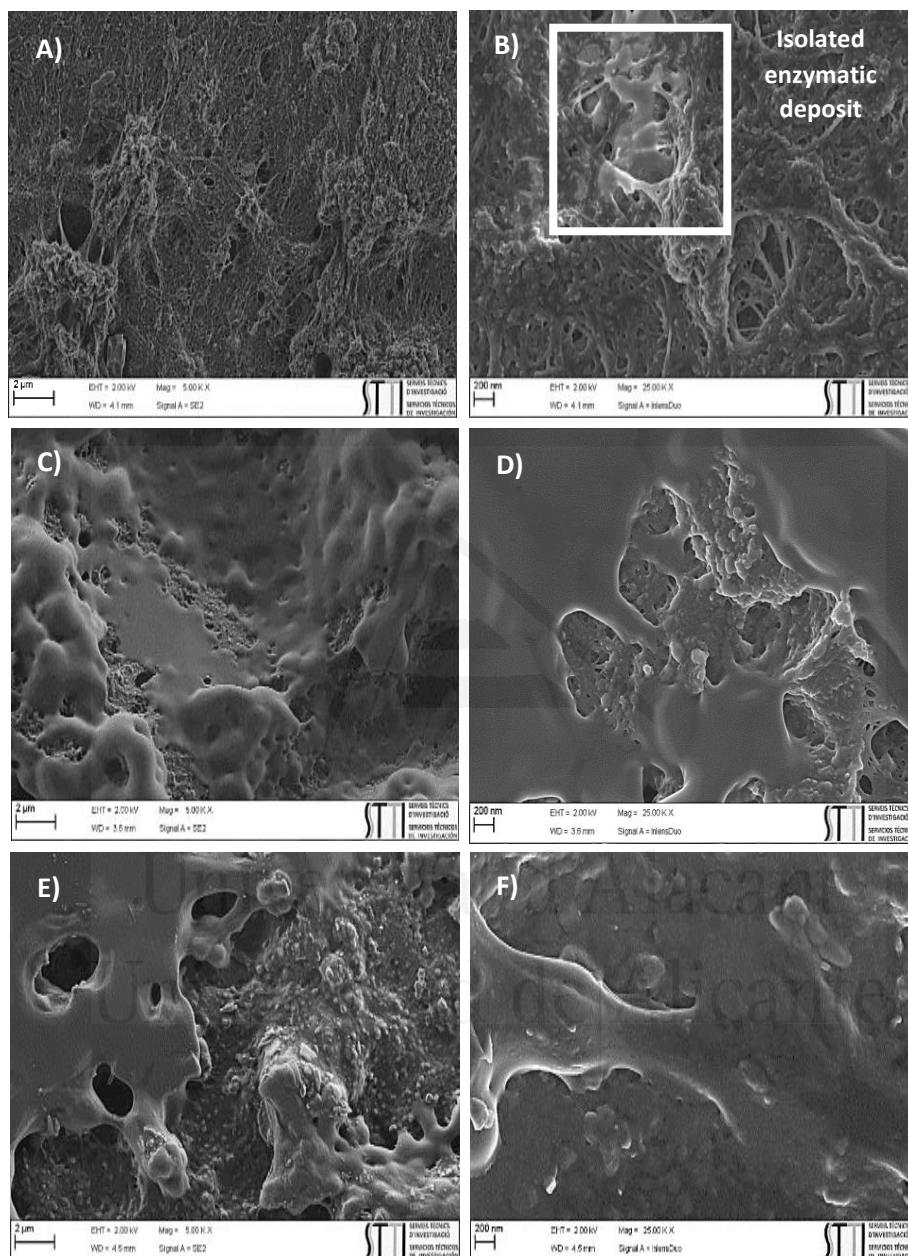


Figure 6.5. FESEM of bioelectrodes SWCNT-APPA-X@PQQ-GDH synthesized at different upper potential limits: A-B) X= 0.75, C-D) X=0.95 and E-F) X=1.15 V. Electrodes were modified under the following conditions: HEPES electrolyte + 5 mg mL^{-1} PQQ-GDH (pH=5.0) at 50 mV s^{-1} for 50 cycles under Ar atmosphere.

3.2.3. Glucose oxidation on SWCNT-APPA-X@GDH-PQQ electrodes

As it was observed in procedure 1, the electrodes synthesized at 0.75 and 0.95 V present a lack of reproducibility, saturation at low concentration of glucose and unstable behavior during the electrocatalytic activity towards glucose oxidation. Then, in the case of procedure 2, the study of the response towards glucose oxidation at different concentrations has only been done with the electrode synthesized at 1.15 V (electrode SWCNT-APPA-1.15@PQQ-GDH). Figure 6.6-A shows the cyclic voltammogram of this bioelectrode in 0.1 M PBS (pH = 7.2) in absence and presence of glucose. In presence of glucose, an additional contribution in the oxidation current is appreciated (471.23 nA at 0.4 V).

Chronoamperometry response of the SWCNT-APPA-1.15@PQQ-GDH electrode (Figure 6.6-B) shows an increase in the oxidation current after each addition of glucose aliquots. The variation of the current referred to the enzyme concentration versus the glucose concentration presents a typical Michaelis-Menten behavior. Lineweaver-Burk fitting allowed determining the value of K_m , which is 0.083 mM (See inset Figure 6.6-C). This value is lower than the obtained with procedure 1, suggesting a stronger interaction between the enzyme and the substrate. Linear detection range of the electrode was determined between 0.4 and 10 mM (See Figures 6.6-C and 6.6-D), obtaining a sensitivity normalized by the enzyme concentration of $4.28 \mu\text{A cm}^2 \text{mol}^{-1} \text{mM}^{-1}$ ($R^2=0.98$). The measured LOD has a value of $5 \mu\text{M}^{20}$.

Universidad de Alicante

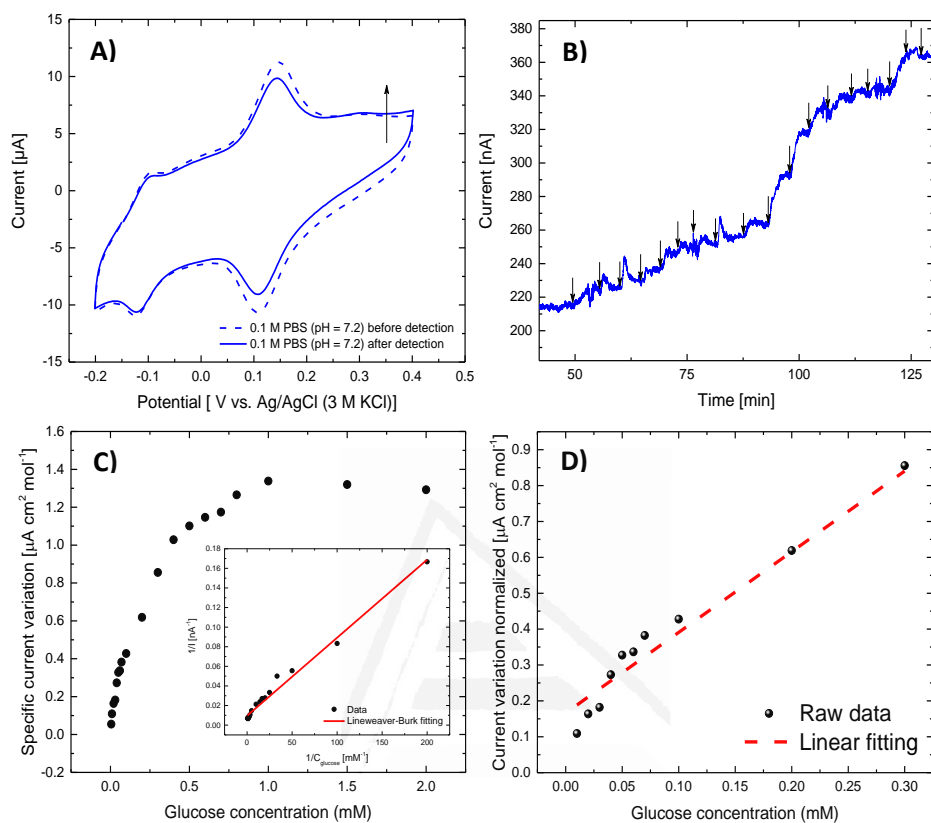


Figure 6.6. A) Cyclic voltammograms of electrode SWCNT-APPA-1.15@GDH/PQQ before and after the detection of glucose, B) Chronoamperometric response of SWCNT-APPA-1.15@GDH/PQQ at 0.35 V for different concentrations of glucose: 0.005, 0.01, 0.02, 0.03, 0.04, 0.05, 0.06, 0.07, 0.1, 0.2, 0.3, 0.4, 0.5, 0.6, 0.7, 0.8, 0.9, 1, 1.5, 2 and 4 mM under room atmosphere conditions, C) Calibration curve. Inset: Lineweaver-Burk fitting for enzyme immobilization by Michaelis-Menten constant and D) Linear regression fitting.

3.2.4. Stability and reproducibility

Reproducibility of the glucose biosensor SWCNT-APPA-1.15@PQQ-GDH was investigated by detection of 10 mM glucose at a constant potential of 0.35 V in 0.1 M PBS (pH = 7.2) in room atmosphere conditions for 3 different electrodes synthesized. As can be observed, electrochemical entrapment and electrochemical characterization in neutral conditions do not show important differences between them (See Figure A-6.11). Relative standard deviation

(RSD) of the current density variation at positive potential of the electrode was 10%, demonstrating a good reproducibility of the electrocatalytic response of the bioelectrode towards glucose oxidation. Cyclic voltammograms (See Figure A-6.12) in absence and presence of 10 mM glucose shows that the electrodes stored for 24 hours present a retention of the 89% (363.5 ± 10.3 nA) in the current density variation at higher potential, in comparison with the fresh-prepared electrode.

3.3. Comparison between both procedures and drop-casting method.

Comparison of the calibration curves for the electrodes prepared by electrochemical entrapment with 4-APPA by both procedures and an electrode modified with 4-APPA at 1.15 V and adding PQQ-GDH by drop-casting (SWCNT-APPA-1.15@PQQ-GDH_{drop-casting} electrode) are presented in Figure 6.7. The voltammogram of the drop-casting prepared electrode and the chronoamperometry profile towards glucose oxidation can be observed in Figure A-6.13.

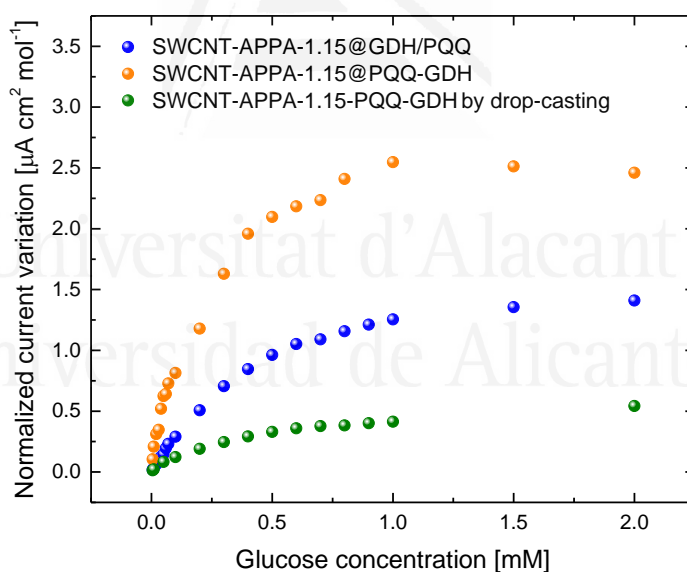


Figure 6.7. Calibration curves for the SWCNT synthesized by electrochemical entrapment of PQQ-GDH with 4-APPA for the two procedures developed and conventional manual procedure (drop casting).

Electrodes synthesized by electrochemical entrapment with both procedures show an important increase in the sensitivity normalized to the

amount of enzyme in the concentration range between 0.04-0.3 mM in comparison with the electrode prepared by drop-casting (see Figure 6.7 and Table A-6.1). Enhancement in the sensitivity values are more notorious in the samples prepared by procedure 2. Therefore, procedure 2 provides a platform to interconnect the enzyme and enhance the electron transfer, which is in agreement with the lower values of K_m obtained. Possibly, the strong interaction between phosphorus functionalities and the enzyme might favor the electron-transfer, what would improve the electrocatalytic activity towards glucose oxidation^{30,45}. It is important to highlight that the proposed method of electrochemical entrapment can produce bioelectrodes employing considerably low amount of enzyme, without affecting analytical parameters such as linear range. Interestingly, the electrode synthesized by drop-casting using the same amount of enzyme (5 mg mL^{-1} PQQ-GDH) presents a catalytic current 6.8 times lower than the observed for the electrochemical method developed in this study.

4. Conclusions

The electrochemical entrapment of either *s*-GDH or PQQ-GDH during oxidation of *para*-aminophenyl phosphonic acid (4-APPA) provides a simple method for the immobilization of the enzyme onto the SWCNT surface. During the electrochemical immobilization, the functionalization of the SWCNT with phosphorus and nitrogen groups also occurs. The adequate interaction between the functionalized SWCNT and the enzyme seems to be determined by the phosphorus groups incorporated in the material during the electrochemical co-deposition films. In the presence of the enzyme substrate a catalytic current is obtained showing the efficient enzyme-electrode contact. These bioelectrodes show an enhancement in the electrocatalytic current density and consequently in the sensitivity towards glucose oxidation in comparison with the electrode prepared by drop-casting. The sensitivity shows a high dependence with the upper potential limit employed for the enzyme immobilization being higher at high potential. The bioelectrode prepared with a one-step process (procedure 2), shows a sensitivity, referred to the amount of enzyme, around double than the electrode prepared using procedure 1 and six times higher than the bioelectrode prepared by drop-casting.

The proposed methodology offers a platform for enzymatic electrode preparation under mild conditions of synthesis on nanostructured carbon-based

materials, employing low loading of enzyme on the electrode surface and with high sensitivity. This methodology could be extended to other soluble enzymes, assuring good reproducibility, scalability and improved direct electron transfer, which may have potential application as anode in biofuel cells.

5. References

- (1) Vilkanauskyte, A.; Erichsen, T.; Marcinkeviciene, L.; Laurinavicius, V.; Schuhmann, W. Reagentless Biosensors Based on Co-Entrapment of a Soluble Redox Polymer and an Enzyme within an Electrochemically Deposited Polymer Film. *Biosens. Bioelectron.* **2002**, *17* (11), 1025–1031.
- (2) Schmidt, H.-L.; Schuhmann, W. Reagentless Oxidoreductase Sensors. *Biosens. Bioelectron.* **1996**, *11* (1), 127–135.
- (3) Ghindilis, A. L.; Atanasov, P.; Wilkins, E. Enzyme-Catalyzed Direct Electron Transfer: Fundamentals and Analytical Applications. *Electroanalysis* **1997**, *9* (9), 661–674.
- (4) Lopez, R. J.; Babanova, S.; Artyushkova, K.; Atanassov, P. Surface Modifications for Enhanced Enzyme Immobilization and Improved Electron Transfer of PQQ-Dependent Glucose Dehydrogenase Anodes. *Bioelectrochemistry* **2015**, *105*, 78–87.
- (5) Schuhmann, W. Amperometric Enzyme Biosensors Based on Optimised Electron-Transfer Pathways and Non-Manual Immobilisation Procedures. *Rev. Mol. Biotechnol.* **2002**, *82* (4), 425–441.
- (6) Albareda-Sirvent, M.; Merkoçi, A.; Alegret, S. Configurations Used in the Design of Screen-Printed Enzymatic Biosensors. A Review. *Sensors Actuators B Chem.* **2000**, *69* (1), 153–163.
- (7) May, S. W. Applications of Oxidoreductases. *Curr. Opin. Biotechnol.* **1999**, *10* (4), 370–375.
- (8) Bartlett, P. N. *Bioelectrochemistry: Fundamental, Experimental Techniques and Applications*. 1st ed., Jhon Wiley & Sons, Ltd, Southampton, UK, **2008**.
- (9) López-Bernabeu, S.; Huerta, F.; Morallón, E.; Montilla, F. Direct Electron Transfer to Cytochrome c Induced by a Conducting Polymer. *J. Phys. Chem. C* **2017**, *121* (29), 15870–15879.

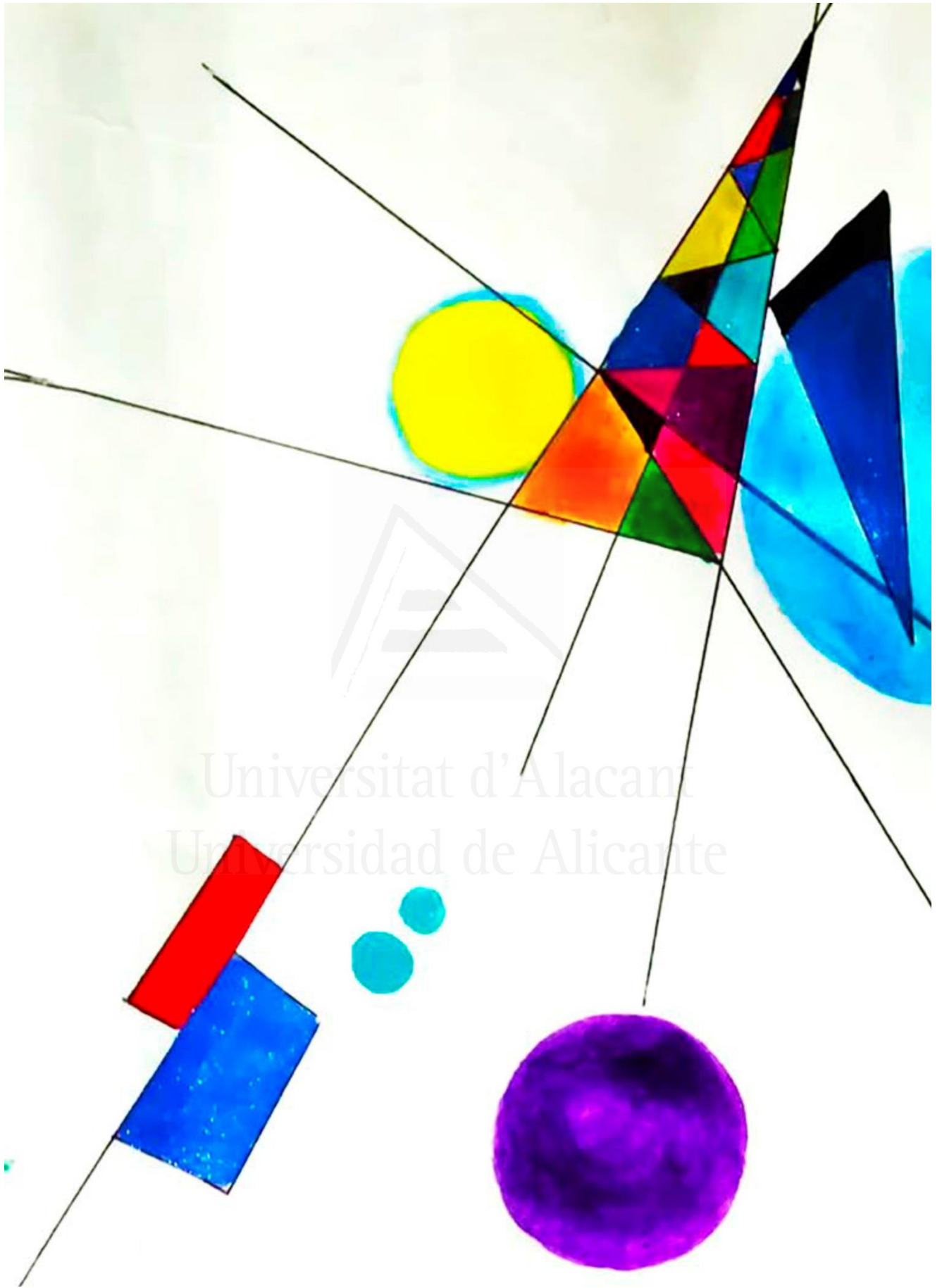
- (10) Tran, D. N.; Balkus, K. J. Perspective of Recent Progress in Immobilization of Enzymes. *ACS Catal.* **2011**, *1* (8), 956–968.
- (11) Shao, M.; Nadeem Zafar, M.; Sygmund, C.; Guschin, D. A.; Ludwig, R.; Peterbauer, C. K.; Schuhmann, W.; Gorton, L. Mutual Enhancement of the Current Density and the Coulombic Efficiency for a Bioanode by Entrapping Bi-Enzymes with Os-Complex Modified Electrodeposition Paints. *Biosens. Bioelectron.* **2013**, *40* (1), 308–314.
- (12) Lötzbeyer, T.; Schuhmann, W.; Schmidt, H.-L. Minizymes. A New Strategy for the Development of Reagentless Amperometric Biosensors Based on Direct Electron-Transfer Processes. *Bioelectrochemistry Bioenerg.* **1997**, *42* (1), 1–6.
- (13) Barwe, S.; Andronescu, C.; Pöller, S.; Schuhmann, W. Codeposited Poly(Benzoxazine) and Os-Complex Modified Polymethacrylate Layers as Immobilization Matrix for Glucose Biosensors. *Electroanalysis* **2015**, *27* (9), 2158–2163.
- (14) Heller, A. Electrical Connection of Enzyme Redox Centers to Electrodes. *J. Phys. Chem.* **1992**, *96* (9), 3579–3587.
- (15) Ramanavicius, A.; Habermüller, K.; Csöregi, E.; Laurinavicius, V.; Schuhmann, W. Polypyrrole-Entrapped Quinohemoprotein Alcohol Dehydrogenase. Evidence for Direct Electron Transfer via Conducting-Polymer Chains. *Anal. Chem.* **1999**, *71* (16), 3581–3586.
- (16) Abidi, M.; López-Bernabeu, S.; Huerta, F.; Montilla, F.; Besbes-Hentati, S.; Morallón, E. Spectroelectrochemical Study on the Copolymerization of O-Aminophenol and Aminoterephthalic Acid. *Eur. Polym. J.* **2017**, *91*, 386–395.
- (17) Wu, F.; Huang, T.; Hu, Y.; Yang, X.; Xie, Q. One-Pot Electrodeposition of a Composite Film of Glucose Oxidase, Imidazolium Alkoxysilane and Chitosan on a Reduced Graphene Oxide–Pt Nanoparticle/Au Electrode for Biosensing. *J. Electroanal. Chem.* **2016**, *781*, 296–303.
- (18) Betancor, L.; Luckarift, H. R. Bioinspired Enzyme Encapsulation for Biocatalysis. *Trends Biotechnol.* **2008**, *26* (10), 566–572.
- (19) Liu, J.; Wang, X.; Wang, T.; Li, D.; Xi, F.; Wang, J.; Wang, E. Functionalization of Monolithic and Porous Three-Dimensional Graphene by One-Step Chitosan Electrodeposition for Enzymatic Biosensor. *ACS Appl. Mater. Interfaces* **2014**, *6* (22), 19997–20002.

- (20) Kausaite-Minkstimiene, A.; Mazeiko, V.; Ramanaviciene, A.; Ramanavicius, A. Evaluation of Amperometric Glucose Biosensors Based on Glucose Oxidase Encapsulated within Enzymatically Synthesized Polyaniline and Polypyrrole. *Sensors Actuators B Chem.* **2011**, *158* (1), 278–285.
- (21) López-Bernabeu, S.; Gamero-Quijano, A.; Huerta, F.; Morallón, E.; Montilla, F. Enhancement of the Direct Electron Transfer to Encapsulated Cytochrome c by Electrochemical Functionalization with a Conducting Polymer. *J. Electroanal. Chem.* **2017**, *793*, 34–40.
- (22) Andronesu, C.; Pöller, S.; Schuhmann, W. Electrochemically Induced Deposition of Poly(Benzoxazine) Precursors as Immobilization Matrix for Enzymes. *Electrochem. commun.* **2014**, *41*, 12–15.
- (23) Tan, Y.; Deng, W.; Chen, C.; Xie, Q.; Lei, L.; Li, Y.; Fang, Z.; Ma, M.; Chen, J.; Yao, S. Immobilization of Enzymes at High Load/Activity by Aqueous Electrodeposition of Enzyme-Tethered Chitosan for Highly Sensitive Amperometric Biosensing. *Biosens. Bioelectron.* **2010**, *25* (12), 2644–2650.
- (24) Habermüller, K.; Ramanavicius, A.; Laurinavicius, V.; Schuhmann, W. An Oxygen-Insensitive Reagentless Glucose Biosensor Based on Osmium-Complex Modified Polypyrrole. *Electroanalysis* **2000**, *12* (17), 1383–1389.
- (25) Brownlee, B. J.; Bahari, M.; Harb, J. N.; Claussen, J. C.; Iverson, B. D. Electrochemical Glucose Sensors Enhanced by Methyl Viologen and Vertically Aligned Carbon Nanotube Channels. *ACS Appl. Mater. Interfaces* **2018**, *10* (34), 28351–28360.
- (26) Topçu Sulak, M.; Gökdoğan, Ö.; Gülce, A.; Gülce, H. Amperometric Glucose Biosensor Based on Gold-Deposited Polyvinylferrocene Film on Pt Electrode. *Biosens. Bioelectron.* **2006**, *21* (9), 1719–1726.
- (27) Ammam, M.; Fransaer, J. Microbiofuel Cell Powered by Glucose/O₂ Based on Electrodeposition of Enzyme, Conducting Polymer and Redox Mediators. Part II: Influence of the Electropolymerized Monomer on the Output Power Density and Stability. *Electrochim. Acta* **2014**, *121*, 83–92.
- (28) Ramanavičius, A.; Ramanavičienė, A.; Malinauskas, A. Electrochemical Sensors Based on Conducting Polymer—Polypyrrole. *Electrochim. Acta* **2006**, *51* (27), 6025–6037.

- (29) Barlett, P. N.; Cooper, J. M. A Review of the Immobilization of Enzymes in Electropolymerized Films. *J. Electroanal. Chem.* **1993**, *362* (1), 1–12.
- (30) Fusco, G.; Göbel, G.; Zanoni, R.; Kornejew, E.; Favero, G.; Mazzei, F.; Lisdat, F. Polymer-Supported Electron Transfer of PQQ-Dependent Glucose Dehydrogenase at Carbon Nanotubes Modified by Electropolymerized Polythiophene Copolymers. *Electrochim. Acta* **2017**, *248*, 64–74.
- (31) Yon-Hin, B. F. Y.; Lowe, C. R. An Investigation of 3-Functionalized Pyrrole-Modified Glucose Oxidase for the Covalent Electropolymerization of Enzyme Films. *J. Electroanal. Chem.* **1994**, *374* (1), 167–172.
- (32) Cosnier, S. Biomolecule Immobilization on Electrode Surfaces by Entrapment or Attachment to Electrochemically Polymerized Films. A Review. *Biosens. Bioelectron.* **1999**, *14* (5), 443–456.
- (33) Pinyou, P.; Ruff, A.; Pöller, S.; Ma, S.; Ludwig, R.; Schuhmann, W. Design of an Os Complex-Modified Hydrogel with Optimized Redox Potential for Biosensors and Biofuel Cells. *Chem. – A Eur. J.* **2016**, *22* (15), 5319–5326.
- (34) Marcinkevičienė, L.; Bachmatova, I.; Semėnaitė, R.; Rudomanskis, R.; Bražėnas, G.; Meškiene, R.; Meškys, R. Purification and Characterisation of PQQ-Dependent Glucose Dehydrogenase from *Erwinia* Sp. 34-1. *Biotechnol. Lett.* **1999**, *21* (3), 187–192.
- (35) Thermo scientific XPS simplified [Online], Thermo scientific XPS, Phosphorus (2020). Available at: <https://xpssimplified.com/elements/phosphorus.php#appnotes> [Accessed 2018 March 3].
- (36) Quintero-Jaime, A. F.; Cazorla-Amorós, D.; Morallón, E. Electrochemical Functionalization of Single Wall Carbon Nanotubes with Phosphorus and Nitrogen Species. *Electrochim. Acta* **2020**, *340*, 135935.
- (37) Quílez-Bermejo, J.; Ghisolfi, A.; Grau-Marín, D.; San-Fabián, E.; Morallón, E.; Cazorla-Amorós, D. Post-Synthetic Efficient Functionalization of Polyaniline with Phosphorus-Containing Groups. Effect of Phosphorus on Electrochemical Properties. *Eur. Polym. J.* **2019**, *119*, 272–280.

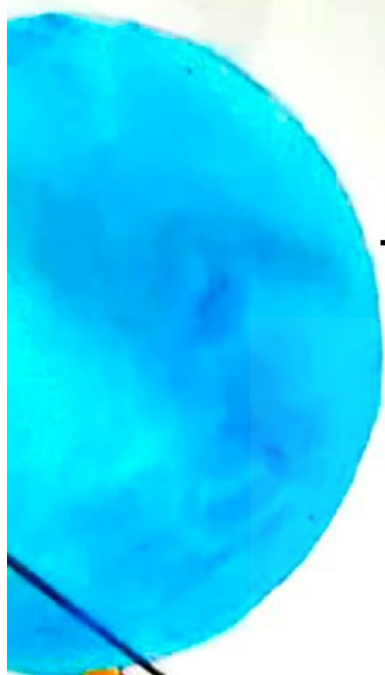
- (38) Quesada-Plata, F.; Ruiz-Rosas, R.; Morallón, E.; Cazorla-Amorós, D. Activated Carbons Prepared through H₃PO₄-Assisted Hydrothermal Carbonisation from Biomass Wastes: Porous Texture and Electrochemical Performance. *Chempluschem* **2016**, *81* (12), 1349–1359.
- (39) Zhang, L.; Miranda-Castro, R.; Stines-Chaumeil, C.; Mano, N.; Xu, G.; Mavré, F.; Limoges, B. Heterogeneous Reconstitution of the PQQ-Dependent Glucose Dehydrogenase Immobilized on an Electrode: A Sensitive Strategy for PQQ Detection Down to Picomolar Levels. *Anal. Chem.* **2014**, *86* (4), 2257–2267.
- (40) Katz, E.; Schlereth, D. D.; Schmidt, H.-L. Electrochemical Study of Pyrroloquinoline Quinone Covalently Immobilized as a Monolayer onto a Cystamine-Modified Gold Electrode. *J. Electroanal. Chem.* **1994**, *367* (1), 59–70.
- (41) Zayats, M.; Katz, E.; Baron, R.; Willner, I. Reconstitution of Apo-Glucose Dehydrogenase on Pyrroloquinoline Quinone-Functionalized Au Nanoparticles Yields an Electrically Contacted Biocatalyst. *J. Am. Chem. Soc.* **2005**, *127* (35), 12400–12406.
- (42) Tanne, C.; Göbel, G.; Lisdat, F. Development of a (PQQ)-GDH-Anode Based on MWCNT-Modified Gold and Its Application in a Glucose/O₂-Biofuel Cell. *Biosens. Bioelectron.* **2010**, *26* (2), 530–535.
- (43) Flexer, V.; Durand, F.; Tsujimura, S.; Mano, N. Efficient Direct Electron Transfer of PQQ-Glucose Dehydrogenase on Carbon Cryogel Electrodes at Neutral PH. *Anal. Chem.* **2011**, *83* (14), 5721–5727.
- (44) Kim, Y.-P.; Park, S. J.; Lee, D.; Kim, H.-S. Electrochemical Glucose Biosensor by Electrostatic Binding of PQQ-Glucose Dehydrogenase onto Self-Assembled Monolayers on Gold. *J. Appl. Electrochem.* **2012**, *42* (6), 383–390.
- (45) Göbel, G.; Schubart, I. W.; Scherbahn, V.; Lisdat, F. Direct Electron Transfer of PQQ-Glucose Dehydrogenase at Modified Carbon Nanotubes Electrodes. *Electrochem. commun.* **2011**, *13* (11), 1240–1243.
- (46) Chen, Y.; Yang, X.-J.; Guo, L.-R.; Li, J.; Xia, X.-H.; Zheng, L.-M. Direct Electrochemistry and Electrocatalysis of Hemoglobin at Three-Dimensional Gold Film Electrode Modified with Self-Assembled Monolayers of 3-Mercaptopropylphosphonic Acid. *Anal. Chim. Acta* **2009**, *644* (1–2), 83–89.

- (47) Yasutaka, K.; Takato, Y.; Takashi, K.; Kohsuke, M.; Hiromi, Y. Enhancement in Adsorption and Catalytic Activity of Enzymes Immobilized on Phosphorus- and Calcium-Modified MCM-41. *J. Phys. Chem. B* **2011**, *115* (34), 10335–10345.
- (48) Sarauli, D. Xu, C. Dietzel, B. Schulz, B. Lisdat, F. A multilayered sulfonated polyaniline network with entrapped pyrroloquinoline quinone-dependent glucose dehydrogenase: tunable direct bioelectrocatalysis. *J. Mater. Chem. B* **2014**, *2*, 3196–3203.
- (49) Sarauli, D.; Riedel, M.; Wettstein, C.; Hahn, R.; Stiba, K.; Wollenberger, U.; Leimkühler, S.; Schmuki, P.; Lisdat, F. Semimetallic TiO₂ Nanotubes: New Interfaces for Bioelectrochemical Enzymatic Catalysis. *J. Mater. Chem.* **2012**, *22* (11), 4615–4618.
- (50) Sarauli, D.; Xu, C.; Dietzel, B.; Schulz, B.; Lisdat, F. Differently Substituted Sulfonated Polyanilines: The Role of Polymer Compositions in Electron Transfer with Pyrroloquinoline Quinone-Dependent Glucose Dehydrogenase. *Acta Biomater.* **2013**, *9* (9), 8290–8298.
- (51) Stevens, J. S.; de Luca, A. C.; Pelendritis, M.; Terenghi, G.; Downes, S.; Schroeder, S. L. M. Quantitative Analysis of Complex Amino Acids and RGD Peptides by X-Ray Photoelectron Spectroscopy (XPS). *Surf. Interface Anal.* **2013**, *45* (8), 1238–1246.

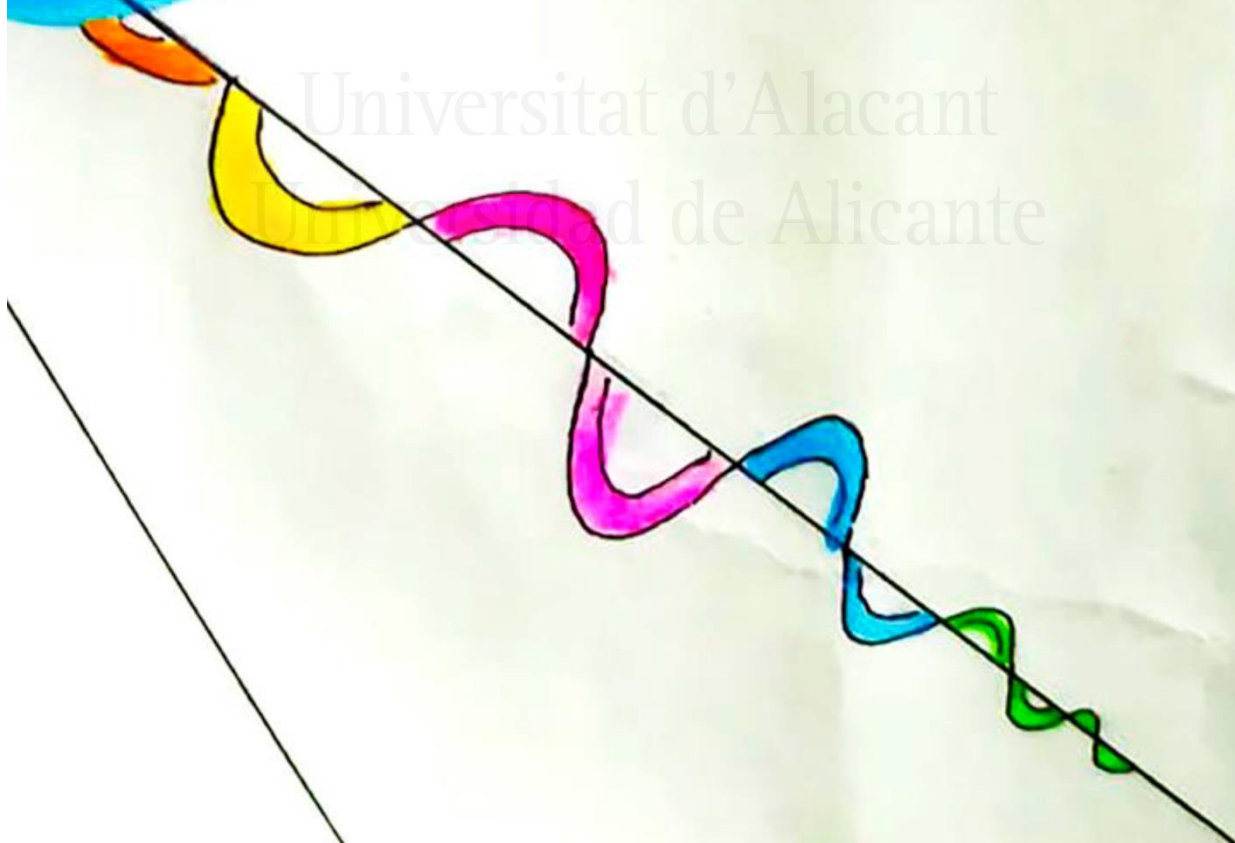


Universitat d'Alacant
Universidad de Alicante

**Annex to Chapter 6
Single Wall Carbon
Nanotubes-based
Bioelectrodes Prepared by
One-step Electrochemical
Enzyme Entrapment**



Universitat d'Alacant
University of Alicante



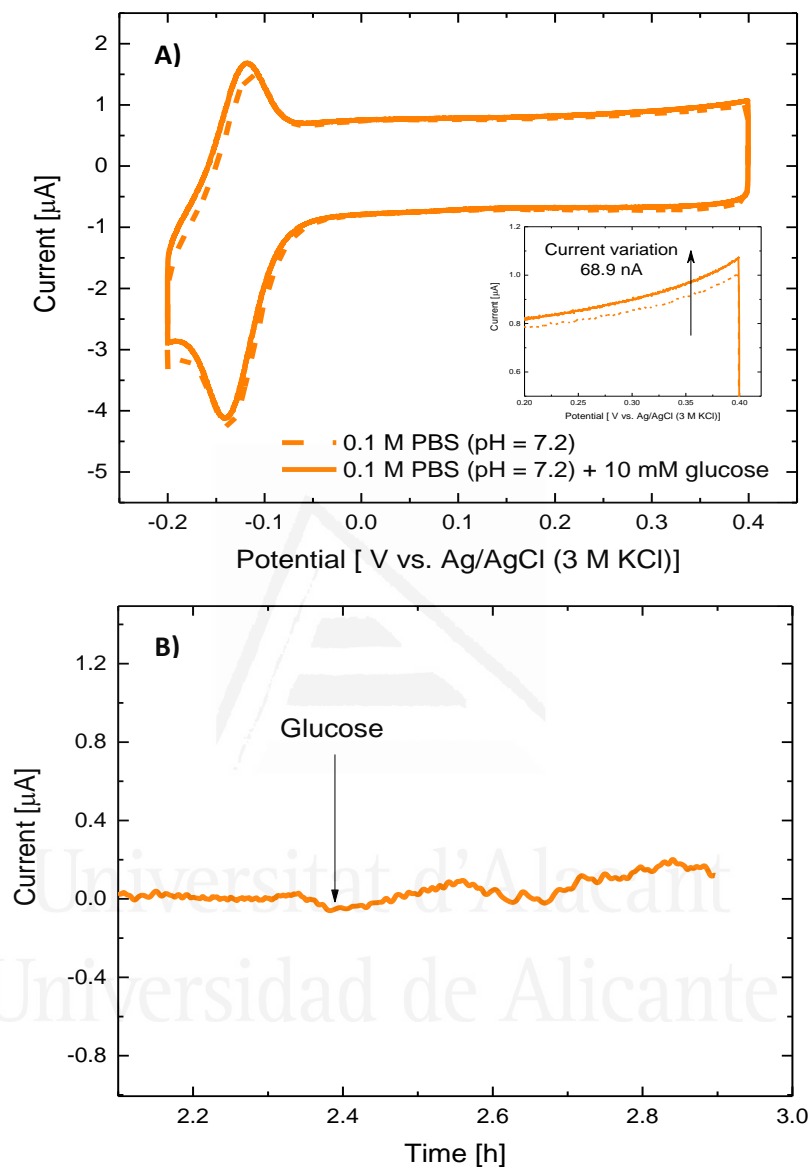


Figure A-6.1. A) Cyclic voltammograms of SWCNT modified with 5 mg mL^{-1} PQQ-GDH by drop-casting incubated in absence (dash line) and presence (solid line) of glucose in 0.1 M PBS (pH = 7.2) under room atmosphere at $5 \text{ mV} \cdot \text{s}^{-1}$ ($n=3$) and B) Chronoamperometry at 0.35 V in 0.1 M PBS (pH=7.2) after addition of 10 mM glucose, under O_2 room atmosphere and stirring condition.

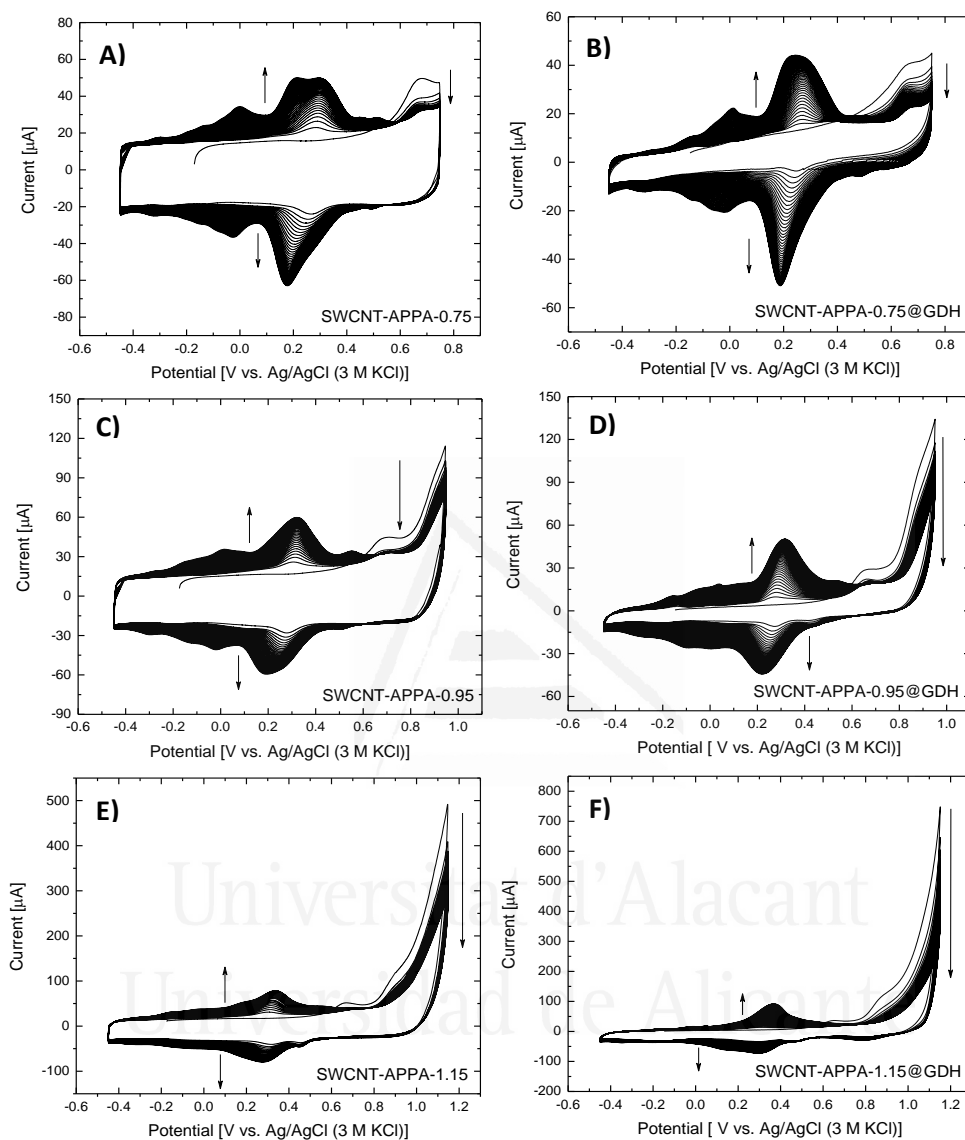


Figure A-6.2. Cyclic voltammograms of electrochemical entrapment in absence of apo-enzyme s-GDH (A, C and E) and presence of 5 mg mL^{-1} of apo-enzyme s-GDH (B, D and F) on SWCNT electrodes at different upper potential limit in HEPES electrolyte at 50 mV s^{-1} for 50 cycles under Ar atmosphere: A-B) 0.75 V, C-D) 0.95 V and E-F) 1.15 V, at 50 mV s^{-1} . All potentials are referred to the Ag/AgCl (3 M KCl) electrode reference at $\text{pH} = 5.0$.

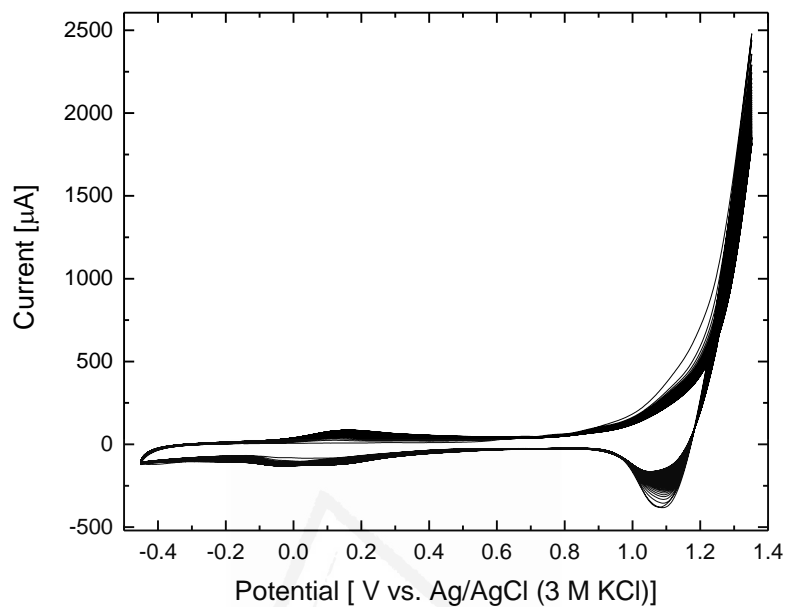


Figure A-6.3. Cyclic voltammogram of electrochemical entrapment in absence of apo-enzyme s-GDH on SWCNT electrodes at 1.35 V in HEPES electrolyte at 50 mV s^{-1} for 50 cycles under Ar atmosphere.

Universitat d'Alacant
Universidad de Alicante

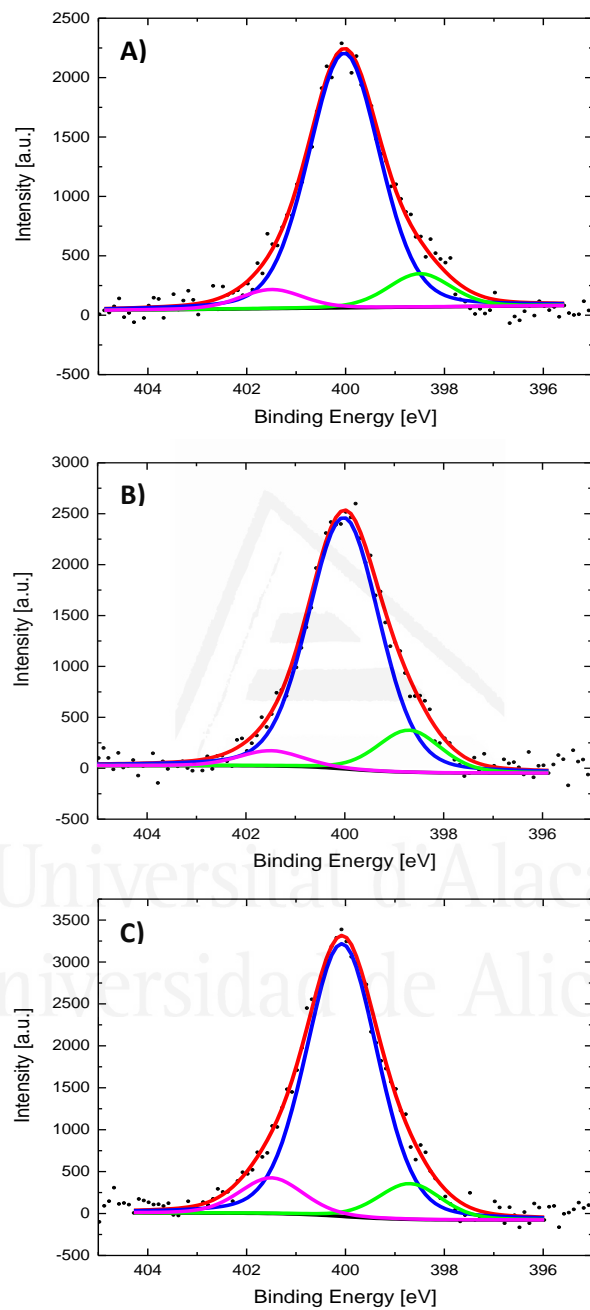


Figure A-6.4. N1s XPS spectra of SWCNT-APPA-X electrodes at different oxidation potentials, being: A) X=0.75 V, B) X=0.95 V, and C) X=1.15 V.

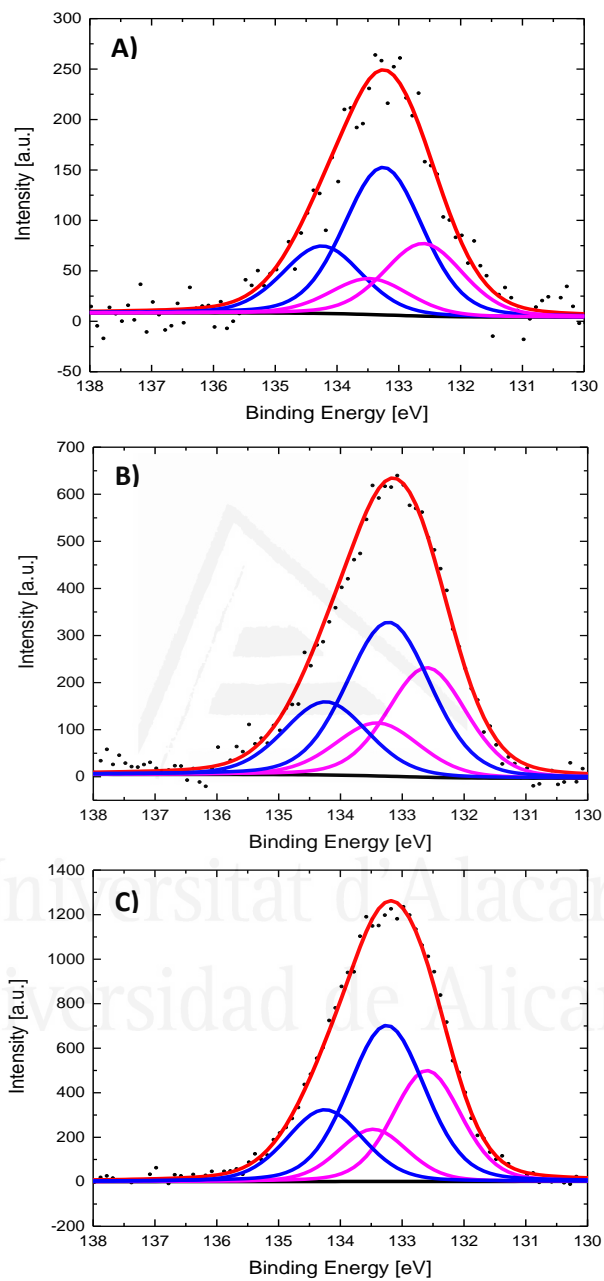


Figure A-6.5. P2p XPS spectra of SWCNT-APPA-X electrodes at different oxidation potentials being: A) X= 0.75 V, B) X= 0.95 V, and C) X= 1.15 V.

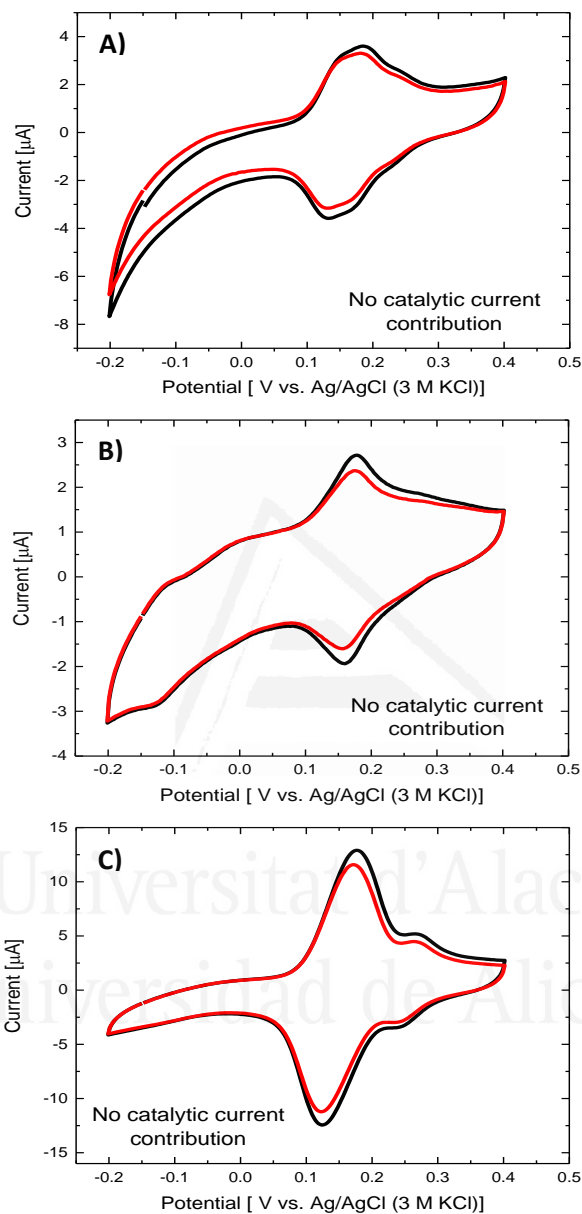


Figure A-6.6. Cyclic voltammograms of SWCNT-APPA-X@GDH electrodes synthesized at different upper potential limit: A) X=0.75, B) X=0.95 and C) X=1.15 V, in absence (black line) and presence (red line) of 4 mM glucose in 0.1 M PBS (pH = 7.2) under room atmosphere at 5 mV s^{-1} (n=3).

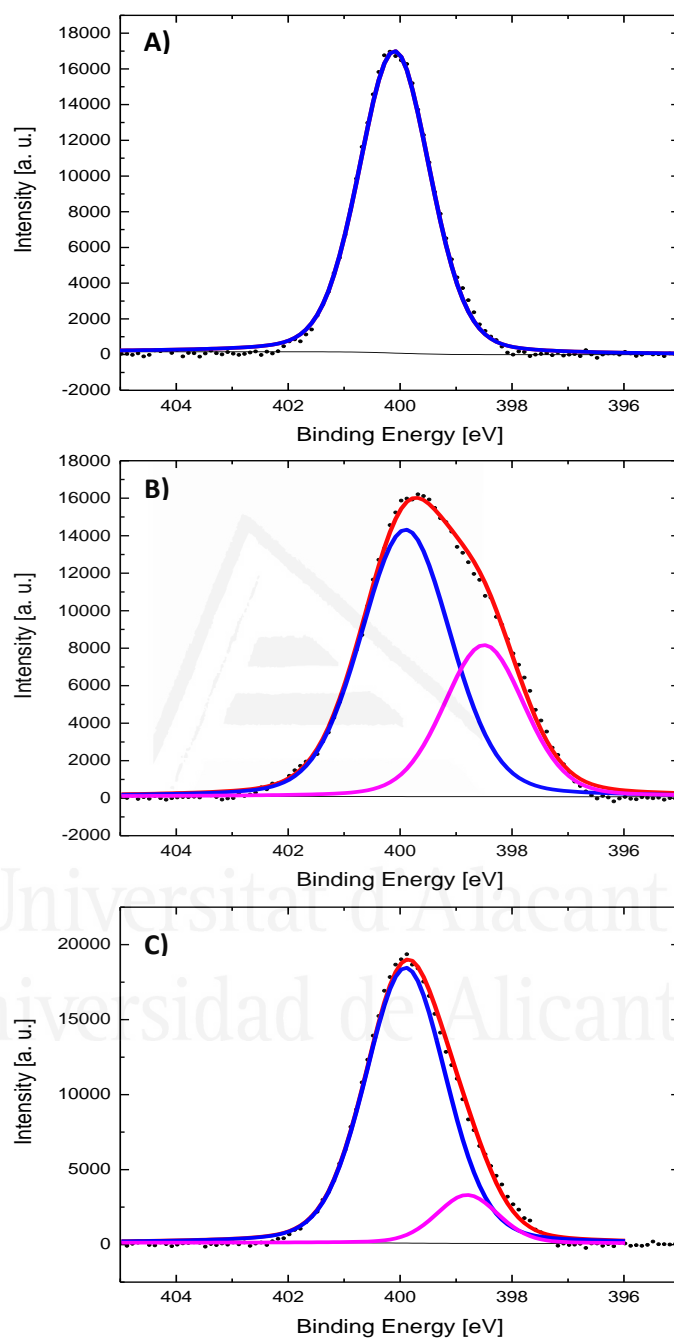


Figure A-6.7. N1s XPS spectra for bioelectrodes SWCNT-APPA-X@PQQ-GDH (red line) at different upper potential limits: A) 0.75, B) 0.95, C) 1.15 V.

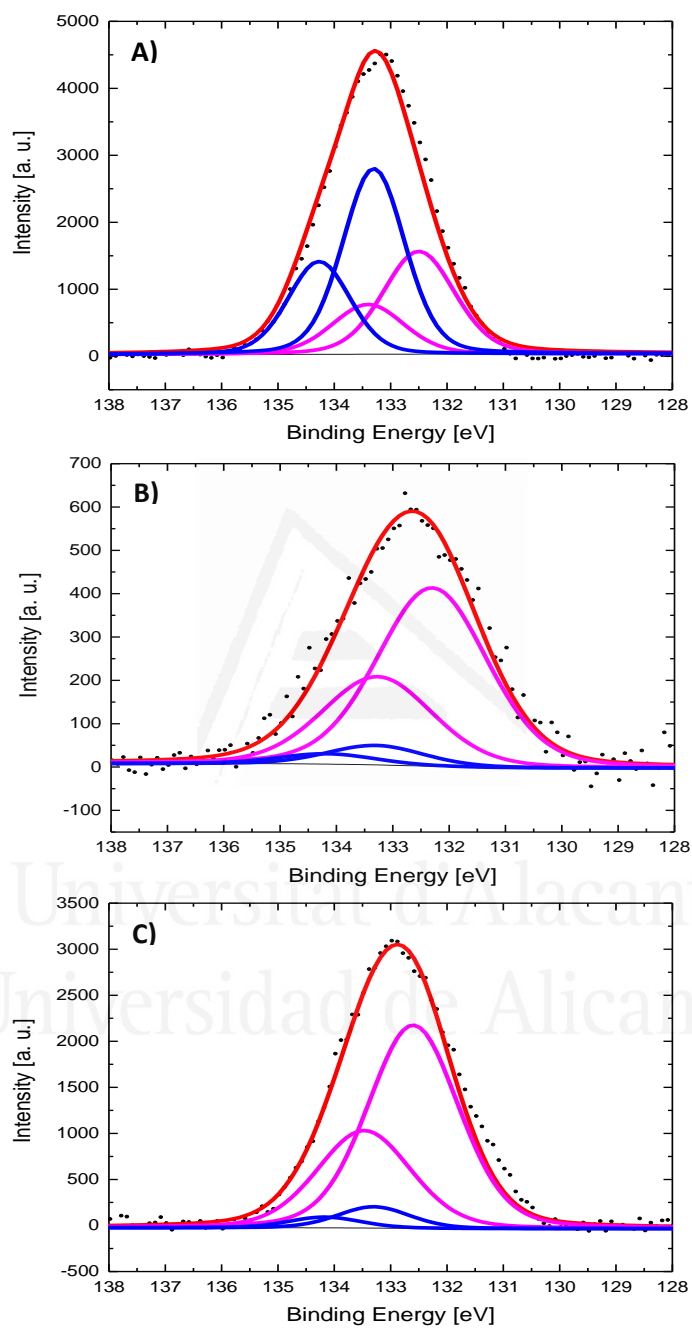


Figure A-6.8. P2p XPS spectra for bioelectrodes SWCNT-APPA-X@PQQ-GDH (red line) at different upper potential limits: A) 0.75, B) 0.95, C) 1.15 V.

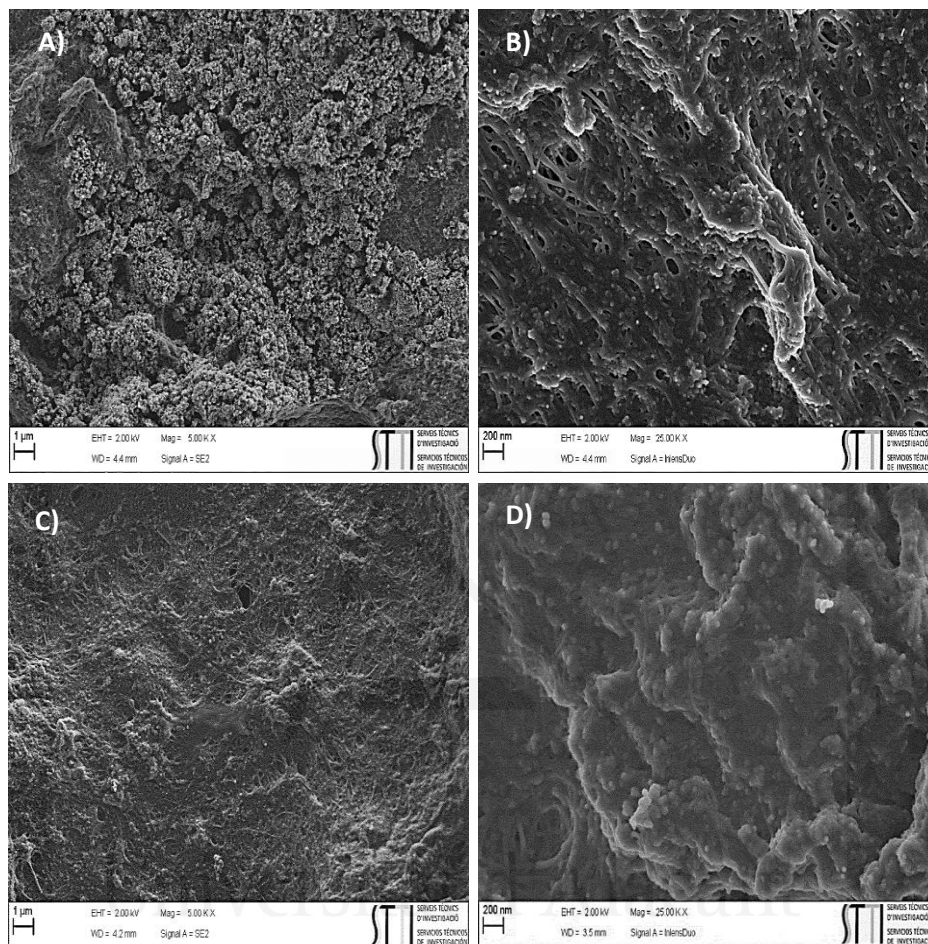


Figure A-6.9. FESEM micrographs of: A-B) SWCNT deposited onto glassy carbon electrode and C-D) SWCNT-APPA-1.15 electrode synthesized under the following conditions: HEPES electrolyte (pH=5.0) at 50 mV s⁻¹ for 50 cycles under Ar atmosphere.

In order to guarantee that deposits observed in SWCNT-APPA-1.15@PQQ-GDH electrode prepared in presence of PQQ-GDH can be correlated with the formation of an enzyme/APPA deposit, a control electrode synthesized at 1.15 V (SWCNT-APPA-1.15) in the same conditions in absence of the enzyme was performed (See Figure A-6.9-C and A-6.9-D). Morphology of this electrode shows that during the electrochemical functionalization, products generated by the electrooxidation of 4-APPA cover homogeneously the surface of the SWCNTs.

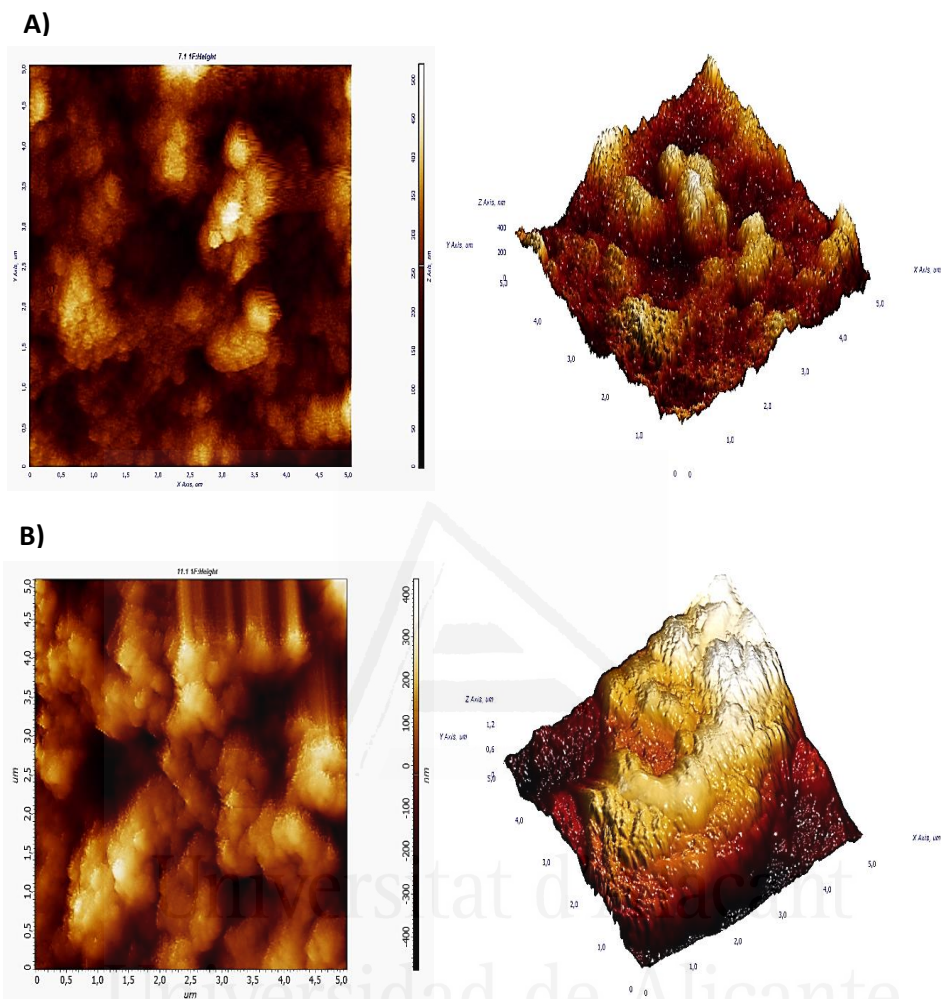


Figure A-6.10. AFM micrographs for A) pristine SWCNT and B) SWCNT-APPA-1.15@PQQ-GDH electrode. Electrode B) was synthesized under the following conditions: HEPES electrolyte in absence (A) and presence (B) of 5 mg mL^{-1} PQQ-GDH (pH=5.0) at 50 mV s^{-1} for 50 cycles under Ar atmosphere.

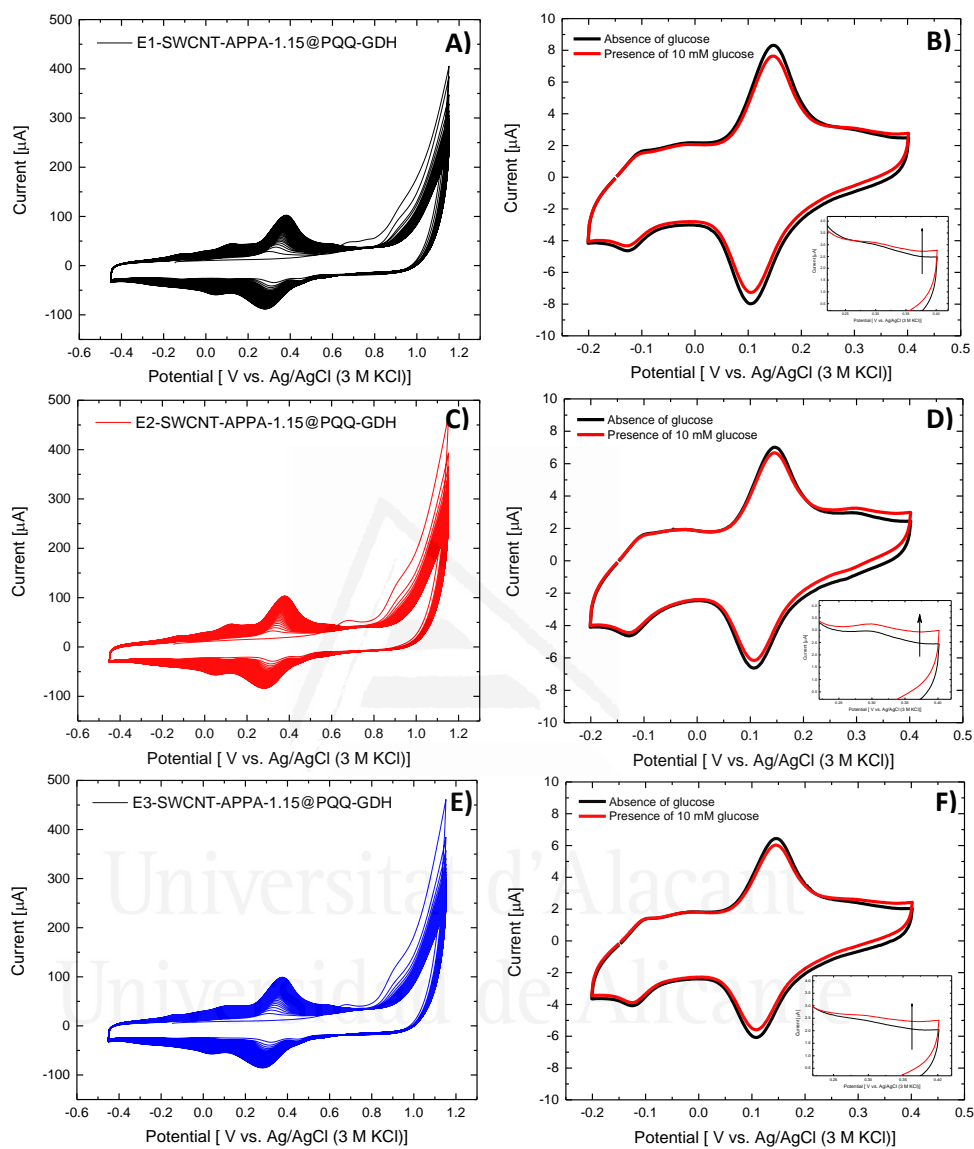


Figure A-6.11. A, C and E) Cyclic voltammograms of electrochemical entrapment of PQQ-GDH in 3 different electrodes synthesized in the same conditions: HEPES electrolyte and 5 mg mL^{-1} of PQQ-GDH at 50 mV s^{-1} for 50 cycles under Ar atmosphere until 1.15 V. B, D and F) Cyclic voltammograms of corresponding 3 electrodes E1, E2 and E3 synthesized at the same conditions (SWCNT-APPA-1.15@PQQ-GDH) in absence (black line) and presence (red line) of 10 mM glucose, in 0.1 M PBS (pH = 7.2) under room atmosphere conditions at 5 mV s^{-1} ($n=3$).

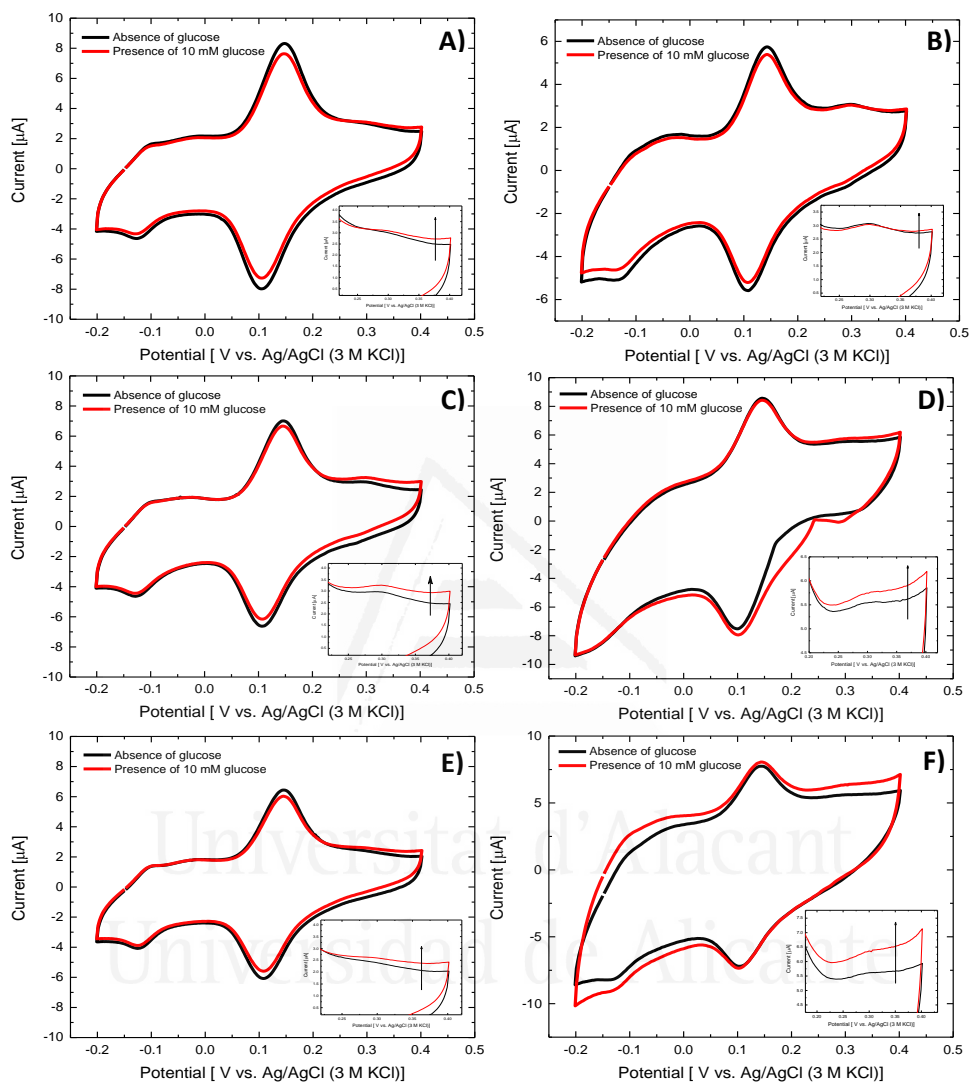


Figure A-6.12. Cyclic voltammograms of three different electrodes of SWCNT-APPA-1.15@PQQ-GDH in absence (black line) and presence (red line) of 10 mM glucose: A), C) and E) freshly prepared and B), D) and F) after 24 hours of storage in 0.1 M PBS (pH=7.2). Inset: Enlargement of the high potential zone.

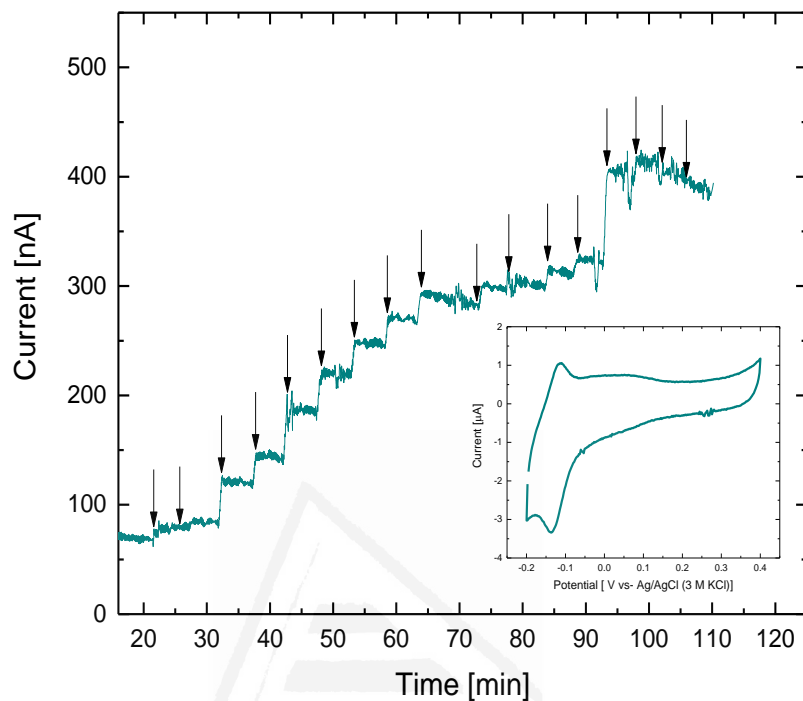
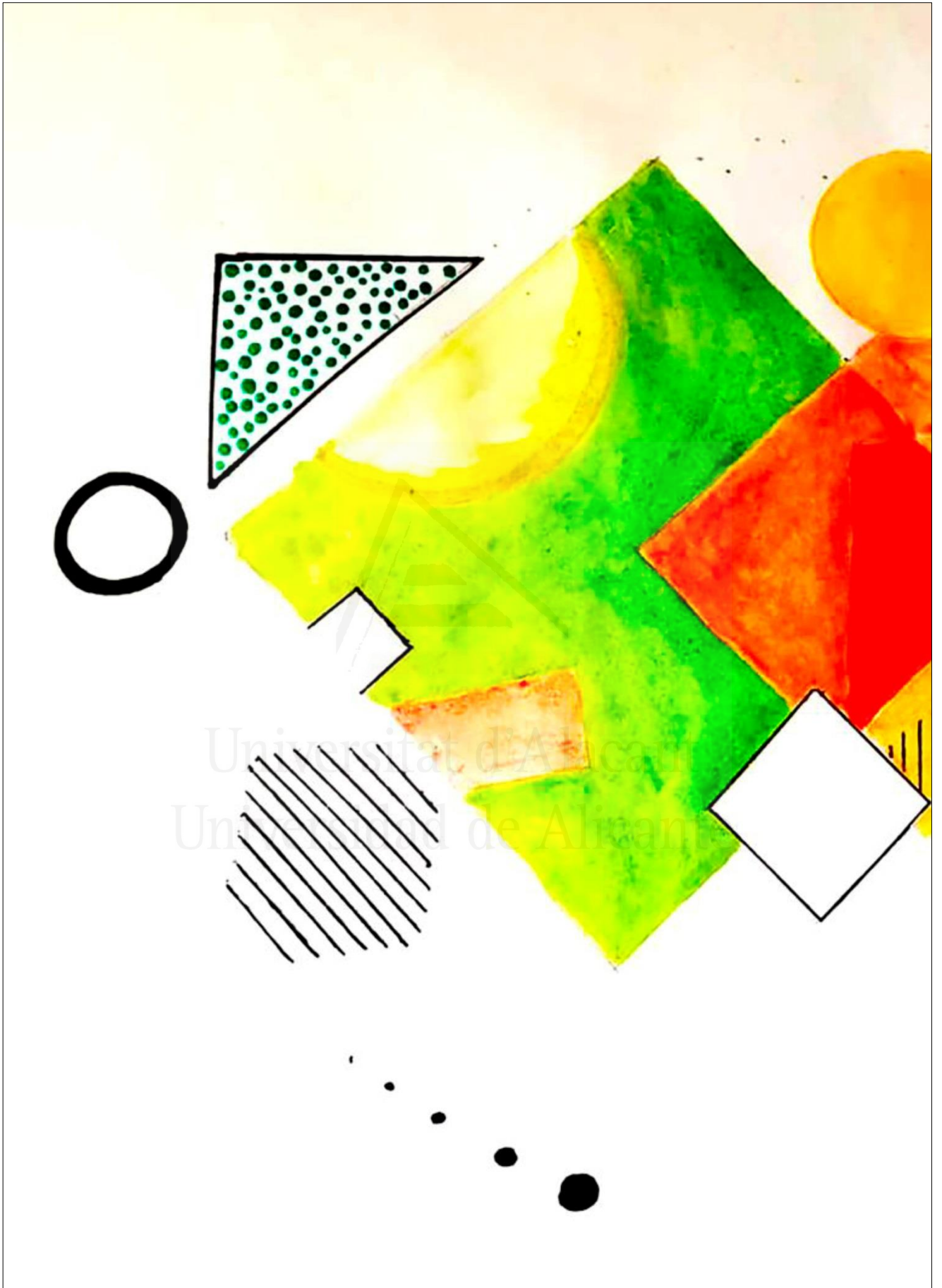


Figure A-6.13. Chronoamperometric curves of SWCNT-APPA-1.15@PQQ-GDH_{drop casting} electrode at 0.35V at different concentrations of glucose under O₂ room atmosphere. Inset: Cyclic voltammograms of the electrode in 0.1 M PBS (pH = 7.2) under room atmosphere at 5 mV s⁻¹ (n=3).

Universidad de Alicante

Table A-6.1. Analytical figures of merit for the quantification of glucose for electrodes prepared by entrapment in this work (procedure 1 and procedure 2) and a control electrode synthesized by drop-casting.

| Parameter | Bioelectrode | | |
|---|--------------------------|--------------------------|--------------------------------------|
| | SWCNT-APPA-1.15@GDH/PQQ | SWCNT-APPA-1.15@PQQ-GDH | SWCNT-APPA-1.15-PQQ-GDH Drop casting |
| Coating of enzyme [mol cm ⁻²] | 2.57 x 10 ⁻¹⁰ | 5.77 x 10 ⁻¹¹ | 6.07 x 10 ⁻¹⁰ |
| Sensitivity [μA cm ² mol ⁻¹ mM ⁻¹] | 2.29 | 4.28 | 0.66 |
| R ² | 0.99 | 0.98 | 0.97 |
| Linear range (mM) | 0.01-0.3 | 0.01-0.3 | 0.01-0.3 |
| K _m ^{app} (mM) | 0.42 | 0.083 | 0.59 |



Chapter 7

Metal Free Electrochemical Glucose Biosensor Based on N-Doped Carbon Material



Mariv

1. Introduction

Glucose concentration is a reliable indicator to identify metabolic disorder in the production of insulin (diabetes) and other diseases in human being; then, monitoring its concentration in physiological fluids has received attention in the last century¹⁻³. Moreover, the determination of glucose is important in a variety of fields such as food chemistry, environmental protection and biotechnology⁴. For that reason, the development of electronic devices for effective detection and accurate quantification of glucose has been extensively studied, being the enzymatic electrochemical biosensors the most developed and commercialized^{3,5}. The enzymatic glucose detection is based on the indirect measurement of generated hydrogen peroxide (H_2O_2), molecular oxygen (O_2) consumption or the oxidation changes generated by an artificial redox mediator species^{6,7}. In this sense, development of different electrocatalytic materials that may provide high sensitivity and selectivity but working at low potentials, to minimize the interference effects, has received substantial interest^{7,8}. Different electrode materials have been used for this application like metal containing electrodes⁹⁻¹¹, conducting polymers¹²⁻¹⁴ and carbon-based modified electrodes¹⁵⁻¹⁷, among others.

Several first generation electrochemical biosensors have demonstrated an outstanding performance for indirect glucose detection^{17,18}. However, a non-effective selectivity, high overpotential and pH-dependence of the catalytic performance have limited the proper applicability of these first generation biosensors¹⁹. One outstanding strategy to reduce the working potential, thus avoiding the effect of external interference, has been proposed by Wang et. al^{10,20,21}, and consists in the use of noble metal nanoparticles, generally platinum (Pt), supported on a carbon-based material, together with the immobilization of the enzyme. Metal nanoparticles provide many advantages like high surface activity, but the strong adsorption of the biomolecules after their immobilization can affect the performance of the biosensors.

The use of carbon materials for the synthesis of biosensors has gained an increasing attention, considering their remarkable catalytic activity, high surface area and easy processing^{22,23}. Additionally, tailoring the surface chemistry of carbon materials by different functionalization procedures provides routes for proper enzyme immobilization, which improve its electrocatalytic activity^{11,24}. Previous works have shown that nanostructured

carbon materials, such as carbon nanotubes (CNTs) and graphene-based materials present a remarkable electrocatalytic activity to promote the detection of glucose, uric acid and ascorbic acid, without interference effect between them^{25,26}. Recently, carbon-based materials doped with heteroatoms have shown outstanding electrocatalytic behavior for oxidation and reduction reactions. The presence of heteroatoms in the carbon network provides active sites for specific oxidation/reduction reactions and an improved electron transfer in the interface electrode/electrolyte²⁷⁻²⁹. For instance, catalytic activity of carbon nanotubes doped with nitrogen towards ascorbic acid and uric acid oxidation, allowed the successful quantification in different physiological fluids of those species without matrix effects³⁰. Additionally, functionalities in carbon materials may have a good interaction with the enzymatic element, acting as an anchoring point with the amino acid residues³¹ or even may connect the cofactor of the enzyme with the electrode facilitating the direct-electron transfer (DET)³².

In this work, we present a low-cost enzymatic metal-free biosensor based on nitrogen doped carbon materials, obtained after thermal treatment of polyaniline, for enzymatic amperometric detection of glucose in real samples like urine and commercial sugary drinks. Interestingly, high sensitivity of the biosensor towards changes in molecular oxygen concentration provides an accurate procedure for glucose determination.

2. Experimental section

2.1. Materials

Chemical synthesis of polyaniline (PANI) was carried out from distilled aniline, ACS reagent ($\geq 99.5\%$). Ammonium persulphate ($\geq 98\%$ -BioXtra), D-(+)-Glucose ACS reagent, D-(+)-Gluconic acid δ -lactone ($\geq 99\%$), Nafion® 117 solution ($\sim 5\%$ in mixture of lower aliphatic alcohols in water), glutaraldehyde (GA) solution (50 wt. % in H₂O), L-Ascorbic acid reagent grade-Crystalline, Uric acid ($\geq 99\%$ -Crystalline), Dopamine hydrochloride ($+98\%$) and glucose oxidase (GO_x) from *Aspergillus Niger* (50K Units), were purchased from Sigma-Aldrich.

Hydrochloric acid (37%) was obtained from VWR Chemicals. Potassium dihydrogen phosphate (KH₂PO₄) and ammonia solution (25%) was obtained from Merck. Dipotassium hydrogen phosphate (K₂HPO₄) was purchased from

VWR Chemicals. Both potassium salts were used to prepare phosphate buffer solutions (0.1 M PBS, pH=7.2). All the solutions were prepared using ultrapure water (18 M Ω cm, Millipore® Milli-Q® water). The gases N₂ (99.999%) and H₂ (99.999%) were provided by Air Liquide.

2.2. Synthesis of PANI-TT

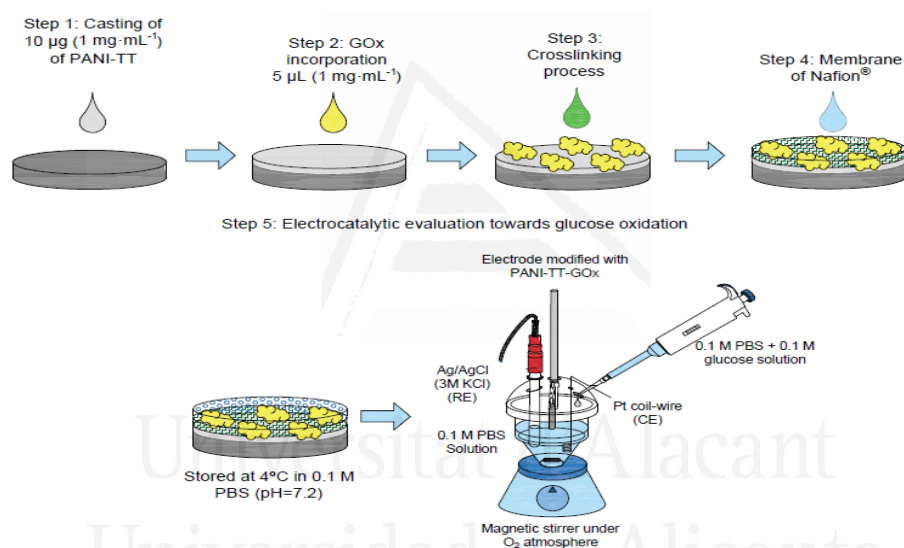
The preparation of the nitrogen doped carbon material was carried out employing PANI that was synthesized by chemical polymerization using the following procedure. In a two-neck bottom flask with 0.67 M of aniline in 1 M HCl solution, ammonium persulphate is added in a stoichiometric ratio. The mixture was put under stirring for 3 hours in an ice-bath system at 0°C. Doped PANI was obtained treating the filtered and dried polymer with 1 M NH₄OH for 24 hours. The synthesized PANI was washed several times with distilled water and dried at 80 °C overnight.

The nitrogen doped carbon material was obtained after thermal treatment of PANI following the procedure published elsewhere³³, which consists on putting 150 mg of PANI in a tubular furnace and applying a two-step thermal treatment. In the first step, PANI is heated at 1000°C for 1h using a heating rate of 5°C min⁻¹ in an oxygen-containing atmosphere (5000 ppm O₂/N₂) with a flow rate of 100 ml min⁻¹. After cooling at 10°C min⁻¹ until room temperature, a second heating step was carried out at 5°C min⁻¹ from room temperature to 1200°C in a nitrogen atmosphere with a flow rate of 100 ml min⁻¹ during the treatment. The nitrogen doped carbon material obtained is named as PANI-TT (polyaniline thermally treated).

2.3. Preparation of PANI-TT-GO_x modified electrode

A schematic diagram of the stepwise assembly procedure of the biosensor is shown in Scheme 7.1. Prior to the modification, a glassy carbon electrode surface (3 mm diameter) was sanded with emery paper and polished using 1 and 0.05 μ m alumina slurries, then rinsed with ultrapure water. PANI-TT was dispersed in a 0.002% of Nafion® solution in water:isopropanol (80:20) in order to attain a concentration of 1mg mL⁻¹, with the aid of ultrasonic bath for 45 minutes and using an ice bath to avoid heating during the sonication. A 5 μ L aliquot of the dispersion was dropped onto the glassy carbon (GC) surface and dried under an infrared lamp to remove the solvents. This procedure was

repeated twice for a total of $10 \mu\text{g}$ of PANI-TT. In the second step, $5 \mu\text{L}$ of 10 mg mL^{-1} GO_x in 0.1 M PBS ($\text{pH} = 7.2$) were added onto the electrode surface and incubated at room temperature till all the drop was dried, reaching an enzyme loading of $5.0 \mu\text{g}_{\text{GO}_x} \mu\text{g}^{-1}_{\text{PANI-TT}}$. The third step includes the immobilization process, which was carried out employing $2 \mu\text{L}$ of 0.25 w/w\% GA in 0.1 M PBS ($\text{pH}=7.2$) to promote crosslinking. Finally, enzymatic coating was entrapped by adding of $2 \mu\text{L}$ of 2.5 w/w\% of Nafion®. This procedure was previously used with carbon nanotubes²². Afterwards, the electrodes are stored in PBS (0.1 M , $\text{pH} = 7.2$) for 24 hours at 4°C previous to its use for electrochemical evaluation. The electrodes are called as PANI-TT- GO_x .



Scheme 7.1. Illustration of the stepwise process for glucose biosensor electrode fabrication and detection of glucose based on PANI-TT- GO_x electrodes.

2.4. Physicochemical characterization

X-Ray photoelectron spectroscopy (XPS) was performed in a VG-Microtech Mutilab 3000 spectrometer using an $\text{Al K}\alpha$ radiation (1253.6 eV). The deconvolution of the XPS peaks for $\text{C}1s$, $\text{O}2p$ and $\text{N}1s$ was done by least squares fitting using Gaussian-Lorentzian curves, while a Shirley line was used for the background determination.

Transmission electron microscopic measurements (TEM) were carried out using JEOL TEM, JEM-2010 model, and GATAN acquisition camera.

Scanning electron micrographs were taken using an ORIOUS SC600 model Field Emission Scanning Electron Microscopy (FE-SEM) and a ZEISS microscope, Merlin VP Compact model. Samples were coated with a thin layer of carbon to avoid decomposition of the enzyme and the different components employed during the fabrication of the biosensor.

The textural properties of the PANI-TT were evaluated by N₂ adsorption isotherms at -196°C in an automatic adsorption system (Autosorb-6, Quantachrome). Prior to the measurements, the sample was degassed at 250°C for 4 hours. Apparent surface area has been determined by BET method (S_{BET}) and total micropore volume (pores of size < 2 nm) has been assessed by applying the Dubinin-Radushkevich (DR) equation to the N₂ adsorption isotherm.

2.5. Electrochemical characterization.

The electrochemical characterization and catalytic activity evaluation was performed employing a conventional 3 electrode cell: the glassy carbon electrode modified with PANI-TT or PANI-TT-GO_x was used as working electrode (WE), a Pt coil-wire was used as counter electrode (CE) and a Ag/AgCl (3 M KCl) was used as reference electrode (RE). Considering the oxygen dependence of the detection process, both oxygen saturated solution and just laboratory atmosphere conditions were selected for the electrochemical evaluation towards glucose determination. The chronoamperometry was performed in a stirring 0.1 M PBS (pH=7.2) solution using the PANI-TT-GO_x as working electrode. Aliquots of glucose solution, from a concentrated glucose solution (0.1 M) prepared in 0.1M PBS, were added to the electrochemical cell to reach the desired concentrations between 0.005 to 20 mM. Between aliquots, 5 minutes are left until current stabilization. Cyclic voltammetry was employed at the beginning and the end of the glucose determination to control changes in the electrode. All the measurements were carried out in triplicate (n=3). All electrochemical measurements were carried out in a BIOLOGIC SP-300 potentiostat.

3. Results and discussion

3.1. Physicochemical characterization of PANI-TT

The synthesis of the N-doped carbon material has been previously published and consists of a double-stage heat treatment of PANI under O₂/N₂ and N₂ atmosphere³³. This procedure promotes the development of porosity during the heat treatment of the polymer precursor. N₂ adsorption isotherm for sample PANI-TT (Figure 7.1-A) corresponds to a type I isotherm typical of microporous solids. The BET surface area of this carbon material is 1360 m² g⁻¹ and the micropore volume is 0.51 cm³ g⁻¹. TEM image in Figure 7.1-B shows that the carbon material has a laminar morphology and that the heat treatment applied up to 1200°C does not produce a relevant increase in the long-range structural order, in agreement with previous results^{34,35}.

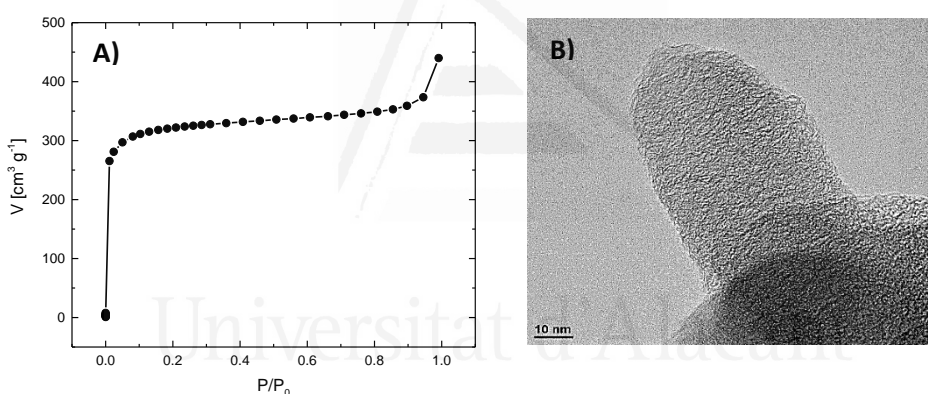


Figure 7.1. A) N₂ adsorption isotherm at 77K of PANI-TT N-doped carbon material and B) TEM image of PANI-TT N-doped carbon material.

It was previously reported that the heat treatment first in an oxygen containing atmosphere and second in N₂ up to 1200 °C, has important effects on the textural and structural properties of the carbon material. This heat treatment program increases both the yield of the process, since stabilization reactions are favored, and the porosity due to the slightly oxidizing atmosphere employed and, finally, it promotes structural changes in the obtained N species, resulting in the conversion of pyridine and pyridone species into quaternary nitrogen species (also named graphitic nitrogen)³³. Figure 7.2 shows the XPS N1s spectrum in which it can be observed that the heat treatment program applied to PANI results in the selective formation of

quaternary nitrogen species with an energy binding at 401.2 eV with a nitrogen content of around 1 atom%. Previous works have shown that the quaternary nitrogen species are responsible for the generation of active sites for the oxygen reduction reaction with a high catalytic activity^{33,34}.

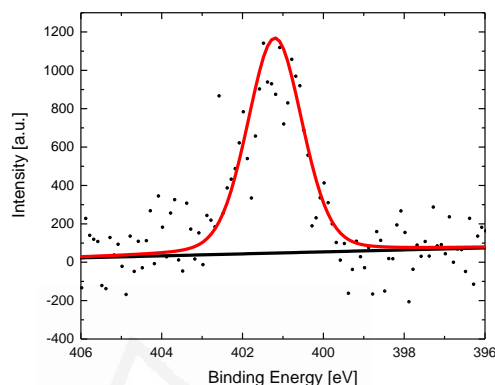


Figure 7.2. N1s XPS spectrum for PANI-TT.

3.2. Electrochemical behavior of PANI-TT-GO_x.

Figure 7.3 shows the electrochemical characterization by cyclic voltammetry of N-doped carbon material (PANI-TT) and PANI-TT-GO_x electrodes in neutral conditions (0.1 M PBS, pH=7.2) and at different atmosphere conditions in order to analyze the electrocatalytic activity to ORR. The voltammogram of PANI-TT electrode presents under N₂ saturated conditions (Figure 7.3-A) a rectangular shape from -0.62 to 0.05 V due to the formation of the electrical double-layer.

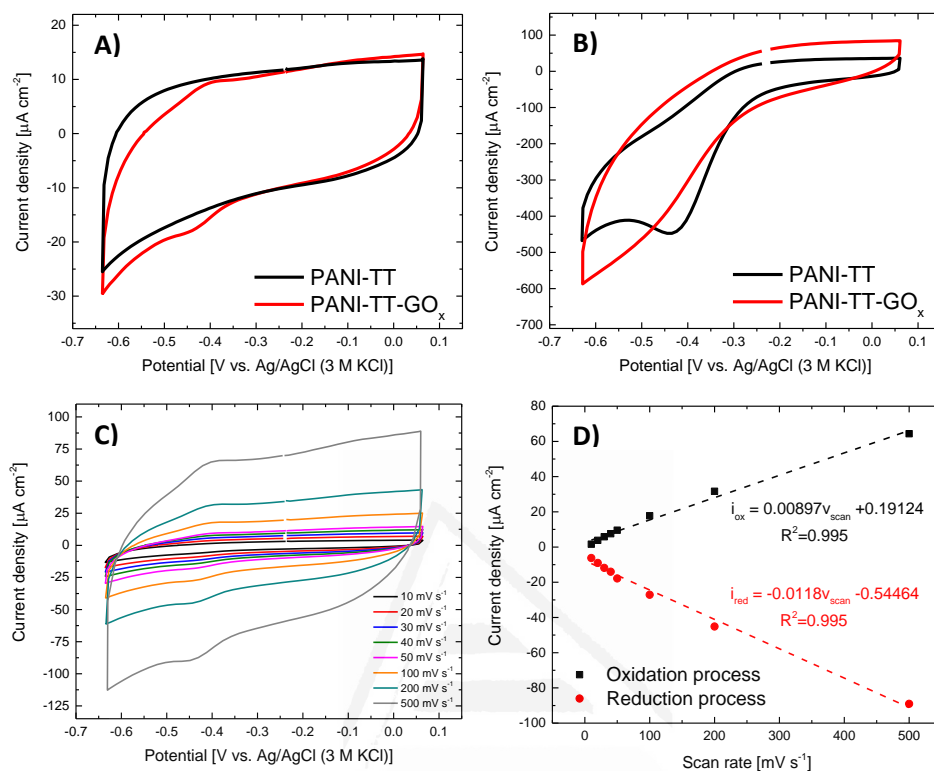


Figure 7.3. Cyclic voltammograms of PANI-TT and PANI-TT-GO_x in 0.1 M PBS (pH = 7.2) at 50 mV s⁻¹: A) solution saturated in N₂, B) solution saturated in O₂, C) Cyclic voltammograms at different scan rates (from 1 to 500 mV s⁻¹) in N₂ saturated solution and D) Plot of peak current against scan rate.

The voltammograms obtained with increasing the upper potential limit can be observed in Figure 7.4-A. Further anodic polarization to potentials higher than 0.6 V produces the electrochemical oxidation of the carbon material. Under O₂-saturated conditions the cyclic voltammograms of PANI-TT (Figure 7.3-B and Figure 7.4-B) presents a reduction peak with an onset potential at around -0.2 V vs. Ag/AgCl (3 M KCl) corresponding to the oxygen reduction reaction (ORR). The PANI-TT-GO_x electrode (Figure 7.3-A) shows a highly reversible redox process ($\Delta E \sim 33$ mV) at around -0.42 V, which can be associated with the redox processes of the two electron-transfer of the GO_x cofactor (FAD/FADH₂)^{15,27}. This process, as can be observed in the Figure 7.3-C and 7.3-D, shows a linear dependence with the scan rate, suggesting that the redox process of FAD/FADH₂ corresponds to a surface-controlled redox

process, what shows the adequate immobilization of the enzyme³⁶⁻³⁸. However, the incorporation of the GO_x results in a decrease in the catalytic activity towards the oxygen reduction reaction, as observed with the shift to less positive potentials of the cathodic peak at around -0.42 V associated to ORR (Figure 7.3-B); which might be a consequence of a partial blocking of the active sites in the carbon material by the enzyme coating³⁹.

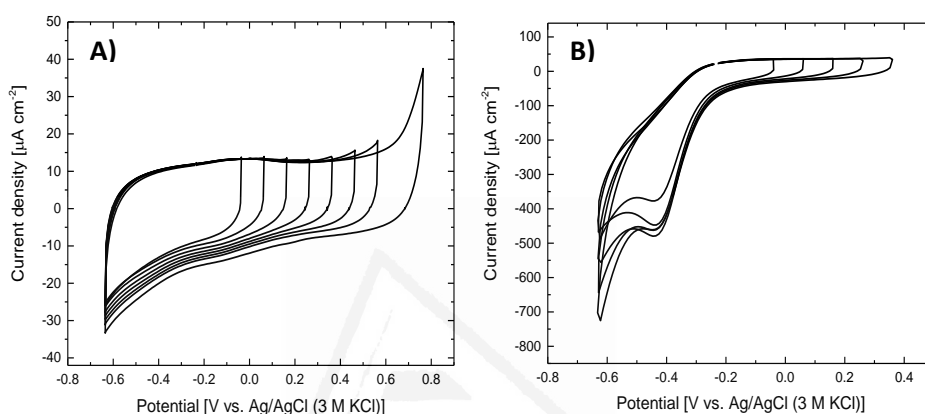


Figure 7.4. Cyclic voltammograms at different potential limits for PANI-TT in 0.1 M PBS (pH = 7.2) at 50 mV s⁻¹: A) under N₂ atmosphere and B) under O₂-saturated conditions.

Morphological characterization of the biosensors was carried out by FESEM (Figure 7.5) and it shows a homogeneous surface coating, during the different steps of preparation of the bioelectrode. Initially, PANI-TT deposited onto the glassy carbon electrode presents a rough surface morphology. Once the enzyme is incorporated in the modified electrode, the presence of a thin layer of the glucose oxidase onto the carbon material is observed that produces a smoother surface. Further cross-linking with glutaraldehyde and Nafion® results in the formation of a thick and homogenous layer onto the electrode surface with presence of cracks that can be generated during drying. The incorporation of these two layers entraps the enzyme, suppressing the leaching of the bioelement. Higher magnifications for both coatings of glutaraldehyde and Nafion® show that the surface presents some roughness and pores (See Figure 7.5-E and 7.5-F) that may facilitate diffusion of the substrate and molecular oxygen towards the PANI-TT-GO_x.

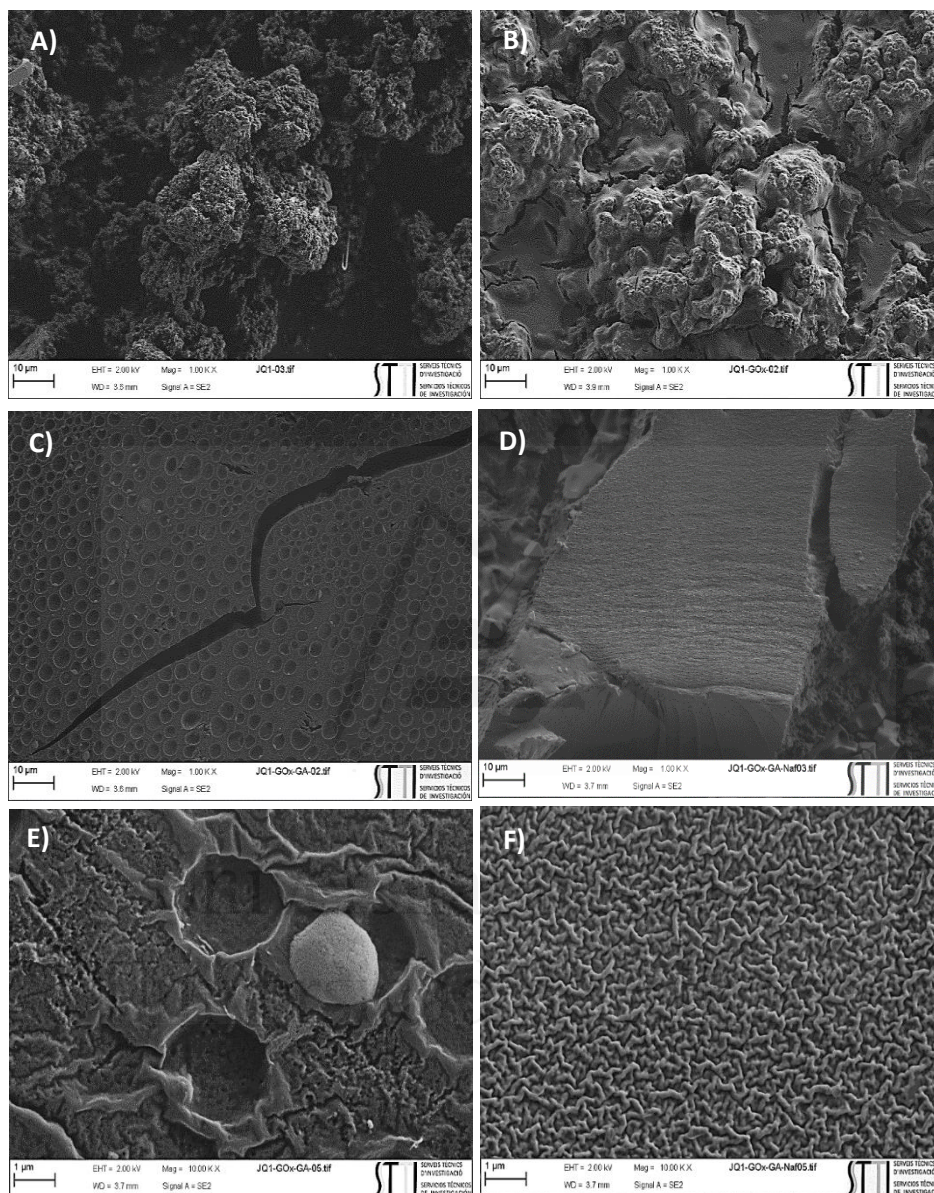


Figure 7.5. FESEM micrographs of glassy carbon electrode modified during the different steps for the glucose biosensor fabrication: A) PANI-TT, B) PANI-TT-GO_x, C) PANI-TT-GO_x-GA, D) PANI-TT-GO_x-GA-Nafion®, E) magnification at 10.000 X of PANI-TT-GO_x-GA and F) magnification at 10.000 X of PANI-TT-GO_x-GA-Nafion®

Figure 7.6 shows the voltammetric response of the PANI-TT-GO_x electrode with different concentrations of glucose. It can be observed that the presence of glucose in solution generates an important decrease in the reduction current associated to the reduction of molecular oxygen, observed at the onset potential of around -0.3 V. This decrease can be related with the decrease of the concentration of molecular oxygen in solution as consequence of the enzymatic reaction. At the same time, an oxidation current at more positive potentials than -0.10 V suggests that the oxidation of H₂O₂ is also produced⁵. In both cases, the enzymatic reaction of glucose involves the molecular oxygen consumption and hydrogen peroxide formation; these results confirm the electrocatalytic activity of the biosensor towards glucose oxidation.

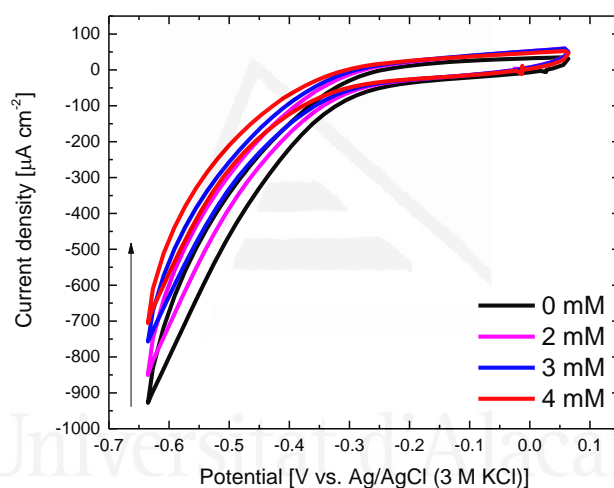


Figure 7.6. Cyclic voltammograms of PANI-TT-GO_x in 0.1M PBS (pH = 7.2) at 50 mV s⁻¹, saturated in O₂ and different concentrations of glucose.

Hydrogen peroxide can be reduced at negative potentials and oxidized at positive potentials as it can be observed in the study done at different concentrations of H₂O₂ (Figure 7.7-A). However, the electrode has a higher sensitivity towards the ORR and the contribution of H₂O₂ reduction is less important than the changes generated in the O₂ reduction, as can be observed by cyclic voltammetry at -0.4 V in presence of glucose (See Figure 7.7-B) and the chronoamperometry detection in Figure 7.7-C and 7.7-D at different potentials. Chronoamperometric detection of glucose at -0.4 V provides higher sensitivity and could decrease the interference effects of other species

normally existing in the sample fluids, which can be oxidized at positive polarization of the electrode^{5,10}.

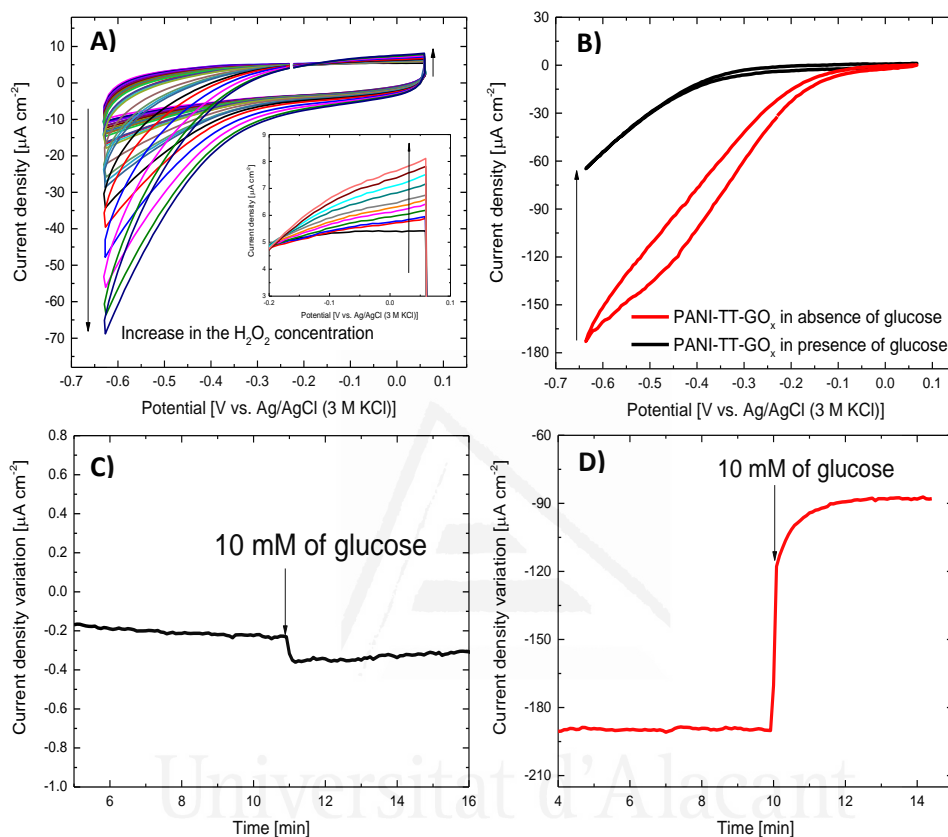


Figure 7.7. A) Cyclic voltammograms for PANI-TT-GO_x in presence of different concentration of H₂O₂. Inset: enlargement of the positive potential region of H₂O₂. B) Cyclic voltammograms for PANI-TT-GO_x in 0.1 M PBS (pH = 7.2) at 50 mV s⁻¹, under O₂-saturated conditions in absence (red line) and presence (black line) of 20 mM glucose. Chronoamperometry profiles of PANI-TT-GO_x electrode at different potentials: A) -0.06 V and B) -0.4 V, under O₂-saturated conditions and under stirring before and after the addition of 10 mM of glucose. 0.1 M PBS (pH = 7.2).

3.3. Electrocatalytic activity towards glucose oxidation

Chronoamperometry experiments were carried out at -0.4 V under stirring conditions and both, with the solution saturated with O₂ (Figure 7.8) and at room atmosphere conditions (Figure 7.9), in a glucose concentration range

between 5 μM and 10 mM in 0.1 M PBS (pH = 7.2). As can be observed in Figure 7.8-A for O_2 -saturated conditions, the presence of glucose in solution generates a rapid decrease in the reduction current associated to ORR, reaching a steady-state value after 25 seconds. Taking into account that during glucose oxidation, the molecular oxygen participates as oxidant in the reaction, the decrease in the current density can be correlated with the decrease of the concentration of oxygen in the electrolyte^{22,40}. Considering that N-doped carbon material has a remarkable activity towards ORR, the decrease in the oxygen concentration is the responsible for the change in the observed current density in the PANI-TT- GO_x electrode.



Universitat d'Alacant
Universidad de Alicante

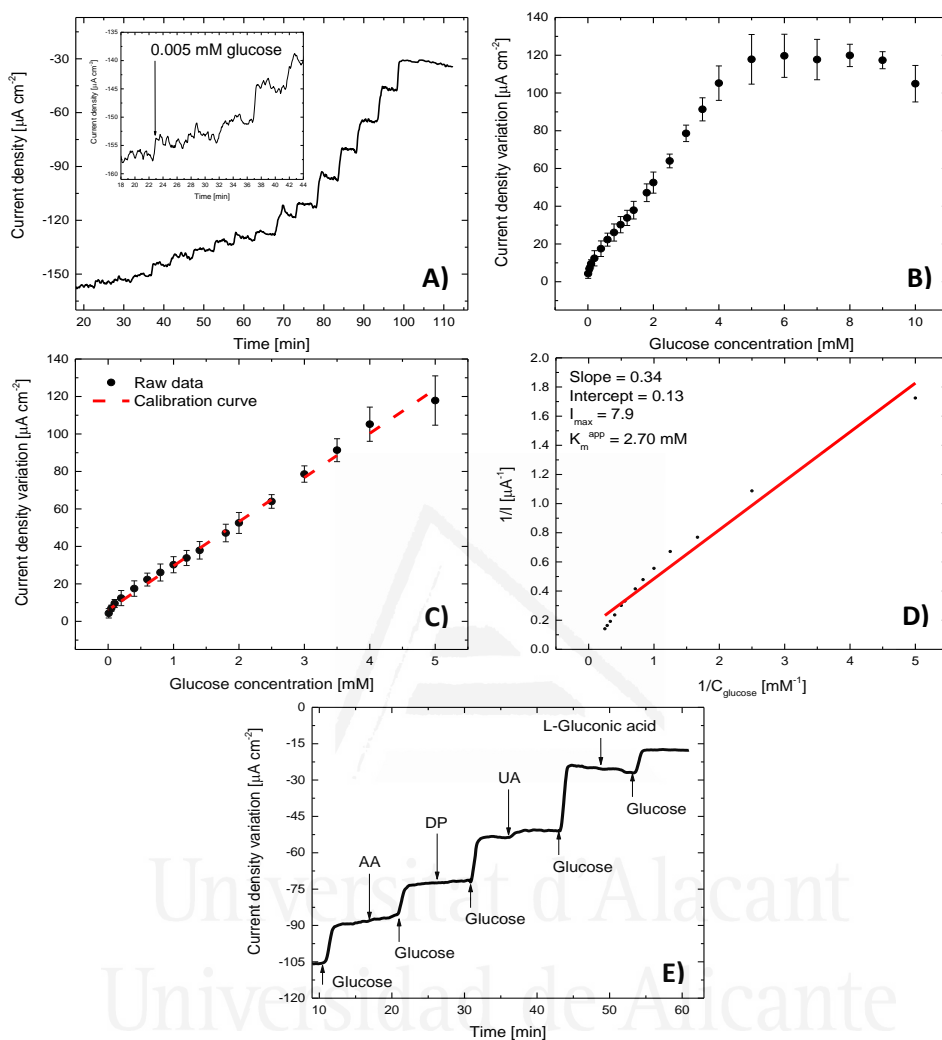


Figure 7.8. A) Chronoamperometric curves of PANI-TT-GO_x at -0.4 V for different concentrations of glucose: 0.001, 0.005, 0.01, 0.05, 0.1, 0.2, 0.3, 0.4, 0.6, 0.8, 1, 1.2, 1.4, 1.8, 2, 2.5, 3, 3.5, 4, 5, 6, 7, 8, 9, 10 mM under saturated O₂ conditions. Inset: enlargement at low concentrations, B) Calibration curve, C) Linear calibration curve obtained for glucose detection, D) Lineweaver-Burk fitting for enzyme immobilization by Michaelis-Menten kinetics and E) Interference study at spiking level of 0.8 mM glucose, 1 μM DP, 1.5 mM glucose, 132 μM AA, 2.5 mM glucose, 833 μM UA, 4 mM glucose, 159 μM L-Gluconic acid and 4.6 mM glucose at -0.4 V under saturated O₂ conditions. 0.1M PBS (pH = 7.2).

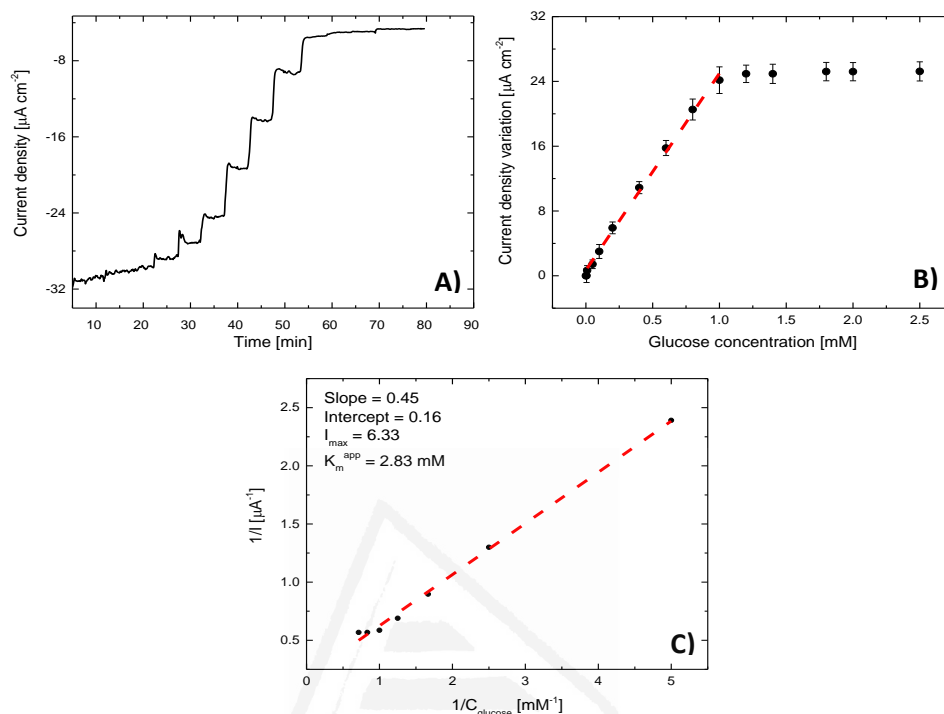


Figure 7.9. A) Chronoamperometric profiles for PANI-TT-GO_x electrode at -0.4 V for different concentrations of glucose: 0.001, 0.005, 0.01, 0.05, 0.1, 0.2, 0.3, 0.4, 0.6, 0.8, 1, 1.2, 1.4, 1.8 and 2, 2.5 mM under room atmosphere conditions, B) Calibration curve obtained for glucose detection and C) Lineweaver-Burk fitting for enzyme immobilization by Michaelis-Menten kinetics. 0.1 M PBS (pH = 7.2).

The calibration curves (Fig. 7.8-B) for the PANI-TT-GO_x biosensor are in agreement with a Michaelis-Menten kinetics behavior, in which an initial linear range of the variation in the catalytic current can be observed before a saturation of the catalytic activity of the enzyme towards glucose oxidation, which is observed as a region with constant current density. Similar electrochemical behavior was observed in the chronoamperometry profiles for the PANI-TT-GO_x electrode tested at room atmosphere conditions; however, the constant current values are reached for lower concentrations (See Figure 7.9-A and 7.9-B). Interestingly, samples in O₂-saturated conditions show a wide linear range between 5 μM and 5 mM as can be observed in Figure 7.9-C, compared to the sample measured under room atmosphere conditions in which both linear range (10 μM to 1.0 mM) and concentration of saturation reach

lower values (See Figure 7.9-B). In case of limit of detection (LOD), it was determined empirically by measuring progressively more diluted concentrations of glucose. The LOD was the lowest concentration whose signal could be clearly distinguished from the blank solution. Electrodes in O₂-saturated conditions present a lower LOD, around 1 μM, ten times lower than at room atmosphere conditions. Based on the previous result, the limit of quantification (LOQ) was calculated as 3.3 times the LOD⁴¹. Regression model of the calibration curve in the linear range was applied to determine the slope and intercept of the linear calibration curve, obtaining close values of sensitivity for O₂-saturated and room atmosphere conditions (23.57±1.77 μA cm⁻² mM⁻¹ and 24.29±1.12 μA cm⁻² mM⁻¹, respectively).

Table 7.1 summarizes the most relevant parameters obtained for the glucose biosensor prepared with PANI-TT-GO_x electrode. Considering the linear detection range and LOD obtained for the proposed sensor of glucose, it may be employed in the detection of glucose in different physiological fluids such as blood (3.9-5.6 mM)⁴², urine (2.8-5 mM)⁴³ and even perspiration (0.0056-2.2 mM)⁴⁴.

Table 7.1. Analytical parameters obtained for the PANI-TT-GO_x towards glucose detection.

| Parameter | O ₂ -Saturated | Room atmosphere |
|---|---------------------------|-----------------|
| Sensitivity [μA mM ⁻¹ cm ⁻²] | 23.57±1.77 | 24.29±1.12 |
| Intercept [μA cm ⁻²] | 6.05±9.17 | 0.7±1.17 |
| R² | 0.994 | 0.997 |
| n | 3 | 3 |
| Linear range [mM] | 5 μM-5 mM | 10 μM -1.0 mM |
| LOD [μM] | 1 μM | 10 μM |
| LOQ [μM] | 3.3 μM | 33 μM |

The apparent Michaelis-Menten constant (K_m^{app}), which is an important parameter related to the interaction between the immobilized enzyme and the substrate, and can be used to evaluate the biological activity of the immobilized enzyme, was calculated by the Lineweaver-Burk fitting (Eq. 7.1), obtaining values of 2.70 mM and 2.83 mM for O₂-saturated and room atmosphere conditions, respectively (Figure 7.8-D and 7.9-C, for O₂ saturated

and room atmosphere conditions, respectively). Similar values are obtained at both atmosphere conditions. This is an expected result because the biosensor is the same and the only difference is the change in oxygen concentration in both conditions. The K_m^{app} obtained suggests that after the immobilization process, the biosensor maintains a proper substrate-enzyme interaction⁴⁵. Moreover, the K_m^{app} is smaller than the values reported previously for other biosensors and nitrogen-doped carbon nanotubes biosensor^{30,37} and the values obtained in solution⁴⁶.

$$\frac{1}{I_{ss}} = \frac{1}{I_{Max}} + \frac{K_m^{app}}{I_{Max}C_{glucose}} \quad \text{Eq. 7.1}$$

Where I_{ss} is the steady-state current reached after glucose addition, $C_{glucose}$ is the glucose concentration and I_{Max} is the maximum current observed at glucose saturation.

The effect of possible interfering species on glucose detection was examined using dopamine, ascorbic acid, uric acid and L-gluconic acid, which can interfere in the electrochemical detection of glucose⁴⁷. Specifically, the following concentrations were studied to check for possible interference: 1 μM Dopamine (DP), 132 μM ascorbic acid (AA) and 833 μM uric acid (UA). Furthermore, effect of the L-gluconic acid produced during the reaction was also evaluated in the performance of the biosensor towards glucose detection by adding an aliquot of this compound until reaching a concentration of 159 μM . Study of interference was carried out by chronoamperometry at the working potential of -0.4 V vs. Ag/AgCl (3 M KCl). Between the additions of each aliquot of interference compound, different amounts of glucose were added to guarantee that the catalytic activity towards glucose oxidation is maintained. As can be observed in the chronoamperometry profile in Figure 7.8-E, no interference effect is observed at the concentrations evaluated for AA, DP and L-Gluconic acid. In contrast, uric acid tends to produce a small interference; however, observed current variation ($\sim 0.18\mu\text{A}$) compared with the signal produced after glucose addition suggests that the main current variation is consequence of the molecular oxygen consumed by the enzymatic reaction. It is important to highlight that concentration levels chosen for the analysis correspond with the highest values presented in physiological fluids like urine⁴³.

3.4. Real samples

Urine samples were collected in the first excretion in the morning before any ingestion of meals from a volunteer (healthy man around thirties) with no medical problems related with diabetes. Urine sample was previously filtrated.

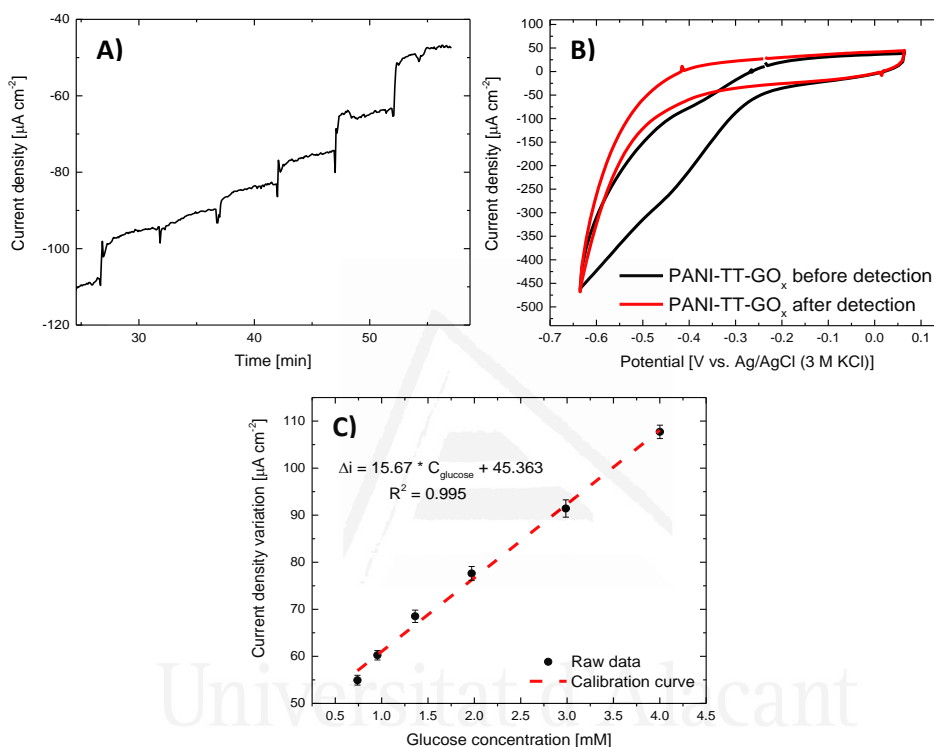


Figure 7.10. A) Chronoamperometric profiles for PANI-TT-GO_x electrode at -0.4 V for different concentrations of glucose in urine samples: 0.75, 0.95, 1.36, 1.97, 2.98 and 4 mM under O₂-saturated conditions by standard addition method, B) Cyclic voltammograms of biosensors before and after the detection of glucose in urine samples and C) Calibration curve for glucose detection in urine.

Determination of glucose concentration in urine sample was done by the standard addition method due to matrix effects and without any need of sample pretreatment except a dilution step⁴⁸. In this sense, calibration curves for glucose were obtained at a working potential of -0.4 V under O₂-saturated conditions (See Figure 7.10). Value of glucose concentration in the sample was 2.89 ± 0.27 mM, a concentration which is within the normal glucose levels of healthy human being [2.8-5.6 mM]⁴³.

Given the high complexity of the urine matrix, glucose detection was carried out in a commercial sugary drink where matrix effects should not affect the biosensor performance (see sample S1 in Figure 7.11). Trueness of the glucose detection was evaluated adding a known concentration of glucose during the chronoamperometry (Figure 7.11).

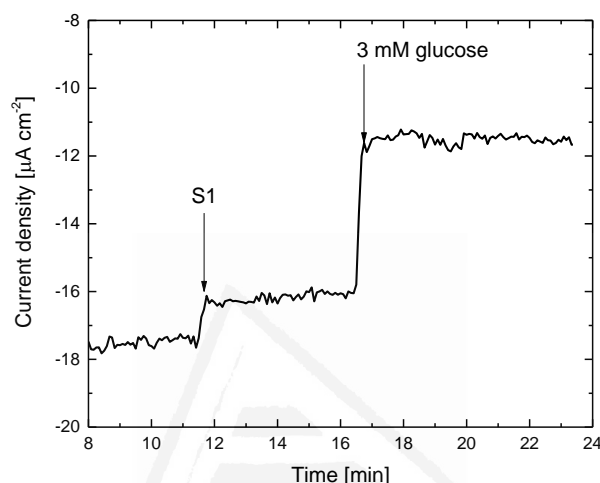


Figure 7.11. A) Chronoamperometry profile for PANI-TT-GOx electrode in S1 solution at -0.4 V vs. Ag/AgCl (3 M KCl) under O_2 -saturated conditions.

Acceptable values of recovery for the analyte studied of around 101% (Table 7.2), proves that in a less complex matrix, external calibration curve can be employed with highly accurate results. Concentration of glucose for sample S1 was determined to be 0.34 M of glucose. According to the nutritional information reported by the company, total concentration of sugar is 0.58 M. Nevertheless, not all the sugar in sample S1 is glucose, in addition, saccharose and fructose contribute to the sugar amount in sample S1.

Table 7.2. Recovery values in the chronoamperometric detection of sample S1 using the PANI-TT-GOx electrode.

| Sample | Dilution | Spiked (mM) | Found (mM) | Recovery (%) |
|--------|----------|-------------|------------|--------------|
| S1 | 1:580 | 3 | 3.39 | 101 |

3.5. Reproducibility and stability of PANI-TT-GOx biosensors

The stability of the electrodes towards glucose detection was tested at different times after their preparation. The glucose detection was investigated in a 4 mM glucose solution at -0.4 V vs. Ag/AgCl (3 M KCl) in O_2 saturated

0.1 M PBS (pH = 7.2). Between measurements, electrode was stored in 0.1 M PBS (pH = 7.2) at 4°C. Relative standard deviation (RSD) of the current density variation of the electrode was 3%, demonstrating a good reproducibility of the biosensor. Additionally, RSD of current density variations for measurements of 4 mM glucose in 3 independently electrodes was 10%, proving an acceptable reproducibility of the biosensor. The electrodes show a good stability and their initial activity is maintained after 15 days stored in 0.1 M PBS (pH = 7.2). Chronoamperometry profiles (see Figure 7.12) after 15 days present a retention of the 91.3% in the current density variation compared to a fresh-prepared electrode.

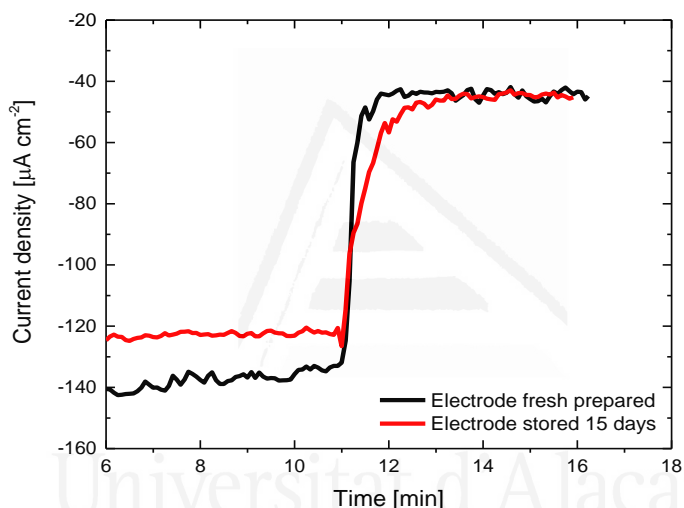


Figure 7.12. Chronoamperometry profiles for PANI-TT-GO_x electrode in 0.1 M PBS (pH= 7.1) and 4 mM glucose at -0.4 V vs. Ag/AgCl (3 M KCl) under O₂ saturated conditions: fresh prepared electrode (black line) and stored 15 days (red line).

Table 7.3 shows a comparison of some analytical parameters obtained in this work, with data published in the literature. In most of the cases, the sensitivity is similar or higher than the published, being the proposed electrochemical biosensor competitive with respect to previously reported electrochemical sensors. Moreover, the obtained sensitivity and LOD are better than those obtained with different N-doped carbon materials MWCNTs^{37, 54}.

Table 7.3. Comparison of analytic parameters for several electrochemical biosensors

| Glucose biosensor | Linear range [mM] | Sensitivity [$\mu\text{A mM}^{-1} \text{cm}^{-2}$] | LOD [μM] | K_m^{app} [mM] | Reference |
|---|-------------------|--|-----------------------|-------------------------|-----------|
| CNS-Nafion-GOx | 0.08-2.04 | 7.31 | 39.1 | -- | 40 |
| SWCNT/GOx/Nafion | 0-6 | 1.06** | 6 | 8.5 | |
| CeO ₂ nanorods-GOx | 2-26 | 0.165 | 100 | 44.6 | 49 |
| Graphene oxide-poly-L-lysine-Nafion | 0.005-9 | 8.00 | 0.002 | -- | 50 |
| Carbon-Ferrocene carboxylic-GOx-MAP | 5.55-22.2 | 1.72 nA mM ⁻¹ | -- | -- | 51 |
| Pt-PVF-GOx-Au | 0.02-36 | 4.17* | 0.02 | 30.4 | 52 |
| GC-PTH-AuNPs-GOx-Chitosan | 0.008-6 | -- | 2 | 0.87 | 53 |
| Al ₂ O ₃ -Pt-PANI-GOx | 0.01-5.5 | 97.18 | 0.3 | 2.37 | 14 |
| GO _x /CN _x -MWCNT | 0.02-1.02 | 13.0 | 10 | 2.2 | 37 |
| GOD/N-CNT@CF | 0.05-15.55 | 15.87 | 5 | -- | 54 |
| PANI-TT-GOx | 0.005-5 | 23.57 | 1 | 2.7 | This work |

*The value registered corresponds with the optimal biosensor

**Sensitivity is reported in $\mu\text{A mM}^{-1}$, because electrode area is not specified

4. Conclusions

An enzymatic glucose biosensor is developed based on glucose oxidase immobilized on a N-doped carbon material, obtained by heat treatment of PANI. This biosensor is a metal free carbon material. N-doped carbon material has a remarkable catalytic activity towards oxygen reduction reaction due to the presence of quaternary N species, even after the immobilization of the glucose oxidase. Surface reversible redox process at -0.42 V vs. Ag/AgCl related with the cofactor FAD/FADH₂ demonstrates the successful immobilization of the enzyme on the electrode.

Indirect glucose detection is carried out following the current density variation of the ORR generated by the increase of the glucose concentration, as consequence of the enzymatic reaction of the GO_x at a potential of -0.4 V vs. Ag/AgCl. Sensitivity of the prepared biosensor exhibits good values towards glucose detection, with no dependence of the oxygen concentration in the solution ($23.57 \pm 1.77 \mu\text{A cm}^{-2} \text{mM}^{-1}$ and $24.29 \pm 1.12 \mu\text{A cm}^{-2} \text{mM}^{-1}$ for O₂-saturated and room atmosphere conditions, respectively). Nevertheless, reaction rate for the recovery of the enzyme from the reduced to the oxidized state conditions, affects the linear detection range of the biosensor, being wider for the O₂-saturated conditions where the re-oxidation of the pristine enzyme is carried out rapidly. Additionally, biosensor shows an acceptable reproducibility, repeatability and stability. Despite small interference effect of uric acid in the detection of glucose, high affinity and sensitivity towards glucose oxidation still allows us the application of this biosensor in the detection of glucose in real samples like urine and commercial sugary drink.

5. References

- (1) Sabu, C.; Henna, T. K.; Raphey, V. R.; Nivitha, K. P.; Pramod, K. Advanced biosensors for glucose and insulin, *Biosens. Bioelectron.* **2019**, 141, 111201.
- (2) Wang, D.; Liang, Y.; Su, Y.; Shang, Q.; Zhang, C. Sensitivity enhancement of cloth-based closed bipolar electrochemiluminescence glucose sensor via electrode decoration with chitosan/multi-walled carbon nanotubes/graphene quantum dots-gold nanoparticles, *Biosens. Bioelectron.* **2019**, 130, 55–64.
- (3) Wang, H.-C.; Lee, A.-R. Recent developments in blood glucose sensors, *J. Food Drug Anal.* **2015**, 23, 191–200.
- (4) Galant, A. L.; Kaufman, R. C.; Wilson, J. D. Glucose: Detection and Analysis, *Food Chem.* **2015**, 188, 149–160
- (5) Lee, W.-C.; Kim, K.-B.; Gurudatt, N.G.; Hussain, K.K.; Choi, C.S.; Park, D.-S.; Shim, Y.-B. Comparison of enzymatic and non-enzymatic glucose sensors based on hierarchical Au-Ni alloy with conductive polymer, *Biosens. Bioelectron.* **2019**, 130, 48–54.
- (6) Rahman, M.M.; Umar, A.; Sawada, K. Development of amperometric glucose biosensor based on glucose oxidase co-immobilized with multi-walled carbon nanotubes at low potential, *Sensors Actuators B*

Chem. **2009**, 137, 327–333.

- (7) Scognamiglio, V. Nanotechnology in glucose monitoring: Advances and challenges in the last 10 years, *Biosens. Bioelectron.* **2013**, 47, 12–25.
- (8) Wang, D.; Tan, Y. Electrodeposition of enzymes-integrated mesoporous composite films by interfacial templating: A paradigm for electrochemical biosensors, *Electrochim. Acta.* **2014**, 116, 495–503.
- (9) Coyle, V.E.; Kandjani, A.E.; Field, M.R.; Hartley, P.; Chen, M.Y.; Sabri, M.; Bhargava, S.K. Co₃O₄ needles on Au honeycomb as a non-invasive electrochemical biosensor for glucose in saliva, *Biosens. Bioelectron.* **2019**, 141, 111479.
- (10) Abellán-Llobregat, A.; Jeerapan, I.; Bandodkar, A.; Vidal, L.; Canals, A.; Wang, J.; Morallón, E. A stretchable and screen-printed electrochemical sensor for glucose determination in human perspiration, *Biosens. Bioelectron.* **2017**, 91, 885–891.
- (11) Wu, F.; Huang, T.; Hu, Y.; Yang, X.; Xie, Q. One-pot electrodeposition of a composite film of glucose oxidase, imidazolium alkoxysilane and chitosan on a reduced graphene oxide–Pt nanoparticle/Au electrode for biosensing, *J. Electroanal. Chem.* **2016**, 781, 296–303.
- (12) Turkmen, E.; Bas, S.Z.; Gulce, H.; Yildiz, S. Glucose biosensor based on immobilization of glucose oxidase in electropolymerized poly(o-phenylenediamine) film on platinum nanoparticles-polyvinylferrocenium modified electrode, *Electrochim. Acta.* **2014**, 123, 93–102.
- (13) Andronesu, C.; Pöller, S.; Schuhmann, W. Electrochemically induced deposition of poly(benzoxazine) precursors as immobilization matrix for enzymes, *Electrochem. Commun.* **2014**, 41, 12–15.
- (14) Wang, Z.; Liu, S.; Wu, P.; Cai, C. Detection of Glucose Based on Direct Electron Transfer Reaction of Glucose Oxidase Immobilized on Highly Ordered Polyaniline Nanotubes, *Anal. Chem.* **2009**, 81, 1638–1645.
- (15) Kang, X.; Wang, J.; Wu, H.; Aksay, I. A.; Liu, J.; Lin, Y. Glucose Oxidase–graphene–chitosan modified electrode for direct electrochemistry and glucose sensing, *Biosens. Bioelectron.* **2009**, 25, 901–905.

- (16) Shan, C.; Yang, H.; Song, J.; Han, D.; Ivaska, A.; Niu, L. Direct Electrochemistry of Glucose Oxidase and Biosensing for Glucose Based on Graphene, *Anal. Chem.* **2009**, 81, 2378–2382.
- (17) Al-Sagur, H.; Shanmuga sundaram, K.; Kaya, E. N.; Durmuş, M.; Basova, T. V.; Hassan, A. Amperometric glucose biosensing performance of a novel graphene nanoplatelets-iron phthalocyanine incorporated conducting hydrogel, *Biosens. Bioelectron.* **2019**, 139, 111323.
- (18) Tan, Y.; Deng, W.; Chen, C.; Xie, Q.; Lei, L.; Li, Y.; Fang, Z.; Ma, M.; Chen, J.; Yao, S. Immobilization of enzymes at high load/activity by aqueous electrodeposition of enzyme-tethered chitosan for highly sensitive amperometric biosensing, *Biosens. Bioelectron.* **2010**, 25, 2644–2650.
- (19) Lin, Y.; Lu, F.; Tu, Y.; Ren, Z. Glucose Biosensors Based on Carbon Nanotube Nanoelectrode Ensembles, *Nano Lett.* **2004**, 4, 191–195.
- (20) Kim, J.; Sempionatto, J. R.; Imani, S.; Hartel, M. C.; Barfidokht, A.; Tang, G.; Campbell, A. S.; Mercier, P. P.; Wang, J. Simultaneous Monitoring of Sweat and Interstitial Fluid Using a Single Wearable Biosensor Platform, *Adv. Sci.* **2018**, 5, 1800880.
- (21) Zhai, Q.; Gong, S.; Wang, Y.; Lyu, Q.; Liu, Y.; Ling, Y.; Wang, J.; Simon, G. P.; Cheng, W. Enokitake Mushroom-like Standing Gold Nanowires toward Wearable Noninvasive Bimodal Glucose and Strain Sensing, *ACS Appl. Mater. Interfaces.* **2019**, 11, 9724–9729.
- (22) González-Gaitán, C.; Ruiz-Rosas, R.; Morallón, E.; Cazorla-Amorós, D. Effects of the surface chemistry and structure of carbon nanotubes on the coating of glucose oxidase and electrochemical biosensors performance, *RSC Adv.* **2017**, 7, 26867–26878.
- (23) Rernglit, W.; Teanphonkrang, S.; Suginta, W.; Schulte, A. Amperometric enzymatic sensing of glucose using porous carbon nanotube films soaked with glucose oxidase, *Microchim. Acta.* **2019**, 186, 616.
- (24) Göbel, G.; Schubart, I. W.; Scherbahn, V.; Lisdat, F. Direct electron transfer of PQQ-glucose dehydrogenase at modified carbon nanotubes electrodes, *Electrochem. Commun.* **2011**, 13, 1240–1243.
- (25) Liu, J.; Wang, X.; Wang, T.; Li, D.; Xi, F.; Wang, J.; Wang, E. Functionalization of Monolithic and Porous Three-Dimensional

Graphene by One-Step Chitosan Electrodeposition for Enzymatic Biosensor, *ACS Appl. Mater. Interfaces*. **2014**, 6, 19997–20002.

- (26) Abellán-Llobregat, A.; Vidal, L.; Rodríguez-Amaro, R.; Canals, A.; Morallón, E. Evaluation of herringbone carbon nanotubes-modified electrodes for the simultaneous determination of ascorbic acid and uric acid, *Electrochim. Acta*. **2018**, 285, 284–291.
- (27) González-Gaitán, C.; Ruiz-Rosas, R.; Morallón, E.; Cazorla-Amorós, D. Functionalization of carbon nanotubes using aminobenzene acids and electrochemical methods. Electroactivity for the oxygen reduction reaction, *Int. J. Hydrogen Energy*. **2015**, 40, 11242–11253.
- (28) Chen, Y.; Wang, J.; Liu, H.; Banis, M. N.; Li, R.; Sun, X.; Sham, T. -K.; Ye, S.; Knights, S. Nitrogen Doping Effects on Carbon Nanotubes and the Origin of the Enhanced Electrocatalytic Activity of Supported Pt for Proton-Exchange Membrane Fuel Cells, *J. Phys. Chem. C*. **2011**, 115, 3769–3776.
- (29) Cruz-Silva, E.; Cullen, D. A.; Gu, L.; Romo-Herrera, J. M.; Muñoz-Sandoval, E.; López-Urías, F.; Sumpter, B. G.; Meunier, V.; Charlier, J. -C.; Smith, D. J.; Terrones, H.; Terrones, M. Heterodoped Nanotubes: Theory, Synthesis, and Characterization of Phosphorus–Nitrogen Doped Multiwalled Carbon Nanotubes, *ACS Nano*. **2008**, 2, 441–448.
- (30) Abellán-Llobregat, A.; González-Gaitán, C.; Vidal, L.; Canals, A.; Morallón, E. Portable electrochemical sensor based on 4-aminobenzoic acid-functionalized herringbone carbon nanotubes for the determination of ascorbic acid and uric acid in human fluids, *Biosens. Bioelectron.* **2018**, 109, 123–131.
- (31) Liu, S.; Cai, C. Immobilization and characterization of alcohol dehydrogenase on single-walled carbon nanotubes and its application in sensing ethanol, *J. Electroanal. Chem.* **2007**, 602, 103–114.
- (32) Sajjadi, S.; Ghourchian, H.; Rahimi, P. Different behaviors of single and multi wall carbon nanotubes for studying electrochemistry and electrocatalysis of choline oxidase, *Electrochim. Acta*. **2011**, 56, 9542–9548.
- (33) Quílez-Bermejo, J.; Melle-Franco, M.; San-Fabián, E.; Morallón, E.; Cazorla-Amorós, D. Towards understanding the active sites for the ORR in N-doped carbon materials through fine-tuning of nitrogen functionalities: an experimental and computational approach, *J. Mater.*

Chem. A. **2019**, *7*, 24239–24250.

- (34) Quílez-Bermejo, J.; Morallón, E.; Cazorla-Amorós, D. Oxygen-reduction catalysis of N-doped carbons prepared via heat treatment of polyaniline at over 1100 °C, *Chem. Commun.* **2018**, *54*, 4441–4444.
- (35) Quílez-Bermejo, J.; González-Gaitán, C.; Morallón, E.; Cazorla-Amorós, D. Effect of carbonization conditions of polyaniline on its catalytic activity towards ORR. Some insights about the nature of the active sites, *Carbon.* **2017**, *119*, 62–71.
- (36) Ratautas, D.; Laurynėnas, A.; Dagys, M.; Marcinkevičienė, .; Meškys, R.; Kulys, J. High current, low redox potential mediatorless bioanode based on gold nanoparticles and glucose dehydrogenase from *Ewingella americana*, *Electrochim. Acta.* **2016**, *199*, 254–260.
- (37) Deng, S.; Jian, G.; Lei, J.; Hu, Z.; Ju, H. A glucose biosensor based on direct electrochemistry of glucose oxidase immobilized on nitrogen-doped carbon nanotubes, *Biosens. Bioelectron.* **2009**, *25*, 373–377.
- (38) Vilian, A. T. E.; Chen, S. M. Direct electrochemistry and electrocatalysis of glucose oxidase based poly(L-arginine)-multi-walled carbon nanotubes, *RSC Adv.* **2014**, *4*, 50771–50781
- (39) Yoon, J.; Lee, S. N.; Shin, M. K.; Kim, K. -W.; Choi, H. K.; Lee, T.; Choi, J. -W. Flexible electrochemical glucose biosensor based on GOx/gold/MoS₂/gold nanofilm on the polymer electrode, *Biosens. Bioelectron.* **2019**, *140*, 111343.
- (40) Li, T.; Li, Y.; Wang, C.; Gao, Z. -D.; Song, Y. -Y. Nitrogen-doped carbon nanospheres derived from cocoon silk as metal-free electrocatalyst for glucose sensing, *Talanta.* **2015**, *144*, 1245–1251.
- (41) Miller, J. N. Basic statistical methods for Analytical Chemistry. Part 2. Calibration and regression methods. A review, *Analyst.* **1991**, *116*, 3–14.
- (42) Wang, J. Electrochemical Glucose Biosensors, *Chem. Rev.* **2008**, *108*, 814–825.
- (43) Zhang, Z.; Chen, Z.; Cheng, F.; Zhang, Y.; Chen, L. Highly sensitive on-site detection of glucose in human urine with naked eye based on enzymatic-like reaction mediated etching of gold nanorods, *Biosens. Bioelectron.* **2017**, *89*, 932–936.
- (44) Moyer, J.; Wilson, D.; Finkelshtein, I.; Wong, B.; Potts, R. Correlation

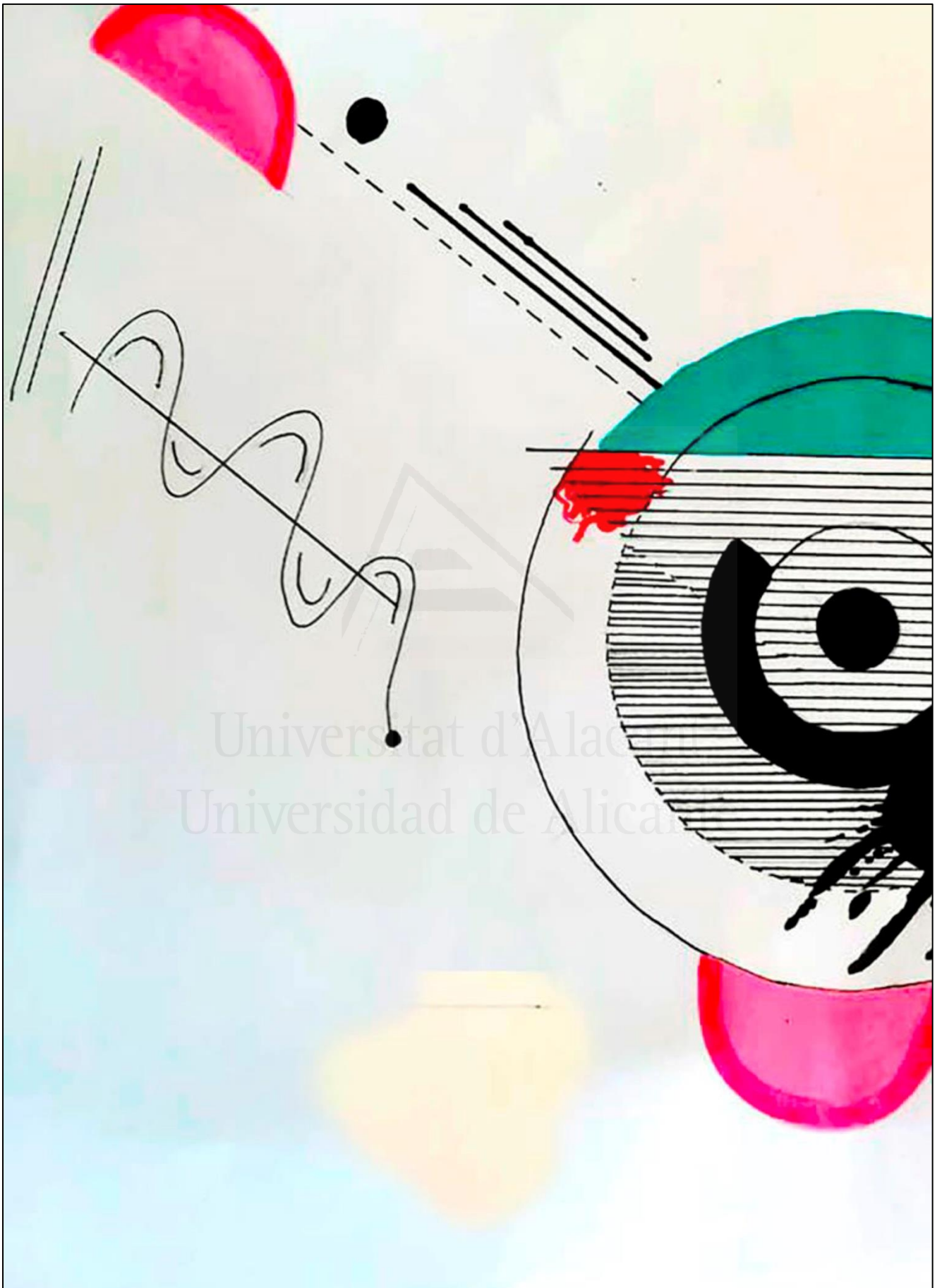
Between Sweat Glucose and Blood Glucose in Subjects with Diabetes, *Diabetes Technol. Ther.* **2012**, 14, 398–402.

- (45) Pingarrón-Carrazón, J. M.; Sánchez-Batanero, S. Química electroanalítica-Fundamentos y aplicaciones, Síntesis S.A., Madrid, España, **2003**.
- (46) Gibson, Q. H.; Swoboda, B. E.; Massey, V. Kinetics and Mechanism of Action of Glucose Oxidase, *J. Biol. Chem.* **1964**, 239, 3927–34.
- (47) Janyasupab, M.; Liu, C. -W.; Chanlek, N.; Chio-Srichan, S.; Promptmas, C.; Surareungchai, W. A comparative study of non-enzymatic glucose detection in artificial human urine and human urine specimens by using mesoporous bimetallic cobalt-iron supported N-doped graphene biosensor based on differential pulse voltammetry, *Sensors Actuators B Chem.* **2019**, 286, 550–563.
- (48) Skoog, D.; Holler, J.; Neiman, T.; Holler, J. Principios de Análisis Instrumental, 6th ed., Mc Graw-Hill S.A., **2000**.
- (49) Patil, D.; Dung, N. Q.; Jung, H.; Ahn, S. Y.; Jang, D. M.; Kim, D. Enzymatic glucose biosensor based on CeO₂ nanorods synthesized by non-isothermal precipitation, *Biosens. Bioelectron.* **2012**, 31, 176–181.
- (50) Zhang, D.; Chen, X.; Ma, W.; Yang, T.; Li, D.; Dai, B.; Zhang, Y. Direct electrochemistry of glucose oxidase based on one step electrodeposition of reduced graphene oxide incorporating polymerized l-lysine and its application in glucose sensing, *Mater. Sci. Eng. C.* **2019**, 104, 109880.
- (51) Kim, K. B.; Choi, H.; Jung, H. J.; Oh, Y. -J.; Cho, C. -H.; Min, J. H.; Yoon, S.; Kim, J.; Cho, S. J.; Cha, H. J. Mussel-inspired enzyme immobilization and dual real-time compensation algorithms for durable and accurate continuous glucose monitoring, *Biosens. Bioelectron.* **2019**, 143, 111622.
- (52) Topçu Sulak, M.; Gökdoğan, Ö.; Gülce, A.; Gülce, H. Amperometric glucose biosensor based on gold-deposited polyvinylferrocene film on Pt electrode, *Biosens. Bioelectron.* **2006**, 21, 1719–1726.
- (53) Huang, Q.; An, Y.; Tang, L.; Jiang, X.; Chen, H.; Bi, W.; Wang, Z.; Zhang, W. A dual enzymatic-biosensor for simultaneous determination of glucose and cholesterol in serum and peritoneal macrophages of diabetic mice: Evaluation of the diabetes-accelerated atherosclerosis risk, *Anal. Chim. Acta.* **2011**, 707, 135–141.

- (54) Pinchao, F.; Lijuan, L.; Qiaohui, G.; Wang, J.; Yang, J.; Guan, X.; Chen, S.; Hou, H. Three-dimensional N-doped carbon nanotube@carbon foam hybrid: an effective carrier of enzymes for glucose biosensors, *RSC Adv.* **2017**, *7*, 26574-26582.

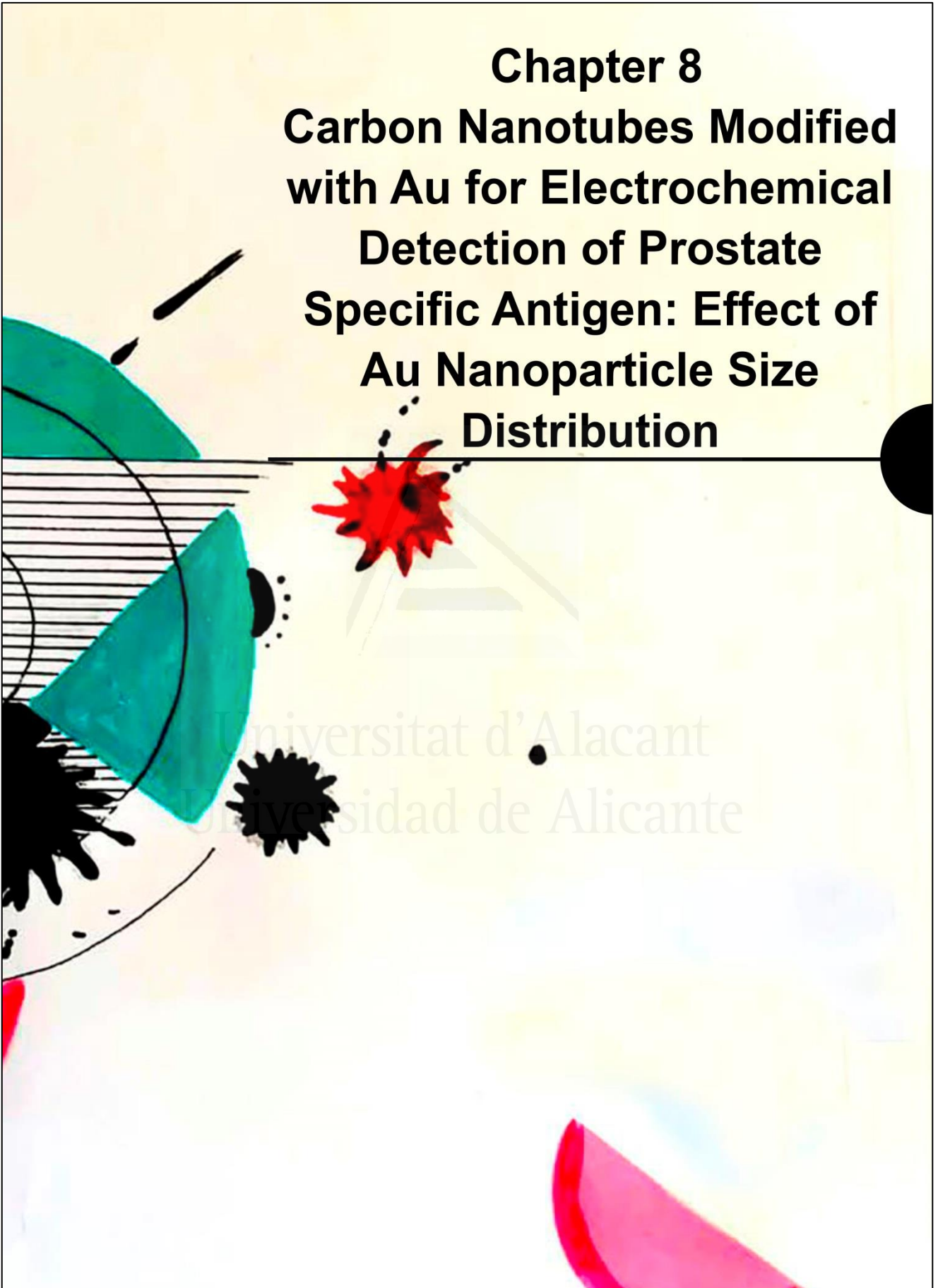


Universitat d'Alacant
Universidad de Alicante



Chapter 8
Carbon Nanotubes Modified
with Au for Electrochemical
Detection of Prostate
Specific Antigen: Effect of
Au Nanoparticle Size
Distribution

Universitat d'Alacant
Universidad de Alicante



1. Introduction

Prostate Specific Antigen (PSA) or Kallikrein related peptidase-3, is a serine protease secreted by the prostate gland to seminal fluid, with a single chain of 32-33 kDa. According to the World Health Organization (WHO), prostate cancer is considered the second cause of death by cancer in men, with 307,000 deaths in 2012^{1,2}. One of the reasons for the high mortality of this illness lies in the application of medical therapy in advanced stages. Normally, blood levels of this protein in healthy men is below 4 ng mL⁻¹; then, higher values in the PSA concentration in blood might be related with development of tumors or initial inflammation in the prostate gland, considering it as a reliable biomarker for early detection of prostate cancer³⁻⁶.

Thus, methods for early detection are required for a proper clinical treatment and control of different human medical disorders. Unfortunately, current methods for cancer diagnosis, such as histological test or screening methods based on immunoassays as ELISA test are time-consuming and require qualified personnel, which implies high cost^{7,8}. Besides, low sensibility and sensitivity makes the detection of the disease difficult, especially in the first stages, where cancer shows an asymptomatic phase and all the biomarkers are mainly in low concentrations⁹. For that reason, many researches are trying to find low-cost techniques and improve the parameters of detection for the specie of interest, decreasing the time-response in the measurement.

Nowadays, sensitive detection and accurate quantification of chemical substances in physiological fluids have been critical factors for a reliable clinical diagnostics of different diseases or medical disorders, for instance, infectious diseases, diabetes mellitus, Alzheimer's disease, DNA mutations and cancer¹⁰. Biomarkers are specific molecules (enzymes, proteins), whose concentrations increase during the development of a disease. Therefore, changes in the levels of a biomarker in physiological fluids might be related to the presence of a specific disease, thus, their measurement could be useful for the early detection, monitoring drug therapy and medical control¹¹.

Certainly, biosensors have been one of the most economical and functional analytical devices utilized in the last decade, as a result of their simple use in the detection of analytes, especially in complex samples; their low-cost and easier handling¹²⁻¹⁴.

Since the commercial implementation of electrochemical biosensors in the quantification of glucose in blood proposed by Clark and Lyons in 1962¹⁵, recent advances in the biosensor field, especially in the application of nanomaterials, have brought a remarkable development in the miniaturization of electrochemical biosensors, translating in a small amount of sample required for the detection and a reduction of costs for manufacturing of the devices. Moreover, given that biological processes occur in nano and micro scales, nanostructured materials have shown an excellent platform to improve the interaction between the biological species of interest (analytes) and the biosensor, guaranteeing an accurate measurement of the concentration. Proof of this concept has been the use of high surface area materials as metal nanoparticles (Au, Pt, Pd, Cu)^{16,17}, carbon materials (carbon nanotubes, graphene and carbon nanohorns)^{18,19}, nanomanufactured electrodes, for instance interdigitated electrodes array (IDA) and screen printed electrodes^{20,21}; producing electrochemical transducers for biosensors with high electroactive area and excellent electron transfer; key properties to provide an excellent sensitivity and correct interaction with the sample. At the same time, these materials might offer anchoring sites to promote the immobilization of the biorecognition elements; or even facilitating the direct electron transfer between the analyte and the electrode without the use of mediators or other species in the medium^{21,22}.

Integration between electrochemistry with other detection methods, such as enzyme immunoassays (EI), has created new platforms for biosensors with high sensibility and selectivity, benefitting from the specificity of the antigen-antibody (Ag-Ab) reaction or the DNA chains hybridization, called electrochemical immunosensors, as several works have reported²³. Depending on the configuration of the immunosensors, two main configurations are present: “label-free” or “sandwich-type”. The first ones employ the interaction of the antibody (Ab) as biorecognition element with the antigen (Ag) to create an immunocomplex (Ab-Ag) onto the surface which will block the surface for electron transfer of some electroactive species in the electrolyte^{24,25}. On the other hand, sandwich-type uses the coupling of a second antibody with antigen immobilized, creating an immunocomplex $Ab_1-Ag-Ab_2$, to increase the electrical barrier of the system. However, several works have developed sandwich type immunosensors with a second antibody labeled with peroxidase

or phosphatase enzymes which catalyzes the hydrogen peroxide reduction, creating an increase in the electrochemical signal^{26,27}.

Even though prostate specific antigen (PSA) detection has been widely studied using different electrochemical techniques, the high time consumption to quantify the concentration of the analyte has not been solved, taking at least 24 hours for its analysis.

In this chapter a label-free electrochemical platform has been studied for the fast measurement of concentrations of PSA for the identification of the biomarker. Then, electrochemical detection of PSA was carried out with glassy carbon electrodes (GC) modified with functionalized multi-wall carbon nanotubes decorated with gold nanoparticles and the immobilization of monoclonal antibodies to the PSA

2. Experimental

2.1. Materials

Multi-Wall Carbon Nanotubes (MWCNT) with purity 95% (8 nm of diameter) and 10-30 μm length were purchased to Cheap Tubes Inc. (Cambridgeport, USA). Nitric acid (65%) from Panreac was employed to functionalize and purify the carbon nanotubes. Purified mouse monoclonal PSA antibody (Ab) (Purified IgG-Ab) and native human prostate specific antigen purified were purchased from Bio-Rad Laboratories (Munich, Germany).

Potassium dihydrogen phosphate (KH_2PO_4) and dipotassium hydrogen phosphate (K_2HPO_4) obtained from Merck and VWR Chemicals, respectively, were used to prepare phosphate buffer solutions (0.01 M PBS, pH=7.2 and 0.1 M PBS, pH=7.2) to dissolve the immunoreagents and as electrolyte, unless otherwise noted. Ferrocenium hexafluorophosphate (Fc-97%), employed as redox probe was purchased from Sigma Aldrich. All the solutions were prepared using ultrapure water (18 M Ω cm, Purelab Ultra Elga equipment). The gases N_2 (99.999%) and H_2 (99.999%) were provided by Air Liquide.

Reagents employed in the gold nanoparticles synthesis included: sodium tetrachloroaurate (III) dihydrate ($\text{NaAuCl}_4 \cdot 2\text{H}_2\text{O}$, 99%),

poly-n-vinylpyrrolidone (PVP, 40K), sodium hydroxide (NaOH, 99.99% purity), anhydrous ethylene glycol and methanol (+98%) and were purchased from Sigma-Aldrich.

2.2. Preparation of the transducer material. Functionalized Multi-Wall Carbon Nanotubes (fMWCNT) with gold nanoparticles (AuNPs)

2.2.1. Functionalization of Multi-Wall Carbon Nanotubes

Multi-Wall carbon nanotubes (MWCNT) were functionalized by oxidation in acid solution accordingly with the same methodology carried out in Chapter 5. 200 mg of MWCNT were added in a two-necked, round bottom flask with 100 mL of 3 M HNO₃ at 120°C for 24 hours under reflux conditions.

MWCNTs were extracted after 24 hours, filtered, washed with ultrapure water until the pH was neutral and dried in vacuum at 60°C for 24 hours, and weighed. Sample was called fMWCNTs. These fMWCNTs were dispersed in water using sonication bath for 10 min, to get a concentration of 1 mg mL⁻¹.

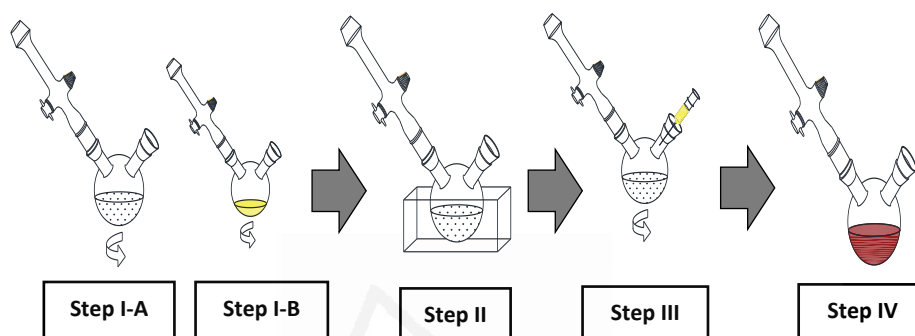
2.2.2. Gold nanoparticles synthesis

Gold nanoparticles were synthesized following the reduction-by-solvent method²⁸, adapting a previously published procedure²⁹. A typical synthesis stepwise procedure is described with details below (See Scheme 8.1).

Solution 1: In a two-necked, round-bottom flask, 6.4 mg of the gold precursor (NaAuCl₄ · 2H₂O) were dissolved in 5 mL of methanol. The resulting solution, light yellow in color, was stirred for 1 hour at room temperature.

Solution 2: In a two-necked, round-bottom flask, the protecting polymer (PVP) was dissolved in 12 mL of ethylene glycol at 80°C for 1 hour, under stirring conditions. Afterwards, solution 2 was cooled at 0°C in an ice bath and solution 1 was added to solution 2, keeping stirring conditions. Immediately, pH of the resulting solution was adjusted to 9-10 with 0.5 mL 1 M NaOH under stirring conditions at 100°C for 2 hours. After a few minutes, the color of the solution turned from yellow to dark red, indicating the reduction of the metal precursor to nanoparticles of zerovalent gold.

Gold nanoparticles (AuNPs) were purified using an excess of acetone to remove excess of capping agent (PVP), solvents and remaining salts used in the synthesis; also, this procedure promotes the flocculation of the nanoparticles at the bottom of the vessel. The nanoparticles were subsequently dispersed in water to achieve a suspension 1 mg mL^{-1} .



Scheme 8.1. Scheme of the gold-nanoparticles synthesis by the reduction-by-solvent method. (Step I): Preparation of solution 2-PVP: Ethylene glycol (Step I-A) and solution 1: $\text{NaAuCl}_4 \cdot 2\text{H}_2\text{O}$ in methanol (Step I-B). (Step II): Cooling at 0°C . (Step III): Mixing of solution 1 and 2, adjusting pH to 9-10 with NaOH 1M. (Step IV): Purification of AuNPs colloid with acetone.

Given that, this procedure allows a control of the nanoparticle size distribution varying the molar ratio PVP/Au. In this PhD Thesis, two syntheses were carried out using two PVP/Au molar ratios (0.5 and 50) in order to generate two different size distribution of the nanoparticles. At the same time, all the chemical reactions during the synthesis were carried out in an inert atmosphere of argon, using a Schlenk system to avoid undesirable reactions.

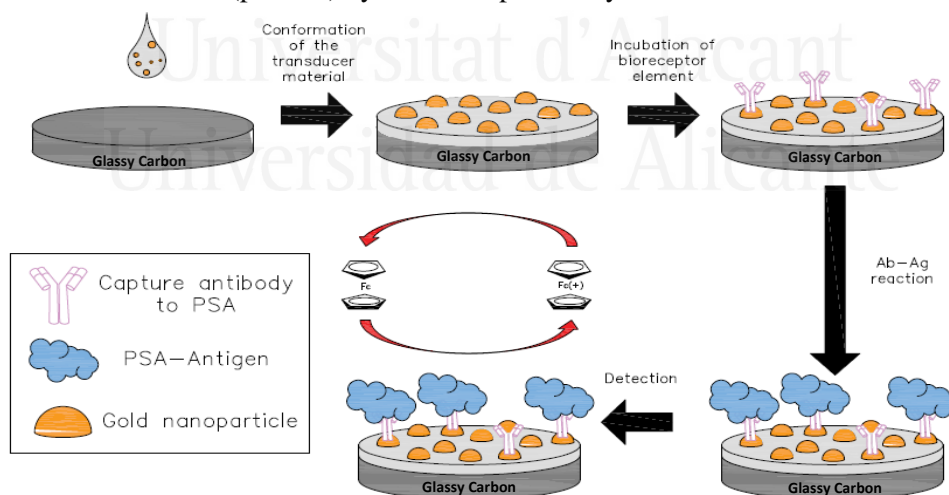
2.2.3. fMWCNT decorated with AuNPs dispersion

Transducer materials were prepared by the impregnation method in liquid phase, where the suspensions of the carbon material were put in contact with the nanoparticles colloid. Suspensions of fMWCNT (1 mg mL^{-1}) were mixed with an appropriate amount of purified gold nanoparticles suspension (1 mg mL^{-1}) to yield 5% (w/w) of metal loading. The dispersions were sonicated and stirred overnight in order to ensure the adsorption of the metal nanoparticles. Samples were filtered in vacuum to remove non-adsorbed nanoparticles and dried in vacuum at 60°C for 24 hours. Based on the ratio PVP/Au used in the synthesis, transducer material will be named as

fMWCNT-AuNPs-0.5 and fMWCNT-AuNPs-50, for 0.5 and 50 ratios respectively.

2.3. Immunosensor electrode preparation

A schematic diagram of the stepwise assembly procedure of the immunosensor is shown in Scheme 8.2. Prior to the modification, glassy carbon electrodes surface (3 mm diameter) was sanded with emery paper and polished using 1 and 0.05 μm alumina slurries, then rinsed with ultrapure water. Ten milligrams of the transducer material (fMWCNT-AuNPs) were dispersed in water with the aid of ultrasonic bath for 45 minutes, using an ice bath to avoid heating during the sonication. A 4 μL aliquot of the dispersion was dropped onto the glassy carbon (GC) surface and dried under an infrared lamp to remove the water. This procedure was repeated 3 times until completing 12 μL of the carbon material suspension on the electrode. Then, 5 μL of monoclonal antibodies solution ($10 \mu\text{g mL}^{-1}$) were added onto the electrode surface and incubated at 4°C for 24 hours, yielding the GC-fMWCNT-AuNPs-Ab electrode with $4.16 \mu\text{g}_{\text{Ab}} \text{g}^{-1}_{\text{fMWCNT}}$ of loading. Subsequently, electrodes were rinsed with PBS (0.01 M, $\text{pH}=7.2$) to remove all non-reacted material. Afterwards, the electrodes were stored in PBS (0.1 M, $\text{pH}=7.2$) solution at 4°C before electrochemical detection of PSA in 0.1 M PBS + 0.5 mM Fc ($\text{pH}=7.2$) by chronoamperometry.



Scheme 8.2. Illustration of the stepwise process for PSA immunosensor electrode fabrication and detection of the cancer biomarker.

2.4. Electrochemical methods.

Electrochemical characterization was performed in an EG&G Princeton Applied Research Model 263A Potentiostat/Galvonostat using a standard three-electrode cell configuration, in which GC-fMWCNT-AuNPs-Ab electrode was the working electrode (WE), a gold wire as counter electrode (CE) and a reversible hydrogen electrode (RHE) introduced in the same electrolyte as reference electrode (RE). All the measurements were carried out in 0.1 M PBS (pH=7.2) and 0.1 M PBS + 0.5 mM Fc (pH=7.2) solutions, deoxygenating the cell during the measurement by bubbling nitrogen. Previously, fMWCNT-AuNPs were submitted to a continuous cycling in 0.1 M PBS (pH=7.2) to be cleaned.

The electrochemical detection of PSA was carried out by chronoamperometry in a BIOLOGIC SP-300 potentiostat, applying a steady potential of 1.0 V in 0.1 M PBS + 0.5 mM Fc (pH=7.2) solution. A total of 8-9 aliquots of PSA solution (500 ng mL⁻¹) were added to the electrochemical cell, achieving concentrations between 1 to 10 ng mL⁻¹. Three minutes of reaction were maintained after the addition of each aliquot. Stirring was maintained during the immunoreaction to ensure a good homogenization of the analyte in the electrolyte and promoting the transport of the PSA to the electrode.

All the calibration curves and the electrochemical characterization, including the immobilization process, were performed by triplicate using 3 different electrodes, synthesized separately. Error bars are incorporated in the calibration curves considering the standard deviation. Afterwards the electrochemical determination of PSA, mass of carbon nanotubes modified with AuNPs were determined using the gravimetric capacitance in PBS; in this way, current was normalized to the mass to avoid effect of mass.

2.5. Physicochemical characterization

Scanning electron micrographs were taken using an ORIUS SC600 model Field Emission Scanning Electron Microscopy (FESEM) and a ZEISS microscope, Merlin VP Compact model, with and EDX Bruker, Quantax 400 model.

Transmission electron microscopic measurements (TEM) were carried out using JEOL TEM, JEM-2010 model, which is equipped with and Oxford X-

ray detector (EDS), INCA Energy TEM 100 model, and GATAN acquisition camera.

X-Ray photoelectron spectroscopy (XPS) was performed in a VG-Microtech Mutilab 3000 spectrometer and Al K α radiation (1253.6 eV). The deconvolution of the XPS Au4f, C1s, S2p and N1s was done by least squares fitting using Gaussian-Lorentzian curves, while a Shirley line was used for the background determination. The S2p spectra have been analyzed considering the spin-orbit splitting into S2p_{3/2} and S2p_{1/2} with a 2:1 peak area ratio and 1.2 eV splitting³⁰. The XPS measurements were done in different parts of a given sample and repeated in two different samples, being the results similar.

To determine metal content, 10 mg of the carbon material modified with AuNPs were digested in an acid solution (1 HNO₃ (65%):3 HCl (37%)). The suspension was sonicated for 20 minutes and heated at 80°C for 6 hours until evaporation. Afterwards, 2 mL of HNO₃ were added and diluted with ultrapure water. Solutions were then analyzed using inductively coupled plasma optical emission spectroscopy (ICP-OES), Perkin-Elmer Optima 4300.

3. Results and discussion

3.1 fMWCNT-AuNPs electrodes characterization

3.1.1 Physicochemical characterization

MWCNT pristine material and fMWCNT were studied by temperature programmed desorption (TPD) to observe the nature of the different oxygen surface groups incorporated during the functionalization treatment and by Transmission Electron Microscopy (TEM) for studying possible morphological changes in the structure of the carbon material. The most relevant results are presented in Chapter 4.

FESEM micrographs in Figure 8.1 show the deposit of the fMWCNT-AuNPs synthesized, onto the surface of the glassy carbon electrode. Firstly, a homogeneous distribution of the carbon material modified with AuNPs is observed in Figure 8.1-A and 8.1-C, covering the entire surface with no bundles or agglomeration of the nanotubes. Secondly, nanoparticles are distinguished of the carbon material using Back-Scattering electrons (BSE),

(See Figure 8.1-B and Figure 8.1-D), showing a good distribution of the catalyst in the material and a smaller nanoparticle size in the synthesis with higher amount of PVP.

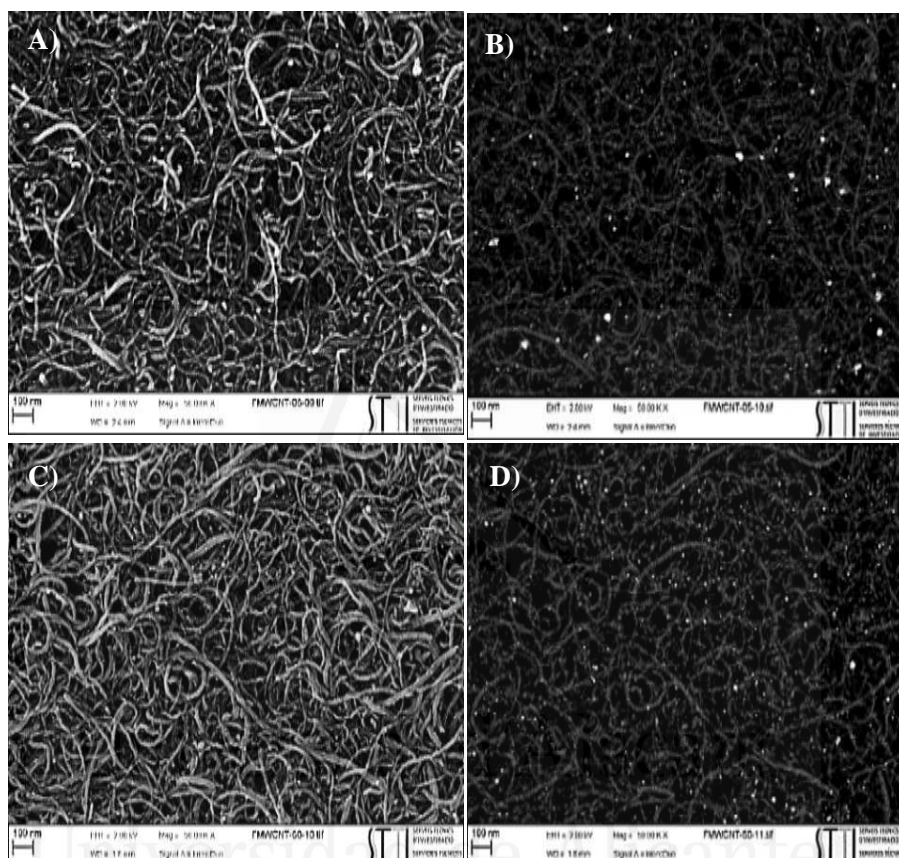


Figure 8.1. FESEM micrographs for fMWCNT-AuNPs onto glassy carbon surface: A) fMWCNT-AuNPs-0.5, B) BSE- fMWCNT-AuNPs-0.5, C) fMWCNT-AuNPs-50 and D) BSE-fMWCNT-AuNPs-50.

Gold loading was quantified by ICP-OES, achieving values of 2.1 wt % and 3.6 wt % for the ratios PVP/Au of 0.5 and 50, respectively (See Table 8.1). Furthermore, XPS spectra for Au4f core level region of our samples in Figure 8.2, shows two doublets at 84.1 and 87.8 eV associated with Au⁰ species and at 84.9 and 88.6 eV related with a higher oxidized state (Au^{+δ} species)^{34,35}. The Au⁰/Au^{+δ} ratio is for both samples 90.5%.

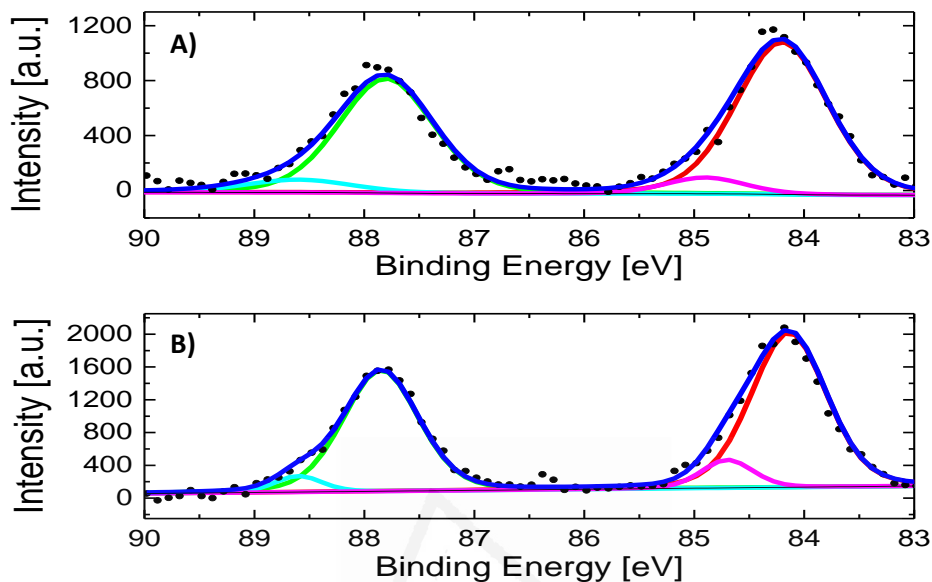


Figure 8.2. XPS spectra for Au4f: A) fMWCNT-AuNPs-0.5 and B) fMWCNT-AuNPs-50 synthesized.

Table 8.1. Amount of Au obtained by ICP and EASA in the fMWCNT-AuNPs and fMWCNT-AuNPs-Ab materials. Amount of S obtained by XPS and percentage of thiol group bound to Au.

| Sample | Au ICP-OES (wt %) | EASA ($\text{m}^2 \text{g}^{-1}$)* | S2p amount by XPS (wt %) | % of Au-S species in the total S2p |
|--------------------|-------------------|--------------------------------------|--------------------------|------------------------------------|
| fMWCNT-AuNP-0.5 | 2.1 | 28.6 | - | - |
| fMWCNT-AuNP-50 | 3.6 | 33.4 | - | - |
| fMWCNT-AuNP-0.5-Ab | - | - | 0.16 | 9 |
| fMWCNT-AuNP-50-Ab | - | - | 0.32 | 28 |

*Amount of gold was determined, considering the gravimetric capacitance and concentration (w/w) obtained by ICP-OES, previously.

Figure 8.3 shows the TEM micrographs of the carbon materials with AuNPs. This figure reveals the distribution and particle size of the AuNPs onto the surface of the carbon nanotubes after the impregnation procedure. As

previously reported, PVP concentration during the synthesis of the metal nanoparticles is a key factor to control the nanoparticle size in the colloid^{36,37}. Figure 8.3-C and 8.3-F show the particle size distribution determined by TEM. As expected, the nanoparticle size distribution decreases to a narrow distribution with the increase of the amount of PVP. The average particle size changes from 9.5 nm to 6.6 nm with the increase in the PVP/Au ratio. Moreover, agglomeration and a non-spherical shape of the nanoparticles is observed for lower PVP/Au ratio.



Universitat d'Alacant
Universidad de Alicante

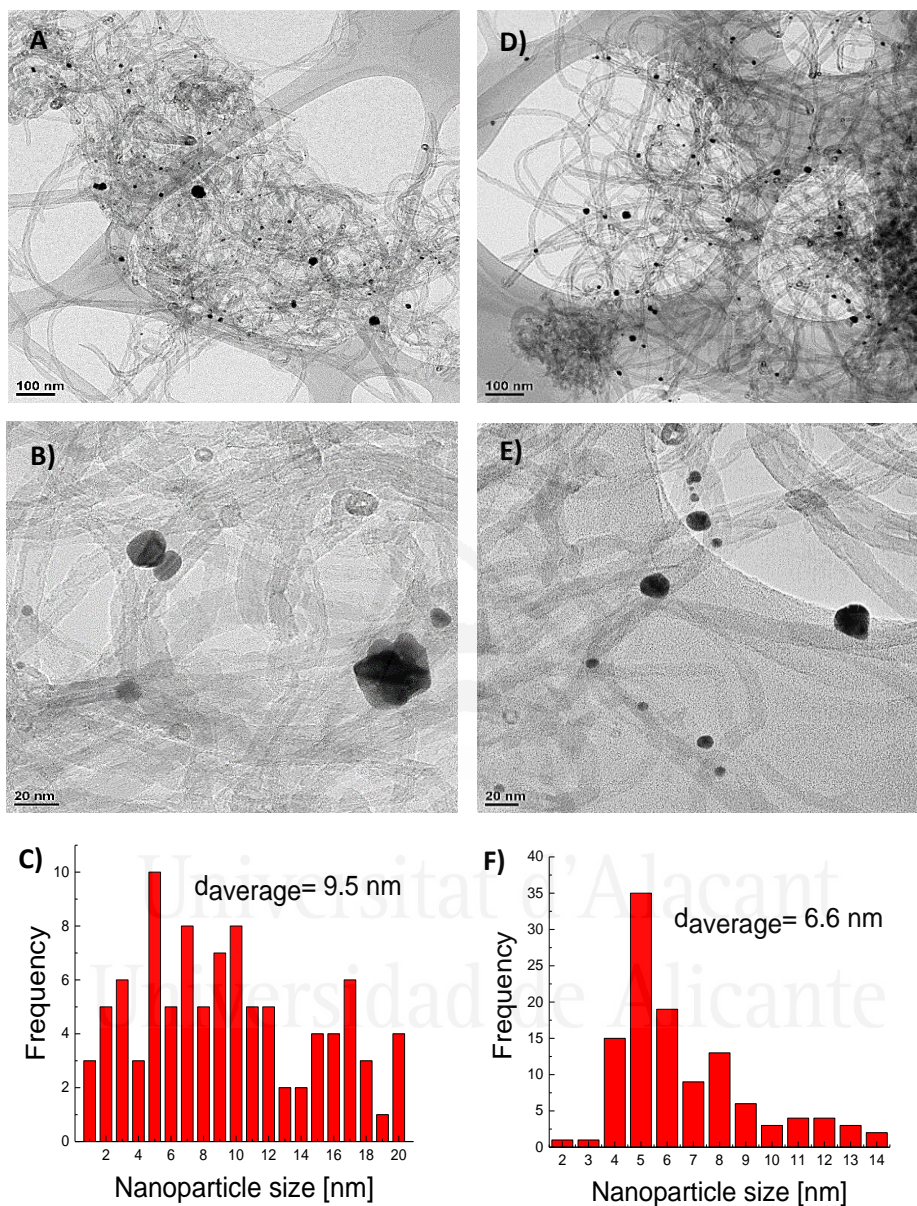


Figure 8.3. HR-TEM micrographs: A) fMWCNT-AuNPs-0.5, B) fMWCNT-AuNPs-0.5 magnified, C) histogram of Au nanoparticle size distribution in fMWCNT-AuNPs-0.5 transducer material, D) fMWCNT-AuNPs-50, E) fMWCNT-AuNPs-50 magnified and F) histogram of Au nanoparticle size distribution in fMWCNT-AuNPs-50 transducer material.

3.1.2 Electrochemical characterization of fMWCNT-AuNPs

Figure 8.4 shows the cyclic voltammograms for fMWCNT and fMWCNT-AuNPs modified GC electrode between 0.1 and 1.8 V. For fMWCNT, voltammogram shows an oxidation peak at approximately 0.6 V, with the corresponding reduction peak at 0.55 V; which are associated with the surface oxygen groups formed during the functionalization treatment. At the same time, the capacitance of these fMWCNTs is 43 F g^{-1} , a value similar to that previously reported in similar conditions²¹. However, incorporation of the gold nanoparticles in the carbon material generates an additional oxidation process at 1.5 V and the corresponding reduction at 1.15 V, corresponding with the oxidation-reduction of the gold oxide on the surface of the nanoparticles³⁸.

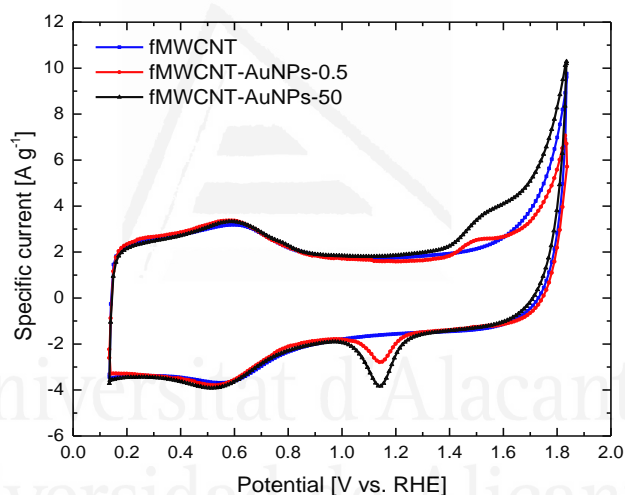


Figure 8.4. Cyclic voltammograms for fMWCNT, fMWCNT-AuNPs-0.5 and fMWCNT-AuNPs-50 in 0.1 M PBS (pH=7.2) and $v_{\text{scan}} = 50 \text{ mV s}^{-1}$.

It is well known that nanoparticle size has an important influence in the electrochemical active surface area (EASA) and smaller nanoparticle size implies an increase in the EASA³⁸⁻⁴⁰. Table 8.1 shows the EASA, which was determined following the Eq. 8.1 for the different transducer material synthesized in this work. It can be observed that the decrease in the particle size implies an increase in the EASA of around 17%.

$$EASA (S_{Au}) = \frac{Q}{m_{Au} \cdot 4.2} \quad \text{Eq. 8.1.}$$

Where EASA is in $\text{m}^2 \text{g}^{-1}$; Q is the charge in C , m_{Au} is the mass of gold in g and 4.2 C m^{-2} corresponds to the theoretical charge of the reduction of gold oxide.

3.2 Electrochemical characterization of the monoclonal antibodies immobilized on the fMWCNT-AuNPs samples

Figure 8.5 shows the cyclic voltammograms for the fMWCNT-AuNP electrode before and after immobilization of antibodies. It can be observed that no significant changes are appreciated on the double layer region of carbon nanotubes between 0.1 and 0.75 V for both materials. This result suggests that the immobilization of the antibody is not produced on the carbon nanotube surface. On the other hand, the redox processes for gold surface oxide shows a decrease in the current, indicating a blockage of the surface area of AuNP and a decrease in the EASA of 16 and 24% for fMWCNT-AuNPs-0.5 (Figure 8.5-A) and fMWCNT-AuNPs-50 (Figure 8.5-B), respectively^{41,42}. The high affinity between thiol groups present in the antibody structure with the gold nanoparticles causes the immobilization of the antibody⁴³, producing the observed decrease in available Au surface area.

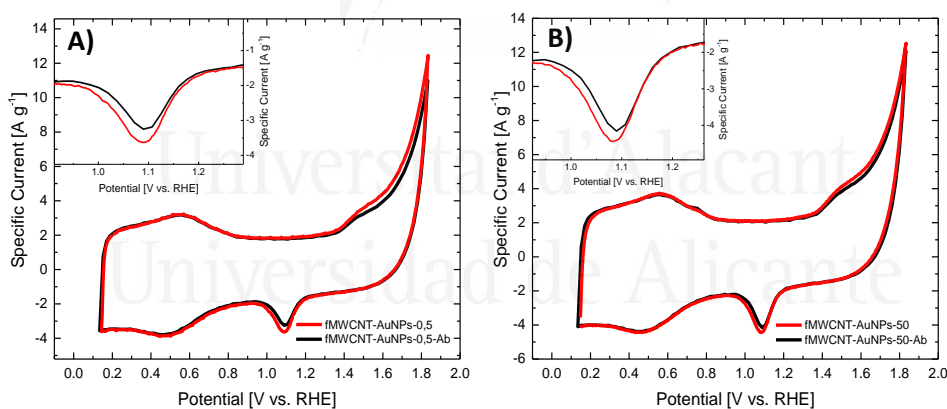


Figure 8.5. Electrochemical behavior of the immunosensor fMWCNT-AuNPs-Ab: A) cyclic voltammogram for transducer material before (red line) and after (black line) the immobilization with monoclonal antibodies of fMWCNT-AuNPs-0.5 in 0.1 M PBS (pH=7.2), $v_{\text{scan}}=50 \text{ mV s}^{-1}$ and B) cyclic voltammogram for transducer material before (red line) and after (black line) the immobilization with monoclonal antibodies of fMWCNT-AuNPs-50 in 0.1 M PBS (pH=7.2), $v_{\text{scan}}=50 \text{ mV s}^{-1}$. Inset: Enlargement of the reduction process of gold oxide

The covalent interaction between gold and the bioreceptor can be observed in the S2p spectra after immobilization (Figure 8.6), where, S2p3/2 peaks at binding energies of 163.9 and 162.7 eV, can be associated unbound and bound thiol groups, respectively³⁰. Considering the low amount of sulphur species, the XPS has significant noise and the deconvolution can only be considered qualitative. The bound thiol species can be associated to the interaction between the antibody and the gold surface⁴⁴⁻⁴⁷. Then, it can be suggested that the interaction between gold nanoparticles and thiol groups promote the covalent immobilization of the antibodies in the material. The samples with PVP/ratio of 50 present a much higher intensity of the peak at 162.7 eV, indicating a higher quantity of thiol groups bonded to AuNPs, in contrast with the AuNPs prepared with a lower PVP/Au ratio. This suggests that a higher amount of antibodies is immobilized on the surface of the electrode which contains the smaller average Au nanoparticle size (Table 8.1). Moreover, the presence of a higher amount of covalently bounded Ab-Au in the fMWCNT-AuNPs-50-Ab samples permits either a proper immobilization or even a better orientation of the bioreceptor in the transducer⁴⁸. Even though the interaction with thiol generates changes in the oxidation states of gold from Au⁰ to Au^{+δ}, authors have observed that the signal of Au⁰ can scatter the intensity of the Au^{+δ}, when low concentration of this latter species is in the electrode. For that reason no significant changes in gold spectra can be observed⁴⁹.

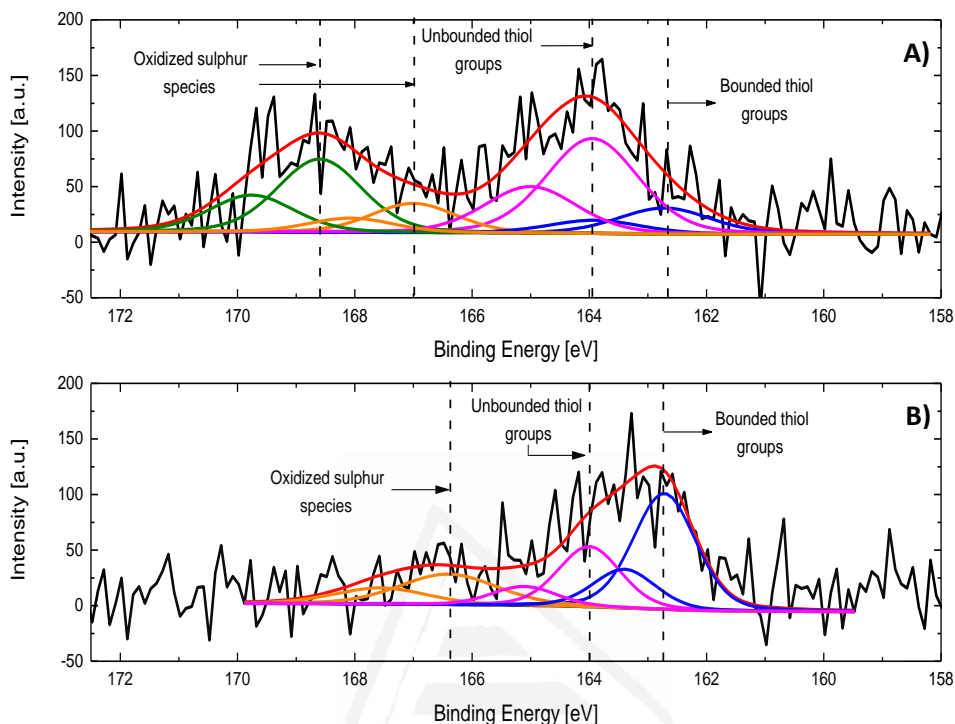


Figure 8.6. XPS spectra for S2p: A) fMWCNT-AuNPs-0.5-Ab and B) fMWCNT-AuNPs-50-Ab synthesized.

Additional signals in the S2p spectra appear at higher binding energies, especially for fMWCNT-AuNPs-0.5-Ab, between 166.4 and 169.6 eV, which can be related with oxidized sulfur species, probably associated with the denaturalization which takes place in the antibody or other direct interactions with the functional groups of the carbon material. These interactions are more probable for the sample with the largest AuNPs size and this produces a larger proportion of inappropriate immobilization of the biorecognition element in the surface of the material^{48,49}.

3.3. Electrochemical performance of the PSA immunosensor

Despite the blocking effect of the Ab antibodies in the AuNPs surface and subsequent formation of the immunocomplex antibody-antigen, which can be used as a label-free platform for detection, application of the high potential to achieve the oxidation-reduction reaction of gold nanoparticles produces the denaturalization and desorption of the bioreceptor (See section 3.2). Then, a

redox mediator could be used in order to decrease the detection potential⁵⁰, for this part ferrocene was used as redox probe mediator for the sensing process of the biomarker.

Figure 8.7-A shows the cyclic voltammograms for the fMWCNT and fMWCNT-AuNPs with different PVP/Au ratios (0.5 and 50) in 0.1 M PBS + 0.5mM Fc solution, where the corresponding oxidation-reduction processes of ferrocene at 0.9 and 0.83 V can be observed. Current density for both processes increases with the incorporation of the AuNPs. Moreover, increasing the PVP/Au ratio causes a growth in the current density for both processes, as a result of a larger EASA.

As reported, the oxidation process of ferrocene in aqueous solution is characterized by a single-electron transfer mechanism preceded by a weak adsorption process⁵¹. In this case, the separation peak for the redox process of ferrocene in fMWCNT at 50 mV s⁻¹ is around 47 ± 1 mV, suggesting that the mechanism for the redox process of ferrocene involves adsorption on the carbon material. On the contrary, incorporation of the AuNPs in the carbon material causes an increase of the separation peak to around 72 ± 1 mV, suggesting that the catalyst avoids the adsorption step during the oxidation process, making the process more irreversible⁵². The electrochemical behavior with the scan rate for the different transducer material synthesized in presence of the Fc can be observed in Figure 8.7. Analysis for the cathodic process show an increase of the peak current linearly in the range of scan rates of 10-200 mV s⁻¹, as can be observed in Figure 8.7-B, suggesting a diffusion-controlled electrochemical behavior for fMWCNT and fMWCNT-AuNPs⁵³. Based on Randles-Sevicks' equation (Eq. 8.2):

$$I_p = 2.69 \times 10^{-5} n^{3/2} A D_0^{1/2} C_0^* v_{scan}^{1/2} \quad \text{Eq. 8.2}$$

where I_p (A) is the peak current of the process, n is the number of exchanged electrons, A is the electroactive area (cm²), D_0 is the diffusion coefficient (cm² s⁻¹), C_0^* is the concentration of the electroactive specie (mol cm⁻³), v_{scan} is the scan rate (V s⁻¹). Slopes of the linear behavior might be associated with the term $2.69 \times 10^{-5} n^{3/2} A D_0^{1/2} C_0^*$, which suggested the electrochemical active area (A) in fMWCNT-AuNPs samples are higher and increase with the concentration of PVP in synthesis, given that the reduction of the nanoparticle size, as was mentioned above.

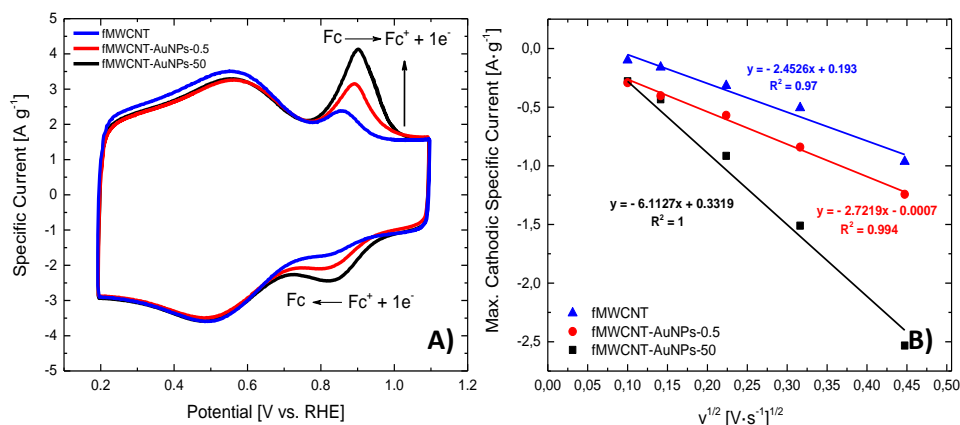


Figure 8.7. Electrochemical behavior of material synthesized in ferrocene: A) cyclic voltammograms at $v_{\text{scan}} = 50 \text{ mV} \cdot \text{s}^{-1}$ for fMWCNT and fMWCNT-AuNP and B) Plot of Maximum cathodic specific current vs. $v_{\text{scan}}^{1/2}$. Electrolyte: 0.1 M PBS + 0.5 mM Fc (pH=7.2).

Figure 8.8-A and 8.8-B show the decrease in the peak current for the oxidation process at 0.9 V for electrodes modified with Ab monoclonal antibodies, suggesting that the Fc redox processes are electrochemically impeded, presenting the higher current drop in fMWCNT-AuNPs-50-Ab biosensors. Some authors have suggested that, steric effects of the different functional groups of the antibodies immobilized on the surface, reduce the electron transfer between the electrode and the electroactive species (Fc) in solution, which might be used as a label-free platform for detection of the biomarker. These results agree with the XPS data and confirm the presence of the Ab on the surface of AuNPs⁴¹.

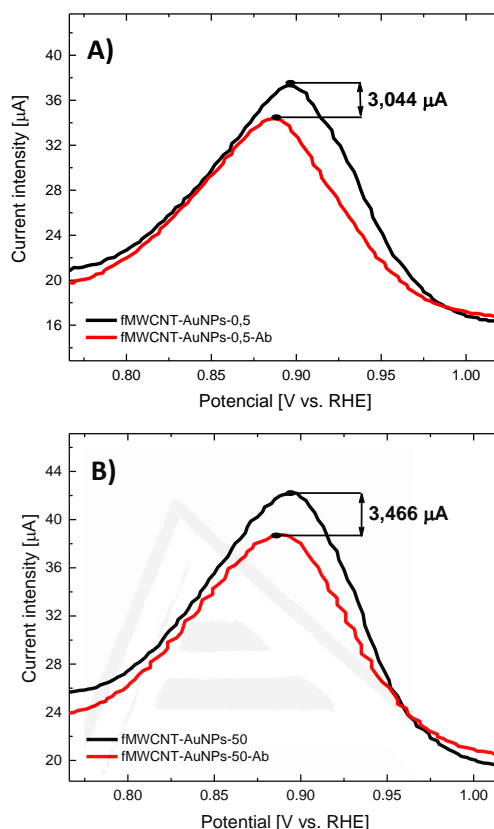


Figure 8.8. Enlargement of the oxidation process of Fc in the transducer material before (black line) and after (red line) of the immobilization with monoclonal antibodies: A) fMWCNT-AuNPs-0.5 and B) fMWCNT-AuNPs-50, in 0.1 M PBS + 0.5 mM Fc (pH=7.2) at $v_{\text{scan}} = 50 \text{ mV s}^{-1}$.

Immunosensor performance was investigated using chronoamperometry at 1 V with different concentrations of PSA in 0.1 M PBS + 0.5 mM Fc solution. Only three minutes were left between the additions of each aliquot for reaction between Ab immobilized in the AuNPs and PSA in solution. A decrease of the oxidation current associated to Fc is obtained with the increase of the PSA concentration. The change of the current with the addition of PSA can be used as electrochemical signal for detection of PSA. Given that antibody-antigen (Ab-Ag) reaction takes place after the addition of PSA in the solution, the immunocomplex Ab-Ag on the surface of the biosensor might increase the steric effects onto the surface of the electrode, which is translated in a decrease

of the current for the ferrocene oxidation process ($\text{Fc} \rightarrow \text{Fc} + 1\text{e}^-$)⁵⁴. The calibration curves for both electrodes are shown in Figure 8.9-A and 8.9-B, with the chronoamperometric profiles (inset). First of all, decrease in the electrical current density of the oxidation process for ferrocene is observed with the increase of the concentration of PSA, demonstrating the blocking of the surface by the Ab-Ag complex which was mentioned above. Furthermore, all immunosensors show a typical Langmuir behavior, where an initial linear range can be observed and a plateau, where the saturation of the biorecognition element takes place. In this case, saturation occurs as a consequence of the interaction of most of the immobilized antibodies with the antigen in solution, therefore, no more active sites are available for an enhanced detection of PSA after achieving this saturation and, thus, no current changes happen. Finally, only an important decrease in the oxidation-reduction processes for ferrocene can be observed in the cyclic voltammograms (Figure 8.9-C and 8.9-D), before and after the sensing process, as result of the immuno-complex onto the surface, which blocks the electron transfer, proving the biosensing activity of the immunosensor synthesized.

The saturation range of the immunosensor takes place at higher concentration values with the increase of PVP/Au ratio, showing at the same time, a higher analytical linear range detection of (0-4 ng mL⁻¹) for fMWNCT-AuNPs-0.5-Ab and (0-6 ng mL⁻¹) for fMWCNT-AuNPs-50-Ab. This behavior can be attributed to the nanoparticle size distribution in the fMWCNT-AuNPs-50-Ab immunosensor, which can provide a higher surface area, promoting a higher amount of biorecognition element immobilized onto the surface, a critical factor in the proper interaction of the fragment antigen-binding (Fab) part of the antibody with the antigen, which is in concordance with the XPS spectra for sulphur observed in section 3.2⁵⁵.

The linear regression of the calibration curve for both electrodes (fMWCNT-AuNPs-0.5-Ab and fMWCNT-AuNPs-50-Ab) were: $\Delta i \text{ (mA/g}_{\text{fMWCNT}}) = 7.112 C_{\text{PSA}} \text{ (ng}_{\text{PSA}} \text{ mL}^{-1}) + 2.478$ and $\Delta i \text{ (mA/g}_{\text{fMWCNT}}) = 4.743 C_{\text{PSA}} \text{ (ng}_{\text{PSA}} \text{ mL}^{-1}) + 1.717$, respectively and with the same correlation coefficient ($R^2=0.96$) for both electrodes. On the other hand, the sensitivity of the immunosensor shows a higher value in fMWNCT-AuNPs-0.5-Ab biosensors, in comparison with the samples with the highest PVP/Au ratio, which can be attributed to the fast decrease in the

amount of antibodies in the electrode during the detection process, which is also supported by the saturation limit of the immunosensor.

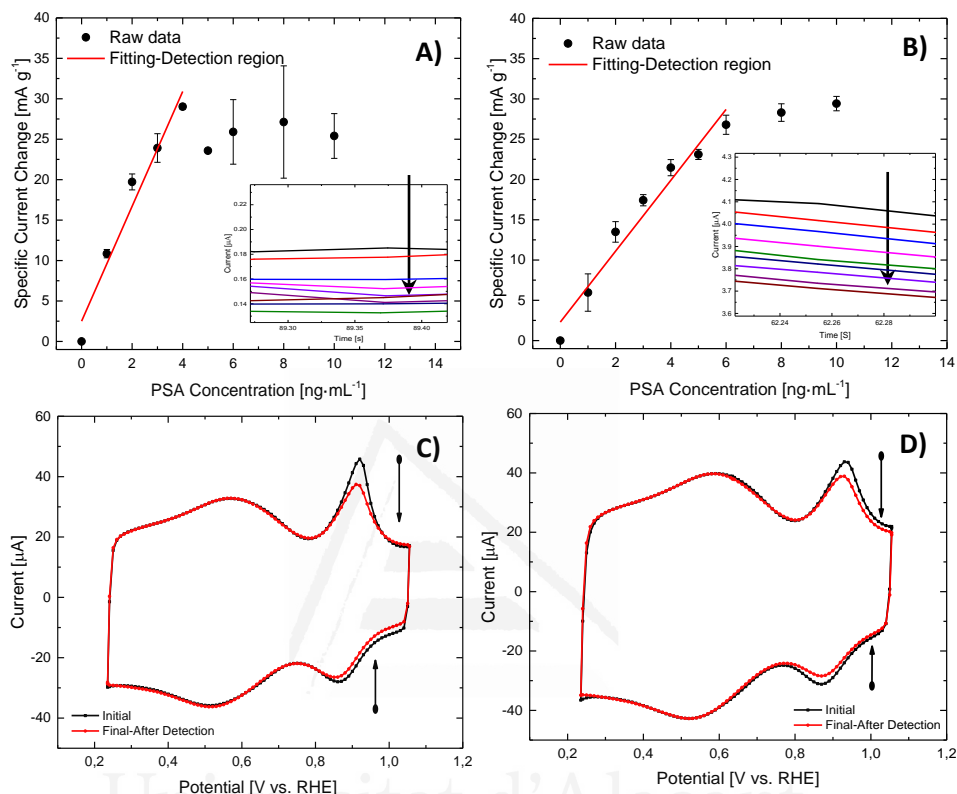


Figure 8.9. Electrochemical detection of the biomarker: A) Calibration curve for fMWNCT-AuNPs-0.5-Ab, B) Calibration curve for fMWNCT-AuNPs-50-Ab. All the measurements were performed in 0.1 M PBS + 0.5 mM Fc (pH=7.2) and $v_{scan}=50 \text{ mV s}^{-1}$, C) cyclic voltammograms for fMWNCT-AuNPs-0.5-Ab before (black line) and after (red line) detection of PSA in 0.1 M PBS + 0.5 mM Fc (pH=7.2) and $v_{scan}=50 \text{ mV s}^{-1}$, D) cyclic voltammogram for fMWNCT-AuNPs-50-Ab before (black line) and after (red line) detection of PSA in 0.1M PBS + 0.5 mM Fc (pH=7.2) at $v_{scan}=50 \text{ mV s}^{-1}$.

Table 8.2 shows the analytical parameters obtained with both immunosensors. It can be observed that the sensitivity is higher for the fMWCNT-AuNPs-0.5 electrodes; however, the linear range is higher for the fMWCNT-Au-50 electrode.

Table 8.2. Analytical figures of merit for the quantification of PSA with both electrochemical modified electrodes (fMWCNT-AuNPs-0.5-Ab and fMWCNT-AuNPs-50-Ab).

| Parameter | Sample | |
|---|--------------------|-------------------|
| | fMWCNT-AuNP-0.5-Ab | fMWCNT-AuNP-50-Ab |
| Sensitivity [(mA g _{fMWCNT} ⁻¹)/ (ng mL ⁻¹)] | 7.11 ± 0.82 | 4.74 ± 0.43 |
| Intercept (ng mL ⁻¹) | 2.48 ± 2.02 | 2.32 ± 1.22 |
| R | 0.96 | 0.96 |
| N | 5 | 7 |
| Linear range (ng mL ⁻¹) | 0-4 | 0-6 |
| LOD (ng mL ⁻¹) | 1 | 1 |
| LOQ (ng mL ⁻¹) | 3.3 | 3.3 |

Table 8.3 shows a comparison of some analytical parameters obtained in this work, with data published in the literature. In most of the cases, the sensitivity is similar or higher than the published, being the proposed sensor competitive with respect to previously reported electrochemical sensors. Moreover, time consumption to detect the PSA is greatly improved with respect to other immunosensors.

Table 8.3. Analytical parameters for different PSA biosensors.

| Electrode | Sample | | | | Reference |
|---|--|---|---|---|-----------|
| | Electrochemical technique (Time to measure) | Detection limit (ng mL ⁻¹) | Concentration range (ng mL ⁻¹) | Sensitivity ($\mu\text{A mL ng}^{-1}$) | |
| fMWCNT-AuNPs-0.5-Ab | Amperometric (5 min) | 1 | 0-4 | 0.085 | This work |
| fMWCNT-AuNPs-50-Ab | Amperometric (5 min) | 1 | 0-6 | 0.056 | This work |
| GC-MWCNT-Reactor | Amperometric (24 hours) | 1 | 0-60 | 0.047 | 56 |
| AuNPs-PANAM dendrimer/MWCNTs/Chitosan/Ionic liquid | Voltammetry (24 hours) | 0.05 | 0.05-2 (Range 1) | 0.0942 | 23 |
| Pt/Ti patterned-SWCNT | DPV (24 hours) | 0.25 | 0-1 | ... | 24 |

4. Conclusions

Electrochemical PSA biosensors based on fMWCNT-AuNPs-Ab with different nanoparticle size distribution were developed. In order to study the effect of the nanoparticle size in the performance of the biosensor, two different syntheses were carried out, controlling the PVP/Au molar ratio to obtain gold nanoparticles with a wide and narrow distribution, and an average diameter of 9.5 nm and 6.6 nm for PVP/Au ratios of 0.5 and 50, respectively. Incorporation of the metal nanoparticles was verified by cyclic voltammetry, which demonstrated that narrow nanoparticle size distribution presents higher EASA.

The prepared transducer materials with Au nanoparticles sizes showed a decrease of the current density of the redox processes associated with the gold oxide formation after the immobilization process of the biorecognition element, as a consequence of the blocking effect of this molecule onto the surface. This behavior was shown for ferrocene (Fc-Fc⁺) employed as redox probe. At the same time, XPS spectra for S2p demonstrated the presence of the S-Au bound, due to the covalent immobilization of the antibodies on the nanoparticle surface. Moreover, narrow Au nanoparticle size distribution promotes a higher immobilization of the antibodies which was seen as an increase in the amount of S-Au bound.

Electrochemical detection of PSA by chronoamperometry provided a fast method for the detection of this compound, which takes profit of the steric effects in the surface of the electrode created by the formation of the immunocomplex antibody-antigen, which acts as a diffusional barrier for the electroactive species, which is translated in a decrease in the current intensity of the oxidation processes. Even though a decrease in current with the increase of PSA concentration can be observed in both biosensors, the lineal range and saturation concentrations is influenced by the nanoparticle size, being fMWCNT-AuNPs-50-Ab the sample which presents the best performance with a higher linear range between 0 to 6 ng mL⁻¹ with a good sensitivity of 4.74 mA ng g_{fMWCNT}⁻¹ mL⁻¹, allowing the detection in human samples.

5. References

- (1) Ryerson, A. B.; Ehemann, C. R.; Altekruze, S. F.; Ward, J. W.; Jemal, A.; Sherman, R. L.; Henley, S. J.; Holtzman, D.; Lake, A.; Noone, A.

- M.; et al. Annual Report to the Nation on the Status of Cancer, 1975-2012, Featuring the Increasing Incidence of Liver Cancer. *Cancer* **2016**, *122* (9), 1312–1337.
- (2) Siegel, R.; Miller, K.; Jemal, A. Cancer Statistics, 2017. *Ca Cancer J.* **2017**, *67* (1), 7–30.
 - (3) Bélanger A, van Halbeek H, Graves HC, Grandbois K, Stamey TA, Huang L, Poppe I, L. F. Molecular Mass and Carbohydrate Structure of Prostate Specific Antigen: Studies for Establishment of an International PSA Standard. *Prostate* **1995**, *27* (4), 187–197.
 - (4) Villoutreix, B. O.; Getzoff, E. D.; Griffin, J. H. A Structural Model for the Prostate Disease Marker, Human Prostate-Specific Antigen. *Protein Sci.* **1994**, *3* (11), 2033–2044.
 - (5) Qu, B.; Chu, X.; Shen, G.; Yu, R. A Novel Electrochemical Immunosensor Based on Colabeled Silica Nanoparticles for Determination of Total Prostate Specific Antigen in Human Serum. *Talanta* **2008**, *76* (4), 785–790.
 - (6) Liu, B.; Lu, L.; Hua, E.; Jiang, S.; Xie, G. Detection of the Human Prostate-Specific Antigen Using an Aptasensor with Gold Nanoparticles Encapsulated by Graphitized Mesoporous Carbon. *Microchim. Acta*, **2012**, *178* (1–2), 163–170.
 - (7) Akter, R.; Rahman, M. A.; Rhee, C. K. Amplified Electrochemical Detection of a Cancer Biomarker by Enhanced Precipitation Using Horseradish Peroxidase Attached on Carbon Nanotubes. *Anal. Chem.* **2012**, *84* (15), 6407–6415.
 - (8) Wang, D.; Zheng, Y.; Chai, Y.; Yuan, Y.; Yuan, R. Target Protein Induced Cleavage of a Specific Peptide for Prostate-Specific Antigen Detection with Positively Charged Gold Nanoparticles as Signal Enhancer. *Chem. Commun.* **2015**, *51* (52), 10521–10523.
 - (9) Altintas, Z.; Uludag, Y.; Gurbuz, Y.; Tohill, I. E. Surface Plasmon Resonance Based Immunosensor for the Detection of the Cancer Biomarker Carcinoembryonic Antigen. *Talanta* **2011**, *86* (1), 377–383.
 - (10) Holliger, P.; Hudson, P. J. Engineered Antibody Fragments and the Rise of Single Domains. *Nat. Biotechnol.* **2005**, *23* (9), 1126–1136.
 - (11) Jayanthi, V. S. P. K. S. A.; Das, A. B.; Saxena, U. Recent Advances in Biosensor Development for the Detection of Cancer Biomarkers. *Biosens. Bioelectron.* **2017**, *91*, 15–23.

- (12) Turner, A. P. F. Biosensors - Sense and Sensitivity. *Science* **2000**, 290 (5495), 1315–1317.
- (13) Ronkainen, N. J.; Halsall, H. B.; Heineman, W. R. Electrochemical Biosensors. *Chem. Soc. Rev.* **2010**, 39 (5), 1747–1763.
- (14) Pisoschi, A. M. Biosensors as Bio-Based Materials in Chemical Analysis: A Review. *J. Biobased Mater. Bioenergy* **2013**, 7 (1), 19–38.
- (15) Wang, J. Glucose Biosensors: 40 Years of Advances and Challenges. *Electroanalysis* **2002**, 10 (1), 107–119.
- (16) Zhou, W.; Gao, X.; Liu, D.; Chen, X. Gold Nanoparticles for in Vitro Diagnostics. *Chem. Rev.* **2015**, 115 (19), 10575–10636.
- (17) Corma, A.; Garcia, H. Supported Gold Nanoparticles as Catalysts for Organic Reactions. *Chem. Soc. Rev.* **2008**, 37 (9), 2096.
- (18) Bo, X.; Zhou, M.; Guo, L. Electrochemical Sensors and Biosensors Based on Less Aggregated Graphene. *Biosens. Bioelectron.* **2016**, 89, 1–20.
- (19) Wang, Z.; Dai, Z. Carbon Nanomaterial-Based Electrochemical Biosensors: An Overview. *Nanoscale* **2015**, 7 (15), 6420–6431.
- (20) Abellán-Llobregat, A.; Vidal, L.; Rodríguez-Amaro, R.; Berenguer-Murcia, Á.; Canals, A.; Morallón, E. Au-IDA Microelectrodes Modified with Au-Doped Graphene Oxide for the Simultaneous Determination of Uric Acid and Ascorbic Acid in Urine Samples. *Electrochim. Acta* **2017**, 227, 275–284.
- (21) González-Gaitán, C.; Ruiz-Rosas, R.; Morallón, E.; Cazorla-Amorós, D. Effects of the Surface Chemistry and Structure of Carbon Nanotubes on the Coating of Glucose Oxidase and Electrochemical Biosensors Performance. *RSC Adv.* **2017**, 7 (43), 26867–26878.
- (22) Santos, J. C. S. D.; Barbosa, O.; Ortiz, C.; Berenguer-Murcia, A.; Rodrigues, R. C.; Fernandez-Lafuente, R. Importance of the Support Properties for Immobilization or Purification of Enzymes. *ChemCatChem* **2015**, 7 (16), 2413–2432.
- (23) Kavosi, B.; Salimi, A.; Hallaj, R.; Amani, K. A Highly Sensitive Prostate-Specific Antigen Immunosensor Based on Gold Nanoparticles/PAMAM Dendrimer Loaded on MWCNTS/Chitosan/Ionic Liquid Nanocomposite. *Biosens. Bioelectron.* **2014**, 52, 20–28.

- (24) Okuno, J.; Maehashi, K.; Kerman, K.; Takamura, Y.; Matsumoto, K.; Tamiya, E. Label-Free Immunosensor for Prostate-Specific Antigen Based on Single-Walled Carbon Nanotube Array-Modified Microelectrodes. *Biosens. Bioelectron.* **2007**, *22* (9-10), 2377-2381.
- (25) Wang, H.; Zhang, Y.; Yu, H.; Wu, D.; Ma, H.; Li, H.; Du, B.; Wei, Q. Label-Free Electrochemical Immunosensor for Prostate-Specific Antigen Based on Silver Hybridized Mesoporous Silica Nanoparticles. *Anal. Biochem.* **2013**, *434* (1), 123-127.
- (26) Yu, X.; Munge, B.; Patel, V.; Jensen, G.; Bhirde, A.; Gong, J. D.; Kim, S. N.; Gillespie, J.; Gutkind, J. S.; Papadimitrakopoulos, F.; et al. Carbon Nanotube Amplification Strategies for Highly Sensitive Immunodetection of Cancer Biomarkers. *J. Am. Chem. Soc.* **2006**, *128* (34), 11199-11205.
- (27) Yan, M.; Zang, D.; Ge, S.; Ge, L.; Yu, J. A Disposable Electrochemical Immunosensor Based on Carbon Screen-Printed Electrodes for the Detection of Prostate Specific Antigen. *Biosens. Bioelectron.* **2012**, *38* (1), 355-361.
- (28) Lu, P.; Teranishi, T.; Asakura, K.; Miyake, M.; Toshima, N. Polymer-Protected Ni/Pd Bimetallic Nano-Clusters: Preparation, Characterization and Catalysis for Hydrogenation of Nitrobenzene. *J. Phys. Chem. B* **1999**, *103* (44), 9673-9682.
- (29) Domínguez-Domínguez, S.; Berenguer-Murcia, Á.; Cazorla-Amorós, D.; Linares-Solano, Á. Semihydrogenation of Phenylacetylene Catalyzed by Metallic Nanoparticles Containing Noble Metals. *J. Catal.* **2006**, *243* (1), 74-81.
- (30) Castner, D. G.; Hinds, K.; Grainger, D. W. X-Ray Photoelectron Spectroscopy Sulfur 2p Study of Organic Thiol and Disulfide Binding Interactions with Gold Surfaces. *Langmuir* **1996**, *12* (21), 5083-5086.
- (31) Romanos, G. E.; Likodimos, V.; Marques, R. R. N.; Steriotis, T. A.; Papageorgiou, S. K.; Faria, J. L.; Figueiredo, J. L.; Silva, A. M. T.; Falaras, P. Controlling and Quantifying Oxygen Functionalities on Hydrothermally and Thermally Treated Single-Wall Carbon Nanotubes. *J. Phys. Chem. C* **2011**, *115* (17), 8534-8546.
- (32) Brender, P.; Gadiou, R.; Rietsch, J.-C.; Fioux, P.; Dentzer, J.; Ponche, A.; Vix-Guterl, C. Characterization of Carbon Surface Chemistry by Combined Temperature Programmed Desorption with in Situ X-Ray Photoelectron Spectrometry and Temperature Programmed Desorption

with Mass Spectrometry Analysis. *Anal. Chem.* **2012**, *84* (5), 2147–2153.

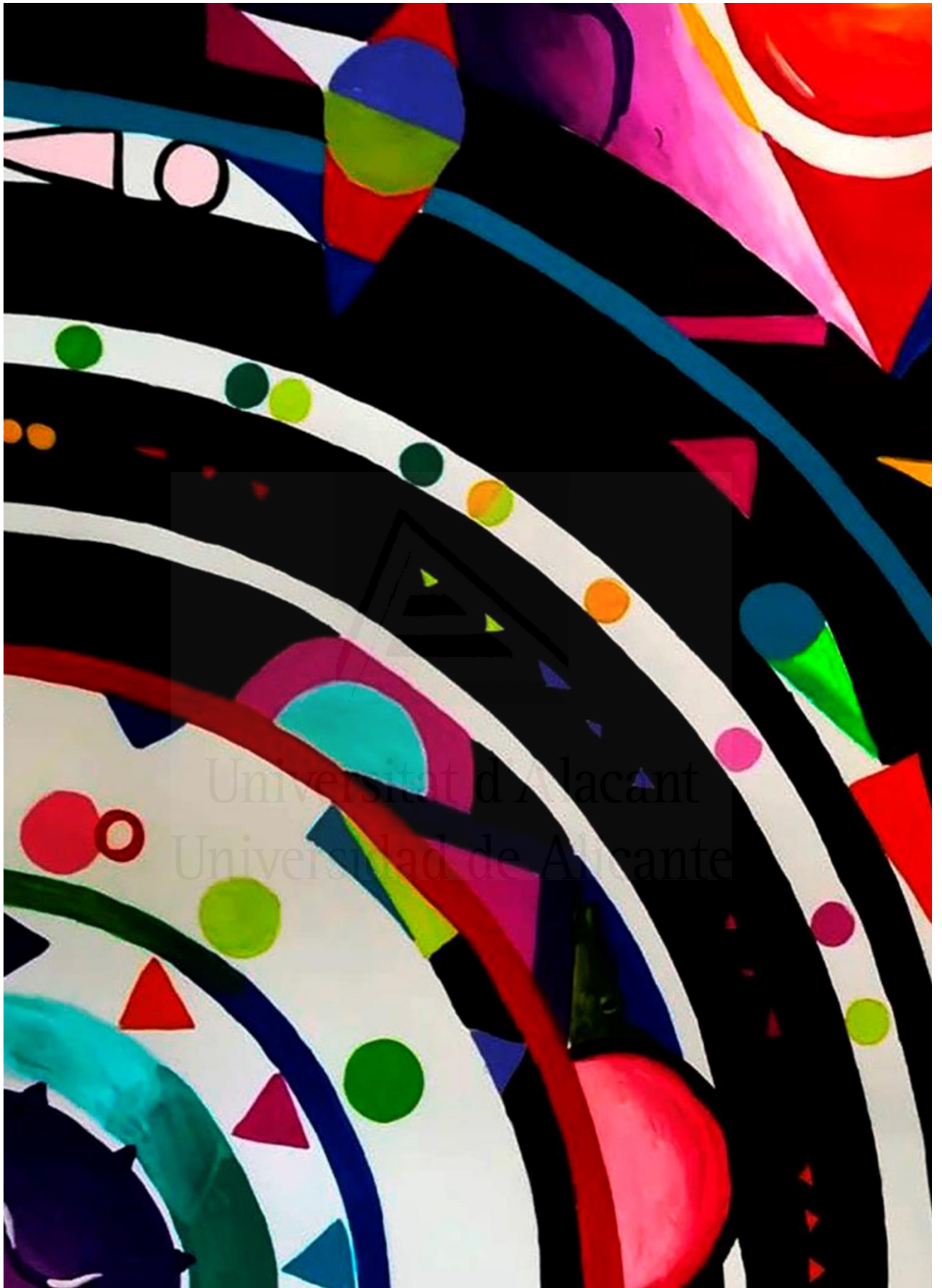
- (33) Berenguer, R.; Marco-Lozar, J. P.; Quijada, C.; Cazorla-Amorós, D.; Morallón, E. Effect of Electrochemical Treatments on the Surface Chemistry of Activated Carbon. *Carbon* **2009**, *47* (4), 1018–1027.
- (34) Jasmin, J.-P.; Miserque, F.; Dumas, E.; Vickridge, I.; Ganem, J.-J.; Cannizzo, C.; Chaussé, A. XPS and NRA Investigations during the Fabrication of Gold Nanostructured Functionalized Screen-Printed Sensors for the Detection of Metallic Pollutants. *Appl. Surf. Sci.* **2017**, *397*, 159–166.
- (35) Liberman, E. Y.; Naumkin, A. V.; Tsodikov, M. V.; Mikhailichenko, A. I.; Kon'kova, T. V.; Grunskii, V. N.; Kolesnikov, V. A.; Pereyaslavtsev, A. Y. Synthesis, Structure, and Properties of a Au/MnOx–CeO₂ Nanocatalyst for Low-Temperature Oxidation of Carbon Monoxide. *Inorg. Mater.* **2017**, *53* (4), 406–412.
- (36) Miguel-García, I.; Berenguer-Murcia, Á.; Cazorla-Amorós, D. Preferential Oxidation of CO Catalyzed by Supported Polymer-Protected Palladium-Based Nanoparticles. *Appl. Catal. B Environ.* **2010**, *98* (3–4), 161–170.
- (37) Bönnemann, H.; Richards, R. M. Nanoscopic Metal Particles – Synthetic Methods and Potential Applications. *Eur. J. Inorg. Chem.* **2001**, *2001* (10), 2455–2480.
- (38) Sukeri, A.; Saravia, L. P. H.; Bertotti, M. A Facile Electrochemical Approach to Fabricate a Nanoporous Gold Film Electrode and Its Electrocatalytic Activity towards Dissolved Oxygen Reduction. *Phys. Chem. Chem. Phys.* **2015**, *17* (43), 28510–28514.
- (39) Ayán-Varela, M.; Ruiz-Rosas, R.; Villar-Rodil, S.; Paredes, J. I.; Cazorla-Amorós, D.; Morallón, E.; Martínez-Alonso, A.; Tascón, J. M. D. Efficient Pt Electrocatalysts Supported onto Flavin Mononucleotide–Exfoliated Pristine Graphene for the Methanol Oxidation Reaction. *Electrochim. Acta* **2017**, *231*, 386–395.
- (40) Zaragoza-Martín, F.; Sopena-Escario, D.; Morallón, E.; de Lecea, C. S. M. Pt/Carbon Nanofibers Electrocatalysts for Fuel Cells. Effect of the Support Oxidizing Treatment. *J. Power Sources* **2007**, *171* (2), 302–309.
- (41) Deiminiat, B.; Rounaghi, G. H.; Arbab-Zavar, M. H.; Razavipanah, I.

A Novel Electrochemical Aptasensor Based on F-MWCNTs/AuNPs Nanocomposite for Label-Free Detection of Bisphenol A. *Sensors Actuators B Chem.* **2017**, *242*, 158–166.

- (42) Dey, A.; Kaushik, A.; Arya, S. K.; Bhansali, S. Mediator Free Highly Sensitive Polyaniline–Gold Hybrid Nanocomposite Based Immunosensor for Prostate-Specific Antigen (PSA) Detection. *J. Mater. Chem.* **2012**, *22* (29), 14763.
- (43) Benvidi, A.; Firouzabadi, A. D.; Moshtaghiun, S. M.; Mazloum-Ardakani, M.; Tezerjani, M. D. Ultrasensitive DNA Sensor Based on Gold Nanoparticles/Reduced Graphene Oxide/Glassy Carbon Electrode. *Anal. Biochem.* **2015**, *484*, 24–30.
- (44) Venditti, I.; Fontana, L.; Scaramuzza, F.; Russo, M.; Battocchio, C.; Carlini, L.; Gonon, L.; Mareau, V.; Fratoddi, I. Nanocomposite Based on Functionalized Gold Nanoparticles and Sulfonated Poly(Ether Ether Ketone) Membranes: Synthesis and Characterization. *Materials* **2017**, p 258.
- (45) Amendola, V.; Scaramuzza, S.; Agnoli, S.; Polizzi, S.; Meneghetti, M. Strong Dependence of Surface Plasmon Resonance and Surface Enhanced Raman Scattering on the Composition of Au–Fe Nanoalloys. *Nanoscale* **2014**, *6* (3), 1423–1433.
- (46) Yam, C. M.; Cho, J.; Cai, C. Preparation, Characterization, and Heck Reaction of Multidentate Thiolate Films on Gold Surfaces. *Langmuir* **2003**, *19* (17), 6862–6868.
- (47) Berner, S.; Lidbaum, H.; Ledung, G.; Åhlund, J.; Nilson, K.; Schiessling, J.; Gelius, U.; Bäckvall, J. E.; Puglia, C.; Oscarsson, S. Electronic and Structural Studies of Immobilized Thiol-Derivatized Cobalt Porphyrins on Gold Surfaces. *Appl. Surf. Sci.* **2007**, *253* (18), 7540–7548.
- (48) Trilling, A. K.; Beekwilder, J.; Zuilhof, H. Antibody Orientation on Biosensor Surfaces: A Minireview. *Analyst* **2013**, *138* (6), 1619–1627.
- (49) Singh, J.; Whitten, J. E. Adsorption of 3-Mercaptopropyltrimethoxysilane on Silicon Oxide Surfaces and Adsorbate Interaction with Thermally Deposited Gold. *J. Phys. Chem. C* **2008**, *112* (48), 19088–19096.
- (50) Chuah, K.; Lai, L. M. H.; Goon, I. Y.; Parker, S. G.; Amal, R.; Justin Gooding, J. Ultrasensitive Electrochemical Detection of Prostate-

Specific Antigen (PSA) Using Gold-Coated Magnetic Nanoparticles as “Dispersible Electrodes.” *Chem. Commun.* **2012**, 48 (29), 3503–3505.

- (51) Salinas-Torres, D.; Huerta, F.; Montilla, F.; Morallón, E. Study on Electroactive and Electrocatalytic Surfaces of Single Walled Carbon Nanotube-Modified Electrodes. *Electrochim. Acta* **2011**, 56 (5), 2464–2470.
- (52) Sieben, J. M.; Ansón-casaos, A.; Montilla, F.; Martínez, M. T.; Morallón, E. Electrochimica Acta Electrochemical Behaviour of Different Redox Probes on Single Wall Carbon Nanotube Buckypaper-Modified Electrodes. *Electrochim. Acta* **2014**, 135, 404–411.
- (53) Sanjuán, I.; Brotons, A.; Hernández-Ibáñez, N.; Foster, C. W.; Banks, C. E.; Iniesta, J. Boron-Doped Diamond Electrodes Explored for the Electroanalytical Detection of 7-Methylguanine and Applied for Its Sensing within Urine Samples. *Electrochim. Acta* **2016**, 197, 167–178.
- (54) Torati, S. R.; Kasturi, K. C. S. B. S. B.; Lim, B.; Kim, C. G. Hierarchical Gold Nanostructures Modified Electrode for Electrochemical Detection of Cancer Antigen CA125. *Sensors Actuators B Chem.* **2017**, 243, 64–71.
- (55) Tajima, N.; Takai, M.; Ishihara, K. Significance of Antibody Orientation Unraveled: Well-Oriented Antibodies Recorded High Binding Affinity. *Anal. Chem.* **2011**, 83 (6), 1969–1976.
- (56) Panini, N. V.; Messina, G. A.; Salinas, E.; Fernández, H.; Raba, J. Integrated Microfluidic Systems with an Immunosensor Modified with Carbon Nanotubes for Detection of Prostate Specific Antigen (PSA) in Human Serum Samples. *Biosens. Bioelectron.* **2008**, 23 (7), 1145–1151.



The background is a vibrant, abstract composition of various colors and shapes. It features thick, curved bands of red, pink, purple, and green, set against a dark, almost black background. There are also smaller, scattered geometric shapes like triangles and circles in blue, yellow, and red. A white circle is partially visible on the right edge.

Chapter 9

General Conclusions

Universitat d'Alacant
Universidad de Alicante

This PhD thesis has been focused on the development of functionalization procedures of carbon materials for bioelectrochemical applications. In this sense, different strategies based on chemical and electrochemical methods have been employed in order to incorporate different functionalities such as, surface functional groups and metal-nanoparticles which subsequently promote the immobilization of bioelements and electron transfer for application in electrochemical devices as biosensors.

Electrochemical Functionalization of Single-Wall Carbon Nanotubes with Phosphorus and Nitrogen Species

Functionalization of SWCNT with N and P functional groups was achieved by electrochemical oxidation of 4-APPA by cyclic voltammetry. The electrochemical oxidation selectively produces oligomer layers that wrap the surface of the SWCNT. Increase in the positive potential of the electrochemical modification demonstrated a high influence in the degree of incorporation of N and P species. Thus, when an upper potential limit of 1.4 V is used, the highest P incorporation is reached and further potential increase causes loss of P-species probably due to hydrolysis reactions. Several surface redox processes that depend on the applied potential are clearly observed in the voltammograms of the functionalized SWCNT. These redox processes present important pH dependence. The well-defined redox processes observed suggests the formation of oligomers with homogenous composition and structure. This conclusion is supported by TEM and Raman spectroscopy. However, the high reversibility and symmetry of the redox processes suggest that covalently bound redox species may also exist.

The high selectivity of the electrochemical process towards monomer oxidation, even at high potentials, and the precise control of the degree of modification of the CNT surface by selecting the electrochemical conditions, make this method an alternative procedure for electrochemical co-functionalization with P and N species with the generation of electroactive materials.

Effect of Surface Oxygen Groups in the Electrochemical Modification of Multi-walled Carbon Nanotubes by 4-amino phenyl phosphonic acid

MWCNTs and fMWCNTs were successfully functionalized with N and P species during electrochemical oxidation of 4-APPA employing cyclic

voltammetry. The oxidation of 4-APPA promotes the formation of electroactive oligomers onto the CNTs surface; however, covalently bonded redox species cannot be discarded. It has been observed a negative effect of the surface oxygen groups in the CNTs in the functionalization degree. Thus, for the fMWCNTs the amount of phosphorus incorporated is lower than in the non-oxidized MWCNTs. However, the amount of P incorporated shows a maximum in both CNTs at an upper potential limit of 1.4 V; further potential increase causes an over oxidation of the oligomers or the oxidation of the phosphorus groups without producing severe damage of the carbon nanotube structure.

In the case of MWCNTs, different redox processes with high reversibility are observed, which produces a remarkable increase in the electric charge stored compared to the pristine MWCNTs. In addition, oligomer chains are clearly observed by TEM. In the case of the fMWCNTs, the oligomerization reaction is not favored compared to pristine MWCNTs. In this material, the presence of electron withdrawing oxygen groups that decrease the π electron density of the CNTs and modify the orientation of the 4-APPA molecule, thus reducing the incorporation of 4-APPA parallel to the surface of the CNTs, impede the oligomerization reaction.

The evolution of I^D/I^G and I^D/I^G Raman band ratios with potential in presence of 4-APPA follows a similar trend for functionalized MWCNTs and functionalized fMWCNTs. For MWCNTs they increase importantly from 1.4 V, indicating that some oxidation of the MWCNTs occurs from this potential, generating defects. However, in the case of fMWCNTs these ratios go through a maximum indicating that some loss of carbon material occurs through carbon gasification reactions or the formation of species in solution. These reactions may also make difficult the functionalization by 4-APPA.

Thus, the presence of surface oxygen groups in the MWCNTs is detrimental to achieve the functionalization through oligomerization reactions, being covalent attachment the prevailing mechanism.

Single Wall Carbon Nanotubes-based Bioelectrodes Prepared by One-step Electrochemical Enzyme Entrapment

The electrochemical entrapment of either s-GDH or PQQ-GDH during oxidation of *para*-aminophenyl phosphonic acid (4-APPA) provides a simple

method for the immobilization of the enzyme onto the SWCNT surface. During the electrochemical immobilization, the functionalization of the SWCNT with phosphorus and nitrogen groups also occurs. The adequate interaction between the functionalized SWCNT and the enzyme seems to be determined by the phosphorus groups incorporated in the material during the electrochemical co-deposition films. In the presence of the enzyme substrate a catalytic current is obtained showing the efficient enzyme-electrode contact. These bioelectrodes show an enhancement in the electrocatalytic current density and consequently in the sensitivity towards glucose oxidation in comparison with the electrode prepared by drop-casting. The sensitivity shows a high dependence with the upper potential limit employed for the enzyme immobilization being higher at high potential. The bioelectrode prepared with a one-step process (procedure 2), shows a sensitivity, referred to the amount of enzyme, around double than the electrode prepared using procedure 1 and six times higher than the bioelectrode prepared by drop-casting.

The proposed methodology offers a platform for enzymatic electrode preparation under mild conditions of synthesis on nanostructured carbon-based materials, employing low loading of enzyme on the electrode surface and with high sensitivity. This methodology could be extended to other soluble enzymes, assuring good reproducibility, scalability and improved direct electron transfer, which may have potential application as anode in biofuel cells.

Electron Transfer Enhancement at Electrochemically Modified Multiwall Carbon Nanotubes based Bioelectrodes

The electrochemical modification of MWCNT with 4-APPA has demonstrated the incorporation of different phosphorus and nitrogen surface species which promote the immobilization of PQQ-GDH. The bioelectrodes have been used in the oxidation of glucose at physiological pH. Depending of the upper potential limit used in the electrochemical modification of MWCNTs, morphological features of the enzymatic coating and interaction with the enzymatic element, improve the electron-transfer kinetics, obtaining values for apparent electron transfer rate constants from 69 to 82 s⁻¹. This good electron transfer could be associated with a better orientation of the redox-active center of the enzyme to the electrode. Moreover, the different

biocatalytic electrodes show different amounts of immobilized enzyme, oxidation catalytic current and sensitivity towards glucose oxidation.

The MWCNT-APPA-1.37-GDH bioelectrode shows the highest values of glucose oxidation current ($1.47 \text{ A}\cdot\text{g}^{-1}$ obtained by cyclic voltammetry and $3.06 \mu\text{A}$ obtained by chronoamperometry). The sensitivity obtained for this electrode is $53.63 \pm 4.72 \text{ mA g}_{\text{MWCNT}}^{-1} \text{ mM}^{-1}$. Therefore, the electrochemical modification of MWCNTs with phosphorus and nitrogen species coming from oxidation of 4-APPA, can be considered as a promising alternative to control and improve the electrochemical performance of biocatalysts for further application as biosensors.

Metal Free Electrochemical Glucose Biosensor based on N-doped Carbon Material

An enzymatic glucose biosensor is developed based on glucose oxidase immobilized on a N-doped carbon material, obtained by heat treatment of PANI. This biosensor is a metal free carbon material. N-doped carbon material has a remarkable catalytic activity towards oxygen reduction reaction due to the presence of quaternary N species, even after the immobilization of the glucose oxidase. Surface reversible redox process at -0.42 V vs. Ag/AgCl related with the cofactor FAD/FADH₂ demonstrates the successful immobilization of the enzyme on the electrode.

Indirect glucose detection is carried out following the current density variation of the ORR generated by the increase of the glucose concentration, as consequence of the enzymatic reaction of the GO_x at a potential of -0.4 V vs. Ag/AgCl. Sensitivity of the prepared biosensor exhibits good values towards glucose detection, with no dependence of the oxygen concentration in the solution ($23.57 \pm 1.77 \mu\text{A cm}^{-2} \text{ mM}^{-1}$ and $24.29 \pm 1.12 \mu\text{A cm}^{-2} \text{ mM}^{-1}$ for O₂-saturated and room atmosphere conditions, respectively). Nevertheless, reaction rate for the recovery of the enzyme from the reduced to the oxidized state conditions, affects the linear detection range of the biosensor, being wider for the O₂-saturated conditions where the re-oxidation of the pristine enzyme is carried out rapidly. Additionally, biosensor shows an acceptable reproducibility, repeatability and stability. Despite small interference effect of uric acid in the detection of glucose, high affinity and sensitivity towards

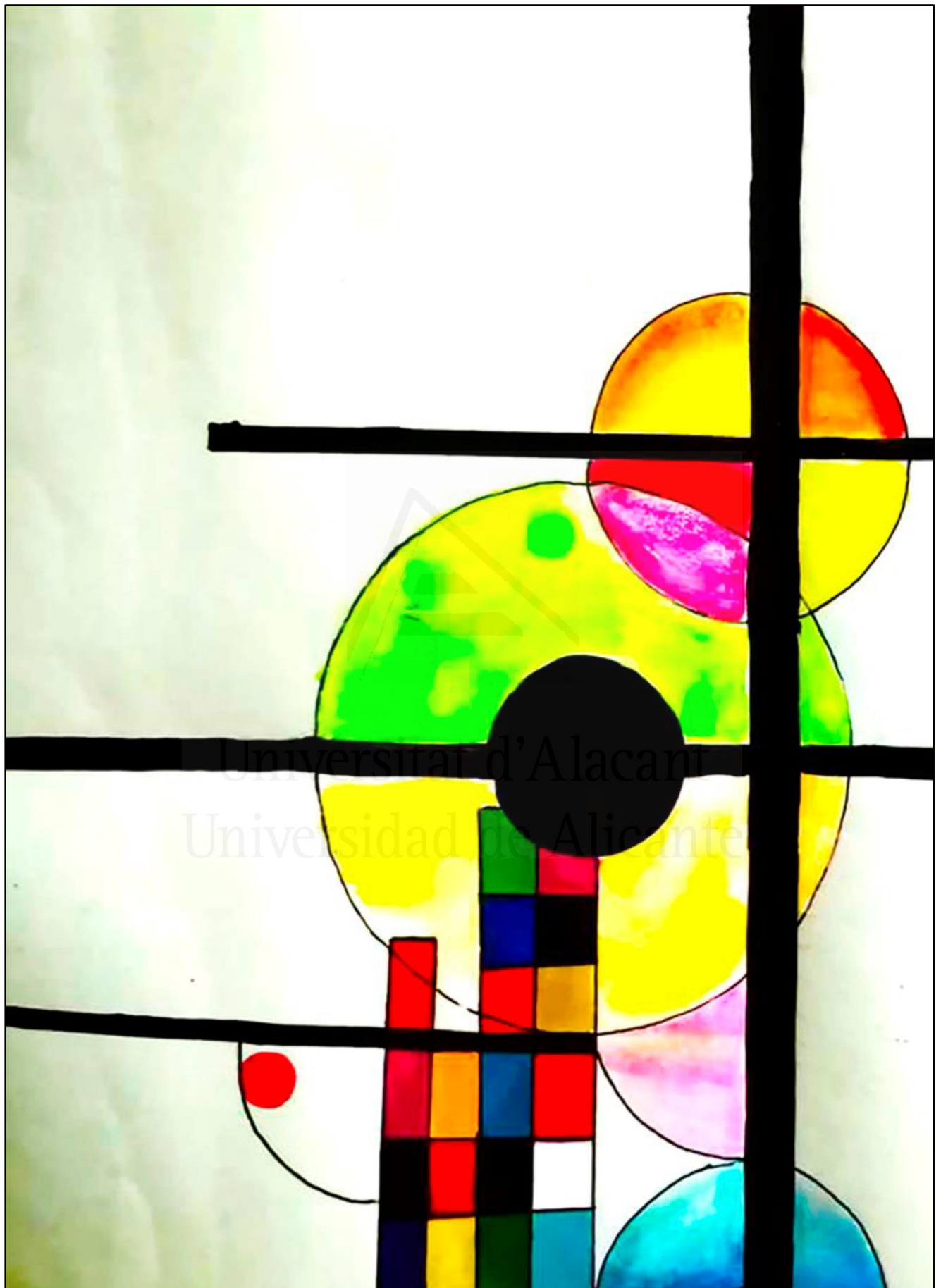
glucose oxidation still allows us the application of this biosensor in the detection of glucose in real samples like urine and commercial sugary drink.

Development of fMWCNT Modified with Gold Nanoparticles for the Chronoamperometric-Immunodetection of the Prostate Specific Antigen

Electrochemical PSA biosensors based on fMWCNT-AuNPs-Ab with different gold nanoparticle size distribution were developed. In order to study the effect of the nanoparticle size in the performance of the biosensor, two different syntheses were carried out, controlling the PVP/Au molar ratio to obtain gold nanoparticles with a wide and narrow distribution, and an average diameter of 9.5 nm and 6.6 nm for PVP/Au ratios of 0.5 and 50, respectively. Incorporation of the metal nanoparticles was verified by cyclic voltammetry, which demonstrated that narrow nanoparticle size distribution presents higher EASA.

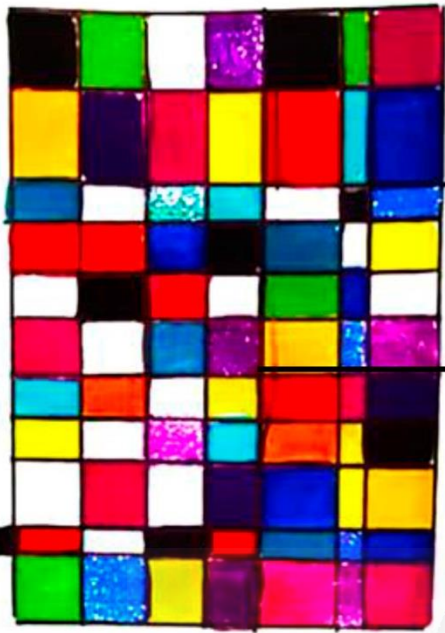
The prepared transducer materials with different Au nanoparticle sizes showed a decrease of the current density of the redox processes associated with the gold oxide formation after the immobilization process of the biorecognition element, as a consequence of the blocking effect of this molecule in the surface. This behavior was shown for ferrocene (Fc-Fc^+) employed as redox probe. At the same time, XPS spectra for S2p demonstrated the presence of the S-Au bond, due to the covalent immobilization of the antibodies on the nanoparticle surface. Moreover, narrow Au nanoparticle size distribution promotes a higher immobilization which was seen as an increase in the amount of S-Au bond.

The electrochemical detection of PSA by chronoamperometry provided a fast method for the detection of this compound, which takes profit of the steric effects in the surface of the electrode created by the formation of the immunocomplex antibody-antigen, which acts as a diffusional barrier for the electroactive species, which is translated in a decrease in the current intensity of the oxidation processes. Even though a decrease in current with the increase of PSA concentration can be observed in both biosensors, the lineal range and saturation concentrations are influenced by the nanoparticle size, being fMWCNT-AuNPs-50-Ab the sample which presents the best performance with a higher linear range between 0 to 6 ng mL^{-1} with a good sensitivity of $4.74 \text{ mA ng} \cdot \text{g}_{\text{fMWCNT}}^{-1} \text{ mL}^{-1}$, allowing the detection in human samples.

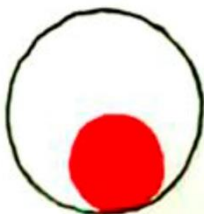


Capítulo 9

Conclusiones generales



Universidad d'Alacant
Universidad de Alicante



Esta tesis doctoral se ha centrado en el desarrollo de procedimientos de síntesis de material de carbono para aplicaciones bioelectroquímicas. En este sentido, se han empleado diferentes estrategias basadas en métodos químicos y electroquímicos para incorporar diferentes tipos de funcionalidades en la superficie de los materiales carbonosos; así como heteroátomos en la red y nanopartículas metálicas; los cuales han facilitado la inmovilización de bioelementos, orientación del bioelemento y la transferencia de electrones con el elemento biocatalizador o de reconocimiento, para su aplicación en dispositivos electroquímicos como sensores y/o bioelectrodos.

Funcionalización electroquímica de nanotubos de carbono de pared simple con especies de fósforo y nitrógeno

La funcionalización de SWCNT con grupos funcionales N y P se logró a partir de la oxidación electroquímica de 4-APPA por voltamperometría cíclica. La oxidación electroquímica produce de forma selectiva la unión de especies electroactivas y la formación de capas de oligómeros que envuelven la superficie de los SWCNT. El incremento en el potencial positivo de la modificación electroquímica demostró tener una alta influencia en el grado de incorporación de especies de N y P. Por lo tanto, cuando se usa un potencial límite superior de 1.6 V vs. RHE, se alcanza la incorporación de P más alta, por encima de dicho potencial se genera la pérdida de especies P probablemente debido a reacciones de hidrólisis. Varios procesos redox superficiales, que depende del potencial aplicado, se observan claramente en los voltamogramas de los SWCNT funcionalizados. Estos procesos redox presentan una importante dependencia con el pH. Los procesos redox bien definidos tras la funcionalización sugieren una buena interacción entre los SWCNT y las especies funcionales unidas al nanotubo, así como los oligómeros adsorbidos homogéneamente en la superficie. Esta conclusión está respaldada por la espectroscopia Raman y las micrografías TEM. Sin embargo, la alta reversibilidad y simetría de los procesos redox sugieren que también existen especies redox unidas covalentemente.

La alta selectividad del proceso de modificación electroquímica hacia la oxidación de monómeros, incluso a altos potenciales, y el control preciso del grado de modificación de la superficie nanotubo de carbono, mediante el control de las condiciones electroquímicas, hacen de este método un

procedimiento alternativo para la co-funcionalización electroquímica con P y N especies en la generación de materiales electroactivos.

Efecto de los grupos de oxígeno de superficie en la modificación electroquímica de los nanotubos de carbono de paredes múltiples por el ácido 4-amino fenil fosfónico

MWCNT y fMWCNT se funcionalizaron con éxito con especies N y P durante la oxidación electroquímica de 4-APPA empleando voltamperometría cíclica. La oxidación del 4-APPA promueve la formación de oligómeros electroactivos que pueden adsorberse en la superficie del nanotubo de carbono; sin embargo, la unión covalente de las especies redox al nanotubo no puede ser descartada. Se ha observado un efecto negativo de los grupos de oxigenados en el grado de funcionalización del nanotubo de carbono. Sin embargo, la cantidad de P incorporada muestra un valor máximo en ambos nanotubos de carbono a un potencial límite superior de 1.4 V vs. RHE, un aumento potencial adicional causa la sobre oxidación excesiva de los oligómeros en la superficie de los nanotubos de carbono o la oxidación de las especies de fósforo sin producir daños significativos en la estructura de los nanotubos de carbono.

En el caso de los MWCNT, se observan diferentes procesos redox con alta reversibilidad, lo que produce un aumento notable en la carga eléctrica de los nanotubos de carbono iniciales. En el caso de los fMWCNT, la presencia de grupos de oxígeno con capacidad de retirar electrones disminuye la densidad de electrones π del nanotubo de carbono y, en consecuencia, el potencial dispersivo, lo que puede resultar en una disminución importante en la adsorción del 4-APPA en la superficie del nanotubo. Además, los grupos oxigenados en la superficie también pueden modificar la orientación de la molécula de 4-APPA, reduciendo así la incorporación de 4-APPA paralela a la superficie de los CNT, impidiendo las reacciones de oligomerización.

La evolución de las relaciones de banda I^D/I^G e I^D/I^G Raman con el potencial de funcionalización sigue una tendencia similar para los MWCNT funcionalizados y fMWCNT. En el caso de los MWCNT aumentan de manera importante desde 1.4 V vs. RHE, lo que indica que cierta oxidación del MWCNT se produce a partir de este potencial, generando defectos en la estructura. Sin embargo, en el caso de fMWCNT, estas relaciones pasan por un máximo que indica que se produce cierta pérdida del material de carbono a

través de reacciones de gasificación o la formación de especies en solución. Estas reacciones también pueden dificultar la interacción con el 4-APPA.

Por lo tanto, la presencia de grupos de oxígeno en la superficie en el MWCNT es perjudicial para lograr la funcionalización a través de reacciones de oligomerización, siendo la unión covalente el mecanismo predominante.

Mejora de la transferencia de electrones en bioelectrodos basados en nanotubos de carbono de pared múltiple modificados electroquímicamente

La modificación electroquímica de MWCNT con 4-APPA ha demostrado la incorporación de diferentes especies de superficie de fósforo y nitrógeno que promueven la inmovilización de PQQ-GDH. Los bioelectrodos se han utilizado en la oxidación de glucosa a condiciones de pH fisiológico. Dependiendo del potencial límite superior utilizado en la modificación electroquímica de los MWCNT, las características morfológicas del recubrimiento enzimático y la interacción con el elemento enzimático mejoran la cinética de transferencia de electrones, obteniendo valores para la constante cinética de la velocidad de transferencia de electrones de 69 a 82 s⁻¹. La mejora en la transferencia de electrones podría asociarse con una mejor orientación del centro activo de la enzima hacia la superficie del electrodo. Además, los diferentes electrodos presentan diferentes cantidades de enzima inmovilizada, corriente catalítica de oxidación y sensibilidad a la oxidación de glucosa.

El bioelectrodo MWCNT-APPA-1.37-GDH muestra los valores más altos de corriente de oxidación de glucosa (1.47 A g⁻¹ obtenida por voltamperometría y 3.06 μA obtenida por cronoamperometría). La sensibilidad obtenida para este electrodo es 53.63 ± 4.72 mA gMWCNT⁻¹ mM⁻¹. Por lo tanto, la modificación electroquímica de MWCNT con especies de fósforo y nitrógeno generadas de la oxidación de 4-APPA puede considerarse una alternativa prometedora para controlar y mejorar el rendimiento electroquímico de los biocatalizadores para aplicaciones adicionales como biosensores.

Bioelectrodos basados en nanotubos de carbono de pared simple preparados electroquímicamente en un paso para el encapsulamiento de enzimas

El atrapamiento electroquímico de s-GDH y PQQ-GDH durante la oxidación del ácido para-amino fenil fosfónico (4-APPA) proporciona un

método simple para la inmovilización de la enzima en la superficie de los SWCNT. Durante la inmovilización electroquímica, también se produce la funcionalización del SWCNT con grupos de fósforo y nitrógeno. La interacción adecuada entre el SWCNT funcionalizado y la enzima parece estar determinada por los grupos de fósforo incorporados en el material durante las películas co-depositadas electroquímica. En presencia del sustrato enzimático, se obtiene una corriente catalítica que demuestra el eficiente contacto enzima-electrodo. Estos bioelectrodos muestran una mejora en la densidad de corriente electrocatalítica y, en consecuencia, en la sensibilidad a la oxidación de la glucosa en comparación con el electrodo preparado por el método convencional de *drop-casting*. La sensibilidad del bioelectrodo muestra una alta dependencia con el límite de potencial límite superior empleado en el proceso de síntesis, siendo mayor la inmovilización enzimática a alto potencial. El bioelectrodo preparado con un proceso de un solo paso (procedimiento 2) muestra una sensibilidad, referida a la cantidad de enzima, aproximadamente el doble que el electrodo preparado usando el procedimiento 1 y seis veces mayor que el bioelectrodo preparado por *drop-casting*.

La metodología propuesta ofrece una plataforma para la preparación de electrodos enzimáticos en condiciones no agresivas de síntesis sobre materiales a base de carbono nanoestructurados, empleando baja cantidad de enzima en la superficie del electrodo y alta sensibilidad. Esta metodología podría extenderse a otras enzimas solubles, asegurando una buena reproducibilidad, escalabilidad y una mejor transferencia directa de electrones, que pueden tener una aplicación potencial como ánodo en células biocombustibles o en aplicaciones como biosensor electroquímico.

Biosensor de glucosa electroquímico sin metal basado en material de carbono N-dopado

Se desarrolló un biosensor enzimático de glucosa basado en glucosa oxidasa inmovilizada en un material de carbono dopado con nitrógeno, obtenido por tratamiento térmico de polianilina. Este biosensor es un material de carbono libre de metal. El material de carbono dopado con N tiene una elevada actividad catalítica hacia la reacción de reducción de oxígeno debido a la presencia de especies N cuaternarias, incluso después de la inmovilización de la glucosa oxidasa. El proceso redox reversible en superficie a $-0,42$ V vs.

Ag/AgCl relacionado con el cofactor FAD/FADH₂ demuestra la inmovilización exitosa de la enzima en el electrodo.

La detección indirecta de glucosa se llevó a cabo siguiendo la variación de la densidad de corriente de la reacción de reducción de oxígeno generada por el aumento de la concentración de glucosa, como consecuencia de la reacción enzimática de la glucosa oxidasa a un potencial de -0.4 V vs. A/AgCl. La sensibilidad del biosensor preparado presenta buenos valores hacia la detección de glucosa, sin dependencia de la concentración de oxígeno en la solución ($23.57 \pm 1.77 \mu\text{A cm}^{-2} \text{ mM}^{-1}$ y $24.29 \pm 1.12 \mu\text{A cm}^{-2} \text{ mM}^{-1}$ para condiciones de saturación de O₂ y atmosféricas, respectivamente). Sin embargo, la velocidad de reacción para la regeneración de la enzima del estado reducido al estado oxidado afecta el rango de detección lineal del biosensor, siendo más amplio para las condiciones de saturación de O₂ donde la re-oxidación de la enzima se lleva a cabo rápidamente. Además, el biosensor muestra una reproducibilidad, repetibilidad y estabilidad, con valores aceptables. A pesar del pequeño efecto de interferencia del ácido úrico en la detección de glucosa, la alta afinidad y sensibilidad hacia la oxidación de la glucosa todavía permite la aplicación de este biosensor en la detección de glucosa en muestras reales como orina y bebidas azucaradas comerciales.

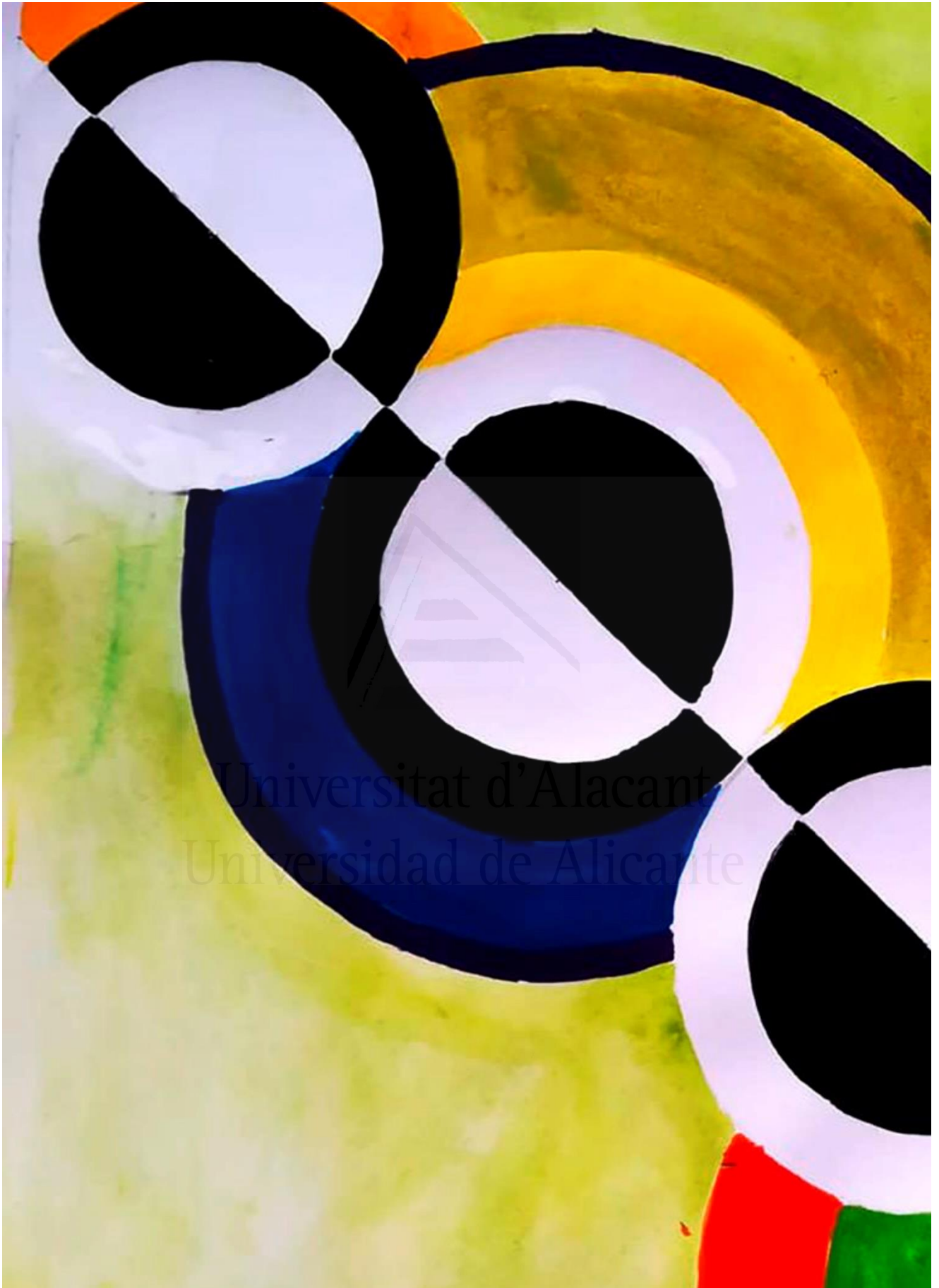
Desarrollo de fMWCNT modificado con nanopartículas de oro para la inmunodetección cronoamperométrica del antígeno prostático específico

Se desarrollaron biosensores electroquímicos del antígeno prostático específico (PSA) basados en fMWCNT-AuNPs-Ab con diferente distribución de tamaño de nanopartículas. Para estudiar el efecto del tamaño de las nanopartículas en el rendimiento del biosensor, se realizaron dos síntesis diferentes, controlando la relación molar PVP/Au para obtener nanopartículas de oro con una distribución ancha y estrecha, y un diámetro promedio de 9,5 nm y 6.6 nm para relaciones PVP/Au de 0.5 y 50, respectivamente. La incorporación de las nanopartículas metálicas se verificó por voltamperometría cíclica, lo que demostró que la distribución estrecha del tamaño de las nanopartículas presenta una mayor área superficial electroquímicamente activa.

Los materiales del transductor preparados con diferentes relaciones PVP/Au mostraron una disminución de la densidad de corriente de los procesos redox asociados con la formación de óxido de oro después del proceso de

inmovilización del elemento de biorreconocimiento, como consecuencia del efecto de bloqueo de esta molécula en la superficie. Este comportamiento también se observó para el ferroceno (Fc-Fc^+) empleado como sonda redox. Al mismo tiempo, los espectros XPS para S2p demostraron la presencia del enlace S-Au, debido a la inmovilización covalente de los anticuerpos en la superficie de las nanopartículas. Además, la distribución estrecha del tamaño de nanopartículas de Au promueve una mayor inmovilización, que se evidenció como un aumento en la cantidad de especie S-Au.

La detección electroquímica del PSA por cronoamperometría proporcionó un método rápido para la detección de este compuesto, que aprovecha los efectos estéricos en la superficie del electrodo creados por la formación del inmunocomplejo entre antígeno y los anticuerpos, que actúa como una barrera difusiva para las especies electroactivas, que se traduce en una disminución en la intensidad actual de los procesos de oxidación. Aunque se puede observar una disminución en la corriente con el aumento de la concentración de PSA en ambos biosensores, el rango lineal y las concentraciones de saturación están influenciados por el tamaño de las nanopartículas, siendo los electrodos fMWCNT-AuNPs-50-Ab los que presenta el mejor rendimiento con un mayor rango lineal entre 0 y 6 ng mL^{-1} y una buena sensibilidad de $4.74 \text{ mA ng}_{\text{PSA}} \text{ g}_{\text{fMWCNT}}^{-1} \text{ mL}^{-1}$, lo que permite la detección en muestras humanas.



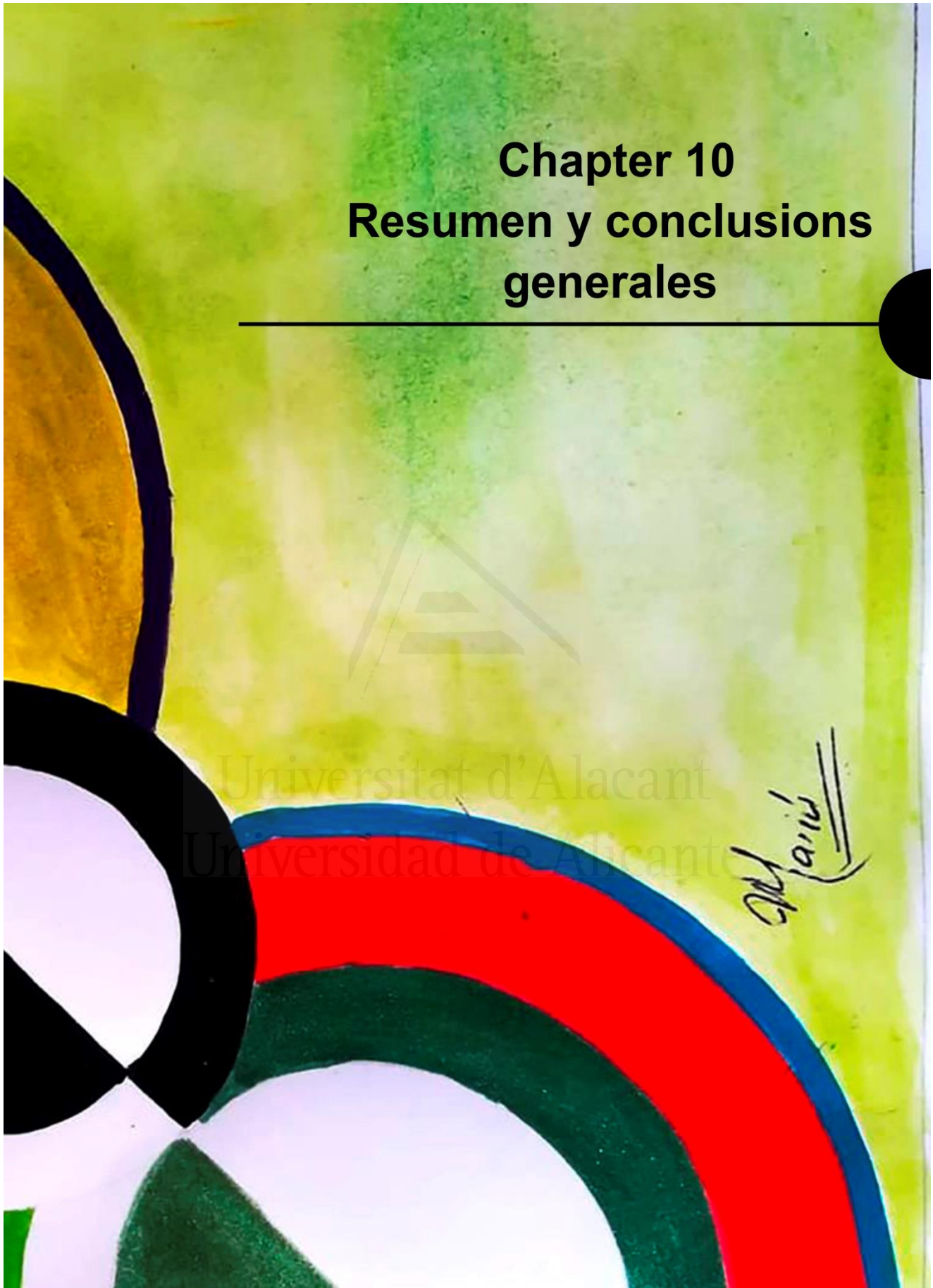
Universitat d'Alacant
Universidad de Alicante

Chapter 10

Resumen y conclusiones generales

Universitat d'Alacant
Universidad de Alicante

Andrés



Los materiales carbonosos presentan una gran versatilidad de propiedades que han despertado gran interés en el desarrollo de nuevas aplicaciones^{1,2}. Su gran abundancia, procedimientos de síntesis escalables y la gran capacidad de adaptar y modificar sus propiedades mediante técnicas de modificación química³⁻⁶, han permitido su aplicabilidad como adsorbente en la eliminación de contaminantes, en el desarrollo de catalizadores de alto rendimiento para la producción de energía, en el almacenamiento de energía, y en aplicaciones biomédicas como en la sustitución de tejidos, liberación de fármacos o en la detección de analitos de interés biológico^{7,8,17,18,9-16}.

Dentro de las aplicaciones más destacables, se encuentran las que implementan sistemas electroquímicos acoplados con elementos biológicos en el desarrollo de tecnologías limpias para la generación de energía (células de combustible bioelectroquímicas-*EBFC*, por sus siglas en inglés) y dispositivos selectivos de detección y cuantificación de sustancias (biosensores electroquímicos)¹⁹⁻²¹. En este sentido, los materiales de carbono nanoestructurados tales como nanotubos de carbono (*CNT*, por sus siglas en inglés) han sido empleados constantemente en el desarrollo de diferentes biocatalizadores, debido a su notable estabilidad química, biocompatibilidad y propiedades catalíticas y electrónicas^{1,22,23}. Una de las propiedades más interesantes de los *CNT* radica en la capacidad de funcionalización y adaptabilidad de las propiedades superficiales, a través de diferentes procedimientos de modificación química que pueden ser no covalentes o covalentes. La incorporación de funcionalidades en superficie se convierte en una ruta sobresaliente para la síntesis de materiales con propiedades mejoradas para aplicaciones específicas.

Los primeros enfoques de funcionalización han sido centrados en la oxidación de los *CNT*, empleando disoluciones ácidas oxidantes para incorporar especies oxigenadas en superficie, como grupos carboxílicos, lactonas, quinonas e hidroxilos²⁴⁻²⁶, los cuales además de mejorar la dispersabilidad de los *CNT* en disolventes de tipo polar como el agua, también pueden servir de anclaje, promoviendo la inmovilización de los bioelementos empleados como biocatalizadores. No obstante, en la actualidad diferentes tipos de funcionalidades han sido incorporadas en nanotubos de carbono, empleando reacciones químicas orgánicas, tales como la amidación, hidrogenación, anclaje (*grafting*) de moléculas y/o polimerización sobre la

superficie de los nanotubos de carbono^{27,28}. En estos procesos de funcionalización, la generación de especies radicales de alta reactividad hacia los átomos de carbono en la estructura del CNT son una parte fundamental en la formación de enlaces covalente con el material carbonoso²⁹⁻³².

Entre los diferentes procedimientos de modificación superficial, ciertamente los procesos de funcionalización electroquímica han demostrado ser una alternativa prometedora³³⁻³⁵. Adicionalmente, la versatilidad que ofrecen los métodos electroquímicos para obtener de manera controlada y selectiva funcionalidades en la superficie del material de carbón, bajo condiciones de síntesis no agresivas y localizadas en la interface electrodo-electrolito, hacen de esta clase de métodos una prometedora ruta para la síntesis de materiales con altas prestaciones en diferentes campos de aplicación^{36,37}. Por ejemplo, la oxidación electroquímica con maleimida sobre electrodos basados en materiales carbonosos genera una capa modular con grupos carboxílicos y amino en la superficie del electrodo carbonoso, los cuales interaccionan covalentemente con una enzima deshidrogenasa. Las características físico-químicas de la superficie del electrodo permiten orientar el centro activo de la enzima sobre la superficie del mismo, reduciendo la distancia para la transferencia de electrones, promoviendo la transferencia directa y una mayor densidad de corriente catalítica, asociada a la oxidación del sustrato³⁸. Así mismo, la modificación de la interacción electrodo-biomolécula ha permitido generar sistemas de transferencia directa entre el centro activo de elementos enzimáticos como la hemoglobina o el citocromo C³⁹⁻⁴¹; aunque también se han observado sistemas de transferencia directa en oxidoreductasas como la glucosa oxidasa³³. Así mismo, la presencia de especies nitrogenadas en la estructura de los materiales carbonosos, además de que pueden facilitar la inmovilización de biomoléculas, proveen una alta actividad catalítica para la oxidación de ácido ascórbico, ácido úrico y peróxido de hidrógeno, debido a la generación de sitios activos para la transferencia de electrones, sirviendo como materiales electródicos en el desarrollo de sensores electroquímicos^{42,43}.

Partiendo del principio de que la correcta interacción electrodo-bioelemento es uno de los aspectos críticos y determinantes en el óptimo desempeño de un dispositivo bioelectroquímico^{44,45}, la presente tesis doctoral ha desarrollado diferentes procedimientos de síntesis y modificación de materiales carbonosos, con el fin de obtener superficies biofuncionales con

diferentes funcionalidades que permitan promover el desarrollo efectivo de bioelectrodos para su aplicación en dispositivos electroquímicos.

Con el fin de obtener superficies activas que faciliten la inmovilización de bioelementos, se ha seleccionado estudiar en la primera etapa de la tesis (capítulos 3 y 4), la funcionalización electroquímica, empleando el ácido 4-amino fenil fosfónico (4-APPA) como agente modificante en medio acuoso, como método de modificación superficial de diversos materiales carbonosos: nanotubos de carbono de pared simple (SWCNTs), nanotubos de pared múltiple (MWCNTs), grafeno y óxido de grafeno. En estos procedimientos de modificación superficial, se generan especies de nitrógeno y de fósforo en la superficie de los materiales carbonosos mediante polarización potenciodinámica (mediante voltametría cíclica) variando el potencial límite superior (1.0, 1.2, 1.4, 1.6 y 1.8 V vs. RHE) en H_2SO_4 0.5M + 4-APPA 1 mM.

Los nanotubos de carbono de pared simple (SWCNT, por sus siglas en inglés), presentan la formación de procesos redox en superficie a bajos potenciales de oxidación (1.0 V), lo cual no se evidencia en los otros nanotubos de carbono (MWCNT). Al incrementar los potenciales de oxidación se presenta una contribución en los valores de densidad de corriente a potenciales positivos, que se encuentra acompañada por la formación de un proceso irreversible alrededor de 1.1 V vs. RHE, aproximadamente, para todos los tipos de nanotubos de carbono empleados, el cual es directamente asociado a la oxidación del 4-APPA. En contraste, el óxido de grafeno (GO por sus siglas en inglés), el óxido de grafeno reducido electroquímicamente (rGO por sus siglas en inglés), y el grafeno, llamado en la presente tesis como K4, muestran un desplazamiento a mayores potenciales para el potencial de inicio y potencial en el máximo del pico de oxidación del 4-APPA; lo cual sugiere que la estructura curva de la lámina en los nanotubos de carbono tiene un mayor efecto catalítico en la oxidación electroquímica del 4-APPA.

Se puede considerar que el 4-APPA puede adsorberse en la superficie de los nanotubos de carbono mediante interacciones π - π y, posteriormente, el incremento de potencial permite producir la oxidación del mismo y el crecimiento de oligómeros en la superficie del nanotubo de carbono. Por tanto, la estructura y la química superficial del material de partida (SWCNT o MWCNT) tienen una influencia muy importante en el proceso de funcionalización electroquímica.

Teniendo en cuenta los mecanismos de oxidación electroquímica de la anilina y sus derivados, que se inicia con la formación de un radical que ataca a una nueva molécula generando un dímero, que crece formando oligómeros y finalmente la polianilina o sus derivados, en este caso, se podría suponer que la formación del radical produce un ataque a la estructura aromática del material de carbón, promoviendo la funcionalización covalente en superficie. A su vez, las reacciones entre las especies radicales generadas, conllevarían a la formación de oligómeros, los cuales pueden crecer en la superficie de los nanotubos de carbono que da lugar a una funcionalización no covalente.

Una vez la oxidación del 4-APPA ocurre en la superficie del electrodo, se observan diferentes procesos redox a menores potenciales en el voltagrama, los cuales presentan un incremento en la densidad de corriente con el aumento del ciclado y el potencial aplicado; lo cual es concordante con el proceso de formación y crecimiento de oligómeros, generados por la oxidación del 4-APPA en la superficie del material carbonoso. En este sentido, los oligómeros pueden adsorberse en la superficie de los nanotubos de carbono dando lugar a una funcionalización no-covalente. Este mecanismo podría explicar la presencia de estructuras aglomeradas no grafénicas sobre las paredes del nanotubo observadas en las micrografías TEM, las cuales concuerdan con la presencia de depósitos de pequeñas cadenas sobre la superficie del material de carbón.

La caracterización electroquímica en ausencia del 4-APPA en medio ácido muestra que las especies electroactivas desarrolladas en la superficie de los nanotubos de carbono corresponden a especies en superficie, las cuales presentan una alta reversibilidad electroquímica y gran simetría; lo cual sugiere que existe una importante interacción entre el nanotubo de carbono y las funcionalidades generadas en superficie, lo cual facilita y promueve la transferencia de carga. No obstante, en los nanotubos de carbono (fMWCNTs) modificados mediante oxidación con ácido nítrico, y que presentan diferentes especies oxigenadas superficiales, los procesos redox consecuencia de la funcionalización, no presentan una contribución significativa en carga y densidad de corriente como lo observado en los SWCNT y MWCNT, de hecho, en algunos casos no se evidencia una respuesta electroquímica diferente al nanotubo de carbono sin modificar, lo cual puede relacionarse con la disminución en la conductividad y la pérdida de la estructura conjugada presente en los nanotubos de carbono. La actividad electroquímica asociada a

las funcionalidades y los valores de capacidad asociada a la doble capa eléctrica en los materiales carbonosos modificados, presentan una disminución significativa con el aumento de pH. En el caso de las funcionalidades a bajos potenciales, estas empiezan a disminuir sus valores de densidad de corriente a pH neutro o alcalino, al mismo tiempo que se observa un incremento en los valores de separación de pico, haciendo más irreversible los procesos redox, de igual forma a lo observado en previos estudios de productos tipo polianilina.

Teniendo en cuenta que los procesos de modificación electroquímica, mayoritariamente ocurren en superficie, el análisis mediante espectroscopia fotoelectrónica de rayos-X (XPS) revela el grado de incorporación en N, O y P, así como la naturaleza química de las especies. Inicialmente, se evidencia que el contenido en oxígeno y nitrógeno presenta un incremento proporcional con el aumento del potencial límite de oxidación, lo cual es concordante con las condiciones oxidativas a dichos potenciales que, como resultado, inducen una mayor formación de cadenas de oligómeros mediante funcionalización no-covalente y un mayor acoplamiento covalente de las funcionalidades. En cuanto al contenido en fósforo se observa un valor máximo de incorporación entre los potenciales de 1.4 y 1.6 V para los nanotubos de carbono, y de 1.5 V para los materiales basados en grafeno. A potenciales superiores ocurre una disminución en la concentración de dicha especie, lo cual puede ser resultado de una degradación y/o desorción de las funcionalidades de fósforo en la estructura. Aunque se ha evidenciado que en los materiales con alto contenido en grupos oxigenados, las especies electroactivas inducidas en el material durante el proceso de modificación electroquímica no presentan importantes contribuciones redox, se observa un mayor grado de incorporación de fósforo (1.14% at en el GO) en comparación con los materiales no oxidados o sometidos a reducción (MWCNT, SWCNT y rGO), sugiriendo que las especies oxigenadas pueden estar interactuando directamente con el 4-APPA y las cadenas de oligómeros generadas.

Los espectros XPS asociados al fósforo muestran dos contribuciones correspondientes a grupos fosfónico y grupos tipo fosfóricos, siendo esta última más significativa a potenciales superiores a 1.4 V. En este sentido, la disminución de la concentración de grupos fosfónico mientras las especies tipo fosfórico incrementan, corroboran que durante el proceso de modificación del material carbonoso ocurre un proceso de oxidación del grupo fosfónico; estos grupos, a potenciales superiores (1.8 V), pueden presentar hidrólisis y por ende

su pérdida en disolución, generando la disminución de la concentración de fósforo. Las especies de nitrógeno generadas corresponden a grupos nitrogenados neutros tipo aminas e iminas, y también especies nitrogenadas cargadas positivamente y que corresponden a especies observadas en la polianilina y sus derivados. Por tanto, corroborarían la presencia de oligómeros del tipo polianilina.

Debido a que los procesos de funcionalización electroquímica con 4-APPA pueden generar modificaciones significativas en la estructura y propiedades de los materiales carbonosos, el grado de modificación en los materiales fue evaluada por espectroscopia Raman. El análisis de las relaciones entre las bandas G y D obtenidas en los espectros, asociadas a las contribuciones de la estructura grafénica sp^2 y la presencia de defectos sp^3 , respectivamente, muestran en todos los casos para los nanotubos de carbono, un incremento de la relación I_D/I_G con el potencial, lo cual demuestra que durante el proceso de modificación electroquímica con 4-APPA existe un incremento de las contribuciones relacionada a estructuras tipo sp^3 , que puede asociarse a la pérdida de estructura grafénica, debido al posible enlace del nanotubo con el radical procedente del 4-APPA. Sin embargo, al analizar la zona de bajas frecuencias para los *SWCNT*, la cual se encuentra asociada a los modos de vibración axial de los nanotubos (*RBM*, por sus siglas en inglés), parámetro altamente sensible a los cambios estructurales que puedan presentar los *SWCNTs*, se observan pocas modificaciones en las diferentes contribuciones, lo cual conllevaría un bajo grado de modificación del material carbonoso, pese a las condiciones de oxidación electroquímica a las cuales fueron sometidos.

Con base en los resultados obtenidos en los capítulos 3 y 4, en los cuales se ha podido desarrollar la modificación electroquímica con N y P sobre la superficie de materiales carbonosos sin alterar significativamente sus propiedades, se propone su utilización en el desarrollo de biocatalizadores para la oxidación de glucosa para su futura utilización como bioanodo o biosensor de glucosa.

De esta manera, se procede a evaluar el efecto del proceso de modificación superficial desarrollado en el capítulo 4 sobre los materiales carbonosos en la síntesis de biocatalizadores. Se seleccionaron *MWCNT* modificados con 4-APPA en diferentes condiciones para evaluar su efecto en la transferencia electrónica de la enzima modelo *PQQ-GDH*. En este estudio, se utilizaron

electrodos de MWCNTs modificados con 4-APPA a 0.97, 1.17 y 1.37 V vs. Ag/AgCl (3 M KCl) en H₂SO₄ 0.5 M + 4-APPA 1 mM durante 10 ciclos a 10 mV·s⁻¹, como electrodos en los que se realiza la inmovilización de la enzima glucosa deshidrogenasa (GDH) dependiente de la pirroloquinolina quinona (PQQ). Tras la modificación, los nanotubos de carbono presentan diferentes procesos redox superficiales a condiciones neutras (pH = 7.2). Posteriormente, fueron modificados con *PQQ-GDH* mediante el método de *drop-casting*. Una vez incorporado el elemento enzimático se aprecia una disminución de la doble capa eléctrica ocasionada por el recubrimiento enzimático. De igual forma, a un potencial de -0.11 V se evidencia la aparición de un proceso reversible asociado a la transferencia de electrones del cofactor (PQQ) del elemento enzimático generado. En este sentido, la concentración determinada de PQQ, asociada a la enzima presente, tiene un valor máximo para las muestras modificadas a 0.97 V, valor en el cual se produce la mayor incorporación de fósforo en el electrodo tras la modificación. En este aspecto, los grupos fosfónicos parcialmente desprotonados pueden estar generando una carga negativa parcial de la superficie de los nanotubos de carbono, lo cual permitiría que una mayor cantidad del elemento enzimático, cuya carga neta es positiva a las condiciones de pH en las cuales ocurre la inmovilización de la enzima, quede retenida en la superficie. De esta manera, las interacciones electrostáticas pueden estar facilitando la inmovilización en el electrodo, lo cual es concordante con las morfologías evidenciadas por microscopía FESEM, en las cuales, a dicho potencial se evidencia un recubrimiento de alta densidad sobre la superficie de los *MWCNT* modificados.

Al analizar la actividad catalítica hacia la oxidación de glucosa voltaméricamente y cronoamperométricamente (polarizando a 0.35 V vs. Ag/AgCl (3 M KCl)), se evidencia que a un potencial de modificación de 1.37 V, los electrodos presentan un aumento considerable en la densidad de corriente asociada a la oxidación de glucosa, lo cual es correlacionado con el incremento en los valores de la constante de transferencia de carga heterogénea que pasa de 69.2 a 81.7 s⁻¹ con el aumento del potencial de modificación. Al analizar las rectas de calibrado, todos los biosensores presentan el comportamiento típico de Michaelis-Menten; sin embargo, el valor de la constante de Michaelis-Menten presenta una disminución con el potencial de modificación, alcanzando valores de 1.36 mM para los electrodos sintetizados a 1.37 V, lo cual sugiere que la interacción

entre el sustrato y la enzima es mucho mayor con el incremento de potencial. En este sentido los valores de sensibilidad en el mismo rango de linealidad de 0.1-1 mM muestran que los electrodos modificados a 1.37 V presentan un incremento de la sensibilidad alrededor del 37%. Lo anterior sustenta la hipótesis de que la elevada interacción entre la interface del material carbonoso y la enzima, puede estar generando una mejor orientación del elemento enzimático en la superficie del electrodo o que los MWCNTs funcionalizados mejoren la transferencia de electrones hacia el electrodo. Este comportamiento también se puede evidenciar con una retención de la corriente de detección en el test de estabilidad realizado durante 15 días. No obstante, la disminución en la actividad catalítica observada en los electrodos enzimáticos, puede ser atribuida a los procesos de protonación de los grupos R-POO- a causa de la disminución local de pH después de la formación de ácido glucónico. Este proceso disminuiría la carga neta de la superficie del electrodo, generando el desacoplamiento de la enzima adsorbida por interacciones electrostáticas.

Teniendo en cuenta que el mecanismo de modificación electroquímica propuesto genera especies funcionales ancladas y/o adsorbidas en la superficie del nanotubo, las cuales facilitan la interacción con el elemento enzimático empleado, se evalúa la utilización de dicho proceso de modificación en la inmovilización enzimática mediante encapsulamiento electroquímico. Inicialmente, se realiza el proceso de oxidación electroquímica del 4-APPA en condiciones menos ácidas (pH=4.08 aproximadamente), en presencia de la enzima, con el fin de no afectar las propiedades catalíticas de esta, observándose el proceso de oxidación irreversible a 0.65 V vs. Ag/AgCl (3 M KCl). Aunque la cinética del proceso se ve ligeramente retardada por las condiciones evaluadas, se conserva el típico comportamiento previamente observado en condiciones de mayor acidez, en el cual tras la oxidación del 4-APPA se observa la formación de distintos procesos redox en superficie, los cuales presentan un incremento en los valores de densidad de carga con el ciclado. En este sentido, una vez incorporado el elemento enzimático modelo empleado (glucosa deshidrogenasa dependiente de pirroloquinoleína quinona-*PQQ-GDH*), se observa que la presencia del elemento enzimático no afecta al proceso de generación de oligómeros, ni a la actividad electroquímica de dichas especies en superficie. Para efectos comparativos se llevó a cabo el encapsulamiento de la enzima activa (con el cofactor PQQ) y no activa (sin

PQQ). En éste último caso, se procede a la incorporación del centro activo una vez encapsulado en el electrodo. En el caso del encapsulamiento de la enzima activa, se aprecia que el elemento enzimático es incorporado en la matriz con el incremento en los valores de densidad de carga de un proceso a bajo potencial llamado A-A', el cual puede estar asociado al cofactor (PQQ) en la enzima. Tras la incorporación, se observa en los bioelectrodos sintetizados, un proceso redox altamente reversible a potenciales cercanos a -0.11 V vs. Ag/AgCl (3 M KCl), lo cual ha sido asociado al proceso redox del cofactor PQQ. Dependiendo de los potenciales de oxidación empleados, se observa que existe una mejora en la sensibilidad del biocatalizador hacia la oxidación de glucosa, vista como un incremento en la corriente catalítica hacia la oxidación de glucosa, siendo las muestras modificadas a 1.15 V vs. Ag/AgCl (3 M KCl) sobre SWCNT las que evidencian una mayor corriente catalítica. Al analizar las condiciones de encapsulamiento, se aprecia que existe una correlación entre el incremento de la corriente catalítica del bioelectrodo con el contenido de fósforo, determinado por XPS, en el cual, los electrodos no presentan importantes modificaciones en la naturaleza de las especies químicas de fósforo. En este sentido la mejora en la actividad catalítica puede estar asociada a que, en realidad, las especies de fósforo durante el proceso de encapsulamiento pueden estar facilitando la interacción con la enzima, promoviendo la transferencia electrónica desde el cofactor hacia el electrodo. De igual manera, la mejora en la actividad catalítica genera valores de sensibilidad superiores a los evidenciados para los electrodos preparados por *drop-casting*, y en los cuales hay presencia de PQQ libre adsorbido en la superficie del electrodo, que puede servir como especie mediadora. Es importante destacar que la diferencia en las cantidades de enzima empleadas durante la síntesis (menores que en el encapsulamiento), demuestran que las muestras encapsuladas presentan un contacto más íntimo entre el electrodo y la enzima, ocasionando una mejor interacción con el electrodo. De igual forma, las muestras electroquímicamente encapsuladas presentan valores bajos de la constante aparente de Michaelis-Menten; lo cual sugiere que existe una importante interacción entre el elemento enzimático y la superficie del electrodo. Lo anterior conlleva a suponer que las diferentes funcionalidades generadas, pueden interactuar con la enzima y promover una mayor velocidad en la transferencia de electrones o inclusive orientar el centro activo de la enzima en una posición más óptima para la transferencia de los electrones con el electrodo.

A partir de polianilina sintetizada químicamente se pueden preparar materiales carbonosos dopados con heteroátomos (nitrógeno), tras un tratamiento térmico en dos etapas. En esta tesis, se propone en el capítulo 7 su uso como transductor y catalizador para la detección indirecta de glucosa, teniendo en cuenta la elevada actividad catalítica del material carbonoso sintetizado hacia la reducción de oxígeno, siendo posible así el desarrollo de un biosensor de glucosa de primera generación. A partir del proceso de síntesis se ha logrado obtener de manera selectiva especies nitrogenadas tipo N-grafítico en el material carbonoso, el cual como se ha observado en previas investigaciones, genera sitios que facilitan la reacción de reducción de oxígeno, siendo altamente sensible a la concentración de oxígeno. En este sentido, se inmovilizó glucosa oxidasa (GOx) en la superficie del material carbonoso dopado con nitrógeno para obtener un bioelectrodo sensible a la oxidación de glucosa. La incorporación del material enzimático genera principalmente un proceso redox a -0.42 V vs. Ag/AgCl (3 M KCl), que presenta una alta reversibilidad electroquímica ($\Delta E \sim 33$ mV), relacionado con el proceso redox del cofactor de la GOx (FAD/FADH₂). Una vez en presencia de glucosa a condiciones aeróbicas, se aprecia una disminución de las corrientes de reducción asociadas a la reducción del oxígeno molecular en disolución, esto como consecuencia a la disminución en la concentración de dicha especie por la reacción enzimática de oxidación de glucosa.

Las rectas de calibrado para los electrodos PANI-TT-GOx-GA-Nafion muestran un comportamiento típico de Michaelis-Menten, con un valor de límite de detección (*LOD*, por sus siglas en inglés) de $1 \mu\text{M}$. Dependiendo de la concentración de oxígeno, condiciones saturadas o atmosféricas, se observa que los rangos de linealidad para el biosensor varían de $5 \mu\text{M}$ - 5 mM a $10 \mu\text{M}$ - 1 mM , respectivamente, sin variaciones en la sensibilidad ($23.57 \pm 1.77 \mu\text{A cm}^{-2} \text{ mM}^{-1}$) hacia la oxidación de glucosa y los valores de la constante aparente de Michaelis-Menten ($K_m^{\text{app}} = 2.74$). Pese a que los estudios de posibles interferentes demuestran que los sensores presentan una cierta influencia hacia el ácido úrico, la sensibilidad del electrodo hacia el ácido úrico, es menos significativa que la señal generada por la glucosa. No obstante, los resultados de determinación de glucosa en muestras de orina mediante el método de adición estándar, demuestran que el biosensor, es una plataforma adecuada para la detección de glucosa en fluidos fisiológicos, con una alta sensibilidad si se compara con otros biosensores desarrollados empleando

catalizadores metálicos. Adicionalmente los valores de reproducibilidad y estabilidad del biosensor, lo hacen una alternativa prometedora para su aplicabilidad en la detección de éste compuesto en otros fluidos como sangre, suero sanguíneo, sudor o bien, en el sector de la alimentación en bebidas azucaradas.

En el capítulo 8 de esta Tesis Doctoral, se han modificado nanotubos de carbono de pared múltiple con nanopartículas de oro para la detección cronoamperométrica del antígeno prostático específico (*PSA*, por sus siglas en inglés), marcador tumoral clásico asociado al cáncer de próstata. En este trabajo se ha sometido inicialmente a los MWCNT a un proceso de funcionalización química en disolución HNO_3 3 M, con el propósito de desarrollar grupos oxigenados en los nanotubos que permitan mejorar su dispersabilidad en agua, obteniendo dispersiones con concentraciones de $1\text{mg}\cdot\text{mL}^{-1}$ de la misma manera que se realizó en el capítulo 4. Teniendo en cuenta que el *PSA* no muestra actividad electroquímica y su respectiva oxidación ocurre a elevados potenciales donde puede generarse la oxidación de otras especies, se realiza la incorporación de un anticuerpo monoclonal específico al *PSA*. Con el fin de promover la inmovilización, los nanotubos de carbono funcionalizados (fMWCNT) son modificados con nanopartículas de oro sintetizadas por el método de reducción por disolvente, el cual, permite controlar la distribución de tamaño de las nanopartículas mediante la variación de la relación entre el polímero protector, polivinilpirrolidona (PVP), y el precursor de oro, obteniendo una distribución de tamaño de partícula ancha para relaciones $\text{PVP}/\text{Au}=0.5$ y distribución de tamaño de partícula estrecha para relaciones $\text{PVP}/\text{Au} = 50$, traducida en nanopartículas de mayor y menor tamaño, respectivamente. Es importante destacar que se obtuvo una mayor cantidad de carga metálica en las muestras con relación $\text{PVP}/\text{Au} = 50$, lo cual a su vez permite obtener mayor área electroactiva (*EASA*, por sus siglas en inglés) de las nanopartículas de oro, observada voltamétricamente en la carga asociada al proceso de reducción del óxido de oro. Los materiales sintetizados fMWCNT-AuNPs-0.5 y fMWCNT-AuNPs-50 son posteriormente modificados con anticuerpos monoclonales, los cuales son adsorbidos y mediante interacciones covalentes a través de los grupos tiol presentes en los residuos de cisteína de las cadenas de aminoácidos, son inmovilizados en los electrodos. El proceso de inmovilización causa una disminución en la carga almacenada del proceso de reducción del óxido de oro, lo cual está asociado a

un bloqueo parcial de la superficie del metal. Adicionalmente, los espectros XPS muestran una mayor contribución de las especies Au-S en las muestras con un tamaño de nanopartículas menor (MWCNT-AuNPs-50), lo cual sugiere que existe una mayor cantidad de especies inmovilizadas en comparación con las muestras de menor relación PVP/Au como corresponde a una mayor área electroactiva.

A partir de los electrodos sintetizados es posible llevar a cabo la detección indirecta del PSA, teniendo en cuenta que la formación del complejo anticuerpo-antígeno (Ab-Ag) genera efectos estéricos que bloquean la transferencia electrónica de las especies electroactivas. Para ello, se empleó como sonda redox el ferroceno hexafluorofosfato (Fc) para la medida indirecta del PSA. En esta medición se evidenció que los electrodos con relación PVP/Au = 50 presentan una mayor densidad de corriente para el proceso redox Fc/Fc⁺ del mediador, lo cual sugiere que la distribución de tamaño de partícula menor, permite que haya mayor área para la oxidación del ferroceno. De igual manera, la incorporación del anticuerpo en la superficie del electrodo genera una disminución de la misma manera que lo observado en los procesos redox asociados al oro, lo cual permite emplear ésta especie como sonda para la detección indirecta del PSA.

Se utilizó la cronoamperometría bajo agitación constante para mejorar el flujo del mediador redox al electrodo. Una vez añadido el analito (PSA), manteniendo un tiempo de reacción aproximado de tres minutos para la formación del inmunocomplejo, se realiza saltos potencioestáticos hasta 1.0 V vs. RHE, en donde se produce la oxidación del Fc. Los valores de densidad de corriente en los perfiles cronoamperométricos muestran que ambos materiales presentan una disminución en la corriente de oxidación del ferroceno conforme incrementa la concentración de PSA. No obstante, al analizar las rectas de calibrado se observa que las muestras con relación PVP/Au = 50 presentan un incremento significativo del rango de linealidad, en comparación con las muestras con relación de 0.5, lo cual podría estar asociado a la mayor cantidad de anticuerpos inmovilizados en superficie, como se observó en los espectros XPS. De igual forma, el comportamiento visto en las rectas de calibrado, sugiere que los electrodos presentan un comportamiento tipo Langmuir en el cual se alcanza la saturación del electrodo por un agotamiento del sitio activo, que en este caso corresponde con el anticuerpo inmovilizado. Adicionalmente, los niveles de sensibilidad y linealidad obtenidos para esta

clase de biosensores se encuentran en valores óptimos y adecuados en su utilización para la detección de dicho analito. Es importante destacar que los resultados obtenidos demuestran que la distribución y tamaño de las nanopartículas de oro tienen un efecto significativo en el desempeño del biosensor y sus parámetros analíticos.

Esta tesis doctoral se ha enfocado al desarrollo de materiales carbonosos nanoestructurados funcionalizados electroquímicamente para aplicaciones bioelectroquímicas. En ese sentido, la funcionalización electroquímica de diferentes tipos de nanotubos de carbono (SWCNT, MWCNT y fMWCNT), así como materiales basados en grafeno, a partir de la oxidación electroquímica del ácido amino fenil fosónico (4-APPA) por voltametría cíclica, ha permitido la incorporación de diferentes grupos funcionales de N y P. El proceso de funcionalización, en el cual oligómeros electroactivos que pueden ser adsorbidos y envolver la superficie de los nanotubos de carbono, así como especies enlazadas covalentemente, favorece la generación de diferentes procesos redox superficiales que dependen del potencial aplicado.

La presencia de grupos oxigenados genera un efecto negativo en la funcionalización de los fMWCNTs, específicamente en las reacciones de oligomerización, las cuales no están tan favorecidas como en los MWCNTs originales. Esto puede ser una consecuencia de la capacidad de los grupos oxigenados de retirar electrones, que disminuye la densidad de electrones π en los CNTs, y provoca una modificación de la orientación de la molécula de 4-APPA que impide las reacciones de oligomerización.

La funcionalización electroquímica de nanotubos de carbono con 4-APPA en presencia de una enzima, permite el encapsulamiento electroquímico de s-GDH y PQQ-GDH durante la oxidación del 4-APPA. Se trata de un método simple para la inmovilización de la enzima en la superficie de los SWCNT en un proceso de síntesis de un paso, al mismo tiempo que se produce la funcionalización de los SWCNTs con grupos de fósforo y nitrógeno. La interacción entre los nanotubos funcionalizados y la enzima parece estar determinada por los grupos de fósforo incorporados en el material durante el depósito electroquímico simultáneo, mejorando la actividad electrocatalítica y la sensibilidad hacia la oxidación de glucosa. Se ha conseguido una sensibilidad, referida a la cantidad de enzima en el bioelectrodo, seis veces mayor que en un bioelectrodo preparado por *drop-casting*.

La presencia de grupos funcionales de N y P, generados electroquímicamente sobre MWCNT, promueve la inmovilización de PQQ-GDH sobre la superficie del electrodo, observándose que presenta una actividad electrocatalítica a la oxidación de glucosa en condiciones de pH fisiológico. La interacción entre el material carbonoso funcionalizado y el recubrimiento enzimático, mejora la cinética de transferencia de electrones, probablemente debido a una mejor orientación del centro activo de la enzima hacia la superficie del electrodo.

El uso de un material carbonoso dopado con especies de nitrógeno cuaternario como elemento transductor, permitió el desarrollo de un biosensor enzimático de primera generación para la detección indirecta de glucosa a un potencial de $-0.4\text{ V vs. Ag/AgCl}$. La presencia del proceso redox reversible en superficie relacionado con el cofactor FAD/FADH_2 demuestra la inmovilización exitosa de la enzima en el electrodo. Teniendo en cuenta la elevada actividad catalítica del material carbonoso a la reducción de oxígeno, la variación de la densidad de corriente de esta reacción, como consecuencia de la reacción enzimática de la glucosa oxidasa, sirvieron para la medición de glucosa en disolución, obteniendo una sensibilidad independiente de la concentración de oxígeno en la disolución, con excelente reproducibilidad, repetitividad y estabilidad. Además, no se observan efectos significativos de interferentes, lo cual permitió la aplicación de este biosensor en la detección de glucosa en muestras reales como orina y bebidas azucaradas comerciales.

Se han desarrollado materiales electródicos de fMWCNT-AuNPs-Ab como biosensores electroquímicos del antígeno prostático específico (PSA). Se han empleado dos distribuciones de tamaño de nanopartículas de oro, obtenidas empleando dos relaciones molares PVP/Au, lo que permite controlar el área superficial electroquímicamente activa. Los materiales transductores sintetizados permitieron la inmovilización de anticuerpos específicos al antígeno prostático específico a través de la formación de enlaces covalentes Au-S. La distribución estrecha del tamaño de nanopartículas de Au promueve una mayor inmovilización, que se evidenció como un aumento en la cantidad de especies S-Au. La disminución de la corriente con el incremento de la concentración de PSA, como resultado de la formación del inmunocomplejo antígeno-anticuerpo, permitió la detección cronoamperométrica del analito, a través del bloqueo de reacción redox del ferroceno (empleado como sonda redox), siendo los electrodos con mayor cantidad de anticuerpos inmovilizados

(fMWCNT-AuNPs-50-Ab) los que presentan el mayor rango lineal (0 y 6 ng mL⁻¹) y mejor sensibilidad (4.74 mA ng g_{fMWCNT}⁻¹ mL⁻¹), lo que permite la detección en muestras humanas.

Referencias

- (1) Xiao, S. X.; Huang, C. S.; Li, Y. L. Carbon Materials. In: Xu, R. Xu, Y, editor. Modern Inorganic Synthetic Chemistry, 2nd edition, Elsevier, Amsterdam, **2017**, pp. 429–462.
- (2) Prasanth, R., Karthika-Ammini, S., Ge, L., Kumari-Thakur, M., Kumar-Thakur, V. Carbon Allotropes and Fascinated Nanostructures-The high-Impact Engineering Materials of the Millennium. In: T. Vijay Kumar, T. Manju Kumari, editor. Chemical Functionalization of Carbon Materials-Chemistry and Applications, Taylor and Francis group, CRC Press, Washington, **2016**, pp. 2-27.
- (3) T.C. Dinadayalane, J. Leszczynski, Comparative Theoretical Study on the Positional Preference for Functionalization of Two OH and SH Groups with (5,5) Armchair SWCNT, *J. Phys. Chem. C* **117** (2013) 14441–14450.
- (4) González-Gaitán, C., Ruíz-Rosas, R., Morallón, E., Cazorla-Amorós, Diego. Electrochemical Methods to Functionalize Carbon Materials. In: T. Vijay Kumar, T. Manju Kumari, editor. Chemical Functionalization of Carbon Materials-Chemistry and Applications, Taylor and Francis group, CRC Press, Washington, **2016**, pp. 230-249.
- (5) Jaisankar, S. N.; Haridharan, N.; Murali, A.; Sergii, P.; Špírková, M.; Mandal, A. B.; Matějka, L. Single-Electron Transfer Living Radical Copolymerization of SWCNT-g-PMMA via Graft from Approach. *Polymer* **2014**, *55* (13), 2959–2966.
- (6) Sun, Y.-P.; Fu, K.; Lin, Y.; Huang, W. Functionalized Carbon Nanotubes: Properties and Applications. *Acc. Chem. Res.* **2002**, *35* (12), 1096–1104.
- (7) Beguin, F. Frackowiak, E. Carbon for Electrochemical Energy Storage and Conversion Systems, Taylor and Francis, CRC Press, Boca Raton, **2010**.
- (8) Nishihara, H.; Kyotani, T. Templated Nanocarbons for Energy Storage. *Adv. Mater.* **2012**, *24* (33), 4473–4498.
- (9) Indrawirawan, S.; Sun, H.; Duan, X.; Wang, S. Nanocarbons in

Different Structural Dimensions (0–3D) for Phenol Adsorption and Metal-Free Catalytic Oxidation. *Appl. Catal. B Environ.* **2015**, *179*, 352–362.

- (10) Eatemadi, A.; Daraee, H.; Karimkhanloo, H.; Kouhi, M.; Zarghami, N.; Akbarzadeh, A.; Abasi, M.; Hanifehpour, Y.; Joo, S. W. Carbon Nanotubes: Properties, Synthesis, Purification, and Medical Applications. *Nanoscale Res. Lett.* **2014**, *9* (1), 393.
- (11) González-Gaitán, C.; Ruiz-Rosas, R.; Morallón, E.; Cazorla-Amorós, D. Effects of the Surface Chemistry and Structure of Carbon Nanotubes on the Coating of Glucose Oxidase and Electrochemical Biosensors Performance. *RSC Adv.* **2017**, *7* (43), 26867–26878.
- (12) Abellán-Llobregat, A.; Vidal, L.; Rodríguez-Amaro, R.; Canals, A.; Morallón, E. Evaluation of Herringbone Carbon Nanotubes-Modified Electrodes for the Simultaneous Determination of Ascorbic Acid and Uric Acid. *Electrochim. Acta* **2018**, *285*, 284–291.
- (13) Scholten, K.; Meng, E. A Review of Implantable Biosensors for Closed-Loop Glucose Control and Other Drug Delivery Applications. *Int. J. Pharm.* **2018**, *544* (2), 319–334.
- (14) Yao, X.; Niu, X.; Ma, K.; Huang, P.; Grothe, J.; Kaskel, S.; Zhu, Y. Graphene Quantum Dots-Capped Magnetic Mesoporous Silica Nanoparticles as a Multifunctional Platform for Controlled Drug Delivery, Magnetic Hyperthermia, and Photothermal Therapy. *Small* **2017**, *13* (2), 1602225.
- (15) Zhao, X.; Liu, L.; Li, X.; Zeng, J.; Jia, X.; Liu, P. Biocompatible Graphene Oxide Nanoparticle-Based Drug Delivery Platform for Tumor Microenvironment-Responsive Triggered Release of Doxorubicin. *Langmuir* **2014**, *30* (34), 10419–10429.
- (16) Bose, S.; Kuila, T.; Mishra, A. K.; Rajasekar, R.; Kim, N. H.; Lee, J. H. Carbon-Based Nanostructured Materials and Their Composites as Supercapacitor Electrodes. *J. Mater. Chem.* **2012**, *22* (3), 767–784.
- (17) Liu, X.-W.; Sun, T.-J.; Hu, J.-L.; Wang, S.-D. Composites of Metal–Organic Frameworks and Carbon-Based Materials: Preparations, Functionalities and Applications. *J. Mater. Chem. A* **2016**, *4* (10), 3584–3616.
- (18) Tang, J.; Liu, J.; Torad, N. L.; Kimura, T.; Yamauchi, Y. Tailored Design of Functional Nanoporous Carbon Materials toward Fuel Cell

Applications. *Nano Today* **2014**, 9 (3), 305–323.

- (19) Gross, A. J.; Holzinger, M.; Cosnier, S. Buckypaper Bioelectrodes: Emerging Materials for Implantable and Wearable Biofuel Cells. *Energy Environ. Sci.* **2018**, 11 (7), 1670–1687.
- (20) Wang, Z.; Dai, Z. Carbon Nanomaterial-Based Electrochemical Biosensors: An Overview. *Nanoscale* **2015**, 7 (15), 6420–6431.
- (21) Abellán-Llobregat, A.; Jeerapan, I.; Bandothkar, A.; Vidal, L.; Canals, A.; Wang, J.; Morallón, E. A Stretchable and Screen-Printed Electrochemical Sensor for Glucose Determination in Human Perspiration. *Biosens. Bioelectron.* **2017**, 91, 885–891.
- (22) Malhotra, B. D., Ali, M.A. Nanomaterials in Biosensors: Fundamentals and Applications. In: Malhotra, B. D.; Ali, M. A. editors, *Nanomaterials in Biosensors: Fundamentals and Applications*, Elsevier, Amsterdam, William Andrew Publishing, **2018**, pp. 1–74.
- (23) De Volder, M. F. L.; Tawfick, S. H.; Baughman, R. H.; Hart, A. J. Carbon Nanotubes: Present and Future Commercial Applications. *Science* **2013**, 339 (6119), 535 – 539.
- (24) Mubarak, N. M., Sahu, J. N., Wong, J. R., Jayakumar, N. S., Ganesan, P., and Abdullah, E. C. Overview on the Functionalization of Carbon Nanotubes. In: Vijay Kumar, T., Manju Kumari, T. editor. *Chemical Functionalization of Carbon Materials-Chemistry and Applications*, Taylor and Francis group, CRC Press, Washington, **2016**, pp. 89-101.
- (25) Ramanathan, T.; Fisher, F. T.; Ruoff, R. S.; Brinson, L. C. Amino-Functionalized Carbon Nanotubes for Binding to Polymers and Biological Systems. *Chem. Mater.* **2005**, 17 (6), 1290–1295.
- (26) Martínez, M. T.; Callejas, M. A.; Benito, A. M.; Cochet, M.; Seeger, T.; Ansón, A.; Schreiber, J.; Gordon, C.; Marhic, C.; Chauvet, O.; et al. Sensitivity of Single Wall Carbon Nanotubes to Oxidative Processing: Structural Modification, Intercalation and Functionalisation. *Carbon* **2003**, 41 (12), 2247–2256.
- (27) Ma, P.-C.; Siddiqui, N. A.; Marom, G.; Kim, J.-K. Dispersion and Functionalization of Carbon Nanotubes for Polymer-Based Nanocomposites: A Review. *Compos. Part A Appl. Sci. Manuf.* **2010**, 41 (10), 1345–1367.
- (28) Holzinger, M.; Abraham, J.; Whelan, P.; Graupner, R.; Ley, L.; Hennrich, F.; Kappes, M.; Hirsch, A. Functionalization of Single-

- Walled Carbon Nanotubes with (R-)Oxycarbonyl Nitrenes. *J. Am. Chem. Soc.* **2003**, *125* (28), 8566–8580.
- (29) Ghanem, M. A.; Kocak, I.; Al-Mayouf, A.; AlHoshan, M.; Bartlett, P. N. Covalent Modification of Carbon Nanotubes with Anthraquinone by Electrochemical Grafting and Solid Phase Synthesis. *Electrochim. Acta* **2012**, *68*, 74–80.
- (30) Mayuri, P.; Huang, S.-T.; Mani, V.; Kumar, A. S. A New Organic Redox Species-Indole Tetraone Trapped MWCNT Modified Electrode Prepared by in-Situ Electrochemical Oxidation of Indole for a Bifunctional Electrocatalysis and Simultaneous Flow Injection Electroanalysis of Hydrazine and Hydrogen Peroxide. *Electrochim. Acta* **2018**, *268*, 150–162.
- (31) Servinis, L.; Beggs, K. M.; Scheffler, C.; Wölfel, E.; Randall, J. D.; Gengenbach, T. R.; Demir, B.; Walsh, T. R.; Doeven, E. H.; Francis, P. S.; et al. Electrochemical Surface Modification of Carbon Fibres by Grafting of Amine, Carboxylic and Lipophilic Amide Groups. *Carbon* **2017**, *118*, 393–403.
- (32) He, M.; Swager, T. M. Covalent Functionalization of Carbon Nanomaterials with Iodonium Salts. *Chem. Mater.* **2016**, *28* (23), 8542–8549.
- (33) Deng, S.; Jian, G.; Lei, J.; Hu, Z.; Ju, H. A Glucose Biosensor Based on Direct Electrochemistry of Glucose Oxidase Immobilized on Nitrogen-Doped Carbon Nanotubes. *Biosens. Bioelectron.* **2009**, *25* (2), 373–377.
- (34) Ivnitski, D.; Artyushkova, K.; Rincón, R. A.; Atanassov, P.; Luckarift, H. R.; Johnson, G. R. Entrapment of Enzymes and Carbon Nanotubes in Biologically Synthesized Silica: Glucose Oxidase-Catalyzed Direct Electron Transfer. *Small* **2008**, *4* (3), 357–364.
- (35) Davis, J. J.; Coleman, K. S.; Azamian, B. R.; Bagshaw, C. B.; Green, M. L. H. Chemical and Biochemical Sensing with Modified Single Walled Carbon Nanotubes. *Chem. – A Eur. J.* **2003**, *9* (16), 3732–3739.
- (36) Liu, J.; Wang, X.; Wang, T.; Li, D.; Xi, F.; Wang, J.; Wang, E. Functionalization of Monolithic and Porous Three-Dimensional Graphene by One-Step Chitosan Electrodeposition for Enzymatic Biosensor. *ACS Appl. Mater. Interfaces* **2014**, *6* (22), 19997–20002.
- (37) Kausaite-Minkstimiene, A.; Mazeiko, V.; Ramanaviciene, A.;

- Ramanavicius, A. Evaluation of Amperometric Glucose Biosensors Based on Glucose Oxidase Encapsulated within Enzymatically Synthesized Polyaniline and Polypyrrole. *Sensors Actuators B Chem.* **2011**, *158* (1), 278–285.
- (38) Al-Lolage, F. A.; Meneghello, M.; Ma, S.; Ludwig, R.; Bartlett, P. N. A Flexible Method for the Stable, Covalent Immobilization of Enzymes at Electrode Surfaces. *ChemElectroChem* **2017**, *4* (6), 1528–1534.
- (39) Chen, Y.; Yang, X.-J.; Guo, L.-R.; Li, J.; Xia, X.-H.; Zheng, L.-M. Direct Electrochemistry and Electrocatalysis of Hemoglobin at Three-Dimensional Gold Film Electrode Modified with Self-Assembled Monolayers of 3-Mercaptopropylphosphonic Acid. *Anal. Chim. Acta* **2009**, *644* (1–2), 83–89.
- (40) Wang, C. H.; Yang, C.; Song, Y. Y.; Gao, W.; Xia, X. H. Adsorption and Direct Electron Transfer from Hemoglobin into a Three-Dimensionally Ordered Macroporous Gold Film. *Adv. Funct. Mater.* **2005**, *15* (8), 1267–1275.
- (41) López-Bernabeu, S.; Huerta, F.; Morallón, E.; Montilla, F. Direct Electron Transfer to Cytochrome c Induced by a Conducting Polymer. *J. Phys. Chem. C* **2017**, *121* (29), 15870–15879.
- (42) Quílez-Bermejo, J.; González-Gaitán, C.; Morallón, E.; Cazorla-Amorós, D. Effect of Carbonization Conditions of Polyaniline on Its Catalytic Activity towards ORR. Some Insights about the Nature of the Active Sites. *Carbon* **2017**, *119*, 62–71.
- (43) Abellán-Llobregat, A.; González-Gaitán, C.; Vidal, L.; Canals, A.; Morallón, E. Portable Electrochemical Sensor Based on 4-Aminobenzoic Acid-Functionalized Herringbone Carbon Nanotubes for the Determination of Ascorbic Acid and Uric Acid in Human Fluids. *Biosens. Bioelectron.* **2018**, *109*, 123–131.
- (44) Vilkanauskyte, A.; Erichsen, T.; Marcinkeviciene, L.; Laurinavicius, V.; Schuhmann, W. Reagentless Biosensors Based on Co-Entrapment of a Soluble Redox Polymer and an Enzyme within an Electrochemically Deposited Polymer Film. *Biosens. Bioelectron.* **2002**, *17* (11), 1025–1031.
- (45) Tran, D. N.; Balkus, K. J. Perspective of Recent Progress in Immobilization of Enzymes. *ACS Catal.* **2011**, *1* (8), 956–968.